THE JOURNAL OF

PHYSICAL CHEMISTRY

(Registered in U. S. Patent Office)

CONTENTS

SYMPOSIUM ON THE WETTING PROCESS, Boston, Mass., April 8, 1959

Notes

THE JOURNAL OF PHYSICAL CHEMISTRY

(Registered in U. S. Patent Office)

WETTING OF SOLIDS BY SOLUTIONS AS A FUNCTION OF SOLUTE ADSORPTION[1,2]

By R. J. Ruch and L. S. Bartell

Institute for Atomic Research and Department of Chemistry, Iowa State University, Ames, Iowa

Received November 11, 1959

The wetting of flat platinum and chromium slides of small surface area by aqueous solutions of decylamine was measured as a function of the adsorption of the amine and the surface tension of the solutions. Adsorption at the solid–solution interface was measured *in situ* by an optical polarimetric method and wetting was determined concurrently by contact angle measurements employing the captive bubble technique. Adsorption and wetting results for platinum were sharply defined but those for chromium were somewhat obscured by erratic kinetic effects. Multilayer adsorption was observed in all cases, and isotherms on platinum in basic solutions exhibited steps. The observed contact angles of the solutions on platinum rose from 0° to a maximum of about 90° as adsorption increased, and then fell, sometimes to 0°, as adsorption proceeded further. A model is proposed to explain the wetting results which provides a semi-quantitative scheme for computing the behavior of the contact angles from the adsorption isotherms.

Introduction

Because of the ability of molecules on a surface to mask the force fields of underlying molecules, the wetting of surfaces may be strongly influenced by adsorption. When orientational effects are present, the dependence of wetting upon surface excess of adsorbate may be complex. While the problem is understood in a qualitative way, and, indeed, is utilized in a wide variety of commercial processes, no theories seem to have been proposed which have allowed the direct calculation of contact angles as a function of adsorption from simple observables. The difficulty in measuring adsorption on small surface areas or of wetting on powders has greatly impeded progress. Several informative studies have been made, nevertheless, which circumvented some of the difficulties by utilizing polished specimens for wetting measurements and crushed specimens for adsorption as, for example, by Gaudin and co-workers.[3]

In the present study an optical polarimetric method[4–6] was used to measure adsorption *in situ*

on flat polished surfaces of small area. Contact angles were measured on the same surfaces by the captive bubble technique. The systems investigated, namely, aqueous solutions of *n*-decylamine on polished platinum and chromium, exhibited contact angles which rose to a maximum and then fell as the concentration of adsorbate was increased.

The purpose of the present investigation was, first, to develop the optical method for studying adsorption of small molecules on flat surfaces, and secondly, to elucidate the structural basis of wetting of solids by solutions.

Experimental Details

Materials.—The same piece of platinum, 20 × 10 × 2 mm., was used for all of the adsorption experiments on platinum. The platinum was polished with wet Behr-Manning emery polishing paper followed by Linde A on a polishing wheel covered with Buehler Ltd. finest quality microcloth. In experiments on chromium, separate chromium plated steel slides having an area of about 2 cm.[2] were cut from commercial ferrotype plates for each adsorption trial. Prior to an adsorption trial, the platinum and chromium slides were cleaned by hand polishing with Linde A or Linde B, flushing in a stream of distilled water, and wiping dry with a benzene dampened Kleenex. The platinum slide was flamed in a Meker burner to a bright red glow and cooled for two minutes after the disappearance of the glow before it was placed in the adsorption medium. The chromium slides were passed through the flame of a Meker burner six times and cooled 35 seconds. The surfaces were assumed to be free of impurities and suitable for adsorption

(1) Work was performed in the Ames Laboratory of the U. S. Atomic Energy Commission.

(2) Based on a dissertation by R. J. Ruch to the Graduate School, Iowa State University, in partial fulfillment of the requirements for the degree of Doctor of Philosophy, 1959.

(3) A. M. Gaudin, "Flotation," 2nd Edition, McGraw-Hill Book Co., Inc., New York, N. Y., 1957, pp. 175, 268.

(4) P. Drude, *Ann. physik. Chem.*, **36**, 532 (1889); **36**, 865 (1889); **39**, 481 (1890).

(5) L. Tronstad, *Trans. Faraday Soc.*, **29**, 502 (1933).

(6) A. Rothen, *Rev. Sci. Instr.*, **16**, 26 (1945).
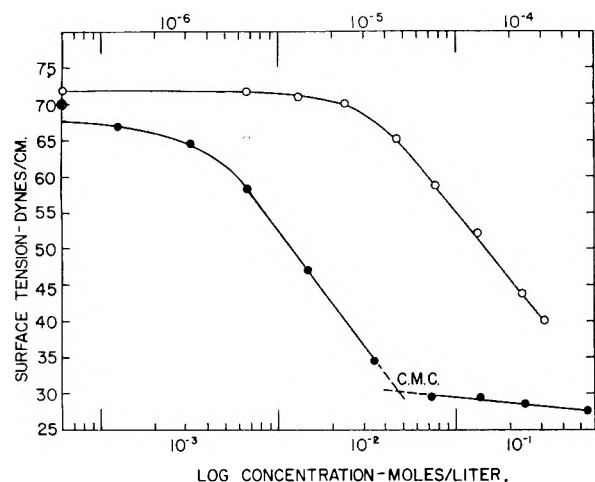
Fig. 1.—Surface tension of aqueous solutions of decylamine hydrochloride: ○ (upper abscissa); pH 10.2; 28°; system buffered with 0.05 M Na₂CO₃ and 0.05 M NaHCO₃. ● (lower abscissa): pH 6.0–6.2; 28.5°; no buffer, acid or base added to system.
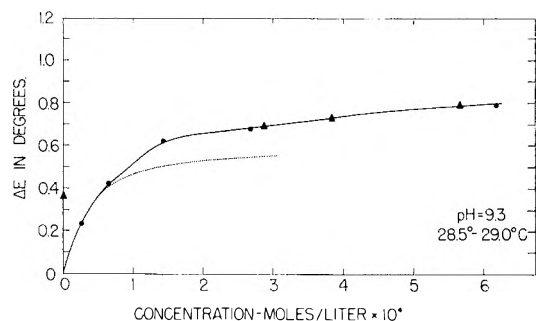
Fig. 2.—Adsorption of decylamine on platinum at pH 9.3. System buffered with 0.01 M Na₂CO₃ and 0.06 M NaHCO₃. Triangular points, explicitly defined in the text, represent sorption cycles later than the initial uptake cycle. The dotted line corresponds to that portion of the adsorbed film estimated to be in the bottom layer.

studies after this cleaning procedure if they were completely wet by the adsorption medium. The platinum was completely repolished whenever heterogeneous adsorption was noted or the surface became too scratched for optical studies.

Doubly distilled water was used in all experiments. Reagent grade sodium carbonate and sodium bicarbonate were used for buffer systems. Neither the water nor the buffer materials had any adsorbable impurities that could be detected by contact angle measurements.

Matheson Co. n-decylamine was used to prepare decylamine hydrochloride. The hydrochloride for all except one stock solution was recrystallized four times and had a melting point of 181.5°. The stock solution for the higher concentrations in runs at a pH of 6 was prepared from a product recrystallized twice, having a melting point of 181–182°.

All glassware and Teflon parts were cleaned before use with a 1:8 nitric acid–sulfuric acid cleaning solution.

Apparatus.—A Cenco–DuNouy tensiometer was employed for surface tension measurements.

The instrument used to measure the amount of material adsorbed was similar in optical arrangement to the ellipsometer described by Rothen[6] except for the half-shade device. A phase-shifting piece of mica was used to obtain half-fields for balancing the instrument. The instrument was used at an angle of incidence of 70° at the solution–metal interface. The setting of the quarter-wave plate was kept constant during the course of any particular run.

The adsorption cell used was a Pyrex turbidity cell, 30 × 30 × 60 mm., obtained from the Phoenix Precision Instrument Company.

Air bubbles for contact angle measurements were formed with a micro-syringe attached to a 0.1 ml. pipet having a flat Teflon tip. The bubbles were viewed with a low-power microscope having a filar micrometer eyepiece. The microscope was mounted in a graduated rotating object-holder and contact angles were measured directly.

Procedures.—The concentration of solutions used for adsorption and for surface tension measurements was increased by pipetting stock solutions of decylamine hydrochloride to known quantities of the adsorption medium. No corrections were made for adsorption on container walls. The error for the most dilute solutions used in adsorption would have been about 10% if unimolecular adsorption had occurred and the glass had a roughness factor of one.

The pH in the basic region was controlled with sodium carbonate–sodium bicarbonate buffer or by using 0.1 N potassium hydroxide and a Radiometer Model TTT 1a automatic titrator. Doubly distilled water from the still had a pH of approximately 6 and was used without buffer, acid or base in adsorption trials at this pH value.

Solutions used for surface tension measurements were stirred for three minutes after the addition of the amine hydrochloride. Readings were taken over a 10 to 20 minute period until the drift of the readings had fallen to a point where the average deviation of the last five to seven readings was about 0.1 dyne/cm.

In studies of adsorption, at least 15 minutes and often more than one hour was allowed for equilibrium to be reached. Optical measurements were taken after contact angle measurements. Fourteen readings were taken for each point on the adsorption curves. The two highest and two lowest readings were discarded and the average of the remaining ten was used for the point. The average deviation in a given series of readings was usually about 0.03°.

Air bubbles of about 4 mm. in diameter were used for contact angle measurements. Each advancing and each receding angle on contact angle curves is the average of measurements taken at three spots on the surface.

All optical, contact angle and surface tension measurements were made at room temperature. The temperature usually did not vary more than a degree throughout a trial.

Results

Surface Tension.—The variation of the surface tension of aqueous solutions of decylamine is illustrated as a function of concentration of amine in Fig. 1 for representative measurements at pH values of 6.0–6.2 and 10.2. The points plotted on the left ordinate correspond to the surface tensions of the adsorption media at zero concentration of amine. The effect of micelle formation is apparent in the curve for the solution at lower pH, where a break occurs at 0.047 M, the critical micelle concentration. In solutions with pH values in the vicinity of 10, the solubility was always exceeded before such a break occurred.

The steep linear segments of the curves indicate that the surface active species were approaching a limiting area per molecule at the air interface. An application of Gibbs' adsorption isotherm, in which activity was assumed to be proportional to total amine concentration, yielded limiting areas ranging from 29 to 35 Å.[2] for the various solutions studied. No systematic variation with pH was observed within the limits of experimental accuracy achieved.

Adsorption.—Adsorption is expressed in terms of ΔE, the difference in degrees between analyzer readings for the clean slide in water or buffer solution and the slide with adsorbed film in the adsorption solution. Previous experiments in air in which optical measurements were calibrated with radiotracer measurements showed that ΔE was proportional to amount adsorbed, even in the case of frac-
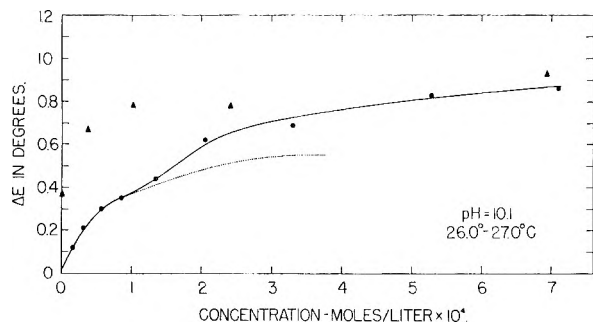
Fig. 3.—Adsorption of decylamine on platinum at pH 10.1. System buffered with 0.07 M Na_2CO_3 and 0.05 M $NaHCO_3$.
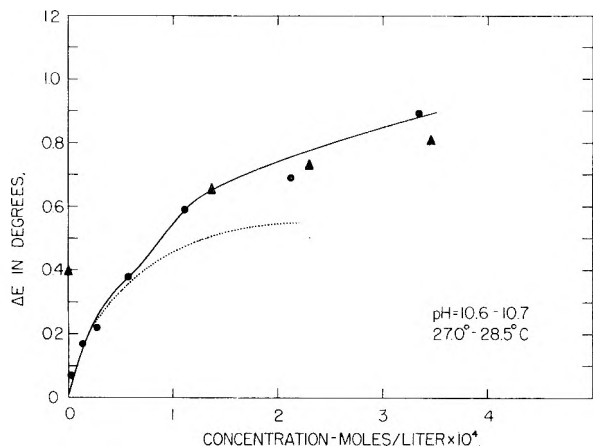
Fig. 4.—Adsorption of decylamine on platinum at pH 10.6–10.7. System buffered with 0.06 M Na_2CO_3 and 0.01 M $NaHCO_3$.

Fig. 5.—Adsorption of decylamine on platinum at pH 10.6. pH adjusted with 0.1 N KOH added by an automatic titrator.
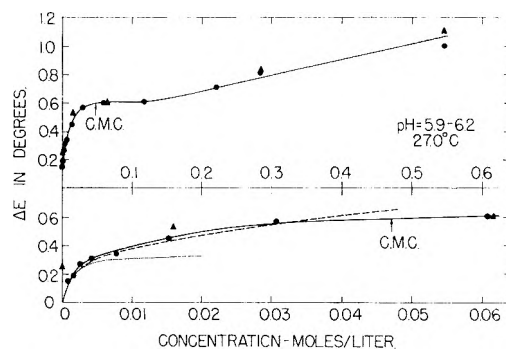
Fig. 6.—Adsorption of decylamine hydrochloride on platinum at pH 5.9–6.2. The dashed line represents the BET calculated curve for three layer adsorption.

tional monolayers.[7] It is not unreasonable to expect ΔE to be approximately proportional to the surface concentration of adsorbate in solutions also, and direct proportionality has been assumed in the following. Experiments with paraffin and octadecylamine films indicated that the sensitivity of measurements, in degrees per Å. of film thickness, was very nearly the same in solution as in air at the same angle of incidence.

Representative adsorption isotherms of decylamine on platinum at various pH values are shown in Figs. 2–6. Characteristic of all eleven isotherms run in basic solution was the stepped shape, which suggested the adsorption of a monolayer followed by the adsorption of a second layer as the concentration was increased. Additional support for this picture was lent by studies of monolayers of decylamine adsorbed from cetane solutions and read in air. These readings indicated that monolayer coverage of similar compactness in the aqueous medium would correspond to a ΔE of about 0.55°. This is just the value that appears to be characteristic of coverage by the first layer in the aqueous studies, and one-half the maximum value achieved at high concentrations of amine. BET plots for two layer adsorption were able to fit the data only in the mean, being insufficiently flexible to follow the steps.

Octadecylamine monolayers on platinum gave a reading of about 1.46° for ΔE. If octadecylamine

(7) L. S. Bartell and J. F. Betts, This Journal, in press.

monolayers are assumed to have areas per molecule on platinum of 21 or 22 Å.[2], then the readings for decylamine suggest an area per molecule of roughly 33 Å.[2] This value agrees well with the crude values obtained at the air interface from surface tension measurements.

The triangular adsorption points in Fig. 2 represent a desorption isotherm which follows the adsorption isotherm until an amount of decylamine corresponding to firm adsorption[8] is reached. The triangular points in Fig. 3–6 were measured after replacing the solution of maximum concentration in the initial adsorption run by water or buffer and repeating the adsorption cycle. If it is assumed that monolayer coverage, ΔE_m, corresponds to 0.55°, the average amount of firm adsorption was about 60% of a monolayer, but varied from run to run. The increase in adsorption noted upon repeating some adsorption cycles may have resulted from coöperative interactions provided by the framework of molecules adsorbed firmly in the preceding cycles.

A comparison of isotherms reveals that the platinum surfaces were not accurately reproducible from run to run, and this variation obscures effects of small changes in pH. A complicating factor in this respect was the apparent interaction of the carbonate buffer with the amine, which appeared to be more specific than a simple salt effect. The buffer decreased the surface tension depression of the amine by several dynes, decreased the adsorp-

(8) The term firm adsorption used by several authors in recent years refers, somewhat arbitrarily, to that part which desorbs at a vastly slower rate than the rest.
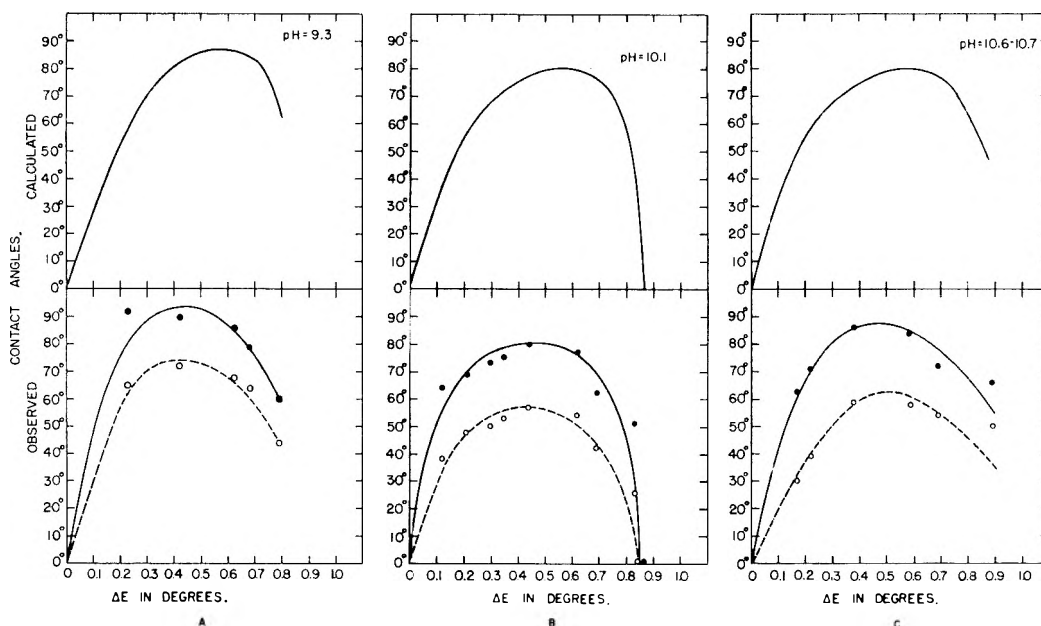
Fig. 7.—Relationship between adsorption and contact angles for aqueous solutions of decylamine on platinum: ●, observed advancing angles; ○, observed receding angles. Calculated curves plotted using $72P - 15R + 57S = \gamma_{LA} \cos \theta$ and $\Delta E_m = 0.55°$: (A) pH 9.3, (B) pH 10.1, (C) pH 10.6–10.7.

tion on platinum, but also decreased the solubility of the amine.

The effect upon the adsorption isotherms of changing from a pH of 10 to a pH of 6 was striking. The isotherms observed in the acidic range were essentially type II isotherms until the critical micelle concentration was reached, whereupon they leveled off sharply. This behavior has been noted in other studies with similar systems, as dodecyl-ammonium chloride on alumina.[9] Unlike the isotherms referred to, however, the present isotherms began to climb again when the solute concentration was increased further. The optical reading corresponding to a monolayer was conspicuously less than that at higher pH values. For want of an independent assessment of the reading for monolayer coverage, ΔE_m, the value of 0.33°, derived from a BET fit of the initial portion of the curve, was assumed. This, when the effect of the chloride ion is considered, represents an area per molecule of approximately twice that of the free amine. A large area also has been found in the analogous system of dodecylamine hydrochloride on alumina by Tamamushi and Tamaki[9] who reported the value of 101 Å.^{2} per molecule. The total concentration of amine required to give adsorption in acidic solutions was one hundred-fold greater than that required at a pH of 10. This was interpreted as indicating that adsorption at pH 10 was principally due to free amine, and that at pH 6, where the concentration of free amine was extremely low, was due to the hydrochloride. It is possible, however, that protonation of a surface oxide layer suppressed the adsorption of amine ions in the acidic region but not in the basic region.

When allowance was made for the effect of the c.m.c., the general aspect of acidic isotherms was more suggestive of a type II isotherm than of the

stepped isotherms obtained at higher pH values. This implies that the adsorbed hydrochloride was not as highly ordered structurally as the free amine.

Adsorption experiments on chromium were much less reproducible than on platinum, and suffered erratic kinetic effects which made the equilibrium readings at lower concentrations very uncertain. The affinity of the amine for chromium at pH 10 was markedly less than for platinum. Adsorption appeared to lag slightly behind adsorption at the air interface, as inferred from surface tension measurements, until a concentration of about 3×10^{-4} mole/liter was reached. At higher concentrations adsorption on chromium rapidly approached a double molecular layer. Firm adsorption on chromium was approximately 40% of a monolayer. This is similar to the firm adsorption found in an earlier study[10] of octadecylamine adsorbed from cetane on chromium and depleted with benzene.

Wetting.—The variation of contact angles with amount of amine adsorbed on platinum is shown in Figs. 7–9 for the systems corresponding to the isotherms in Figs. 2–6. Contact angles increased, approaching a maximum at the coverage corresponding approximately to a statistical monolayer, and then decreased, sometimes to 0°, as adsorption proceeded. The maximum values reached were about 90° for advancing angles. Hysteresis quickly rose to 30° at perhaps 0.3 of a monolayer, and then slowly dropped to 15° before dropping precipitously to zero when complete wetting occurred at slightly less than a double molecular layer.

The contact angle curves for chromium surfaces were similar to those for platinum. Maximum contact angles were 10° or 20° less than on platinum, however. This undoubtedly was associated with the lower surface tension of the solution at comparable stages of adsorption on chromium,

(9) B. Tamamushi and K. Tamaki, *Proc. 2nd Intern. Congr. Surface Activity*, **3** 449 (1957).

(10) L. S. Bartell and R. J. Ruch, THIS JOURNAL, **60**, 1231 (1956).
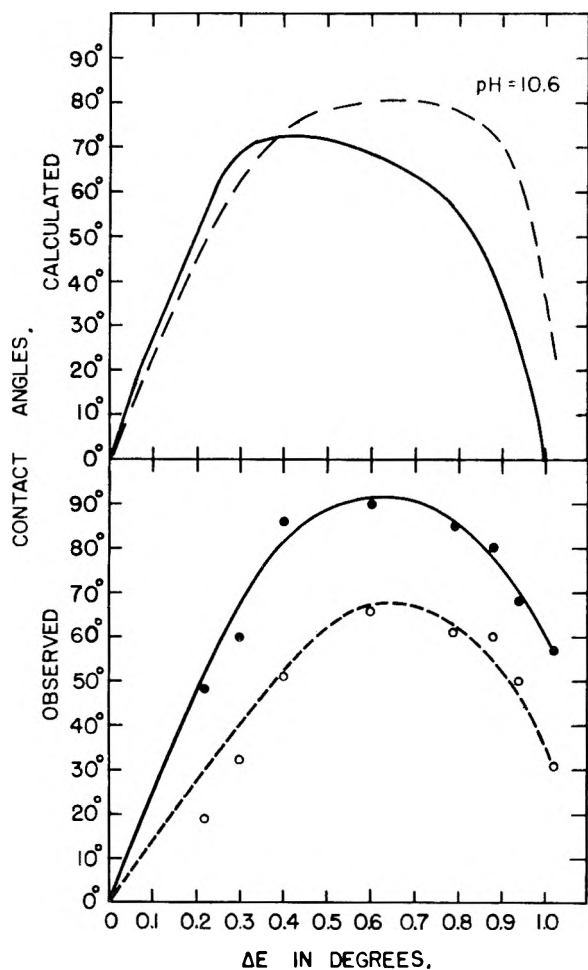
Fig. 8.—Contact angles for aqueous solutions of decyl-amine on platinum at a pH of 10.6: ●, observed advancing angles; ○, observed receding angles. Both calculated curves plotted using $72P - 15R + 57S = \gamma_{LA} \cos \theta$. ΔE_m was 0.55° for the solid calculated curve and 0.65° for the dashed calculated curve.
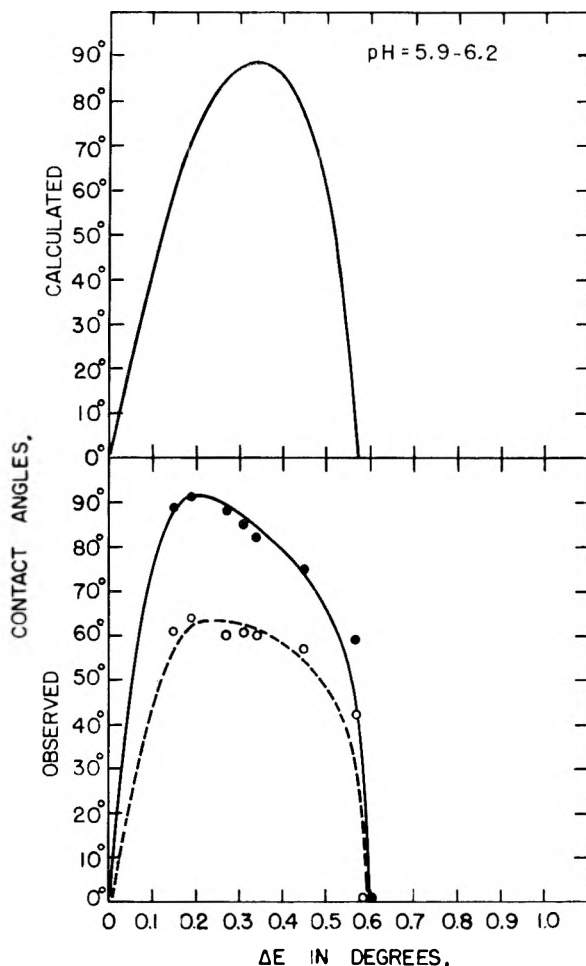
Fig. 9.—Contact angles for aqueous solutions of decyl-amine hydrochloride on platinum at a pH of 5.9 to 6.2°: ●, observed advancing angles; ○, observed receding angles. Calculated curve plotted using $72P - 15R + 57S = \gamma_{LA} \cos \theta$ and $\Delta E_m = 0.33°$.

which exhibited a lower affinity for the amine. Measurements on chromium were much more erratic than on platinum, for contact angles as well as for adsorption. In many cases it was necessary for air bubbles to remain in contact with the chromium surfaces for a minute or longer before the bubbles became attached and measurements could be made. On platinum adhesion of the air bubbles to the surface usually took place in seconds.

Proposed Model of Wetting

The revealing shape of the adsorption isotherms and closely correlated behavior of the contact angles suggests a simple model of the wetting process. The model, illustrated schematically in Fig. 10, makes use of the familiar Young equation

$$\gamma_{SA} - \gamma_{SL} = \gamma_{LA} \cos \theta \quad (1)$$

The contact angle θ can be calculated if the appropriate boundary tensions, γ_{ij} are known. The surface tension of the solution, γ_{LA}, is measured directly. In the proposed model the other tensions are derivable from the adsorption isotherm as follows.

In basic solutions it is considered that the surface of the solid is divided into regions variously covered with adsorbed water, adsorbed decylamine monolayer, and adsorbed decylamine double molecular layer. It is proposed that the fraction of each present, P, R and S, respectively, can be inferred, at any concentration, from the adsorption isotherm. The amine molecules in the first layer are presumed to be attached to the solid principally by their polar groups such that their hydrocarbon chains are exposed to the adsorption medium. The molecules in the second layer are postulated to adsorb on those of the first in the opposite orientation, with polar groups directed toward the adsorption medium. The effective boundary tensions are considered to be the area average of the individual tensions of the regions present. Representative regions of each type are assumed to be of sufficient size that edge effects can be ignored. Equation 1 then becomes

$$P(\gamma_{WA} - \gamma_{WL}) + R(\gamma_{MA} - \gamma_{ML}) + S(\gamma_{DA} - \gamma_{DL}) = \gamma_{LA} \cos \theta \quad (2)$$

where the subscripts W, M and D refer to adsorbed water, monolayer of amine and double molecular layer of amine, respectively.

The adsorbed multilayer of water is assumed to be essentially liquid-like, and hence ($\gamma_{WA} - \gamma_{WL}$) be-

$$\gamma_{SA} - \gamma_{SL} = \gamma_{LA} \cos \theta$$

YOUNG'S EQUATION

P + R + S = 1
O = WATER
O—— = POLAR-NON-POLAR
             MOLECULE
W = WATER
M = MONOLAYER
D = DOUBLE MOLECULAR LAYER

$$P(\gamma_{WA} - \gamma_{WL}) + R(\gamma_{MA} - \gamma_{ML}) + S(\gamma_{DA} - \gamma_{DL}) = \gamma_{LA} \cos \theta$$

MODIFIED YOUNG'S EQUATION
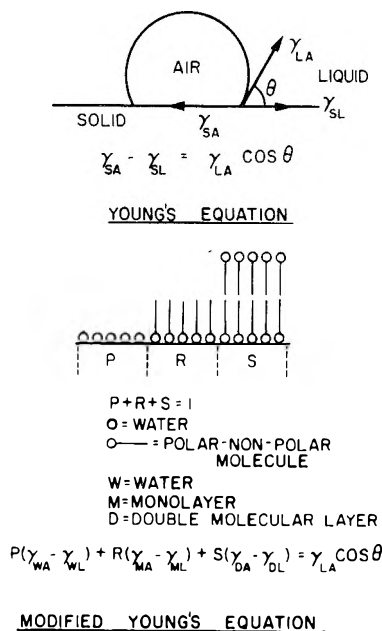
Fig. 10.—Proposed model for calculating contact angles.

comes simply the surface tension of water, γ_{WA}. The value of 72 dynes/cm. was taken.

The value of $(\gamma_{MA} - \gamma_{ML})$ may be estimated from the contact angle of water on various types of hydrocarbon surfaces with the aid of Young's equation. The surface involved should in many respects be intermediate between close-packed methyl surfaces such as are found in crystalline hydrocarbons, and methylene surfaces found in polyethylene. Alternatively they should resemble monolayers of n-octadecylamine, although the packing is not as compact in the shorter compound. The contact angles of water on these surfaces of 111°, 94° and 102° reported by Zisman, et al.[11,12] suggest that a plausible value for $(\gamma_{MA} - \gamma_{ML})$ is −15 dynes/cm., the average for the three surfaces.

The hydrated surface of the double adsorbed layer may be considered to have a composition similar to that of concentrated ammonium hydroxide. The interfacial tension between such a surface and water should be low. Hence, $(\gamma_{DA} - \gamma_{DL})$ was taken for the purpose of comparison as 57 dynes/cm., the surface tension of concentrated ammonium hydroxide.

The remaining variables, P, R and S, are not uniquely defined by the isotherm, but may be estimated to within small limits if the asymptotic value corresponding to ΔE_m, the monolayer reading, is assumed to be known. Plausible values, ΔE_u, representing adsorption of molecules in the first layer, were inferred from curves constructed to connect smoothly the initial portions of the isotherms with the asymptotic line, ΔE_m. The dotted lines in Fig. 2–4, and the dot dashed line in Fig. 5 correspond to these estimates of ΔE_u for an assumed asymptote of 0.55°. The fraction P then equals $(\Delta E_m - \Delta E_u)/\Delta E_m$, S equals $(\Delta E - \Delta E_u/\Delta E_m$, and R equals $1 - (P + S)$. In calculations, ΔE values were taken from the smooth curves drawn through experimental points.

(11) H. W. Fox and W. A. Zisman, *J. Colloid Sci.*, **7**, 428 (1952).
(12) E. G. Shafrin and W. A. Zisman, *ibid.*, **7**, 166 (1952).

A comparison between calculated and observed contact angles is presented in Fig. 7 and 8. The solid calculated curves are based on a value of ΔE_m of 0.55°. In Fig. 8 the effect of varying the choice of ΔE_m from 0.55 to 0.65° is shown. On the whole the agreement between experiment and calculation is surprisingly good considering the simplicity of the model. No attempt has been made to vary the parameters of the model arbitrarily to obtain an optimum fit.

As discussed above, the structure of the film adsorbed from acid solutions appears less well defined than the film at pH 10. Accordingly, the wetting model cannot be expected to apply as accurately to acidic films. A rote application of the model, assuming $\Delta E_m = 0.33°$, gives a better fit, as shown in Fig. 9, than might have been anticipated, but a fit inferior to that at pH 10. The faster increase of θ in the experimental acidic curves probably results from a faster blanketing of the surface by the haphazardly tipped amine ions than by the more nearly vertical amine molecules, at a given number of molecules per square centimeter.

When slides with films thicker than a monolayer were withdrawn from the adsorption medium it was sometimes observed that the film, in air, was thinner than in solution, but never thinner than a monolayer. If the receding solution quantitatively removed the molecules beyond the first layer, the quantity $(\gamma_{DA} - \gamma_{DL})$ would perhaps correspond more nearly to the surface tension of a hydrocarbon than to that of an ammonia solution. Wetting curves indicate no great need for such a correction, and direct optical measurements, difficult to compare precisely in two different media, indicate only partial removal. It cannot be expected, however, that the stability in air of an amine layer with its polar group outward, would be very great.

Finally, it may be noted that the model does not account for hysteresis. It perhaps would have been preferable to have averaged the tensions around the periphery of the drop rather than taking a direct area average. That such an average might be different, and account at least partially for the hysteresis, can be explained as follows. The periphery of an advancing droplet would tend to move spontaneously over the high energy patches and come to rest on low energy patches of monolayer. The periphery of a receding drop would tend to be held back on high energy patches of adsorbed water or amine double molecular layer, and lower the contact angle. It is clear that the magnitude of the hysteresis would depend upon the geometric distribution of such patches. No quantitative treatment of this has been devised.

Conclusions

It is possible, using optical methods, to measure concurrently both adsorption isotherms from aqueous solutions and contact angles of the solutions on small flat metal slides. Isotherms of n-decylamine on platinum have a stepped shape corresponding to the adsorption of a first layer with functional groups down, and of a second layer with functional groups up. Decylamine hydrochloride also exhibits multilayer adsorption but is not as

strongly ordered as the free amine. A simple quantitative model, relating the variation of contact angles with concentration to the adsorption isotherm, correctly represents the wetting data.

Acknowledgments.—It is a pleasure to ack-

nowledge helpful discussions with Professors R. S. Hansen and F. E. Bartell. We are grateful to the American Petroleum Institute for a Grant-in-Aid which contributed materially to the equipment used.

CONSTITUTIVE RELATIONS IN THE WETTING OF LOW ENERGY SURFACES AND THE THEORY OF THE RETRACTION METHOD OF PREPARING MONOLAYERS[1]

By Elaine G. Shafrin and William A. Zisman

U. S. Naval Research Laboratory, Washington 25, D. C.

Received November 11, 1959

Earlier systematic studies of the angle of contact (θ) exhibited by drops of liquid on plane, solid surfaces of low surface energy have revealed a regular linear variation in cos θ with the surface tension (γ_{LV}) of a large variety of liquids; this led to the concept of the critical surface tension of spreading (γ_c) and its use in characterizing the wettability of organic solids and of high energy surfaces coated with adsorbed organic films. Effects of the nature and packing of the atoms or organic radicals in the organic surface in determining the wetting of the solid are summarized. Simple and useful correlations have been found between γ_c and the constitution of low energy solid surfaces. It is concluded that usually atoms more than a few atom diameters below the surface have no influence on wetting. The "retraction method" of preparing monomolecular films from solutions on solids is shown to be a direct consequence of the above constitutive law of wetting. The same analysis can be applied to a pure liquid also, and it results in the explanation of the behavior of the autophobic liquids at room temperature and of the process of depositing a monolayer on a solid by retraction from the melt over a range of temperatures.

Introduction

Since the tendency for a drop of liquid to spread over a plane solid surface increases as the contact angle θ decreases, the contact angle provides a useful, inverse measure of wettability. Providing suitable precautions are taken to employ smooth, clean, solid surfaces and pure, well-defined materials, there is no difficulty in obtaining reliable, reproducible measurements of θ. When the solid low energy surface is plane, smooth and non-porous,[2] the slowly advancing and receding contact angles are equal. In all cases here, reference is to the slowly advancing contact angle.

Systematic studies have been reported[2-13] earlier for the contact angles of a wide variety of pure liquids on low energy solid surfaces[2-10,13] and high energy surfaces.[11,12] These have revealed significant regularities in the wettability of organic crystals and polymers as well as of high energy surfaces modified by the adsorption of monolayers of oriented organic molecules. A rectilinear relation has been established empirically between the cosine of the contact angle and the surface tension (γ_{LV}) for each homologous series of

organic liquids. This has led to the useful concept of the critical surface tension for spreading (γ_c) for each series, as defined by the intercept of the straight line plot of cos θ *vs.* γ_{LV} with the cos $\theta = 1$ axis. This concept also has proved useful in approximately describing the spreading behavior of a much greater variety of liquids.

Close correlations have been discovered between γ_c and the constitution of the solid surface.[2-14] The purpose of this paper is to summarize the constitutive law found to describe the wettability of low energy surfaces and to show that it leads to a rational explanation of the retraction method of preparing condensed monolayers at the solid–air interface.

The Constitutive Law of Wettability.—The striking regularities in the contact angles exhibited by pure liquids on low energy surfaces are exemplified by the data for the homologous series of liquid *n*-alkanes on several types of fluorinated solid surfaces. In Fig. 1 is plotted cos θ for each alkane on a given solid against the surface tension (γ_{LV}) of the liquid; each curve thus represents the wetting behavior of a single surface. Curve A of Fig. 1 is a plot of the data for the *n*-alkanes (from pentane to hexadecane) on smooth, clean polytetrafluoroethylene (Teflon), and it exemplifies the rectilinearity of the cos θ *vs.* γ_{LV} plot. The lower the γ_{LV} of the wetting liquid, the smaller θ is and the more wettable the surface; below a critical value of the surface tension of the liquids, denoted as γ_c, the contact angle is zero.

Curve B of Fig. 1 presents recent data[15] for a new commercial copolymer of tetrafluoroethylene and

(1) Presented at the Spring Meeting of the Division of Colloid Chemistry of the American Chemical Society in Boston, Massachusetts, April 8, 1959.

(2) H. W. Fox and W. A. Zisman, *J. Coll. Sci.*, **5**, 514 (1950).

(3) (a) H. W. Fox and W. A. Zisman, *ibid.*, **7**, 109 (1952); (b) **7**, 428 (1952).

(4) E. G. Shafrin and W. A. Zisman, *ibid.*, **7**, 166 (1952).

(5) F. Shulman and W. A. Zisman, *ibid.*, **7**, 465 (1952).

(6) H. W. Fox, E. F. Hare and W. A. Zisman, *ibid.*, **8**, 194 (1953).

(7) A. H. Ellison, H. W. Fox and W. A. Zisman, This Journal, **57**, 622 (1953).

(8) E. F. Hare, E. G. Shafrin and W. A. Zisman, *ibid.*, **58**, 236 (1954).

(9) A. H. Ellison and W. A. Zisman, *ibid.*, **58**, 260 (1954).

(10) A. H. Ellison and W. A. Zisman, *ibid.*, **58**, 503 (1954).

(11) E. F. Hare and W. A. Zisman, *ibid.*, **59**, 355 (1955).

(12) H. W. Fox, E. F. Hare and W. A. Zisman, *ibid.*, **59**, 1097 (1955).

(13) E. G. Shafrin and W. A. Zisman, *ibid.*, **61**, 1046 (1957).

(14) W. A. Zisman, "Relation of Chemical Constitution to the Wetting and Spreading of Liquids on Solids" in "A Decade of Basic and Applied Science in the Navy," Office of Naval Research, published by the U. S. Government Printing Office, Washington, D. C., 1957.

(15) M. K. Bernett and W. A. Zisman, to be published.
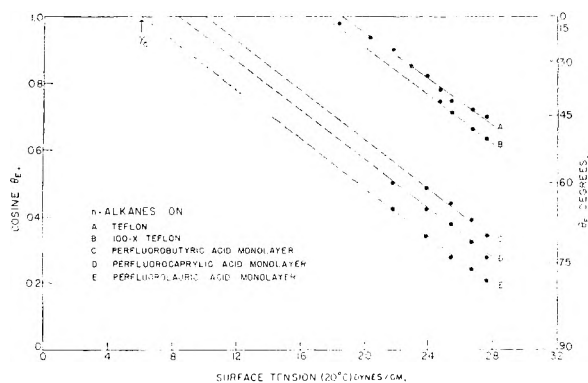
Fig. 1.—Wettability of several fluorinated low energy surfaces by the n-alkanes.

hexafluoropropylene (100-X Teflon).[16] Curves C, D and E describe the wetting behavior of a normally completely wettable, high-energy surface (clean platinum) modified by the adsorption of an oriented close-packed unimolecular layer of a fluorinated organic acid. All of these surfaces exhibit remarkably similar wetting properties, and they exemplify the conclusion that the presence of a condensed adsorbed monolayer of organic polar–non-polar molecules transforms a high-energy surface into one with the wetting properties characteristic of a low-energy surface of the same surface composition and packing.

From the intercepts of the rectilinear graphs of Fig. 1, it is evident that γ_c has a value of about 18 dynes/cm. for the n-alkanes on the surface of Teflon; a value of about 17 dynes/cm. is obtained from curve B for 100-X Teflon.[15] As was expected, the introduction of the perfluoromethyl group as side chains in the polymer reduces γ_c. The reduction becomes greater, however, when the surface contains a higher concentration of exposed $-CF_3$ groups. An adsorbed close-packed monolayer of a perfluorinated acid is an example of such a surface.[5,7] The critical surface tensions for such surfaces are therefore much lower than for the $-CF_2-$ surfaces. The closer the packing of the aliphatic chains of the adsorbed molecules, the closer the packing of the exposed terminal $-CF_3$ groups, and hence the lower γ_c. Thus, the value for a condensed monolayer of perfluorolauric acid is only 6 dynes/cm., and this surface is the least wetted by the alkanes of any surface ever encountered.

Even when cos θ is plotted against γ_{LV} for a variety of non-homologous liquids, the points lie close to a straight line or tend to collect around it in a narrow rectilinear band. On some low energy surfaces this band exhibits curvature for values of γ_{LV} above 50 dynes/cm. But in those cases it has been shown that such curvature results when weak hydrogen bonds form between the molecules of liquid and those in the solid surface. This is most likely to happen with liquids of high surface tension, because these always are hydrogen-donating liquids. Therefore, the working hy-

pothesis has evolved that the graph of cos θ vs. γ_{LV} for any low-energy surface is always a straight line (or a narrow rectilinear band) unless the molecules in the solid surface form hydrogen bonds or otherwise strongly associate with the liquid.[7,9]

When rectilinear bands are obtained in these groups of cos θ vs. γ_{LV} data points, the intercept of the lower limb of the band at cos $\theta = 1$ is chosen as the critical surface tension (γ_c) of the solid. Although this intercept is less precisely defined than the critical surface tension of an homologous series of liquids, nevertheless, it is an even more useful parameter, because it is a characteristic of the *solid only*.

In general, the wettability of organic surfaces is determined by the nature and packing of the surface atoms or exposed groups of atoms of the solid and is otherwise independent of the nature and arrangements of the underlying atoms and molecules. This exemplifies the extreme localization of the attractive field of force around covalent bonded atoms which are responsible for the adhesion of liquids to organic solids. The basic explanation is that the surface atoms in both classes of solids and liquids attract each other by highly localized attractive force fields such as the London dispersion forces,[17] which decrease in intensity with the sixth power of distance. The influence of such a field of force becomes unimportant at a distance of only a few atom diameters; hence, there is little contribution to the force of adhesion by atoms below the surface layer of atoms in the solid and liquid. However, when the constitution of the solid, or of the adsorbed monolayer, is such that either ions or uncompensated permanent dipoles are located in the outermost portion of the surface, the field of force emanating from the surface is much less localized. A recent example will be found in the wetting behavior of terminally fluorinated monolayers of fatty acids and amines.[13] Langmuir[18,19] many years ago emphasized the extreme localization of surface forces encountered in observing the mechanical properties of insoluble organic monolayers on water and referred to this concept as "the principle of independent surface action." Our studies of wetting demonstrate that although the proposed principle does not always hold,[13] it is usually true to a good first approximation.

Survey of Results of Studies of γ_c vs. Solid Constitution.—The widespread occurrence of the rectilinear relationship between cos θ and γ_{LV} in the now large body of experimental data[7-15] and the fact that these graphs do not cross has made it possible to use γ_c to characterize the wettability of each low energy surface.

In Table I are presented the results of values of γ_c obtained from studies of the wettability of a number of well-defined, low energy, solid surfaces. In the first column is given the constitution of the atoms or organic radicals in the solid surface arranged in the order of increasing values of γ_c. Literature references are given in the third column.

(16) R. S. Mallouk and W. B. Thompson, "Teflon 100-X Perfluorocarbon Resin, A New Melt-Extrudable Fluorocarbon Resin," p. 782, Vol. IV, Technical Papers, Soc. Plastics Engnrs., 14th Annual Meeting, Detroit, Mich., January, 1958.

(17) F. London, *Trans. Faraday Soc.*, **33**, 8 (1937).

(18) I. Langmuir, *J. Am. Chem. Soc.*, **38**, 2286 (1916).

(19) I. Langmuir, "Third Colloid Symposium Monograph," Chem. Catalog Co., Inc., New York, N. Y., 1925.

For reasons that will be apparent, the data have been grouped under subheadings emphasizing the atomic components of primary interest: fluorocarbons, hydrocarbons, chlorocarbons, or nitrated hydrocarbons.

A. Fluorocarbons.—The surface of lowest energy, and hence lowest γ_c, is that comprised of closest packed $-CF_3$ groups.[5,8] The effect of the replacement of a single fluorine atom by a hydrogen atom in a terminal $-CF_3$ group is to more than double γ_c. Thus, the value γ_c of 6 dynes/cm. obtained for a condensed adsorbed monolayer of perfluorolauric acid is to be compared with that of 15 dynes/cm. for a condensed adsorbed monolayer of ω-monohydroperfluoroundecanoic acid (CF_2H-$(CF_2)_9COOH$).

A parallel and regular increase in γ_c has been observed with progressive replacement of fluorine by hydrogen atoms in the surfaces of bulk polymers. In Table I the data for Teflon ($-CF_2-CF_2-$), polytrifluoroethylene ($-CF_2-CFH-$), polyvinylidene fluoride ($-CF_2-CH_2-$), and polyvinyl fluoride ($-CFH-CH_2-$) are listed in the order of increasing values of γ_c, which is also the order of decreasing fluorine content. If each of these polymers is considered a fluorinated derivative of polyethylene, a plot of γ_c against the atom per cent. replacement of hydrogen in the monomer by fluorine results in a straight line (Fig. 2); the decrease in γ_c is approximately 3 dynes/cm. for each successive 25% replacement.

B. Hydrocarbons.—Results in Table I of studies of the wetting of hydrocarbon surfaces reveal that the lowest values of γ_c and the least wettability are found in a surface comprising close-packed, oriented methyl groups.[4,14] The low value of γ_c of 20–22 dynes/cm. results when the methyl groups are packed in the close-packed array found in the easiest cleavage plane of a single crystal of n-hexatriacontane. Wettability of the less closely packed arrangement found in a condensed adsorbed monolayer of a high molecular weight fatty acid is characterized by a value of γ_c of 22–24 dynes/cm. The great sensitivity of wettability, and hence of γ_c, to such subtle changes in the packing of the methyl groups comprising the surface of the solid is not only remarkable but has much significance in technological aspects of wetting and adhesion phenomena. It should be noted that the transition from a surface comprised of $-CH_3$ groups to one of $-CH_2-$ groups results in an increase in γ_c of some 10 dynes/cm.; this is to be compared with the increase of 12 dynes/cm., observed in going from a surface of $-CF_3$ to one of $-CF_2-$ groups.

The presence of aromatic carbon atoms in the hydrocarbon surface also serves to increase γ_c. Thus, the introduction of a significant proportion of phenyl groups in the surface in going from polyethylene to polystyrene raises γ_c from 31 to 33 dynes/cm. A further increase to 35 dynes/cm. results when the surface is composed solely of phenyl groups, edge on, as in the cleavage surface of naphthalene or anthracene single crystals.[6]

C. Chlorocarbons.—Graphs of cos θ vs. γ_{LV} for the chlorinated hydrocarbons polyvinyl chloride ($-CH_2-CHCl-$) and polyvinylidene chloride ($-CH_2-$
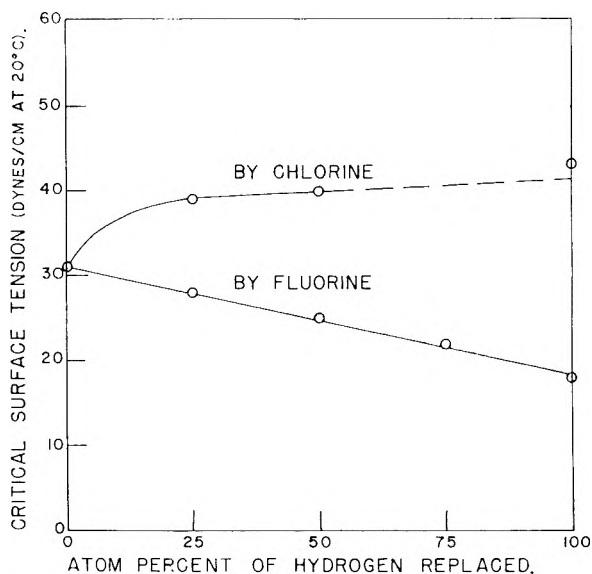
Fig. 2.—The effect of progressive halogen substitution on the wettability of polyethylene-type surfaces.

TABLE I

CRITICAL SURFACE TENSIONS (γ_c) OF LOW ENERGY SURFACES

Surface constitution	γ_c (dynes/cm. at 20°)	Ref.
A. Fluorocarbon surfaces		
$-CF_3$	6	8
$-CF_2H$	15	7
$-CF_3$ and $-CF_2-$	17	15
$-CF_2-$	18	2
$-CH_2-CF_3$	20	13
$-CF_2-CFH-$	22	9
$-CF_2-CH_2-$	25	9
$-CFH-CH_2-$	28	9
B. Hydrocarbon surfaces		
$-CH_3$ (crystal)	20–22	3b
$-CH_3$ (monolayer)	22–24	4
$-CH_2-$	31	3b
$-CH_2-$ and $=CH=$	33	10
$=CH=$ (phenyl ring edge)	35	6
C. Chlorocarbon surfaces		
$-CClH-CH_2-$	39	9
$-CCl_2-CH_2-$	40	9
$=CCl_2$	43	9
D. Nitrated hydrocarbon surfaces		
$-CH_2ONO_2$ (crystal) $\{110\}$	40	20
$-C(NO_2)_3$ (monolayer)	42	20
$-CH_2NHNO_2$ (crystal)	44	20
$-CH_2ONO_2$ (crystal) $\{101\}$	45	20

CCl_2-) are narrow, rectilinear bands. The corresponding polytrichloroethylene polymer has not been studied. The completely chlorinated analog, polytetrachloroethylene, never has been prepared and probably cannot be, owing to steric hindrances resulting from the large atomic diameter of covalent chlorine. In Fig. 2, values of γ_c for polyethylene, polyvinyl chloride and polyvinylidene chloride are plotted against the atom per cent. replacement of hydrogen by chlorine, since the two chlorinated polymers can be considered derived from poly-

ethylene by 25 and 50 atom % replacement, respectively. Although the introduction of the first chlorine atom in the monomer causes γ_c to rise from 31 to 39 dynes/cm., the addition of a second chlorine only increases γ_c to 40 dynes/cm. There are striking differences, therefore, in the effects on γ_c (and wettability) observed with fluorine and chlorine replacement of hydrogen, both as to the effect of progressive halogenation and the direction of the change.

Although polytetrachloroethylene does not exist, an organic coating with an outermost surface comprised of close-packed covalent chlorine atoms has been prepared by adsorbing a condensed, oriented monolayer of perchloropentadienoic acid (CCl_2=CCl—CCl=CCl—$COOH$) on the clean polished surface of glass.[9] Not only is the graph of cos θ vs. γ_{LV} for such a surface quite similar to those of the above-mentioned chlorinated polyethylenes, but the corresponding value of γ_c (43 dynes/cm.) is shifted in the appropriate direction (i.e., to higher values of γ_c). Extrapolation of the line defined by the experimental points for the two chlorinated polymers in Fig. 2 to the value of γ_c for 100% hydrogen replacement indicates a value of 42 dynes/cm. Thus, the hypothetical polytetrachloroethylene surface should have a critical surface tension of wetting of 42 dynes/cm., which is only 1 dyne/cm. less than the experimental value found for the perchloropentadienoic acid monolayer. This shows how closely the latter surface approximates a fully chlorinated polymeric surface in its wetting properties. When the monolayer was adsorbed on polished platinum, the results were the same.

An interesting but more specialized example of the relation of γ_c to constitution is the plot of cos θ of water vs. % chlorination of polyethylene. This graph is a good straight line over the range 0 to 100%.[9]

D. Nitrated Hydrocarbons.—The last group in Table I presents results of wettability studies on organic solids having surfaces rich in nitro groups.[20] These include the natural crystal faces of single crystals of pentaerythritol tetranitrate (–CH_2ONO_2) and of cyclotrimethylene trinitramine (–CH_2-$NHNO_2$) as well as of a condensed, oriented monolayer of trinitrobutyric acid adsorbed on glass. The presence of the nitro groups makes all of these surfaces more wettable (i.e., all have higher values of γ_c than hydrocarbon surfaces). The variation of 5 dynes/cm. in γ_c for the {110} and {101} faces of pentaerythritol tetranitrate is significant and results from differences in the surface density of the –NO_2 groups.

Critical Surface Tensions of Solid Polymers.—Results of wettability studies on clean, smooth, plasticizer-free polymeric solids of widespread interest have been summarized in Table II. Data are arranged in order of increasing γ_c.

In general, the introduction of covalent chlorine atoms markedly increases the wettability of a surface. Thus, in a series of copolymers of polytetrafluoroethylene and polytrifluorochloroethylene,[3a] there is a regular increase in γ_c with chlorination in

(20) H. W. Fox and O. Levine, private communication.

TABLE II

CRITICAL SURFACE TENSIONS (γ_c) OF COMMON POLYMERIC SOLIDS

Polymer	γ_c (dynes/cm. at 20°)	Ref.
Polytetrafluoroethylene (Teflon)	18	2
Polytrifluoroethylene	22	9
Polyvinylidene fluoride	25	9
Polyvinyl fluoride	28	9
Polyethylene	31	3b
Polytrifluorochloroethylene (Kel-F)	31	3a
Polystyrene	33	10
Polyvinyl alcohol	37	21
Polyvinyl chloride	39	9
Polyvinylidene chloride	40	9
Polyethylene terephthalate	43	10
Polyhexamethylene adipamide (Nylon 6, 6)	46	10

going from the fully fluorinated surface ($\gamma_c = 18$ dynes/cm.) to that having 25 atom % chlorine substitution ($\gamma_c = 31$ dynes/cm.). Similarly, a large increase in γ_c of 8 dynes/cm. was observed on replacing 25% of the hydrogen atoms in polyethylene by chlorine.

Included in Table II is the value for polyvinyl alcohol ($\gamma_c = 37$ dynes/cm.) which was reported recently by Ray, et al.[21,22] The same investigators reported a range in γ_c of 40 to 45 dynes/cm. for a series of hydroxyl-rich surfaces of the starch polymer type. These values of γ_c are in reasonable agreement with that of 43 dynes/cm. reported for the oxygen-rich surface of polyethylene terephthalate.[10]

Contact angles and surface tensions for the wetting of the smooth surfaces of various waxes, resins and cellulose derivatives have been reported by Bartell, et al.[23–25] If the cosines of their contact angles are plotted against γ_{LV}, good straight lines are obtained. The values for γ_c for those resin surfaces rich in exposed oxygen-containing groups fit in well with the data presented here on the relative wettability of oxygen-rich surfaces.

Nylon, with its many exposed amide groups, has the highest value of γ_c of the common plastics reported.[10] Since γ_c for all the polymers of Table II are well below the surface tension of water (72.8 dynes/cm.), all are hydrophobic.

Figure 3 presents a "wettability spectrum" on which are indicated values of γ_c for over twenty different types of low-energy organic surfaces. The position of each symbol in the bar chart indicates the relative wettability of a given solid while the form of the symbol denotes its physical state. The data in each row correspond to surfaces comprised of the same atomic constituents, without regard to their relative proportions or chemical function. Figure 3 serves to emphasize the dependency

(21) B. R. Ray, J. R. Anderson and J. J. Scholz, THIS JOURNAL, **62**, 1220 (1958).

(22) J. J. Scholz, B. R. Ray and J. R. Anderson, ibid., **62**, 1227 (1958).

(23) F. E. Bartell and O. H. Greager, Ind. Eng. Chem., **21**, 1248 (1929).

(24) F. E. Bartell and H. H. Zuidema, J. Am. Chem. Soc., **58**, 1449 (1936).

(25) F. E. Bartell and B. R. Ray, ibid., **74**, 778 (1952).

γ_c = CRITICAL SURFACE TENSION (DYNES/CM AT 20° C).
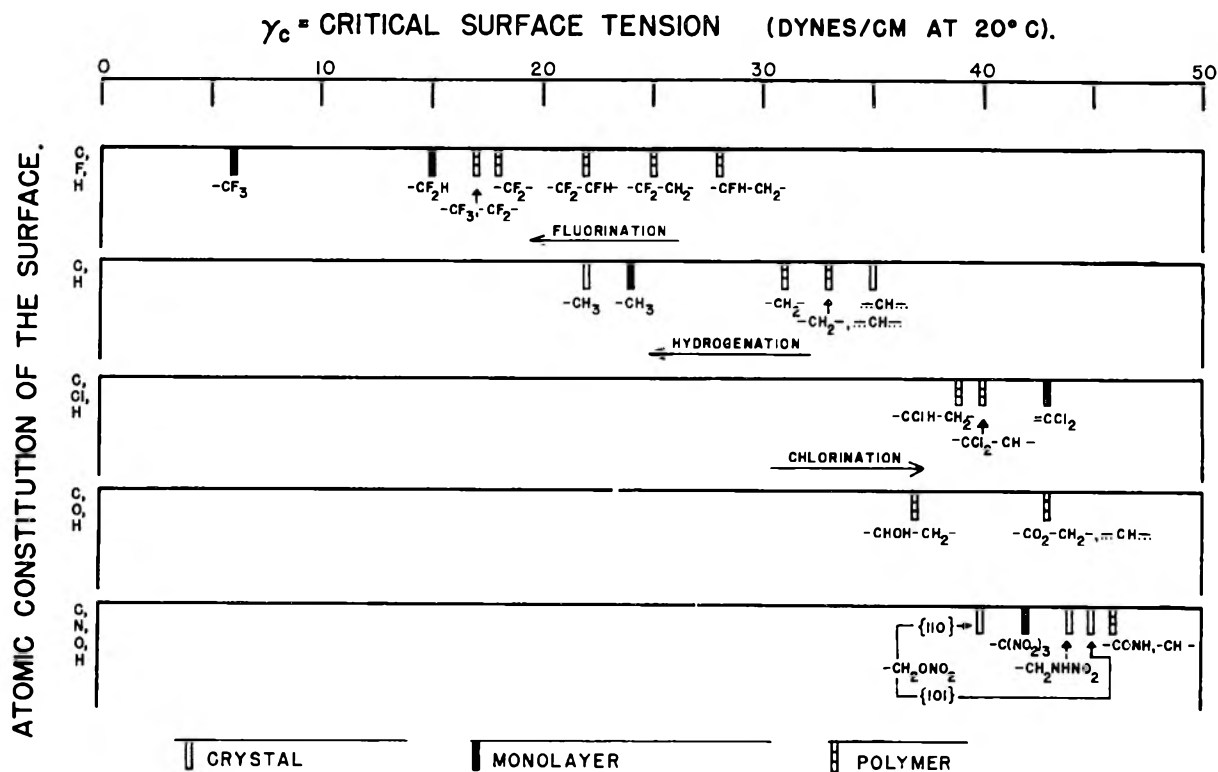
Fig. 3.—The wettability "spectrum" for selected low energy surfaces.

of wetting properties on the chemical structure and physical packing of the atomic groupings in the outermost layer of the surface.

For hydrocarbons (Fig. 3, row C, H) the sequence of chemical structures of the atomic groupings corresponding to decreasing values of γ_c parallels that for progressive hydrogenation of the surface: aromatics to saturates, methylene to methyl groups. This sequence corresponds to an increase in the ratio of hydrogen to carbon atoms and the direction of increasing H/C has been indicated by an arrow.

Where a sufficient number of members of the series of halogen-containing surfaces are available, similar correlations are found with γ_c; the corresponding directions of increase in the ratio halogen/carbon are indicated. The reversal in the effect on γ_c of fluorination vs. chlorination has been discussed earlier.

Thus, it is seen that values of γ_c for surfaces of related atomic composition tend to fall within a relatively narrow band in the wettability spectrum, while the introduction of another atomic constituent results in a shift of the band to a different, but still restricted, range of values. The several rows of data in Fig. 3 have been arranged in accordance with the order of increasing group values of γ_c for related surfaces. The effectiveness of substitution of individual atomic species in increasing the wettability of organic surfaces is

$$F < H < Cl < (Br) < (I) < O < N$$
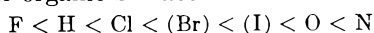
Theory of the Retraction Method.—The concepts developed in the previous section make it possible to prove that the now widely used retraction method of preparing monolayers is a direct consequence of the constitutive law of wetting. The

retraction method[26-31] is a process by which a clean, high energy, plane surface is contacted with a liquid containing adsorbable polar–nonpolar molecules; adsorption occurs at the solid–liquid interface and the surface is covered with a film which converts it to a lower energy surface. When the coated solid is approximately vertical during withdrawal from contact with the bulk liquid phase, the adhering layer of liquid exhibits an appreciable contact angle and then peels back or retracts leaving the withdrawn, solid, low energy surface dry but still coated with the monolayer.

The monolayer-coated surface can be removed from the liquid unwetted only when the contact angle θ of the liquid with the solid is greater than zero, and the permissible rate of removal can be faster the greater the value of θ. However, θ exceeds zero only for those liquids having surface tensions greater than the critical surface tension of the solid. Therefore, the necessary condition for retraction is that $\gamma_{LV} > \gamma_c$. Adsorbed monolayers can thus be isolated from any liquid having a surface tension γ_{LV} greater than the value of γ_c of the low energy surface created by the initial adsorption process.

This explanation provides helpful guidance about

(26) W. C. Bigelow, D. L. Pickett and W. A. Zisman, *J. Coll. Sci.*, **1**, 513 (1946).

(27) W. C. Bigelow, E. Glass and W. A. Zisman, *ibid.*, **2**, 563 (1947).

(28) E. G. Shafrin and W. A. Zisman, *ibid.*, **4**, 571 (1949).

(29) H. R. Baker, E. G. Shafrin and W. A. Zisman, THIS JOURNAL, **56**, 405 (1952).

(30) E. G. Shafrin and W. A. Zisman, "Hydrophobic Monolayers and Their Adsorption from Aqueous Solution" in "Monomolecular Layers," edited by H. Sobotka, AAAS Symposium Publication, Washington, D. C., 1954.

(31) O. Levine and W. A. Zisman, THIS JOURNAL, **61**, 1068 (1957).

the solvents that may be used in the preparation of films by retraction from solution. The principal requirement is that γ_{LV} exceed γ_c; the greater the difference between γ_{LV} and γ_c, the larger the contact angle and the easier it is to perform the retraction operation and isolate the adsorbed film on the solid. An example of this was pointed out in an early study of adsorbed monolayers of branched or cyclic polar molecules.[6] In order for the adsorbed monolayer to emerge from the solution of adsorbate unwetted, it proved advantageous to choose a solvent with a surface tension enough greater than γ_c of the monolayer that the solution would exhibit a contact angle with the coated solid of 35° or more.

The same argument explains the behavior of "autophobic" liquids,[11] which are pure polar–non-polar liquid compounds having no ability to spread on clean high energy surfaces at room temperature. Each such liquid always adsorbs on the solid to form an oriented monolayer of low surface energy; because the liquid surface tension is greater than the value of γ_c of its own adsorbed film, $\theta > 0°$ and spreading does not occur.

A method described earlier[27] of preparing adsorbed monolayers on solids by retraction from the molten pure compound represents the more general case of an autophobic liquid; these compounds are non-spreading at all temperatures in the liquidus range of the polar material at which the liquid surface tension exceeds γ_c of the adsorbed monolayer. A temperature limit (τ) has been found experimentally above which it is no longer possible to use the retraction method to isolate the monolayer from the molten compound. The values of τ for each homologous series of aliphatic compounds indicate that a rectilinear relation exists between the temperature limit and chain length.[27]

For most pure homologous liquids not too near the critical temperature, the surface tension vs. temperature relations can be represented by a series of straight lines of negative slope. In contrast, the effect of raising the temperature of an adsorbed film by a few degrees is to decrease the surface density and lateral adhesion very little; hence, γ_c increases only slightly per degree of rise. At a sufficiently high temperature, the condition will be reached at which $\gamma_{LV} \not> \gamma_c$ and retraction will not

be possible. The temperature limit τ corresponds to the condition when γ_{LV} of the molten compound equals γ_c of the adsorbed film.

For the homologous series of fatty acids, only small variations were found in the value of γ_c characteristic of the acid monolayer at the temperature τ. Whereas an increase in chain length in going from octanoic to octadecanoic acid resulted in a rise in τ from 23 to 106°, the corresponding change in γ_c was only to decrease from 28 to 25 dynes/cm. Since these values do not greatly exceed the value of γ_c characteristic of hydrocarbon surfaces in closest packing, they indicate that wetting of the adsorbed film by the melt occurs at temperatures at which the adsorbed films are still relatively intact.

Table III summarizes the results on the wettability of a coated solid of using a variety of techniques to adsorb and isolate by retraction a condensed monolayer of n-octadecylamine on high energy surfaces such as platinum, stainless steel and Pyrex. The identical packing of methyl groups in the condensed monolayer formed under each condition is demonstrated by the nearly constant value of the contact angle exhibited by methylene iodide. The maximum variation in the contact angle is only 2°, and this is the experimental error of the measurement of θ. Methylene iodide is used as the wetting liquid here because the size and shape of its molecules are not consistent with penetration of and adlineation in the monolayer.[32] It can be concluded, therefore, that the various methods of isolating adsorbed condensed monolayers by retraction all result in identical monolayers.

TABLE III

EQUIVALENCE OF VARIOUS RETRACTED MONOLAYERS OF OCTADECYLAMINE

Method of isolating adsorbed film on solid	Methylene iodide contact angle at 25°	Ref.
Retraction from molten amine	69°	31
Retraction from hexadecane soln.	70	31
Retraction from dicyclohexyl soln.	68 (at 20°)	13
Retraction from nitromethane soln.	69	31
Retraction from aq. soln. of $C_{18}H_{37}NH_3Cl$	69	31

(32) O. Levine and W. A. Zisman, THIS JOURNAL., **61**, 1188 (1957).

A RADIOACTIVE TRACER STUDY OF THE ADSORPTION OF FLUORINATED COMPOUNDS ON SOLID PLANAR SURFACES.
II. $C_8F_{17}SO_2N(C_2H_5)CH_2COOH$

By John P. Ryan, R. J. Kunz and J. W. Shepard

Contribution No. 114 from Central Research Department, Minnesota Mining and Manufacturing Company, St. Paul, Minnesota

A C-14 labeled fluorochemical acid $(C_8F_{17}SO_2N(C_2H_5)CH_2C^*OOH)$ was adsorbed from an n-decane solution onto solid planar surfaces. Platinum, quartz, glass and aluminum were studied. Rates of adsorption and solution isotherms were determined. Physical adsorption took place on platinum, quartz and glass, while extensive chemisorption took place on aluminum. Pretreating the samples at 450° in a nitrogen atmosphere gave the most reproducible results. Desorption of the adsorbed film occurred at an appreciable rate from platinum, quartz and glass. Desorption from aluminum was much slower. No desorption from aluminum was observed with non-polar decane, and very little with water. Use of adsorption data to calculate roughness factors is discussed. Values of about 1.0 were obtained for platinum, quartz and glass. An interesting exchange was observed between the adsorbed molecules and those in solution on all surfaces except aluminum. This phenomenon was reported previously for adsorbed films of perfluoroöctanoic acid.

Introduction

Previous studies[1,2] with carbon-14 tagged perfluoroöctanoic acid on planar glass and aluminum surfaces gave evidence of chemisorption. This made determination of roughness factor values for these surfaces uncertain. For platinum and quartz substrates physical adsorption appeared to take place and reasonable roughness factor values were obtained. As an extension of this work some C-14 tagged N-ethyl-N-perfluoroöctanesulfonylglycine, a weaker acid than perfluoroöctanoic acid, was prepared.[3] This acid was expected to be less reactive and thus provide more reliable data for calculating roughness factor values.

To obtain roughness factor values (or surface area) from solution adsorption data, two assumptions are made: (1) the surface is occupied by a closely packed, oriented, monomolecular film; (2) the area occupied by each molecule is the same as on an aqueous substrate. The latter assumption is necessary because molecular area values obtained from film balance measurements are used in the calculations. Other investigators[4] have shown that surface area values obtained on powders using long chain hydrocarbon carboxylic acids and esters are in good agreement with values obtained by independent methods.

Experimental

Materials. A. Labeled Acid.—The radioactive solutions were prepared from a sample of tagged acid purified by recrystallization and vacuum sublimation. The material had a melting point of 163 ± 1° and carbon, fluorine and nitrogen analyses showed very good agreement with the calculated values.

The specific activity of the acid (0.92 millicurie/g.) was determined by counting weightless samples of the compound in a windowless Q-gas counter. This value was checked by measurements of toluene solutions of the acid in a liquid scintillation counter.

A saturated stock solution of the acid ($C_0 = 4.0 \times 10^{-6}$ molar) in n-decane was prepared by dissolving excess acid in 100 cc. of the solvent. The solutions used in this study were prepared by appropriate dilution of this stock solution. Concentrations were checked by radiochemical assay of aliquots of the adsorption solutions.

B. Solvents.—Polar impurities were removed from all non-polar solvents by passing the liquids through a column of activated alumina and silica gel. The solvents were checked for the absence of polar impurities by placing a drop on neutral, acidic and basic substrata.

C. Surfaces.—The surfaces used in this study were (1) platinum (20 mil rolled), (2) quartz ($1/16''$ ground and polished plate), (3) glass (Corning optical cover glasses), and (4) aluminum (40 mil Alcoa flat sheet standard -2S, one side bright finished).

The surfaces were given the following pretreatment: (1) acetone wash, (2) detergent (Dreft) wash, (3) tap water rinse, (4) five minute boil in distilled water, (5) five minute boil in acetone, (6) heat treatment for five hours at 450° in a purified nitrogen atmosphere.

Procedure.—The procedure has been described previously.

Experimental Results

A. Adsorption Isotherms.—The extent of adsorption of N-ethyl-N-perfluoroöctanesulfonylglycine on various surfaces was studied as a function of time and concentration. Results for platinum, quartz and glass were similar and only the data for platinum are shown (Fig. 1).

Concentrations are reported in C/C_0 units where C is the solution concentration and C_0 is the concentration of a saturated solution (4.0×10^{-6} M). Each point represents the average of four samples while the vertical limits show the range. About 75% of the adsorption took place in one hour or less, but five hours were required for complete saturation of the surface. At lower concentrations, saturation was never obtained although an equilibrium condition was observed. No rate data are given for aluminum since saturation was never observed—even after as much as 48 hours in the solution. The glycine compound reacted continuously with the aluminum surface until the adsorbate was completely consumed.

Adsorption isotherms for surfaces of platinum, quartz and glass are presented in Fig. 2, 3, and 4. For dip times of greater than 15 minutes, adsorption on these surfaces became independent of concentration above the range 0.4–0.6 C_0. Except for the adsorption on platinum from a saturated solution, autoradiographs showed a uniform deposit of

(1) J. W. Shepard and J. P. Ryan, This Journal, **60**, 127 (1956).

(2) J. W. Shepard and J. P. Ryan, *ibid.*, **63**, 1729 (1959).

(3) We are indebted to Mr. T. N. Lahr of the Nuclear Research Section for the synthesis of the tagged compound.

(4) W. D. Harkins and D. M. Gans, This Journal, **36**, 86 (1932); W. W. Ewing, *J. Am. Chem. Soc.*, **61**, 1317 (1939); H. A. Smith and J. F. Fuzek, *ibid.*, **68**, 229 (1946); E. B. Greenhill, *Trans. Faraday Soc.*, **45**, 625 (1949); W. Hirst and J. K. Lancaster, *Research*, **3**, 336 (1950); S. H. Maron, E. G. Bobalek and S. M. Fok, *J. Colloid Sci.*, **11**, 21 (1956).
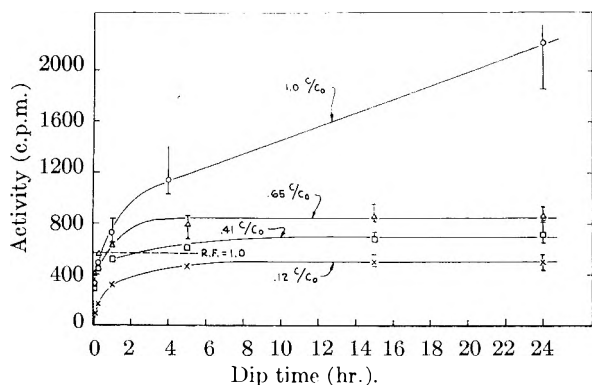
Fig. 1.—Rate of adsorption of $C_8F_{17}SO_2N(C_2H_5)CH_2C^*OOH$ on platinum; temp., 29°.
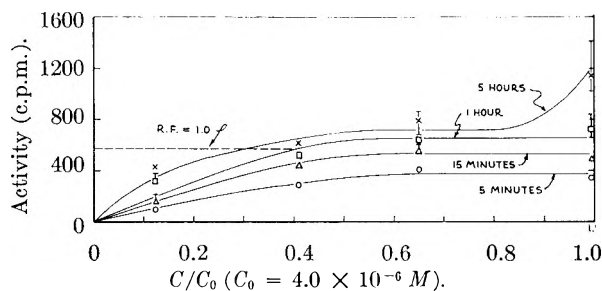
Fig. 2.—Isotherms for adsorption of $C_8F_{17}SO_2N(C_2H_5)CH_2 C^*OOH$ on platinum; temp., 29.°
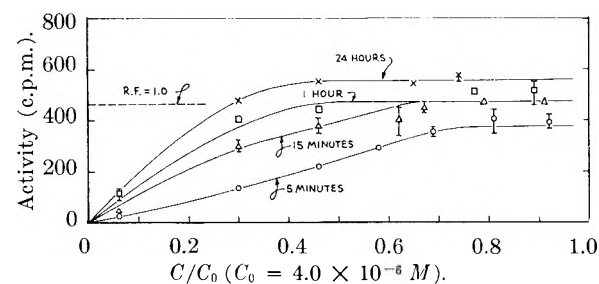
Fig. 3.—Isotherms for adsorption of $C_8F_{17}SO_2N(C_2H_5)CH_2 C^*OOH$ on quartz; temp., 29.°
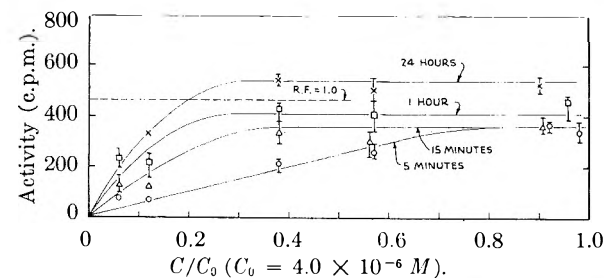
Fig. 4.—Isotherms for adsorption of $C_8F_{17}SO_2N(C_2H_5)CH_2 C^*OOH$ on glass; temp., 29°.

adsorbate. Platinum was quite sensitive to dip time in the saturated solution and showed a continuous increase of adsorbate with time. Autoradiographs showed that for dip times greater than 15 minutes localized build-up of adsorbate was obtained, probably because of precipitation of the acid from the saturated solution.

The isotherms for adsorption of the acid on aluminum indicated chemisorption and subsequent continued reaction (Fig. 5). Autoradiographs showed uniform adsorbate coverage. Experiments at various times and concentrations gave no indication of adsorption becoming independent of concentration.

Autoradiographs of films adsorbed on aluminum from a saturated solution provided insight into an unexpected course of adsorption at this concentration. The autoradiographs for short dip times revealed localized "hot spots" on the substrate, while those for 24 hour dip times showed a uniform adsorbate distribution. Apparently when the aluminum sample was first dipped into the saturated solution, the chemisorption process was accompanied by precipitation of solute at discrete spots on the surface. As the chemisorption process continued, the solution concentration was lowered. Chemisorption on an aluminum sample reduced the C/C_0 from 1.0 to less than 0.01[5] in 24 hours. The precipitated solute then redissolved in the solvent and re-entered the chemisorption process. With a sufficiently long dip time all the glycine acid was chemisorbed rather than locally deposited, and a uniform coverage resulted.

These adsorption results contrast in several ways with those obtained previously with perfluorooctanoic acid.[2] On the unreactive surfaces (platinum and quartz) the adsorption of $C_7F_{15}COOH$ proceeded at a faster rate than the glycine compound. With both platinum and quartz, adsorption of $C_7F_{15}COOH$ became independent of concentration at a much lower value than did the glycine compound. No localized buildup of the $C_7F_{15}COOH$ absorbate was observed on platinum. Results on glass with perfluorooctanoic acid indicated chemisorption with continued reaction, whereas physical adsorption was indicated with the glycine compound. Both compounds underwent reaction with aluminum surfaces, but the glycine compound reacted faster and to a greater extent than the $C_7F_{15}COOH$.

B. Roughness Factor Values.—Roughness factor values can be obtained from solution adsorption data using a tagged adsorbate if the following data are available: (1) the area occupied by an adsorbed molecule, (2) the specific activity of the radioactive acid, (3) the counting efficiency of the counter, and (4) the area of the sample counted. The value used for the molecular area of N-ethyl-N-perfluorooctanesulfonylglycine was 63 Å.[2],[6] This value was obtained from film balance measurements on an aqueous substrate. The specific activity of the acid was 0.92 millicuries/g. The counting efficiency of the Q-gas flow counter was calculated using a 50% geometry correction and backscattering factors of 23% for aluminum, glass and quartz, and 52% for platinum.[7] The unmasked area was 2.40 cm.[2]. Using these data, values of 461 c.p.m./monolayer for quartz, glass and aluminum and 570 c.p.m./monolayer for platinum were obtained. Roughness factor values obtained for the N-ethylglycine derivative are shown in Table I along with values previously reported for perfluorooctanoic acid.

In the case of glass, where a roughness factor of one again seems realistic, the glycine acid data

(5) 0.01 C_0 corresponds to 3 c.p.m. above background which we took as our detection limit.

(6) J. A. Mann and J. W. Shepard, to be published.

(7) H. Sobotka and S. Rosenberg, "Monomolecular Layers," Publ. Am. Assn. Adv. Sci. 1951, p. 175, 192 1954.

bear out the conclusion that physical adsorption is taking place. This contrasts with the perfluoro-octanoic acid adsorption which indicated chemisorption and, therefore, is a poor measure of surface roughness. For aluminum, it is obvious that the chemisorption of the glycine acid is no measure of the surface roughness, whereas the data for the perfluoroöctanoic acid may be "reasonable."

C. Desorption by Solvents.—Figure 6 presents data on desorption of N-ethyl-N-perfluoro-octanesulfonylglycine by pure decane from various substrates under static conditions. Only aluminum showed no desorption. These results differ from those obtained with perfluoroöctanoic acid where desorption by decane was negligible for all surfaces.

Typical desorption curves using other solvents are shown for quartz in Fig. 7. Results for platinum and glass were similar. The desorption data provide additional evidence for physical adsorption of the N-ethyl-N-perfluoroöctanesulfonyl glycine on platinum, quartz and glass.

Data for films on aluminum (Fig. 8) showed that desorption was markedly slower than for the non-reactive surfaces for all solvents studied and provides additional evidence for a chemisorption process. The behavior of water is especially noteworthy.

TABLE I
ROUGHNESS FACTORS

Surface	Soln. concn. C/C_0	Dip time	Apparent roughness factor $C_7F_{15}COOH$	$C_8F_{17}SO_2N-(C_2H_5)-CH_2COOH$
Platinum	0.5	5 min.	1.15	
		1 hr.	1.07	
		6 hr.	1.04	
Platinum	.90	5 min.		0.47
		1 hr.		0.98
	.46	4 hr.		1.04
Quartz	.2	5 min.	0.86	
		1 hr.	1.10	
		6 hr.	0.80	
Quartz	.9	5 min.		0.85
		1 hr.		1.12
		13 hr.		1.14
Glass	.5	5 min.	2.7	
		1 hr.	4.2	
		6 hr.	4.5	
		24 hr.	7.3	
Glass	.92	5 min.		0.79
		1 hr.		0.81
		6 hr.		0.90
		24 hr.		1.14
Aluminum	.5	5 min.	3.3	
		1 hr.	4.1	
		6 hr.	4.2	
		24 hr.	4.4	
Aluminum	.7	5 min.		1.12
		1 hr.		6.2
		6 hr.		21.3
		24 hr.		65.0

D. Exchange.—When a quartz, glass or platinum surface containing an adsorbed film of $C_8F_{17}SO_2N(C_2H_5)CH_2C^*OOH$ is immersed in pure n-
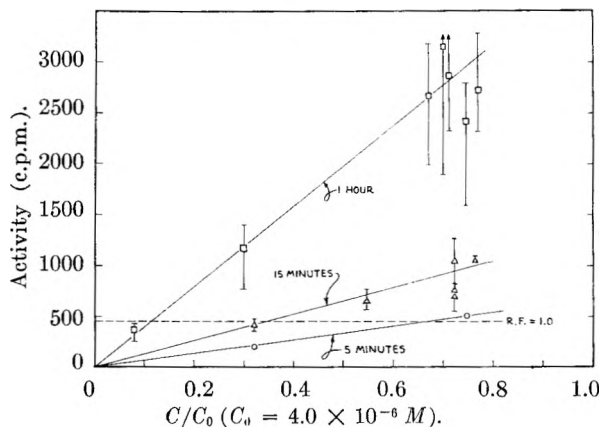
Fig. 5.—Isotherms for adsorption of $C_8F_{17}SO_2N(C_2H_5)CH_2$ C^*OOH on aluminum; temp., 29°.
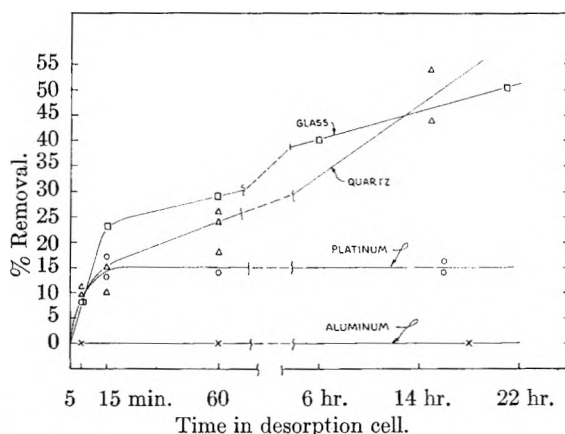
Fig. 6.—Decane desorption of $C_8F_{17}SO_2N(C_2H_5)CH_2C^*$ OOH from planar surfaces; temp., 29°; no agitation.
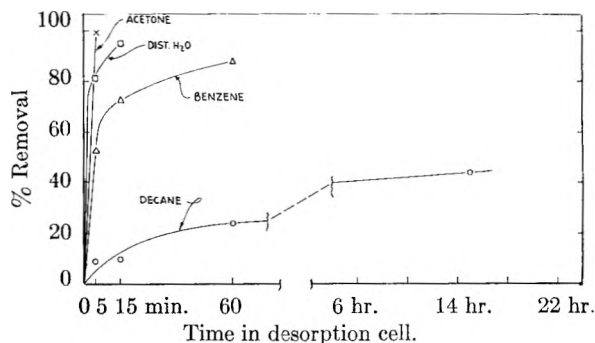
Fig. 7.—Desorption of $C_8F_{17}SO_2N(C_2H_5)CH_2C^*OOH$ from quartz; temp., 29°; no agitation.
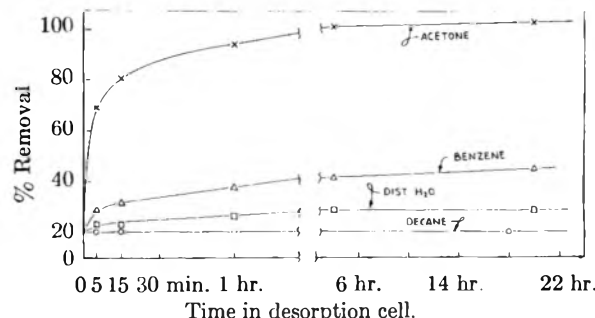
Fig. 8.—Desorption of $C_8F_{17}SO_2N(C_2H_5)CH_2C^*OOH$ from aluminum; temp., 29°; no agitation.
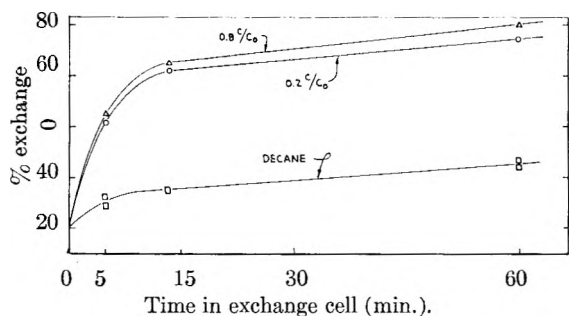
Fig. 9.— Exchange rate of $C_8F_{17}SO_2N(C_2H_5)CH_2C*OOH$ on quartz; temp., 29°.
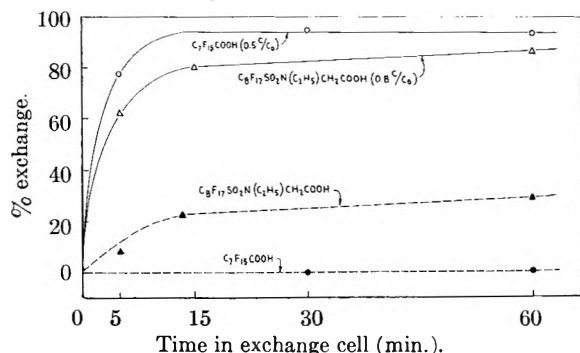
Fig. 10.—Comparison of exchange rates of $C_8F_{17}SO_2N$ $(C_2H_5)CH_2C*OOH$ and $C_7F_{15}C*OOH$ on glass: temp., 29°; ———, exchange with non-active solutions of the acids; – – –, desorption in pure decane.
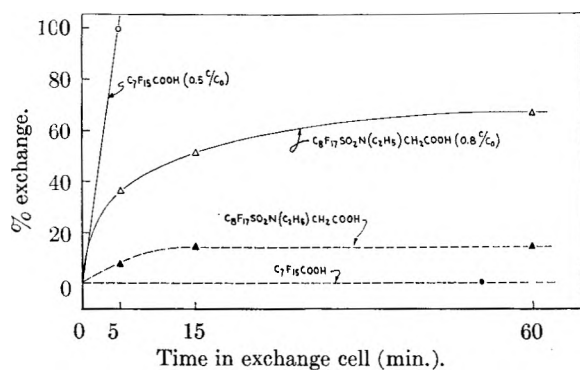
Fig. 11.—Comparison of exchange rates of $C_8F_{17}SO_2N$ $(C_2H_5)CH_2C*OOH$ and $C_7F_{17}C*OOH$ on platinum; temp., 29°; ———, exchange with non-active solutions of the acids; – – – –, desorption in pure decane.

decane, the adsorbed film is slowly removed (about 20% in one hour). In contrast, if a sample containing an adsorbed layer of the tagged acid is immersed in a solution of the non-tagged glycine compound, the activity changes at a greater rate (40–80% in 15 minutes). Interaction between the molecules in solution and those on the surface resulted in an exchange phenomenon. Contact angles showed no depletion of the adsorbed film. The rate of exchange for an adsorbed film on quartz is shown in Fig. 9. The values reported are the per cent. decrease of tagged acid for a given immersion time in the non-tagged acid solution under static conditions. Desorption data in pure n-decane are shown for reference. Obviously the presence of the compound in solution has a pronounced effect.

Data for exchange on glass are presented in Fig. 10. Curves obtained for perfluoroöctanoic acid are presented for comparison.

Exchange results for both acids on platinum surfaces are shown in Fig. 11. The rate of exchange is considerably greater for perfluoroöctanoic acid.

No exchange was observed for the chemisorbed N-ethyl-N-perfluoroöctanesulfonylglycine on aluminum. Data obtained with perfluoroöctanoic acid on aluminum also indicated a chemisorption process but in this case exchange was observed.

Comparison of the exchange rates of the two acids on the various surfaces indicates that when the type of adsorption is the same, i.e., physical (platinum) or chemisorption (glass), the rate for perfluoroöctanoic acid is much faster than for the N-ethylglycine compound. When the octanoic acid film has been deposited via chemisorption and the N-ethyl acid via physical adsorption (glass), the rates are approximately the same.

E. Contact Angles.—Advancing contact angles using hexadecane and methylene iodide were used to verify the difference between exchange and desorption. In exchange, where radioactive molecules were replaced by non-radioactive molecules of the same compound, the contact angle did not change. On the other hand, in desorption, where N-ethylglycine derivative molecules were replaced by solvent molecules, the contact angles decreased an amount depending upon the extent of desorption.

Contact angles were also determined for complete coverage of the N-ethylglycine acid on various substrates. These values, along with values previously obtained with perfluoroöctanoic acid, are given in Table II. The extremely high values on aluminum were unexpected. Further work is under way to elucidate the phenomenon.

TABLE II

Substrate	Advancing contact angle (degrees) Perfluoro-octanoic Hexadecane	N-Ethylglycine Hexadecane	Methylene iodide
Platinum	63	63	90
Quartz	..	67	93
Glass	72	67	93
Aluminum	74	110	160

Discussion

The surfaces used in this study were composed of oxide films with the possible exception of platinum. This work is part of a program to study adhesion on surfaces encountered in industrial processes. As such, it is these surfaces that are of interest. The pretreatment used was designed to give reproducible results with a wide variety of surfaces. Water contact angles showed the effectiveness of the cleaning procedure (Table III).

TABLE III

ADVANCING WATER CONTACT ANGLE VALUES FOR PRE-TREATED AND NON-PRETREATED SURFACES

Surface	Water contact angle value, degree Before treatment	After pretreatment
Platinum	85	28
Glass	27	<10
Quartz	47	15
Aluminum	95	<10

As is shown by contact angle values, the pretreatment contributes significantly to removal of pre-

adsorbed contaminants, chiefly organic in nature. Previous experiments using flaming treatments gave lower contact angles but reproducibility was very poor.

Tingle[8] and Daniel[9] have discussed adsorption from solution on various metal substrates. They pointed out that reliable surface area values could not be obtained from data on substrates which have thick permeable oxide layers capable of reacting with the adsorbate. While perfluorooctanoic acid data provided reliable estimates of roughness factors for quartz and platinum substrates, reaction with subsequent buildup of adsorbate on glass and aluminum surfaces precluded placing any degree of certainty on roughness factor values for these surfaces. The data for the N-ethylglycine compound used in this research provides reasonable estimates for roughness factors on platinum, quartz, and glass, but the surprising reactivity found with aluminum makes the calculated roughness factor values meaningless. The greater reactivity of the N-ethyl compound relative to perfluorooctanoic acid, the difference in the exchange properties, and the unusual wetting properties of the N-ethylglycine compound film on aluminum are indeed perplexing. Additional investigation of the character of this interaction is warranted.

It should be noted that when using a compound as relatively insoluble in decane as the N-ethylglycine compound, slight variation in temperature can alter the solubility noticeably. This was borne out in the cases of platinum and aluminum where localized "precipitation" occurred when these substrates were dipped in saturated solutions. In both cases it was possible that the "saturated" solutions were really supersaturated owing to slight temperature fluctuations during the solution preparation process. In the case of platinum the amount removed by physical adsorption was so slight that the solution concentration was not lowered enough to redissolve the "precipitated" solute. In the case of aluminum, where extensive chemisorption took place, the solution was depleted enough to redissolve the precipitate. If the aluminum dip solution were truly saturated and not supersatu-

rated the slight temperature drop caused by the immersion of the sample could have caused temporary precipitation. Considerable care is required when working with relatively insoluble compounds. The autoradiographic technique as an aid to normal radiochemical counting techniques has proven invaluble in this work.

Rideal and Tadayon[10] have studied the effect of polar liquids in causing the carboxyl group of stearic acid molecules buried in a paraffin substrate to come to the surface. When water was placed on a solidified mixture of paraffin and stearic acid, the contact angle decreased as a function of time, indicating reorientation of the stearic acid molecules. Some correlation of solvent desorption efficiency for perfluorooctanoic acid films with solvent polarity was possible.[2] With the N-ethylglycine compound, desorption efficiency again appeared to correlate with solvent polarity. Solubility seemed to be of secondary importance. The dipole moments of the solvents and the solubility of the glycine acid in these solvents are presented along with desorption data in Table IV.

TABLE IV

SOLVENT CHARACTERISTICS AND DESORPTION EFFICIENCY FOR N-ETHYLGLYCINE FILMS ON VARIOUS SUBSTRATES

Solvent	Dipole moment (Debyes)	Solubility at 29° ($\times 10^{-6}$ mole/l.)	% of film desorbed in 5 min.			
			Quartz	Glass	Platinum	Aluminum
Acetone	2.8	430,000	99	98	83	49
Distilled water	1.8	8	81	91	47	3
Benzene	0	220	53	19	56	9
Decane	0	4	9	8	8	0

The interaction of the polar N-ethylglycine compound in solution with the molecules in the adsorbed film could also provide a mechanism for the exchange process. As has been suggested, the adsorbate molecules in the decane could interact to bring about the overturning and subsequent desorption of the film molecules.

Further work is planned in the areas of exchange and contact angle vs. coverage.

(8) E. D. Tingle, Trans. Faraday Soc., 46, 93 (1950).

(9) S. G. Daniel, ibid., 47, 1345 (1951).

(10) E. Rideal and J. Tadayon, Proc. Roy. Soc. (London), 225A, 346 (1954).

FREE ENERGIES, HEATS AND ENTROPIES OF WETTING OF GRAPHITE

BY J. J. CHESSICK, A. C. ZETTLEMOYER AND YUNG-FANG YU

Surface Chemistry Laboratories, Lehigh University, Bethlehem, Penna.

The heats of monolayer formation of toluene, carbon tetrachloride, *n*-heptane, cyclohexane and 1-propanol on graphite were determined by measuring the heats of immersional wetting of the bare and monolayer covered surface. From previously determined free energies of adsorption,[1,2] entropies of monolayer formation were calculated. Serious difficulties arose. The heats of immersion of the graphite coated with monolayers of toluene, carbon tetrachloride and cyclohexane were considerably below the known surface enthalpies of the corresponding liquids. Even more surprising, the heat of immersion of graphite covered with a monolayer of alcohol was greater than for the immersion of the bare surface. Since for heptane no such unexpected results were obtained, inaccessible area (nitrogen) or reduction by pore filling by the other organic molecules is an unlikely explanation. Furthermore, the results cannot be explained on the basis of customary adsorption thermodynamics.

Introduction

Thermodynamic functions of adsorbed molecules have received a great deal of attention in the last decade since they are not only a measure of strength of interaction, but also a criterion for determining the state and orientation of the adsorbed molecules. However, experimental endeavor, particularly in immersional calorimetry, has been restricted to the determination of the heat of adsorption. There is a paucity of values of free energies and entropies of immersional wetting and adsorption, especially for organic adsorbates. In addition, the assumption that heats of adsorption obtained from immersional calorimetry and from adsorption isotherms at several temperatures are equivalent needs verification.

In the present work, heats of immersional wetting in five organic liquids have been determined on bare and on monolayer covered graphite. By subtraction of the corresponding results, the heats of formation of the monolayers could be calculated. Since the free energies of adsorption had been determined previously by Bartell and co-workers, the entropies of monolayer formation also could be calculated.

Experimental

The graphite sample was prepared by the Acheson Colloid Company and was furnished in a pre-treated condition by Bartell.[1] The graphite was designated "Graphite A" by Craig, Van Voorhis and Bartell[2] and had a surface area of 386 m.²/g. Samples were evacuated at 25° for 12 hours, and finally at 250° for 2 hours, before heats of immersional wetting were determined.

The organic liquids employed were toluene, carbon tetrachloride, *n*-heptane, cyclohexane and 1-propanol. All liquids were reagent grade supplied by the Matheson Co., and were dried and distilled prior to each run; the middle fraction of the distillates was used.

The heat of wetting calorimeter has been described previously.[3] To prepare monolayer-covered samples, the graphite was first activated and then equilibrated with the desired organic liquid thermostated at the temperature at which the vapor pressure of each liquid equalled the equilibrium pressure required to form monolayer on the graphite surface at 26°. Monolayer values were calculated from adsorption data using the BET equation by F. E. Bartell.[1] These values differed slightly from values reported previously[2] because of minor changes in graphite pre-treatment conditions.

These V_m values and the co-areas of organic molecules at monolayer coverage calculated from these data are listed in Table I. For comparison, the molecular cross-sectional areas calculated from liquid densities and the ratio of the two are listed.

TABLE I

MONOLAYER VALUES FOR THE ADSORPTION OF ORGANICS ON GRAPHITE AT 25°

	V_m, moles/g. $\times 10^3$	p/p_0	Co-area,[a] Å.²	C.S.A.,[b] Å.²	$\frac{\text{Co-area}}{\text{C.S.A.}}$
Toluene	1.34	0.036	47	34.4	1.37
Carbon tetrachloride	1.40	.082	47	32.3	1.46
n-Heptane	1.04	.073	61	42.7	1.42
Cyclohexane	1.22	.078	52	34.6	1.50
1-Propanol	1.74	.119	37	27.3	1.35

[a] From V_m and nitrogen area. [b] From liquid density.

Results and Discussion

If the surface area Σ of a solid is known, the heat evolved when a clean solid is immersed into a liquid can be put on a unit area basis, and

$$\frac{\Delta H_I}{\Sigma} = h_{I(SL)} = h_{SL} - h_{S}^{\circ} \qquad (1)$$

where h_{S}° and h_{SL} are surface enthalpies of the solid surface and the solid–liquid interface, respectively. The integral heat of adsorption of N_A moles of adsorbate from the vapor state at equilibrium pressure p and temperature T is

$$h_{ads} = h_{I(SL)} - h_{I(SfL)} + \Gamma \Delta H_L \qquad (2)$$

where $h_{I(SfL)}$ is the heat liberated on immersion of a solid pre-covered with N_A moles of adsorbed molecules at a surface concentration $\Gamma = N_A/\Sigma$ and ΔH_L is the molar heat of liquefaction. If the entire entropy change can be attributed to the adsorbate, Jura and Hill[4] showed that the difference in entropy of the adsorbed film S_A and the entropy of the bulk liquid S_L is given by the equation

$$T(S_A - S_L) = [h_{I(SL)} - h_{I(SfL)}]/\Gamma + \varphi/\Gamma - kT \ln x \qquad (3)$$

Here x is the relative equilibrium pressure and φ the spreading pressure, $\gamma_{S}^{\circ} - \gamma_{SV}^{\circ}$.

Bartell and co-workers[2] supplied from their adsorption isotherms the free energy values $\gamma_{S}^{\circ} - \gamma_{SV}^{\circ}$ at monolayer coverage ($\theta = 1$) for the various organic vapors on graphite. In the present in-

(1) F. E. Bartell, private communication.

(2) R. G. Craig, J. J. Van Voorhis and F. E. Bartell, THIS JOURNAL, 60, 1225 (1956).

(3) A. C. Zettlemoyer, G. J. Young, J. J. Chessick and F. H. Healey, *ibid.*, 57, 649 (1953).

(4) G. Jura and T. L. Hill, *J. Am. Chem. Soc.*, 74, 1598 (1952).

<div align="center">TABLE II</div>

THERMODYNAMIC FUNCTIONS OF IMMERSIONAL WETTING AND ADSORPTION FOR ORGANICS ON GRAPHITE AT 25°

	$-h_{I(SL)}$	———ergs./cm.²——— $-h_{I(S_1L)}, \theta = 1$	h_L	$(\gamma_{S^0} - \gamma_{SV^0})$	$[h_{I(SL)} - h_{I(S_1L)}]$ cal./mole	$S_A - S_L,$ e.u.
Toluene	123.0 ± 2	29.6 ± 0.5	40.5	28.0	-6400	-8.3
Carbon tetrachloride	113.0 ± 2	$38.3 \pm .6$	62.9	25.1	-5100	-6.5
n-Heptane	122.5 ± 0.5	$78.2 \pm .4$	49.9	27.6	-3933	0.4
Cyclohexane	102.0 ± 2	$32.8 \pm .5$	~50	23.5	-5215	-6.4
1-Propanol	90.5 ± 0.5	$105.2 \pm .1$	~70	30.7	$+782$	14.5

vestigation the heats of immersion of the evacuated (clean) and monolayer-covered surfaces of graphite in these same organic liquids were measured. Through use of the results of these free energy and heat values, integral entropies of adsorption at $\theta = 1$ were calculated. These and the other pertinent values are listed in Table II.

The heat values per unit nitrogen area for the immersion of monolayer-covered samples in toluene, cyclohexane and carbon tetrachloride are less than the surface enthalpies of the respective wetting liquids, h_L. These unusual results might be caused by the presence of small pores in the graphite inaccessible to the larger organic molecules, but accessible to nitrogen. Considerable loss of area during monolayer formation is unlikely, however, in view of a monolayer heat value greater than h_L obtained for the immersion experiments with heptane, a molecule which possesses the largest C.S.A. in the liquid state among those studied.

If the rapid heat evolution on immersion is followed by a slow process undetectable with the calorimeter used, then possibly lower than h_L values could also be determined. This latter effect, however, would be expected to be much more serious for the evacuated sample. Non-equilibrium heat of immersion values, at least for the evacuated sample, also appear unlikely since Bartell and Suggitt[5] found very nearly the same heat values for the immersion of both 8.4 m.²/g. and 86 m.²/g. Acheson graphites in the same liquids. The value of 61 Å.² for the cross-sectional area of n-heptane might possibly be too large, but it agrees well with the value found by Kiselev[6] for adsorption on a somewhat more homogeneous surface, Spheron 6, graphitized at 1700° in hydrogen. Indeed, large C.S.A.'s for

the adsorption of organics on graphites are common.[7] In view of these circumstances, these results cannot be explained on the basis of conventional adsorption thermodynamics as developed by earlier workers.[8]

Likewise, the large heat value found for the immersion of the alcohol-covered sample cannot be ascribed to the filling of small pores. Surprisingly, the heat value measured for the monolayer-covered solid was greater than that for the evacuated sample. Conceivably, more hydrogen bonds are broken during the immersion of the evacuated sample compared to the same process for the monolayer-covered sample. The results could be explained if the monolayer film formed from the vapor phase possesses fewer hydrogen bonds than a liquid-like layer would possess. It is interesting to note that the area occupied by propanol out of aqueous solution onto Graphon was found[9] to be only 22 Å.²

More work on these systems is needed and is in progress. Specifically, heats of wetting lower than h_L near monolayer coverage must be explained if the effect of pores is absent at such low coverages. If the effect of pores is present, a more reliable estimate of monolayer capacities for complex organic adsorbates than provided by the BET equation must be developed. The anomalous effects found for the immersion of graphite samples in the alcohol must be explained. There is no doubt that the relationship between vapor adsorption and immersion in liquids is more complex than previouly suspected.

(5) F. E. Bartell and R. M. Suggitt, THIS JOURNAL, **58**, 36 (1954).

(6) A. V. Kiselev, "Proceedings of the Second International Congress of Surface Activity," Vol. II, Academic Press, New York, N. Y., 1957, p. 168.

(7) See for example, J. H. de Boer, *Advances in Catalysis*, **VIII**, 82 (1956).

(8) W. D. Harkins, "The Physical Chemistry of Surface Films," Reinhold Publ. Corp., New York, N. Y., 1952.

(9) Donald Graham and Robert S. Hansen, THIS JOURNAL, **60**, 1153 (1956).

FREE ENERGIES OF IMMERSION FOR CLAY MINERALS IN WATER, ETHANOL AND n-HEPTANE

BY C. S. BROOKS

The free energies of immersion for several clay minerals—pyrophyllite, kaolinite and montmorillonite—in water, ethanol and n-heptane at 30° and for illite in water at 20° have been calculated from vapor sorption isotherms by application of the Gibbs adsorption equation. The thermodynamic validity of free energies of immersion calculated from vapor sorption isotherms on clay minerals has been examined, particularly in regard to (a) hysteresis in the isotherms, and (b) selection of a realistic vapor–solid interfacial area. The influence of exchangeable cation and of sample preparation (in particular, the water left on the montmorillonite surface) on the accessibility of the intralattice surfaces for adsorption of polar vapors has been demonstrated. The same degassing conditions that leave calcium montmorillonite platelets separated by one molecular layer of water adsorbate collapse sodium montmorillonite so that rehydration by water vapor sorption at low relative humidity is drastically reduced. This demonstrates the effect of strong van der Waals interaction at platelet–platelet separations less than 3 Å., which is a result of the lower free energy of hydration of the sodium exchange cation. It was considered especially significant that the surface-charge densities of clay minerals as varied in morphology, chemical composition and particle size as pyrophyllite, kaolinite, illite and montmorillonite were all of the order of 20–23 × 10^{-8} meq. of CEC/cm.^{2} when referred to water and ethanol surface areas. Comparison of free energies of immersion for clays with those for quartz and for sodium ion-exchange resins demonstrated the contribution of the cation exchange capacity; for three clays—sodium illite, calcium illite and calcium montmorillonite—a quantitative estimate was obtained for the contribution of the cation-exchange capacity to the total free energy of hydration. Reference of free energies of immersion calculated from vapor isotherms to the cation-exchange capacity, rather than to the often indeterminate vapor–solid interfacial area, was shown to have considerable utility for polar adsorbates on clay minerals.

Introduction

Surface tensions and oil-water interfacial tensions are susceptible to direct measurement, but vapor–solid and liquid–solid interfacial tensions cannot be evaluated directly. By application of the Gibbs adsorption equation[1] to vapor isotherms, the difference between the solid surface tension and the liquid–solid interfacial tension can be estimated. This difference has been defined as the free energy of immersion of the solid in the liquid.

Several studies have been made in which the free energies of immersion of mineral surfaces in liquids were determined by this method from vapor sorption isotherms.[1-5] These investigations were made with water, n-heptane and nitrogen vapors on hydrophilic mineral surfaces, such as silica, calcite, mica and anatase, and on hydrophobic mineral surfaces, such as graphite.

In this study the free energies of immersion of several clay minerals—pyrophyllite, kaolinite and montmorillonite—in water, ethanol and n-heptane at 30° and of illite in water at 20° were determined from vapor sorption isotherms.

Of particular interest were the dependence of the free energy of adsorption at vapor activities less than 1 upon the cation-exchange capacity and the exchangeable cation, the amount of water present on the clay surface, the vapor polarity, and the conditions of adsorbent preparation and accessibility of clay surfaces.

The free energies of immersion of these clay minerals in water, ethanol and n-heptane are discussed in the light of similar studies made by other investigators for vapor sorption on mineral surfaces,[1-5]

particularly silica, and for water vapor sorption on ion-exchange resins.[3-9]

Experimental

Apparatus and Procedure.—The sorption isotherms were measured with helical spring balances.[10]

The construction of the apparatus and the operating procedures have been described elsewhere.[11]

Adsorbents.—The pyrophyllite, kaolinite, illite and montmorillonite used in this study were portions of clay minerals from API Research Project 49 on Reference Clay Minerals. The chemical analyses and physical properties of these clays have been reported by that project.[12]

Pyrophyllite	API Sample No. 47	Robbins, N. C.
Kaolinite	API Sample No. 3	Macon, Ga.
Illite	API Sample No. 35	Fithian, Ill.
Montmorillonite	Same source as API Sample No. 26	Clay Spur, Wyo.

Pyrophyllite and kaolinite were used in their native condition with whatever exchangeable cations were originally present (predominantly Ca^{2+} and Mg^{2+}).

The sodium and calcium illites and the calcium montmorillonite were prepared by conversion on ion-exchange resin columns.[13]

The Wyoming montmorillonite was a stock sample used for colloid investigations in this Laboratory and was supplied by the Baroid Division, National Lead Company. The native (sodium) montmorillonite was used in its untreated condition, in which approximately 90% of the exchangeable cation was sodium.

The quartz was a high-purity sample with a surface area of 1.8 m.^{2}/g.

The polystyrene ion-exchange resins had varying degrees of sulfonation, which provided cation exchange capacities

(6) H. P. Gregor, B. R. Sundheim, K. M. Held and M. H. Waxman, *J. Colloid Sci.*, **7**, 511 (1952).

(7) B. R. Sundheim, M. H. Waxman and H. P. Gregor, THIS JOURNAL, **57**, 969 (1953).

(8) B. R. Sundheim, M. H. Waxman and H. P. Gregor, *ibid.*, **57**, 974 (1953).

(9) E. Glueckauf and G. P. Kitt, *Proc. Roy. Soc. (London)*, **A228**, 322 (1955).

(10) J. W. McBain and A. M. Bakr, *J. Am. Chem. Soc.*, **48**, 690 (1926).

(11) C. S. Brooks, "Gravimetric Vapor Sorption Apparatus," to be published.

(12) "Reference Clay Minerals," API Research Project 49, Columbia Univ., New York, N. Y., Jan. 1951.

(13) D. R. Lewis, *Ind. Eng. Chem.*, **45**, 1782 (1953).

(1) G. J. Jura and W. D. Harkins, *J. Am. Chem. Soc.*, **66**, 1356 (1944).

(2) G. E. Boyd and H. K. Livingston, *ibid.*, **64**, 2383 (1942).

(3) N. Hackerman and A. C. Hall, THIS JOURNAL, **62**, 1212 (1958).

(4) W. D. Harkins, G. Jura and E. H. Loeser, *J. Am. Chem. Soc.*, **68**, 554 (1946).

(5) D. H. Bangham and S. Mosallam, *Proc. Roy. Soc.(London)*, **A166**, 558 (1938).

ranging from 0.62 to 4.78 meq. per gram of dry hydrogen equivalent.

All the sodium resins were prepared by sulfonation of the same inert copolymer, polystyrene cross-linked with approximately 10% divinylbenzene, by Dr. Monroe Waxman.

The resins were thoroughly washed to remove all the salts retained in the interstitial pore spaces and were dried to constant weight at 57° before introduction into the adsorption system. In preparation for the adsorption experiments the resins were evacuated for at least 24 hours under a high vacuum (10^{-5} mm. pressure). The water sorption capacities were based on the weight of the dry sodium resin at the end of the adsorption experiments after evacuation to constant weight at 30°.

Adsorbates.—An absolute, high-purity ethanol (Commercial Solvents Corporation) and a research-grade, high-purity (99.9 mole %) n-heptane (Phillips Petroleum Company) were used without further refinement except for being dried over desiccant silica gel. Ordinary, singly distilled water was used to provide water vapor. All the adsorbates were deaerated by several successive freeze-outs with liquid nitrogen and by evacuation under high vacuum.

Adsorbent Preparation.—The adsorption capacities were based on the final weights after the resins were degassed in a vacuum of 10^{-5} mm. pressure at the specified time and temperature. In the present experiments we used a mild degassing preparation which consisted of partially dehydrating the adsorbent by evacuating at 25° for 16 hours and a second more rigorous degassing preparation which consisted of evacuating for 8 hours at 110°. The selection of the mild degassing condition was entirely arbitrary. The second degassing condition was selected so that removal of physically adsorbed hydration water would be essentially complete.

Results

Isotherms—Pyrophyllite, Kaolinite and Illite.

—The isotherms for water, ethanol and n-heptane on kaolinate are characteristic of the isotherms that we obtained for pyrophyllite and illite with these vapors (Fig. 1). The magnitude of the sorption capacity of pyrophyllite for these vapors was appreciably lower than that of illite, owing to the much larger average effective particle size of pyrophyllite.

All of these clay minerals gave some low-order hysteresis between the adsorption and desorption isotherms for water vapor over at least a portion of the range of relative vapor pressures.

Isotherms—Calcium Montmorillonite.—Desorption isotherms for calcium montmorillonite for water, ethanol and n-heptane are given (Fig. 2).

An unheated portion of calcium montmorillonite equilibrated at $\sim$0.8 p/p_0 adsorbed two complete molecular layers of intralattice water (Fig. 2), as indicated by X-ray diffraction basal spacing of 15.5 Å. compared with 9.6 Å. for dehydrated clay.

In the case of mildly degassed clay portion, the BET monolayer[14] surface-area estimate based on the water desorption isotherm approximated one-half the amount of water which would have been necessary to form two complete intralattice layers (X-ray diffraction).

Appreciable hysteresis was observed between the adsorption and desorption isotherms for water and ethanol for the portions degassed at 110°, but there was hysteresis only at high values of P/P_0 with water for the portion degassed at 25°.

Isotherms—Native (Sodium) Montmorillonite.—

Adsorption and desorption isotherms for water and ethanol on native (sodium) montmorillonite are given (Fig. 3).

(14) S. Brunauer, P. H. Emmett and E. Teller, *J. Am. Chem. Soc.*, **60**, 309 (1938).
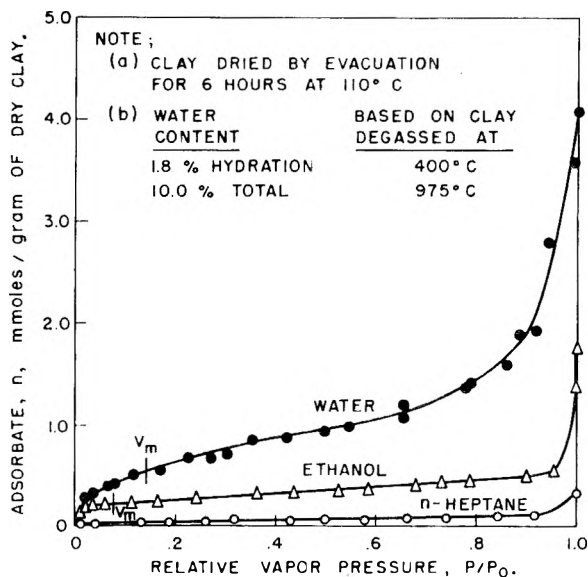
Fig. 1.—Sorption of water, ethanol and n-heptane on kaolinite at 30° (desorption isotherm).
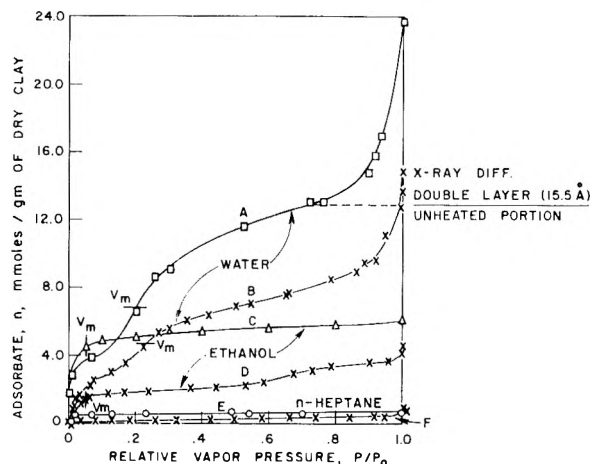
CLAY PREPARATION	SYMBOL	WATER CONTENT HYDRATION	TOTAL	BASED ON CLAY DEGASSED AT
EVACUATED UNDER HIGH VACUUM AT 25°C FOR 16 HOURS	A, C, E	10.5 %	—	400° C
			15.1 %	950°C
EVACUATED UNDER HIGH VACUUM AT 110°C FOR 6 HOURS	B, D, F	1.5 %	—	400° C
			6.1 %	950° C

Fig. 2.—Sorption of water, ethanol and n-heptane on calcium montmorillonite at 30° (desorption isotherms).

An unheated portion, equilibrated at $\sim$0.8 P/P_0, yielded a complete intralattice water monolayer, as indicated by the X-ray diffraction basal spacing of 12.5 Å. compared with 9.6 Å. for the dehydrated clay.

In the case of native (sodium) montmorillonite, the BET water-vapor surface area based on the desorption branch shows quite poor agreement with the monolayer value for water based on the X-ray diffraction basal spacing of an unheated portion of this clay. This demonstrates that even though the clay was exposed for several days to high water vapor pressures ($\sim$0.99 P/P_0), only partial rehydration of the intralattice clay surfaces occurred.

The marked hysteresis between water and ethanol adsorption and desorption isotherms demon-
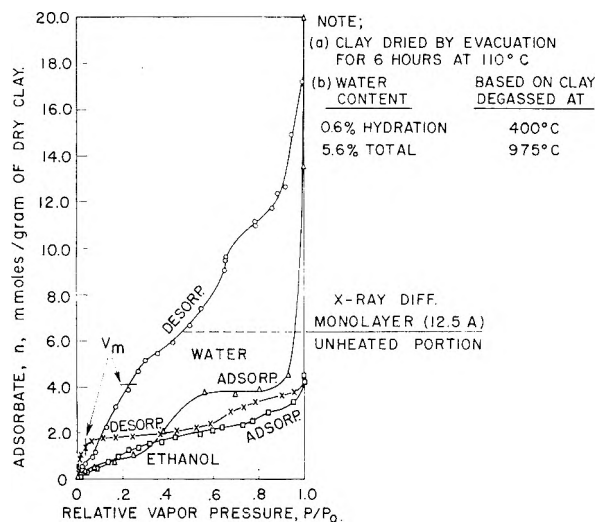
Fig. 3.—Sorption of water and ethanol on native (sodium) montmorillonite at 30°.

strates the difficulty with which even highly polar adsorbates penetrate the dehydrated intralattice surfaces of sodium montmorillonite.

Free Energy Calculations

Derivation of the Gibbs adsorption equation as applied to estimation of the free energy of adsorption at vapor–solid interfaces has been given elsewhere[7,15-17] and will not be presented here. The relations used for calculation of the free energies of immersion are

$$\Delta F_v = -\frac{RT}{A} \int_{P/P_0=0}^{P/P_0} \frac{n}{P/P_0} \, d(P/P_0) +$$
$$nRT \ln (P/P_0) \quad (1)$$
$$\gamma_{so} - \gamma_{sl} = \Delta F_v + \gamma_{lv} \cos \theta_{lv} \quad (2)$$

ΔF_v is defined as the free energy of vapor adsorption and $\Delta F_v = \gamma_{so} - \gamma_{sv}$ when $P/P_0 = 1$, but not otherwise. γ_{so} is the surface tension of the clean, dry, solid surface; γ_{sv} is the surface tension of the solid covered with the adsorbate film at P/P_0; R is the gas constant; T is the absolute temperature; n is the moles of adsorbate per gram of solid at relative vapor pressure P/P_0; γ_{sl} is the surface tension of the solid immersed in the liquid; γ_{lv} is the normal surface tension of the liquid against its own vapor; and $\cos \theta_{lv}$ is the contact angle for the solid with a multilayer adsorbate film against its own vapor at $P/P_0 = 1$.

The first term on the right side of equation 1 is the form in which vapor adsorption data are graphically integrated. Uncertainty due to graphical integration with good vapor adsorption data from 0.02 to 0.99 P/P_0 should not exceed 5 ergs/cm.^{2}.

The second term on the right side of equation 1 is the work for isothermal compression of vapor at P to P_0.

Equation 2 gives the total free energy of immersion, $\gamma_{so} - \gamma_{sl}$, for the solid covered with adsorbate film in the liquid. The normal liquid–vapor surface tension γ_{lv} was used. $\cos \theta_{lv}$ was taken as 1 at

(15) D. H. Bangham, *Trans. Faraday Soc.*, **33**, 805 (1937).

(16) T. L. Hill, *J. Chem. Phys.*, **17**, 520 (1949).

(17) D. H. Bangham and R. J. Razouk, *Trans. Faraday Soc.*, **33**, 1463 (1937).

$P/P_0 = 1$, since silicate surfaces form multilayer adsorbate films for which zero contact angle with saturated vapor can be assumed to apply.

Discussion

Assumptions and Limitations Applicable to Free Energy Calculations.—The thermodynamic validity of ΔF_v calculated from a vapor sorption isotherm on a clay requires examination. Two considerations which will be examined are (1) hysteresis in the isotherms, and (2) the vapor–solid interfacial area.

(1) **Hysteresis.**—One of the most serious limitations imposed upon these free energy calculations is that the hysteresis between adsorption and desorption vapor isotherms on many of the clay minerals raises the question of thermodynamic reversibility, which is necessary for rigorous application of these equations.

The observed hysteresis cannot be eliminated; in many instances, especially with the montmorillonites, the adsorption branch cannot consistently be reproduced to the extent possible with rigid porous solids. This apparently is due to variations in the structure of the clay aggregates each time the sample is rigorously dried, resulting in variations in the subsequent rehydration when a second adsorption isotherm is measured.

Many polar organic fibers provide a non-rigid adsorbent structure which is characterized by appreciable hysteresis between adsorption and desorption isotherms throughout essentially the entire range of P/P_0 for polar vapors. The sorption behavior of such fiber aggregates bears a striking resemblance to the sorption behavior of clay platelet aggregates.[18,19]

If the aggregates of platelets which constitute the clay mineral adsorbent are considered to form an unstable gel network in which restraints opposing free swelling may vary with the extent of the platelet–platelet contact surfaces, the observed failure to obtain consistently reproducible adsorption isotherms for polar adsorbates on a clay mineral such as montmorillonite is understandable.

In view of our inability to apply rigorously the condition that equilibrium adsorption can be approached by either adsorption or desorption throughout the isotherm, desorption isotherms which have a high order of reproducibility have been used. In all isotherms characterized by hysteresis, ΔF_v calculated for isotherm data in the hysteresis region must at best correspond to a metastable equilibrium state.

(2) **Interfacial Area.**—In view of the hysteresis in these vapor isotherms, caution must be used in selection of the vapor–solid interfacial area of reference for ΔF_v.

The higher order of reproducibility of the desorption isotherms for polar adsorbates provides greater assurance that for a given P/P_0 there is a well-defined vapor–solid interfacial area for the given adsorbent. Estimates of this interfacial area based on desorption isotherms of the given vapor are con-

(18) W. M. Barkas, *ibid.*, **38**, 194 (1942).

(19) J. L. Morrison and M. A. Dzieciuch, *Can. J. Chem.*, **37**, 1379 (1958).

sidered more reasonable than those based on adsorption isotherms.

Further support for selection of the surface areas estimated from the vapor-desorption isotherms is provided by consideration of the accessibility of the cation-exchange sites to the given vapor.

We can consider that a cation-exchange capacity (CEC) determined by ammonium ion exchange in an aqueous solution[20] provides a measure of the maximum concentration of cation-exchange sites at the vapor–clay interface for the most polar adsorbate water.

Examination of the BET surface areas estimated from water and ethanol vapor desorption isotherms referred to the CEC (Table I) demonstrates that, except for the sodium montmorillonite degassed at either 25 or 110°, and calcium montmorillonite degassed at 110°, the area available per exchange site lies within the range 70–140 A.[2]. This range is based on the surface area from X-ray diffraction crystal structure data for montmorillonite and kaolinite.[21,22] Values appreciably lower than 70 A.[2] per exchange site based on BET surface areas, calculated from adsorption data below 0.4 P/P_0 indicate that some exchange sites are inaccessible for adsorption of these vapors. This was particularly evident for montmorillonite.

NOTE;

(a) BASED ON DESORPTION ISOTHERMS AT 30° C

(b) CLAY DEGASSED BY EVACUATION FOR 6 HOURS AT 110°C

Fig. 4.—ΔF_v for kaolinite in water, ethanol and n-heptane.

TABLE I

AREA PER CATION-EXCHANGE SITE FROM WATER AND ETHANOL VAPOR DESORPTION ISOTHERMS

Clay	CEC, meq./ g.	—Water— Area, m.²/g.	Area/ cation ex- change site × 10¹⁶ cm.	—Ethanol— Area, m.²/ g.	Area/ cation ex- change site × 10¹⁶ cm.	Ad- sorbent pre- pared by evacu- ation
Kaolinate	0.06	34	94	31	86	110°
Pyrophyllite	.01	4.6	76	3.2	53	110°
Sodium illite	.22	106[a]	80			110°
Calcium illite	.22	115[a]	87			110°
Native (sodium)	.87	262	50	202	39	110°
montmorillonite	.87	234	45	252	48	25°
Calcium mont-	.87	295	56	205	39	110°
morillonite	.87	428	82	489	93	25°

[a] From isotherm at 20°, all other isotherms at 30°.

It was considered especially significant that the surface-charge densities[23] for clay minerals as varied in morphology, chemical composition, and average particle size as pyrophyllite, kaolinite, illite and montmorillonite, calculated from the CEC and vapor surface areas from Table I, show a very restricted range—20 ± 1.6 (av. dev.) × 10⁻⁸ meq. of

(20) Official Methods of Analysis of the Association of Official Agricultural Chemists 41, 43-44, 1950, Assoc. of Off. Ag. Chemists, P. O. Box 540, Benjamin Franklin Sta., Washington 4, D. C.

(21) S. B. Hendricks, THIS JOURNAL, 45, 65 (1941).

(22) R. E. Grim, "Clay Mineralogy," McGraw-Hill Book Co., New York, N. Y., 1953, p. 134.

(23) In the case of sodium montmorillonite degassed at 25 and 110° and of calcium montmorillonite degassed at 110°, it was necessary to correct for the external surface area of the platelet aggregates, ∼50 × 10⁴ cm.²/g., and for one molecular layer of intralattice water adsorbed between two platelet surfaces to obtain

$$\frac{\text{meq. of CEC}}{\text{cm.}^2} = \frac{\text{CEC in meq./g.}}{2\left[\text{total vapor area}\frac{\text{cm.}^2}{\text{g.}} - 50 \times 10^4\right]}$$

Fig. 5.—ΔF_v for sodium and calcium illites, sodium and calcium montmorillonites and quartz in water vapor.

CEC/cm.[2] (water area), and 23 ± 4.2 (av. dev.) × 10⁻⁸ meq. of CEC/cm.[2] (ethanol area).

Only the external surfaces of the dehydrated clay aggregates are accessible for adsorption of vapors of low polarity, such as n-heptane or nitrogen; in the case of montmorillonite, this is less than 10% of the total surface of the clay mineral platelets.

In the case of pyrophyllite, kaolinite and illite, there is far less evidence of dependence of the vapor–solid interfacial area upon the vapor polarity and upon the hydration water retained on the clay surface, so that there should be little ambiguity involved in considering the same surface area to be accessible for high-polarity adsorbates such as water or low-polarity adsorbates such as nitrogen or n-heptane.

Free Energy of Adsorption at $p/p_0 < 1$. ΔF_v for water, ethanol and n-heptane on kaolinite over the entire isotherm have been plotted (Fig. 4). ΔF_v was referred to the BET surface area calculated from desorption isotherms in all cases.

Dependence of ΔF_v upon vapor polarity is evident. It is also evident that ΔF_v for kaolinite increases to a value appreciably greater than the value for quartz as P/P_0 approaches 1.

The ΔF_v curves for kaolinite are, in general, characteristic of those obtained for all the clay minerals.

ΔF_v for water vapor on quartz, sodium and calcium illites, and sodium and calcium montmorillonites are plotted up to $P/P_0 = 1$ (Fig. 5).

ΔF_v were based on the water desorption areas, except for the lower ΔF_v curves for the illites, in which the nitrogen surface area (85 m.^{2}/g.) was used. ΔF_v above 0.4 to 0.6 P/P_0, when the most reliable areas were used, were appreciably greater for the clays than for quartz. This was true only when the nitrogen areas were used for the illites. In the case of the montmorillonites, water desorption areas must be used to obtain meaningful results.

The larger ΔF_v for the clay minerals compared with quartz is due presumably to a greater interaction energy per molecule for hydration water about the exchangeable cation.

If the increase in ΔF_v for clay minerals over quartz is assumed to be primarily due to the presence of the exchange capacity, the free energy of hydration per equivalent of CEC can be estimated. This was done for illite with sodium and calcium as exchange cations.

$$-\Delta F_{hyd} = \frac{2.389 \times 10^{-11}\,[\pi^{clay*} - \pi^{SiO_2*}]P/P_0 = 1}{*\text{equiv. of CEC per cm.}^2} \quad (3)^{24}$$

The calcium montmorillonite data were treated in the same manner, except that ΔF_v and the surface concentration of CEC were based on the surface areas estimated from the water desorption isotherms (adsorbent degassed at 25° (Table II).

TABLE II

FREE ENERGY OF HYDRATION PER EQUIVALENT OF CEC FOR CLAYS AND ION-EXCHANGE RESINS

Adsorbent	Cation	ΔF_{hyd}, kcal./equiv. of CEC at $P/P_0 = 1$
Illite	Na	3.8
Illite	Ca	7.3
Montmorillonite	Ca	3.4
Ion-exchange resin	Na	4.5–6.2
Ion-exchange resin	Na	5.8[a]
Ion-exchange resin	Ca	7.1[a]

[a] Sulfonated polystyrene with 10% DVB–4.80 meq./g. Gregor, Sundheim, Held and Waxman, *J. Colloid Sci.*, **7**, 511 (1952).

The quartz surface resembles the exposed surfaces of the three-layer clays, such as illite and montmorillonite, inasmuch as these surfaces are formed by silica tetrahedra. The principal difference between the quartz and silicate surfaces is that the latter bears a net negative charge due to isomorphous substitution, *e.g.*, of divalent magne-

(24) * referred to N$_2$ surface area.

TABLE III

FREE ENERGIES OF IMMERSION FOR CLAY MINERALS IN WATER, ETHANOL AND n-HEPTANE[a]

Mineral surface	Free energy of immersion $\gamma_{so} - \gamma_{sl}$, ergs./cm.^{2} Water A	Water B	Ethanol A	Ethanol B	n-Heptane A	n-Heptane B	Temp. of isotherm, °C.
Pyrophyllite	348	331	154	150	97	105	30
Kaolinite	356	292	155	156	89	52	30
Native (sodium) montmorillonite	296	219	138	136	59	76	30
Calcium mont.	294	226	133	150	71	77	30
Sodium illite	263 (307)						20
Calcium illite	265 (346)						20
Quartz	266						30
Quartz	C 275(125°) C 303(700°)				D 59		25

[a] (A) clay prepared by evacuation under high vacuum for 16 hours at 25°; (B) clay prepared by evacuation under high vacuum for 6 hours at 110°; (C) data from ref. 3; (D) data from ref. 2.

sium for trivalent aluminum. In montmorillonite this substitution occurs predominantly in the octahedral alumina layer sandwiched between the two silica tetrahedral layers, but in illite the isomorphous substitution may be principally in the silica tetrahedral layers.

ΔF_{Hyd} computed from equation 3 for these clays can be compared with total ΔF_{Hyd} based on water vapor sorption data on ion-exchange resins. In the case of the resins the primary factor is hydration of the exchange sites. The contribution of the hydrocarbon resin chain network to the water vapor sorption capacity of the resins is considered to be of minor importance. Support for this conclusion is provided by the extremely low order water sorption capacity of the resin chain network before introduction of the exchange capacity by sulfonation.

Glueckauf and Kitt,[9] in their treatment of water vapor sorption data on ion-exchange resins, proposed a model in which hydration water is divided between the anionic exchange site and the exchange cation. Formulation of an equivalent model for the clay-water vapor system was considered too speculative in the light of our present understanding of clay mineral hydration. The major change in magnitude of ΔF_{Hyd} (Table II, column 3) with a change in exchange cation in the case of both the clays and the ion-exchange resins justifies the qualitative observation that the major factor in hydration is the exchange cation.

The agreement between the ΔF_{Hyd} for calcium illite and the calcium resin is good. The value for sodium illite is somewhat lower than that for the sodium resin. No explanation can be offered for this discrepancy.

The calcium montmorillonite value corresponds to the free energy of hydration for the second layer of intralattice hydration water and is comparable to the value estimated for sodium illite rather than for calcium illite.

This simplified treatment provides a straightforward manner of accounting for the variations in the hydration of a given clay mineral dependent upon the nature of the exchange cation by attributing these hydration differences entirely to the varia-

tions in the free energy of hydration of the cations. Van Olphen[25] has pointed out, however, that the true geometric positions of the cations relative to the silicate lattice have not yet been determined unequivocally, so that the present treatment based entirely on vapor adsorption measurements requires further confirmation by establishment of the true steric relation of the exchange cations to the silicate lattice.

Free Energy of Immersion, $\gamma_{so} - \gamma_{sl}$.—The free energies of immersion, $\gamma_{so} - \gamma_{sl}$, calculated from equation 2 for pyrophyllite, kaolinite, sodium and calcium illites, sodium and calcium montmorillonites, and quartz are summarized in Table III.

$\gamma_{so} - \gamma_{sl}$ for all the clay minerals ranges from 219 to 352 ergs/cm.^{2} for water. $\gamma_{so} - \gamma_{sl}$ for quartz not degassed above 125° ranges from 266 to 275 ergs/cm.^{2}. High-temperature annealing of quartz at 700° raises this value appreciably.[3]

The values of $\gamma_{so} - \gamma_{sl}$ for all the clays range from 133 to 156 ergs/cm.^{2} for ethanol .

$\gamma_{so} - \gamma_{sl}$ for the clay minerals ranges from 52 to 105 ergs/cm.^{2} for n-heptane and can be compared with the value of 59 ergs/cm.^{2} for quartz obtained by Boyd and Livingston.[2]

$\gamma_{so} - \gamma_{sl}$ for the illites based on the nitrogen areas shown in parentheses in Table III is greater than the corresponding values for quartz by amounts of the order of 41 ergs/cm.^{2} for sodium and 80 ergs/cm.^{2} for calcium. These increases indicate the contribution of the CEC and primarily the exchange cation to hydration of the illite surface.

Free Energy of Adsorption Referred to CEC.— An alternative to referring ΔF_v to the vapor–solid interfacial area is to substitute CEC for A in equation 1.

A plot was made of ΔF_v per equivalent of CEC vs. P/P_0 for sodium montmorillonite and sodium illite degassed at 110°, sodium montmorillonite

(25) H. van Olphen, "Interlayer Forces in Bentonite," paper presented at 2nd National Conference on Clays and Clay Minerals, 1953, Pub. Natl. Acad. Sci. and Natl. Res. Council, 1954.

degassed at 25° and two sodium ion exchange resins degassed at 30°.

This type of plot is particularly appropriate for the ion-exchange resins, where the ion-exchange sites are the primary sites of hydration and the exchangeable cation is the predominant factor.

It was apparent from these plots that if the hydration of the resins were attributed exclusively to the exchange cation, and if the hydration of the sodium cation on the resins and on the clay mineral were of the same magnitude, the exchange cation would be responsible for $^1/_5$–$^1/_3$ of the total free energy of hydration of the clays.

Comparison of the curves of ΔF_v vs. P/P_0 for sodium illite with the plots for sodium montmorillonite degassed at 25 or 110° indicated that for montmorillonites an appreciable portion of the exchange sites must be inaccessible for water vapor sorption.

ΔF_v for ethanol at low values of P/P_0 was comparable in magnitude with ΔF_v for water for montmorillonite degassed at 25°, indicating that adsorption on the montmorillonite at low vapor activities was comparable for the two vapors. Ethanol showed preferential adsorption on montmorillonite degassed at 110°.

The resin with the lower CEC demonstrated a larger $\Delta F_{Hyd.}$ of ~1.5–2 kcal. per equivalent of CEC over most of the isotherm due, no doubt, to some structural changes in the resin network with more extensive sulfonation. It also may be due, in part, to some mutual interference in hydration of adjacent sulfonate groups for the high-exchange-capacity resin.

CORRELATION BETWEEN THE ADHESION TENSION OF AQUEOUS SOLUTIONS OF DETERGENTS AND PROTECTIVE COLLOIDS AND THEIR EFFECT ON THE STABILITY OF COLLOIDS*

BY HERMANN LANGE

Henkel & Cie, G.m.b.H., Düsseldorf, Germany

Received November 11, 1959

Detergents and protective colloids are capable of stabilizing hydrophobic suspensions or sols in water even at high electrolyte concentrations where the electrical repulsion between the particles is essentially suppressed. In this case the stabilizing effect is due to the hydration of the protective colloids on the particle surface. Hence it is expected that there is some correlation between the influence of detergents on the adhesion tension and on the sol stabilization. This correlation has been verified by experiments on the influence of detergents on the adhesion tension of water at solid paraffin and on the stability of an aqueous paraffin sol at high electrolyte concentration. Contrariwise macromolecular, surface inactive protective colloids exhibiting a marked stabilization of the sol show only little influence on the adhesion tension. This may be explained by assuming that the work of desorption is small for the protective colloids. The stabilizing action of these agents may be based upon the low speed of desorption caused by the size of these molecules.

Introduction

The stability of lyophobic sols or suspensions is in most cases mainly due to a repulsion between the particles caused by the electrical double layers surrounding them. For sols stabilized by protective colloids or surface active agents an additional stabilizing influence is exerted by the solvation of the adsorbed molecules or ions. At high ionic strength the electrical repulsion is nearly completely suppressed. If a sol is stable even at high ionic strength the stability is caused almost exclusively by the solvation. For that reason observations on the stabilization of sols at high ionic strength make it possible to investigate the efficacy of the solvation uninfluenced by electrical phenomena.

The solvation of a solid surface immersed in a liquid—whether or not under the influence of an adsorbed protective colloid or detergent—takes part in lowering the free surface energy of the solid and therefore in increasing the adhesion tension. Hence it is expected that a certain correlation exists between the influence of detergents and protective colloids on the adhesion tension and on the stabilization of sols.

Particularly this correlation results from the following considerations. The extent of the stabilizing action of a solute is expected to depend chiefly on the strength of the solvation of the adsorbed molecules or ions. Furthermore, the free energy of adsorption will be important. Only if this energy is sufficiently high (negative) will the concentration of stabilizing agent at the sol particle surface be sufficient for stabilization. Moreover, a high energy of adsorption is essential for the stabilization because it prevents a local desorption of the stabilizing agent at the collision of two sol particles.

Regarding the influence of the solute on the adhesion tension for receding liquid j_R or—as Guastalla[1] calls it—on the work of dewetting per cm.[2] one has to distinguish between two possibilities depending on whether or not an adsorbed film of the solute is left behind on the solid surface. If a film remains a desolvation occurs at the emersion. The influ-

ence of the solute on the work of dewetting therefore depends on the free energy of solvation of the film. If, on the other hand, the film is desorbed at the emersion the energy of desorption will be decisive. The work of dewetting therefore in any case depends on one of the two quantities which determine the sol stabilization.

The following investigation may be a contribution to an experimental examination of the expected correlation between the work of dewetting and the stabilization of a sol. Solid paraffin has been chosen as the solid phase. Accordingly, the stabilization of an aqueous sol of solid paraffin by different detergents and protective colloids has been investigated at high ionic strength. At the same time, the work of dewetting of surfaces of solid paraffin has been measured with the same solutions.

Because the characteristics of the measurements described here consist in the suppression of the electrical interaction between the sol particles by a high and constant ionic strength these investigations are not comparable with the interesting earlier works of other authors[2-5] on the influence of detergents upon the stability of hydrophobic sols. These works clearly show the coöperation of electrical and van der Waals forces.

Experimental

The paraffin sol was prepared by the method described by Tuorila,[6] using "paraffinum solidum DAB6," m.p. 68–70° and deionized water. It contained 0.19 g. per liter. The coagulation of the sol produced by electrolytes was observed by measuring the turbidity using a photoelectric turbidimeter. Readings were taken an hour after addition of the electrolyte or a mixture of an electrolyte and a stabilizing agent.

Figure 1 shows the turbidity T as a function of the concentration of added NaCl and $MgCl_2$, resp. The rising parts of the curves correspond to increasing coagulation, the upper horizontal parts indicate complete coagulation. $MgCl_2$ causes a coagulation of the negatively charged sol at much lower concentrations than NaCl, in accordance with the Schulze–Hardy rule.

The experiments on the stabilizing action of detergents and protective colloids are based on a concentration of NaCl of 0.5 N. At this concentration the sol is completely coagu-

(1) J. Guastalla, *J. Colloid Sci.*, **11**, 623 (1956).

(2) K. Meguro, *J. Chem. Soc. Japan, Pure Chem. Sect.*, **77**, 77 (1956).

(3) J. F. Hazel and J. O. Strange, *J. Colloid Sci.*, **12**, 529 (1957).

(4) B. Tamamushi, *Kolloid-Z.*, **150**, 44 (1957).

(5) E. Matijević and R. H. Ottewill, *J. Colloid Sci.*, **13**, 242 (1958).

(6) P. Tuorila, *Kolloidchem. Beihefte*, **27**, 44 (1928).
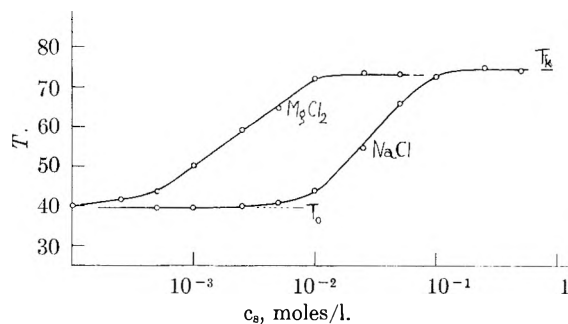
Fig. 1.—Turbidity T of a paraffin sol as a function of the concentration c_s of added electrolytes. T_0 and T_k mark the turbidities of the original and the completely coagulated sol, resp.
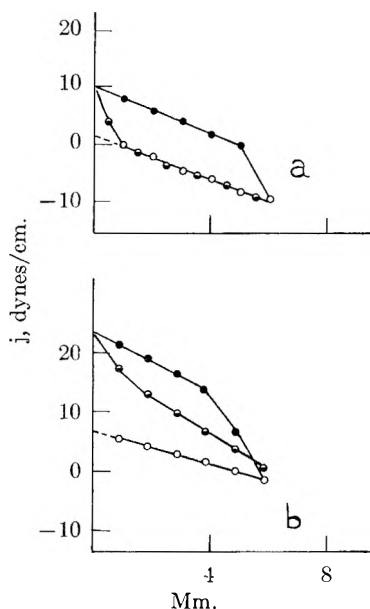
Fig. 2.—Measurement of the adhesion tension by the Guastalla method: $\bigcirc$, first immersion; $\bullet$, emersion; $\ominus$, second immersion. (a) The adhesion tension j_v is equal for the first immersion and for the second one. (b) j_v is higher for the second immersion as compared to the first one.

Fig. 3.—Diminution $\Delta T = T_k - T$ of the turbidity of a paraffin sol produced by the addition of sodium alkyl sulfates in the presence of NaCl; sum of concentrations 0.5 mole/l.

Fig. 4.—Relative diminution of the turbidity of a paraffin sol and work of dewetting j_R at a paraffin surface for sodium alkyl sulfates in the presence of NaCl; n = number of carbon atoms in the alkyl group; sum of concentrations 0.5 mole/l. (top and bottom curves) $\bullet$, 10^{-3} mole/l.; $\odot$, 10^{-4} mole/l.; $\bigcirc$, 10^{-5} mole/l.

lated if no stabilizing agent is present as is shown by the diagram. It can be concluded from Tuorila's measurements that the electrophoretic mobility of the paraffin particles is almost zero at this high concentration of NaCl. In order to investigate the stabilizing action of ionic detergents the NaCl was stepwise substituted by the detergent in such a manner that the total ionic concentration remained 0.5 N. The stabilizing effect expressed itself by a reduction ΔT of the turbidity as compared with the value T_K for the completely coagulated sol. Non-ionic detergents were investigated in a similar manner. They were added gradually while the NaCl concentration was kept constant at 0.5 N.

The work of dewetting was measured by the vertical plate method as described by Guastalla.[7] Thin glass slides covered with solid paraffin were used. Applying this method it is possible at the same time to decide whether or not an adsorbed film of the stabilizing agent is left behind. If no film remains on the solid surface the adhesion tension for the second immersion equals the value for the first immersion. In the opposite case one observed different values of the adhesion tension for the first and for the second immersion. This may be demonstrated by two examples shown in Fig. 2. The vertical force exerted on the plate partly immersed in the liquid is plotted against the depth of immersion. No correction for buoyancy is applied in this diagram. The cycle shown above—measured with an aqueous solution of a polyethylene oxide in 0.5 N NaCl—is closed, i.e.,

no adsorbed film remains. The cycle shown below—obtained with a solution of an alkyl polyglycol ether—is not closed. The adhesion tension is higher for the second immersion than for the first one. This indicates an adsorbed film left behind on the paraffin surface. The latter occurred in almost all cases where the solute caused a distinct increase of the work of dewetting.

The sodium alkyl sulfates used in this work had been extracted with petroleum ether. As a criterion of purity, they showed no minima in the surface tension curves.

Non-ionic detergents had been prepared by reaction of pure long chain alcohols with ethylene oxide.

As protective colloids sodium carboxymethylcellulose with a degree of substitution of 0.69, methylcellulose with a degree of substitution of 0.52 and polyethylene oxide with a hydroxyl number of 12 were used.

Sodium chloride and magnesium chloride were of A.R. grade. The water for preparing the solutions was deionized by an ion-exchange column.

Results and Discussion

Figure 3 shows the stabilizing action—as expressed by the lowering of the turbidity ΔT—of sodium alkyl sulfates. The curves are shifted to lower concentrations as the length of the alkyl chain is increased. The stabilizing action of the dodecyl and of the tetradecyl sulfate begins at about 10^{-6} mole/l. The octyl sulfate evidently

(7) J. Guastalla and L. Guastalla, Compt. rend., 226, 2054 (1948).
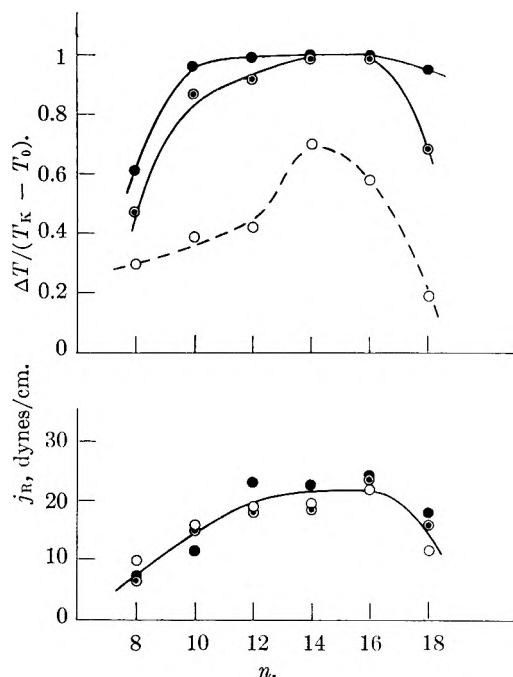
Fig. 5.—Relative diminution of the turbidity of a paraffin sol and work of dewetting j_R at a paraffin surface for condensation products of ethylene oxide and long chain alcohols in the presence of 0.5 mole/l. NaCl; n = number of carbon atoms of the alcohol; 9 moles of ethylene oxide per mole alcohol; ●, 3×10^{-5} mole/l.; ☉, 1×10^{-5} mole/l.; ○, 3×10^{-6} mole/l.
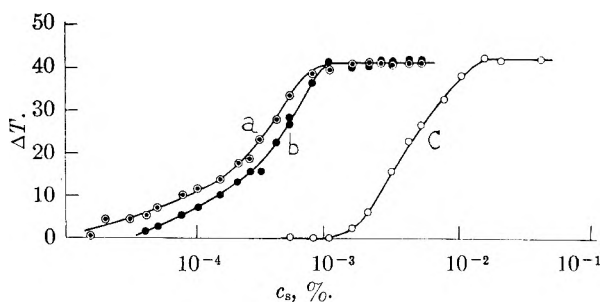
Fig. 6.—Diminution of the turbidity of a paraffin sol produced by protective colloids in the presence of 0.5 mole/l. NaCl: (a) carboxymethylcellulose; (b) methylcellulose; (c) polyethylene oxide.

inhibits the coagulation of the sol only incompletely even at high concentrations.

In the upper part of Fig. 4 the sol stabilizing action—as expressed by the relative lowering of the turbidity—is plotted against the chain length of the alkyl sulfate for different concentrations. In the lower part of the diagram the work of dewetting is plotted in an analogous manner. The curves of both the stabilizing action and the work of dewetting show a similar rise with increasing chain length.

Because the hydrophilic group is the same in the homologous series of the sodium alkyl sulfates the hydration of each adsorbed ion will also be constant. Hence the increase of the stabilizing action and of the work of dewetting are due to a rise in energy of adsorption.

Further investigations were made with nonionic detergents, especially with condensation products of ethylene oxide and long chain alcohols.
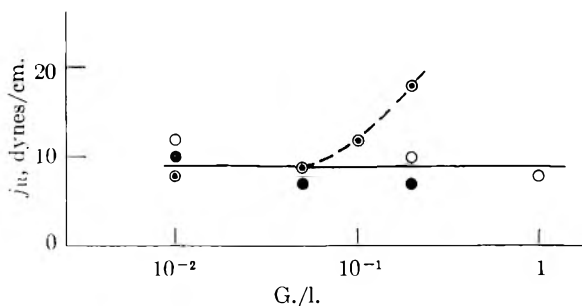
Fig. 7.—Work of dewetting at a paraffin surface for aqueous solutions of protective colloids in the presence of 0.5 mole/l. NaCl: ☉, carboxymethylcellulose; ●, methylcellulose; ○, polyethylene oxide.
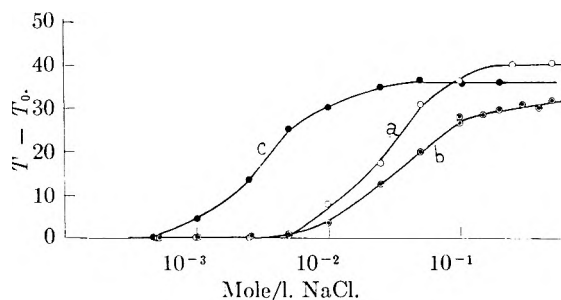
Fig. 8.—Increase of turbidity of a paraffin sol produced by NaCl: (a) no additive; (b) with $5 \times 10^{-5}\%$ carboxymethylcellulose; (c) with $5 \times 10^{-5}\%$ methylcellulose.

Figure 5 shows results obtained with a homologous series in which the length of the alkyl chain varied whereas the number of ethylene oxide units was kept constant. The curves for the relative lowering of the turbidity and for the work of dewetting as a function of the chain length have a very similar shape. They show a common maximum at 14 to 16 carbon atoms per alkyl chain. In this case it is also suggested on account of the constant hydrophilic group that the dependence of the chain length is determined by the adsorption. It is remarkable in this connection to note that the surface activity of the same compounds also increases only up to 14 C-atoms per alkyl chain.[8]

Protective colloids which are not distinctly surface active show a quite different behavior. Methylcellulose, sodium carboxymethylcellulose and a polyethylene oxide have been investigated. As Fig. 6 shows all these agents display a pronounced stabilizing action for the paraffin sol with 0.5 N NaCl. Nevertheless, the same agents have but little influence on the work of dewetting, as is shown in Fig. 7. Only carboxymethylcellulose causes a rise of the work of dewetting, but only at concentrations much higher than necessary for complete stabilization of the sol.

This result—somewhat surprising at first sight—may be explained by assuming that the work of dewetting is essentially a static quantity whereas the stabilization is a kinetic phenomenon. As the protective colloids investigated here have no strong lipophilic group they have a very low energy of adsorption on the paraffin surface. Hence the work required for the desorption of the adsorbed layer when the paraffin plate emerges sufficiently slowly

(8) H. Lange, Kolloid-Z., 163, 9 (1959).

from the solution is low. The work of dewetting is therefore little influenced by the protective colloid. For sol stabilization, however, not only the work of desorption but also the speed of desorption is important. For macromolecular protective colloids the speed of desorption may be so low that two colliding sol particles are separated by the Brownian movement before a local desorption has occurred. The stabilizing power is maintained in this case in spite of the low work of desorption.

The nearly identical sol stabilizing power of methylcellulose and carboxymethylcellulose in 0.5 N NaCl clearly demonstrates the influence of suppressing the electrical interaction between the sol particles by the high ionic strength. At low ionic strength where the electrical interaction is not suppressed methylcellulose and carboxymethyl cellu-

lose behave quite differently. In Fig. 8 the increase of turbidity caused by addition of NaCl is plotted as a function of the NaCl concentration, and that without any additive and with constant concentrations of methylcellulose and of carboxymethylcellulose. At NaCl concentrations lower than 0.1 N carboxymethylcellulose inhibits the coagulation whereas methylcellulose causes a coagulation at NaCl concentrations where the sol is stable in absence of any additive. This result is in accordance with the fact that the electrokinetic potential at solid–aqueous solution interfaces is increased by carboxymethylcellulose and decreased by methylcellulose.[9,10]

(9) W. Kling and H. Lange, *Kolloid-Z.*, **127**, 19 (1952).

(10). M. v. Stackelberg, W. Kling, W. Benzel and F. Wilke, *ibid.*, **135**, 67 (1954).

WETTING OF POLY-(METHYL METHACRYLATE) AND POLYSTYRENE BY WATER AND SALIVA

By R. G. Craig, G. C. Berry and F. A. Peyton

School of Dentistry, University of Michigan, Ann Arbor, Michigan

Received November 11, 1959

The wetting properties of poly-(methyl methacrylate) (PMMA) and polystyrene (PS) in contact with distilled water and saliva were determined by contact angle measurements. The advancing contact angles θ_a for distilled water and saliva on PMMA were measured to be 78 ± 1° and 75 ± 1° and on PS were 86 ± 1° and 79 ± 1°. The receding contact angles θ_r for distilled water and saliva on PMMA were 50 ± 1° and 0° and on PS were 64 ± 2° and 0°. Pigments and opacifiers used in dental PMMA or PS did not alter the contact angles appreciably except in the case of θ_r for water on PS which was reduced approximately 20°. Certain components of the saliva appeared to be strongly adsorbed by PS and PMMA since θ_a for water and saliva on the plastic surfaces stored in saliva for 48 hours decreased. Values for θ_a on plastic surfaces contaminated with saliva were 57 to 65° although the values for θ_r were 0°. The force required to separate PMMA or PS from a glass surface with an intervening film of water or saliva was determined and compared with values calculated on the basis of capillarity using the above data. The calculated and experimental values agreed within experimental error, supporting the use of the capillary equation for liquids which form a finite contact with the solids.

The wetting properties of solids by liquids are of great importance in many fields of science. In dentistry the wetting properties of denture base plastics by human saliva is of interest since the extent of wetting has an effect on the retention of the denture. The denture base serves two purposes, first it supports the artificial teeth in a normal functional position and second it is contoured to the shape of the oral tissues to provide retention of the dental structure during normal mastication.

The retention of a denture base has been attributed to a number of factors such as physical, physiological, psychological, mechanical and surgical. This study was limited to an investigation of the physical factors related to denture retention. Forces of cohesion, adhesion and capillarity, at one time or another, have been cited as the main reason for denture retention. It was, therefore, the purpose of this investigation to study the fundamental wetting properties of water and saliva on plastic surfaces. The surface tension of the saliva was determined by the ring method and the wetting properties of saliva on poly-(methyl methacrylate) and polystyrene denture base plastics were evaluated by contact angle measurements. In addition, the purpose was to determine the force required to separate a plastic surface from a glass surface with an intervening film of saliva and to compare these

experimental values with values calculated according to the equation expressing the force needed to separate two parallel solid surfaces with an intervening film of liquid.

Experimental

Materials.—Heat-activated poly-(methyl methacrylate) and polystyrene (Jectron) denture base plastics as well as commercial clear poly-(methyl methacrylate) and polystyrene, free from any solid lubricants such as zinc stearate, were used in this study.

The distilled water for this study had a surface tension of 72.3 dynes/cm. at 25° as measured with a du Noüy tensiometer.

The human saliva was collected by chewing paraffin wax and only that portion collected after the first 100 ml. was used. The surface tension of the saliva also was determined with a du Noüy tensiometer and values from 53.4 to 57.0 dynes/cm. at 25° were obtained. Saliva with a surface tension of 53.4 dynes/cm. was used in the contact angle measurements. Fresh saliva was used in all cases and was refrigerated when not in actual use. It should be noted that saliva is generally composed of 99.3% water, 0.2% inorganic salts (mainly K^+ and PO_4^- ions) and 0.5% organic material (mainly mucin, a gluco-protein, 0.4%).

Contact Angle Measurements.—The shadow box technique was used to determine the contact angles of water and saliva on the plastic surfaces. The contact angles were measured directly from an enlargement of a photographic negative of the drop profile. The contact angles were measured at 25° in the presence of the saturated vapor of the liquid forming the drop. The stable advancing and receding contact angles were measured in all cases and are reported in Table I.
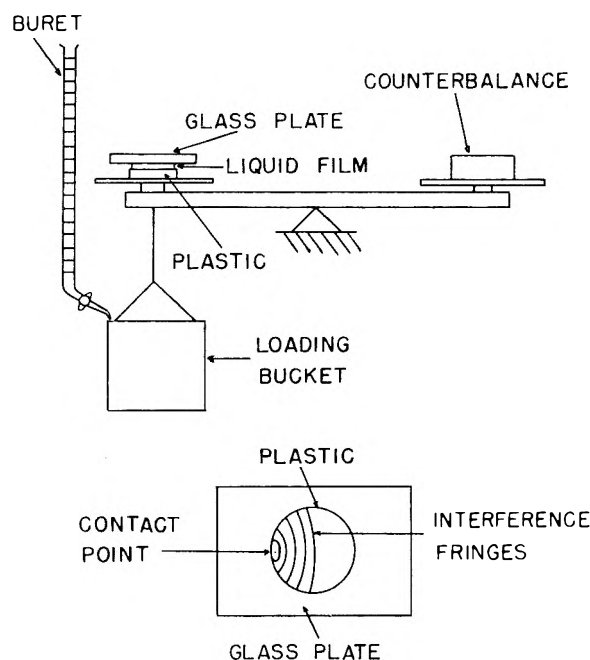
Fig. 1.—Sketch of equipment used for determining separating force values.

TABLE I

CONTACT ANGLES OF WATER AND SALIVA[a] ON PMMA AND PS AT 25°

Liquid drop	Solid surface	Surface treatment	θ_a, degrees	θ_r, degrees
		Paraffin wax		
H_2O	Commercial wax	Clean	109 ± 1	99 ± 1
		Poly-(methyl methacrylate)		
H_2O	Clear	Clean	78 ± 1	50 ± 1
H_2O	Pigmented	Clean	76 ± 1	51 ± 1
Saliva	Clear	Clean	75 ± 1	0
Saliva	Clear	Saliva[b]	68 ± 3	0
H_2O	Clear	Saliva[b]	65 ± 5	0
		Polystyrene		
H_2O	Clear	Clean	86 ± 1	64 ± 2
H_2O	Pigmented	Clean	83 ± 1	45 ± 2
Saliva	Clear	Clean	79 ± 1	0
Saliva	Pigmented	Clean	80 ± 2	0
Saliva	Clear	Saliva[b]	56 ± 5	0
Saliva	Pigmented	Saliva[b]	58 ± 5	0
H_2O	Clear	Saliva[b]	57 ± 5	0

[a] Surface tension of saliva was 53.4 dynes/cm. [b] The surfaces were stored in saliva for 48 hours and superficially washed with distilled water just prior to making the contact angle measurements.

Retention Force Measurements.—The attractive force between two parallel plates separated by a liquid film which extends to the edge of the plates and forms a zero contact angle with the plates has been expressed by Bikerman[1] in the equation

$$f = \frac{2\gamma A}{d} \qquad (1)$$

where f represents the attractive force, γ the surface tension of the liquid film, A the surface area, and d the liquid film thickness. If the liquid forms a finite contact angle with the solid, the attractive force would be reduced, presumably by a factor representing the cosine of the contact angle and, therefore, equation 1 may be modified in the manner

(1) J. J. Bikerman, "Surface Chemistry for Industrial Research," Academic Press, Inc., New York, N. Y., 1948, pp. 31-32.

$$F = \frac{2\gamma A \cos \theta}{d} \qquad (2)$$

The attractive force F should also represent the force required to separate the surfaces if the receding contact angle $\cos \theta_r$ is substituted for $\cos \theta$. These equations assume that the viscosity of the liquid is low and thus the rate of load application may be neglected.

The equipment used to measure the separating forces is shown in Fig. 1. The plastic surface to be tested was placed on one of the pans of a trip balance and a liquid film formed between the plastic and a glass plate supported above the balance pan. The glass plate was used to simulate the hydrophilic oral tissues although it was hard and unyielding compared to the tissues.

The pans of a trip balance move in such a manner that the direction of movement is nearly a straight line over small distances and thus it may be assumed that movement was a straight line from the start of the load application until rupture occurred. The glass plate was aligned parallel to the plastic surface by observing the interference fringes as indicated in Fig. 1.

The separating force was measured by the following procedure. The liquid film was formed between the parallel surfaces and a set load of 150 g. was applied to the counterbalance pan. The excess liquid was removed and water added to the loading bucket until the surfaces separated. The load obtained was found to be essentially independent of the loading rate.

The separating force F with a saliva film may be calculated from equation 2 if the film thickness d is known, since all other quantities either are known or have been determined. If the value of d is constant, and the same area A is used, then the separating forces measured for two different liquids should be a function of the surface tension and $\cos \theta_r$. The separating forces for two liquids should be such that

$$\frac{F_1}{\gamma_1 \cos \theta_1} \times \frac{\gamma_2 \cos \theta_2}{F_2} = 1 = R \qquad (3)$$

where F_1 and F_2, γ_1 and γ_2, and θ_1 and θ_2 represent the separating forces, surface tensions and contact angles, respectively, for the two systems. The entire expression has been denoted as a ratio R. Thus, if the surfaces are aligned using one liquid for which it is known that the separating force is due to capillary attraction, then the film thickness can be computed from equation 2 and a separating force predicted for some other liquid. Alternately, the separating forces can be substituted into equation 3, and the deviation of the value of R from unity used as a measure of the presence of some retention force other than the capillary attraction.

To test the accuracy of this method, the separating forces for two glass plates were measured with methanol and water as the two liquids. It should be remembered that the cross-sectional area of the film changes as the surfaces part, as does the film thickness. If one computes d from the measured force and cross-sectional area by using equation 2, the d computed is some effective film thickness which is a function of the rate of change of the film area and the degree to which the plates have been oriented. Thus, for fluids whose viscosities are similar, the measured forces should be in the ratio of equation 3 so long as the orientation of the surface is not varied from one force measurement to the next. The measured forces for methanol and water with glass plates were such that $R = 0.942$. Since it can be assumed that capillary attraction is the only force operating, this indicated a 6% error in the measurement.

The average values for R obtained with methanol or water as one liquid and saliva as the second liquid and using glass and PMMA or PS surfaces are reported in Table II. These values were within experimental error of unity, and therefore it was assumed that capillary attraction was the principal force involved in the separating force measurements.

Results and Discussion

The contact angles for distilled water and saliva on poly-(methyl methacrylate) and polystyrene are listed in Table I. In addition, the advancing and receding angles for distilled water on paraffin wax were determined as a check on the experimental

TABLE II

FORCE REQUIRED TO SEPARATE SOLIDS FROM A GLASS
SURFACE WITH AN INTERVENING SALIVA FILM AT 25°

Solid surface	R	d, μ	F_{obs}, g. force	F_{calc}, g. force	F/A at 25 μ g. force/cm.^{2}
Glass	0.925	17.3	176	162	50 ± 3
PMMA	1.056	21.7	140	148	43 ± 2
PS	1.006	25.2	117	117	45 ± 1

procedure and also are reported in Table I. The contact angles for water on paraffin wax of 109 and 99° for θ_a and θ_r, respectively, were in close agreement with the values of 110 and 99° obtained by Bartell and Shepard[2] on smooth paraffin wax surfaces.

The advancing contact angles of 78 and 76° for water on clear and pigmented (dental grade) poly-(methyl methacrylate), PMMA, were within experimental error. The receding contact angles of 50 and 51° for water on clear and pigmented PMMA also agreed and were approximately 25° less than the advancing angles. The advancing angles of 75 and 68° for human saliva on clean and saliva contaminated clear PMMA indicated that the wetting by saliva was very similar to distilled water and that the contaminated surface was more easily wetted by saliva. The receding contact angles for saliva on PMMA could not be measured since complete spreading occurred and thus the angles are denoted as zero angles. The advancing and receding angles for water on saliva contaminated PMMA were approximately the same as for saliva on the contaminated PMMA, indicating that an adsorbed film was controlling the system.

The advancing contact angles for water and saliva on clean surfaces of clear and pigmented (dental grade) polystyrene, PS, indicated that the wetting of the two liquids was very similar. The advancing angle of 86° for water on a clean surface of clear PS is somewhat lower but close to the value of 91° reported by Ellison and Zisman.[3] The receding angle for water on clear PS was approximately 20° lower and on pigmented PS was about 40° lower than the corresponding advancing contact angles. As with PMMA, the receding contact angles for saliva on PS were always zero. The advancing angles for saliva or water on saliva contaminated PS were within experimental error, having an average value of 57°. Thus, it appears that some component of the saliva such as mucin is adsorbed on the PMMA and PS surfaces and results in the receding contact angle being zero.

In general, the contact angle results showed that the wetting properties of PMMA and PS by water and saliva were similar in spite of the fact that the former has ester groups while the latter has phenyl groups extending off the main polymer chain. Since it is generally recognized that the phenyl group is more easily wetted by water than the methyl group, the similarity in wetting properties of PMMA and PS may be due to an alteration of

(2) F. E. Bartell and J. W. Shepard, THIS JOURNAL, **57**, 211 (1953).
(3) A. H. Ellison and W. A. Zisman, *ibid.*, **58**, 503 (1954).

the wetting properties of the methyl group by the attached oxygen. The moderately large hysteresis effect noted with water on PMMA and PS suggests that adsorption effects as well as frictional effects, surface heterogeneity or surface roughness are responsible for the contact angle hysteresis of 20 to 25°. The large hysteresis effect observed with saliva on PMMA and PS is of particular interest and indicates the formation of strongly adsorbed films on the plastic surfaces. The fact that the advancing angles for water on plastic surfaces having an adsorbed film of some saliva component were 57 to 65°, while the receding angles were zero is possibly due to an additional adsorbed layer inverting the nature of the film. In regard to the use of these plastics for denture base materials, it was of considerable importance that the hysteresis observed with saliva was 75 to 79° and that the receding angles for saliva on these plastics were always zero since the receding angle is the angle formed when a force tends to remove a denture base. Thus, cos θ_r has the maximum attainable value of 1 and contributes its maximum effect to the separating force F in equation 2.

The experimental separating forces F_{obs} required to separate glass, PMMA and PS from a glass surface with an intervening film of saliva are recorded in Table II. Also listed are the ratios R, the film thickness d, the calculated separating force F_{calc}, and the separating force per unit area at a corrected film thickness of 25 μ. The film thickness d was determined by using methanol and water as liquids and substituting into equation 2 the experimental separating forces and the receding contact angles for the liquids against the solid. The values of the film thicknesses obtained were between 17 and 25 μ which are within the experimental error. The fact that approximately the same film thickness was obtained with different liquids and solids indicates that surface irregularities of the various types of surfaces were similar or alignment conditions were consistent.

The values for the ratio R shown in equation 3 were calculated using water or methanol as fluid 1 and saliva as fluid 2. The values obtained for R were within experimental error of unity and the observed separating forces were in close agreement with the corresponding separating forces calculated from equation 2. The separating force per unit area for the system glass–saliva–glass was little different from the values for the systems glass–saliva–PMMA and glass–saliva–PS. As would be expected from the similarity of the wetting properties of PMMA and PS, no difference was observed in the separating force per unit area for these two plastics.

These results show that capillary forces are the main physical forces involved in the separation of parallel plates with an intervening liquid film. The separating force measurements also substantiate the use of equation 2 for liquids forming a finite contact with the solid surface.

THE RHEOLOGICAL PROPERTIES OF FILMS AT CRUDE PETROLEUM–WATER INTERFACES

By Charles G. Dodd

The Pure Oil Company and University of Oklahoma, Norman, Oklahoma

Received November 11, 1959

The rheological properties of films at liquid surfaces (gas–liquid interfaces) have been investigated by numerous workers, but little work has been done on films at crude petroleum–water interfaces or other oil–water interfaces. Elastic properties of films at oil–water interfaces have been measured by oscillating disk viscometers, but rotating cylinder viscometers designed for measuring general rheological properties, including time-dependent properties, of interfacial films have not been described in the literature. This paper describes the development and use of an interfacial film viscometer designed especially for rheological investigations at oil–water interfaces. Critical design factors pertinent to interfacial film work are summarized. The viscometer has been used to study diffusion-controlled reactions at crude oil–water interfaces and the nonequilibrium, time-dependent rheological properties acquired by films as a result of such interactions. Control of aqueous substrate composition and pre-treatment of oil samples permit some interpretations of film structure and of interaction mechanisms. The most significant rheological properties of crude petroleum–water interfacial films appear to be the pseudo-thixotropic phenomena which depend upon time elapsed after formation of the interface. Evidence is presented which indicates the film structures involve free naphthenic acids, acid anions and their salts. Geochemical implications of the data are discussed.

The first measurements of surface viscosity apparently were made by Wilson and Ries,[1] who employed a torsional or oscillating disk type of surface viscometer. Subsequent workers using similar instruments have studied the plasticity of films at air–water interfaces in more detail.[2-4] Other investigators have employed slit and canal viscometers to study insoluble monolayers.[5-7] Neither the oscillating disk nor the slit type of surface viscometer permits the attainment of controlled rates of shear, held constant during measurements, which are necessary for the characterization of thixotropic, viscoelastic, and other time-dependent rheological properties. The oscillating disk method detects departures from Newtonian rheological behavior only in a qualitative manner. The slit or canal viscometers, two-dimensional analogs of capillary instruments, permit the rate of shear to be calculated only at the wall and suffer from a varying rate of shear across the slit unless the material undergoing test is in the "plug flow" regime.

The Couette–Hatschek- or Searle-type of rotational viscometer is the preferred surface viscometer for the study of time-dependent rheological properties. The first such rotational surface viscometer appears to have been described by Van Wazer.[8] An improved instrument was designed by Brown, Thuman and McBain.[9] The interfacial film viscometer used in the work described herein was patterned after the latter instrument. Appropriate modifications were made to adapt the instrument for measurements at the oil–water interface.

The colloidal nature of crude petroleum has long been a subject of discussion and speculation. Various exploratory investigations have been concerned with dispersed material in petroleum, the films that form at crude oil–water interfaces, the interfacially active constituents in petroleum, and the ability of petroleum to alter the preferential wettability of reservoir rock. Each of the workers in this field has been concerned with but a few aspects of the over-all problem. Bartell and Niederhauser[10] and Denekas, Carlson, Moore and Dodd[11] were interested in the formation of films at oil–water interfaces, the isolation and identification of the film material, and the significance of this material with respect to its role in petroleum production, especially in flooding with water. In addition to devising a novel method of isolating the oil–water interfacial film substance, Bartell and Niederhauser followed the removal of the film-forming constituents from petroleum by measuring interfacial tensions of oil–water systems before and after extraction of the film-forming constituents. They used the pendent drop interfacial tension instrument for this purpose and for relatively crude, semi-quantitative observations of interfacial film strength. Denekas, et al.,[11] used the same techniques. Dodd, Moore and Denekas[12] showed that the interfacial films contained trace metals in amounts considerably concentrated relative to those in the original crude oil. Ray, Witherspoon and Grim[13] demonstrated, by use of an ultracentrifuge, that some Illinois Basin crude oils actually did contain colloidally dispersed materials. Witherspoon[14] has reviewed the current status of this field.

The first significant study of the mechanical properties of petroleum–water interfacial films was

(1) R. E. Wilson and E. D. Ries, "Surface Films as Plastic Solids," Colloid Symposium Monograph, University of Wisconsin Press, Madison, Wisc., 1923, p. 145–173.

(2) I. Langmuir and V. J. Schaefer, *J. Am. Chem. Soc.*, **59**, 2400 (1937).

(3) E. J. Burcik and R. C. Newman, *J. Colloid Sci.*, **12**, 10 (1957).

(4) D. W. Criddle and A. L. Meader, Jr., *J. Appl. Phys.*, **26**, 838 (1955).

(5) W. D. Harkins and J. G. Kirkwood, *J. Chem. Phys.*, **6**, 53 (1938).

(6) L. Fourt and W. D. Harkins, This Journal, **42**, 897 (1938).

(7) G. C. Nutting and W. D. Harkins, *J. Am. Chem. Soc.*, **62**, 3155 (1940).

(8) J. R. Van Wazer, *J. Colloid Sci.*, **2**, 223 (1947).

(9) A. G. Brown, W. C. Thuman and J. W. McBain, *ibid.*, **8**, 491 (1953).

(10) F. E. Bartell and D. O. Niederhauser, "Film Forming Constituents of Crude Petroleum Oils," Fundamental Research on Occurrence and Recovery of Petroleum, 1946–1947, Am. Petroleum Inst., New York, p. 57–80, 1949.

(11) M. O. Denekas, F. T. Carlson, J. W. Moore and C. G. Dodd, *Ind. Eng. Chem.*, **43**, 1165 (1951).

(12) C. G. Dodd, J. W. Moore and M. O. Denekas, *ibid.*, **44**, 2585 (1952).

(13) B. R. Ray, P. A. Witherspoon and R. E. Grim, This Journal, **61**, 1296 (1957).

(14) P. A. Witherspoon, "Studies on Petroleum with the Ultracentrifuge," Report of Investigations 206, Illinois State Geol. Survey, Urbana, Ill., 1958.

that of Lawrence and Killner[15] who were interested in fuel oil demulsification problems. They measured elastic properties of the films and found effective viscosities many orders of magnitude larger than the bulk viscosities of either water or crude petroleum, but they did not measure rheological properties of the films effectively. The instrument used in their investigations was of the oscillating disk type with which they could measure only bulk elastic properties of the interfacial phase. Sears[16] also used an oscillating disk viscometer to make an exploratory study of the transition temperatures of crude oil–water interfacial films and the effect of "aging" on the elastic properties of the films. Sears speculated that the interfacial films might have a structure such as that postulated for the sodium soap solution films described by Burcik, Sears and Tillotson,[17] and by Burcik and Newman.[3]

In this paper we wish, first, to examine the requirements for rotational viscometers designed for interfacial rheology; second, to present results of experimental measurements; and, third, to interpret the data from a geochemical point of view.

Experimental

Crude Oil–Water Rotational Viscometer.—A commercially available MacMichael rotational viscometer, used in the paint, varnish and other related industries, was converted to an interfacial film viscometer following the general features of the design suggested by Brown, Thuman and McBain.[9] Their instrument, an adaptation of the Couette–Hatchek-type of rotational viscometer, consisted essentially of an inverted cylinder-type of bob suspended on a torsion wire. The tapered edge of the bob dipped through the surface of the liquid sample held in a dish mounted on a rotating pan on the base of the instrument. As the pan was rotated at a constant rate, the shearing stress was indicated by the angular deflection of the inner, suspended bob.

The following factors were found to be essential for the development of an instrument applicable to studies of petroleum–water interfacial films.

1. The rotational speed of the outer turntable must be adjustable continuously and smoothly over a range from about 0.1 r.p.m. to about 50 r.p.m., and the rate of rotation must remain constant once it is set. This requires that the motor and gear train or other driving and speed control mechanism must operate without vibration and substantially without backlash.

2. The axes of rotation of the sample vessel and of the bob suspended on the torsion wire must be co-axial. Provision must be made for lowering the bob to a predetermined and reproducible depth of submersion through the upper oil phase, interfacial film, and lower aqueous phase. This setting must be reproduced easily for each measurement.

3. The lower edge of the cylindrical viscometer bob must be tapered sharply to minimize end effects in the lower phase.

4. The bob must be constructed of a material which will be wet by the two bulk liquids under test. Clean brass is suitable, for example, unfinished or coated with a baked lacquer, but plastics having extremely low surface energies, such as Teflon and other fluorocarbon plastics, should not be used. The contact angle with which the upper phase wets the bob should, preferably, be less than 90 degrees.

5. The moment of inertia of the bob and the torsion wire constant should be optimized for application of the apparatus to crude oil–water interfacial films. Brady and Brown[18] recommend that the moment of inertia of the bob be
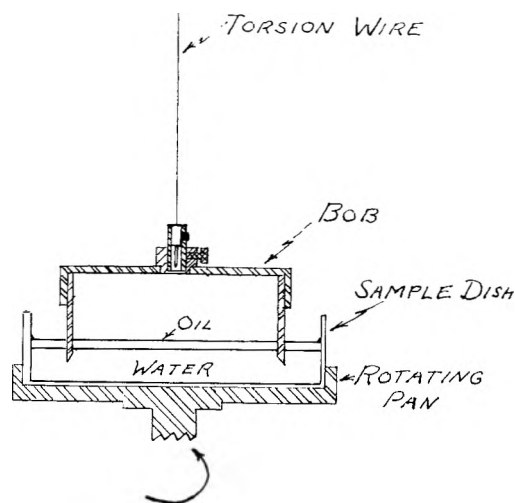
Fig. 1.—Interfacial viscometer.
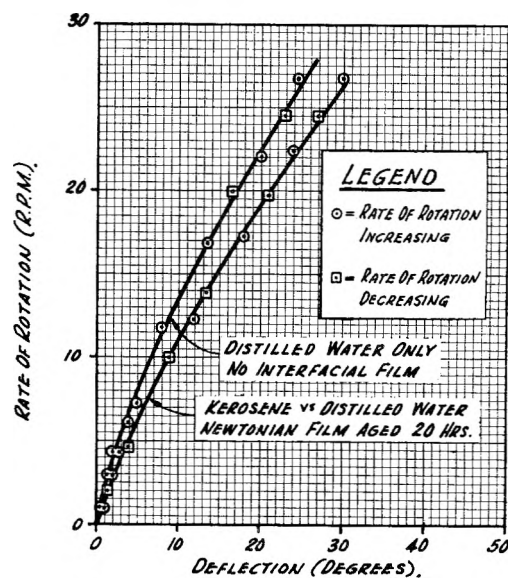
Fig. 2.—Calibrations with Newtonian liquids.
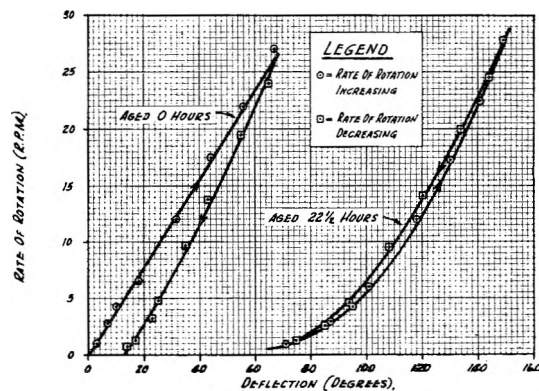
Fig. 3.—Cypress crude vs. distilled water.

adjusted to provide for slight under-damping, and that the suspension wire be selected to provide sufficient sensitivity for the materials under study. Too great a sensitivity leads to difficulties in bringing the bob to a reproducible point of measurement. A 34-gauge wire was used for this work.

(15) A. S. C. Lawrence and W. Killner, *J. Inst. Petr.*, **34**, 821 (1948).

(16) J. R. Sears, "A Fundamental Investigation of Surface Viscosity and Surface Plasticity," M. Petr. Engr. Thesis, Univ. of Oklahoma, Norman, Okla., 1952.

(17) E. J. Burcik, J. R. Sears and A. Tillotson, *J. Colloid Sci.*, **9**, 281 (1954).

(18) A. P. Brady and A. G. Brown, "Mechanical Properties of the Surface Films on Aqueous Solutions of Detergents," Monomolecular Layers, H. Sobotka, Ed., Am. Assoc. Adv. Sci., Washington, D. C., p. 33–62, esp. p. 55, 1954.
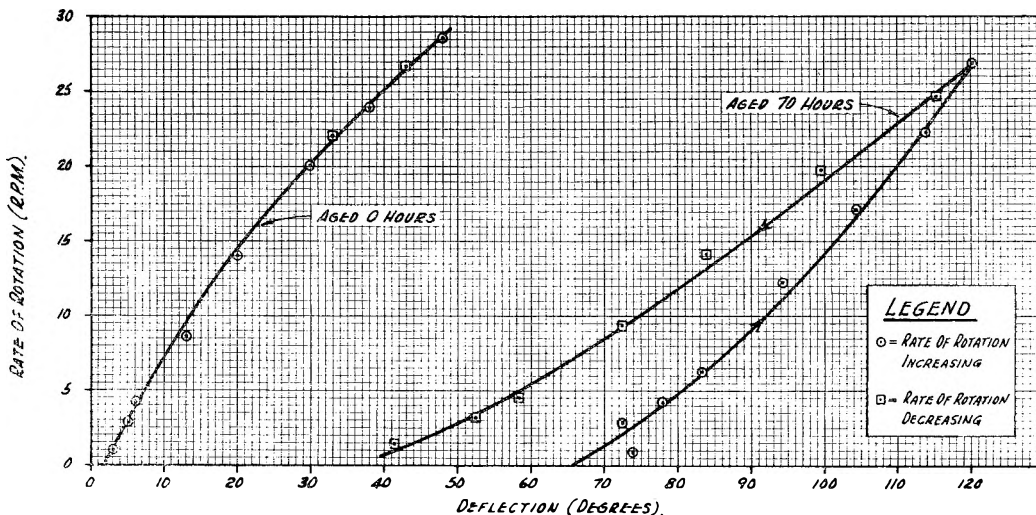
Fig. 4.—Cypress crude *vs.* 2% NaCl solution.
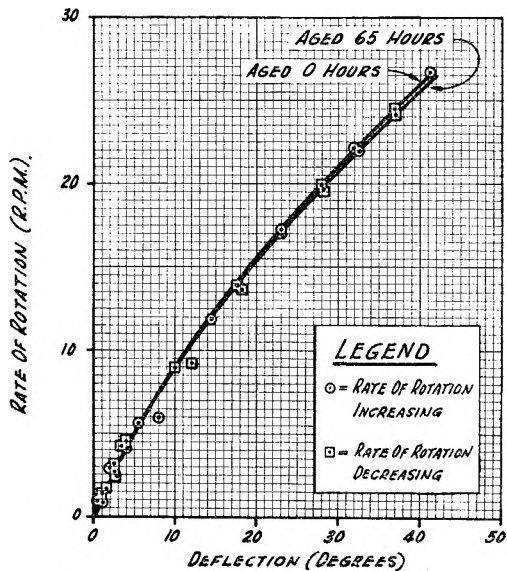
Fig. 5.—Cypress crude *vs.* 1% NaOH solution.
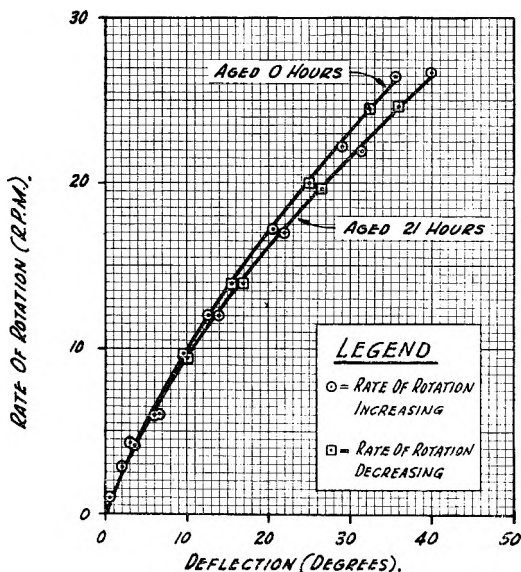
Fig. 6.—Cypress crude *vs.* 2% NaCl + 0.01% NaOH solution.

In the application of this instrument it was found necessary to mount it on a vibration-free base and to protect it from air currents in a suitable cabinet. Temperature control was found to be necessary for reproducibility and for observations of transition temperatures. The most satisfactory type of temperature control is that described by Brown, Thuman and McBain[9] which utilized a hollow-walled cabinet through which thermostated water was allowed to flow from a constant-temperature reservoir.

Experimental Procedures.—In making a measurement with the viscometer, glass dishes, similar to Petri dishes, were filled uniformly with 50 ml. of the aqueous phase followed by a covering of 10 ml. of the oil under study. The sample in the dish then was set aside for the desired period of aging before measurement or, in the case of the 0-hour measurements, was placed immediately in the outer rotatable pan of the viscometer. The clean viscometer bob then was lowered to the predetermined depth of submersion through the oil and interfacial film and into the lower aqueous phase, a total of 5 mm. in most runs. After the viscometer bob had come to rest, the angular rest position was recorded and, if all materials had previously been brought to the desired temperature of the measurement, rotation was started at a slow rate, usually a little less than 1 r.p.m. A reading of the angular deflection of the bob was taken as soon as it was steady, and the rate of rotation of the outer dish immediately was increased to determine the next point on the curve. A typical run consisted of about eight points measured at successively increasing rates of rotation starting at a little less than one and going up to 25 or 30 r.p.m., preferably in uniform increments, followed immediately by six to eight measurements at successively decreasing rates of rotation, ending at approximately one r.p.m. This procedure permitted one to obtain reproducible curves readily interpretable with respect to characterization of time-dependent rheological properties of the interfacial film. Absolute values of Newtonian, apparent, or plastic viscosities, Bingham yield values, or bulk interfacial phase elastic moduli cannot be determined directly by this procedure. It was convenient, however, to compare the curves with those obtained when 60 ml. of a Newtonian liquid, or 50 ml. of water and 10 ml. of a hydrocarbon oil, were in the cup. A subtraction of the viscometer bob deflection due to Newtonian liquids having the same bulk viscosities from corresponding data obtained with film-forming oil–water pairs permitted approximate film flow curves to be plotted but these difference curves are not presented in this paper.

The procedure of continuously increasing rates of rotation was found necessary because it was difficult to reproduce the rest point deflection when the instrument was stopped after each reading. Apparently, this difficulty was due to the time-dependent film properties and, possibly, the imperfect elasticity of the torsion wire.

A schematic drawing of the instrument is shown in Fig. 1.

Materials.—Experimental work was done on two fresh crude oil and water samples obtained from Southern Illinois Fields. One sample was from the Veit No. 8 well in
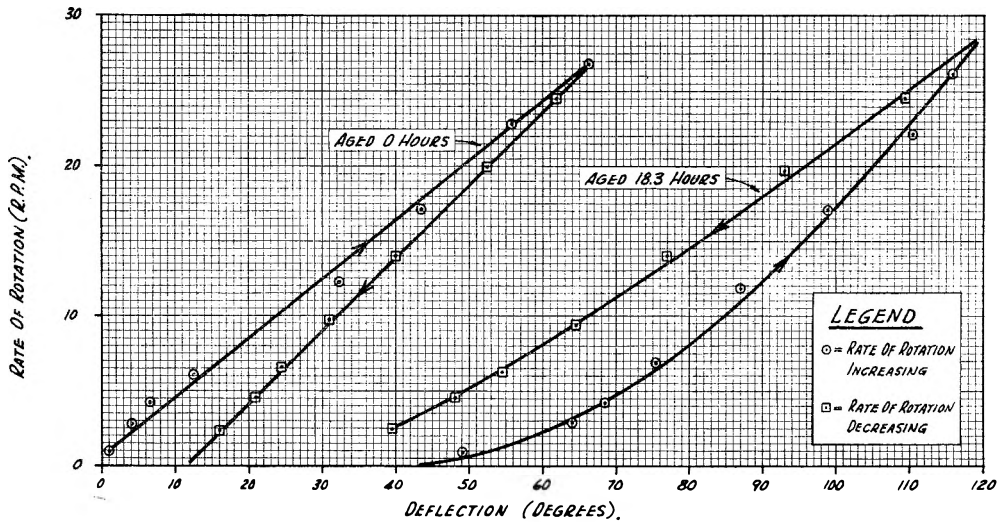
Fig. 7.—Cypress crude *vs.* 2% NaCl + 0.001% NaOH solution.

the Noble district producing from the Cypress formation. The other was obtained from J. O. Coen No. 43 well in the Noble district producing from the McClosky formation.

Results of Rheological Measurements

Significant differences were found in the rheological behavior of the crude oil–water interfacial films studied with respect to the type of water that was used in the viscometer with a given crude oil and as a function of the time that the film was permitted to age before measurements were started. The important time-dependent rheological characteristics of these curves appear to be the thixotropic properties as indicated by the degree of hysteresis, that is, non-reproducibility of the data at increasing and decreasing rates of shear. If other factors are held constant, the degree of thixotropy in a system is indicated by the area of the hysteresis loop.[19,20]

Newtonian Curves.—Some of the films studied were essentially Newtonian. Whenever curves representing Newtonian behavior were obtained it was assumed that the rigidity of any film formed at the oil–water interface was negligible and the rheological properties of the oil–water system were essentially those of the bulk liquid phases.

A calibration curve (shown in Fig. 2) was obtained using a volume of water equal in volume to the combined volume of water and crude oil used normally in the viscometer dish. This gave an indication of the type of curve to be expected for a Newtonian liquid of approximately one centipoise viscosity. When 50 ml. of water was covered by 10 ml. of kerosine, essentially the same curve was obtained, as shown in Fig. 2 also. Similar curves, representing Newtonian behavior and essentially no film strength, were measured on films of some of the crude oil–water systems under study.

It is true that the rheological diagram for a Newtonian liquid should be represented by a straight line intersecting the origin of the diagram. The calibration curves referred to in the last paragraph have a slight curvature convex to the rate-of-shear axis. The curvature is believed to be caused by an

(19) R. N. Weltman, *J. Soc. Cosmetic Chemists*, **7**, 599 (1956).
(20) H. Green and R. N. Weltman, *Colloid Chem.*, **6**, 328 (1946).
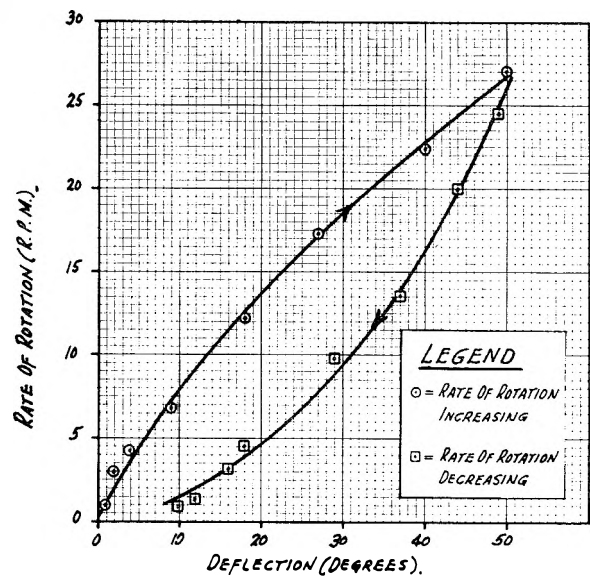
Fig. 8.—Cypress crude *vs.* formation water; aged 0 hours
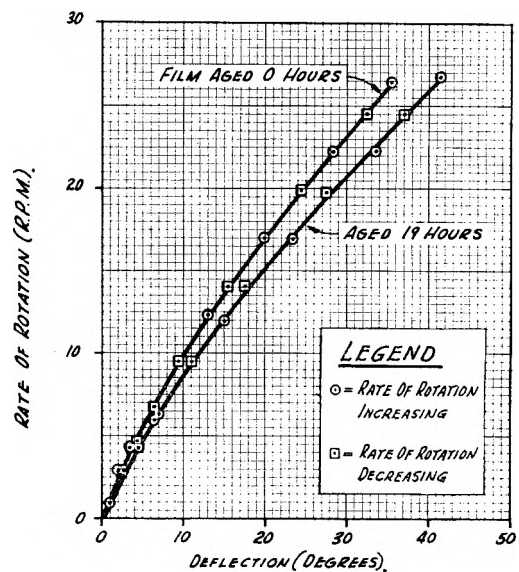
Fig. 9.—Cypress crude *vs.* 2% NaCl + 0.1% Igepal CO-630 Newtonian film.
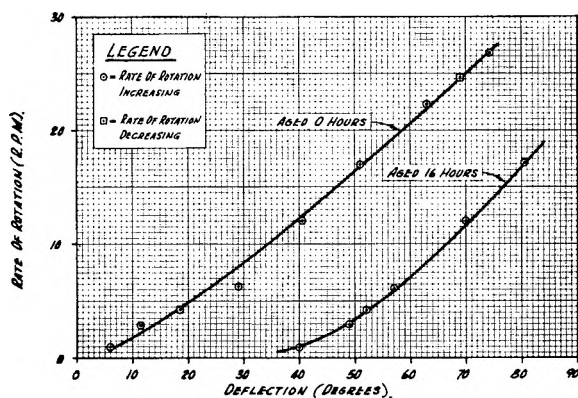
Fig. 10.—Cypress crude washed with 10% NaOH solution and distilled water vs. distilled water.

not to determine absolute rheological properties with the instrument. The important information sought was the relative shapes of the curves, degrees of hysteresis, and relative amounts of deflection at varying rates of shear. As long as the instrumental constants were the same for different runs, their rheological diagrams could be compared. If thicknesses of the interfacial films were known, it would have been possible to calculate the elastic constants of these essentially bulk film phases, using the calibration curves to obtain instrumental constants. The important point that should be recognized at this stage is that one can differentiate clearly between the rheological behavior of a Newtonian liquid in the sample dish and essentially the same system with a more or less rigid interfacial film at the oil–water interface. The fact that sig-

Fig. 11.—Cypress crude washed with (1) methanol containing 3% NH$_4$OH and (2) distilled water vs. 2% NaCl solution.
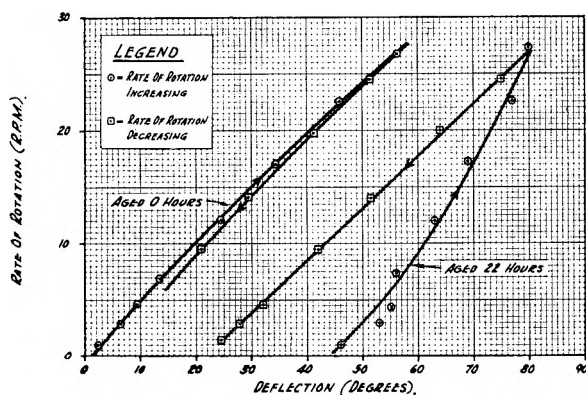
Fig. 12.—McClosky crude vs. distilled water.

artifact resulting in part from the measurement procedure referred to above, but largely to imperfect centering of the bob in the sample dish. Suspended on the torsion wire, the bob was free to oscillate about its axis; furthermore, the glass dishes used were not precisely circular. At higher rates of rotation the bob was more nearly centered. All of the rheological curves obtained with crude oil–water systems might have been corrected to a degree sufficient to straighten out the calibration curves measured with Newtonian liquids. The corrections were not made because the object was

nificant differences can be recognized on the curves indicates that these crude oil–water interfacial films have unusually high rigidities, as reported by Lawrence and Killner.[15]

Crude Oil–Water Interfacial Films.—Many of the crude oil–water interfacial films studied were non-Newtonian, and most were time-dependent. Most were found to have effective viscosities many times that of water. The effective viscosity of a non-Newtonian liquid or dispersion at a given rate of shear is proportional to the slope of the line drawn from the origin of the rheological diagram to the point on the curve measured at the desired rate of shear. The effective viscosity of such a system was found to be a transient quantity dependent, among other factors, upon the past history of the particular sample.

The crude oil–water films were strong enough to make the use of more delicate surface (air–water) viscometers, such as the instrument used by Brady, Thuman and McBain,[9] entirely unnecessary and useless in this work. A relatively insensitive instrument is required compared to the instruments designed to measure surface viscosities on aqu ous detergent solutions.

The rheological diagrams obtained with two Illinois basin crude oils are shown in Figs. 3–15 inclusive. Examination of the curves discloses a

wide variety of rheological behavior encountered in the various interfacial films. Some of the systems demonstrate relatively simple Newtonian behavior, but many of the interfacial films show definite non-Newtonian properties and most of these demonstrate irreversible time-dependent phenomena. The extent of irreversibility, and, presumably, the degree of thixotropy or pseudothixotropy, is essentially proportional to the size of the hysteresis loop.

Another characteristic of these data is illustrated by the difference between the curve obtained with distilled water against Cypress crude and that against McClosky crude. Compare Fig. 3 and 12. Most systems, however, were Newtonian when the pH of the water phase was high; see Fig. 5, 6, 7 and 14.

The power of sodium hydroxide solutions, of high pH, to eliminate or minimize non-Newtonian properties of the films was investigated further by extracting one sample of the Cypress crude oil with a 10% sodium hydroxide solution and another sample with a 3% ammonium hydroxide solution in methanol. The rheological curves obtained with the extracted Cypress crude samples against distilled water are shown in Fig. 10 and should be compared with Fig. 3. These data indicate that some but not all of the film-forming materials in the Cypress crude oil was extracted by the alkaline solutions. More of the film-forming substance, however, was extracted by the sodium hydroxide solution than by ammonium hydroxide in methanol.

Figures 6 and 7 show the effect of various concentrations of sodium hydroxide plus 2% salt in the aqueous phase against Cypress crude oil. At a concentration of 0.01% NaOH the film demonstrated Newtonian behavior whereas non-Newtonian time-dependent thixotropic properties were observed with 0.001% NaOH.

Figures 9 and 15 show the results obtained with aqueous substrates containing 2% salt plus various non-ionic surfactants of the type used as detergent additives for water flooding. All of the rheology curves, both 0-hour and aged curves, are Newtonian. The curves for the various surfactants almost coincide.

Figure 8 is of particular interest because it indicates 0-hour thixotropic behavior with the Cypress crude oil against its own formation water. Some crude oils studied later did not demonstrate thixotropic behavior against their own formation water, while others resembled the Cypress system.

Discussion

For the first time it has been possible to measure the thixotropic, or pseudo-thixotropic, and other rheological properties of interfacial films in a semiquantitative manner. The rheological diagrams obtained appear to be the best means known at this time of characterizing time-dependent rheological properties of these colloidal systems. The results obtained tie in nicely with the data of earlier workers, cited above, which showed that crude petroleum contains colloidally dispersed materials and that these materials are concentrated at oil–water interfaces to form more or less rigid interfacial films. Dunning, Moore and
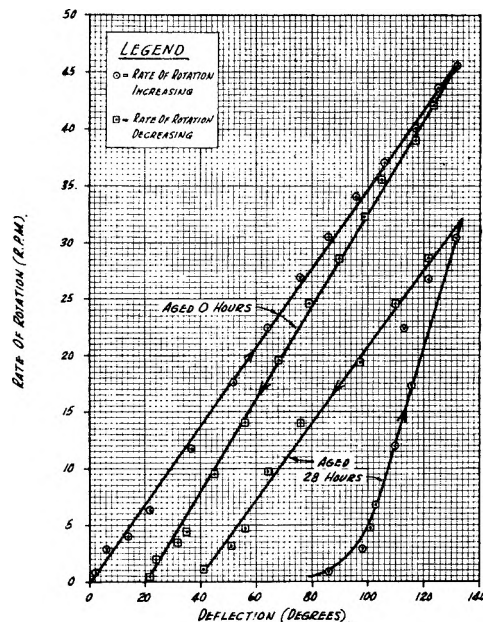
Fig. 13.—McClosky crude vs. 2% NaCl solution.
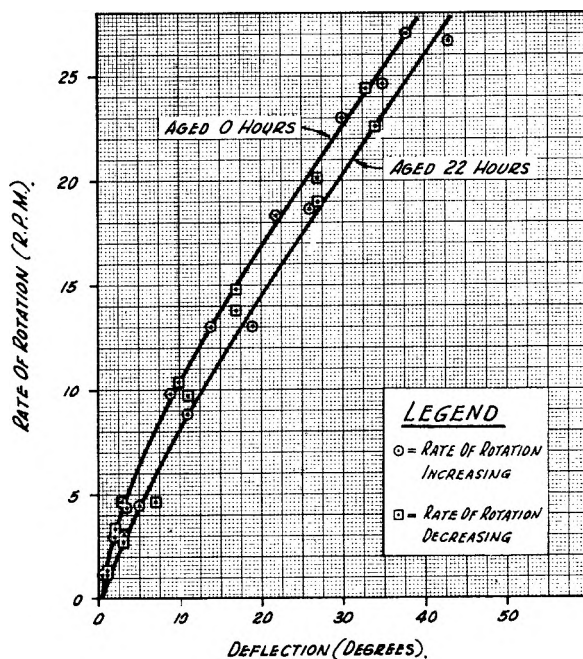
Fig. 14.—McClosky crude vs. 2% NaCl + 1% NaOH solution.

Denekas[21] believed that most crude oil–water interfacially active films having low interfacial tensions contained relatively large amounts of porphyrins. Dodd, Moore and Denekas[12] found that films which were less interfacially active often were stronger or more rigid films. The degree of interfacial activity was measured by the decrease in interfacial tension as determined by an instrument such as the pendent drop tensiometer. If a rigid interfacial film that constitutes essentially a third phase, separating oil and water, is formed at the interface, the basis for the calculation of interfacial tension by the pendent drop or any other classical

(21) H. N. Dunning, J. W. Moore and M. O. Denekas, Ind. Eng. Chem., 45, 1759 (1953).
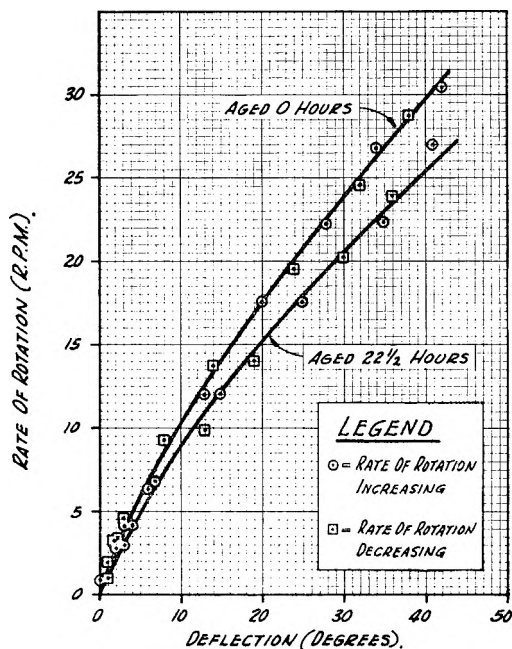
Fig. 15.—McClosky crude *vs.* 2% NaCl + 0.01% Igepal CO-630 solution.

method is invalidated. Thus these earlier estimates of interfacial activity may be of limited validity. Dodd, Moore and Denekas found that vanadium was present in greater concentrations in the films that showed the greatest mechanical rigidity and the least interfacial activity whereas other trace metals such as nickel, copper and zinc were present in greater quantities in the films demonstrating a higher degree of interfacial activity. More recently Radchenko and Sheshina[22] showed that crude oils containing large amounts of vanadium also invariably contained large amounts of sulfur and asphaltic materials whereas the oils containing a predominance of nickel were more paraffinic in nature and contained relatively small amounts of asphaltic material.

The work reported herein indicates that the rigid interfacial films probably contain materials such as naphthenic acids. It is assumed that the acidic substances occur in combination with resins and various sulfur-bearing asphaltic substances, such as are present in the asphaltene fractions of petroleum, and, frequently, high molecular weight hydrocarbons of a waxy nature. In combination with naturally occurring connate waters, which contain salts, the naphthenic acids form soaps which hydrolyze to varying degrees depending on the salt content and *p*H of the water. Hydrolysis of naphthenic acid soaps would form a complex including free acids, soaps and acid anion, and such a complex probably forms the backbone of the interfacial film structure in a manner analogous to the fatty acid soap films observed by Burcik and Newman.[3] In the present work no effort was made to explore in more detail the nature of the naphthenic acid groups nor the molecular structure of the films.

The evidence found for the presence of naphthenic acids in interfacial film supports the con-

cepts of Baker[23] relative to the migration of petroleum by solubilization in water. Baker assumed the existence of naturally occurring naphthenic acid soaps in crude oils. He assumed the soaps solubilized hydrocarbons in water and could account for the transportation of relatively large quantities of hydrocarbons in water in comparison with the low solubilities of hydrocarbons in water. It is likely that naphthenic acids participate in the colloidal structure of crude petroleum as suggested by Witherspoon,[14] but this supposition might prove difficult to establish experimentally. Baker did present a good argument, however, for the solubilization of hydrocarbons in water by naphthenic acid soaps. He showed experimentally that synthetic soaps such as sodium laurate solubilize hydrocarbons in large quantities relative to their solubilities in water. What is more significant, he showed that the relative amounts of different hydrocarbons solubilized by sodium laurate corresponded to the relative amounts of these same hydrocarbons found in crude petroleum.

The concept of a complex interfacial film made up from free naphthenic acids, naphthenic acid soaps and naphthenic acid anions, in combination with resins, waxes and asphaltenes is in harmony with modern theories of emulsion stability and surface film viscosity. Schulman and Cockbain,[24] for example, have proposed that many emulsion systems are stabilized by closely packed, rigid interfacial films made up of a condensed complex of two or more emulsifying agents.

The packing of molecules in the films observed in the present work is thought to depend on steric factors in addition to hydrogen bonding and van der Waals bonding. The process of crude oil–water interfacial film formation probably involves steps similar to those involved in the dimerization of fatty acids, which process depends on hydrogen bonding. The extent of hydrolysis and film formation, and hence the strength of the interfacial films, was found to be dependent upon both acidity and the ionic atmosphere in the aqueous phase.

The fact that the pseudo-thixotropic properties of crude oil–water interfacial films appear to be time sensitive, and that they demonstrate different degrees of time sensitivity with different crude oil–water systems, may indicate that the naphthenic acids are of varying molecular or particle weights, resulting in varying rates of diffusion to the interface. The observed time sensitivity probably depends, also, on an orientation process at the interface. Both of these proposed steps are irreversible rate processes requiring an activation energy and, thus, they would be temperature dependent; hence, the occurrence of transition temperatures. After a given complexity of film structure were attained, the film would be disrupted irreversibly, to an increasing extent, as rates of shear were increased in the viscometer cup.

(22) O. A. Radchenko and L. S. Sheshina, *Doklady Akad. Nauk S.S.S.R.*, **105**, 1285 (1955) (Assoc. Tech. Services Translation No. RJ-480).

(23) E. G. Baker, *Science*, **129**, 871 (1959). Also see "Crude Oil Composition and Hydrocarbon Solubility," paper presented as part of a symposium on Chemical Aspects of the Origin, Migration, and Accumulation of Oil, Amer. Chem. Soc. Meeting, Chicago, Sept. 7–12, 1959 (Paper preprinted by Div. of Petroleum Chemistry).

(24) J. H. Schulman and E. G. Cockbain, *Trans. Faraday Soc.*, **36**, 651 (1940).

EFFECT OF WETTABILITY ON THE ELECTRICAL RESISTIVITY OF CARBONATE ROCK FROM A PETROLEUM RESERVOIR

BY S. A. SWEENEY AND H. Y. JENNINGS, JR.

California Research Corporation, La Habra, California

Resistivity measurements were made on porous carbonate rock which contained varying amounts of electrolyte and aliphatic hydrocarbon. The porous rock was treated so as to make the carbonate surface preferentially water-wet and then preferentially oil-wet. Resistivity data on preferentially water-wet samples were considerably different from the data on preferentially oil-wet samples. The results are discussed in terms of the effect of changes in wettability on porosity and water saturation values derived from electric well logs.

Introduction

Accurate information concerning the porosity and water saturation of subsurface porous rock formations is of importance to those engaged in the exploration and production of gas and oil. Porosity and water saturation of oil-bearing formations are estimated from the interpretation of electric well logs. To aid in the interpretation of electric logs resistivity measurements are made in the laboratory on rock samples taken from the formation of interest. From the measurements the ratio of the resistance of a water-saturated rock to the resistance of the water with which it is filled is obtained. The ratio, commonly called Formation Factor, can be expressed as: $F = R_o/R_w$. The ratio of the resistance of a rock containing water and oil or gas, R_t, to the resistance of the same rock 100% saturation with water is also obtained. This ratio, commonly called Resistivity Index, I, can be expressed as $I = R_t/R_o$.

Early advances in the quantitative interpretation of electric logs were made by Archie.[1] Archie concluded that a study of the resistivity of formations when all the pores are filled with water was of basic importance in the detection of oil and gas by the use of an electric log. Archie, and Wyckoff and Botset,[2] among others, also studied the variation in the resistivity of sands due to the percentage of water contained in the pores. The study was done by displacing varying amounts of conducting water from the pores with non-conducting fluids such as gas or oil. These early investigators considered the effect of distribution of water and oil on the resistivity values but their results did not show distribution to be a significant factor. More recent investigators including Keller[3] and Moore[4] have shown that the resistivity measurements made on sandstones were a function of the manner in which the water was distributed. The changes in distribution were caused by changing the wettability of the sandstone surface.

The purpose of the study reported in this paper was to determine how changes in wettability affect the resistivity of porous carbonate rocks. Although carbonate rock reservoirs account for more than half of the world's oil production the study was delayed because of the difficulty with which carbonate surfaces are made preferentially oil-wet in the laboratory. We recently developed a treatment for making carbonate surfaces strongly oil-wet based upon contact angle work published by Benner and Bartell.[5] With this treatment it was possible to carry out the proposed study.

Experimental

Materials.—Twenty-five one-inch diameter carbonate core plugs 3 inches long were selected which covered a range of porosity from 11.8 to 31.5%. The samples varied widely in texture but consisted for the most part of clastic carbonate fragments of sand size or larger. Cementation varied from poor to strong and dolomitization ranged from 10 to 75%.

The electrolyte solution was the same composition as that associated with the carbonate rock in the reservoir. It contained 182 g. of $NaCl$, 30 g. of $CaCl_2$ and 14 g. of $MgCl_2$ per liter and had an electrical resistivity of 0.053 ohm-meters at 23.5°. The oil was kerosene, boiling point range 179–252°, which had been purified by the method described by Craig, *et al.*,[6] for toluene.

Measurement of Electrical Resistivity. Apparatus.—The electrical resistance of the cores was measured by a two electrode method.[3,7] In the past the two electrode method had one major disadvantage, polarization. Polarization at current carrying metal electrodes produces both "contact resistance" and "contact capacitance." The amount of polarization at the current carrying electrodes depends upon the electrolyte in contact with electrode, the electrode metal and the current frequency. It was found that by using gold-plated or Monel-metal electrodes and a 1000-cycle current the contact resistance became negligible. The contact capacitance was compensated for in the measurement of resistivity.

The power source imposes a 1000-cycle signal directly on the horizontal deflection plates of the oscilloscope. The power source also imposes, through an isolating transformer, a 1000-cycle signal on the Wheatstone bridge. The legs of the bridge comprise two 1000-ohm resistors, the core electrode assembly and a combination variable resistor and capacitor. When the variable resistance and capacitance match the resistance and capacitance of the core-electrode assembly, no signal is impressed on the vertical deflection plates of the oscilloscope. When the magnitude of the admittance of the variable capacitor is small compared to that of the variable resistance, no significant error in resistance is involved in balancing a series capacitor–resistor combination in the core against a parallel arrangement in the reference.

Procedure.—The core plugs were refluxed in toluene for 24 hours or until fresh toluene no longer became discolored. After refluxing, the cores were dried in a vacuum oven and then were leached with distilled water to remove residual salt. The leached samples were saturated 100% with 0.053 ohm-meter water and placed between the electrodes for resistance measurement.

The remainder of the resistivity data were obtained at

(1) G. E. Archie, *Am. Inst. Mining Met. Engrs., Petroleum Division, Trans.,* **146**, 54 (1942).

(2) R. D. Wyckoff and H. G. Botset, *J. Applied Phys.,* **7**, 325 (1936).

(3) G. B. Keller, *Oil and Gas J.,* **51**, 63, Jan. 5 (1953).

(4) J. C. Moore, *Producers Monthly,* **22**, 30, March (1958).

(5) F. C. Benner and F. E. Bartell, "The Effect of Polar Impurities upon Capillary and Surface Phenomena in Petroleum Production," API Drilling and Production Practice, 1941, p. 341.

(6) R. G. Craig, J. J. Van Voorhis and F. E. Bartell, THIS JOURNAL, **60**, 1225 (1956).

(7) P. B. Lorenz, *ibid.,* **57**, 430 (1953).
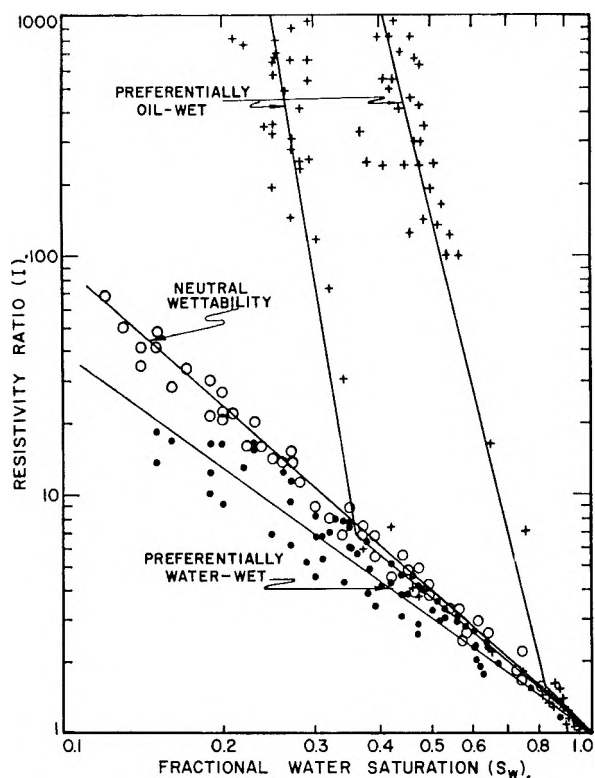
Fig. 1.—Summary of resistivity ratio data.

saturations other than 100%. The cores were placed in capillary pressure cells which have capillary diaphragms attached to Monel plates for electrical contact. The capillary diaphragms were porous plates having pores about 1 micron in diameter. When a preferentially water-wet diaphragm is completely saturated with water, oil cannot enter the pores of the diaphragm unless the applied pressure is great enough to overcome the entry pressure of the porous diaphragm. At pressures less than the entry pressure, water will flow through the diaphragm and preferentially exclude the non-wetting fluid, oil.

In the experiments reported here, a 100% water saturated core was placed in contact with a preferentially water-wet diaphragm. Capillary contact was achieved between the core and the diaphragm with a diatomaceous earth–water mixture. The core was completely surrounded by oil and pressure was applied to the oil. Water displaced from the core passed through the diaphragm into a receiver where its volume was measured.

Cores contain pores of various sizes. Each of these pores will permit oil to enter at its characteristic capillary entry pressure. This pressure depends upon the pore radius, interfacial tension and the wetting properties of the solid matrix. As oil enters a pore, water is displaced and the water saturation decreases. The cores are allowed to stand at several predetermined capillary pressures until water production has stopped. The electrical resistance then is measured. The maximum capillary pressure reached in these tests was 20 p.s.i.

Changes of Wettability.—Water–oil imbibition tests were performed by saturating the core 100% with one phase and then completely immersing the core in the other phase. Displaced fluid was measured in a calibrated buret at regular time intervals. When neither water or oil was displaced, the core was said to have neutral wettability. For preferentially water-wet cores only oil was displaced and for preferentially oil-wet cores only water was displaced.

Measurements on more than a hundred toluene extracted limestone cores of the type used in this study showed them to be of neutral wettability. It was concluded in an earlier study[8] that the surfaces of some cores from oil-bearing formations were preferentially oil-wet because of a highly tenacious, sorbed layer of organic material. It was further

established that in every case the cores were made preferentially water-wet by heating in an oxidizing atmosphere.

The first series of resistivity tests were made on the toluene extracted weather cores of neutral wettability. At the completion of these tests the cores were muffled for one hour at 450°. At 500° the dissociation pressure of calcium carbonate is 0.11 mm.,[9] a value less than the partial pressure of carbon dioxide in ordinary air. The average weight loss was 0.5 g. per core. This treatment gave imbibitions up to 72% pore volume water starting with the core 100% saturated with oil.

Attempts to make a carbonate rock strongly preferentially oil-wet by treatment with silicon[10,11] were unsuccessful. We prepare preferentially oil-wet sandstone surfaces by coating the surface with a silicone material. Such a surface represents an extreme oil-wet condition. A technique was finally developed for carbonate using a solution of high molecular weight organic acid in benzene. The most successful treatment consisted of saturating the core with 10% solution of Eastman practical grade Naphthenic Acids (P2388) in benzene. The core was refluxed in the solution for 30 minutes. Excess solution was gas driven from the core and the remaining benzene was removed in a vacuum oven. At the present time this treating procedure represents the extreme preferentially oil-wet condition yielding imbibitions of oil up to 56% pore volume starting with the core 100% saturated with water.

The ideal treatment would cover all the carbonate surface with a monolayer of acid which would alter the wettability of the surface but would cause a negligible change in the physical dimensions of the matrix. The average increase in weight of rock due to the naphthenic acid treatment was 0.13 g. per core. Surface area measurements using low temperature krypton adsorption by the BET method on samples of this core material gave values of 0.50 sq. meter per gram. A monolayer of stearic acid on all the surfaces of an average core would weigh about 0.08 g.

Experimental Results

The results of the resistivity measurements on the cores in three conditions of wettability are summarized in Fig. 1. The straight lines drawn through these points were obtained by the method of least squares. The equation for these straight lines on log-log coördinates may be written

$$I = S_w{}^{-n}$$

where n is defined as the saturation exponent and S_w is the fractional water saturation of the core.

The equations relating resistivity index to water saturation for neutral and preferentially water-wet cores are $I = S_w{}^{-1.92}$ and $I = S_w{}^{-1.61}$, respectively. The data for the preferentially oil-wet condition separated into two distinct curves. The equations for the lower water saturation portion of these curves are $I = 0.000027\ S_w{}^{-12.27}$ and $I = 0.37\ S_w{}^{-8.09}$, respectively.

The equation of the straight line relating the formation factor of a rock to its porosity may be written

$$F = \phi^{-m}$$

where ϕ is the porosity and the exponent m is defined as the cementation factor. The m values for the curves relating formation factor with porosity are as follows: neutral, 1.92; preferentially water-wet, 1.57; and preferentially oil-wet, 2.01.

Discussion

The data obtained in this study show the striking

(8) H. Y. Jennings, Jr., *Producers Monthly*, **21**, 20, March (1957).

(9) H. H. Willard and A. W. Boldyreff, *J. Am. Chem. Soc.*, **52**, 1888 (1930).

(10) W. P. Gilliam, H. A. Liebhafsky and A. F. Winslow, *ibid.*, **63**, 801 (1941).

(11) C. G. Dodd, J. W. Davis and F. D. Pidgeon, THIS JOURNAL, **55**, 684 (1951).

influence that the wettability of the rock surfaces has on the resistivity of the rock. The data show that at a given fractional water saturation the resistivity is greater when the surface is preferentially oil-wet than when the surface is preferentially water-wet. It can be concluded that in the oil-wet system a portion of the water exists in discrete non-connected globules which are unable to assist with the conduction of current. This concept has been developed in some detail by Keller[3] and by Moore[4] to explain their results on sandstone cores.

Significant differences are apparent, however, in the results obtained for carbonate rocks and those published for sandstone.

Keller[3] shows a break in the water saturation-resistivity index curve for preferentially water-wet sandstones in an air–water system occurring at a water saturation of 30%. It was concluded that below the critical saturation of 30% more and more of the water becomes separated in discrete drops which are not available for current conduction resulting in a more rapid increase in resistance. No such break was observed in the carbonate results though data were obtained at saturations as low as 8%. Apparently the critical saturation does not exist in the water–oil–carbonate system or, if it does, it exists at a water saturation lower than that which can be attained in the laboratory by normal capillary pressure displacement.

The preferentially oil-wet resistivity index–saturation curve for carbonate shows a break as does Keller's curve for sandstone. However, the sandstone curve slopes less steeply after a break at 55% whereas the carbonate slopes more steeply after the break. Keller concludes that the water saturation in the interconnecting pores is reduced first because the water content is forced out into the larger pores by capillary pressure. On further water reduction the water becomes discontinuous but is present in stringers through the center of the larger pores. The resistance does not increase as rapidly after the break because the water that remains is present mainly in the large pores whose water content does not so greatly affect the total resistivity.

The difference in behavior between preferentially oil-wet carbonates and sandstones may be due to a difference in pore size distribution. Studies of formation rock through interpretation of mercury injection curves show that carbonate rocks have complex but characteristic pore size distributions. Apparently the cores used in this study had large pores and large interconnecting pores which remained saturated at high water saturation. However, after a critical saturation was reached the water in these pores became disconnected and the resistivity increased more rapidly. Additional support to the pore size distribution interpretation is found in the separation of the oil-wet curves.

An interesting result of this study was the separation of the preferentially oil-wet data into two distinctly separate curves. Inspection of the samples which fell in the two groups showed that they possessed other distinguishing properties. For example, a separation into the same two groups could be made by analysis of the pore size distribution and by petrographic examination. The separation of curves suggests the use of resistivity measurements on preferentially oil-wet samples as a classification method for carbonate material. Further study of oil-wet carbonate resistivity curves and pore size distribution information will undoubtedly shed more light on the capillary pressure desaturation mechanism.

The formation factor of a porous medium is the simplest resistivity quantity that can be measured. Archie[1] found empirically that m in the equation $F = \phi^{-m}$ was related to the degree of consolidation of the rock. A soft, friable sandstone had an m value of 1.3 while a highly cemented sandstone had an m value of 2.0. The treatment used in this study also changed the value of m. The decreased resistivity observed after muffling the cores could be attributed to the resulting increase in water saturation. But the subsequent decrease in water saturation as a result of depositing naphthenic acid in the core is not sufficient to account for the $m = 2.01$ curve. Apparently the uniform coating of naphthenic acid is more effective in partially sealing off the necks of pores containing water which had previously been contributing to current flow.

It is apparent from the data obtained in this study that a knowledge of the wettability of the formation being penetrated by the well is essential to accurate determination of porosity and water saturation from electric logs. Laboratory resistivity measurements should be made on samples that have the same wettability as the formation being logged.

PARAMAGNETIC RESONANCE OF CHLOROPHYLL CRYSTALS AND SOLUTIONS

By S. S. Brody,[1] G. Newell and T. Castner

Photosynthesis Laboratory and Department of Physics, University of Illinois, Urbana, Illinois

Received January 16, 1959

A light induced resonance is observed both in chlorophyll crystals and solutions. It is shown that the final product in the photoreduction of chlorophyll, by ascorbic acid in pyridine, is not paramagnetic. The quantum yield of spin formation, *q*-value, line width and order of magnitude for the relaxation time are given for crystals of chlorophyll *a*, chlorophyll *b*, and methyl chlorophyllide *a* and plus *b*, and chlorophyll in pyridine. The possible origins of the resonance is discussed.

I. Introduction

This paper describes a study of paramagnetic resonance in certain chlorophyll solutions and in crystalline chlorophyll.

Krasnovsky[2] has postulated the transient formation of a free (ionized) radical as an intermediate in the photochemical reduction of chlorophyll by ascorbic acid in pyridine; he has also assumed that the final, relatively stable pink reduction product ("eosinophyll") itself is a (neutral) radical. According to him the absorption of a light quantum by chlorophyll probably breaks one of the double bonds in the conjugated system, thus producing a biradical, which may tend to either accept or donate an electron (or H-atom). Ascorbic acid, according to Krasnovsky, donates an electron to this biradical, converting it into a semiquinone ion, the latter is converted into a neutral semiquinone-monodehydroascorbic acid by the uptake of an H^+-ion.

Whether "eosinophyll" is a radical can be determined by measurements of paramagnetic resonance. Our results indicate that it is not. While a weak resonance is observed in solutions of chlorophyll upon illumination, it was found to occur not only in the presence but also in the absence of the reductant, ascorbic acid.

An electron spin resonance (e.s.r.) study was then made on chlorophyll crystals. These crystals exhibited paramagnetic properties after exposure to light; the light induced e.s.r. survived for a long time in darkness.

II. Materials and Methods

A V58 Klystron, operating at 9400 Mc. with a modified Pound F.F. frequency stabilization, served as the microwave source in the magnetic resonance spectrometer. The sample was placed between the poles of a Varian V4012A 12″ magnet with a 3¼″ gap. The sensitivity of the spectrometer was estimated, by calibration with Mn^{++} solution, as being better than 10^{12} spins for one gauss line width and one c.p.s. amplifier band width. The spectrometer consisted of a half wave length cavity, forming one arm of a microwave bridge; the bridge was balanced in the absence of resonance. The magnetic field was modulated at eight c.p.s. by separate magnet coils. When resonance occurred, the bridge was unbalanced, and the resulting signal was detected by push–pull bolometers; the eight cycle component was amplified in an eight cycle lock-in amplifier. The microwave bias power for the bolometers, which is analogous to the local oscillator signal in a superheterodyne detection system, was supplied through a separate channel from the same Klystron, and permanently set for optimum detection sensitivity. This permitted independent control of the phase and the power level at the sample. In normal operation, the derivative of the absorption line was recorded. The samples were irradiated while they were in the microwave cavity, through a ¼″ hole in the end of the cavity. To minimize the effect of the dielectric constant of the sample on the Q of the spectrometer, the sample was located in the center and against the end wall of the cavity, where the electric field is at a minimum.

The chlorophylls *a* and *b*, and the methyl chlorophyllide *a* + *b*, were prepared in crystalline form according to the method described by Jacobs and Holt.[3] The concentration of the chlorophyll solutions usually was sufficient for complete absorption of the incident light.

The light source used for illumination was a 1000 watt tungsten lamp; the image of the filament was focused on the sample in the cavity. A solution of $CuSO_4$ was used as a filter to eliminate infrared light. The intensity of the light impinging upon the sample was 0.3 cal./(cm.² min.); the vessel had a cross sectional area of 10 mm.²; therefore, the number of photons absorbed by the chlorophyll sample was about 10^{14}/sec.

The extent of bleaching of the chlorophyll–ascorbic acid mixture was measured with a Beckman model DU spectrophotometer. Two identical samples were prepared for these experiments; one was used in the microwave cavity, while the optical density of the other was measured in the Beckman spectrophotometer before and after illumination with a light source similar to that used in the cavity.

III. E.s.r. in Crystalline Chlorophyll

Large paramagnetic resonance effects were observed when chlorophyll micro-crystals were exposed to light. Invariably, a small resonance could be detected before the crystals were illuminated (even if they had been held in the dark for months)—see Fig. 1. Upon illumination of a sample of chlorophyll *a* in the apparatus described in Section II, a concentration of greater than 10^{15} spins could be produced, with a steady state being reached after about two minutes of illumination (Table I).

The increase of spin concentration as a function of time of illumination could be approximated by the equation $C = C_0 (1 - e^{-kt})$. The constant *k* was evaluated to be 9×10^{-3}/sec., giving a time constant $\tau = 110$ seconds. (Calvin, Sogo, *et al.*,[4] found that spin production *in vivo* involves several time constants. Our precision was not high enough to evaluate more than one time constant.) In a typical experiment, the *final* number of free spins, C_0, was 8×10^{14}. The initial rate of spin production, at $t = 0$, is then

$$\left(\frac{dc}{dt}\right)_{t=0} = C_0 k = 7 \times 10^{12} \text{ spins/sec.}$$

In these experiments, 1.1×10^{14} photons/sec. were absorbed by the chlorophyll sample. Thus

(1) Air Force Cambridge Research Center, Geophysics Directorate, Bedford, Mass.

(2) A. A. Krasnovsky, *Compt. rend. (Doklady), Acad. Sci., USSR,* **60,** 421 (1948).

(3) E. Jacobs and A. S. Holt, *Am. J. Bot.,* **41,** 710 (1954).

(4) M. Calvin and P. Sogo, *et al.,* Brookhaven Meeting, Proceedings, 1958.

TABLE I

PROPERTIES OF E.S.R. INDUCED BY LIGHT IN CHLOROPHYLL
in Vitro

	Chlorophyll soln.	Crystalline chlorophyll a
Rise time, min.	~3	2
Decay time, hr.	>30	2
Line width, gauss	10	See Table II
g	$2.0 \pm 2\%$	See Table II
Spin concn., %	0.1	~0.1
Cor.[a] spin concn., %	....	~20
$\dfrac{10^2}{I_0}\left(\dfrac{dc}{dt}\right)_{t=0}$	~3	7
T_1 light room temp., sec.	~10^{-4}	$<5 \times 10^{-5}$
T_1 dark room temp., sec.	....	10^{-4}
T_1 dark liquid N_2 temp., sec.	....	10^{-2}
I_0, photons/sec.	~10^{14}	~10^{14}

[a] In the crystalline samples, a correction must be made for the mutual shading of chlorophyll crystals.

the initial quantum yield of spin formation was about 7%.

On the other hand, the maximum number of free spins produced by light was only about 0.1% of the total number of chlorophyll molecules present. However, this value needs to be corrected for the mutual light shading of the chlorophyll crystals in the sample vessel. For, unlike solutions in which all the molecules can be exposed to light by the process of energy transfer (at high concentrations) or diffusion, in the crystalline samples only those crystals which comprise the peripheral layer continuously receive full intensity of light. Light intensity is reduced by a factor of one hundred after traversing the first or peripheral layer of crystals (which contains about 100 molecular layers and an extinction coefficient of 0.02/layer; Jacobs, et al.,[5]). Accordingly, it will take the second layer of crystals 100 times longer to reach spin saturation than it took the first peripheral layer. Therefore, it is believed that e.s.r. was induced only in this peripheral layer which contains about 0.5% of the chlorophyll molecules in the sample vessel. Applying this correction raises to 20% the number of chlorophyll molecules which give rise to e.s.r.

There is some evidence that the resonance band of the e.s.r. produced in the light is narrower (Fig. 2) than that in the dark. This light-induced e.s.r. disappeared in the dark with a half-life of about two hours.

The summary of g-values, line widths, etc., is given in Table II. The resonance lines observed in chlorophyll a and b are quite similar, and differ

TABLE II

LINE WIDTHS AND g-VALUES FOR CRYSTALLINE AND AMORPHOUS CHLOROPHYLL

	g-Value $\pm$ 0.0003		Line width, gauss	
	Dark	Light	Dark	Light
Chlorophyll a	2.0030	2.0027	12 ± 1	6 ± 1
Chlorophyll b	2.0033	2.0025	11 ± 1	7 ± 1
Methyl chlorophyllide a + b	2.0029	2.0028	6 ± 0.5	4 ± 0.5
Amorphous chlorophyll b	2.0035	2.0038	11 ± 1	11 ± 1

(5) E. Jacobs, A. S. Holt, R. Kromhout and E. Rabinowitch, Arch. Biochem. Biophys., 72, 495 (1957).
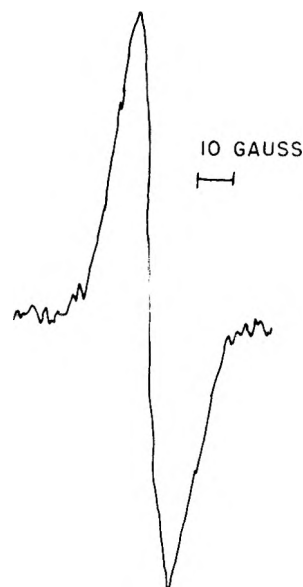
Fig. 1.—Electron spin resonance for crystalline chlorophyll a before irradiation.
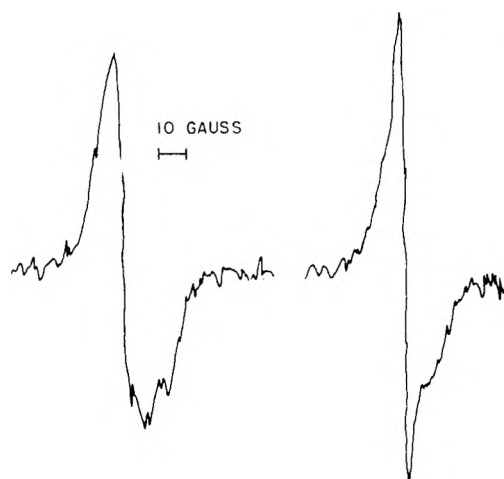
Fig. 2.—E.s.r. for crystalline chlorophyll a (left) and chlorophyllide a + b (right) after irradiation showing the asymmetric superposition of a broad and a narrow resonance line.

from the results obtained with mixed methyl chlorophyllide a + b. The sharpness of the X-ray diffraction pattern of the chlorophyllide showed it to have a much higher degree of crystallinity than the chlorophyll a or b. Two samples of chlorophyll b were studied; by X-ray analysis it was found that one of the samples was almost amorphous. The amorphous sample had a broader resonance line (11 gauss) than the more crystalline sample (7 gauss). Furthermore, the amorphous sample did not show the narrower resonance line after illumination.

A microwave saturation effect was observed; however, not enough data were obtained to ascertain whether the resonance line saturates as a homogeneously or inhomogeneously broadened line.[6] For chlorophyll a, in light, the relaxation time T_1 was 5×10^{-4} sec., or less, while in the dark it was 10^{-4} sec.

(6) T. Castner, Thesis, University of Illinois, 1958.

Microwave saturation of the e.s.r. was more readily observed at the temperature of liquid nitrogen. For chlorophyll a, the dark relaxation time was of the order of 10^{-2} sec.; the line width and the g-value were the same as at room temperature.

While it is known[7] that oxygen quenches molecules in the metastable state, or removes radicals, it was observed that the presence of oxygen had no significant effect on the strength of the induced e.s.r., the g-value, or the line width in the chlorophyll crystals.

IV. E.s.r. in Chlorphyll Solutions

Samples used in the search for a paramagnetic "Krasnovsky intermediate" were prepared by dissolving ethyl chlorophyllide crystals or chlorophyll crystals and excess ascorbic acid in pyridine. (Usually water was added to the solution.) No resonance, or only a very low one, was found upon examination before illumination. When the solution was illuminated, e.s.r. rose to a maximum within three minutes; further illumination for 30 minutes had no affect. The photostationary bleaching of chlorophyll reached 50% or more in a parallel experiment. However, it was soon learned that neither water nor ascorbic acid had any effect on or were required to obtain the light-induced e.s.r.!

The e.s.r. observed had a $g = 2$ (within $\pm 2\%$), a line width of 10 gauss, and a signal to noise ratio of about 25. The shape of the resonance band, the line width and the lack of fine structure were similar to that of the resonance band observed by Commoner[8] and Calvin, et al.,[9] in chloroplasts. A saturation effect also was observed in solution; the T_1 was of the order of 10^{-4} sec. (Table I).

When the total number of chlorophyll molecules in the solution was 3×10^{17}, the number of free spins produced by light was $3 \pm 2 \times 10^{14}$. Thus, the photostationary concentration of unpaired electrons was only 0.1% of the number of chlorophyll molecules—a very low value compared to the simultaneous photostationary concentration of reduced chlorophyll, which exceeded 50%. A comparison of these figures (50 and 0.1%) shows that the reduced form of chlorophyll and photoproduct giving rise to the e.s.r. are different.

To estimate the initial yield of radical formation, a first-order process was assumed, and the experimentally measured values are

$$k \cong \frac{2}{180 \text{ sec.}}$$

$C_0 = 3 \times 10^{14}$ and $I_0 = 1.1 \times 10^{14}$ photons/sec.

Thus

$$\% \text{ yield} = \frac{10^2 \times \left(\frac{dc}{dt}\right)_{t=0}}{I_0} = 3\%$$

This is comparable to the yield measured in crystals.

Because of light shading in highly concentrated chlorophyll solutions, it was thought that stirring

(7) H. Kautsky, et al., Chem. Ber., 66, 1588 (1933).

(8) B. Commoner, J. Heise and J. Townsend, Nat. Acad. Sci., 42, 710 (1956).

(9) M. Calvin and P. Sogo, Science, 125, 499 (1957).

might help to expose more chlorophyll molecules to light. However, gentle stirring did not increase the photostationary spin concentration. In fact, stirring the chlorophyll solution, in a vessel open to air, slightly reduced this concentration.

That the reduced form of chlorophyll in the Krasnovsky reaction does not give rise to an e.s.r. is also readily shown by the large difference between the life times of the e.s.r. (hours) and the reduced form of chlorophyll (minutes). When the light was extinguished, the e.s.r. signal persisted in an oxygen-free atmosphere, without change, for up to 30 hours. After four days, no spin resonance could be detected. On the other hand, the life time of the reduced form of chlorophyll is not longer than one-half hour (even if no oxidant, other than the dehydroascorbic acid formed in the reaction, is present). When the solutions were exposed to air, the e.s.r. disappeared in about an hour.

The spin resonance induced by light in chlorophyll solutions occurs with approximately the same yield both in the presence and absence of ascorbic acid and of water, and in solutions which have not been de-oxygenated. Both chlorophyll a and methyl chlorophyllide give essentially the same results.

V. Discussion

The experimental results reported above give rise to several matters which require elaboration. First, the e.s.r. observed in solutions and in crystals might arise from some impurity in the "chromatographically pure" chlorophyll. An impurity with a maximum concentration of 1% is quite possible. (The most likely impurity is β-carotene; we have found commercial β-carotene to exhibit a strong e.s.r. However, light has little, if any effect on its e.s.r.). In crystals, the fact that the e.s.r. concentration exceeds 10% rules out the impurity possibility.

Assuming for the moment that an impurity is present, the paramagnetic impurity either must have an absorption band in the visible light region (for direct activation by light) or else be photochemically activated by light absorbed by chlorophyll. In the former case, the pigment present as an impurity might be some degradation product of chlorophyll, if not a carotene. In the latter case, activation of the impurity necessitates some mechanism of energy transfer. The transfer of energy by resonance, exciton and electron conduction requires that either the energy migrate among similar molecules or be transferred to a molecule having a lower energy state—therefore, the absorption maximum of an "impurity" is at a wave length greater than 680 mμ. Furthermore, a high transition probability for energy transfer requires that there be considerable overlapping between the fluorescence spectrum of the energy donor and the absorption maximum of an "impurity" is close to 680 mμ. Such a band was postulated to be characteristic of chlorophyll aggregates[10,11] both in solution and in vivo.

The e.s.r. is observed clearly only in solutions having concentrations greater than 10^{-3} M.

(10) J. Lavorel, THIS JOURNAL, 61, 1600 (1957).

(11) S. S. Brody, Science, 128, 838 (1958).

At these concentrations, quenching of fluorescence is observed, presumably because of the formation of a non-fluorescent dimer.[12] Furthermore, in the solutions used for e.s.r. experiments it is estimated that the concentration of chlorophyll dimer is one-fifth to one-tenth that of the monomer. (The effective dimer concentration was estimated from data of fluorescence yield as a function of concentration,[13] by assuming that the decrease in yield of fluorescence was attributable to the energy being absorbed *and transferred* to a non-fluorescent dimer). If the e.s.r. is associated only with dimers and not with monomers, then the estimated yield of formation of paramagnetic molecules in solution should be raised 5 to 10 times (to about 1%).

If the impurity is activated by electron transfer involving chlorophyll, it would leave the chlorophyll molecule with an uneven number of electrons, so that the chlorophyll molecule itself would also become paramagnetic (both in crystals and in solution).

A few remarks are called for regarding the difference in the e.s.r. observed in crystals in the dark and the e.s.r. induced by light. The two resonances probably arise from different sources. The resonance induced in the light may be "exchange narrowed" if the electron is transferred among the chlorophyll molecules in the crystal lattice. The narrower e.s.r. in the dark for the highly crystalline methyl chlorophyllide may also be due to exchange narrowing.

The resonances observed in the *dark* in crystals and in chlorophyll solutions have similar g-values, line widths and relaxation times. The difference in the life time of this "dark" resonance in crystals and solutions may be due to the fact that in the solution there is much higher probability of deactivation (by collision) of the paramagnetic molecules—thus limiting the life time to days, while in the crystal, the paramagnetic molecule is protected by the surrounding chlorophyll molecules—permitting a life time of months. Perhaps the long-lived resonances observed in the dark originate in the body of the crystal and the shorter lived resonance—induced by light—is a property of the surface molecules. The latter resonance should be more readily deactivated by surrounding gases.

It is of interest to compare the e.s.r.'s reported here, for chlorophyll crystals and solutions, with those observed *in vivo*. It is possible that the paramagnetic species detected in solutions of chlorophyll is the same as that reported by Commoner[8] and Calvin[4] in chloroplasts. However, since the observed resonance is lacking in fine structure, it is impossible at this time to make an exact identification. The only properties of the resonance that we can compare are the line width, g-value, yield of spin formation and relaxation time (T_1). Of the information available (line width, g-value and yield), the results are in agreement, within experimental error, with the findings in chloroplasts. Decay or life times of e.s.r. do not constitute a good basis for comparing the spin resonance observed *in vivo* and *in vitro*. The life times of the e.s.r. depends on the number of mechanisms (and their rate constants) returning the free electron to its original state, and these will be quite different *in vivo* and *in vitro*.

Using data obtained from photosynthetic bacteria Calvin, *et al.*,[4] tried to correlate both the final spin concentration with the size of the photosynthetic unit, and the initial yield of e.s.r. with the yield of photosynthesis. However, these correlations may not necessarily be significant since we find the spin concentration and initial yield to be of the same order of magnitude for chlorophyll *in vitro*, where there is neither photosynthesis nor a photosynthetic unit. Perhaps the final spin concentration should be correlated—not with the photosynthetic unit—but with the concentration of aggregated chlorophyll molecules *in vivo*.

In regard to the photoreduction of chlorophyll in the Krasnovsky reaction, it may be concluded that the free semiquinone form of chlorophyll either does not exist, or, if it does, it reacts so rapidly to form the "pink" compound (absorbing at 520 mμ), that it is only present in solution in very small amounts. Furthermore, the "pink" form of chlorophyll itself is not paramagnetic. The substance giving use to the spin resonance which we have observed in chlorophyll solutions may be the precursor of further photochemical reactions.[14,15]

(12) T. Förster, "Fluoreszenz Organischer Verbindungen," Göttingen, Vendenhoeck and Ruprecht, 1951, p. 243.

(13) W. Watson and R. Livingston, *J. Chem. Phys.*, **18**, 802 (1950).

(14) S. S. Brody, *J. Am. Chem. Soc.*, **82**, 1570 (1960).

(15) A. A. Krasnovsky and A. V. Umrikheina, *Biofisika*, **3**, 547 (1958).

HYDROGEN OVERPOTENTIAL ON CADMIUM

By I. A. AMMAR AND M. HASSANEIN

Department of Chemistry, Faculty of Science, University of Cairo, Cairo, Egypt, U.A.R.

Received June 15, 1959

Hydrogen overpotential has been measured on Cd in 0.01, 0.05, 0.1 N HCl, and in 0.01, 0.05, 0.1 and 0.5 N NaOH. Measurements have been carried out at 20, 30, 40 and 50°. The results have been statistically analyzed and the confidence limits have been computed. It has been observed that the Tafel slope lies between 0.16 and 0.18 v., the maximum confidence limits being ±0.01 v. The results have been compared with the results of previous authors.

Introduction

Very few overpotential measurements have been carried out on Cd. The early work of Hickling and Salt[1] indicates the occurrence of a Tafel line slope of 0.19 v., and an exchange current density of 10^{-7} amp./cm.^{2} in 1.0 N HCl at 16°. In 2 N H$_2$SO$_4$, Pecherskaya and Stender[2] have reported values of 0.3 and 10^{-5} amp./cm.^{2} for the transfer coefficient α, and the exchange current density i_0, respectively. More recently, Belmondi[3] has reported the hydrogen overpotential measurements on Cd in 1.0 N HCl, 1.0 N H$_2$SO$_4$, 1.0 N HClO$_4$ and 0.5 N HClO$_4$ + 0.5 N HCl. In HCl solution the Tafel equation is valid down to 10^{-4} amp./cm.^{2}, with a Tafel slope of 0.137 v. Below 10^{-4} amp./cm.^{2} the overpotential tends to a stationary value. In HClO$_4$ and H$_2$SO$_4$ solutions, the Tafel slope is 0.144 and 0.137 v., respectively. In 0.5 N HCl + 0.5 N HClO$_4$, the Tafel line is linear only at high current densities, while at low current densities it shows a sigmoid behavior. Overpotential measurements on Cd in alkaline solutions have been carried out by Genta and Belmondi.[4] The authors observe that the Tafel slope decreases from 0.16 v. in 1 N KOH to 0.099 v. in 8 N KOH. Moreover, the Tafel lines intersect each other between 10^{-3} and 10^{-4} amp./cm.^{2}. Owing to the disagreement between the results of the above authors, a revision of the overpotential measurements on Cd in both acid and alkaline solutions is necessary. HCl and NaOH solutions have been chosen for the present investigation in order to be able to compare the parameters of hydrogen evolution on Cd with those on other metals.

Experimental

Cadmium electrodes were prepared from spectroscopically pure Cd in an atmosphere of pure and dry hydrogen. The metal was introduced into a glass apparatus consisting of a wide glass tube in which hydrogen was passed and then was allowed to escape to the atmosphere. The glass apparatus was provided with a side arm (3 mm. diameter) having a Pt wire sealed in the middle. Cd was melted under hydrogen and the melt was introduced in the side arm over the Pt wire. The apparatus was then left to cool with hydrogen still passing. The side arm was quickly cut off. The glass around Cd was removed thus exposing the required area, the electrode was sealed to the electrode holder, and it was then inserted in the electrolytic cell. This was done so quickly such that the electrode surface did not contact air for more than 0.5 minute. The electrode surface then was reduced cathodically in the pre-electrolyzed solution as will be described later on.

The overpotential cell was similar to those previously described,[5,6] and the hydrogen electrode was used as a reference. HCl and NaOH solutions were prepared following the procedure of Bockris and Potter,[6] and then were purified by pre-electrolysis at 10^{-1} amp./cm.^{2} for 30 hours. The direct method of measurements and the rapid technique were employed. Measurements were carried out in unstirred solutions. It was at first observed that, below 10^{-6} amp./cm.^{2}, the overpotential was numerically smaller than the values obtained by extrapolating the measurements at high current densities. This behavior was similar to the effect of depolarization. An appreciable time effect was also observed in this region. The Tafel line was improved after keeping the test cathode polarized at about 10^{-3} amp./cm.^{2} for about 10 hours in the previously pre-electrolyzed solution in the cathode compartment. As a result of this procedure, the time effect was diminished and the reproducibility was improved (±5 mv.). Current densities were calculated using the apparent surface area. The potential was measured with a valve pH meter millivoltmeter, and the current with a microammeter. At very low polarizing currents, the current was checked by measuring the p.d. across a standard resistance.

Results and Discussion

Hydrogen overpotential has been measured in 0.01, 0.05, 0.1 N HCl, 0.01, 0.05, 0.1 and 0.5 N NaOH. For each concentration, measurements have been carried out at 20, 30, 40 and 50°. Several Tafel lines have been measured, in separate experiments, for each concentration and temperature studied, and the mean Tafel lines have been computed. Examples for the mean Tafel lines are given in Figs. 1 and 2 for 0.01 N HCl and 0.01 N NaOH, respectively. Figure 1 indicates that, in HCl solutions, the Tafel line tends to a stationary potential at low current densities, and this is probably due to the dissolution of Cd in HCl. In NaOH solutions (Fig. 2) the overpotential, at low current densities, decreases asymptotically toward the potential of the reversible hydrogen electrode. In this region the relation between overpotential and current density is linear (Fig. 3). The relation between the mean overpotential (at a constant current density) and the pH of solution is linear for both HCl and NaOH solutions. In HCl solutions η increases numerically with the increase of pH, while in NaOH solutions η decreases numerically with the increase of pH and this is in accordance with the previous results on other metals.[6] The relation between the logarithm of the mean exchange current density and the reciprocal of absolute temperature is also linear for both HCl and NaOH solutions.

The parameters of hydrogen evolution have been analyzed statistically and the 95% confidence limits have been computed. It has been observed that the maximum confidence limits for the Tafel

(1) A. Hickling and F. Salt, *Trans. Faraday Soc.*, **36**, 1226 (1940).

(2) K. Pecherskaya and Stender, *J. Appl. Chem., U.R.S.S.*, **19**, 1303 (1946).

(3) G. Belmondi, *Gazz. chim. ital.*, **85**, 124 (1955).

(4) V. Genta and G. Belmondi, *ibid.*, **85**, 111 (1955).

(5) J. O'M. Bockris, *Chem. Revs.*, **43**, 525 (1948).

(6) J. O'M. Bockris and E. C. Potter, *J. Chem. Phys.*, **20**, 614 (1952).

line slope do not exceed ±0.01 v. The results are given in Tables I and II for HCl and NaOH solutions, respectively. Values of the electron number λ[6,7] have been calculated from the slope of the relation between η and the current density (Fig. 3), and these are given in Table II together with the 95% confidence limits. The heat of activation at the reversible potential ΔH_0^* has been calculated from the slope of the relation between the logarithm of the exchange current density and the reciprocal of absolute temperature according to

$$\left(\partial \log i_0 / \partial \frac{1}{T} \right) = \Delta H_0^* / 2.303 R$$

The results are given in Tables III and IV for HCl and NaOH solutions, respectively.

TABLE I

MEAN PARAMETERS OF HYDROGEN EVOLUTION ON CADMIUM IN HCl SOLUTIONS AND THE CONFIDENCE LIMITS

Concn., N	Temp., °C.	b, v.	i_0, amp./cm.²
0.01	20	0.18	$(9.21 \pm 0.53) \times 10^{-10}$
	30	.17	$(1.08 \pm .04) \times 10^{-9}$
	40	.17	$(1.72 \pm .13) \times 10^{-9}$
	50	.16	$(2.49 \pm .06) \times 10^{-9}$
0.05	20	.17	$(1.62 \pm .17) \times 10^{-9}$
	30	.17	$(2.55 \pm .25)$
	40	.17	$(3.39 \pm .11)$
	50	.17	$(5.64 \pm .39)$
0.1	20	.16	$(1.44 \pm .12) \times 10^{-9}$
	30	.16	$(2.29 \pm .19)$
	40	.16	$(3.55 \pm .32)$
	50	.16	$(5.69 \pm .43)$

TABLE II

MEAN PARAMETERS OF HYDROGEN EVOLUTION ON CADMIUM IN NaOH SOLUTIONS AND THE CONFIDENCE LIMITS

Concn., N	Temp., °C.	b, v.	i_0, amp./cm.²	λ
0.01	20	0.17	$(1.34 \pm 0.06) \times 10^{-8}$	1.0 ± 0.1
	30	.17	$(1.83 \pm .14)$	$0.8 \pm .0$
	40	.17	$(2.08 \pm .08)$	$1.1 \pm .1$
	50	.17	$(2.76 \pm .17)$	$1.0 \pm .1$
.05	20	.18	$(3.10 \pm .17) \times 10^{-8}$	$0.9 \pm .0$
	30	.18	$(4.06 \pm .25)$	$1.1 \pm .0$
	40	.18	$(5.54 \pm .07)$	$1.2 \pm .0$
	50	.18	$(8.07 \pm .17)$	$1.2 \pm .0$
.1	20	.18	$(4.79 \pm .22) \times 10^{-8}$	$1.0 \pm .5$
	30	.18	$(5.63 \pm .14)$	$1.1 \pm .1$
	40	.18	$(7.88 \pm .1)$	$1.1 \pm .0$
	50	.18	$(9.55 \pm .3)$	$1.2 \pm .5$
.5	20	.18	$(7.42 \pm .29) \times 10^{-8}$	$1.0 \pm .5$
	30	.18	$(9.27 \pm .43) \times 10^{-8}$	$0.9 \pm .0$
	40	.18	$(1.2 \pm .08) \times 10^{-7}$	$1.0 \pm .0$
	50	.18	$(1.54 \pm .07) \times 10^{-7}$	$1.1 \pm .0$

TABLE III

HEAT OF ACTIVATION FOR HYDROGEN EVOLUTION ON CADMIUM IN HCl SOLUTION

Concn., N	$-\left(\partial \log i_0 / \partial \frac{1}{T} \right)$	ΔH_0^*, kcal.
0.01	1.58×10^3	7.3
.05	2.04×10^3	9.4
.1	2.00×10^3	9.2

(7) J. O'M. Bockris and E. C. Potter, *J. Electrochem. Soc.*, **99**, 169 (1952).
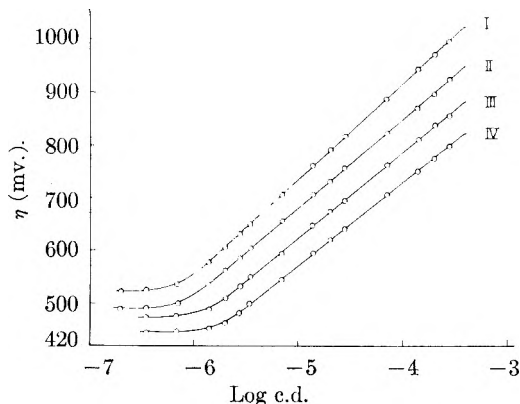
Fig. 1.—Mean Tafel lines on Cd in 0.01 N HCl: I, 20°; II, 30°; III, 40°; IV, 50°.
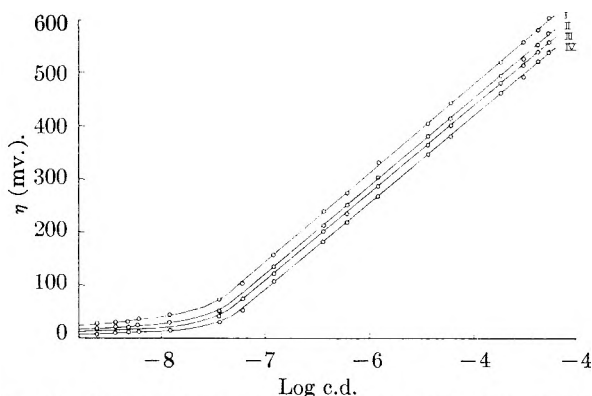
Fig. 2.—Mean Tafel lines on Cd in 0.01 N NaOH: I, 20; II, 30°; III, 40°; IV, 50°.
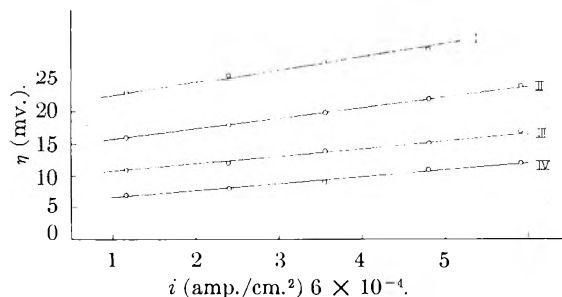
Fig. 3.— Relation between mean η and the current density for Cd in 0.01 N NaOH at low values of η: I, 20°; II, 30°; III, 40°; IV, 50°.

TABLE IV

HEAT OF ACTIVATION FOR HYDROGEN EVOLUTION ON CADMIUM IN NaOH SOLUTIONS

Concn., N	$-\left(\partial \log i_0 / \partial \frac{1}{T} \right)$	ΔH_0^*, kcal.
0.01	0.99×10^3	4.6
.05	1.38×10^3	6.4
.1	0.99×10^3	4.6
.5	1.1×10^3	5.1

The results of the present investigation on Cd in HCl solutions indicate, in a manner similar to the results of Belmondi,[3] the occurrence of a region of stationary potential at the low current density range (Fig. 1). However, the Tafel line slope lies between 0.16 and 0.18 v. (Table I). These values are higher than the values given by Belmondi[3] for Cd in acid solutions, and lower than the values

quoted by Hickling and Salt,[1] and by Pecherskaya and Stender.[2] Moreover, Table I indicates that the exchange current density lies between 9.21 $\times$ 10^{-10} and 5.69 $\times$ 10^{-9} amp./cm.[2]. These values are also intermediate between the results of Belmondi[3] and those of previous authors.[1,2] In NaOH solutions (Table II), the Tafel slope lies between 0.17 and 0.18 v., and the exchange current density between 1.34 $\times$ 10^{-8} and 1.54 $\times$ 10^{-7} amp./cm.[2]. Values of the slope are higher than those observed by Genta and Belmondi[4] in KOH solutions. The above authors have pointed out that, in KOH solutions, the overpotential is higher in more dilute solutions at high current densities. At low current densities, however, the overpotential in concentrated solutions is higher than the values observed in dilute solutions, with the result that the Tafel lines intersect each other at intermediate current densities.[4] Such a behavior has not been observed in the present investigation. The fact that λ is very near to unity (Table II) indicates a slow discharge mechanism. However, it is difficult to ascribe a Tafel slope of >0.12 v. to the slow discharge mechanism assuming symmetrical energy barriers. It is, therefore, possible that the effective energy barrier for the hydrogen evolution on Cd is not symmetrical. Furthermore, it is also possible that this symmetry factor changes with the condition of the electrode surface, i.e., with the method of electrode preparation. This may, therefore, account for the difference between the results of the present investigation, particularly in acid solutions, and those of Belmondi[3] since the methods of electrode preparation are different in both cases. Thus, whereas Belmondi[3] and Genta and Belmondi[4] have prepared their electrodes in vacuo, Cd electrodes have been prepared in the present investigation under an atmosphere of pure hydrogen as already described. Another possibility exists for the explanation of the high Tafel slopes obtained on Cd. This is based on proton tunneling as suggested by Conway.[8] The author concludes that Tafel slopes higher than those required by the

(8) B. Conway, Can. J. Chem., 37, 178 (1959).

classical theories of overpotential could be explained on the basis of tunneling effects.

Considering the influence of acid or base concentration on η in the light of the double layer effect, one may refer to the work of Frumkin.[9,10] It follows from Frumkin's treatment[3] that, in pure dilute acid solutions under the condition when Stern's theory[11] is applicable, the overpotential should be independent of the acid concentration. According to Stern's theory the potential ξ, at the Helmholtz double layer, is directly proportional to the logarithm of the bulk activity of H_3O^+ ions when specific adsorption of ions is absent, and when the electrode potential is far from that of the electrocapillary maximum (e.c. max.). The mean pH effect observed in the present investigation for Cd in pure HCl solutions is $(\partial\eta/\partial pH)\ i = -100$ mv., and this value does not agree with the predictions of Frumkin's theory. It may, therefore, be possible that the direct proportionality between ξ and log $a_{H_3O}^+$ is not applicable for Cd in the concentration and potential ranges under which the overpotential measurements have been carried out. In alkaline solutions, the discharge of hydrogen probably takes place from H_2O molecules. Under this condition a complex pH effect is theoretically expected.[6] With the assumption that the activity of H_2O molecules in the double layer is equal to that in the bulk of solution, one gets in pure dilute solutions in absence of specific adsorption and at potential conditions far from that of the e.c. max.

$$(\partial\eta/\partial pH)i = 120 \text{ m.v. at } 30°$$

When the potential conditions at the electrode approach those of the e.c. max. $(\partial\eta/\partial pH)i$ lies between 60 and 120 mv. at 30°. The mean pH effect observed for Cd in pure NaOH solutions is $(\partial\eta/\partial pH) = 75$ mv. and this value lies well within the theoretical values expected in the neighborhood of the e.c. max.

The authors wish to express their thanks to Prof. A. R. Tourky for his interest in this work.

(9) A. N. Frumkin, Z. physik. Chem., 164, 121 (1933).
(10) A. N. Frumkin, Zhur. Fiz. Khim., 24, 244 (1950).
(11) O. Stern, Z. Elektrochem., 30, 508 (1924).

A THEORY FOR ESTIMATION OF SURFACE AND INTERFACIAL ENERGIES. III. ESTIMATION OF SURFACE ENERGIES OF SOLIDS FROM CONTACT ANGLE DATA

By ROBERT J. GOOD AND

Convair Scientific Research Laboratory, San Diego, California

L. A. GIRIFALCO

National Aeronautics and Space Agency, Cleveland, Ohio

Received July 13, 1959

A theory is proposed by which the surface free energy of certain solids can be estimated from the contact angles of liquids on them. The method is verified using contact angle and surface tension data from the literature, for benzene and α-methylnaphthalene on liquid and solid fractions of a fluorinated lubricating oil. The method is then applied to data on the contact angles of various liquids on Teflon and on an octadecylamine monolayer. The surface tensions of these solids are estimated to be, respectively, about 28 and 30 ergs/cm.^{2} A theoretical basis is given for the method of Fox and Zisman, of plotting the cosine of the contact angle θ vs. the surface tension of the liquid, to obtain the "critical surface tension" (at which $\theta = 0$) which gives an approximation to the surface tension of the solid.

Introduction

Equilibrium contact angles of liquids on solids are customarily discussed in terms of Young's equation[1-3]

$$\cos \theta = \left(\frac{\gamma_{sv} - \gamma_{sl}}{\gamma_l} \right)$$
$$= 1 \quad \text{if} \left(\frac{\gamma_{sv} - \gamma_{sl}}{\gamma_l} \right) > 1 \quad [4] \qquad (1)$$

where θ is the equilibrium contact angle, γ_l is the surface tension of the liquid, γ_{sl} is the interfacial tension between liquid and solid, and γ_{sv} is the surface tension of the solid in equilibrium with the saturated vapor of liquid l. The expression in terms of the adhesion tension, $A \equiv \gamma_{sv} - \gamma_{sl}$ and the equilibrium spreading pressure, π_e, is

$$A = \gamma_l \cos \theta = \gamma_s - \gamma_{sl} - \pi_e \qquad (2)$$

where γ_s is the surface tension of the bare solid and $\pi_e = \gamma_s - \gamma_{sv}$.

If one is seeking a means of measuring the surface energy or surface tension of the solid, then the contact angle method suffers from the drawback that one cannot in general isolate γ_s as a function of variables which can be measured experimentally. In principle, π_e can be measured by means of adsorption studies; but up to the present it has not been possible in general to do more than measure the difference, $\gamma_s - \gamma_{sl}$.

Zisman and co-workers[5] have pointed out that an estimate of the surface tension of certain solids can be made, as follows: If for a given solid, with a homologous series of liquids, $\cos \theta$ is plotted vs. the surface tension of the liquid, then the "critical surface tension" γ_c, the value of γ_l for which $\cos \theta = 1$, gives a measure of the surface tension of the solid. The basis of this method[5] is the assumption that as

$\theta \to 0$, $\gamma_{sl} \to 0$ and $\pi_e \to 0$ in a smooth and orderly fashion.

We wish to propose the application of a theory, which was suggested[6] previously for the estimation of surface and interfacial energies, to the calculation of the surface tension of certain solids from contact angle data. Equation (3) had been proposed, and tested for liquid–liquid systems

$$\gamma_{ab} = \gamma_a + \gamma_b - 2\Phi(\gamma_a \gamma_b)^{1/2} \qquad (3)$$

The subscripts a and b refer to the two phases, which may be liquid or solid. In the zeroth order approximation, Φ is equal to unity. In the first approximation, it has been shown[6a] that for "regular" interfaces, the value of Φ is given by the equation

$$\Phi = \frac{4(V_a V_b)}{(V_a^{1/3} + V_b^{1/3})^2} \qquad (4)$$

where V refers to molar volume. When V_a and V_b are not extremely different, the value of Φ is close to unity.[7] A regular interface was defined as one for which the intermolecular energies for pairs both of like and unlike molecules follow a Lennard-Jones[8] potential. A somewhat more general definition would be that the energy of attraction between the unlike molecules be the geometric mean of the energies of attraction between pairs of like molecules.

Equations 3 and 4 were confirmed for liquid–liquid systems conforming to the definition of "regular." It was found[6] that experimental values of Φ fell within about 1 to 10% of those given by equation 4, being uniformly on the low side. (Systems of organic liquids vs. water do not fit the

(1) T. Young, *Trans. Roy. Soc. (London)*, **95**, 65 (1805).

(2) N. K. Adam, "Physics and Chemistry of Surfaces," 3rd edition, Oxford, 1941.

(3) W. D. Harkins, "The Physical Chemistry of Surface Films," Reinhold Publ. Corp., New York, N. Y., 1952.

(4) This proviso is always implicit in Young's equation. We will hereafter consider it to be understood without further repetition. Equation 1 also neglects effects due to roughness or lack of homogeneity of the solid. See R. N. Wenzel, *Ind. Eng. Chem.*, **28**, 988 (1936); THIS JOURNAL, **53**, 1466 (1949); also R. J. Good, *J. Am. Chem. Soc.*, **79**, 5041 (1952).

(5) H. W. Fox and W. A. Zisman, *J. Colloid Sci.*, **7**, 428 (1952).

(6) (a) L. A. Girifalco and R. J. Good, THIS JOURNAL, **61**, 904 (1957); (b) R. J. Good, L. A. Girifalco and G. Kraus, *ibid.*, **62**, 1418 (1958).

(7) If $\Phi = 1$, equation 3 can be put in the form

$$\gamma_{ab} = (\gamma_a^{1/2} - \gamma_b^{1/2})^2$$

which bears an obvious resemblance to the Hildebrand–Scatchard equation for energy of mixing for non-electrolytes with equal molar volumes

$$\overline{\Delta E}^M = x_b^2 [(\Delta E_a^V)^{1/2} - (\Delta E_b^V)^{1/2}]^2$$

See below, under Discussion.

(8) J. E. Lennard-Jones, *Proc. Roy. Soc. (London)*, **A159**, 229 (1924).

definition of "regular"; and no generalizations which could be applied to liquid–solid interfaces could be made as to the value of Φ for such systems. For this reason we will not attempt to apply our theory to systems involving strongly hydrogen-bonding liquids, e.g., water, formamide, or the polyhydric alcohols, in contact with solids. The same restriction applies to metal–non-metal liquid systems.)

Application to Contact Angles of Liquids on Solids.—If the solid surface is homogeneous and smooth, then we may combine equations 2 and 3 and solve for γ_s

$$\gamma_s = \frac{[\gamma_l(1 + \cos\theta) + \pi_e]^2}{4\Phi^2\gamma_l} \qquad (5)$$

If π_e can be neglected

$$\gamma_s = \frac{\gamma_l(1 + \cos\theta)^2}{4\Phi^2} \qquad (6)$$

Rearranged, equations 5 and 6 become

$$\cos\theta = 2\Phi\sqrt{\frac{\gamma_s}{\gamma_l}} - 1 - \frac{\pi_e}{\gamma_l} \qquad (7)$$

$$\cos\theta = 2\Phi\sqrt{\frac{\gamma_s}{\gamma_l}} - 1 \qquad (8)$$

Since π_e cannot be greater than γ_s (and indeed π_e may be considerably less than γ_s) the approximation of neglecting π_e is likely to be a good one when $\gamma_s < \gamma_l$, as pointed out by Fox and Zisman[5]; cf. Fowkes and Sawyer.[9]

A test of equation 6 can be made using data of Fowkes and Sawyer,[9] who measured the contact angle of benzene and of α-methylnaphthalene on a glassy solid fluorocarbon obtained by fractionating a perfluorinated lubricating oil. They also measured the surface tension of the four lower, liquid fractions from the same material. Since there was no significant trend of surface tension with molecular weight, they were able to estimate the surface tension of the glassy solid; the result was 22.4 ergs/cm.[2]. From their measurements of interfacial tension of benzene and of α-methylnaphthalene vs. the four liquid fluorocarbon fractions, it was possible[6] to estimate the value of Φ for benzene and α-methylnaphthalene vs. the glassy fluorocarbon solid. If we accept the authors' very reasonable assumption that π_e was negligible for the system we may test equation 6, as shown in Table I.

TABLE I

ESTIMATION OF SURFACE FREE ENERGY OF GLASSY FLUOROCARBON FRACTION

	γ_l	θ^a	$\frac{\gamma_l(1 + \cos\theta)^2}{4}$	Φ^b	$\gamma_s = \frac{\gamma_l(1 + \cos\theta)^2}{4\Phi^2}$
Benzene	28.5	57 ± 2	17.0 ± 0.09	0.86	23.0 ± 1.3
α-Methyl naphthalene	37.2	76 ± 2	14.4 ± 1.3	0.81	21.8 ± 1.9
Estimate of γ_s by extrapolation from lower-molecular-weight fractions					22.4

^{a} Data of Fowkes and Sawyer, ref. 9. ^{b} Value estimated from data on lower fractions.

It may be seen that the values of γ_2, as estimated in the last column, agree with the value obtained by extrapolation from the lower fractions, within

(9) F. M. Fowkes and W. M. Sawyer, J. Chem. Phys., **20**, 1650 (1952).

the experimental error. This corroborates the experimental confirmation previously reported[6] for the theory.

It may be seen from an examination of equations 5 to 8 that, in order for a given liquid to have an equilibrium contact angle $\theta > 0$ on a given (smooth, homogeneous) solid, one or more of the following conditions must hold

(a) π_e is large
(b) $\gamma_l \gtreqqless \gamma_s$ (9)
(c) Φ is appreciably less than 1

These three cases will be taken up one at a time. The necessary and sufficient condition for $\theta > 0$, as will be shown, is that at least one of the three be true.

Consider first the case[10] where (a) is true, but not (b) or (c): $\pi_e > 0$, $\gamma_l < \gamma_s$, $\Phi = 1$. Harkins[3] defines the initial spreading coefficient, $S_{l/s}$, as

$$S_{s/l} \equiv \gamma_s - (\gamma_l + \gamma_{ls})$$

Initially the solid-gas interface is free from adsorbed molecules of the substance comprising the liquid phase. From equation 3, with $\Phi = 1$

$$S_{l/s} = 2\gamma_s(1 - \sqrt{\gamma_l/\gamma_s}) \qquad (10)$$

Since $\gamma_l < \gamma_s$, $S_{l/s} > 0$.

If we neglect the solubility of the solid in the liquid, and the adsorption of molecules from the solid at the liquid-gas interface, the definition[3] of the final spreading coefficient is

$$S_{l'/s'} \equiv \gamma_{sv} - (\gamma_l + \gamma_{sl}) = S_{l/s} - \pi_e$$

Substituting the value of $S_{l/s}$ into this definition of $S_{l'/s'}$ yields

$$S_{l'/s'} = 2\gamma_s(1 - \sqrt{\gamma_l/\gamma_s}) - \pi_e \qquad (11)$$

If $\pi_e > 2\gamma_s(1 - \sqrt{\gamma_l/\gamma_s})$, then $S_{l'/s'} < 0$, and $\theta > 0$. Thus it is possible to predict the minimum value of π_e for which $\theta > 0$, for a given liquid-solid system.

Consider, second, the case where condition (b) holds, $\gamma_l \gtreqqless \gamma_s$. If $\Phi \leq 1$, and regardless of π_e (but a fortiori if $\Phi < 1$ and π_e appreciable) then $\theta > 0$. Conversely, if $\Phi = 1$ and $\pi_e \ll \gamma_l$, then $\theta = 0$ if and only if $\gamma_l \leq \gamma_s$. Thus theoretical confirmation is given of the hypothesis of Fox and Zisman[5] that the surface tension of a solid is given approximately by the "critical surface tension" (see above).

Consider, third, the case where (c) is true, but not (a) or (b), i.e., $\Phi < 1$, but $\pi_e = 0$, and $\gamma_l < \gamma_s$. Then equation 8 shows that the contact angle is zero ($\cos\theta = 1$) if

$$2\Phi\sqrt{\gamma_s/\lambda_l} \geq 2 \text{ or } \gamma_l/\gamma_s \geq \Phi^2 \qquad (12a)$$

and that the contact angle is greater than zero ($\cos\theta < 1$) if

$$\Phi^2\sqrt{\gamma_s/\gamma_l} < 1 \text{ or } \gamma_l/\gamma_s < \Phi^2 \qquad (12b)$$

For example, suppose $\Phi = 0.5^{12}$ and $\pi_e = 0$, then $\cos = 1$ when $\gamma_s > 4\gamma_l$; and $\theta > 0$ if $\gamma_s < 4\gamma_l$.

(10) Bangham and Razouk[11] first reported the non-spreading of an organic liquid on a high-energy solid under conditions where an adsorbed film of molecules from the liquid was present on the solid. In their experiments, π_e was large, $\gamma_l < \gamma_s$, the mutual solubilities of the two phases were negligible, and no precise estimate of Φ can be made, though very probably $\Phi < 1$.

(11) D. H. Bangham and R. I. Razouk, Trans. Faraday Soc., **33**, 1459, 1463 (1937); Proc. Roy. Soc. (London), **A166**, 572 (1938).

According to equations 7 and 8, if for a given solid $\cos\theta$ for a series of liquids is plotted vs. $1/\sqrt{\gamma_1}$, a straight line should result, *provided* Φ is constant and $\pi_e \ll \gamma_1$. The neglect of π_e is probably valid for most organic liquids on Teflon at room temperature. The constancy of Φ is not so certain: equation 4 predicts values ranging from unity down to 0.9 in practical cases; and empirically (see above) a further reduction of 5 to 10% should be made.[13] Since values of Φ ranging from about 0.80 to 0.85 can be expected with organic liquids on Teflon a simple plot of $\cos\theta$ vs. $\sqrt{1/\gamma_1}$ should yield a straight line with a scatter of about 5% superimposed on the scatter due to experimental error. Figure 1 shows the result of this plot, and it may be seen that (particularly in view of the variations in Φ) the fit to a straight line is quite satisfactory. The line is drawn corresponding to the equation $\cos\theta = 2\sqrt{19.0/\gamma_1} - 1$.

Table II summarizes the treatment of the data for the various series of organic liquids, with a typical member of each series treated in detail, *e.g.*, hexadecane representing the alkanes. The calculated values of $\gamma_1(1+\cos\theta)^2/4$ for the various members of any series were found to group within

Fig. 1.—Contact angle vs. $1/\sqrt{\gamma_1}$ for various liquids on polytetrafluoroethylene: ○, alkanes; ▽, alkylaryl compounds; +, di-n-alkyl ethers; ▲, esters; ●, alcohols; □, fatty acids; ✕, halogenated hydrocarbons; △, polysiloxanes.

TABLE II

ESTIMATION OF SURFACE FREE ENERGY OF POLYTETRAFLUOROETHYLENE FROM CONTACT ANGLE DATA, USING EQUATION 5

Liquid	γ_1, ergs/cm.^{2}	θa, deg.	Approx. $\gamma_s b$	Est. Φ for series	γ_s Calcd. by eq. 6
Hexadecane	27.6	46	19.8		
Av., 9 alkanes			19.3	0.85	26.3
Ethylbenzene	29.0	48	20.3		
Av. 7 alkylaryl compounds			19.8	.85	27.4
Tricresyl phosphate	40.9	75	16.2		
Av., 8 esters			16.7	.80	26.1
Butyric acid	26.8	42	20.3		
Av., 5 fatty acids			18.8	.80	29.4
n-Octyl alcohol	27.6	48	19.2		
Av., 5 primary alcohols			19.4	.80	30.3
Dibutyl ether	22.8	31	19.8		
Av., 5 dialkyl ethers			19.3	.85	26.8
Carbon tetrachloride	26.8	36	21.9		
Methylene iodide	50.8	88	13.6		
Av., 11 halogenated hydrocarbons and CS$_2$			18.6	.8	29.1
Polymethyl siloxane (hexamer)	18.5	24	17.5		
Av., 11 polysiloxanes			17.1	.8	26.7

^{a} Data of Fox and Zisman, ref. 15. ^{b} Approximate γ_s calculated by the formula $\gamma_s \simeq 0.25 (\gamma_1 + \cos\theta)^2$, *i.e.*, assuming $\Phi = 1$ in equation 6.

(12) *Cf.* ref. 6a: for tetradecane vs. water, $\Phi = 0.53$. Experimentally,[14] tetradecane forms a lens on water. Since this hydrocarbon has no polar end group to "attach" to water forming an oriented monolayer, π_e should be small. When the observed surface tension of tetradecane, 25.6, is substituted into equation 12, it is found that $\gamma_1/\gamma_s = 0.355$, vs. $\Phi^2 = 0.28$. So $\theta > 0$, in agreement with the observed non-spreading.

(13) D. J. Donahue and F. E. Bartell, THIS JOURNAL, **50**, 480 (1952).

(14) But note that for regular interfaces, Φ cannot be considered a freely adjustable parameter.

(15) H. W. Fox and W. A. Zisman, *J. Colloid Sci.*, **5**, 520 (1950); **7**, 109 (1952); E. G. Shafrin and W. A. Zisman, *ibid.*, 166 (1952); A. H. Ellison, H. A. Fox and W. A. Zisman, THIS JOURNAL, **57**, 622 (1953); see U. S. Naval Research Laboratory Report No. 4932, by W. A. Zisman.

about 0.5 erg/cm.^{2} of the average, for each series. The halogenated hydrocarbons comprised an exception to this close grouping, as illustrated by the difference between CCl$_4$ and CH$_2$I$_2$. But this exception might be considered predictable, in view of the wide range of dipole moments and polarizabilities, among the halogenated hydrocarbons that were included, and hence a wide range of values of Φ that are to be expected in this series.

The values given in the fourth column agree (as would be expected) with the values obtained from Zisman's limiting contact angles. Equations 5 and 6 show that a further correction, of dividing by Φ^2, is required in order to obtain the surface free energy of the solid. Since we have found[6a] that Φ is above unity only for certain systems of water vs. "orienting" organic liquids (such as alcohols) we can be quite confident that the surface free energy is above 19, which is the average value obtained from the contact angle data when Φ is set equal to unity. Sufficient data are not available to make any precise predictions of the values of Φ for the above organic liquids vs. polytetrafluoroethylene; but it is reasonable, based on the data referred to above, to expect values in the range 0.8 to 0.85. The values of Φ for the eight groups of liquids, as estimated from structural considerations of molar volume and polarity, are given in the fifth column. Using these values of Φ, we have calculated the values of γ_s in the last column. Hence we can conclude provisionally that γ_s is between 26 and 30 ergs/cm.^{2}, and probably about 28.[16] This value for Teflon may be compared with the value of 22.4 for the glassy fluorocarbon fraction of Fowkes and Sawyer. Bondi[17] has pointed out that the surface energy of a crystalline solid should be greater than that of the supercooled liquid, and Teflon largely crystalline. So it seems reasonable that of the two substances, the surface tension of Teflon should be the higher.

(16) In paper II of this series, the surface entropy of Teflon was estimated to be 0.17 ergs/deg./cm.^{2}, using the value of the surface energy $\epsilon = 69$ ergs/cm.^{2}, from heat of immersion data, and the surface free energy, $\gamma = 18$ ergs/cm.^{2} from the critical surface tension for zero contact angle. Since it now appears that the surface free energy of Teflon is nearer to 28, a recalculation of the surface entropy is in order: $\sigma = (\epsilon - \gamma)/T = 0.14$ ergs/deg./cm.^{2}

(17) A. Bondi, *Chem. Revs.*, **52**, 417 (1953).

For a monolayer such as octadecylamine (on various substrates) a treatment can be given similar to that reported above for Teflon. The resulting graph is similar to Fig. 1, with about the same scatter about a straight line fitting the equation $\cos \theta = 2\sqrt{24.4/\gamma_l} - 1$. Table III, with arrangement similar to Tables I and II, summarizes the treatment of the data of Shafrin and Zisman[15] for various liquids on a monolayer of octadecylamine. As in the case of column 5, Table II, the values of Φ were estimated on the basis of molecular structure, except for the perfluorinated hydrocarbons, for which the empirical value obtained with benzene vs. a perfluorinated lubricating oil[9] was used.

TABLE III

ESTIMATION OF SURFACE FREE ENERGY OF AN OCTADECYL-AMINE MONOLAYER, FROM CONTACT ANGLE DATA

Liquid	γ_l	$\theta,^a$ deg.	Approx. $\gamma_s{}^b$	Est. Φ for series	γ_s calcd. by eq. 6
Hexadecane	27.6	36	22.6		
Av., 6 alkanes			23.1	0.97	24.5
Dibutyl ether	22.8	8	22.6		
Av., 5 dialkyl ethers			23.6	.95	26.2
Ethylbenzene	29.0	26	26.2		
Av., 7 alkylaryl compounds			26.1	.95	28.9
Tricresyl phosphate	40.9	56	24.8		
Av., 9 esters			23.4	.9	28.9
Perfluorinated hydrocarbon FDG-329 (b. r. 130–180° at 76 cm.)	18.3	16	17.6		
Av., 3 high MW fluorocarbons			18.5	.85	31.5
Carbon tetrachloride	26.7	12	26.1		
Methylene iodide	50.8	60	28.5		
Av., 8 halogenated hydrocarbons			28.4	.9	35.1

^{a} Data of Shafrin and Zisman, ref. 15. ^{b} Approximate γ_s by the formula $\gamma_s = 0.25\,\gamma_l\,(1 + \cos\theta)^2$, i.e., assuming $\Phi = 1$.

It is interesting that the contact angle data for the n-alkanes and the di-n-alkyl ethers lead to markedly lower values of $\gamma_l(1+\cos\theta)^2/4\Phi^2$ than do the other liquids. (This is in obvious contrast to the last column of Table II.) This difference may be due to interaction between the liquid and the adsorbed monolayer, which might be called "monolayer penetration" (or, more metaphorically, "infiltration"), and an increase in the value of π_e, so that it cannot be neglected as in equation 6; cf. the discussion of Bartell and Ruch.[18] Compounds such as alkylbenzenes, CCl$_4$, fluorocarbons, etc., should be less able to enter a two-dimensional solution with the octadecylamine in the monolayer, than would n-alkanes or n-alkyl ethers.

From Table III, and in view of the discussion just given of "monolayer penetration," we may estimate the surface free energy of the octadecylamine-coated solid to be about 28 to 32 ergs/cm.^{2}, and probably close to 30.

While a treatment of this type could be carried out for all the contact angle data that are available, on a very wide variety of solids, we do not feel that such would be justified in this communi-

cation in view of the lack of precision in estimates of Φ that can be made at this time.

Discussion

The linear correlation observed by Zisman and co-workers for series of liquids on various solids, plotting $\cos\theta$ vs. γ_l, might at first sight be considered in conflict with our conclusions. An examination of the graphs of Zisman, et al., and a comparison with Fig. 1 (or similar graphs for other solids), show that the scatter of data is rather wide for both types of plots. The fit of data to a straight line is only a little better for the plot of $\cos\theta$ vs.$1/\sqrt{\gamma_l}$.[19] The scatter is no doubt due in part to the well known difficulties of contact angle measurement, particularly the hysteresis. But the differences in Φ's, to be expected among the various molecular types, should lead to various homologous series falling on more or less parallel lines. Different trends in Φ, for different series, should lead to different slopes of the lines for the various series. And trends in π_e, resulting from monolayer penetration for certain series of liquids, should lead to points for some series of liquids falling on lines of distinctly different slope, as was actually observed[5,15] by Zisman, et al. So within the experimental accuracy, and within the range of deviations expected owing to different values of Φ and of π_e a scatter of data is to be expected such that simple correlations of $\cos\theta$ vs.γ_l or vs.$1/\sqrt{\gamma_l}$ could well be just about as good, over the range of data available. Hence there is no conflict between the theory here presented and the correlation of Zisman, et al.; and indeed, this treatment adds support to Zisman's proposition that γ_c gives a measure of the surface tension of the solid.

Deacon[20] has proposed an interesting treatment of contact angle data, based on an analogous application of the theory of solution of non-electrolytes to the surface phases. We feel that the extension of solubility theory to the "surface phases" alone is not a correct treatment. Indeed, our treatment (which has the same basis in pair-interaction theory as does the solubility theory)[21–24] constitutes a first-order approximation, while Deacon launches into the second-order approximation without including the first-order term.

Hildebrand and Scott[24] reported a semi-empirical correlation of surface tension and solubility parameter

$$\delta = 4.1(\gamma/V^{1/3})^{0.43} \qquad (13)$$

If we ascribe a solubility parameter, δ_s, to the solid surface, then equation 5 can be put in the form

$$\delta_s = 2.05(\gamma_l/V_n^{1/3})^{0.43} \times \frac{(1 + \cos\theta)}{\Phi} \qquad (14)$$

The value that should be used for V_s for poly-

(18) (a) L. S. Bartell and R. J. Ruch, THIS JOURNAL, 60, 1231 (1956); (b) 63, 1045 (1959).

(19) But note that in Zisman's treatment, the slope is a freely adjustable variable, but not in our treatment.

(20) R. F. Deacon, Trans. Faraday Soc., 53, 1014 (1957).

(21) D. Berthelot, Compt. rend., 126, 1703, 1857 (1898).

(22) G. Scatchard, Chem. Revs., 8, 321 (1931).

(23) J. H. Hildebrand and S. E. Wood, J. Chem. Phys., 1, 817 (1933).

(24) J. H. Hildebrand and R. L. Scott, "Solubility of Non-Electrolytes," 3rd Ed., Reinhold Publ. Corp., New York, N. Y., 1950.

tetrafluoroethylene is uncertain, but using $V_8 = 100$, a solubility parameter of about 8.9 is obtained for the solid. This is of the right order of magnitude, being a bit higher than the values of δ for liquid fluorocarbons, which are in the range of 5.7 to 6.0 for substances such as perfluorononane and perfluorocyclohexane. Thus we must regard Deacon's linear correlation of $\gamma_l(1 - \cos\theta)$ with $V(\delta_l - \delta_s)^2$ as fortuitous and resulting from the narrow range of surface tensions in the homologous series he employed.

Conclusions

The treatment discussed above shows that it is possible to estimate the surface free energy of certain solids from a single measurement of the contact angle of a suitable liquid on the solid. The estimate will be reliable provided the liquid and solid constitute a "regular" system, as defined above, since then the value of the constant Φ in equations 5 to 8 can be estimated using equation 2 or a value no more than 10% below the value calculated by that equation. (For such systems, it usually turns out that π_e is negligible too—which fact further simplifies the estimation of the surface energy).

Conversely, equation 5 may be regarded as giving a complete phenomenological account of contact angles, in terms of three constants: the surface tension of the solid γ_s; the spreading pressure π_e; and the constant Φ. The latter may be estimated by equation 2, or empirically, from analogous liquid-liquid systems.

THE DIELECTRIC PROPERTIES OF MERCURIC CHLORIDE AND MERCURIC BROMIDE IN DIOXANE

By A. R. Tourky, H. A. Rizk and Y. M. Girgis

Department of Chemistry, Faculty of Science, University of Cairo, Egypt

Received August 17, 1959

Dielectric constant measurements on mercuric chloride and mercuric bromide in dioxane yield dipole moment values for the two halides comparable with those obtained in benzene indicating that dioxane behaves in this case as an inert solvent. The enthalpy of activation for dipole relaxation of the two compounds in dioxane are approximately 3.1 and 3.4 kcal., respectively. The dielectric loss decreases first in the frequency range 300–4000 kc./sec. due to d.c. conductivity and then increases toward maximum energy absorption at higher frequencies.

Dioxane has been used as an inert solvent for electric moment measurements of a number of compounds with which it does not form addition products.[1] Crenshaw[2] suggested that such addition compounds would be formed if the solutes were "mercury compounds," whereas Curran and Wenzke[3] found that the dipole moment of diphenylmercury in dioxane was equal to that determined by Hampson[4] in benzene and in decalin. Curran and Wenzke[3] also determined the dipole moments of mercuric chloride and mercuric bromide in dioxane and obtained values as low as 1.29 and 1.06 *D*, respectively. These values compare satisfactorily with the values 1.23 and 0.95 *D* subsequently determined by the present authors[5] in benzene.

This investigation has as its aim the determination of the enthalpy of activation for the dipole relaxation of these two halides in dioxane and the variation of the dielectric loss with frequency. Before so doing, it was deemed desirable to reevaluate their dipole moments in this solvent using the temperature solution method.

Experimental

Materials.—Dioxane of grade "AnalaR" was dried with successive portions of potassium hydroxide pellets and then refluxed with sodium until the latter remained bright. It was thereafter distilled from sodium through a long fractionating column. The fraction of constant boiling point 101.3° was used; it has the constants

$$d^{30}{}_4 = 1.02229 \text{ (g./cm.}^3\text{)}, \quad \epsilon_{30}{}^\circ = 2.2005, \quad n^{30}{}_D = 1.4179$$

Mercuric chloride was prepared by recrystallization of "AnalaR B.D.H." grade followed by thorough drying and then distillation under vacuum. Mercuric bromide was synthesized according to the method of Baker and Watson.[6]

Measurements.—The dielectric constant measurements were made with a superheterodyne apparatus. The crystal oscillator had a quartz crystal with a frequency 1800 kc./[7] sec., and the beats after amplification were made visible on a cathode ray tube. The precision condenser used for the dielectric constant determinations of the solutions, permitted fine adjustments and allowed a sensitivity of the order of 10^{-6}. The platinum foil in the test condenser was sealed on glass free of tension, namely, Ruhrglass, type AR. Calibration of the cell was made by liquids of standard dielectric constants. The dielectric loss ϵ'' was measured in a frequency range 300 to 5000 kc./sec. only, since higher frequencies were not available; the method employed was the difference substitution method and the sensitivity was of the order of 10^{-5}. The measurements of densities, composition of solutions, and the calculation of the polarization of solute at infinite dilution were made as previously described.[7]

(1) J. W. Williams, *J. Am. Chem. Soc.*, **52**, 1838 (1930).

(2) J. L. Crenshaw, *ibid.*, **60**, 2308 (1938).

(3) W. J. Curran and H. H. Wenzke, *ibid.*, **57**, 2162 (1935).

(4) G. C. Hampson, *Trans. Faraday Soc.*, **30**, 877 (1934).

(5) A. R. Tourky and H. A. Rizk, *Canad. J. Chem.*, **35**, 630 (1957).

(6) H. B. Baker and W. H. Watson, *J. Chem. Soc.*, **105**, 2530 (1914).

(7) A. R. Tourky and H. A. Rizk, THIS JOURNAL, **61**, 231 (1957).

TABLE I
MERCURIC CHLORIDE IN DIOXANE

w_2	ϵ_{12} 30°	40°	50°	d_{12} (g./cm.³) 30°	40°	50°	p_2 (cm.³) 30°	40°	50°
0	2.2005	2.1835	2.1665	1.02229	1.01120	1.00009	0.24249	0.23218	0.22707
.0018912	2.2020	2.1849	2.1677	1.02341	1.01234	1.00123	.23700	.23011	.22555
.0042286	2.2045	2.1869	2.1695	1.02540	1.01404	1.00277	.23515	.22956	.22589
.0051777	2.2057	2.1879	2.1704	1.02628	1.01484	1.00350	.23509	.22933	.22508
.0067445	2.2070	2.1891	2.1714	1.02731	1.01581	1.00445			

$M_2 = 271.52$ $\epsilon_{12} = \epsilon_1 + \alpha w_2$ $d_{12} = d_1 + \beta w_2$ $p_{12} = A + \gamma w_2$

$P_{2\infty}$ (graph.) 30°	40°	50°	$P_{2\infty}$ (Hedestrand) 30°	40°	50°	$P_{2\infty}$ (Palit–Banerjee) 30°	40°	50°
65.98	64.49	63.40	64.24	62.68	61.05	63.35	62.14	61.26

$\alpha = 0.96540 \quad 0.82743 \quad 0.72739$ $A = 0.27959 \quad 0.27977 \quad 0.27994$

$\beta = 0.74433 \quad 0.68374 \quad 0.64584$ $\gamma = -0.046259 \quad -0.050905 \quad -0.054321$

$P_{2\infty}$ 30°	40°	50°	$P_{2\infty} \times \frac{1}{T}$ 30°	40°	50°
64.52	63.10	61.90	0.21282	0.20149	0.19154

$$P_{2\infty} = A + (B/T); \quad A = 27.27; \quad B = 10606$$

	D^{P2} (cm.³) (R-Method)	μ (D.)	D^{P2} (cm.³) (T-Method)	μ (D.)
Bergmann and Engel[8]	30.36	...	...	...
Braune and Linke[9]	22.9	...	29.2	...
Curran and Wenzke[3]	...	1.29	...	...
Tourky and Rizk[7]	32.61	1.23	...	...
Present paper	...	...	27.27	1.31

TABLE II
MERCURIC BROMIDE IN DIOXANE

w_2	ϵ_{12} 30°	40°	50°	d_{12} (g./cm.³) 30°	40°	50°	p_2 (cm.³) 30°	40°	50°
0	2.2005	2.1835	2.1665	1.02229	1.01120	1.00009	0.20820	0.20840	0.20308
.0018214	2.2020	2.1850	2.1677	1.02367	1.01253	1.00135	.20708	.20326	.20344
.0024834	2.2024	2.1853	2.1680	1.02412	1.01298	1.00170	.20595	.20615	.20282
.0028526	2.2028	2.1857	2.1684	1.02445	1.01326	1.00203	.20515	.20321	.20106
.0043102	2.2040	2.1867	2.1693	1.02557	1.01430	1.00302	.20599	.20435	.20269
.0054364	2.2049	2.1875	2.1702	1.02642	1.01512	1.00389			

$M_2 = 360.44$

$P_{2\infty}$ (graph.) 30°	40°	50°	$P_{2\infty}$ (Hedestrand) 30°	40°	50°	$P_{2\infty}$ (Palit–Banerjee) 30°	40°	50°
75.69	75.15	74.61	74.43	74.52	72.90	75.64	74.03	73.26

$\alpha = 0.80629 \quad 0.74544 \quad 0.66176$ $A = 0.27959 \quad 0.27977 \quad 0.27994$

$\beta = 0.75759 \quad 0.72074 \quad 0.68611$ $\gamma = -0.069724 \quad -0.074373 \quad -0.076697$

$P_{2\infty}$ 30°	40°	50°	$P_{2\infty} \times \frac{1}{T}$ 30°	40°	50°
75.25	74.57	73.59	0.24821	0.23811	0.22771

$$A = 52.27; \quad B = 6818.2$$

	D^{P2} (cm.³) (R-Method)	μ (D.)	D^{P2} (cm.³) (T-Method)	μ (D.)
Bergmann and Engel[8]	55.30	...	...	...
Braune and Linke[9]	29.3	...	36.5	...
Curran and Wenzke[3]	...	1.06	...	...
Tourky and Rizk[7]	60.49	0.95	...	...
Present paper	...	...	52.27	1.05

The viscosities were measured by the Ostwald–Poiseuille apparatus. The working temperatures were 30, 40 and 50° ± 0.002°. Dipole moments were calculated by Debye's equation $P_2 \infty = A + B/T$ using the method of least squares.

On the basis of precisions of ±0.0005 in dielectric constants (the individual values of ϵ were reproducible to ±0.00005), ±0.0001 in densities and ±0.1% in solution concentrations, the dipole moments are believed reliable to ±0.03 D.

The data obtained together with those of previous authors are shown in Tables I and II.

(8) E. Bergmann and L. Engel, Z. physik. Chem., B13, 247 (1931).

(9) H. Braune and R. Linke, ibid., B13, 12 (1935).

Discussion

The experimental result that mercuric chloride and mercuric bromide have dipole moments from dielectric constant measurements in dioxane very near to those in benzene, indicates that dioxane as a solvent produces no special effect on these halides. If, however, addition products were formed, much higher dipole moment values would have been obtained. This point was emphasized by Curran[10]

(10) W. J. Curran, J. Am. Chem. Soc., 64, 830 (1934).
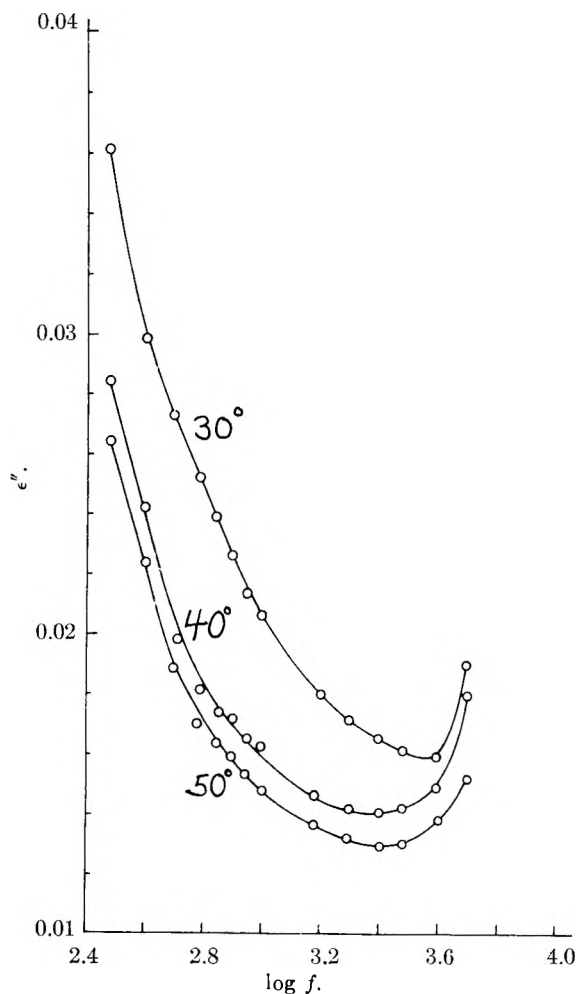
Fig. 1.—Variation of ϵ'' with log f for mercuric chloride in dioxane ($w_2 = 0.0018912$).
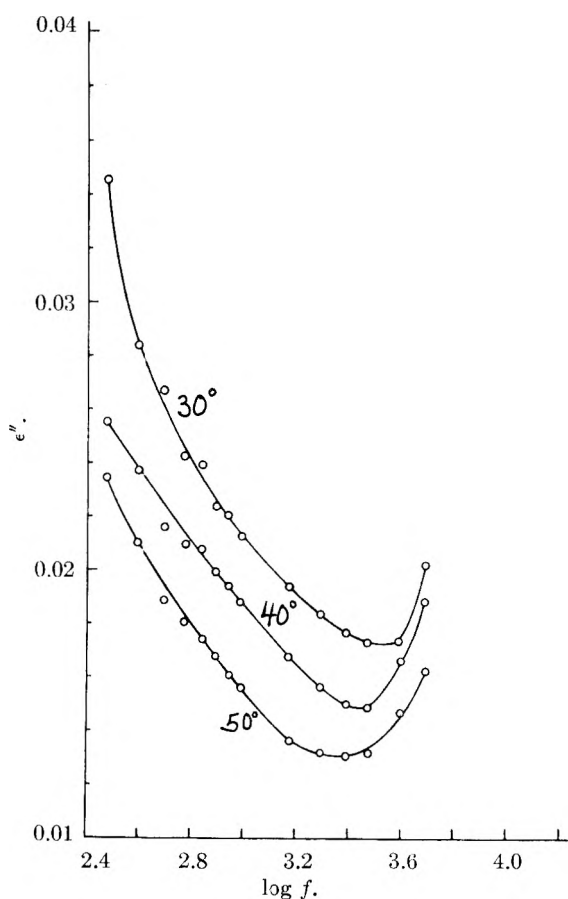
Fig. 2.—Variation of ϵ'' with log f for mercuric bromide in dioxane ($w_2 = 0.0028526$).

in investigating the dipole moments of organometallic halides in dioxane.

To get approximate values of the relaxation time from viscosity measurements, Debye's equation[11] ($\tau = 8\pi\eta a^3/2KT$) was employed. The results obtained are

	HgCl₂ ($w_2 = 0.0018912$)			HgBr₂ ($w_2 = 0.0024834$)		
	30°	40°	50°	30°	40°	50°
$\eta \times 10^5$ (poise)	1079	957	854	1072	923	822
$\tau \times 10^5$ (sec.)	3.3	2.8	2.4	3.3	2.7	2.3

The decrease of τ with temperature evidently is due to an increase of randomness of motion, so that a decrease in dipole orientation takes place. The gradient[12] of the plot ln τ vs. $1/T$, gives an approximate value of ΔH of 3.1 kcal. for mercuric chloride and of 3.4 kcal. for mercuric bromide.

Representative curves for the frequency variation of the dielectric loss in the range 300–5000

kc./sec. for the compositions $w_2 = 0.0018912$ (HgCl₂) and $w_2 = 0.0024834$ (HgBr₂) at 30, 40 and 50°, are shown in Fig. 1 and 2. The observed decrease in ϵ'' with increase of frequency till about 4000 kc./sec. at each temperature in both cases, cannot be in any way connected to the relaxation process of dipole orientation, and it is probably due to a d.c. conductivity which may arise from the dielectric properties of the mixed medium. After acquiring a minimum value at about 4000 kc./sec. the loss increases, thus indicating the start of disappearance of orientation polarization at this point. The increase of ϵ'' in the range 4000–5000 kc./sec. is lower at 50 than at 40 or 30°. This is because the increase of temperature increases the agitation of molecules, and consequently the relaxation of the dipoles begins at higher rather than smaller values of frequency. The decrease of ϵ'' with increase of temperature is due to the increase in the freedom of dipole orientation, which thus gives rise to a decrease in the phase lag or the energy absorption.

(11) P. Debye, Trans. Faraday Soc., 30, 679 (1934).

(12) S. Glasstone, K. J. Laidler and H. Eyring, "Theory of Rate Processes," McGraw-Hill Book Co., New York, N. Y., 1941.

THE CHARGE EFFECT IN SEDIMENTATION[1]

By Jack H. Tremaine[2,3] and Max A. Lauffer

Department of Biophysics,[4] University of Pittsburgh, Pittsburgh 13, Pennsylvania

Received August 28, 1959

A detailed experimental study was carried out on Southern bean mosaic virus (SBMV) for the purpose of investigating the charge effect in sedimentation. This material was chosen because its particles are essentially spherical; it is moderately stable; it has a relatively large sedimentation rate; and it can be obtained without extreme difficulty. The effects of pH, ionic strength and concentration on the sedimentation rate were studied. Auxiliary measurements were made on electrophoretic mobility and valence. All of these data were analyzed in terms of existing theories of the charge effect. The most widely known equation, that of Tiselius, seriously underestimated the effect observed in the present study. The increase of the charge effect with virus protein concentration was linear as predicted. The theory of Booth predicted an unrealistically small charge effect. Furthermore, the prediction of variation of the charge effect with concentration of colloidal material did not agree with the experimental results.

Introduction

The generation of an electric field when a suspension of glass beads is allowed to settle was observed by Dorn[5] in 1880. Presumably the negatively charged glass beads sediment faster than the partner cations, establishing an electric field in the solution.

Smoluchowski[6] derived an equation predicting the magnitude of the electric field generated by sedimentation of charged particles. He also noted that this field would reduce the sedimentation velocity of the charged particles, and derived an equation for this charge effect.

Tiselius[7] derived an equation for the primary charge effect in sedimentation

$$s' = s \left[1 - \frac{\sigma v n F}{k_s} \right]$$

where s' is the sedimentation rate of the charged particle, and s is the sedimentation rate of the uncharged particle, σ and v are the valence and electrophoretic mobility of the particle, n is the concentration of the particle in moles/ml., F is the faraday constant, and k_s is the specific conductivity of the solution. The equation was found to agree with experimental data obtained with phykoerythrin.

Pedersen[8] studied the charge effect on the sedimentation rate of egg albumin and of bovine serum albumin. He found that the primary charge effect was inversely related to the conductivity of this solution and directly related to the concentration of protein, as predicted by the Tiselius equation.

By a consideration of the dipole field which arises from a distortion of the ionic atmosphere of a charged particle when the particle is sedimented away from its ionic atmosphere, Booth[9] derived an equation predicting the magnitude of the charge

effect on the sedimentation velocity of a single particle. Solution of this equation for a suspension of many particles is possible when the sedimenting boundary is an infinitely thin sheet. An approximation of this condition might be obtained in the cell of the analytical ultracentrifuge.

The purpose of the present investigation was to study the magnitude of the charge effect, to measure the parameters involved in the Tiselius and Booth equations and in this manner to test the validity of these equations. The colloidal particle employed was chosen for several reasons. The secondary charge effect, which is independent of the sedimentation rate of the colloidal ion,[8] was considered to be small in comparison with the large primary effect attributable to the high sedimentation rate of SBMV, the particles of which are known to be essentially spherical. Information concerning the sedimentation rate, partial specific volume and molecular weight is available.[10,11]

Materials and Methods

Preparation of Concentrated Southern Bean Mosaic Virus (SBMV).—The virus nucleoprotein was prepared from infected *Phaseolus vulgaris* L. variety Bountiful bush bean plants which had been ground and frozen at the time of harvesting.

The purification procedure was adapted from the centrifugation procedure of Price[12] and the chromatographic procedure of Shainoff and Lauffer.[13] Plant juice expressed from thawed material was clarified in a Servall angle centrifuge (15 minutes at 5,000 r.p.m). and then concentrated in a Spinco model L centrifuge (three hours) at 20,000 r.p.m. in a No. 20 rotor. The pellets were resuspended in 0.1 ionic strength phosphate buffer at pH 6.7 and then subjected to two cycles of alternate clarification and sedimentation. A dark brown pigment was observed in the virus preparation after this centrifugation procedure. The pigment was removed from the virus preparation by column chromatography. A column of Amberlite CG 400 ion-exchange resin was adjusted to a pH of 6.70 with a buffer composed of 0.008 M phosphate and 0.064 M sodium chloride. The pigmented virus preparation was adsorbed onto the column, and a white virus solution was eluted with the buffer, leaving the pigment adsorbed to the column.

Before each sedimentation coefficient determination, the virus solution was dialyzed against the buffer used in the experiment. After the dialysis, the preparation was clarified by low speed centrifugation, filtered, and the preparation was divided into three samples. One sample was centrifuged to determine the sedimentation rate of the virus; one was

(1) Presented at the 131st meeting of the American Chemical Society, Miami, Florida, April 7–14, 1957.

(2) Canada Department of Agriculture, Science Service, on educational leave-of-absence during the course of this work.

(3) Abstracted from a thesis submitted by J. H. T. to the Graduate School of the University of Pittsburgh in partial fulfillment of the requirements for the degree, Doctor of Philosophy.

(4) Publication No. 73 of the Department of Biophysics.

(5) E. Dorn, *Ann. Physik*, **10**, 46 (1880).

(6) M. V. Smoluchowski, *Graetz Handbuch der Elektrizität und des Magnetismus Leipzig*, **2**, 385 (1921).

(7) A. Tiselius, *Kolloid Z.*, **59**, 306 (1932).

(8) K. O. Pedersen, referred to in "The Ultracentrifuge," Oxford University Press, 1940, p. 26; This Journal, **62**, 1282 (1958).

(9) F. Booth, *J. Chem. Phys.*, **22**, 1956 (1954).

(10) G. A. Miller and W. C. Price, *Arch. Biochem.*, **10**, 467 (1946).

(11) M. A. Lauffer, N. W. Taylor and C. C. Wunder, *Arch. Biochem. Biophys.*, **40**, 453 (1952).

(12) W. C. Price, *Am. J. Botany*, **33**, 45 (1946).

(13) J. R. Shainoff and M. A. Lauffer, *Arch. Biochem. Biophys.*, **64**, 315 (1956).

used to determine the specific conductivity of the solution, and the remaining sample was used for pH determination at 15 minute intervals during the centrifugation of the first sample. To complete the experiment, density and concentration measurements were made on the pooled samples.

Ultracentrifugation Studies.—Sedimentation studies on SBMV nucleoprotein were carried out in a Spinco Model E ultracentrifuge at room temperature. The temperature of each run was taken as the mean of the initial and final temperatures of the rotor as determined with a thermocouple. The difference was usually less than 0.5°. Sedimentation rates were corrected to a standard state, $s^{20}w$, by the usual method employing an apparent partial specific volume of 0.700 reported by Lauffer, et al.[11]

Density and Viscosity.—The densities of all the solutions studied in the ultracentrifuge were determined with a 2-ml. pycnometer at two temperatures above and below the average temperature of the centrifuge run.

Viscosities of the solvents were determined in an Ostwald–Cannon viscometer. The viscometer was calibrated with water at 20, 25 and 30° and the relationship determined that $\eta = 1.773 \times 10^{-2} \, dt$, where d is the solution density and t is the outflow time.

The viscosity of the solvent and density of the solution at the temperature of the centrifuge run were determined by interpolation from measurements above and below that temperature.

pH and Conductivity.—The pH measurements were made using a Beckman glass electrode model G pH meter. These measurements were made at room temperature on one sample of virus solution every 15 minutes during the centrifugation of another sample. After the centrifugation of the first sample, the pH of the virus solution in the centrifuge cell was measured with a one-drop electrode assembly. The pH value used in the calculations was the arithmetic mean of the pH values found for all the measurements of both samples.

The pH measurements made on the virus solution in a single run never varied more than 0.07 of a pH unit. The fluctuation in the pH measurements produces rather large differences in the product of valence and electrophoretic mobility, but greater pH control cannot be obtained easily with low ionic strength buffers because of the low buffering capacity.

Conductivities were measured on other samples with a Shedlovsky cell and a model RC1B conductivity bridge, manufactured by Industrial Instruments, Incorporated. This apparatus was calibrated using standard KCl solutions and has a cell constant of 12.20 cm.$^{-1}$. The conductivity measurements have an error of less than 3%.

The conductivity of the solution at the average temperature of the centrifuge run was interpolated from the values at temperatures above and below.

Electrophoretic Mobility and Valence.—The variation of electrophoretic mobility with pH of SBMV solution at 0.002 ionic strength was determined in a Spinco electrophoresis apparatus. Samples having a nucleoprotein concentration of approximately 0.7 % were dialyzed for at least 24 hours with two changes of buffer. Subsequent conductivity measurements showed no significant differences between samples and dialysate for any of the samples. Conductivity measurements were made at 25° although the electrophoresis water-bath was maintained at 0.9°. The mobility is reported at 25° since sedimentation rate determinations were made at room temperature. Watanabe, et al.,[14] found an error of approximately 10% by the use of this procedure with horse serum albumin at pH 7.7. The pH was determined at room temperature (approximately 25°) with a Beckman Model G pH meter.

The virus was titrated to determine the valence of the nucleoprotein in the pH range employed in sedimentation studies.

The virus solution was dialyzed five days against distilled water with three changes of dialysate. The virus solution was removed from the dialysis bag and split into three 5-ml. aliquots. The pH of one of the 5-ml. aliquots was measured after the addition of 0.1-ml. portions of 0.01 N NaOH. This procedure was repeated with another 5-ml. aliquot employing 0.01 N HCl. The remaining aliquot was employed to determine the concentration of the virus (grams/unit volume) by measuring the refractive index differences between

the virus solution and the dialysate. An additional titration in 0.002 ionic strength NaCl was carried out in the same manner.

The number of OH$^-$ or H$^+$ ions bound per virus particle was calculated by the following method. The concentration of SBMV in moles/liter [V] was determined by employing a molecular weight[11] of 6.1 × 10^6. The concentration of free OH$^-$ or [OH]$_F$ (moles/liter) was calculated from the observed pH. The concentration of free and bound OH$^-$ or

$$p(\mathrm{OH}) = 14.00 - p\mathrm{H} = -\log\ [\mathrm{OH}]_F\,{}^{15}$$

[OH]$_{F\,+\,B}$ (moles/liter) was calculated from the volume (V_a) and titer, 0.01 N, of added NaOH and the total volume of virus solution after addition of NaOH (V_t).

$$[\mathrm{OH}]_{F\,+\,B} = \frac{0.01 V_a}{V_t}$$

The base bound [OH]$_B$ moles/liter was determined by subtracting [OH]$_F$ from [OH]$_{F\,+\,B}$. The number of OH$^-$ ions bound per particle was obtained from the base bound and the molar concentration of virus present. A similar method of calculation was employed in the acid titration.

Determination of Virus Nucleoprotein Concentration.—Virus concentrations were determined by differential refractometry. The refractive index difference between the virus solution and the dialysate was determined for each experiment. The concentration of the virus in the solution in g./100 ml. was obtained by dividing this refractive index difference by the specific refractive increment, i.e., the refractive index difference between the solvent and a solution containing 1 g. of virus per 100 ml. of solution.

Two determinations of the specific refractive increment were made on the virus preparation. Values of 0.00176 and 0.00173 (100 ml./g.) were found. A value of 0.00175 was used during the present study. The results are in good agreement with the specific refractive increments of nearly all proteins and of nucleic acids, which were found[17] to lie within 10% of a mean value of 0.0018.

Results

Variation of Electrophoretic Mobility with pH.— A study of the variation of electrophoretic mobility with pH was made for SBMV using phosphate buf-

TABLE I

THE MOBILITY OF SBMV IN 0.002 IONIC
STRENGTH PHOSPHATE BUFFERS

pH	Electrophoretic velocity, cm./sec. × 10^{-4}	Field strength, v./cm.	Mobility, cm.^{2}/v. sec. × 10^5
5.60	+4.36	8.19	+5.32
6.00	0	. . .	0
6.28	−3.07	8.90	−3.45
6.45	−4.99	7.90	−6.32
6.50	−6.18	8.63	−7.16
6.75	−8.80	9.41	−9.35
7.20	−11.65	9.48	−12.29
7.50	−13.48	8.61	−15.65

(15) The titration herein reported covered the pH range from 5.95 to 7.62, a range in which binding is almost complete. Since the amount bound is the amount added minus that remaining free and since only the very small concentration of unbound H$^+$ or OH$^-$ is determined from the pH measurement, it is obvious that the simple procedure here used is entirely adequate. At extreme pH values, where the fraction of added H$^+$ or OH$^-$ bound is low, it is obvious that activity coefficients, liquid junction electromotive forces and glass electrode errors must be determined and used to calculate the concentration of unbound H$^+$ or OH$^-$ from pH measurements. Tanford[16] has considered this matter critically and has stated that such corrections should be applied at pH values below 4 and above 10. Since no measurements were made in these pH ranges, these precautions were not necessary in the present study.

(16) C. Tanford, in "Electrochemistry in Biology and Medicine," edited by T. Shedlovsky, 1955, p. 248.

(17) P. Doty and J. T. Edsall, Advances in Protein Chem., 6, 54 (1951).

(14) I. Watanabe, N. Ui and M. Nakamura, THIS JOURNAL, 54, 1366 (1950).

fers of 0.002 ionic strength. The pH was limited to the range of the sedimentation studies.

The resulting values of the mobility of SBMV are given in Table I. As discussed previously, the mobility is reported at 25°.

The Titration of SBMV.—The results of the acid–base titration of SBMV in distilled water are presented in Table II. The virus nucleoprotein concentration was 1.48 × 10⁻⁶ mole/liter. The titration carried out in 0.002 ionic strength NaCl yielded within experimental error the same change in H⁺ or OH⁻ bound per unit change in pH.

TABLE II

THE TITRATION OF SBMV

V_a, ml.	pH	V_t, ml.	[H]F or [OH]F, moles/l. × 10⁸	[H]F+B or [OH]F+B, moles/l. × 10⁴	[H]B or [OH]B, moles/l. × 10⁴	H⁺ or OH⁻ ions bound per virus particle
0.05	5.95	5.05	112	0.990	0.979	66
0	6.17	5.00	0	0	0	0
.05	6.35	5.05	2.24	0.990	0.990	67
.10	6.56	5.10	3.63	1.961	1.961	133
.15	6.87	5.15	7.41	2.913	2.912	197
.20	7.30	5.20	19.95	3.846	3.844	260
.25	7.62	5.25	41.69	4.762	4.758	321

The isoelectric point was determined to be 6.00 in 0.002 ionic strength phosphate buffers. The surface charge, σ,[18] employed in testing the Tiselius and Booth charge effect equations at a particular pH value was taken to be the algebraic difference between the number of ions bound per virus particle interpolated from the data of Table II for that pH and the number interpolated from the data of Table II for the isoelectric point, pH 6.00.

Sedimentation Studies.—The results of sedimentation studies on SBMV in buffers of various pH and ionic strength values and at various concentrations are shown in Table III. Analyses of the data employing the Tiselius and Booth equations are also presented in Table III.

1. Sedimentation Studies on SBMV in 0.1 Ionic Strength Phosphate Buffers.—Miller and

(18) The valence calculated from titration curves is not necessarily the true valence because proteins bind ions other than hydrogen. Hartman and Lauffer[19] showed that the isoelectric point of Southern bean mosaic virus in phosphate buffers varies strongly with ionic strength. The most probable interpretation is that the virus protein selectively binds negative ions. Our method of determining valence, however, eliminates a large fraction of this potential error because we employ as valence the difference between the number of hydrogen ions bound at a given pH and the number bound at the isoelectric point in a buffer with the same ionic strength. Any errors in the valence due to ion binding then must be due to changes in other ion binding as a function of pH. While data relative to this question are scanty, the studies of Scatchard, et al.,[20] indicate that in sodium chloride solutions with an ionic strength of 0.002 the change in chloride binding by human serum albumin is probably only a few per cent. of the change in hydrogen ion binding when the pH is altered. This result gives us confidence that the valences determined by our method are not grossly different from true valences.

True valence should be less than valence determined from hydrogen ion binding alone. The results of Scatchard, et al., confirm this expectation. Thus, if our valences are in error, they are probably too large. Accordingly, any probable error in the valence cannot be the reason for the failure of the theories under consideration to predict correct charge effects.

(19) R. E. Hartman and M. A. Lauffer, J. Am. Chem. Soc., **75**, 6205 (1953).

(20) G. Scatchard, I. H. Scheinberg and S. H. Armstrong, ibid., **72**, 535 (1950).

Price[10] carried out sedimentation studies on SBMV at various virus nucleoprotein concentrations in 0.1 M phosphate buffer. They obtained data fitting the equation

$$\frac{1}{s^{20}\text{w}} = 0.00047c_0 + 0.00866$$

where $s^{20}\text{w}$ is the sedimentation coefficient of SBMV corrected to 20° and c_0 is the initial virus nucleoprotein concentration in g./100 ml. Sedimentation data obtained by Lauffer, et al.,[11] with SBMV in 0.1 M phosphate and acetate buffers were found to agree with this equation and indicated no variation in $s^{20}\text{w}$ with pH.

Sedimentation experiments were carried out in 0.1 ionic strength buffers at pH 7.00 and 6.70 on the preparation of SBMV used in this investigation. The results, runs 1 and 3 shown in Table III, are not significantly different from those obtained by Miller and Price.

To ascertain the magnitude of the charge effect in subsequent experiments in low ionic strength buffers, the sedimentation coefficient of the charged particle must be compared with the sedimentation coefficient of the uncharged particle. The sedimentation coefficient of SBMV in 0.1 M buffers was assumed to be the same as the sedimentation coefficient of the uncharged particle. This assumption is justified, because Lauffer, et al.,[11] found no variation with pH of the sedimentation coefficient in 0.1 M buffers.

2. The Effect of Virus Nucleoprotein Concentration upon the Sedimentation Coefficient of SBMV in 0.002 Ionic Strength Phosphate Buffers.—Sedimentation experiments were carried out on virus solutions containing 1 to 4% nucleoprotein in pH 6.90 phosphate buffer at 0.002 ionic strength to study the effect of virus nucleoprotein concentration upon the reduction of the sedimentation coefficient. The results are presented in Table III, runs 6, 10, 13, 14, 15, 17 and 18. As the concentration of virus nucleoprotein increased, the sedimentation coefficient decreased.

A measure of the charge effect can be obtained by calculating $1 - s'/s$ where s' is the observed sedimentation coefficient and s is the sedimentation coefficient when the charge effect is absent for the same initial virus nucleoprotein concentration. It was assumed that s'/s at temperature T is equal to $s^{20'}\text{w}/s^{20}\text{w}$. $s^{20'}\text{w}$ values are shown in Table III. $s^{20}\text{w}$ values were taken for the corresponding initial virus concentrations from the data of Miller and Price[10] obtained with 0.1 M buffers.[21] Variation of $1 - s'/s$ with initial virus nucleoprotein concentration is illustrated in Fig. 1. The plot is linear and extrapolates to zero charge effect at infinite virus dilution.

3. The Effect of pH of Virus Solution upon the Sedimentation Coefficient in 0.002 Ionic Strength

(21) This procedure is valid to the extent that lowering ionic strength causes no change in volume, shape, non-ionic interaction, etc. The fact that the sedimentation rate of the virus protein in 0.002 ionic strength buffer at the isoelectric point (Fig. 2) is the same as that in high ionic strength buffers for the same virus protein concentration supports the validity of this procedure. The assumption that s'/s at temperature T is equal to $s^{20'}\text{w}/s^{20}\text{w}$ is as valid as the universally used method of correcting sedimentation coefficients to water at 20°.

TABLE III

A COMPARISON OF THE EXPERIMENTAL AND PREDICTED CHARGE EFFECT IN SOLUTIONS OF SBMV

Run	T, °C.	pH	Initial virus nucleoprotein concn. g./100 ml.	Specific conductivity mho/cm. $\times 10^{-4}$	$s^{20}{}'_w$	σv_{te} cm.^{2} v.-sec. $\times 10^4$	σv_s cm.^{2} v.-sec. $\times 10^4$	$\sigma v_s/\sigma v_{te}$ ratio	$-q_3{}^*v_3{}^*$ (b) $\times$ 10^3	$q_3{}^*81\beta\varphi S_3{}^{*2}$ (b) b^{-2} $\times 10^3$
1	23.9	7.00	1.81	50.0	103.8					
3	25.6	6.70	4.90	50.0	95.0					
4	24.6	7.45	3.97	1.93	70.8	524	893	1.71	5.35	2.55
5	26.0	7.20	3.79	2.14	74.4	430	898	2.09	4.82	2.30
16	24.0	7.10	1.65	1.47	91.9	365	958	2.62	7.02	1.40
11	25.0	7.00	3.91	1.64	67.2	327	881	2.70	6.26	2.95
12	26.7		3.38	1.74	74.2	339	992	2.72	5.90	2.41
19	26.1		2.89	3.52	85.7	230	1258	5.48	5.66	1.53
6	26.3	6.90	3.70	1.87	74.7	288	831	2.88	5.51	2.45
10	24.7		4.04	1.50	69.9	278	665	2.39	6.85	3.33
13	24.0		3.10	1.64	79.6	274	752	2.74	6.26	2.33
14	26.5		2.65	1.95	86.1	290	812	2.80	5.28	1.69
15	25.8		2.07	1.94	90.9	285	878	3.08	5.31	1.33
17	25.9		1.57	1.78	93.2	286	1040	3.48	5.77	1.09
18	26.1		0.96	1.66	102.8	287	904	3.15	6.20	0.72
20	26.5		2.90	3.74	88.2	199	1145	5.76	5.33	1.04
21	25.3		2.77	2.62	86.0	237	997	4.21	5.84	1.39
7	23.5	6.63	3.69	1.67	80.3	156	550	3.54	6.17	1.97
8	24.0	6.25	3.75	1.66	95.2	34	22	0.65	6.20	2.02

Phosphate Buffers.—Sedimentation experiments were carried out on virus solutions containing approximately 3.7% nucleoprotein in buffers of pH 6.25 to 7.45 and 0.002 strength. The results are presented in Table III, runs 4, 5, 6, 7 and 8. Higher values of pH were found impossible to maintain. Lower values of pH caused precipitation of the virus. At higher pH values, a greater reduction of the sedimentation coefficient was observed. The reduction decreased as the isoelectric point was reached. In Fig. 2, the experimental values of $1 - s'/s$ are plotted as a function of pH.

4. The Effect of Specific Conductivity of SBMV Solution upon the Sedimentation Coefficient.—Sedimentation experiments were carried out on SBMV solutions in pH 6.90 and 7.00 phosphate buffers of increasing ionic strength. The results are presented in Table III, runs 1, 3, 11, 12, 14, 19, 20 and 21. As the conductivity increased, the sedimentation rate increased in every case. The appropriate data are plotted in Fig. 3.

Discussion

The Tiselius Equation.—One of the main objectives of this research was to test the Tiselius equation, which relates the primary charge effect to the pH, conductivity and concentration of the virus solution. One obvious way to accomplish this end is to hold two of the three independent variable constants and measure

$$1 - \frac{s'}{s}$$

as a function of the third. This was attempted and the appropriate results are summarized in the Experimental section. However, in all cases the results suffer from lack of constancy of the restrained variables.

Because of the sector-shape of the cell, the con-
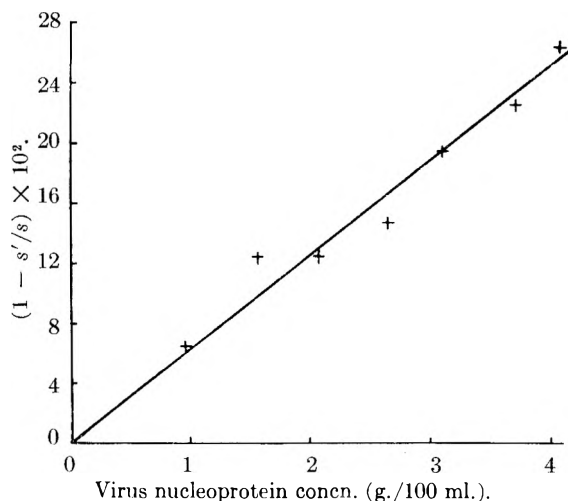
Fig. 1.—The variation of the primary charge effect ($1 - s'/s$) with the initial concentration of virus nucleoprotein in 0.002 ionic strength buffer at pH 6.90.

centration is a function of the boundary position[22] according to the equation

$$\frac{c_0}{c_t} = \left(\frac{x_0}{x_t}\right)^2$$

where c_0 and c_t are the concentrations initially and at time t and x_0 and x_t are the corresponding boundary positions. This concentration change with cell boundary position affects the sedimentation coefficient in low ionic strength buffers in two ways. In addition to the effect described by Lauffer,[23] there is also the concentration dependent charge effect described here.

It can be shown that for the case in which the total variation of s' with c can be described by the equation

(22) T. Svedberg and H. Rinde, *J. Am. Chem. Soc.*, **46**, 2677 (1924).
(23) M. A. Lauffer, *ibid.*, **66**, 1195 (1944).
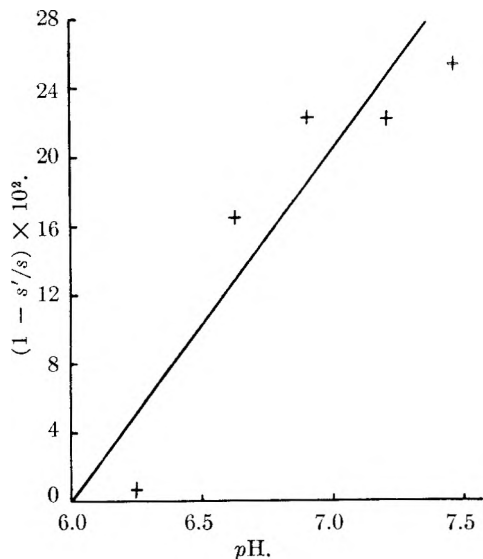
Fig. 2.—The variation of the primary charge effect $(1 - s'/s)$ with the pH of the virus solution in 0.002 ionic strength buffers.
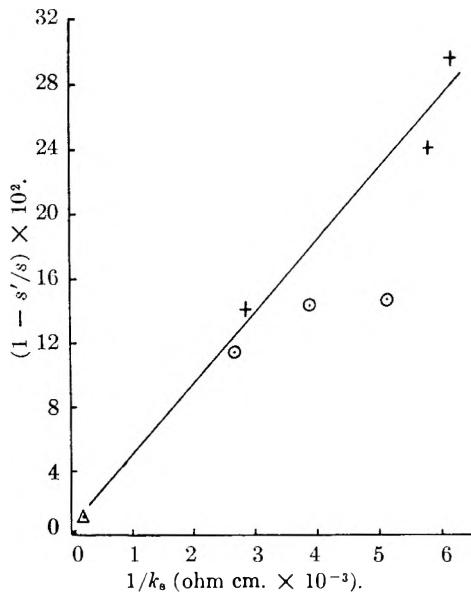
Fig. 3.—The variation of the primary charge effect $(1 - s'/s)$ with the specific conductivity of the virus solution. Experimental points designated by $+$ were obtained at pH 7.00 and the points designated by $\bigcirc$ were obtained at pH 6.90. The point $\triangle$ represents measurements made at 0.1 ionic strength which were independent of pH.

$$s' = s(1 - kc)$$

where k is a constant, the exact integrated form of the dependence of x upon t is

$$\ln x^2 - kc_0x_0^2 = \ln (x_0^2 + kc_0x_0^2) + 2sw^2t$$

where w is the angular velocity. For values of k which are appropriate to the experimental data presented in this paper, the plot of $\ln x$ against t deviates only very slightly from linearity. Experimental plots of $\ln x$ against t were not observed to deviate from linearity. It can be shown mathematically that, if a representative value of s' is calculated from such a graph by employing the formula

$$s' = \frac{1}{w^2} \left(\frac{\ln x_2 - \ln x_1}{t_2 - t_1} \right)$$

where x_1 and t_1 are the boundary position and time at the first measurement after the centrifuge is at speed and x_2 and t_2 are the boundary position and time at the last measurement employed, this sedimentation coefficient corresponds with a satisfactory degree of approximation to a concentration calculated by the formula

$$c = \frac{c_0x_0^2}{2} \left(\frac{1}{x_1^2} + \frac{1}{x_2^2} \right)$$

This concentration was employed in the subsequent analysis of the data. However, for the purpose of evaluating $s^{20}{}_w$ in

$$\left(1 - \frac{s^{20\prime}{}_w}{s^{20}{}_w} \right)$$

c_0 was used because the result of Miller and Price[10] expresses $s^{20}{}_w$ as a function of c_0.

To circumvent the lack of constancy of the two restrained variables, a more sophisticated test was carried out. The product, σv_s, was determined by the Tiselius equation employing s', s, n and k_s values obtained in each run. This value was compared with the product of valence σ, obtained by titration, and electrophoretic mobility v, obtained by electrophoresis, denoted as σv_{te}. The electrophoretic mobility measurements were corrected for viscosity to the temperature of the centrifuge run. The electrophoretic mobility measurements in runs 19, 20 and 21 were corrected to the ionic strength of the buffer.[24]

The ratio

$$\sigma v_s / \sigma v_{te}$$

was approximately 1.7 to 5.7. Since the errors in valence and mobility determinations are not of this order of magnitude, it was concluded that the theory underestimated the charge effect.[25] The highest ratios occurred at intermediate conductivities (runs 19, 20 and 21) and at low pH values (except run 8).

The Booth Equation.—Booth's equation[9] can be written

$$s' = s \left[1 + d_2 \left(\frac{\zeta e}{kT} \right)^2 \right]$$

where e is the electronic charge, ζ is the electrokinetic potential, k is the Boltzmann constant, and T is the absolute temperature. The value of d_2 is

$$q_3^*(V_3^*(b) - 81\beta\varphi S_3^{*2}(b)b^{-2})$$

where b is the product of the Debye-Hückel parameter K, and the radius of the particle r; $V_3^*(b)$ and $S_3^*(b)$ are functions of b given in Fig. 1 of Booth's paper[9]; β is a constant of value $8(\pi/3)$ for sedimentation in which the sedimenting boundary is a thin horizontal sheet; φ is the volume fraction of solute and q_3^* is

(24) D. C. Henry, Proc. Roy. Soc. (London), **A133**, 106 (1931).

(25) One could defend the proposition that v in the Tiselius equation should be the mobility at the concentration c characteristic of the sedimentation experiment. Little is known about the variation of v with c in general and no data are available for SBMV in particular. However, what studies are available indicate that v varies inversely with c. If this is true, the mobilities used in the calculation of σv_{te} were in all cases too high. Therefore, the correct values of σv_{te} should be even lower than those recorded in Table III and the true discrepancy between theory and observation should be even greater than that indicated.

$$\frac{DkT \ \Sigma \ n_i z_i v_i{}^{-1}}{e^2 \pi \eta \ \Sigma \ n_i z_i{}^2}$$

where D and η are the solvent dielectric constant and viscosity, and n_i, z_i and v_i are the concentration, valence and mobility of the ions in solution. If we assume that all of the ionic mobilities are equal, then according to Booth (see page 1966, equation 5.10 of Booth's publication[9])

$$1/k_a = \frac{\Sigma \ n_i z_i v_i{}^{-1}}{e^2 (\Sigma \ n_i z_i{}^2)^2}$$

and $q_3{}^*$ reduces to

$$\frac{DkT \ \Sigma \ n_i z_i{}^2}{\pi \eta k_a}$$

As can be seen in Table III, the value of the portion of d_2 which is independent of concentration of SBMV

$$q_3{}^* V_3{}^*(b)$$

was found by computation to be greater than the portion of d_2 which is dependent on virus concentration

$$q^*{}_3 81 \beta \varphi S_3{}^{*2}(b) b^{-2}$$

This result is inconsistent with the experimental data shown in Fig. 1.

The zeta potential is employed in the Booth charge effect equation.[9] The zeta potential can be calculated from the electrophoretic mobility by means of the Henry equation[21] or of the more elaborate Booth electrophoresis equation.[26] These and other equations assert that the mobility is proportional to $D\zeta/\eta$. The mobilities recorded in the present study fall in the range in which the Booth equation reduces to the Henry equation. Because of the fact that η in the neighborhood of a charged particle is probably greater than that of

(26) F. Booth, *Proc. Roy. Soc. (London)*, **A203**, 514 (1950).

the solvent in bulk, such calculation underestimates ζ.

The potential at the surface of a charged sphere, which is related to ζ but always greater than it because the shear plane in electrophoresis is located at some unknown distance from the surface where the potential is lower than at the surface, can be calculated from the charge and the radius of the virus particles by means of the Debye–Hückel theory, or with greater accuracy by the method of Loeb, Wiersema and Overbeek.[27] The latter method is strictly applicable only to symmetrical electrolytes and thus is not completely valid for phosphate buffers.

For the virus particle in 0.002 ionic strength, pH 6.9, buffers $\zeta e/kT$ was found to have a value of about 1 when ζ was calculated from electrophoretic mobility. When surface potentials computed from charge were used as estimates of ζ, $\zeta e/kT$ for the same conditions had values of 3.2 and 2.3, depending on whether the computation was made for uni-univalent or di-divalent electrolytes. In view of the unsatisfactory state of electrokinetic theory, one can say no more than that $\zeta e/kT$ is of the order of magnitude of 2 for the virus in 0.002 ionic strength phosphate buffer at pH 6.9. The values at other pH values would be somewhat more or somewhat less, depending upon valence or mobility.

Since the values of d_2 for the virus protein in 0.002 M phosphate buffer at pH 6.9, obtained by adding the numbers in the two right columns of Table III, are about -10×10^{-3}, the values of s' computed from the Booth equation are only about 4% less than s. Booth[9] pointed out that his equation predicts charge effects that reduce s by only a few per cent. Thus, the Booth equation underestimates the observed charge effect.

(27) A. L. Loeb, P. H. Wiersema and J. Th. G. Overbeek, referred to in "Electrophoresis," edited by M. Bier, 1959, p. 23.

KINETICS AND MECHANISM OF THE AIR OXIDATION OF THE DITHIONITE ION (S₂O₄⁻) IN AQUEOUS SOLUTION

By Robert G. Rinker, Thomas P. Gordon, David M. Mason,[1] Roy R. Sakaida and William H. Corcoran

Chemical Engineering Laboratory, California Institute of Technology, Pasadena, California

Received September 16, 1959

A study of the air oxidation of sodium dithionite was conducted in aqueous solution which was 0.1 M in sodium hydroxide. The concentration of the dithionite was measured as a function of time at 30, 40, 50 and 60°. Initial concentrations varied from 5×10^{-3} to 20×10^{-3} M. Under conditions in which diffusion of air was not controlling it was found that the oxidation was half order with respect to dithionite and first order with respect to molecular oxygen. The half order mechanism was attributable to the presence of the SO₂⁻ radical ion as an intermediate.

Introduction

Probably the earliest air oxidation study of dithionite was conducted by Meyer[2] in 1903. He studied the oxidation of sodium dithionite by observing the oxygen uptake in shaken flasks containing aqueous dithionite solution. His re-

(1) Division of Chemical Engineering, Stanford University, Stanford, California.
(2) J. Meyer, *Z. anorg. Chem.*, **34**, 43 (1903).

sults showed that the products of reaction were sulfite and sulfate. He proposed a primary reaction to be

$$H_2S_2O_4 + H_2O + O_2 = H_2SO_4 + H_2SO_3 \quad (1)$$
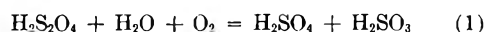
Also, he found that a competing reaction was

$$2H_2S_2O_4 + 2H_2O + O_2 = 4H_2SO_3 \quad (2)$$
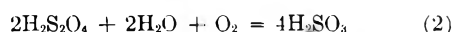
From the over-all reaction rates, he computed first-

order rate constants but found that they drifted over a wide range.

Bassett and Durrant[3] in 1927 studied the reaction between dithionite and molecular oxygen. Their explanation of the oxidation mechanism was based upon arguments that dithionite exists in three isomeric forms. Each isomer was believed to decompose in a way such that all of the observed reaction products could be explained by one or more of the mechanisms. Although Bassett and Durrant's work is of considerable value as a compilation of experimental observations of dithionite reactions, subsequent work has invalidated their interpretations.

Nicloux[4] in 1933 was interested in determining the over-all stoichiometry of the reaction between dithionite and oxidizing agents of varying strengths. With a comparatively weak oxidizing agent such as silver ion, the dithionite was oxidized to sulfite. With molecular oxygen, an equimolar mixture of sulfite and sulfate was formed. Finally, with a very strong oxidizing agent, sulfate was the only product. No experimental details were given. The results of Lynn[5] suggested that the atmospheric oxidation of $Na_2S_2O_4$ proceeded according to a first-order mechanism with respect to dithionite and that the rate increased with temperature. He stated that the over-all stoichiometry was described by the equation

$$Na_2S_2O_4 + O_2 + H_2O = NaHSO_4 + NaHSO_3 \quad (3)$$
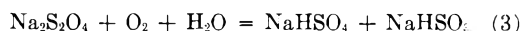
An examination of his data at 50° showed that the oxidation rate increased with an increase in air flow which meant that the diffusion rate of oxygen was a contributing factor. Without correcting for diffusion his results for the actual oxygen–dithionite reaction were, therefore, only approximate. His experiments did show that in the presence of 0.1 M sodium bisulfite the oxidation rate was extremely high. In the presence of 0.1 M sodium hydroxide the rate was inhibited, and the reaction proceeded smoothly.

Experimental

Apparatus.—The air oxidation of the sodium dithionite was carried out in a glass reactor with a volume of approximately 600 cc. Air was bubbled at a rate of 2500 to 3000 cc./min. into the reaction mixture near the bottom of the reactor through a medium-coarse glass frit which could be inserted or removed through a standard-taper opening on the reactor. During the reaction, the frit was always immersed in the liquid contents.

Before the air entered the frit, it was passed first through an Alundum-stone trap to remove suspended solids and aerosols, next through a molecular-sieve dryer, and finally through a temperature-conditioning coil. The air flow was measured by means of a wet-gas meter placed on the downstream side of the reactor.

Mixing was accomplished by means of a glass stirrer having two impellers. The stirrer was supported and sealed through a mercury-in-glass bearing. Stirring speeds could be varied up to 1100 revolutions per minute, which was the speed used throughout the experiments.

The reactor and the temperature-conditioning coil were thermostated in a 28-liter water-bath, which maintained the temperature within ± 0.02°. Heaters in the water-bath were energized by an electronic-relay circuit which in turn received its signal from a mercury-expansion switch immersed in the water.

(3) H. Bassett and R. G. Durrant, *J. Chem. Soc.*, **2**, 1401 (1927).

(4) M. Nicloux, *Compt. rend.*, **196**, 616 (1933).

(5) S. Lynn, Ph.D. Thesis, California Institute of Technology, 1954.

Samples were taken from the reactor through an opening in the top. A syringe needle or pipet was inserted into the reacting mixture, and the sample then was removed.

Commercial-grade nitrogen was the source of supply for the oxygen-free atmosphere required in preparing the sample of fresh sodium dithionite to be charged to the reactor. The nitrogen contained approximately 0.01% oxygen by volume and this amount proved excessive. Hence, most of the oxygen was removed by passing the nitrogen through two scrubbing towers in series. Each contained 0.2 M chromous chloride solution in 1.0 N hydrochloric acid. Acid and water vapors were subsequently removed by passing the nitrogen through a 0.1 M sodium hydroxide solution and then through a calcium chloride dryer.

Concentration of Dithionite as a Function of Time.— Chemically pure sodium dithionite (Baker Chemical Company, Batch No. 3712, Lot No. JTB6113) was the starting point for the source of dithionite ions. In preparing the dithionite for a typical run, approximately 25 g. of the powder was placed in an oxygen-free flask into which a stream of oxygen-free nitrogen had been passed for several minutes. Then, approximately 100 cc. of distilled water, free of oxygen and carbon dioxide, was injected into the flask through a rubber serum-bottle-cap. The mixture was heated to 60° with constant agitation until a saturated solution was obtained. With great care to avoid contact with oxygen, a 60-cc. sample of the saturated solution was withdrawn with a syringe and injected into a side-armed test-tube already filled with nitrogen. The tube with its contents then was cooled to 0° in an ice-bath while maintaining the pressure of the nitrogen constant at slightly above one atmosphere. At the lower temperature the liquid became supersaturated with sodium dithionite. With sufficient agitation, crystals of $Na_2S_2O_4 \cdot 2H_2O$ were formed. Again, with great care, practically all the liquid was removed from the tube leaving the white crystals settled at the bottom. Approximately 4 cc. of distilled water at 0° and free of carbon dioxide and oxygen was injected into the tube to wash the crystals. This washing process was repeated once again to obtain reasonably pure crystals. The final saturated solution with a volume of approximately 20 cc. was used to supply the reactor with an initial concentration of dithionite.

Before injection of the dithionite, the reactor was filled with 505.0 cc. of 0.1 M sodium hydroxide solution. The reactor was then immersed in the water-bath and allowed to reach steady conditions of temperature, stirring rate and air flow. The time of initial air flow was noted in order to account for evaporation losses from the reactor. At steady conditions, 5.00 to 15.00 cc. of the saturated dithionite solution, depending upon the initial concentration desired, was injected into the reactor. Since the delivery times of large syringes are of the order of several seconds, the time at which half of the sample was injected was taken as the initial time of the reaction.

Without delay, 1.00 or 2.00 cc. samples were removed from the reactor with a calibrated syringe and injected into 150-cc. flasks containing a mixture of 50 cc. of 0.1 M potassium hydroxide and 15 cc. of methyl alcohol. Also, the flasks contained a nitrogen atmosphere which was maintained during titration. The solutions in the titration flasks were stirred magnetically. The time at which half the sample from the reactor had been injected into a titration flask was recorded as the injection time.

The concentration of dithionite in the titration flasks was determined by titration with a standardized aqueous solution of methylene blue having a concentration in the range of 9.0×10^{-4} to $9.3 \times 10^{-4} M$.

Usually, the total time required to obtain a sample and titrate it was 40 sec. At the maximum temperature of 60° and at the minimum initial concentration of $5 \times 10^{-3} M$, the time for completion of the reaction was a minimum. Under these conditions, at least five titrations were accomplished before the end of the reaction.

As soon as all the dithionite had been oxidized, the airflow was stopped, and the time was noted. The reactor was removed from the water-bath, and the volume of its contents was measured. A material balance, coupled with the knowledge of the air-flow rate and the assumption that the exit air was saturated with water vapor, made it possible to calculate the loss of water by evaporation prior to and during the reaction.

In the analysis of the dithionite samples, the methylene blue was reduced quantitatively on an equimolar basis from

an intense blue color to an almost colorless leuco-form. It was found in agreement with Lynn's work,[5] that the leuco-form was relatively insoluble in water at room temperature; and unless it was dissolved, it apparently adsorbed unreacted methylene blue during the titration. This resulted in a lowered over-all rate of reaction because of the time required for the dithionite to diffuse to the solid surface before reaction could occur. The purpose of the addition of the methyl alcohol in the titration flasks was to dissolve the solid leuco-compound and hence speed up the titrations. When titrated quickly, any thiosulfate and sulfite present in a sample did not interfere in the reaction between dithionite and methylene blue for the temperature range 0–30°. The end-point was sharp and was attained rapidly at room temperature.

Standardization of the methylene blue was done according to the method of Welcher[6] and Kolthoff.[7] Briefly, the methylene blue was titrated into a standard water-solution of 0.005 M picrolonic acid which was buffered at a pH of about 6. Periodic removal of the dark green product, methylene blue picrolonate, from the water phase was necessary in order to detect the end-point. This was accomplished by extraction of the methylene blue picrolonate with chloroform. Neither the picrolonic acid nor the methylene blue was soluble in the chloroform. Near the end-point, only 2 or 3 drops of methylene blue were titrated into the acid between successive extractions with chloroform. The end-point occurred when a blue color persisted in the water phase after addition of one drop of methylene blue, but with no color in the chloroform phase. When carefully applied, this method gave results accurate to ±0.5% compared with ±2% for the classical iodine-precipitation method.[8]

Solubility of Dithionite at 0°.—A solution of sodium dithionite saturated at 0° was prepared as described in the previous section. The saturation concentration of the dithionite, however, far exceeded the desired value for titrations with reasonable volumes of methylene blue. Therefore, 5.00 cc. of the saturated solution was injected through a scrum-bottle cap into a 1-liter vessel which contained 500.0 cc. of 0.1 M sodium hydroxide maintained under a nitrogen atmosphere and at a temperature of 0°. Several 2.00-cc. samples of the resulting solution were titrated with methylene blue under conditions similar to those stated in the previous section. From these results, the solubility of the dithionite at 0° was calculated.

End-Products of the Dithionite Oxidation Reaction.—A knowledge of the types and quantities of the oxidation products of dithionite was important in determining a mechanism for the reaction. For the qualitative tests, a decomposed sample of dithionite was prepared by adding 0.20 g. of the purified powder to 100 cc. of 0.1 M sodium hydroxide solution through which air was bubbled until a test showed no reduction of methylene blue. A sample of the reaction mixture was acidified with hydrochloric acid to a pH of about 2, then lead acetate was added. A white precipitate resulted which indicated the absence of sulfide from the mixture. For the conditions here of small amounts of chloride ion, a black precipitate of lead sulfide would have appeared had sulfide been present. Another sample, when mixed with potassium triiodide at a pH of about 5, decolorized the iodine, indicating the presence of thiosulfate and/or sulfite. Still another sample at that pH was treated with barium chloride to remove sulfite and sulfate, if present, as barium sulfite and barium sulfate. The white precipitate was filtered. The filtrate was then titrated with potassium triiodide which showed a positive test for thiosulfate. Treatment of the precipitate with strong hydrochloric acid resulted in the evolution of sulfur dioxide to give a positive test for sulfite. The fact that a portion of the precipitate was essentially unattacked by an excess of acid showed the presence of sulfate as barium sulfate.

The procedure for the quantitative analysis was based upon the results of the qualitative findings. The principal ions of interest were sulfite, sulfate and thiosulfate. Any complexes of these ions or the presence of other ions were considered highly unlikely or in concentrations too low to be detected. The quantitative results substantiate this assumption.

Samples for quantitative analysis were taken from two sources, both of which were different from the source used in the qualitative analysis. The first source was contained in a flask which originally was charged with 500 cc. of 0.1 M sodium hydroxide at 30° and with 7 cc. of saturated dithionite solution. Oxygen entered the liquid bulk only by molecular diffusion through the surface of the liquid. This mixture was checked for completion of dithionite oxidation before other components were studied. The second source was contained in the reactor following a usual run at 30° as described previously.

In both cases, the method of analysis for end-products was the same. Four separate analyses were made on four separate samples from each source. These were: (1) iodometric titration to determine the sum of the concentration of thiosulfate and sulfite; (2) iodometric titration to determine only the concentration of thiosulfate; (3) barium chloride titration to determine the sum of the concentration of sulfite and sulfate; and (4) barium chloride titration to determine only the concentration of sulfate.

In the iodometric analysis for the sum of the sulfite and thiosulfate, a 10 to 25-cc. sample was buffered with a solution which was 0.5 M in sodium acetate and 0.4 M in acetic acid. Usually, a volume of the buffer solution equal to the volume of the sample was added to give a constant pH of about 5. Using a starch end-point, the solution was titrated with a standardized solution of approximately 0.01 N triiodide. In case of excess addition of triiodide, back-titration was done with a standard thiosulfate solution which was approximately 0.01 N in thiosulfate.

In the iodometric analysis for only the thiosulfate ion, a 10 to 25-cc. sample was buffered to a pH of about 5. To this was added a volume of 37 weight % formaldehyde in water equal to about half the volume of the sample. The purpose of the formaldehyde was to form a complex with the bisulfite according to the reaction

$$\begin{matrix} H \\ \diagdown \\ \diagup \\ H \end{matrix} C{=}O \ + \ HSO_3Na \longrightarrow CH_2(OH)SO_3Na \quad (4)$$
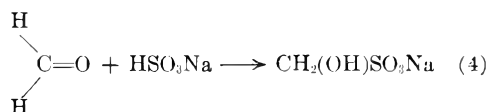
The mixture was stirred for 15 minutes at room temperature to allow sufficient time for the complexing to occur. The unreacted thiosulfate then was determined with the standard triiodide solution.

The use of barium chloride in a titration method to determine sulfate was suggested in the literature by Fritz and Freeland.[9] This method depends upon a color change in the indicator Alizarin Red-S which acts as an adsorption indicator in the presence of a barium sulfate precipitate. In solution the alizarin anion was yellow; but on the surface of suspended barium sulfate and in the presence of excess barium ion, the alizarin complexed with the barium ion to give a red color to the suspended solid. In using the procedure outlined by Fritz and Freeland, however, the method was limited to concentrations of sulfate greater than 20×10^{-3} M. It was necessary, then, to modify the procedure in applying it to the concentrations of sulfate down to 4×10^{-3} M. After several tests, it was noted that the limit of detection of sulfate was determined by the amount of precipitate available for adsorption of alizarin. Too small a quantity of precipitate, although colored red with complexed alizarin, was not perceptible through the yellow color of the alizarin in solution. Therefore, by adding a quantity of semi-colloidal barium sulfate suspended in methyl alcohol to the titration mixture, it was possible to detect the end-point with an accuracy of 1 or 2%. A further improvement in detecting the end-point was to pass an intense light beam through the suspension during the titration. This aided in bringing out color changes more sharply.

To determine the sum of the sulfite and sulfate concentration by the above method, it was first necessary to oxidize the sulfite to sulfate by means of the triiodide ion. The amount of triiodide needed was determined by a starch end-point; but there was some uncertainty as to the effects of the starch on the subsequent sulfate titration. Therefore, it was decided to avoid using the starch by first running a blank to determine the exact triiodide requirement and then adding

(6) F. J. Welcher, "Organic Analytical Reagents," D. Van Nostrand Co., New York, N. Y., 1948.

(7) I. M. Kolthoff and G. Cohn, J. Biol. Chem., 148, 711 (1943).

(8) J. Rosin, "Reagent Chemicals," D. Van Nostrand, New York, N. Y., 1937.

(9) J. S. Fritz and M. Q. Freeland, Anal. Chem., 26, 1593 (1954).
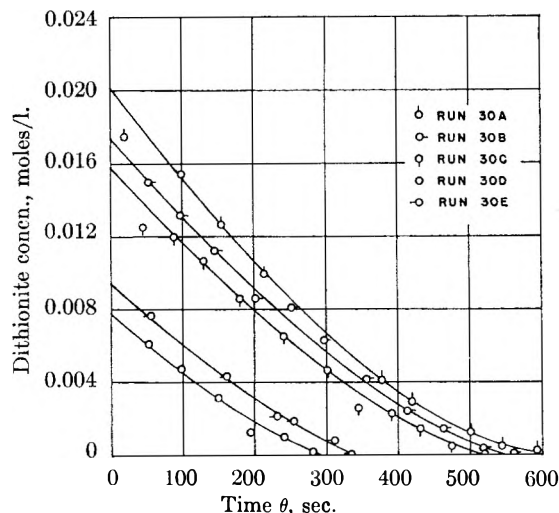
Fig. 1.—Dithionite concentration vs. time in air oxidation at atmospheric pressure and 30°.
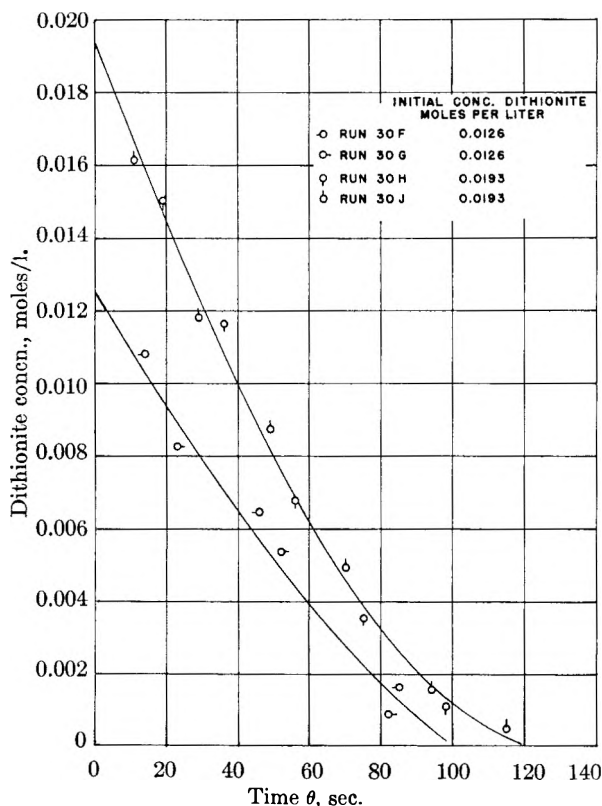
Fig. 2.—Dithionite concentration vs. time at 30° using pure oxygen at atmospheric pressure.

the same amount in the absence of starch to a fresh sample buffered at a pH of about 5 as specified above. Following the oxidation of the sulfite, the buffered solution was acidified to a pH of about 3.5 with 20 weight% acetic acid. The volume of acetic acid required was about equal to the volume of the original sample. Then methyl alcohol containing a semi-colloidal suspension of barium sulfate was added in an optimal amount equal to 38% by volume of the final mixture. With constant stirring, 90% of the estimated 0.1 M barium chloride requirement was added rapidly followed by 3 to 5 drops of 0.020 weight % alizarin-red solution. The final titration was performed slowly with an interval of 3 to 5 sec. between drops of barium chloride solution.

Finally, in determining the concentration of sulfate alone, the sulfite was complexed by addition of formaldehyde. The subsequent barium chloride titration was not affected adversely by the presence of the formaldehyde.

All the standard solutions used in the foregoing analyses were prepared and standardized according to the procedures outlined by Swift.[10]

Results

Rate Studies.—Rate data obtained at 30° are shown in Fig. 1, in which the concentration of dithionite in moles per liter is plotted against time in seconds. A tabulation of these data along with results at 40, 50 and 60° is available.[11] Initial concentrations of dithionite ranged from 5×10^{-3} to 20×10^{-3} mole/liter. The rate of change of concentration was large in the initial stages but decreased continuously and rapidly as the concentration decreased.

In the determination of the order of the reaction with respect to dithionite, the oxygen concentration was held constant for a given temperature. Only for those experiments in which the order with respect to oxygen was to be determined was the oxygen concentration varied. Still maintaining atmospheric pressure, pure oxygen was used as a replacement for air to give nominally a fivefold increase in oxygen concentration. For an assumption of Henry's law, the concentration ratio of dissolved oxygen in equilibrium with the pure gas at atmospheric pressure to dissolved oxygen in equilibrium with air at atmospheric pressure would be 4.8. This same ratio was assumed for the very dilute dithionite solutions in which the total gas pressure was at the atmospheric level. For the equipment used, this method of varying the partial pressure of the oxygen in the gas phase was preferred to a method in which the total pressure on the system would have been varied.

It was found experimentally that the initial rate of the reaction was increased by a factor of 5 when pure oxygen was substituted for air, all other conditions remaining the same. Therefore, the reaction was believed to be first order with respect to molecular oxygen. Figure 2 shows rate data obtained at 30° when pure oxygen was bubbled through the system with the total pressure being atmospheric. Those results have also been tabulated.[11] The figure may be compared with Fig. 1 for the case in which air was used.

Two procedures were available for analyzing the data in the determination of initial rates. An initial concentration could have been established by use of solubility data obtained as explained in Experimental Procedure. Also an initial concentration could have been obtained by extrapolation of the concentration–time curve back to zero time. Inasmuch as sampling of the reactor was usually begun only 30 to 50 sec. after zero time, the use of the extrapolation technique was satisfactory. The extrapolation method was preferred because of the need for exact control of equilibrium conditions in the event that the solubility data were used.

(10) E. H. Swift, "Systematic Quantitative Analysis," Prentice-Hall, New York, N. Y., 1939.

(11) R. G. Rinker, T. P. Gordon, D. M. Mason, R. R. Sakaida and W. H. Corcoran, Am. Doc. Inst., Washington 25, D. C., Document 6104 (1959). A copy of this document may be secured by citing the document number and by remitting $2.50 for photoprints or $1.75 for 35 mm. microfilm. Advance payment is required. Make checks or money orders payable to: Chief, Photoduplication Service, Library of Congress.

After the initial concentration was determined by extrapolation, initial rates were obtained by plotting slopes of concentration–time curves as a function of time for each initial concentration. Extrapolation to zero time produced the initial rates. These compared satisfactorily with the values obtained by drawing tangents to the concentration–time curves at zero time.

From a knowledge of the initial rates and concentrations, the order n of the reaction with respect to dithionite was obtained. The relationship used in this determination applied at time zero was

$$-\frac{dC}{d\theta} = k_c[C]^n \qquad (5)$$

in which C is the concentration of dithionite in moles per liter; θ is the time in seconds; and k_c is the specific reaction rate constant which includes the constant concentration of oxygen.

A plot of log C vs. log $(-dC/d\theta)$ for initial conditions is shown in Fig. 3 for runs at 30°, and the data have been recorded[11] along with those obtained at 40, 50 and 60°. The slopes of the best straight lines through the points at each temperature were calculated to be 0.50 ± 0.04, which was near enough to 0.5 to indicate that the reaction was one-half order with respect to dithionite. The purpose of obtaining n for conditions at zero time was to eliminate any possible effects of reaction products or side reactions in masking the true order of the initial reaction. A discussion of these effects is given later in the section on Product Analysis.

The integrated form of equation 5 was used to obtain values of k_c as a function of time, and the unsmoothed data were used in the computations. Integration of equation 5 gives

$$k_c = \frac{2}{\theta}[C_0^{1/2} - C^{1/2}] \qquad (6)$$

It was found that k_c calculated from equation 6 drifted slightly as a function of time when calculated for various points up to 50% completion of the reaction, but the variation was smooth and linear. A typical plot for data at 30° is shown in Fig. 4, and tabulations of these results together with those at 40, 50 and 60° have been made.[11] The curves for k_c, when extrapolated to time zero, converge to a range of values well within experimental accuracy. Because the values for k_c varied with reasonable smoothness the procedure of using unsmoothed data in the calculation appeared satisfactory. Figure 4 also shows a value of $k_{c_{av}}$, which is the arithmetic average of k_c at zero time and includes the concentration of oxygen. The oxygen dependence can be eliminated, however, by dividing $k_{c_{av}}$ by the saturation concentration of oxygen, which for the dilute solutions studied here was taken as the saturation concentration in pure water.[12] That calculation was made, and the resulting value of specific reaction rate at zero time and independent of the oxygen concentration was designated as k_c^0. Its value at

(12) N. A. Lange, "Handbook of Chemistry," 7th edition, Handbook Publishers, Inc., Sandusky, Ohio, 1949.
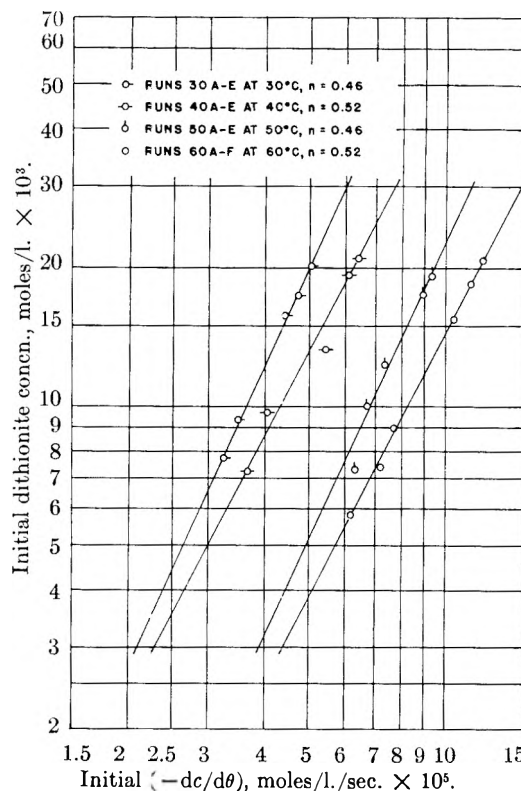
Fig. 3.—Log C vs. log $(-dc/d\theta)$ for initial conditions at 30, 40, 50 and 60° at atmospheric pressure.

30° is listed in Fig. 4 and also in Table I with values at 40, 50 and 60°.

TABLE I

MEAN VALUES OF k_c^0, SPECIFIC REACTION CONSTANT AT ZERO TIME AND INDEPENDENT OF OXYGEN CONCENTRATION

$t,$ °C.	$k_c^0,$ (moles/l.)$^{-1/2}$ sec.$^{-1}$
30	0.151
40	.214
50	.372
60	.565

A correlation of the rate constants with temperature was made by use of the Arrhenius equation. The simple form of the equation was used where

$$k_c^0 = Ae^{-\Delta E/RT} \qquad (7)$$

The constants were evaluated by use of a plot of the data in Table I. A value of 9.3 kcal./mole was obtained for ΔE, and the frequency factor was found to be 7.2×10^5 (moles/l.)$^{-1/2}$ sec.$^{-1}$.

Product Analyses.—Table II lists the experimental results for the analyses of end products. As indicated in the Experimental Procedure, data were obtained from reactions conducted in flasks and in the reactor vessel. For the reactions conducted in the flasks, the molal ratio of sulfite to sulfate was found to be 2.3. In the case of the analyses of the end products in the reactor, the ratio was more nearly 3.0. Such a large difference between the two ratios was due primarily to the difference in reaction time. Whereas the flask reactions required approximately 29 hours for completion, the reactor runs were completed

Fig. 4.—k_c vs. time at 30°.

Fig. 5.—Concentration of sulfite and thiosulfate vs. time in air oxidation at atmospheric pressure and temperatures of 30 and 60°.

in about 300 seconds. During the relatively long time in the flasks, the oxidation of sulfite to sulfate was undoubtedly significant. In comparison to the rate of dithionite oxidation, under identical conditions, the oxidation of pure sulfite was quite slow as may be noted by comparing Fig. 1 with Fig. 5. This lower rate was also observed when at the completion of dithionite oxidation the air flow was allowed to continue for 10 to 15 minutes with no significant change in the sulfite–sulfate ratio. There was no real assurance, however,

END PRODUCT ANALYSES

Air oxidation of dithionite at room temperature and atmospheric pressure, concentrations in moles per liter

		Run EP-A[a]	Run EP-B[b]	Run EP-C[b]
Initial	$[S_2O_4^-]$	10.30×10^{-3}	9.50×10^{-3}	10.10×10^{-3}
Final	$[SO_4^-]$	5.72×10^{-3}	4.16×10^{-3}	4.26×10^{-3}
Final	$[SO_3^-]$	13.14×10^{-3}	13.16×10^{-3}	11.90×10^{-3}
Final	$[S_2O_3^-]$	1.60×10^{-3}	0.42×10^{-3}	1.00×10^{-3}
Final	$\dfrac{[SO_3^-]}{[SO_4^-]}$	2.3	3.16	2.78

[a] Reaction time of 29 hr. in non-stirred flasks. [b] Experiments conducted with agitation and air flow so that diffusion was not controlling. Analysis for EP-B was corrected for 8.8% thermal decomposition and that for EP-C for 21%.

that in the presence of dithionite ions or transient intermediates the sulfite oxidation was not catalyzed. Indeed, the oxidation of sulfite to sulfate by molecular oxygen has been shown to be catalyzed by free radicals.[13] The presence of appreciable amounts of sulfate in the reaction products suggests that catalysis was occurring. The observed ratio of sulfite to sulfate of 3 to 1 sets an upper limit of 25% conversion of sulfite to sulfate by catalyzed air oxidation.

As shown in Table II, thiosulfate in small but measurable quantities was also among the products. There seems to be no explanation of its formation unless it is assumed that a secondary reaction involving thermal decomposition occurred simultaneously with the air oxidation. As the product of a secondary reaction, it accounted for nearly 10% of the dithionite disappearance for a temperature of 30°. This is based upon the stoichiometry of the thermal decomposition in which the two major products are sulfite and thiosulfate. Prob-

(13) H. N. Alyea and H. L. J. Backstrom, J. Am. Chem. Soc., 51, 90 (1929).

ably the secondary reaction was the greatest single factor contributing to the drift in the rate constant k_c.

The stability of thiosulfate in the basic solution and in the presence of molecular oxygen was established by the absence of sulfide and tetrathionate in the end products, and also by the fact that the thiosulfate concentration in the flask reactions remained constant up to 100 hours after the depletion of the dithionite. Further evidence for the very slow oxidation of thiosulfate was obtained when a 0.028 M solution was subjected to the same conditions of temperature, stirring, and air flow in the reactor that existed for dithionite oxidations. No significant oxidation was measured for times up to 15 minutes as may be seen in Fig. 5. Data for runs at both 30 and 60° have been recorded.[11]

Diffusion Effects.—As stated in the experimental procedure, the rate of air or oxygen discharge through the frit into the reacting mixtures was varied from 2500 to 3000 cc./min. Preliminary tests showed, however, that an air rate of only 1200 cc./min. was sufficiently high to oxidize the dithionite independently of the air rate. Therefore, reproducibility of tests was not affected by variable air rates greater than 1200 cc./min. The rate of stirring (approximately 1100 r.p.m.) in the reactor was rapid enough to maintain an isothermal, homogeneous mixture. A stirring rate of only 800 r.p.m., coupled with an air rate of 1200 cc./min. gave the same results within experimental error as a stirring rate of 1100 r.p.m. and an air rate of 2500 cc./min., all other conditions being the same. Figure 6 shows the effects of stirring rate and air flow in the dithionite oxidation, and tabular data are also available.[11] In the figure, the concentration of dithionite as a function of time for the same initial concentration at 60° and a stirring speed of 800 r.p.m. is shown for different air rates. As the air rate increased to 1200 cc./min., the curves moved close to an asymptotic curve which established the lower limits of operation. Data obtained at 2500 cc./min. and 1100 r.p.m. are shown for comparison. The fact that the curves of Fig. 6 differed indicated that diffusion of oxygen to a point in the system was a controlling factor in the rate of oxidation for air rates less than the asymptotic value of 1200 cc./min. at the stirring speed of 800 r.p.m. In the oxidation of the dithionite, the greatest demand for oxygen occurred at the highest temperature, which was 60°, and at the maximum initial concentration of dithionite, which was approximately 20 × 10⁻³ M. The tests represented by Fig. 6 were performed at nearly the extreme conditions of demand, as noted above, except that the initial concentration was only 12 × 10⁻³ M. The experimental data for the runs at concentrations higher than 12 × 10⁻³ M were consistent with data obtained for runs below this concentration. It was therefore assumed that for the air rates and stirring speeds used throughout the experimental work the diffusion of oxygen was not a controlling factor.

Effects of Ionic Strength.—Data obtained at 60°, as shown in Fig. 7 and recorded elsewhere,[11] show that the rate of reaction did not change upon
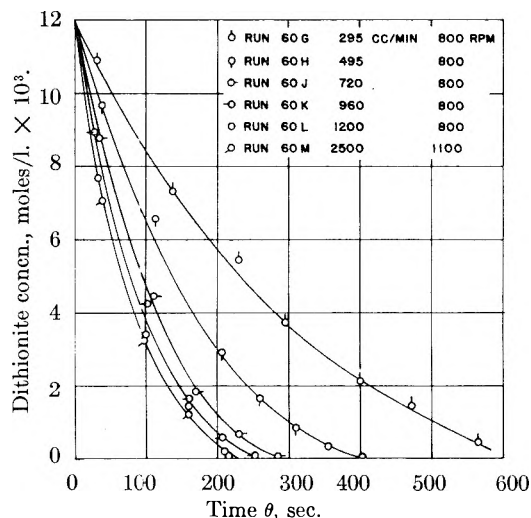
Fig. 6.—Effects of air flow and stirring rate on concentration of dithionite as function of time in oxidation at atmospheric pressure and 60°.
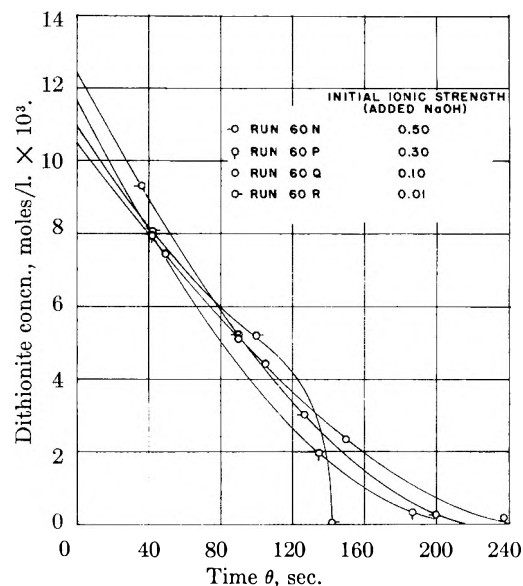
Fig. 7.—Effects of ionic strength in air oxidation of dithionite at atmospheric pressure and 60°.

increasing the concentration of sodium hydroxide, and hence the ionic strength, by factors of three and five. The result in that figure for an experiment conducted in 0.01 M sodium hydroxide appears anomalous. It is almost certain that the different course of reaction resulted from thermal decomposition when the hydrogen ion which was generated neutralized the sodium hydroxide.

pH and Effects of Metal Ions.—The pH of the dithionite solutions changed approximately from 13 to 12.8 for the highest initial concentration of 20 × 10⁻³ M. This change indicated that hydrogen ion was generated as one of the products of reaction. No detailed study of the variation in pH was made for the air oxidation of dithionite.

No careful study was made to determine the effects of metal ions on the oxidation of dithionite. It was observed, however, in a qualitative way, that mercury in minute quantities caused the reaction to become erratic. A reasonable suggestion

is that the mercury reacted to form complexes such as $Hg(SO_3)_2^{=}$.

Solubility Studies.—In measurements of the solubility of sodium dithionite in water at $0°$, the average value of 11 determinations was found to be 13.20 g. per 100 g. of water with a standard deviation of 1.08 g. per 100 g. of water or about 8%. Yost[14] lists a value of 12.85 g. per 100 g. of water at $1°$, and Rao and Patel[15] list 11.86 g. per 100 ml. of solution at $0°$. Neither of those experimenters give any limits of error.

Discussion

A mechanism which satisfies the established order of reaction with respect to dithionite and oxygen and in which the initial step was dissociation of dithionite[16] is given as

$$S_2O_4^- \rightleftharpoons 2SO_2^- \tag{8}$$

$$SO_2^- + O_2 \longrightarrow \text{Products} \tag{9}$$

The first step which is shown as equation 8 reaches equilibrium rapidly, and the second step presented as equation 9 is relatively slow and thus rate determining. Thus the observed reaction rate may be described as

$$r_{obsd} = k_2[SO_2^-][O_2] \tag{10}$$

where r_{obsd} is the reaction rate in moles per liter per second; k_2 is the specific rate constant in moles-liters-seconds units; $[SO_2^-]$ is the concentration of SO_2^- in moles per liter, and $[O_2]$ that of oxygen in moles per liter.

A relationship between the observed experimental specific reaction rate constant, k_c^0, and the rate constant given in equation 10 may be obtained by noting the rapid achievement of equilibrium for the reaction given in equation 8 and the rate-determining character of the reaction given by equation 9. For equation 8 the equilibrium constant may be written as

$$K_c = \frac{[SO_2^-]^2}{[S_2O_4^-]} = \frac{k_1}{k_{-1}} \tag{11}$$

In this relationship K_c has the units of moles/liter. If the value for the quantity $[SO_2^-]$ obtained from equation 11 is substituted in equation 10, the rate expression may be written as

$$r_{obsd} = k_2K_c^{1/2}[S_2O_4]^{1/2}[O_2] \tag{12}$$

The experimentally determined rate constant, k_c^0, is then related to k_2 and K_c by the expression

$$k_c^0 = k_2K_c^{1/2} \tag{13}$$

As noted in the section on Results the variation of k_c^0 with temperature permitted the calculation of an Arrhenius activation energy of 9.3 kcal./mole and a frequency factor of 7.2×10^5 (moles/l.)$^{-1/2}$ sec.$^{-1}$. If it is assumed that the rate-determining step involved an electron transfer to form O_2^- and SO_2, the observed activation energy of 9.3 kcal./mole would appear high. Uri[17] has correlated data for a number of exothermic elec-

(14) D. M. Yost and H. Russell, "Systematic Inorganic Chemistry," Prentice–Hall, Inc., New York, N. Y., 1944.

(15) M. R. A. Rao and C. C. Patel, *Proc. Nat. Inst. Sci. India,* **19**, 211 (1953).

(16) R. G. Rinker, T. P. Gordon, D. M. Mason and W. H. Corcoran, This Journal, **63**, 302 (1959).

(17) N. Uri, *Chem. Revs.,* **50**, 375 (1952).

tron-transfer-reactions and found typical activation energies to lie between 0 and 5 kcal./mole. The experimentally observed value of 9.3 kcal./mole, however, does include a contribution from the equilibrium step described by equation 8. If approximate values of frequency factors obtained from Frost and Pearson[18] are used, order-of-magnitude calculations can be made for the limiting contributions of the equilibrium and rate-determining steps to the observed activation energy. The calculations are

$$k_c^0 = k_2K_c^{1/2} = \frac{k_2k_1^{1/2}}{k_{-1}^{1/2}} \tag{14}$$

Then in the Arrhenius form, equation 14 may be rewritten as

$$A_c^0 e^{-\Delta E_c^0/RT} = A_2 e^{-\Delta E_2/RT} \left[\frac{A_1 e^{-\Delta E_1/RT}}{A_{-1} e^{-\Delta E_{-1}/RT}} \right]^{1/2} \tag{15}$$

If the logarithm is taken of both sides, equation (16) results

$$\ln A_c^0 - \frac{\Delta E_c^0}{RT} = \ln A_2 - \frac{\Delta E_2}{RT} +$$
$$\tfrac{1}{2} \ln \left(\frac{A_1}{A_{-1}} \right) - \tfrac{1}{2} \left[\frac{(\Delta E_1 - \Delta E_{-1})}{RT} \right] \tag{16}$$

A combination of terms then gives

$$\Delta E_c^0 - RT \left[\ln \frac{A_c^0}{A_2} - \tfrac{1}{2} \ln \frac{A_1}{A_{-1}} \right] =$$
$$\Delta E_2 + \tfrac{1}{2}(\Delta E_1 - \Delta E_{-1}) \tag{17}$$

Frost and Pearson suggest a value of 10^6 to 10^7 (moles/l.)$^{-1/2}$ sec.$^{-1}$ for A_2, 10^{13} sec.$^{-1}$ for A_1, and 10^5 to 10^6 (moles/l.)$^{-1/2}$ sec.$^{-1}$ for A_{-1}. If the value of 9.3 kcal./mole is substituted for ΔE_c^0 and a rounded value of 7×10^5 (moles/l.)$^{-1/2}$ sec.$^{-1}$ for A_c^0, then

$$\Delta E_2 + \tfrac{1}{2}(\Delta E_1 - \Delta E_{-1}) = 15 \text{ kcal./mole} \tag{18}$$

These order-of-magnitude calculations place limits on the value of ΔE_2 and $(\Delta E_1 - \Delta E_{-1})$ as

$$0 \leqslant \Delta E_2 \leqslant 15 \text{ kcal./mole} \tag{19}$$
$$0 \leqslant (\Delta E_1 - \Delta E_{-1}) \leqslant 30 \text{ kcal./mole}$$

If a mean value is assumed for ΔE_2 based on Uri's[17] values of 0–5 kcal./mole, for an electron-transfer reaction, a rough estimate can be made of K_c and k_2 in the equation given above. If a value of 3 kcal./mole is assumed for ΔE_2, then K_c is found to be 8×10^{-11} mole/l. and k_2 is therefore 2×10^4 (moles/l.)$^{-1}$ sec.$^{-1}$. These values for K_c and k_2 are, at best, order-of-magnitude estimates.

The order of reaction of the air oxidation with respect to dithionite and molecular oxygen determines the composition of the transition state in the rate-determining step. That is, the activated complex must consist of one molecule of SO_2^- and one molecule of O_2. Further information about the geometry of the activated complex or the products which result from its decomposition cannot be inferred with certainty from the present data. Knowledge of the composition of the transition state and the composition of the end products does, however, place a reasonable limit on the number of mechanisms which might be proposed for the intermediate steps. Two

(18) A. A. Frost and R. G. Pearson, "Kinetics and Mechanism," John Wiley and Sons, Inc., New York, N. Y., 1953.

possibilities are suggested immediately for the rate-determining step

$$SO_2^- + O_2 \rightleftarrows complex\ A \xrightarrow{k_2} SO_4^- \quad (20)$$

or

$$SO_2^- + O_2 \rightleftarrows complex\ B \xrightarrow{k_2} SO_2 + O_2^- \quad (21)$$

It is not inconceivable that both of these mechanisms could occur. Both free radical intermediates, SO_4^- and O_2^-, have ample precedent in the literature.[17] End product analysis does, however, exclude the mechanism given in equation 20 from being the only mechanism by which the activated complex is decomposed. Subsequent steps would almost certainly be of the type

$$SO_4^- + SO_2^- \longrightarrow SO_4^- + SO_2 \quad (22)$$
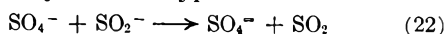
which would lead to a sulfite-to-sulfate ratio of unity in the reaction products. The mechanism given by equation 21 leads to a series of free-radical intermediates of hydrogen peroxide. The following series of reactions may be written as a suggestion

$$S_2O_4^- \rightleftarrows 2SO_2^-$$

$$SO_2^- + O_2 \rightleftarrows complex\ B \xrightarrow{k_2} SO_2 + O_2^-$$

$$SO_2^- + O_2^- \xrightarrow{k_3} SO_2 + O_2^-$$

$$O_2^- + H_2O \xrightarrow{k_4} HO_2^- + OH^-$$

$$HO_2^- + SO_2^- \xrightarrow{k_5} SO_4^- + OH^- \quad (23)$$

$$HO_2^- + SO_2^- \xrightarrow{k_6} SO_3^- + OH$$

$$OH + SO_2^- \xrightarrow{k_7} SO_2 + OH^-$$

$$SO_2 + OH^- \xrightarrow{k_8} SO_3^- + H^+$$

$$^1/_2SO_3^- + ^1/_4O_2 \xrightarrow{k_9} ^1/_2SO_4^-$$
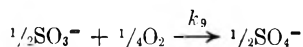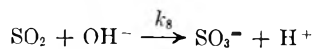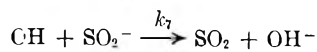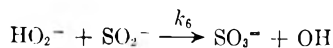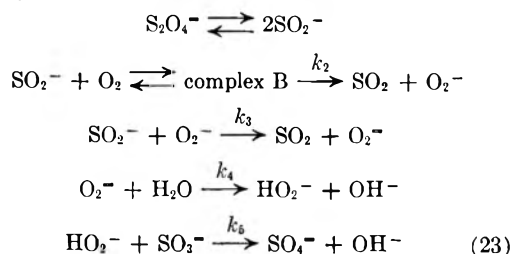
These equations lead to the observed over-all stoichiometry and by suitable choice of kinetic constants could be shown to be kinetically consistent. The summation of the scheme is that the peroxide intermediates which are formed on a mole for mole basis by the decomposition of dithionite can react either with sulfite molecules already formed to form sulfate or with SO_2^- radical ions to form more sulfite and regenerate peroxide intermediates. Since the concentration of sulfite ions in solution greatly exceeds that of SO_2^- ions after the first second of the reaction, the preponderance of sulfite rather than sulfate in the products requires that $k_6 \gg k_5$ in the above scheme. A steady-state concentration of intermediates need not be postulated in this hypothetical analysis.

REACTIONS OF POLYSOAPS WITH CHLORIDE AND BROMIDE IONS[1]

By Dietrich Woermann and Frederick T. Wall

Noyes Chemical Laboratory, University of Illinois, Urbana, Illinois

One polyelectrolyte and five polysoaps with chloride and bromide counterions have been prepared from poly-4-vinylpyridine by quaternizing 0, 4.9, 5.8, 8.1, 13.9, 31.8% of its nitrogen with n-dodecyl groups and the remainder with ethyl groups. The solution viscosities of these chloride and bromide polymers have been studied in the presence of 0.0223 N KCl and 0.0223 N KBr solutions, respectively. Characteristic differences exist between the reactions of the chloride and bromide forms of the polysoaps and polyelectrolytes. The results can be explained by Strauss' concept of a "critical dodecyl group content" of the polysoaps, corresponding to a critical separation of the soap groups. When the critical content is exceeded, by increasing the dodecyl group content, the soap groups exhibit a tendency to form aggregates and the intrinsic viscosity drops considerably. The critical dodecyl group content is analogous to the critical micelle concentration of ordinary soaps. Corresponding to the differences between the critical micelle concentrations of ordinary chloride and bromide soaps, the critical dodecyl group content of the chloride form of the polysoaps is greater than that of the bromide form.

Introduction

The gradual transition from typical polyelectrolytes to polysoaps (*i.e.*, polymers to whose chain structure cationic or anionic soap molecules are chemically attached) has been investigated extensively in recent years. Especially careful study has been given to systems of polyvinylpyridine derivatives prepared by quaternizing some of its nitrogen atoms with n-dodecyl bromide and the remainder with ethyl bromide.[2,3] Viscosity measurements of aqueous solutions of these polymers show that there is an analogy between the properties of polysoaps and ordinary soaps. The results can be explained by Strauss' concept of a "critical dodecyl group content" of the polysoaps analogous to the critical micelle concentration of ordinary soaps.

The purpose of this study was to investigate by means of viscosity measurements the different reactions of the chloride and bromide forms of a typical polyelectrolyte and of five polysoaps, prepared by quaternizing some of the nitrogen of poly-4-vinylpyridine with n-dodecyl bromide (0, 4.9, 5.8, 8.1,

(1) This work was supported by a grant from the National Science Foundation.

(2) U. P. Strauss, N. L. Gershfeld and E. H. Crook, This Journal, **60**, 577 (1956).

(3) A. I. Medalia, H. H. Freedman and S. Sinha, *J. Polymer Sci.*, **40**, 15 (1959).
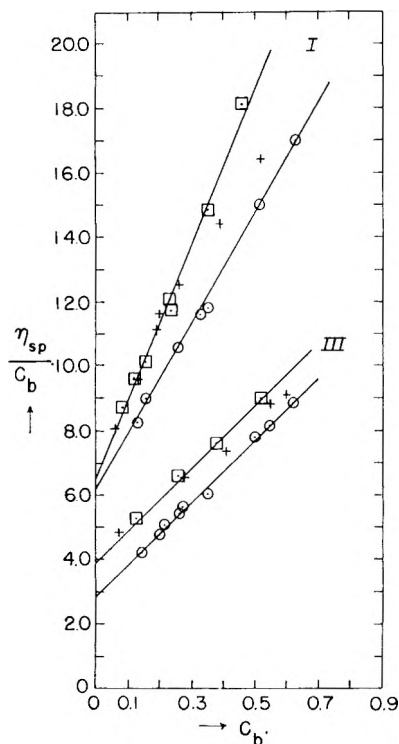
Fig. 1.—Graph of η_{sp}/C_b for polyelectrolytes and polysoaps with chloride and bromide counterions as function of concentration C_b in 0.0223 N KCl and 0.0223 N KBr solutions at 25° (C_b denotes grams of organic cation per 100 ml. of solution.): □, denotes chloride form in presence of chloride salt; O, denotes bromide form in presence of bromide salt; +, denotes bromide form in presence of chloride salt; I, refers to polymer with 0% dodecyl groups; III, refers to polymer with 5.8% dodecyl groups.

13.9, 31.8% of the dodecyl groups) and the remainder with ethyl bromide. (Subsequently, the bromide ions are exchanged with chloride ions.) The polyvinylpyridine quaternized only with ethyl bromide is, of course, a typical polyelectrolyte.

Experimental Part

Materials.—The preparation of poly-4-vinyl-N-ethylpyridinium bromide, henceforth denoted by PVEP-Br, was carried out essentially by the method described by Fuoss and Strauss[4] (substituting ethyl bromide for butyl bromide). The synthesis of the polysoaps has been described previously by Strauss and Gershfeld.[5] Table I gives the chemical composition of the materials used in this investigation. The degree of polymerization[6] of the poly-4-vinylpyridine from which these 6 compounds were prepared was estimated, from the intrinsic viscosities in 100% ethanol, to be about 100,000.

TABLE I

CHEMICAL COMPOSITION OF THE MATERIAL

| | Meq. Br g. | % of pyridine groups substituted with | | | |
		n-$C_{12}H_{23}Br$	C_2H_5Br	HBr	Free
I	4.35	0	95.6	3.4	1.0
II	3.85	4.9	91.1	1.8	2.2
III	3.75	5.8	92.2	2.0	0.0
IV	4.05	8.1	86.5	5.4	0.0
V	4.00	13.9	81.7	1.8	2.6
VI	3.75	31.8	63.3	3.4	1.5

(4) R. M. Fuoss and U. P. Strauss, *Ann. N. Y. Acad. Sci.*, **51**, 836 (1949).

(5) U. P. Strauss and N. L. Gershfeld, THIS JOURNAL, **58**, 747 (1954).

(6) J. B. Berkowitz, M. Yamin and R. M. Fuoss, *J. Polymer Sci.*, **28**, 69 (1958).

Measurement of Viscosities.—Viscosity measurements were performed at 25° using two different Ostwald capillary viscosimeters. The efflux times for water were 37.5 and 83.7 sec., respectively. The number of grams of organic polycations in 100 ml. of solution, denoted by C_b, is a convenient concentration unit for comparison of the influence of chloride and bromide counterions on the reduced viscosities of these polymers. C_b can be calculated from the weight concentration of the polymer knowing its halogen content from microanalysis (Table I).

Preparation of the Polysoap Solutions.—The aqueous solutions of PVEP-Br and of the bromide form of the polysoaps in the presence of 0.0223 N KBr were prepared by weighing the polymers in a volumetric flask and filling to the mark with 0.0223 N KBr solution. The solutions were heated for 1 day at 45° and then held at the viscosimeter bath temperature of 25° for another day, after which their viscosities were measured.

Aqueous solutions of poly-4-vinyl-N-ethylpyridinium chloride, henceforth denoted by PVEP-Cl, and of the chloride form of the polysoaps, each in the presence of 0.0223 N KCl, were prepared by first weighing the bromide form of the polymers in a volumetric flask and filling to the mark with a 0.0223 N KCl solution. (After these solutions were heated in the manner indicated above, their viscosities were likewise determined.) To replace the bromide ions more completely by chloride ions, the solutions were next placed in contact with a strong basic anion-exchange resin ("Dowex 1–X10"; 3.2 meq. per dry gram) charged with chloride ions in a sealed erlenmeyer flask and stirred for two days. The resin had been allowed to come to equilibrium with a 0.0223 N KCl solution before use and had an exchange capacity 10 times larger than the number of equivalents of bromide ions present in the solution. The solutions were subsequently separated from the resin by means of a sintered glass funnel. These solutions were then also heated in the manner indicated above, after which their viscosities were determined. Since the exchange resin absorbed small quantities of the polymer, the concentration of polymer in the solutions after treatment with exchange resin was determined by potentiometric titration. This involved a larger error than determination by weight. Because this could adversely affect the extrapolation of the reduced viscosity to zero concentration (to get the intrinsic viscosity), the reduced viscosity of the bromide form of these polymers in the presence of 0.0223 N KCl also was determined as mentioned above. In this case, the polymer concentration was determined by weight. For the limit of zero polymer concentration, the value of the relative viscosity of the chloride form of the polymer measured in the presence of KCl and the value for the bromide form measured in the presence of KCl were found to be equal as expected. The concentrations of the KCl and KBr solutions, as determined by potentiometric titration, were not measurably different.

Results and Discussion

The circles (o) in Figs. 1 and 2 represent the measured specific viscosities of PVEP-Br and the bromide form of three of the polysoaps in the presence of 0.0223 N KBr solution. The crosses (+) in Figs. 1 and 2 represent the measured specific viscosities of PVEP-Br and the bromide form of the same polysoaps in the presence of 0.0223 N KCl solution. Finally, the squares (□) in Figs. 1 and 2 represent the measured specific viscosities of PVEP-Cl and the chloride form of the same polysoaps in the presence of 0.0223 N KCl solution.

In studying the interactions of the related polyelectrolyte–polysoap systems with chloride and bromide ions, it was of interest to investigate the influence of different counterions on the size of these polymer chains in aqueous solution. The extrapolation of the specific viscosities to infinite dilution of polymer to get intrinsic viscosities can be done effectively for polyelectrolytes and polysoaps only in the presence of added electrolyte; hence, all of the viscosity measurements were car-

ried out at the aforementioned constant concentration of electrolyte, namely, 0.0223 N.

The effect of the dodecyl group content on the intrinsic viscosity of the bromide form of the polysoaps is shown in Fig. 3. There is a marked decrease of the intrinsic viscosity when the percentage of the soap groups attached to the polyvinylpyridine exceeds a certain value. This effect was first described and analyzed by Strauss and co-workers.[2] They interpreted their results by suggesting the existence of a "critical dodecyl group content" of the polysoaps analogous to the critical micelle concentration of ordinary soaps.

At a low percentage of dodecyl groups, the interaction between the soap-like groups, which will be separated by fairly large distances, is small compared with the repulsive coulomb forces between the positively charged pyridinium groups. The macromolecules are almost as extended as the chains of polyvinylpyridine quaternized only with ethyl bromide and hence they behave like normal polyelectrolytes. The difference between the relative viscosities of PVEP-Br and the polysoaps is small. With increasing dodecyl group content the distance between the soap groups diminishes and their interaction increases. At a certain critical distance, which is reached at the critical dodecyl group content, the interactions between the soap-like groups more than compensate for the repulsive forces between the positively charged pyridinium groups; thus, aggregates are formed by the hydrophobic dodecyl groups. Probably the same forces are of importance here as are responsible for the formation of micelles in solutions of ordinary soaps. As a consequence, the polymer chains shrink together and the relative viscosity drops considerably.

The influence of different counterions on the properties of polysoaps can be learned by comparing the viscosities of the bromide form of the polysoaps and of PVEP-Br with corresponding values of the chloride forms measured in the presence of KBr and KCl, respectively. The differences between PVEP-Br and the bromide form of the polysoaps and the chloride form of these polymers can be summarized as: (1) the intrinsic viscosities of the polyelectrolytes, PVEP-Br and its chloride form, are equal within the accuracy of our measurements; (2) the intrinsic viscosity of the chloride form of the polysoaps is greater than that of the bromide form; (3) the "critical dodecyl group content" of the chloride form of the poly-soaps is greater than that of the bromide form.

The larger critical dodecyl group content for the chloride form of the polysoaps compared with that of the bromide form is of special interest because it has a parallel in the differences between the critical micelle concentrations of ordinary soaps with different counterions (but the same soap ion). In these cases the critical micelle concentration increases with increasing size of the hydrated counterions.[7-9] (For example, the critical micelle concentration of dodecylpyridinium salts increases in the direction I<Br<Cl.)[10] The more precisely one
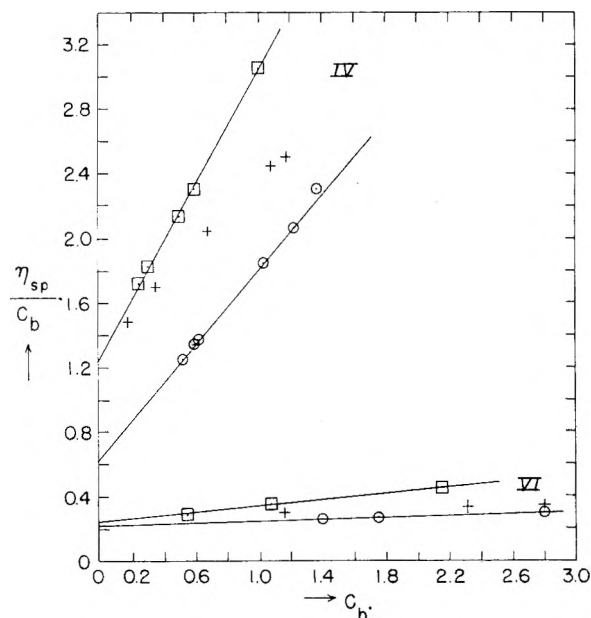
Fig. 2.—Graph of η_{sp}/C_b for polyelectrolytes and polysoaps with chloride and bromide counterions as function of concentration C_b in 0.0223 N KCl and 0.0223 N KBr solutions at 25° (C_b denotes grams of organic cation per 100 ml. of solution): □, denotes chloride form in presence of chloride salt; O, denotes bromide form in presence of bromide salt; +, denotes bromide form in presence of chloride salt; V, refers to polymer with 8.1% dodecyl groups; VI, refers to polymer with 31.8% dodecyl groups.
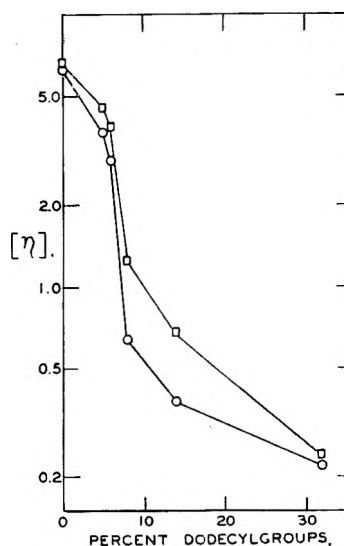
Fig. 3.—Intrinsic viscosities [η] of polyelectrolytes and polysoaps with chloride and bromide counterions as functions of dodecyl group content in 0.0223 N KCl and 0.0223 N KBr solutions, respectively. The intrinsic viscosities are plotted as ordinates using a logarithmic scale; □ denotes chloride form and O denotes bromide form.

can maintain equal distances between the dodecyl groups along the polyvinylpyridinium chains, the sharper will be the transition from the expanded to the coiled form of the polysoap chains when the critical soap group content is reached. Furthermore, the difference between the critical dodecyl group content of the polysoaps in their chloride and bromide forms would be sharper. In the case of

(7) E. D. Goddard, O. Harva and T. G. Jones, Trans. Faraday Soc., 49, 980 (1953).

(8) C. S. Samis and G. H. Hartley, ibid., 34, 1288 (1938).

(9) J. F. Voeks and H. V. Tartar, THIS JOURNAL, 59, 1190 (1955).

(10) H. Lange, Kolloid Z., 121, 66 (1951).

exactly equal distances, the polysoap can be regarded as being built of only one kind of soap molecule with only one critical micelle concentration for chloride counterions and one for bromide counterions. From the nature of the synthesis of our polysoap, we must assume that the distances will vary about an average value. This means that the polysoaps must be regarded as being built of a number of different kinds of soap molecules, each with different critical micelle concentrations. The actual critical dodecyl group content for either the chloride or the bromide form is some kind of mean value. With increasing dodecyl group content, the critical distance is not reached in all parts of the polymer chains at the same time. Consequently, the transition from the expanded form to the coiled form of polysoaps with chloride or bromide counterions is spread out over a range of compositions. In addition, the stiffness of the polymer chains may also contribute to the effect. This picture is further complicated by the fact that by changing the degree of quaternization of polyvinylpyridine with dodecyl groups, not only the distance between the soap-like groups is changed, but also

the ratio of hydrophobic to hydrophilic groups. This ratio determines, in the case of ordinary soaps, the critical micelle concentration and the solubility.[11,12]

We must bear in mind that the critical micelle concentrations for ordinary soaps are influenced by the presence of added electrolyte.[10,11] Accordingly, it is conceivable that the critical dodecyl group contents and their difference for the chloride and bromide forms of the polysoaps are also influenced by the presence of added salt. If we plot an effective length of the chains of the polyelectrolyte and the different polysoaps, derived from the intrinsic viscosity, against their dodecyl group content, it can be seen immediately that the poly-soaps with a dodecyl group content in the critical range represent a system converting chemical energy into mechanical by exchanging their bromide counterions with chloride and the reverse.[13,14]

(11) E. K. Goette, J. Colloid Sci., 4, 467 (1949).

(12) H. V. Tartar and K. A. Wright, J. Am. Chem. Soc., 61, 539 (1939).

(13) W. Kuhn, Angew. Chem., 70, 58 (1958).

(14) D. Woermann, Z. physik. Chem., Neue Folge, 19, 65 (1959).

THE ADSORPTION OF PHOTOGRAPHIC DEVELOPERS BY METALLIC SILVER

By R. J. Newmiller and R. B. Pontius

The adsorption by metallic silver of five common photographic developers has been measured. Adsorption isotherms of the Langmuir type have been obtained at 20 and 40° for 4-amino-3-methyl-N-ethyl-N-(β-methylsulfonamidoethyl)-aniline (I), 4-amino-3-methyl-N,N-diethylaniline (II) and p-methylaminophenol (Elon). Simple p-phenylenediamine was found to adsorb but did not follow a Langmuir-type isotherm. No adsorption of hydroquinone by silver could be detected. Developers I and II were found to adsorb with a heat of adsorption of 12 kcal. per mole. Elon and p-phenylenediamine were adsorbed more weakly with heats of adsorption of 3 and 6 kcal. per mole, respectively.

Introduction

It has long been realized that developer adsorption plays an important part in the mechanism of photographic development. The adsorption may take place on silver, silver halide or both, depending upon the developer being used. This paper deals with the adsorption of developers by metallic silver.

A study of developer adsorption by metallic silver is important for two reasons. First, in some theories of direct chemical development proposed in the literature from time to time, adsorption of the developer by the latent image has been regarded as a key step.[1-3] The adsorption of quinone by silver has been investigated by Staude and Brauer[4] and the question of the part played in photographic development by the adsorption of de-

veloper by silver has been discussed recently by Eggert[5] and by Klein.[6]

Second, in the study of physical development, knowledge of adsorption is important to the investigation of the catalytic effect exerted by silver, whereby the activation energy for the reduction of silver ion at the surface is lowered below that of the homogeneous, uncatalyzed solution reaction.[7]

Little work has been reported in the literature concerning the direct measurement of developer adsorption by silver. Rabinovitch[2,3] attempted to measure the adsorption of hydroquinone by colloidal silver, and reported that hydroquinone was strongly adsorbed. Later, Perry, Ballard and Sheppard,[8] using an improved method, attempted to measure the adsorption of hydroquinone and Elon[9] to silver, but found no indication of adsorption with these developing agents.

(1) A. J. Rabinovitch, S. S. Peissachovitch and L. Minaev, "Ber. über d. VIII Internat. Kongress f. wiss., u. angew. Photographie," Dresden, 1931, p. 186.

(2) A. J. Rabinovitch, Z. wiss. Phot., 33, 57 (1934).

(3) A. J. Rabinovitch and S. S. Peissachovitch, ibid., 33, 94 (1934); Acta Physicochim. U.R.S.S., 4, 705 (1936); Trans. Faraday Soc., 34, 920 (1938).

(4) H. Staude and E. Brauer, Z. Elektrochem., 58, 129 (1954).

(5) J. Eggert, Phot. Sci. Eng., 1, 94 (1958).

(6) E. Klein, Z. Elektrochem., 62, 505 (1958).

(7) S. E. Sheppard, Phot. J., 59, 135 (1919).

(8) E. S. Perry, A. Ballard and S. E. Sheppard, J. Am. Chem. Soc., 63, 2357 (1941).

(9) Trademark of N-methyl-p-aminophenol sulfate, sold by the Eastman Kodak Company.

No data have ever been published concerning the direct measurement of adsorption of a p-phenyl-enediamine-type color developer by silver. Kinetic evidence, however, has seemed to point to the fact that these developers are adsorbed quite strongly.[10,11]

In view of the conflicting results which have been obtained with black-and-white developers, it is clear that any technique to be used to measure the adsorption must be considerably more sensitive than those used previously. Two requirements are essential for the system. First, the silver surface to be used should be clean, free of oxide, and reproducible, and, second, the developer must be protected from oxidation at all times. Thus, a method is needed in which the entire process can be carried out in an enclosed system. Conway, Barradas and Zawidzki[12] have described a method for determining adsorption of organic materials to metals, employing an ultraviolet spectrophotometric method of analysis. The system to be described here utilizes a similar method of analysis.

Experimental

Apparatus.—A fine silver wire (0.001 inch in diameter), drawn by Engelhard Industries of Newark, New Jersey, from better than 99.98% pure silver (as verified by spectrographic analysis) was used as the adsorbent. The wire had a specific geometric surface of about 160 cm.^{2}/g. Between 30 and 35 g. of silver was used in each experiment. Adsorption measurements were made in a flow system (Fig. 1), utilizing a spectrophotometric analysis of the developer solution. A Beckman DU Spectrophotometer, equipped with dual thermospacers for better temperature control, was used in the system. A special silica flow cell for the spectrophotometer was constructed from a design by Sweet and Zehner.[13] All other glassware in the system was Pyrex. The silver chamber was a 24/40 standard taper joint which had been sealed off at the lower end and a small tube attached. The silver wire was unspooled, extracted in a Soxhlet extractor with anhydrous ether for 10 hr. and packed in the chamber. A Teflon gland with a glass tube through it was inserted in the top.

Two short lengths of neoprene tubing were used to connect the silver chamber to the hydrogen inlet and exhaust. The lower portion of the chamber was inserted in a muffle furnace until all the silver was inside. Hydrogen was then slowly passed through the chamber and the temperature raised to 500°. After about 1 hr., the chamber was removed from the furnace and allowed to cool with the hydrogen still flowing. Pinch clamps then were placed on the short lengths of tubing and the hydrogen was disconnected. The chamber now was installed in the adsorption system, as shown in Fig. 1. No deleterious effects could be detected from the use of Pyrex in the 500° hydrogenation.

The system used a Sigmamotor pump to circulate the solution. All connecting tubing was $^1/_8$-inch i.d. neoprene. It was found that Tygon tubing gave off products at alkaline pH which interfered with the ultraviolet analysis of the developer, and therefore could not be used.

Buffer.—Reagent grade sodium carbonate was used as a buffer in the experiments. The buffer solution was prepared by dissolving 1.68 g. of the monohydrate in a liter of water. In most experiments, 25 ml. of the buffer was used with 25 ml. of the acid developer solution. This combination yielded a pH of about 10.8 for the mixed developer. Slight variations in pH had no effect on the adsorption.

Preparation of the Adsorption Apparatus.—The construction of the developer and silver chambers was such that they could be set up immersed in a water-bath to obtain the desired temperature control. The rest of the system was connected as shown in the diagram. The amount of buffer
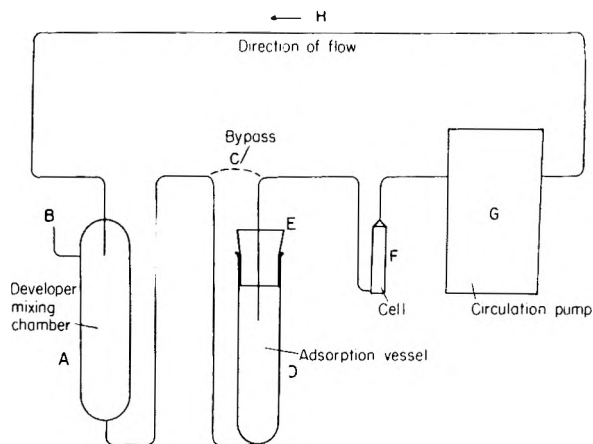
Fig. 1.—Adsorption apparatus: A, developer mixing chamber; B, developer inlet tube; C, bypass; D, adsorption vessel; E, Teflon gland; F, flow cell in spectrophotometer; G, circulation pump; H, direction of flow. All portions except pump and connecting leads thermostated; thermostat not shown.
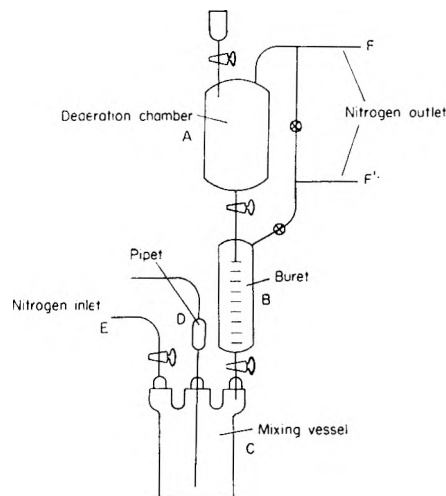
Fig. 2.—Enclosed system for preparation of developer: A, chamber for deaeration of distilled water; B, buret for measurement of water used; C, mixing vessel; D, pipet; E, nitrogen inlet; F,F', nitrogen outlet.

necessary for the experiment was placed in the mixing chamber and pure nitrogen passed through the system. This was done in such a manner as to deaerate the buffer and flush the system free of oxygen.

Preparation of the Developer.—The developer solution was prepared in the system shown in Fig. 2. Distilled water was deaerated in vessel A for about 1 hr. with pure nitrogen. The developer powder was weighed out on an analytical balance and placed in the three-necked flask C. Nitrogen then was passed through vessels B and C for 30 min. to free them of any air. The desired amount of water now was measured out in vessel B and run into C. When the developer had dissolved completely, the desired amount of solution was drawn into the pipet (D) and transferred to the developer inlet tube in the adsorption apparatus. The short contact with air, which the tip of the pipet encounters in transferring the solution, did not cause any oxidation of the developer, which, at this stage, was still acidic. The solution was then allowed to come to temperature equilibrium before any measurements were made.

Measurement of the Adsorption.—The pump was started with the bypass open and pinch clamps still in place on the short rubber tubes leading to the silver chamber. The system was run for about 3 min. to assure uniform temperature and the optical density of the solution read at a suitable wave length. The pump then was stopped, the bypass closed, and the pinch clamps removed. The solution now
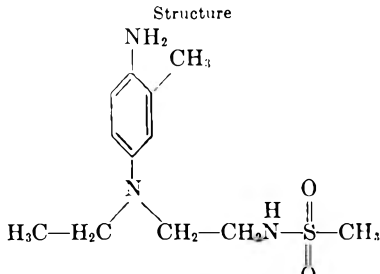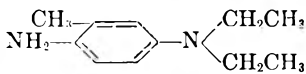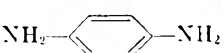
(10) (a) T. H. James, THIS JOURNAL, **45**, 223 (1941); (b) A. Weissberger and D. S. Thomas, Jr., *J. Am. Chem. Soc.*, **64**, 1561 (1942).

(11) G. I. P. Levenson and T. H. James, *J. Phot. Sci.*, **2**, 172 (1954).

(12) B. E. Conway, R. G. Barradas and T. Zawidzki, THIS JOURNAL, **62**, 676 (1958).

(13) T. R. Sweet and J. Zehner, *Anal. Chem.*, **30**, 1713 (1958).

TABLE I

Adsorption of Developers by Silver, per Cent. Coverage and Heat of Adsorption

Developer	Structure	Calcd. amt. for monolayer cover. moles/cm.²	Actual amt. for monolayer cover. moles/cm.²	% Coverage at 20°	Isoteric heat of adsorption in kcal./mole
4-Amino-3-methyl-N-ethyl-N-(β-methyl-sulfonamidoethyl)-aniline (I)	NH_2 ... CH_3 ... H_3C-H_2C $CH_2-CH_2N-S-CH_3$ (structure)	10×10^{-11}	10×10^{-11}	100	12 to 13
4-Amino-3-methyl-N,N-diethylaniline (II)	CH_3, NH_2 ...—N$\big\langle$$CH_2CH_3$ / CH_2CH_3	15×10^{-11}	15.5×10^{-11}	100	11 to 12
p-Methylaminophenol (III)	HO— —N$\big\langle$$CH_3$ / H	20×10^{-11}	4.6×10^{-11}	23	Approx. 3
p-Phenylenediamine (IV)	NH_2— —NH_2	23×10^{-11}	No plateau within present measurements	>30	5 to 6
Hydroquinone (V)	HO— —OH	23×10^{-11}	None	None	.....
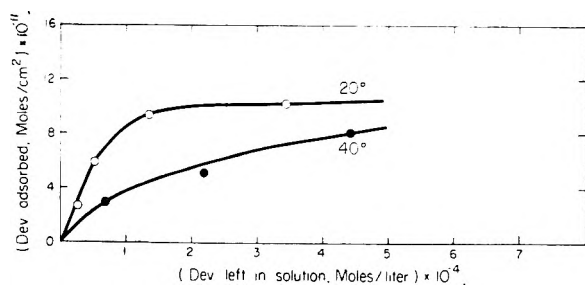
Fig. 3.—Adsorption isotherms for adsorption of developer (I) to silver at 20 and 40°: developer adsorbed in moles/cm.² × 10⁻¹¹ (y-axis) vs. developer remaining in solution in moles/l. × 10⁻⁴ (x-axis).
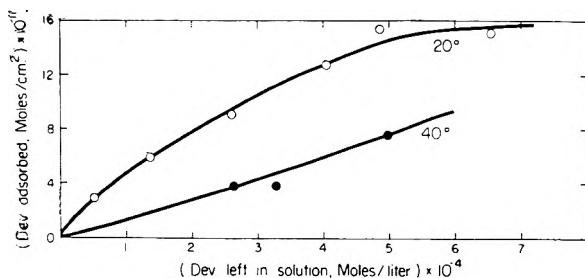
Fig. 4.—Adsorption isotherms for adsorption of developer (II) to silver at 20 and 40°: developer adsorbed in moles/cm.² × 10⁻¹¹ (y-axis) vs. developer remaining in solution in moles/l. × 10⁻⁴ (x-axis).

could flow through the bundle of silver wire. The pump was started again and the optical density determined at the same wave length until an equilibrium was attained. This usually required not more than 5 to 10 min. Longer times did not change the values obtained. The developer adsorbed was assumed to be proportional to the change in the optical density of the solution. The solution optical densities were read in the ultraviolet around 300 mμ, the exact wave length depending on the developer and concentration being used. Blank runs with no silver present showed no adsorption to the glass or tubing.

Developer Purification.—Five developers were used in the experiments. The p-phenylenediamine was Eastman Organic Chemical No. 207 White Label Grade. It was used without further purification. The Elon and hydroquinone were pure samples of standard Kodak developers.

Developer I was purified by converting Kodak Color Developing Agent, Type CD-3 (4-amino-3-methyl-N-ethyl-N-(β-methyl-sulfonamidoethyl)-aniline sesquisulfate monohydrate) to the free base, warming in activated carbon and filtering. The free base was extracted with chloroform and recrystallized by adding an equimolar quantity of dilute sulfuric acid, thus forming the monosulfate salt. This was then dried in a vacuum desiccator.

Developer II was purified by recrystallizing Kodak Color Developing Agent, Type CD-2 (4-amino-3-methyl-N,N-diethyl aniline hydrochloride) in boiling ethyl alcohol and filtering. The solution then was cooled to 20° and the solid filtered off. The developer was washed in isopropyl alcohol, then acetone, and dried in a vacuum desiccator.

Results

All five developers used showed some evidence of adsorption by silver, with the exception of hydroquinone. A number of runs with hydroquinone showed no detectable adsorption for various concentrations at 20°. The adsorption isotherms obtained for the remaining developers are shown in Figs. 3 to 7. I and II exhibit similar isotherms. Both developers were adsorbed strongly and showed strong dependence on temperature. Elon was adsorbed much more weakly and showed very little temperature - dependence. p - Phenylenediamine was adsorbed, but the adsorption isotherms are quite different in appearance from those of I and II. No plateau was obtained within the sensitivity of present measurements and only a moderate dependence on temperature was seen. Data are listed in Table I for equilibrium coverage at 20° and for per cent. of surface covered. The flat, projected area of the developer molecules was computed from van der Waals radii and by using scale molecular models. The silver surface was determined by assuming the surface of the wire to be smooth and calculating the geometrical area. While it was realized that the developer may not always be adsorbed flat and the wire may not have a completely smooth surface, good agreement in the cases of I and II was obtained in this manner. It was considered, therefore, that this procedure

gives a good comparison of the different developers tried.

In order to determine whether the adsorption isotherms were of the Langmuir type, which characteristically exhibit monomolecular coverage at equilibrium, the Langmuir equation was rearranged to the form[14]

$$\frac{P}{Y} = \frac{1}{k_1} + k_2 P$$

where P is the pressure of the adsorbate present, Y is the amount of material in the adsorbed phase, and k_1 and k_2 are constants. It is apparent that the quantity corresponding to the pressure is the concentration of developer in the solution phase not adsorbed, while Y corresponds to the amount of material per unit area adsorbed. Both of these quantities can be taken from the adsorption isotherms. If the concentration of developer left in solution is plotted against the ratio of concentration left in solution to the amount adsorbed, a straight line should result, provided the adsorption is of the Langmuir type. Figure 7 shows this type of plot for the 20° isotherms. All developer data except those for p-phenylenediamine yield straight lines.

Reproducibility of experimental values using the present method is about $\pm 5\%$. It is believed that this may be improved by refinements in technique.

Isoteric heats of adsorption for the developers were calculated from the Clausius–Clapeyron equation, with data from the adsorption isotherms. The values given in Table I are an average of a number of values from 50 to 80% surface coverage.

Time Required for Adsorption

The present system was not constructed to measure rates of adsorption but some information can be obtained from the data. It was found that equilibrium adsorption occurred in less than 5 min. after contact with the silver. This represents the time required for the solutions in the apparatus to come to equilibrium. Solutions, which were allowed to circulate over the silver for as long as an hour, showed very little or no additional change in concentration.

Discussion

The primary object of the present experiments was to resolve some of the speculation concerning the mechanism of photographic development. The system which has been used does not actually measure adsorption by developed silver, but the clean, hydrogenated surface of the silver wire is believed to be similar to the surface of freshly reduced silver.

In photographic practice, the presence of a protective colloid and of silver ions may result in a competition with the developer molecules for adsorption sites. The relative amounts of the different species adsorbed must depend upon their heats of adsorption and relative concentrations. In the absence of direct measurements of the heat of adsorption of gelatin and of silver ion to silver, the effects of this competitive adsorption on photographic development cannot be assessed exactly.

(14) J. H. deBoer, "The Dynamical Character of Adsorption," Oxford University Press, New York, N. Y., 1953, p. 58.
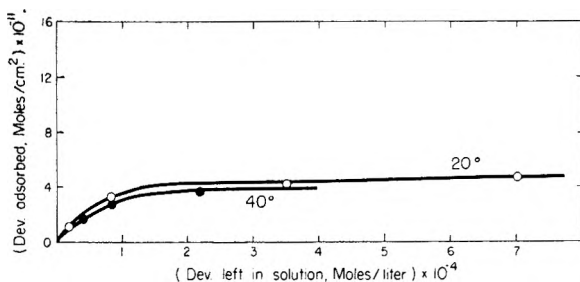
Fig. 5.—Adsorption isotherms for adsorption of p-methylaminophenol (Elon) to silver at 20 and 40°: developer adsorbed in moles/cm.^{2} $\times$ 10^{-11} (y-axis) vs. developer remaining in solution in moles/l. $\times$ 10^{-4} (x-axis).
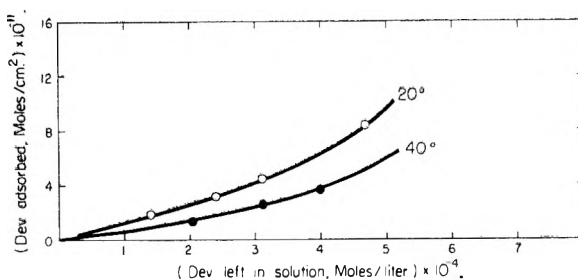
Fig. 6.—Adsorption isotherms for adsorption of p-phenylenediamine to silver at 20 and 40°: developer adsorbed in moles/cm.^{2} $\times$ 10^{-11} (y-axis) vs. developer remaining in solution in moles/l. $\times$ 10^{-4} (x-axis).
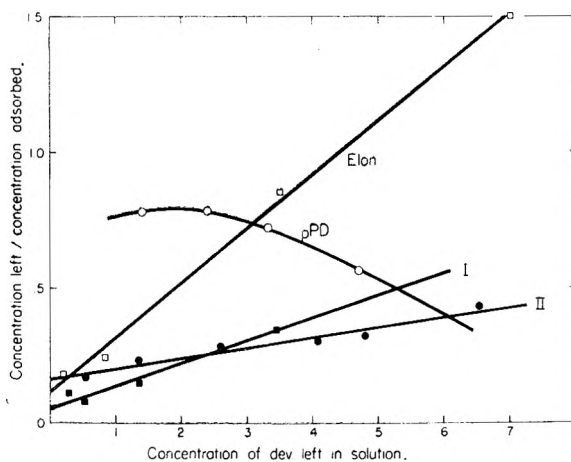
Fig. 7.—Test for conformation of adsorption isotherms to Langmuir-type adsorption: concentration of developer remaining/concentration of developer adsorbed (y-axis) vs. concentration of developer remaining in solution (x-axis).

The data substantiate Perry, Ballard and Sheppard's[8] criticism of the work of Rabinovitch,[3] who concluded that hydroquinone is adsorbed by silver. Perry, Ballard and Sheppard may have been entirely correct in their conclusion that Elon is not adsorbed, since ionization of the developer may play a part in adsorption. At a pH of 9.0, used by these authors, Elon, which has a pK of 10.25,[15] is not ionized. Weak adsorption of Elon was found in the present experiments carried out at the higher pH of 10.8, at which value the Elon molecule is ionized. However, hydroquinone, which also is ionized at pH 10.8, showed no adsorption. The possibility that the adsorption of hydroquinone might require the prior adsorption of silver ions

(15) R. W. Henn, PSA Journal (Phot. Sci. Technique), 18B, 90, (1952).

was not investigated, since oxidation of the developer would interfere with the analysis. Evidently silver ions are, however, not necessary to effect the adsorption of the p-phenylenediamines and Elon.

Levenson and James[8-11] state that developers containing amino groups are able to be adsorbed by silver bromide because of their ability to form a covalent complex with silver ion. Of the five developers studied, those that are adsorbed by silver do contain amino groups. The ability of the amino nitrogen to form a covalent complex with silver ion, and thus to promote adsorption by silver halide, is indicative of a property of the amino group which may or may not also be responsible for the adsorption of these developers by silver in the absence of silver ion. The heat of adsorption for I and II is too large for the adsorptive forces to be of the van der Waals type, and shows that some type of strong interaction between developer and metallic silver occurs. It is believed that the 3-methyl group on the I and II molecules[16] increases the electron-releasing ability of the free amino group and this electromeric effect may contribute to the adsorptive forces. The weaker adsorption of simple p-phenylenediamine may be due to its symmetrical structure which causes a uniform distribution of charge over the molecule. Elon had a very weak adsorption which would be expected from an N-substituted-p-aminophenol. Hydroquinone, having no amino groups, is not adsorbed.

In studying the rate of reduction of silver ions by

hydroquinone and p-phenylenediamine in alkaline solution, James[9] states that the rate of reaction for hydroquinone is proportional to a fractional power of the silver-ion concentration. For p-phenylenediamine, however, the rate of reaction is dependent on the developer concentration to a fractional power. This is also very strong evidence that silver-ion adsorption is necessary for hydroquinone to act as a reducing agent, while p-phenylenediamines may be adsorbed without silver ion on the surface.

In studying postfixation physical development, Pontius and Thompson[17] found, in the case of I, that the rate was proportional to the developed silver to the $^1/_2$ power. This is consistent with James's postulates. Other reports[11,18,19] give similar theories involving non-adsorption of black-and-white developers and adsorption of p-phenylenediamine by silver.

These measurements of adsorption of developers by silver therefore confirm the evidence derived from the study of the kinetics of physical development. The method used for these measurements readily can be adapted to measurement of adsorption of other substances.

(16) R. L. Bent, et al., J. Am. Chem. Soc., 73, 3100 (1951).

(17) R. B. Pontius and Joan S. Thompson, Phot. Sci. Eng., 1, 45 (1957).

(18) T. H. James, J. Chem. Ed., 23, 595 (1946).

(19) T. H. James and W. Vanselow, Phot. Engineering, 6, 183 (1955).

THERMODYNAMIC PROPERTIES OF HIGHER FLUORIDES. I. THE HEAT CAPACITY, ENTROPY, AND HEATS OF TRANSITION OF MOLYBDENUM HEXAFLUORIDE AND NIOBIUM PENTAFLUORIDE[1]

By A. P. Brady, O. E. Myers and J. K. Clauss

Contribution from Stanford Research Institute, Menlo Park, Cal.

The third-law entropy of liquid molybdenum hexafluoride at 25° was found experimentally to be 60.6 ± 0.7 e.u.; calculated from extant spectral data and estimates of the heat of vaporization, it is 60.1 e.u. A hitherto unreported solid–solid transition at −9.6°, $\Delta H = 1.96$ kcal./mole, was found. The experimental heat of fusion, at +17.5°, was found to be 1.06 kcal./mole, much less than estimates in the literature. The entropy of solid niobium pentafluoride at 25° was found to be 38.3 ± 0.7 e.u. The heat of fusion, determined from drop calorimetry, was 2.92 kcal./mole at ∼77°.

Introduction

General data on the physical properties of both MoF_6 and NbF_5 are relatively sparse. Of the two, more is known about MoF_6. The density, boiling point and vapor pressure curve have been determined by Ruff and Ascher.[2] The heats of fusion and of vaporization have been calculated by Ruff and Ascher from the vapor pressure data and recalculated, with a somewhat different result, from the same data by Kelley.[3] The infrared, ultraviolet and Raman spectra also have been measured.[3-6] Data are more scattered in the case

of NbF_5. Reported values for its melting point vary from 72 to 80°.[7-10] The National Bureau of Standards compilation[11] lists 75.5° for the melting point and 225° for the boiling point, with a heat of vaporization of 11.1 kcal./mole. More recently available data[9,10] tend to favor a melting point

(1) This work was supported in part by the Materials Laboratory, Wright Air Development Center.

(2) O. Ruff and E. Ascher, Z. anorg. allgem. Chem., 196, 413 (1931).

(3) K. K. Kelley, U. S. Bur. Mines Bull. No. 476, 1949.

(4) K. Tanner and A. E. F. Duncan, J. Am. Chem. Soc., 73, 1164 (1951).

(5) T. G. Burke, D. F. Smith and A. H. Nielson, J. Chem. Phys., 20, 447 (1952).

(6) J. Gaunt, Trans. Faraday Soc., 49, 1122 (1953).

(7) O. Ruff, J. Zedner, E. Schiller and A. Heinzelmann, Ber., 42, 492 (1909).

(8) V. Schomaker and R. Glauber, Nature, 170, 290 (1952).

(9) F. Fairbrother and W. C. Frith, J. Chem. Soc., 3051 (1951).

(10) J. H. Junkins, R. L. Farrar, Jr., E. J. Barker and H. A. Bernhardt, J. Am. Chem. Soc., 74, 3464 (1952).

(11) National Bureau of Standards, Circular 500, 1952.

close to 79°, a boiling point of about 234°, and heat
of vaporization of the order of 12.7 kcal./mole at
the boiling point. The heat of fusion has been
estimated to be 8.6 kcal./mole by analysis of
experimental heating curves[10] and 4.2 kcal.[12]
by application of the "rule" that the entropy of
fusion of un-ionized salts is about 2 e.u. per gram
atom.

Experimental

1. **Materials.**—Commercial molybdenum hexafluoride
(General Chemical Division, Allied Chemical and Dye
Corporation) was subjected to a number of single-plate dis-
tillations over sodium fluoride in a thoroughly dried all-glass
system.[4] The sodium fluoride is necessary to tie up HF to
interrupt the chain

$$MoF_6 + 3H_2O \longrightarrow MoO_3 + 6HF$$
$$6HF + 3/2SiO_2 \longrightarrow 3/2SiF_4 + 3H_2O, \text{ etc.}$$
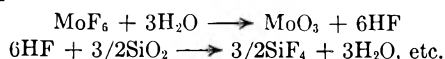
The center cut was water-white and the premelting curve
(Fig. 1) indicated less than 0.02 mole % impurity.

The niobium pentafluoride used for the bulk of the experi-
mental work was prepared by reaction of dry HF gas with
powdered niobium metal[13] contained in a nickel reactor at
250°. The niobium metal was Fansteel "High Purity,"
analyzing less than 0.2% vanadium. The progress of the
reaction was followed by measuring the volume of hydrogen
evolved. When hydrogen evolution ceased, at about 99%
of the theoretical volume, the reactor was placed in an
evacuable dry-box and the product transferred under dry he-
lium. Analysis indicated 0.9% impurity of metallic niobium,
which has been corrected for in the calorimetric work.
Some check experiments were made with the distillate from
a commercially prepared sample which had been exposed to
air during shipment, since this provided a sample with a
totally different history.

2. **Temperature Measurement.**—The central instru-
ment for temperature measurement was a precision recording
microvolt potentiometer built in these laboratories. This
will be described in detail elsewhere. It is a double poten-
tiometer operating on the Lindeck principle, a system which
is particularly adaptable to servomechanisms. An input of
10 microvolts results in an output of 10 millivolts, which can
be recorded on a standard 12-millivolt strip-chart recorder
(to less than 0.02 microvolt).

For temperature measurements below room temperature,
copper–constantan thermocouples were used. The ther-
mocouples were calibrated by comparison with a platinum
thermometer and with a copper thermometer. The plati-
num resistance thermometer (Weiller Instruments Corpora-
tion) was of the Myers construction and comparison with the
standard thermometers of the National Bureau of Standards
therefore justified. Its calibration data, as furnished by the
manufacturer and verified in this Laboratory to 0.05% or
less at the ice point and at the boiling point of nitrogen, indi-
cates that it is of slightly higher purity than the Bureau of
Standards "L" series. For the region between the boiling
point of nitrogen and the sodium point calibration data
furnished by the manufacturer were used. From the nitro-
gen point to −223°, the temperature scale was established
by matching the observed resistance with the tabulated data[14]
for the Bureau of Standards L-6 thermometer. As a further
check comparison was made with a copper thermometer,
using the data published by Dauphinee and Preston-
Thomas.[15] The maximum difference observed between the
copper and platinum therometers was 0.1°. This dis-
crepancy probably should be ascribed mostly to errors in the
copper thermometer, but at any rate sets an upper limit to
errors in absolute temperature. Temperature differences,
of course, could be measured much more accurately—to
about 0.002° at 50°K. and to 0.0005° at room temperature.

Temperatures above room temperature were measured

---

(12) L. Brewer, "National Nuclear Energy Series," Vol. IV, 19B,
Ed. by L. L. Quill, McGraw-Hill Book Co., New York, N. Y., 1951.

(13) V. Gutman and H. J. Emeleus, *J. Chem. Soc.*, 1046 (1946).

(14) American Institute of Physics, "Temperature. Its Measure-
ment and Control in Science and Industry," Reinhold Publ. Corp.,
New York, N. Y., 1941.

(15) T. M. Dauphinee and H. Preston-Thomas, *Rev. Sci. Instr.*, **25**,
884 (1954).
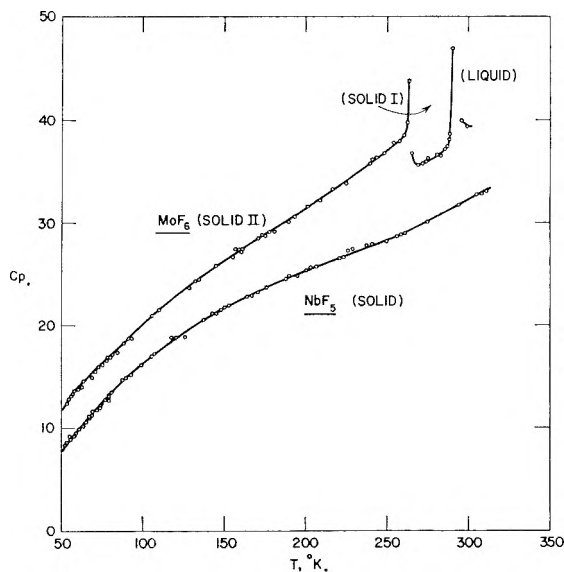
Fig. 1.—Heat capacity of MoF_6 and of NbF_5 below room
temperature

with a platinum–platinum, 10% rhodium thermocouple,
calibrated by the Bureau of Standards. Again the esti-
mated accuracy is 0.1°.

The calibration data for the copper–constantan thermo-
couples were expressed conveniently as a cubic equation in
temperature.[13] Solving an implicit cubic equation is tedious
and time-consuming; accordingly, for each thermocouple a
program was prepared for an IBM Card-Programmed-
Computer. The program accepts the initial and final ther-
mocouple potential (extrapolated to the mid-point of energy
input) and the input energy and yields the temperatures in-
volved and the heat capacity of the system.

Energy input values were determined by preparing smooth
curves of potential and current from the strip-chart record in
order to obtain a coincident product. It turns out that the
input power was generally constant to within a few hun-
dredths of a per cent. for a given run.

3. **Calorimeters.**—The low temperature cryostat assem-
bly was essentially the same as that described by Kelley,
Naylor and Shomate[16] and its details will be omitted here.
Higher temperature heat contents were determined by
conventional drop-calorimetry but with some unusual fea-
tures in gating.

The drop control mechanism is a $7/8$-in. brass tube, 28 in.
long, containing a brass plunger provided with an Alnico V
insert. Holes are drilled in the tube to permit air to escape
until the plunger reaches a point 5.5 in. from the bottom.
Thereafter the flow of air is constricted so that by suitable
adjustment of the constriction the fall is gently and quickly
slowed for the remainder of the drop. There is nearly free
fall (0.9 g.) to the constriction, and a smooth drop can be
completed in 600 milliseconds. The capsule is attached to
the plunger by the proper length of No. 32 platinum–
platinum, 10% rhodium wire which passes through a stain-
less steel hypodermic tube in the upper steel sections of the
furnace.

Before the drop takes place, the plunger supports the cap-
sule in the isothermal region of the furnace. It is held in
place by a pin passing through a wire loop attached to the
plunger. The pin is pulled by a solenoid actuated by a mi-
croswitch on the water-cooled gate. As the magnet in the
plunger passes through the core area of one of two induct-
ances mounted on the brass tube, an electrical pulse is created.
The pulses are applied to the input of a flip-flop circuit so
that as the plunger passes the upper coil a relay is closed.
The pulse from the lower coil opens the relay. This relay
controls a solenoid which pulls open the two lids of the calor-
imeter assembly through a mechanical linkage of Nylon
string. The inductances can be positioned along the brass
tube to reduce to an absolute minimum the time the lids are

(16) K. K. Kelley, B. F. Naylor and C. H. Shomate, U. S. Bureau of
Mines Technical Paper 686, 1946.
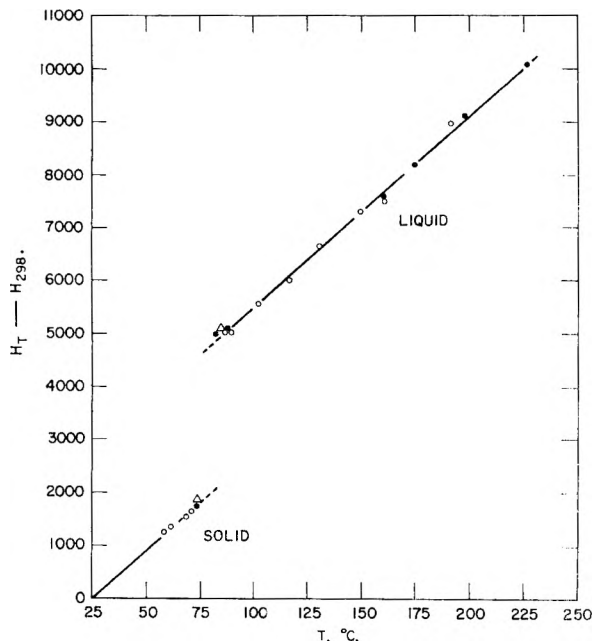
Fig. 2.—Heat content of NbF_5 from room temperature to approximately the boiling point.

TABLE I

LOW TEMPERATURE HEAT CAPACITY OF MoF_6 AND NbF_5 AT ROUNDED TEMPERATURES

T, °K.	C_p, cal./mole-deg. MoF_6	NbF_5	T, °K.	C_p, cal./mole deg. MoF_6	NbF_5
50	11.81	7.82	180	29.43	24.12
60	13.77	9.67	200	31.48	25.45
70	16.50	11.53	220	33.65	26.62
80	17.10	13.32	240	35.97 (SII)	27.82
90	18.67	14.85	260	...	29.03
100	20.12	16.34	273.15	36.17 (SI)	30.16
120	22.52	18.68	280	36.68	30.73
140	25.14	20.83	298.15	39.61 (L)	32.23
160	27.30	22.52	320	...	34.08

TABLE II

MOLAR HEAT CONTENT AND ENTROPY INCREMENTS FOR NbF_5 ABOVE 298.16°

T, °K.	$H_T - H_{298}$	$S_T - S_{298}$
350.7 (S)	1870	5.77
350.7 (L)	4790	14.10
400	6440	18.44
450	8250	22.68
500	10160	26.71

open. The water-cooled gate and the calorimeter lids have milled slots to accommodate the supporting wire.

For the low temperature work with MoF_6, a nickel calorimeter was used. It was attached to the vacuum system of the purification train by means of a nickel screw-cap and a Teflon gasket. The cap was welded to Kovar-to-glass seal. After the usual blank run to obtain the heat capacity of the empty calorimeter, the proper amount of MoF_6 was distilled into the calorimeter (approximately 160 g.) and closure was effected by inserting and tightening a small machine screw in the threaded orifice with a magnetically operated screw device contained within the vacuum system. The closure was quite effective over the approximate month the material was in the calorimeter as judged by constancy of weight, premelting, and the complete volatility of the calorimeter contents at the close of the experiment.

Solid NbF_5 is much less reactive than liquid MoF_6, so a much more convenient copper calorimeter was used for low temperature work, loaded in an evacuable dry box under helium. For drop calorimetry, where the fluoride was liquid part of the time, nickel capsules were used.

Results

Heat Capacities and Heat Contents.—The experimental heat capacities below room temperature for MoF_6 and NbF_5 are plotted in Fig. 1 and are listed for rounded temperatures in Table I. The curve for NbF_5 has no distinguishing features in the temperature range of Fig. 1; that for MoF_6 shows the expected solid → liquid transition at 290.7°K. and a hitherto unreported solid → solid transition at 263.6°K. This transition is quite sharp and reproducible when approached from the low temperature side, although there is some tendency to supercool when it is approached from above. The existence of such a transition should perhaps have been anticipated, since WF_6 is reported to undergo one at 265.0°K.[11] and Ruff and Ascher's vapor pressure curves for MoF_6 show a slight but definite break in the general region of the transition temperature observed here.

Figure 2 gives the experimental heat content relative to 298.2°K. for NbF_5 approximately up to its normal boiling point; values at rounded temperatures and at the solid → liquid transition

(approximately 350.7°K.) are given in Table II.

Heats of Transition.—The solid → solid transition for MoF_6 at 263.6°K. was determined to be 1957 ± 10 cal./mole and the solid → liquid transition to be 1059 ± 10 cal./mole. This latter value is far lower than estimates of about 2,500 cal./mole from vapor pressure data,[2,3] but, as mentioned above, these estimates entail fairing through the solid → solid transition.

The heat of fusion of NbF_5 was determined from the data plotted in Fig. 1 to be 2920 ± 15 cal./mole. The three separate series of runs, two with fillings made on separate occasions with the preparation of these laboratories and the third with the distillate from a commercial preparation, are in essential agreement. The measured value is far less than the 8600 cal./mole reported by Junkins, Farrar, Barker and Bernhardt[10] and appreciably less than Brewer's estimate of 4200 cal./mole.[11] However, the experimental entropy of fusion, 1.62 e.u./g. atom, seems quite reasonable.

Entropies.—For MoF_6 the logical extrapolation function would be a Debye function with six degrees of freedom and Einstein functions with frequencies near those found in Raman and infrared spectra. However, an even approximate fit for the points at the lower temperatures cannot be obtained by this combination of functions. By using a Debye function of eight degrees of freedom ($\theta_D = 133$°K.) a fit of ± 0.6% was obtained to 200°K. There appears to be no justification other than a pragmatic one for the use of eight degrees of freedom, although its use has been found expedient by others.[17]

The calculation steps for obtaining the entropy of MoF_6 at 298.15°K. are summarized in Table III. The entropy of the liquid was found to be 60.6 ± 0.7 cal./deg. mole. The "experimental" standard entropy of the ideal gas at one atmosphere

(17) R. D. Taylor and J. E. Kilpatrick, J. Chem. Phys., 23, 1232 (1955).

TABLE III

MOLAL ENTROPY AT 25° OF MoF_6 AND NbF_5

	S, cal./mole deg.	
	MoF_6	NbF_6
0–50°K. (extrap.)	8.15	4.27
50–263.6° $\int C_p$ d ln t	36.50	
Transition	7.72	
263.6–290.6°K.		
$\int C_p$ d ln t	3.56	
Fusion	3.65	
290.6–298.15°K.	1.04	(50–298.16)
$\int C_p$ d ln t	——	34.02
$S_{298.15°K.}$	60.6 (liquid)	38.3 (solid)
Vaporization 6000/298.15	20.1	
Gas imperfection	0.2	
Compression R ln (645/760)	−0.3	
$S_{298.15°K.}$ (exp.)	80.6 (ideal gas)	
(calcd.)	80.05	

was obtained by use of Kelley's estimate[2] for the heat of vaporization, a crude (but relatively unimportant) correction for gas imperfection using a modified Berthelot equation (taking $T_c/T_B = 1.55$ and $b = 80$ cc.), and Ruff and Ascher's[2] vapor pressure data. The result of 80.6 cal./deg. mole is to be compared with 80.05 cal./deg. mole calculated by Gaunt[18] from infrared and Raman spectra. The spectroscopic value is to be preferred for the gas, but not necessarily for the liquid, principally because of the uncertainty in the entropy of vaporization.

Table III also lists the entropy for solid NbF_6 at 298.15, 38.3 cal./mole deg. For the extrapolation from 50 to 0°K. there are no data to guide the choice of Einstein functions; a Debye function of 6 degrees of freedom ($\theta_D = 170°K.$) and eight Einstein functions ($\nu = 247$ cm.$^{-1}$) were found to reproduce the smoothed experimental curve to ± 0.2% between 50 and 100°K.

Acknowledgments.—The help of Mr. C. I. Glassbrook in the fundamental design of apparatus and of Mr. Glassbrook and Mr. L. A. Cavanagh in construction is gratefully acknowledged.

(18) J. Gaunt, *Trans. Faraday Soc.*, **49**, 1122 (1953).

THERMODYNAMIC PROPERTIES OF HIGHER FLUORIDES. II. THE HEATS OF SOLUTION AND OF FORMATION OF MOLYBDENUM HEXAFLUORIDE, TUNGSTEN HEXAFLUORIDE AND NIOBIUM PENTAFLUORIDE[1a]

BY O. E. MYERS AND A. P. BRADY[1b]

Contribution from Stanford Research Institute, Menlo Park, Cal.

Received October 21, 1959

From solution calorimetry, ΔH_{298}^0 for $MoF_6(l)$ was found to be −388.6 kcal./mole and that for $WF_6(g)$ −416 kcal./mole. No clear cut thermodynamic cycle could be found for NbF_5, but the average for three approaches giving entirely different end products, and fairly concordant results, was −432 kcal./mole. These data, together with previously obtained entropies, permit calculation of the free energies of formation of the three compounds.

Introduction

Estimates of the thermodynamic functions for the higher fluorides of molybdenum, tungsten and niobium[2-4] have been largely intelligent guesswork. Entropies of the ideal gas have been calculated for MoF_6 and WF_6 from Raman and infrared spectra[5-7] but other data have been completely lacking. In a preceding paper[8] from these laboratories, experimental third law entropies were given at 298.15 for liquid MoF_6 and solid NbF_5 and $S_T − S_{298}$ up to approximately the normal boiling point for NbF_5.

(1) (a) This work was supported in part by the Materials Laboratory, Wright Air Development Center; (b) to whom inquiries about this article should be sent.

(2) O. Kubaschewski and E. Evans, "Metallurgical Thermochemistry," Academic Press, New York, N. Y., 1951.

(3) A. Glassner, "The Thermochemical Properties of the Oxides, Fluorides, and Chlorides for 2500°K.," ANL-5750, 1957.

(4) L. Brewer, "National Nuclear Series," Vol. IV, 19B, Ed. by L. L. Quill, McGraw-Hill Book Co., New York, N. Y., 1951.

(5) K. N. Tanner and A. B. F. Duncan, *J. Am. Chem. Soc.*, **73**, 1164 (1951).

(6) T. G. Burke, D. F. Smith and H. A. Nielsen, *J. Chem. Phys.*, **20**, 447 (1951).

(7) J. Garnet, *Trans. Faraday Soc.*, **34**, 358 (1953).

(8) A. P. Brady, O. E. Myers and J. K. Clauss, THIS JOURNAL, **64**, 588 (1960).

The present paper records the results of heats of solution experiments which, together with the data now extant, permit calculation of the free energy functions of the three fluorides.

Experimental

Materials.—The molybdenum hexafluoride, purified by trap to trap distillation in glass over sodium fluoride, was the same material used for the heat capacity determinations discussed in the previous paper.[8] Tungsten hexafluoride, also obtained from the General Chemical Division, Allied Chemical and Dye Corporation, was purified in a similar manner. It is worthy of note that the use of Monel valves with Teflon packing for isolating the traps was found to be much more convenient than Fluorolube-lubricated glass stopcocks, which had a bad tendency to stick, previously used in the MoF_6 purification train. The preparation of the NbF_5, from metallic Nb and gaseous HF, has been described in the previous paper. It contained 0.9% Nb metal as an impurity, which has been corrected for in the calorimetric work.

The MoO_3 used was a hand-picked lot assaying 100.0%, supplied by the S. W. Shattuck Co. It was dried at 250° for six hours prior to use. All other reagents were C.P. grade.

Temperature Measurement.—The temperature of the calorimeter was measured by a Westinghouse 14B thermistor in a bridge circuit. The voltage supply (a 1.3-v. mercury cell) and ratio arms were immersed in a thermostat. The variable arm (a decade box) was in a constant temperature
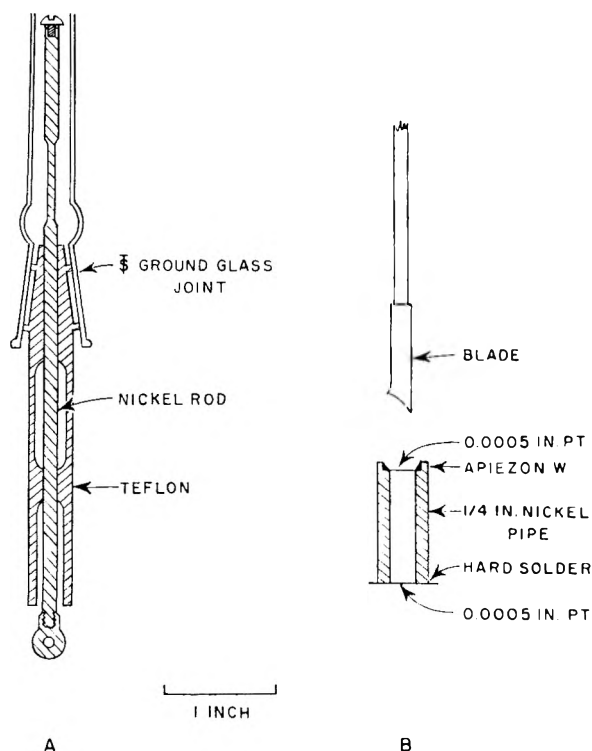
Fig. 1.—Mixing devices: A, Teflon-nickel pipe used for MoF$_6$; B, platinum–nickel ampule and plunger used for WF$_6$ and NbF$_5$

room. A Brown recorder modified to read 500 v. full scale was used as a null and drift indicator. The thermistor was calibrated electrically before and after each run; changes corresponding to about 0.1 cal. (ca. 10^{-4} °) could be detected easily.

Calorimeters.—The solution calorimeters were of conventional type, consisting of a dewar vessel equipped with an insulated closure through which was led a shaft for a stirrer, leads for a manganin heater of known resistance and the thermistor, and a shaft for a capsule-emptying device. The whole was immersed in a constant temperature bath. The MoF$_6$ experiments were run in an all-glass calorimeter; because of a change in the design of the method for introducing the sample (see below) the WF$_6$ and NbF$_5$ experiments were run in a dewar with a glass body but with metal shields for the heater and a metal stirrer. Metallic parts leading out of the calorimeter were of thin-walled Kovar to minimize heat losses.

For ordinary materials (such as MoO$_3$), a frangible glass bulb, containing the sealed-off sample and attached to the bottom of the stirring rod by Apiezon W, served as a convenient method of mixing for starting the solution process. For the higher fluorides, however, this method is objectionable for two reasons: the moisture released during the sealing-off process would start a cyclical reaction with the glass, and momentary high concentrations of fluoride in the presence of an appreciable glass surface area at the instant of breaking might lead to a not inconsequential side reaction. In order to overcome this difficulty two methods for sample introduction were devised. The first, shown in Fig. 1A in the filling position, was a pipet with a Teflon body and a nickel plunger. Approximately 0.075 ml. could be trapped in the annular space between nickel and Teflon by withdrawing the plunger to the intermediate position. The pipet then was withdrawn from the filling assembly, cleaned externally and placed in the solution calorimeter. The liquid was discharged through the machined slot in the Teflon by further withdrawal of the plunger after drift rates had been established. The actual amount of MoF$_6$ discharged from the pipet was determined at the end of the experiment by direct analysis of the solution by the Jones reduction methods.

The second method for sample introduction is illustrated in Fig. 1B. The capsules were sections of nickel pipe, with

platinum foil caps at both ends, which were attached to the vacuum system for filling by means of $^3/_{32}$-in. platinum tubes hard-soldered to copper Housekeeper seals to Pyrex. The ampoules were removed from the vacuum line by pinching off the small platinum tube. For emptying the ampoules in the calorimeter, a plunger was constructed so that the blade forced both foils downward, but during the withdrawal process the upper flap is pulled out.

The Teflon pipet, used for MoF$_6$, had the advantage of positive filling to a prechosen amount, but if the nickel rod became corroded enough not to have a high luster, the subsequent emptying operation was a difficulty. The metal ampoules gave positive emptying, but filling to a convenient level was difficult because they could be weighed only after removal from the vacuum line.

Results

The results of the heat of solution runs are listed in Table I, in terms of the reacting condensed phase, the solution in the calorimeter (before the ampoule is broken), and the heat of reaction per mole of condensed phase. The subscripts used below refer to the reaction numbers in Table I.

TABLE I

HEATS OF SOLUTION

Reac-tion no.	Condensed phase	Solution	Temp., °C.	ΔH, kcal./ mole of con-densed phase
1	0.1759 g. MoF$_6$ (1)	400 ml. 0.1075 f NaOH	25.0	−154.7
2	.2485 g. MoO$_3$	Same	24.9	− 17.6
3	.2434 g. NaF	Same plus 0.2672 g. MoO$_3$	25.0	+ 0.09
4	2.2780 g. WF$_6$ (1)	750 ml. 0.1133 f NaOH	15.0	−149.4
5	2.5138 g. WF$_6$ (1)	750 ml. 0.1084 f NaOH	25.0	−150.8
6	0.7750 g. NbF$_5$	750 ml. 0.1123 f NaOH	24.8	− 97.0
	0.6716 g. NbF$_5$	Same	24.9	− 96.8
7	1.1050 g. NbF$_5$	750 ml. 0.100 f NH$_4$OH	25.1	−100.3
8	0.5604 g. NbF$_5$	750 ml. 2.98 f H$_2$SO$_4$	24.4	− 5.61

Molybdenum Hexafluoride.—The solution reaction 1 corresponds to the skeleton reaction

$$MoF_6(l) + 7NaOH = Na_2MoO_4 + 6NaF + 4H_2O$$
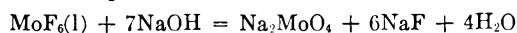
The heat of formation of MoF$_6$, ΔH_{MoF_6} then is given by

$$\Delta H_{MoF_6} = \Delta H_{Na_2MoO_4} \text{ (in soln.)} - \Delta H_1$$

The chosen reaction conditions were such that the concentration of the NaOH is in a range where its heat of formation is nearly constant, −112.12 kcal./mole at the initial concentration, −112.14 kcal. at the final.[9] The heat of formation of liquid water should then suffice, and was taken as ΔH_{H_2O} = −68.32 kcal./mole.[8] Reaction 2 was used in combination with reaction 3 to estimate $\Delta H_{Na_2MoO_4}$ (in solution) via

$$\Delta H_{Na_2MoO_4} \text{ (in soln.)} = \Delta H_2 + 2\Delta H_{NaOH} \text{ (in soln.)} + \Delta H_{MoO_3} - \Delta H_{H_2O}$$

The heat of formation of MoO$_3$ was taken as −178.0 kcal./mole.[10] Reaction 3 was used to estimate ΔH_{NaF} (in soln.) via

$$\Delta H_{NaF} \text{ (in soln.)} = \Delta H_3 + \Delta H_{NaF}$$

The heat of formation of NaF was taken as −136.0 kcal./mole.[8] The results obtained were

$\Delta H_{Na_2MoO_4}$ (solution) = −357.6
ΔH_{NaF} (solution) = −135.9
ΔH_{MoF_6} = −388.6 ± 4 kcal./mole

(9) National Bureau of Standards, Circular 50C, 1951.

(10) B. A. Staskiewicz, J. P. Tucker and P. E. Snyder, J. Am. Chem. Soc., **77**, 2987 (1955).

The value for ΔH_{NaF} (solution) is very close to that reported[9] for ΔH_{NaF} (aq.), -135.84 kcal./mole, so there appears to be little ionic interaction in solution. Neglecting the heat of dilution, the data permit an estimate of -237.0 kcal./mole for the heat of formation of aqueous MoO_4^- (taking $\Delta H_{Na^+} = -57.3$). This is over 17 kcal. less negative than the value given in the Bureau of Standards compilation, but is in reasonable agreement with the more recent value of -238.2 kcal./mole, obtained by Graham and Hepler[11] at a somewhat higher concentration.

Tungsten Hexafluoride.—Solution reactions 4 and 5 in Table I are analogous to reaction 1. Because the second type of ampoule was used here, a small correction for WF_6 in the vapor phase was necessary (0.2 and 0.3 kcal./mole for reactions 4 and 5, respectively); the data of Ruff and Ascher[12] were used. The reaction analogous to reaction 2 could not be carried out in a reasonable length of time within the temperatures accessible to our calorimeter. However, the molybdenum data indicate a lack of strong interactions in solution; indeed, use of the best values for the heat of formation of the aqueous ions together with ΔH_1 would have led to an error of less than 0.5 kcal. in the estimation of ΔH_{MoF_6}. Consequently, the use of such a procedure with tungsten should yield a value reliable to about 2 kcal. Taking the aqueous heats of formation of OH^-, F^- and WO_4^- as -54.96, -78.66, and $-2.66.6$ kcal./mole,[9] together with the average of reactions 4 and 5 of -150.1 kcal./mole (correcting for the temperature difference is not justified), the estimate for ΔH_{WF_6} (liquid) is -422 ± 4 kcal./mole. The estimate of the error includes both that from the heat of solution measurements and that from the use of heats of formation at infinite dilution.

Niobium Pentafluoride.—At the time of these experiments, the only reasonable possibilities for completing a thermodynamic cycle in the solution calorimetry of NbF_5 were solution of the metal or of Nb_2O_5. As in the case of tungsten, solution was too slow to be practical; among solvents tested were NaOH, NH_4OH, KOH, HF, citric acid and tartaric acid. So little is known of the solution chemistry of niobium that the difficulty cannot be circumvented as in the case of tungsten. As a consequence, the series of solution reactions 6–8 was conducted to afford an improved estimate of the heat of formation of NbF_5.

In reaction 6 the soluble niobium species was assumed, by analogy with vanadium,[13] to be the metaniobate ion, according to the skeleton reaction

$$NbF_5(l) + 6OH^- = 1/3Nb_3O_9^- + 5F^- + 3H_2O$$

The heat of formation of the putative metaniobate ion is unknown, but from the chemistry of vanadium and niobium it should be somewhat greater than the heat of formation of metavanadate (-673.5 kcal./mole[9]) multiplied by the ratio of the heat of formation of the two pentoxides, or greater than

-835 kcal./mole. Consideration of the systematics of the neighboring groups, i.e., the Cr–Mo and Ti–Zr pairs, leads to a value of -800 ± 25.

In reaction 7 the precipitate was assumed to be $3Nb_2O_5 \cdot 2H_2O$ or $H_4Nb_6O_{17}$,[13,14] according to the reaction

$$NbF_5(c) + 5OH^- = 1/6H_4Nb_6O_{17} + 5F^- + 13/6H_2O$$

The heat of formation of hydrated niobium oxide was estimated by averaging all available increases in heats of formation per water molecule in hydrated oxides.[9] The average is -71.5 kcal./mole H_2O (excluding hydrous ZrO_2, whose heat of formation was questioned by Latimer[13]). One would expect the water in niobium oxide to be somewhat more tightly bound than this, and the value -73 kcal./mole H_2O has been selected. Combined with the heat of formation of the pentoxide (-463.2 kcal./mole[9]) this leads to a heat of formation of hydrous niobium oxide of -1536 ± 15 kcal./mole.

In reaction 8 the soluble niobium species was assumed to be[13] $Nb(OH)_4$ according to the reaction

$$NbF_5 + 4H_2O = Nb(OH)_4^+ + 5F^- + 4H^+$$

From solubility measurements[15] the free energy of solution of Nb_2O_5 in 3 M H_2SO_4 is about $+3$ kcal.[12] Estimating the entropy of $Nb(OH)_4$ to be about $+50$ cal./degree gives the heat of solution as $+25$ kcal./mole, leading to a value of -320 ± 10 kcal./mole for the heat of formation of $Nb(OH)^+$.

From the considerations in the preceding paragraphs, three estimates can be given for ΔH_f of NbF_5

From reaction 6 $\Delta H_f = -439 \pm 8$, (7) -423 ± 10, (8) -435 ± 8

Discussion

For convenience the thermodynamic properties at 298°K. of the three fluorides are summarized in Table II. Conversion from liquid to vapor in MoF_6 and WF_6 was through the heats of vaporization listed by Kelley.[16] For calculation of ΔF_{298} the entropies of Mo, W, Nb and F_2 were taken as 6.83, 8.0, 8.3 and 48.60 cal./deg.[9] A single value of the free energy is given for the liquid and gas in the case of MoF_6 and WF_6, since the energy of compression or expansion is well within experimental error.

TABLE II

SUMMARY OF THERMODYNAMIC PROPERTIES

Substance	ΔH^0_{298}, kcal./mole	S^0_{298}, cal./deg.	ΔF^0_{298}, kcal./mole	Cp^0, cal./deg.
$MoF_6(l)$	-388.6	60.6^a	-361.2	39.6^a
(g)	0382.0^b	80.95^c		28.35^c
$WF_6(l)$	-422	60.0^b	-397	....
(g)	-416^b	81.75^c		28.44^c
$NbF_5(c)$	(-432)	38.3	(-405)	31.6^a

^{a} From reference 7. ^{b} Computed from ref. 15 and other values in the table. ^{c} From reference 6.

The principal sources of error in the case of MoF_6 and WF_6 have been discussed in this and a previous paper.[8] In the case of NbF_5, it is felt that the limits of error in the estimates of the heat of formation already given are realistic, provided that the

(11) R. L. Graham and L. G. Hepler, *J. Am. Chem. Soc.*, **78**, 4846 (1956).

(12) O. Ruff and E. Ascher, *Z. anorg. Chem.*, **72**, 329 (1931).

(13) W. M. Latimer, "Oxidation Potentials," 2nd Ed., Prentice-Hall, Inc., New York, N. Y., 1952.

(14) P. Süe, *Compt. rend.*, **194**, 1745 (1932).

(15) S. J. Kiehl and D. Hart, *J. Am. Chem. Soc.*, **50**, 2237 (1928).

(16) K. K. Kelley, U. S. Bureau of Mines Bulletin 383, 1935.

assumptions as to the chemistry involved are reasonably correct. Not enough is known to appraise this last source of error. Some reassurance is given by the relative concordance of the estimates from experiments with entirely different end-products, but obviously a more direct check is desirable. This actually now is possible, since the heat of formation of $NbCl_5$ has been determined in at least two laboratories,[17] although not yet published at this writing, since the work described in the present paper was carried out. It is hoped that such a check will be carried out in the near future.

(17) P. Gross, Fulmer Research Institute, Ltd., private communication.

SUCCESSIVE DIFFERENTIAL ABSORPTIONS OF VAPORS BY GLASSY POLYMERS

By Akira Kishimoto and Hiroshi Fujita

Department of Fisheries, University of Kyoto, Maizuru, Japan

and Hisashi Odani, Michio Kurata and Mikio Tamura

Department of Industrial Chemistry, University of Kyoto, Kyoto, Japan

Received October 26, 1959

Successive differential sorptions were measured on the following six pairs of polymer and organic penetrant at temperatures well below the glass transition points of respective polymers: (1) polymethyl methacrylate + methyl acetate (30°), (2) atactic polystyrene + benzene (25 and 35°), (3) cellulose nitrate + acetone (25°), (4) cellulose acetate + methyl acetate (20°), (5) isotactic polystyrene of low crystallinity + benzene (35°), (6) isotactic polystyrene of high crystallinity + benzene (35°). The first two systems were chosen as models of amorphous polymer + organic vapor and the last four as models of crystalline polymer + organic vapor. In all cases investigated the successive differential sorptions showed three types of non-Fickian anomalies, i.e., sigmoid type, pseudo-Fickian type, and two-stage type. For amorphous polymers the process was Fickian type above a certain initial concentration, while for crystalline polymers no transition from non-Fickian to Fickian processes was observed up to the highest of the initial concentration studied. It was found that such a transition occurs at the concentration where the polymer–vapor mixture undergoes glass transition at the temperature of the experiment. The second stage portion of the two-stage process shifts to the short time region as the initial concentration of each step increases. It was found that the rates of this shift are much faster for amorphous polymers than for crystalline polymers. In this respect the isotactic polystyrene of low crystallinity was intermediate between the atactic polystyrene and the isotactic polystyrene of high crystallinity.

Recent works[1-8] on the absorption and desorption of low-molecular-weight substances by polymer solids have revealed that when the polymer is in the glassy state these processes exhibit various features which cannot be explained in terms of Fick's diffusion equation with a diffusion coefficient depending upon penetrant concentration alone. These features usually are referred to as non-Fickian anomalies. Attempts[2,7] have been made to interpret such anomalies in terms of a history-dependent diffusion mechanism but only partial success has been obtained. Some correlations have been pointed out to exist between the molecular structural characters of glassy polymers and the non-Fickian absorption behavior. However, it appears that more experimental material is needed before attempting any systematic theoretical interpretation of the observed facts. This is because the types of non-Fickian anomalies so far reported show a considerable variety and little is yet known about what factors are mainly responsible for the occurrence of those anomalies.

Bagley and Long[9] and later Newns[10] have observed for cellulosics that when a glassy polymer is allowed to absorb a vapor successively by small amounts the resulting series of curves exhibits various non-Fickian anomalies changing in a continuous and systematic manner. The purpose of the present paper is to report results from similar absorption experiments which we have made for other polymer–penetrant combinations. The main object of our experiments was to find out how the structural features of polymer solids affect the successive absorption behavior. To this end we have studied two amorphous polymers and four crystalline polymers. The penetrants chosen for these polymers were all organic substances.

Experimental

Materials.—Two amorphous polymers, polymethyl methacrylate (PMMA) and atactic polystyrene (A-PS), and four partially crystalline polymers, cellulose nitrate (CN), cellulose acetate (CA), isotactic polystyrenes (I-PS) of low and high crystallinities, were studied.

PMMA.—This sample was furnished from the Department of Textile Chemistry, University of Kyoto, through the courtesy of Professor H. Kawai. It had been bulk-polymerized without catalyst at room temperature from purified methyl methacrylate monomer. The polymer was precipitated from a 2% acetone solution by the addition of water. The viscosity-average molecular weight estimated by using Bischoff–Desreux's equation[11] was 6.0×10^5.

Films of the polymer were obtained by slow evaporation of solvent from a 2% acetone solution cast on a clean mercury surface. Final traces of acetone were removed by prolonged leaching in distilled water, followed by drying in a vacuum oven at room temperature. The films obtained were annealed at a temperature 120° for an appropriate

(1) L. Mandelkern and F. A. Long, *J. Polymer Sci.*, **6**, 457 (1951).

(2) J. Crank and G. S. Park, *Trans. Faraday Soc.*, **47**, 1072 (1951).

(3) R. J. Kokes, F. A. Long and J. L. Hoard, *J. Chem. Phys.*, **20**, 1711 (1952).

(4) P. Drechsel, J. L. Hoard and F. A. Long, *J. Polymer Sci.*, **10**, 241 (1953).

(5) F. A. Long and R. J. Kokes, *J. Am. Chem. Soc.*, **75**, 2232 (1953).

(6) G. S. Park, *J. Polymer Sci.*, **11**, 97 (1953).

(7) J. Crank, *ibid.*, **11**, 151 (1953).

(8) L. J. Thompson and D. B. Fordyce, *ibid.*, **22**, 509 (1956).

(9) E. Bagley and F. A. Long, *J. Am. Chem. Soc.*, **77**, 2172 (1955).

(10) A. C. Newns, *Trans. Faraday Soc.*, **52**, 1533 (1956).

(11) J. Bischoff and V. Desreux, *J. Polymer Sci.*, **10**, 437 (1953).

interval of time. The film thickness was determined from the known weight and area, using a value 1.21 g./ml.[12] for the density of PMMA. The films used for sorption measurements were approximately 1.7×10^{-3} cm. thick.

A-PS.—A commercial product "Lustrex hi-flow 77-234" was used after it had been purified twice by precipitation from a 5% benzene solution by the addition of methanol. Its viscosity–average molecular weight estimated by Flory's equation[13] was 2.2×10^5. Films of this polymer were prepared following a procedure similar to that for PMMA. The casting solvent and the leaching reagent were methylene chloride and methanol, respectively. The films used for sorption measurements were about 2.4×10^{-3} cm. thick. A value of 1.05 g./ml.[5] was used for the density of atactic polystyrene in calculating these film thicknesses.

CN.—This was a sample obtained from Fuji Photo Co. It was purified twice by precipitation from a 4% acetone solution with water as non-solvent. The intrinsic viscosity in acetone at 20° and the nitrogen content (determined by the Lunge method) of the purified material were 2.51 dl./g. and 11.95%, respectively. The casting solvent and the leaching liquid used in preparing films of this polymer were acetone and distilled water, respectively. Annealing of the films was effected at 55° in a vacuum oven. The films of about 2.5×10^{-3} cm. thick were used for sorption experiments; a value of 1.66 g./ml. was used for the density of the polymer.

CA.—This also was obtained from Fuji Photo Co., and was purified by precipitation of a 3% chloroform solution with ethanol as precipitant, followed by successive washing with ethyl ether and water. The intrinsic viscosity in chloroform at 25° and the acetyl content were 1.24 dl./g. and 60%, respectively. Films of this polymer were prepared in essentially the same manner as for PMMA; chloroform and n-hexane were used, respectively, as the casting solvent and the leaching reagent. Films of about 2.2×10^{-3} cm. thick were employed for sorption measurements. A value 1.257 g./ml. was used for the density of CA in calculating film thicknesses.

I-PS.—An isotactic polystyrene was furnished from Professor J. Furukawa of this university, who used a stereo-specific polymerization with Ziegler's catalyst. This sample was precipitated from a 3% chlorobenzene solution with methanol as non-solvent, then washed with methanol, and dried in vacuo for three days at room temperature. After the dried polymer had been boiled in heptane for 30 hours, it was separated into isotactic and atactic fractions by extracting the latter with cold methyl ethyl ketone.

Films of this isotactic fraction were prepared by using chlorobenzene as casting solvent (cast about 60°). Two different degrees of crystallinity were obtained by annealing the films at two different combinations of temperature and period. Thus the combinations were 120° and two hours for a low crystallinity and 180° and half an hour in Wood's metal for a high crystallinity. The crystallinities of the two I-PS films were estimated by the X-ray method, giving a few per cent. and 40 to 50%, respectively. The thickness was about 2.4×10^{-3} cm. for all films thus prepared.

Organic Penetrants.—For PMMA and CA methyl acetate was used as penetrant, and for CN acetone was studied. These organic liquids were extensively purified by using a procedure relevant to each. A benzene of A. R. grade was used for polystyrenes, without purification.

Apparatus and Procedure.—The sorption apparatuses employed at the two laboratories were practically the same except for that a tungsten spring balance was used by Kishimoto and Fujita and a quartz spring balance by Odani, Kurata and Tamura. The sensitivities of the two balances were approximately identical. For the six polymers we have studied both integral and differential sorptions under a variety of conditions. In this paper, the term "differential" is used to denote experiments in which the difference between initial and final pressures is sufficiently small, while the term "integral" refers to experiments in which this pressure difference is relatively large. The temperatures at which the measurements were conducted are

PMMA + methyl acetate at 30°
A-PS + benzene at 25 and 35°

(12) T. G. Fox and S. Loshaek, *ibid.*, **15**, 371 (1955).

(13) P. J. Flory, "Principles of Polymer Chemistry," Cornell Univ. Press, Ithaca, N. Y., 1953, p. 312.
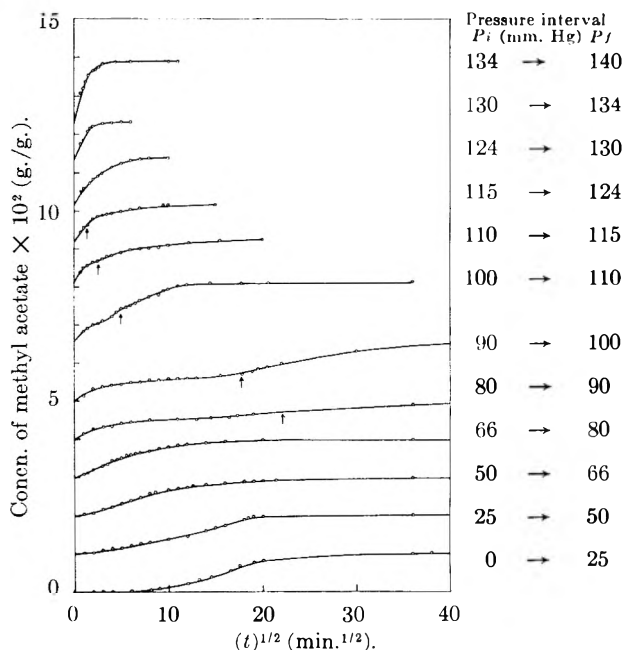
Fig. 1.—Successive differential absorptions of the system PMMA + methyl acetate at 30°. Initial and final pressures, p_i and p_f, of each step are given in the right columns.

CN + acetone at 25°
CA + methyl acetate at 20°
I-PS of low crystallinity + benzene at 35°
I-PS of high crystallinity + benzene at 35°

These temperatures are well below the glass transition temperatures of the respective polymers in their dry state.[14,15]

Results and Discussion

In view of a fairly large amount of data obtained we shall here confine ourselves to reporting only results from successive differential sorption measurements.

Amorphous Polymers.—Figure 1 gives results of a series of successive differential absorption experiments for the system PMMA + methyl acetate at 30°. The increments of methyl acetate concentration in successive steps were approximately the same, about 1×10^{-2} g. penetrant per gram of dry polymer. The general character of this family of curves is similar to that obtained by Bagley and Long[9] for the system CA + acetone at 30° and also that by Newns[10] for the system regenerated cellulose + water at 15°. However there are some important differences from these previous studies.

For the first three steps the absorptions start with a low rate, increase rather rapidly in the intermediate stage, and then gradually approach equilibria. Thus the behavior in this low pressure region is of the sigmoid type, now accepted as one of the most typical of non-Fickian sorption features. With increasing initial concentration the inflection point of the sigmoid curve shifts toward the short time region and at the same time the initial rate is increased. At the fourth step the absorption turns to be almost linear in the initial stage and exhibits no inflection. This behavior resembles ordinary Fickian absorption, but the limited linear initial

(14) H. Mark and A. V. Tobolsky, "Physical Chemistry of High Polymeric Systems," Interscience Pub., Inc., New York, N. Y., 1950, p. 347.

(15) G. Natta, *Makromol. Chem.*, **16**, 213 (1955).

Pressure interval P_i (mm. Hg) P_f	
156	→ 166
150	→ 156
141	→ 150
130	→ 141
115	→ 130
96	→ 115
79	→ 96
63	→ 79
51	→ 63
36	→ 51
18	→ 36
8.5	→ 18
0	→ 8.5
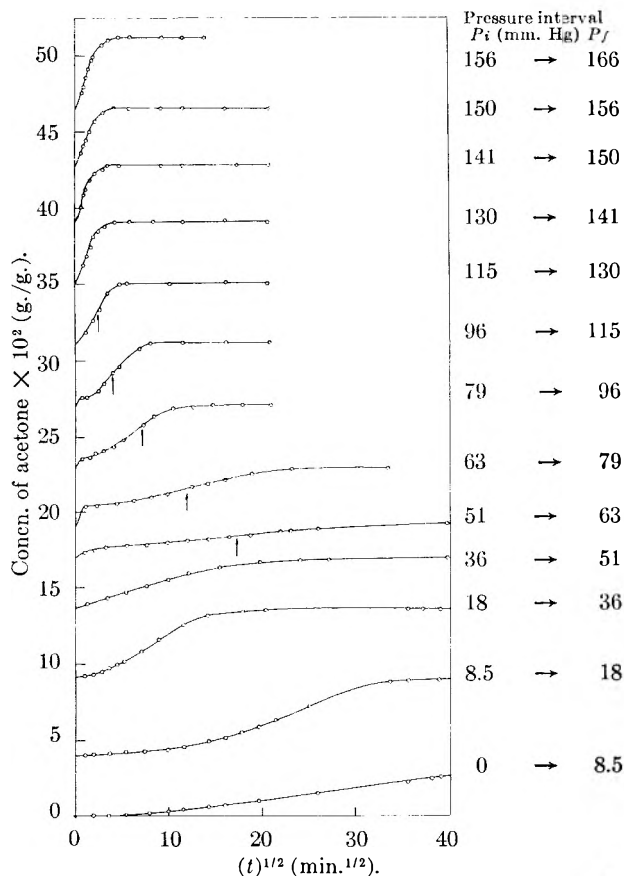
Fig. 2.—Successive differential absorptions of the system CN + acetone at 25°.

portion and the very slow approach to equilibrium indicate that this differential absorption is yet non-Fickian. In this paper we refer to this type of absorption as "pseudo-Fickian." When entering the fifth step a two-stage process appears. At this stage, however, the sigmoid character of the second-stage portion is less noticeable and the contribution of the second stage to the total concentration increment is very small. With further increase of initial concentration the second stage portion shifts rapidly to the short time region, gains a higher rate, and gives a greater contribution to the total concentration increment. Eventually at pressures around 125 mm. the second stage dominates the entire process and the shape of the curve again looks pseudo-Fickian. This systematic change in shape of the two-stage process is essentially similar to that reported by Newns[10] for the system cellulose + water at 15° but differs from the observations by Bagley and Long[9] for the system CA + acetone at 30°. The latter investigators found that the shape and position of the two-stage process were practically independent of initial concentration. We did not observe the behavior of this type in any of the polymer–penetrant combinations studied.

Figure 1 shows that the two-stage process changes to a normal Fickian process *via* a pseudo-Fickian step when the initial pressure passes through about 130 mm. Long, *et al.*,[3,5] have demonstrated that the transition from non-Fickian to Fickian absorption occurs when the concentration of pene-

trant in the polymer reaches a value at which the glass transition temperature of the mixture just equals the temperature of the experiment. If this is the case, the glass transition point of the PMMA + methyl acetate mixture at the concentration corresponding to p_i (initial pressure) = 130 mm. should be in the vicinity of 30°. From the isotherm of this system (not shown in this paper) we find that the weight fraction of methyl acetate in the mixture for the pressure 130 mm. is 0.100. This compares well with the value 0.102 interpolated for the temperature 30° from Jenckel's data[16] for the glass transition temperatures of PMMA + methyl acetate mixtures. Neither Newns' data for cellulose + water nor Bagley and Long's data for CA + acetone referred to above exhibit any evidence of the transition of the two-stage process to the normal Fickian process.

The successive differential absorption data for A-PS + benzene at 25 and 35° showed the general features which are very similar to those of PMMA + methyl acetate described above. However the data for A-PS did not show the existence of a pseudo-Fickian process in the transition from the two-stage to normal Fickian process. It soon became apparent that this was due to the fact that the pressure intervals used for these runs had been too large. In fact, a typical pseudo-Fickian absorption appeared in this transition region when a smaller pressure difference was used.

For A-PS + benzene the concentration of benzene at which the transition from non-Fickian to Fickian absorption occurred was 0.191 g. per gram of dry polymer at 25° and was 0.150 g. at 35°. These values are well consistent with the data interpolated from dilatometric studies by Fox[17] and from sorption experiments by Long and Kokes.[5]

Our generalization from the above results is that the change in type of successive differential absorptions for amorphous polymer + organic penetrant with concentration is represented in terms of a scheme such that

sigmoid type → pseudo-Fickian type → two-stage type → pseudo-Fickian type → Fickian type

The Fickian absorption may appear when the initial concentration attains a value at which the polymer–penetrant mixture changes from glassy to rubbery state at the temperature of the experiment. Odani's data for A-PS + benzene at 50° to be reported in a forthcoming publication also confirm these conclusions.

Partially Crystalline Polymers.—Figure 2 shows the data from successive differential absorptions for CN + acetone at 25°. Although the general features of this family of curves are similar to those for amorphous polymers described above, one may notice several significant differences between the two.

First the second-stage portion of the two-stage process for this system shifts to the short time much more slowly than in the case of PMMA + methyl acetate or of A-PS + benzene. Second the two-stage curves for CN have remarkably distinct plateaus between their first and second stage por-

(16) E. Jenckel and R. Heusch, *Kolloid Z.*, **130**, 89 (1953).

(17) T. G Fox, *Phys. Rev.*, **86**, 652 (1952).

tions and their initial slopes are extremely steep. As seen from Fig. 1, in the case of amorphous polymer the separation of the first and second stages of the two-stage curve is less apparent, and no particular enhancement of the initial slope occurs as the initial concentration increases. Third the successive differential absorptions for CN do not change the type from two-stage to normal Fickian as the initial concentration is larger. Instead, the two-stage process eventually changes to a sigmoid curve and then further increase in initial concentration merely gives rise to a vertical shift of this sigmoid curve with its shape practically unchanged. At the highest of the initial concentrations indicated in Fig. 2 the polymer film could hardly support its own weight from the spring balance. It was thought, therefore, that the polymer must have been in an almost liquid-like state at this concentration of acetone. Nevertheless, no definite evidence is observed in Fig. 2 that the sorption process tends to Fickian type as this concentration region is approached.

The successive differential sorptions for the system CA + methyl acetate at 20° were similar in general trend to those for the system CN + acetone described above. The main differences between these two cellulosics are described. The data for CA start with a pseudo-Fickian curve (i.e., the sigmoid process does not appear in the region of low concentrations) and soon shift to the two-stage type. In the region of initial concentrations where the two-stage process appears the initial slope is much less steep than in the case of CN + acetone and the separation of the first and second stage portions is as less apparent as in the case of PMMA + methyl acetate. Above a certain initial concentration the shapes of successive curves for CA are all of pseudo-Fickian type, as contrasted to the sigmoid type in CN + acetone. However, as in CN + acetone, only a vertical shift of such pseudo-Fickian curves occurs as the initial concentration is increased, and no evidence is observed that the process changes to normal Fickian type at higher concentrations.

Summarizing the data for CN and CA, we may sketch the changes in type of successive differential sorption curves for these cellulosics according to the schemes

CN + acetone sigmoid type → pseudo-Fickian type → two-stage type → sigmoid type

CA + methyl acetate pseudo-Fickian type → two-stage type → pseudo-Fickian type

It is not clear to us what factors are responsible for these differences. We may note that the CA sample used merely swelled in methyl acetate (probably because of its high acetyl content), while the CN sample dissolved readily in acetone.

The data of successive differential absorptions obtained for I-PS of high crystallinity (hereafter designated as high I-PS) + benzene are given in Fig. 3. It is seen that the successive curves change type following a scheme similar to that obtained for CN + acetone. That is, sigmoid type → pseudo-Fickian type → two-stage type → sigmoid type. The corresponding data for I-PS of low crystallinity (designated as low-I-PS) exhibited
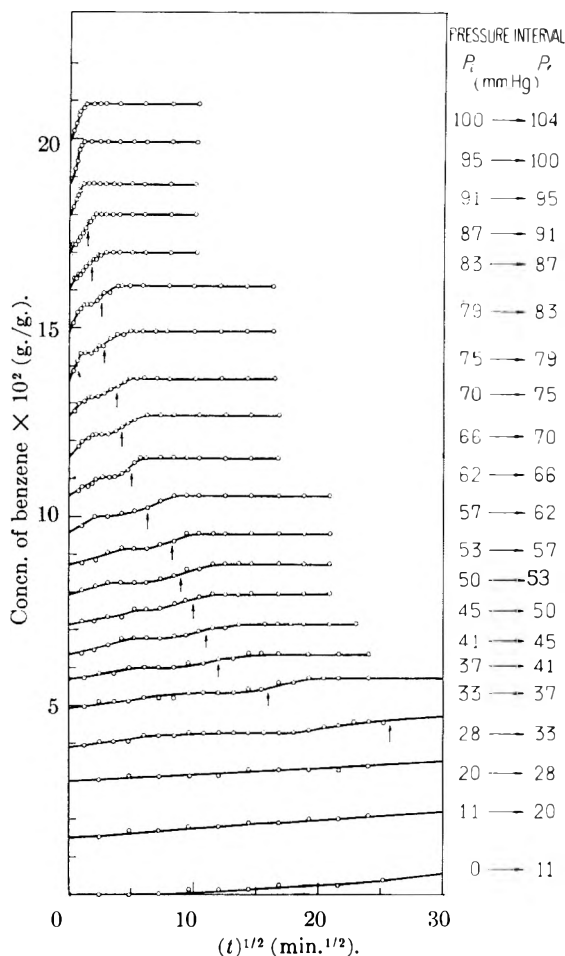
Fig. 3.—Successive differential absorptions of the system high-I-PS + benzene at 35°.
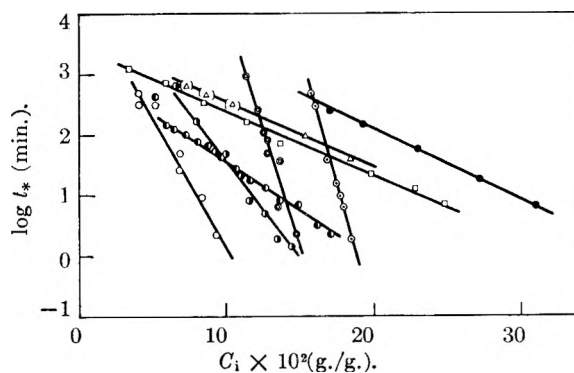
Fig. 4.—Logarithmic correlation plots of t_* and initial concentration C_i for some polymer + vapor systems. t_* is the time corresponding to the inflection point of the second stage of the two-stage process. O, PMMA + methyl acetate at 30°; ⊙, A-PS + benzene at 25°; ◉, A-PS + benzene at 35°; ●, CN + acetone at 25°; □, CA + methyl acetate at 20°; ◑, low-I-PS + benzene at 35°; ◐, high -I-PS + benzene at 35°; △, regenerated cellulose + water at 15°.[10] (The values enclosed by parentheses have been estimated by suitable extrapolations of the experimental curves recorded in Fig. 1b of Newns' paper.[10])

similar features to those for high-I-PS but were intermediate between high-I-PS and A-PS in some respects. For example, it was observed that the initial concentration at which the change from sigmoid to pseudo-Fickian occurred became lower in

the order A-PS, low-I-PS, high-I-PS. The solubility of polystrene in benzene should decrease with increasing crystallinity. Therefore, it appears that the poorer the solubility to a given organic penetrant the lower is the concentration at which the sigmoid to pseudo-Fickian transition occurs. Bagley and Long[3] observed with CA that such a transition occurred at a lower concentration for methanol than for acetone. Since the former is a poorer solvent than the latter for CA, these observations of Bagley and Long are consistent with the above-mentioned conjecture. Further support of this is the fact that the successive sorption curves for CA + methyl acetate started with a pseudo-Fickian process. As noted above, our CA sample merely swelled in this organic liquid. The data for three polystyrenes also show that the minimum initial concentration for the appearance of the two-stage process decreases with increasing crystallinity.

Concentration Dependence of the Second-stage Mechanism.—Studies by Bagley and Long[9] and by Newns[10] have demonstrated that the first-stage portion of a two-stage process is controlled by a purely Fickian diffusion mechanism. Thus it is described by Fick's diffusion equation with an appropriate diffusion coefficient, and in case where the concentration at the end of the first stage can be determined accurately, the value of such a diffusion coefficient may be estimated from the measurement of the initial slope of the curve. For the second stage of the two-stage absorption various investigators[9,10,18—20] agree in that its rate is not diffusion-controlled but governed by the rate at which the network of polymer chains changes configuration under swelling pressure. If this is the case, it is expected that the position of the second stage on the time axis may be related to an average relaxation time of the molecular rearrangements which occur during this absorption process.

As a measure to characterize the position of the second stage portion on the time axis we choose the time t_* corresponding to the inflection point of the curve. In general the t_* must vary with both the

(18) J. G. Downes and B. H. Mackay, *J. Polymer Sci.*, **28**, 45 (1958).

(19) F. A. Long and I. Watt, *ibid.*, **21**, 554 (1956).

(20) G. S. Park, *J. chim. phys.*, **55**, 134 (1958).

initial concentration C_i and the pressure (or concentration) interval Δp of each differential experiment. From a number of systematic integral and differential sorption measurements in which C_i was fixed and Δp was varied we found that for as small Δp values as used in all of the present successive differential experiments the values of t_* may be regarded as being characteristic of the initial concentrations of respective experiments. These separate sorption measurements yielded interesting information about the characteristic dependence of respective systems upon the initial concentration and the pressure interval, and will be reported elsewhere.

Values of t_* were determined from all the successive sorption data we obtained and also from Newn's corresponding data[10] for the system cellulose + water, and are plotted semi-logarithmically against C_i in Fig. 4. The arrow signs indicated in Figs. 1, 2 and 3 show the positions of the inflection points at which the desired t_* values have been taken. We see that the plots are all approximately linear and that the slopes of the lines for the amorphous polymers, PMMA and A-PS, are steeper than those for the crystalline polymers. Of interest is the fact that the slopes for the cellulosics and high I-PS are nearly equal while the slope for low-I-PS is between those for high-I-PS and A-PS. Thus the slope of the plot for log t_* $vs.$ C_i decreases with increasing crystallinity when the chemical composition of the polymer and the penetrant species are given. The real implication of these results is not known to us. However there is no doubt that some definite correlation exists between the concentration dependence of the second-stage rate and the molecular structural features of a given polymer such as crystallinity and regular orientation of repeating units.

THE HEAT CAPACITY OF AQUEOUS POTASSIUM OCTANOATE SOLUTIONS[1]

BY P. WHITE[2] AND G. C. BENSON

Division of Pure Chemistry, National Research Council, Ottawa, Canada

Received October 30, 1959

The heat capacities of aqueous potassium octanoate solutions containing 0.0420 m KOH have been measured in an adiabatic calorimeter over a concentration range 0–0.7 m and at temperatures from 25 to 55°. Partial molal heat capacities of potassium octanoate and relative partial specific heat capacities of the solvent were calculated from the experimental results and the change in the partial molal heat capacity considered in relation to the structural aspects of solute–solvent interaction in micellar solutions.

I. Introduction

Recently Goddard, Hoeve and Benson[3] deduced from specific heat data for aqueous solutions of potassium octanoate at 25° that the partial molal heat capacity of the hydrocarbon portion of the solute molecule increased by a factor of nearly 3 in going from the micellar to the single ion state. In the micelle, the partial molal heat capacity of the hydrocarbon chain was about the same as that of a normal liquid paraffin. To explain these results it was suggested that the non-polar part of a single detergent molecule may promote "iceberg" formation in the surrounding water, in the sense used by Frank and Evans[4] and that extra specific heat was required for the "melting" of these structures.

According to this picture the apparent decrease in the heat of micellization (ΔH_M) with increasing temperature, which has been reported by several authors[5-9] may be related to a diminution in the tendency of the non-polar parts of the single detergent molecule to promote icebergs at the more elevated temperatures. The present determination of the specific heat of potassium octanoate solutions as a function of temperature as well as concentration was undertaken to provide further information on this aspect.

II. Experimental

Heat capacity measurements were made in the adiabatic calorimeter assembly described by Benson, Goddard and Hoeve.[10] The stainless steel vessel used previously was replaced by one made of silver. This was suspended by Nylon loops inside the copper adiabatic shield. Two copper–constantan thermocouples each consisting of 4 junctions were attached between the inner surface of the shield and small copper studs on the outside of the vessel. These thermocouples were used to control the shield heaters and to maintain the calorimetric system (calorimeter vessel plus contents) in an adiabatic state. The temperature of the system was measured with a 100 ohm coiled filament

platinum resistance thermometer.[11] A heater, 100 ohms of manganin wire, was wound on the outside of the thermometer capsule and electrically insulated from it. This heater–thermometer combination was mounted in Cliché metal in a well recessed in the bottom of the silver vessel and a protective copper cover soldered over the protruding end. The filling port in the top of the vessel was closed with a Teflon plug which was covered with a copper disc soldered in place. The vessel when sealed in this way was vacuum tight. Care was taken after each filling to make the weight of the vessel the same by the addition or removal of a small amount of solder and thus to keep the heat capacity of the vessel a unique function of the temperature.

The heat capacity of the calorimetric system was determined in a series of heating periods carried out around mean temperatures of 25, 35, 45 and 55°. The procedures followed in these measurements were similar to those described in previous publications.[10,12] The contents of the vessel were stirred by tipping during the equilibrating and heating periods; corrections were applied for the energy introduced by tipping. The assembly was not tipped during the fore- and after-rating periods. The temperature of the calorimetric system was raised 1 to 1.5° during a heating period. The system was kept in an adiabatic state throughout the determination by adjustment of the shield heating currents; also at the same time the temperature of the external oil bath was raised. The heat capacity of the system was always of the order of 300 cal./°C. and about 6% of this was contributed by the vessel. The heat capacity of the vessel was determined from measurements on the vessel containing a known amount of conductivity water.

Preparation of the potassium octanoate has been described previously.[3,13] The concentration range covered in the present study was 0–0.7 m. In all cases the solvent was a 0.0420 m potassium hydroxide solution.

III. Results

The temperature variation of the specific heat (c_p) of a series of potassium octanoate solutions is shown in Fig. 1. Most of the curves appear to have a minimum value of c_p in the vicinity of 45°. From these data isothermal plots of specific heat against molality were constructed for 25, 35, 45 and 55°. The results at 25° agreed with those obtained previously[3] to within ±0.1%. At all four temperatures the results could be fitted quite well by a pair of straight lines joined by a small curved section in the region of the critical micelle concentration c.m.c. (*i.e.*, 0.35–0.45 m). Values of the constants a and b for the equations of these lines written in the form

$$c_p = a + bm \qquad (1)$$

are given in Table I. A prime is used to indicate the line at concentrations below the c.m.c. and a double prime for the one above the c.m.c.

The smoothed isotherms were used to calculate the partial molal heat capacity $\bar{C}_{p2}$ of the potassium

(1) Issued as N.R.C. No. 5642. Paper presented in part at the General Session of the Division of Colloid Chemistry, 136th National Meeting of the American Chemical Society, Atlantic City, N. J., September 18th, 1959.

(2) National Research Council of Canada Postdoctorate Fellow, 1956–1958.

(3) E. D. Goddard, C. A. J. Hoeve and G. C. Benson, THIS JOURNAL, 61, 593 (1957).

(4) H. S. Frank and M. W. Evans, *J. Chem. Phys.*, 13, 507 (1945).

(5) G. Stainsby and A. E. Alexander, *Trans. Faraday Soc.*, 46, 587 (1950).

(6) B. D. Flockhart and A. R. Ubbelohde, *J. Colloid Sci.*, 8, 428 (1953).

(7) E. D. Goddard and G. C. Benson, *Can. J. Chem.*, 35, 986 (1957).

(8) E. Matijevic and B. A. Pethica, *Trans. Faraday Soc.*, 54, 587 (1958).

(9) P. White and G. C. Benson, *ibid.*, 55, 1025 (1959).

(10) G. C. Benson, E. D. Goddard and C. A. J. Hoeve, *Rev. Sci. Instr.*, 27, 725 (1956).

(11) C. H. Meyers, *J. Research Natl. Bur. Standards*, 9, 807 (1932).

(12) G. C. Benson and G. W. Benson, *Rev. Sci. Instr.*, 26, 477 (1955).

(13) P. White and G. C. Benson, *J. Colloid Sci.*, 13, 584 (1958).
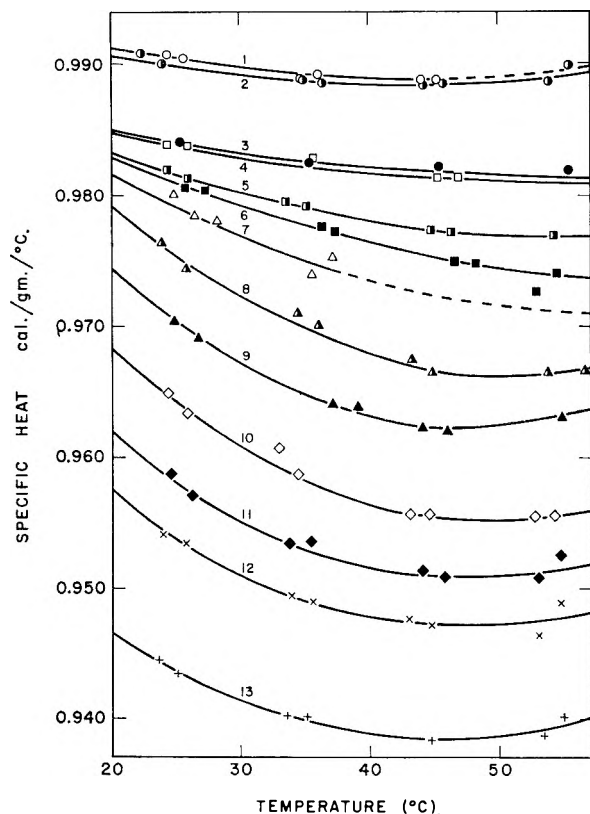
Fig. 1.—Plots of the specific heat of potassium octanoate solutions as a function of temperature. Molalities for the various curves are (1) 0.1047, (2) 0.1367, (3) 0.2552, (4) 0.2735, (5) 0.3479, (6) 0.3988, (7) 0.4119, (8) 0.4620, (9) 0.5187, (10) 0.5625, (11) 0.6296, (12) 0.6684 and (13) 0.7383. The solvent for all solutions is 0.0420 m KOH.
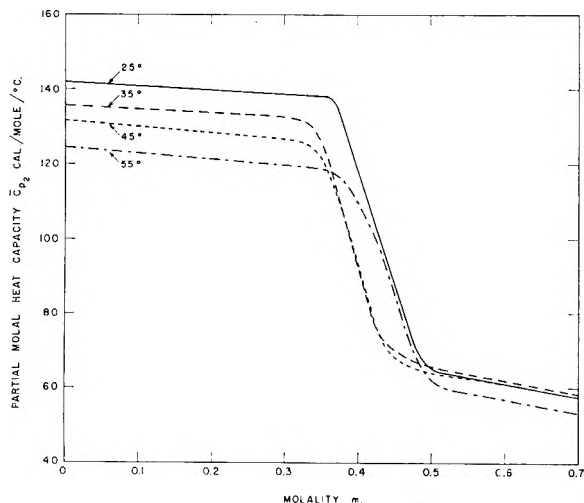
Fig. 2.—Partial molal heat capacity $\bar{C}_{p_2}$ of potassium octanoate plotted as a function of molality at four temperatures.

TABLE I

SUMMARY OF CONSTANTS FOR EQ. 1 AND OF RESULTS CALCULATED FROM EQ. 3-6

Temp., °C.	Below c.m.c. a'	b'	Above c.m.c. a''	b''	m^* = c.m.c.	$\Delta\bar{C}_{p_2}$, cal. mole⁻¹ deg.⁻¹	$\Delta\bar{j}_1$, cal. g.⁻¹ deg.⁻¹
25	0.9946	−0.0380	1.0217	−0.1018	0.42₅	−69	0.029
35	.9944	− .0442	1.0168	− .1013	.39₂	−61	.024
45	.9948	− .0492	1.0157	− .1023	.39₃	−57	.022
55	.9963	− .0563	1.0180	− .1054	.44₂	−53	.023

octanoate and the relative partial specific heat $\bar{j}_1$ of the solvent from the relations

$$\bar{C}_{p_2} = M_2 c_p + (1000 + m M_2)\frac{\partial c_p}{\partial m} \qquad (2)$$

and

$$\bar{j}_1 = c_p - c_p^0 - \frac{m}{1000}(1000 + m M_2)\frac{\partial c_p}{\partial m} \qquad (3)$$

respectively, where M_2 is the molecular weight of the solute and c_p^0 is the specific heat of the solvent. The results of these calculations at each of the four temperatures are shown in Fig. 2 and 3.

Values of the c.m.c. (denoted by m^*) were calculated from the equation

$$m^* = (a' - a'')/(b'' - b') \qquad (4)$$

and the heights of the "steps" in Figs. 2 and 3 were estimated from the equations

$$\Delta\bar{C}_{p_2} = (1000 + M_2 m^*)(b'' - b') \qquad (5)$$

and

$$\Delta\bar{j}_1 = -m^* \Delta\bar{C}_{p_2} \times 10^{-3} \qquad (6)$$

The results of these calculations are also given in Table I.

IV. Discussion

The dependence of specific heat on concentration found for potassium octanoate solutions at a fixed temperature is formally similar to that reported by Bury and Davies[14] for aqueous n-butyric acid solutions at 25° and is probably fairly typical of the thermal behavior of micelle forming systems. There are, however, very few other data in the literature on which to base such a generalization.

The results for the c.m.c. listed in Table I are somewhat higher than values obtained from conductivity measurements[9] but are well within the range of values determined from other physical measurements.[15-17] The variation of the c.m.c. with temperature (i.e., a decrease and subsequent increase) is similar to that observed for a number of detergent systems.[5-9]

The general shapes of the plots of partial molal heat capacity of potassium octanoate and relative partial specific heat of the solvent displayed in Figs. 2 and 3 are qualitatively understandable in terms of the picture of iceberg formation mentioned earlier. According to this each single detergent ion has associated with it a relatively stable (low energy) structure in the surrounding solvent and hence has a higher partial molal heat capacity than in the micellar state. A plot of $\bar{C}_{p_2}$ against concentration thus contains a negative "step." On the other hand addition of solvent to a solution containing a fixed amount of potassium octanoate has very little effect on the partial specific heat of the solvent below the c.m.c. but above this concentration dilution leads to the formation of more single ions with heat capacity larger than in the micellar state. Thus

(14) C. R. Bury and D. G. Davies, J. Chem. Soc., 2413 (1932).

(15) H. B. Klevens, This Journal, 52, 130 (1948).

(16) D. G. Davies and C. R. Bury, J. Chem. Soc., 2263 (1930).

(17) D. Moule, P. White and G. C. Benson, Can. J. Chem., 37, 2086 (1959).

the plot of $\bar{j}_1$ against molality exhibits a positive "step."

Previously,[3] in discussing the heat capacities of potassium octanoate solutions at 25°, a rough estimate of the partial molal heat capacity of the hydrocarbon part of the solute molecule was obtained by a comparison with specific heats of potassium acetate solutions. However, since the temperature dependence of the latter data is uncertain it seems better to limit the present considerations to the changes observed in the partial molal heat capacity of potassium octanoate itself. The values of $\Delta \bar{C}_{p_2}$ listed in Table I correspond roughly to the change in heat capacity when a $-(CH_2)_6 \cdot CH_3$ group is removed from a hydrocarbon medium and placed in aqueous surroundings. This change which amounts to nearly 10 cal. deg.$^{-1}$ for a $-CH_2$ group at 25° is of the same order of magnitude as the excess heat capacity reported by Frank and Wen[18] for tetra-n-butylammonium bromide. With increasing temperature the heat capacity of a normal hydrocarbon liquid increases; however, the changes observed in $\Delta \bar{C}_{p_2}$ are much larger than can be accounted for on this basis and probably result mainly from the decrease in iceberg formation as the temperature is raised.

Finally the present heat capacity data were used to evaluate the expression $\int_{25}^{50} \bar{C}_{p_2} \, dT$ and thus to calculate a curve of the partial molal enthalpy $\bar{H}_2$ at 50° from that obtained for $\bar{H}_2$ at 25° from calorimetric measurements.[3] The result is plotted in Fig. 4 (curve B) and may be compared with curve A which is derived from heat of dilution measurements at 50°.[9] To allow for the different initial concentrations involved in the experimental work curve B has been displaced vertically to coincide with A at $m = 0.1$. Considering the uncertainties involved in deriving both these curves from the primary data the agreement in Fig. 4 is quite reasonable.

Acknowledgments.—The authors wish to thank Mr. P. D'Arcy for invaluable assistance in the

(18) H. S. Frank and W. Wen, *Disc. Faraday Soc.*, **24**, 133 (1957).
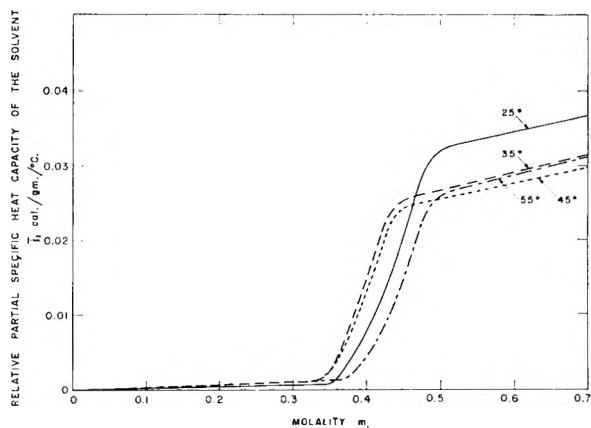
Fig. 3.—Relative partial specific heat of the solvent $\bar{j}_1$ in potassium octanoate solutions plotted as a function of molality at four temperatures.
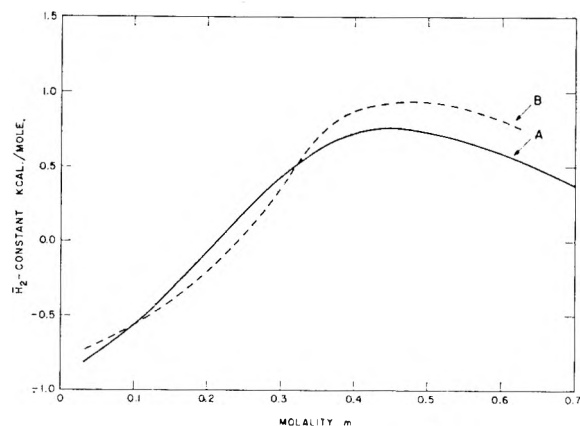
Fig. 4.—Plot of partial molal enthalpy $\bar{H}_2$ ($-$a constant) against molality; curve A, from heats of dilution at 50° (ref. 9); curve B, from heats of dilution at 25° (ref. 3) calculated to 50° using the heat capacity data of the present paper.

calorimetric measurements. They are also indebted to Dr. C. A. J. Hoeve of the Mellon Institute, Pittsburgh, for a stimulating discussion of the results.

KINETICS OF THE GAS PHASE OXIDATION OF HYDROGEN CHLORIDE AND OF HYDROGEN BROMIDE BY NITROGEN DIOXIDE[1]

By WILLIS A. ROSSER, JR., AND HENRY WISE

Chemical Physics Department, Stanford Research Institute, Menlo Park, California

Received November 6, 1959

The oxidations of HCl and of HBr by NO_2 have been studied in the temperature range from 100 to 420°. Both reactions lead to the over-all reaction stoichiometry $NO_2 + 2HX = NO + H_2O + X_2$ where HX is either HCl or HBr, and X_2 is either Cl_2 or Br_2. The rate of reaction varies with the reactant concentrations as shown by the equation $-d(NO_2)/dt = k_X(HX)(NO_2)$. The temperature variation of the two specific reaction rates k_X may be summarized by $k_{Cl} = 10^{11.6} e^{-23,400/RT}$ cc./mole sec. and $k_{Br} = 10^{11.0} e^{-13,000/RT}$ cc./mole sec. Reaction mechanisms are proposed.

Introduction

In the course of kinetic studies involving the reactants H_2, NO_2, Cl_2 and Br_2, it became apparent that NO_2 reacts rapidly at moderate temperatures with the halogen acids HCl and HBr. Both reactions consequently were examined in sufficient detail to determine their essential features since neither of these reactions has been studied previously.

Experimental Apparatus

The various experiments were carried out using an apparatus previously described.[2] The essential elements of the system are: (a) a reaction vessel housed in a cylindrical resistance furnace, (b) a tungsten lamp operated by storage batteries, (c) a Beckman DU monochromator to select light of the desired wave length which then is detected by a photomultiplier tube, (d) a silicone-oil manometer for measuring low pressures, and (e) a Bourdon gauge for measuring higher pressures. The Bourdon gauge consisted of a Vycor spiral to which was attached a small mirror. Movement of the mirror was detected by means of a reflected light beam.

Two cylindrical reaction vessels of a comparable size were used, one made of quartz and the other of Pyrex. The dimensions of the quartz vessel (diameter $\sim$ 4 cm., length $\sim$ 60 cm.) correspond to a surface to volume ratio of 1 cm.$^{-1}$. The Pyrex vessel of similar dimensions was partially filled with borosilicate–glass beads to give an over-all surface to volume ratio of about 5 cm.$^{-1}$. The monitoring light beam passed 1 to 2 mm. above the bed of beads which occupied the lower third of the reaction vessel. The lines connecting the reaction vessel to the other portions of the experimental apparatus were electrically heated by heating tapes to prevent the condensation of water, a reaction product.

In order to obtain temperature uniformity within the reaction vessel, the furnace was heated by four resistance windings, each independently regulated by hand adjustment of a variable voltage supply. The reaction vessel was housed within a heavy-walled aluminum liner. The temperature of the reaction vessel was measured by six external chromel–alumel thermocouples distributed uniformly along the length of the reaction vessel. By adjusting the voltage applied to each of the four heater windings, one could easily limit the temperature range indicated by these six thermocouples to less than two degrees. The temperature within the reaction vessel was considered to be the average of the temperatures indicated by the external thermocouples.

The Reaction between NO_2 and HCl.—The reaction between NO_2 and HCl was studied by observing photometrically the disappearance of NO_2 as a function of time, reactant concentrations and temperature. The initial concentrations of each reactant and the temperature of reaction were varied in the indicated ranges: $(NO_2)_i$ from 1×10^{-3} to 1×10^{-7} mole/cc., $(HCl)_i$ from 1×10^{-6} to 1×10^{-5} mole/cc., and temperature from 250 to

(1) Sponsorship of this work by the Physical and Biological Sciences Division of Stanford Research Institute is gratefully acknowledged.

(2) W. A. Rosser, Jr., and H. Wise, THIS JOURNAL, **63**, 1753 (1959).

420°. Commercially available[3] NO_2 and HCl were used in most experiments. Impurities non-condensable at the temperature of liquid nitrogen were removed by evaporation. The traces of NO present in commercial NO_2 were converted to NO_2 by dry O_2 and the excess O_2 subsequently removed by evaporation at the temperature of liquid nitrogen.

In all experiments the reactants were admitted separately to the reaction vessel from a small manifold between the reaction vessel and the various gas storage vessels. Premixing is not possible because NO_2 and HCl react rapidly at room temperature. In a typical experiment the minor reactant, NO_2, was admitted first to the reaction vessel and its initial pressure measured with the oil manometer. The oil manometer connection was then closed and an excess of HCl added. The total pressure and the pressure change were measured by means of the Bourdon gauge. The rate of disappearance of NO_2 was measured either at 5000 or at 4200 Å. At 4200 Å. it is necessary to correct the observed absorption for the contribution by Cl_2, a reaction product.

Of the feasible over-all stoichiometries only

$$NO_2 + 2HCl = NO + H_2O + Cl_2 \qquad (1)$$

is consistent with the following observations. At temperatures high enough to prevent the formation of significant quantities of NOCl from NO and Cl_2, the reaction proceeds without observable pressure change ($\delta p < 0.2$ mm.). The final change in optical density at 3300 Å., where both NO_2 and Cl_2 absorb light strongly, agrees precisely ($\pm 2\%$) with that implied by eq. 1. At temperatures less than about 300° the formation of some NOCl results in a slight pressure decrease as implied by the reaction

$$2NO + Cl_2 = 2NOCl \qquad (2)$$

At temperatures greater than about 300° the reaction kinetics are uncomplicated. The rate of disappearance of NO_2 was found to be proportional to the product of the concentrations of NO_2 and of HCl

$$\frac{-d(NO_2)}{dt} = k_{Cl}(NO_2)(HCl) \qquad (3)$$

The reaction order for each component was determined in this manner. When the concentration of HCl is much greater than that of NO_2, the quantity $-\ln(NO_2)$ decreases linearly with time. It also is

(3) The Matheson Co., Inc., E. Rutherford, New Jersey.

found that the rate of decrease of $-\ln(NO_2)$ is proportional to the concentration of HCl and independent of the initial concentration of NO_2. Accordingly, the differential rate equation has the form shown in eq. 3. The constant k_{Cl} was determined from the slope of a plot $-\ln(NO_2)$ vs. time. Even when the concentration of HCl changed slightly during reaction, this procedure was used although it was necessary in deriving k_{Cl} to use an average concentration of HCl during the time interval in question.

Equivalent results were obtained at two wave lengths, 5000 and 4200 Å., using either commercial HCl or that prepared in the laboratory from NaCl and H_2SO_4. Moreover, the rate of disappearance of NO_2 is not affected by the reaction products when these are initially present at concentrations comparable to that of NO_2. The presence of N_2 at a concentration comparable to that of the excess reactant HCl likewise does not affect the experimental results. Experiments using the packed Pyrex vessel failed to reveal any dependence on the nature or amount of vessel surface. In view of these observations it may be concluded that the reaction is substantially homogeneous.

The temperature variation of the specific rate constant k_{Cl} can be summarized (see Fig. 1) by the Arrhenius expression

$$k_{Cl} = 10^{11.6}\, e^{-23,400/RT} \text{ cc./mole sec.} \quad (4)$$

The experimental observations are consistent with a reaction mechanism involving the initiation step

$$NO_2 + HCl \longrightarrow HNO_2 + Cl \quad \Delta H = 23 \text{ kcal.} \quad (5)$$
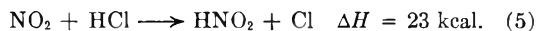
Succeeding steps which involve HNO_2 cannot be unambiguously specified. However, either the sequence

$$HNO_2 \longrightarrow NO + OH \quad (6)$$
$$OH + HCl \longrightarrow H_2O + Cl \quad (7)$$
$$2Cl \longrightarrow Cl_2 \quad (8)$$

or

$$NO_2 + HNO_2 \longrightarrow HNO_3 + NO \quad (9)$$
$$HNO_3 \longrightarrow NO_2 + OH \quad (10)$$
$$\text{etc.}$$
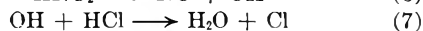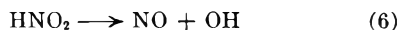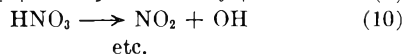
leads to the observed stoichiometry and to the identification of k_{Cl} with k_5. Above 300° the decomposition of HNO_3 is believed to proceed as written.[4] The analogous decomposition of HNO_2 is assumed. Where given, heats of reaction are based on heats of formation from ref. 5 and 6.

The experimental activation energy is only slightly larger than the standard enthalpy increase of reaction 5. Accordingly, the inverse of reaction 5 involves little or no activation energy. Inasmuch as the average collision frequency in the experimental temperature range is about $10^{14.5}$, the pre-exponential factor in eq. 4 implies a steric factor of about 10^{-3}. Equivalently, the pre-exponential factor in eq. 4 when considered in terms of transition-state theory[7] indicates that the formation of the

(4) H. S. Johnston, L. Foering and R. J. Thompson, THIS JOURNAL, 57, 390 (1953).

(5) F. D. Rossini, et al., Circ. No. 500, Natl. Bur. of Standards, 1952.

(6) W. A. Rosser, Jr., and H. Wise, J. Chem. Phys., 26, 571 (1957).

(7) S. Glasstone, K. J. Laidler and H. Eyring, "The Theory of Rate Processes," McGraw-Hill Book Co., New York, N. Y., 1941, p. 21.
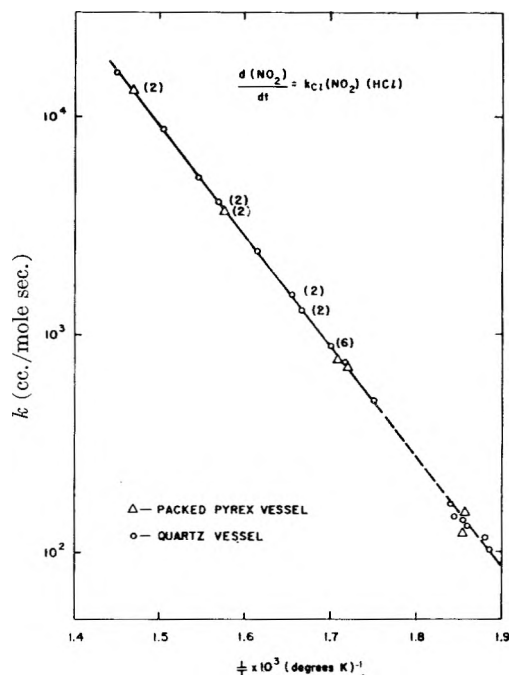
Fig. 1.—NO_2–HCl; specific reaction rate as a function of temperature.

activated complex $NO_2 \cdot HCl$ involves a standard entropy decrease (concentration units) of about eleven units, a reasonable value for such a complex.[8]

At temperatures less than about 270° the reaction acquires some complexity. The order of reaction with respect to NO_2 varies slightly during the course of reaction although it is still approximately one. Too, in this temperature region the products of reaction do have some effect on the reaction. An initial concentration of Cl_2 near that of NO_2 inhibits the reaction slightly while the same amount of NO increases the reaction rate. These features, however, were not investigated in detail.

The Reaction between NO_2 and HBr.—The reaction between NO_2 and HBr was studied in a manner analogous to that used in studying the reaction between NO_2 and HCl. The experimental parameters were varied in the indicated ranges: $(NO_2)_i$ from 1×10^{-8} to 1×10^{-7} mole/cc., $(HBr)_i$ from 5×10^{-8} to 5×10^{-7} mole/cc., and temperature from 90 to 310°. Commercially available NO_2 and HBr were used in these experiments.

The experimental procedure was similar to that used in studying the reaction between NO_2 and HCl except that the rate of disappearance of NO_2 was measured at 3400 Å. where the absorption constant of NO_2 is about ten times as large as that of Br_2, a reaction product. At appreciably longer wave lengths Br_2 and NO_2 absorb light to about the same extent.

The rate of reaction between NO_2 and HBr is inconveniently high for the range of variables permitted by the apparatus and associated experimental techniques. For this reason the HBr reaction was not studied in as great detail as was the HCl reaction.

(8) A. A. Frost and R. G. Pearson, "Kinetics and Mechanism," J. Wiley and Sons, Inc., New York, N. Y., 1953, p. 92.
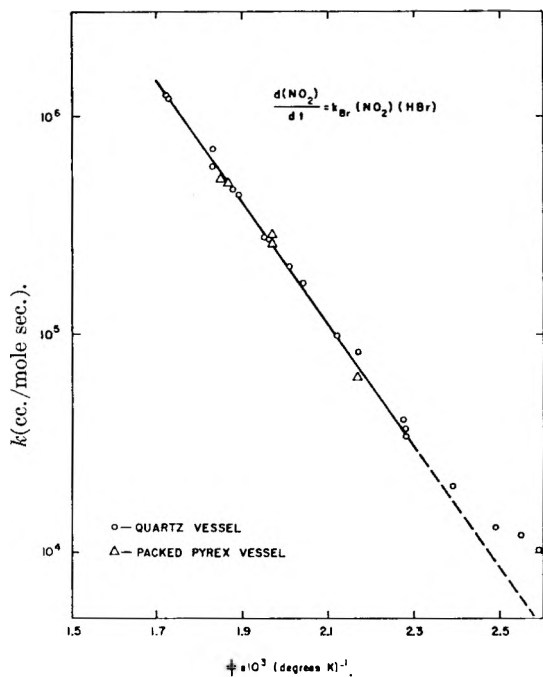
Fig. 2.—NO₂–HBr; specific reaction rate as a function of temperature.

The reaction stoichiometry

$$NO_2 + 2HBr = NO + H_2O + Br_2 \qquad (11)$$
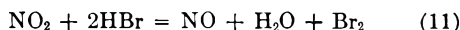
is indicated by a number of observations: (a) the reaction proceeds without observable pressure change at temperatures sufficiently high to prevent the formation of significant quantities of NOBr by the reaction

$$2NO + Br_2 = 2NOBr \qquad (12)$$

(b) when the initial concentration of NO₂ is more than twice as large as that of HBr the amount of NO₂ which disappears is $1/2$ (HBr)$_i$; (c) observation of the optical density at 4200 Å., where NO₂ and Br₂ have nearly equal absorption constants, indicates that one mole of Br₂ is produced for each mole of NO₂ consumed.

Above about 180° the NO₂–HBr reaction appears to be uncomplicated. The rate of disappearance of NO₂ is described by the expression

$$\frac{-d(NO_2)}{dt} = k_{Br}(NO_2)(HBr) \qquad (13)$$

The specific reaction rate k_{Br} was derived in the same manner as was k_{Cl}. In this case, however, a plot of $-\ln(NO_2)$ *versus* time is not a straight line because the concentration of HBr decreases during the course of reaction. By means of the stoi-

chiometry, eq. 12, one may compute and make allowances for the decrease in the concentration of HBr. Equivalent results were obtained using either the quartz vessel or the packed Pyrex vessel.

Below 180° a low temperature reaction contributed to the rate of disappearance of NO₂. The temperature coefficient of the low temperature reaction was observed to be negative. Accordingly, for initial concentrations of NO₂ and HBr of about 1×10^{-7} mole/cc. and 5×10^{-7} mole/cc., respectively, the rate of disappearance of NO₂ passes through a minimum at about 100°. The low temperature reaction, however, was not investigated in detail, only to the extent necessary to determine the temperature above which it could be neglected.

The observed temperature variation of k_{Br} is shown in Fig. 2. The indicated line corresponds to the expression

$$k_{Br} = 10^{11.0}\, e^{-13,000/RT} \text{ cc./mole sec.} \qquad (14)$$

and refers to the high temperature reaction alone· The effect of the low temperature reaction on the apparent specific rate constant is evident from the results shown.

The various experimental observations are consistent with a reaction mechanism like that proposed for the system NO₂–HCl.

$$NO_2 + HBr \longrightarrow HNO_2 + Br \quad \Delta H = 7 \text{ to } 8 \text{ kcal.} \quad (15)$$
$$HNO_2 \longrightarrow NO + OH \qquad (6)$$
$$NO_2 + HNO_2 \longrightarrow HNO_3 + NO \qquad (9)$$
$$HNO_3 \longrightarrow NO_2 + OH \qquad (10)$$
$$OH + HBr \longrightarrow H_2O + Br \qquad (16)$$
$$2Br \longrightarrow Br_2 \qquad (17)$$
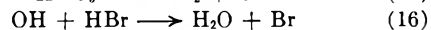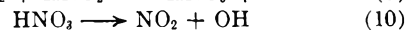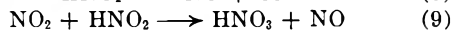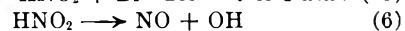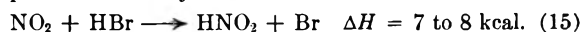
It is possible that some of the reactions which follow eq. 15 are heterogeneous. The decomposition of HNO₃, for instance, is known to include surface decomposition below 300°.

According to the proposed mechanism the observed rate constant refers to the initiation reaction, eq. 15. The observed activation energy is 5 to 6 kcal. greater than the standard enthalpy change of reaction 15. Accordingly, the inverse reaction must have an activation energy of 5 to 6 kcal., whereas the corresponding reaction involving Cl rather than Br has an activation energy of 0 to 1 kcal. Qualitatively, these two values are reasonable ones. The Hirschfelder rules[9] for instance predict a value of about 4 kcal. for both reactions.

The pre-exponential factor in eq. 14 is about the same as the corresponding factor in Eq. 4. Similarly, the steric factors are about the same (10^{-3}) as are the entropy decreases (11 e.u.) associated with the formation of the activated complexes NO₂·HX.

(9) J. O. Hirschfelder, *J. Chem. Phys.*, **9**, 645 (1941).

ELECTRIC PROPERTIES OF MACROMOLECULES. V.
THEORY OF IONIC POLARIZATION IN POLYELECTROLYTES

By Chester T. O'Konski

Department of Chemistry, University of California, Berkeley 4, California

Received November 10, 1959

Ionic transport phenomena are shown to be important to the dielectric constant, as well as the dispersion and conductivity of polyelectrolyte solutions. The effects of the excess conductivity arising from mobility of ions at the interface, and—with thin ion atmospheres—the charge transport due to counterions, may be expressed in terms of a two-dimensional conductivity. The electrical boundary value problem is formulated in terms of this surface conductivity, the dielectric constant and volume conductivity of the medium, and an anisotropic dielectric constant and volume conductivity for the particle. These parameters have important physical significance for macromolecular structures. It is proposed that this model is more appropriate for polyelectrolytes than either the Debye–Falkenhagen or Maxwell–Wagner models. Isotropic spheres are considered in detail, to show the effects of a surface conductivity on the internal field, the induced polarization, and the dielectric constant, dispersion, and conductivity of dilute systems. Reasonable approximations were found which obviate detailed treatment of the boundary-value problems for the generalized ellipsoid and the limiting forms of a cylinder. Anisometric particles of uniform surface conductivity are shown to be electrically equivalent to particles of anisotropic volume conductivity. Equations are given for the complex dielectric constant, the relaxation times, and the low and high frequency dielectric and conductivity increments of dilute systems of ellipsoidal particles. Numerical calculations of the increments are made for randomly and completely oriented ellipsoids of revolution over a wide range of parameters appropriate to dilute aqueous media. Important differences between needle and disk-shaped particles are found. In oriented systems of anisometric particles, counterion transport produces a strong anisotropy of the low frequency dielectric increment, and an anisotropy of conductivity apart from the contribution due to anisotropy of the frictional coefficient of the polyion. Further, the internal field depends upon orientation, and this effect on polyion mobility may greatly exceed the frictional coefficient effect discussed by Eigen and Schwarz. The results indicate that essentially all of the known dielectric properties of aqueous proteins, nucleic acids, nucleoproteins, and charged colloids are explicable in terms of this model. It is shown that polarization of the counterion atmosphere reduces the internal field and thus diminishes permanent dipole polarization. Available experimental data, generally incomplete for the present interpretation, are discussed in as far as possible. The need for further experiments to test the theory is indicated, and some crucial ones are suggested. It is predicted that biological effects in intense high frequency fields may be enhanced by the use of pulsed radiation.

1. Introduction

Of the many types of systems for which the frequency-dependent dielectric properties have been investigated, perhaps the least understood are solutions of polyelectrolytes and colloidal electrolytes. These classes include the proteins, nucleic acids, synthetic polyelectrolytes, micelles and many colloidal dispersions. Formulation of an adequate theory of the dielectric constant and conductivity of these systems requires treatment of the charge transport processes arising from the motion of the ions or other charge carriers in the solvent, in the ion atmosphere, and in the solutes or the suspended phase. Neglect of these effects can lead to serious errors in the interpretation of dielectric constant and conductivity. A recent interpretation evidently in error will be discussed below.

There exists no general theory of dielectric constant and conductivity rigorously applicable to polyelectrolytes. Debye and Falkenhagen[1] treated the dielectric constant of simple electrolytes in terms of a model involving point charges in a dielectric continuum. Several investigators[2] have treated the conductivity of simple electrolytes and in recent years there have been some significant refinements[2b,3] which are in accord with experimental results well above the low concentrations for which the Debye–Hückel limiting law is valid. But the refinements are not adequate for polyelectrolytes, where particle dimensions and shape are important constants of the system.

A central concept in the treatment of simple electrolytes is the existence of an ion atmosphere. In external fields, the ion atmosphere becomes polarized; by this we refer to the production of a dipole moment by displacement of the center of atmospheric charge from the center of the charge about which the atmosphere is formed. This results in a retarding local field which depresses the equivalent conductivity of an ion below the infinite dilution value, often referred to as the "asymmetry effect" or the "relaxation effect." For highly charged polyelectrolytes with many neighboring counterions, and a greater distance for them to move, we may anticipate that this effect will be larger than in simple electrolytes. To treat it, we wish to adopt a tractable model in which mobilities enter naturally, and which depicts the sharp gradient of ion concentrations in the strong electric field of the polyelectrolyte. It was proposed recently[4] that the introduction of a surface conductivity in treating the electrical boundary-value problems of polyelectrolyte systems may be helpful in explaining some of the interesting dielectric behavior of protein solutions. This model is treated mathematically here.

The concept of a surface conductivity apparently was first introduced by Smoluchowski,[5] who recognized the importance of the mobility of the ions of the diffuse layer at a charged surface, and employed this concept in discussing electrophoresis of colloidal particles. The idea subsequently was elaborated by Havestadt and R. Fricke,[6] Bikerman,[7] H. Fricke and Curtis[8] and Henry.[9] In fact,

(1) (a) P. Debye and H. Falkenhagen, *Physik. Z.*, **29**, 121, 401 (1928); (b) *Z. Elektrochem.*, **34**, 562 (1928).

(2) (a) L. Onsager, *Physik. Z.*, **27**, 388 (1926); **28**, 277 (1927); (b) R. M. Fuoss and L. Onsager, *Proc. Natl. Acad. Sci.*, **41**, 274, 1010 (1955); This Journal, **61**, 668 (1957).

(3) (a) R. M. Fuoss, *J. Am. Chem. Soc.*, **81**, 2658 (1959); (b) H. Falkenhagen, M. Leist and G. Kelbg, *Ann. Physik*, [6] **11**, 51 (1952).

(4) C. T. O'Konski, *J. Chem. Phys.*, **23**, 1559 (1955).

(5) M. von Smoluchowski, "Electric Endosmosis and Streaming Current," in "Two Monographs on Electrokinetics," trans. by P. E. Bocquet [Ann Arbor] Engineering Research Institute, University of Michigan, 1951, pp. 51–159.
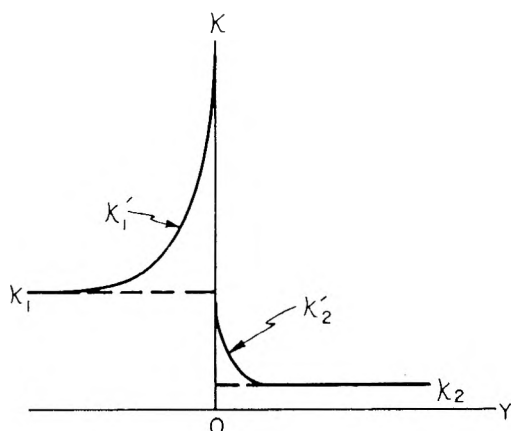
Fig. 1.—Physical situation prompting introduction of a surface conductivity. The primed quantities show the conductivity variation in the vicinity of a planar charged "interface." A contribution from an infinitely thin layer, or a "true" surface conductivity, would correspond to a singularity at $y = 0$.

Miles and Robertson[10] proposed very early that the electric properties of colloidal particles with an electric double layer might be explained in terms of a model involving a sphere surrounded by a concentric shell of higher conductivity, and developed equations for the complex conductivity of a dilute system. But the parameters were not evaluated and the dielectric increment was not discussed. Bikerman[7b] obtained an approximate expression for the dielectric constant of a dilute suspension of cylindrical rods with surface conductivity. Subsequently, the theory of Maxwell–Wagner polarization was extended to homogeneous ellipsoids by Fricke,[11] but a surface conductivity was not incorporated in the model.

In the present study, the concept of a surface conductivity is generalized to include contributions from all species in the ion atmosphere, and other charge carriers, such as protons, electrons or holes, which are confined to a thin region on or near the surface. Equations are then obtained for the dielectric constant and conductivity of dilute systems of variously shaped particles of arbitrary dielectric constant, volume conductivity and surface conductivity, completely oriented or randomly oriented, in a solvent of arbitrary dielectric constant and conductivity, at arbitrary frequency. Various special cases are examined and predictions are made for some systems of particular interest. It is shown that remarkably high dielectric increments, conductivity increments and a broad range of relaxation behavior can be explained in terms of this model. It is concluded that the model has a useful range of validity in interpreting the behavior of solutions of large rigid macromolecules and colloidal electrolytes, and that it provides a system of

(6) (a) L. Havestadt and R. Fricke, *Z. anorg. allgem. Chem.*, **188**, 357 (1930); **196**, 120 (1931); (b) R. Fricke, *Kolloid Z.*, **66**, 166 (1931).

(7) (a) J. J. Bikerman, *Z. physik. Chem.*, **A171**, 209 (1934); (b) *J. chim. phys.*, **32**, 285 (1935); (c) *Kolloid-Z.*, **72**, 100 (1935); (d) *Trans. Faraday Soc.*, **36**, 154 (1940).

(8) H. Fricke and H. J. Curtis, THIS JOURNAL, **41**, 729 (1937).

(9) D. C. Henry, *Trans. Faraday Soc.*, **44**, 1021 (1948).

(10) J. B. Miles and H. P. Robertson, *Phys. Rev.*, **40**, 583 (1932).

(11) H. Fricke, THIS JOURNAL, **57**, 934 (1953).

equations to facilitate further investigation of mobile charges in the ion atmosphere and on surfaces, through dielectric constant and conductivity studies.

2. The Surface Conductivity Model and Ion Atmosphere Polarization

The surface conductivity may be defined by means of the relation

$$dq_e/dt = \lambda E_t l \qquad (2.1)$$

where the first term is the rate of transfer of charge along a surface of specific conductivity λ through a line element of length l in an electric field with a component E_t along the surface and perpendicular to the line element. The charge carriers may be ions, electrons or holes. If u_i is the mobility of a carrier of type i, then the contribution to λ from all carriers in the surface is

$$\lambda_s = \sum_i s_i u_i z_i \qquad (2.2)$$

where s_i is the number of carriers per unit surface area, and z_i is the absolute value of the valence.

In the more general case, carriers will not necessarily be restricted to a surface, but may be transported through the bulk media as well. Furthermore, their concentrations will be functions of position with respect to the surface. When the region of conductivity variation is thin compared to the dimensions of the particles the local conductivity at each point may be regarded as the sum of a bulk value, i.e., a value characteristic of the phase at a specified distance from the surface, and a value to be associated with the surface. Then the surface conductivity may be written as the sum of λ_s, defined above, and λ_a, the contribution to be evaluated from the excess conductivity due to the ion atmosphere. Consider, for example, a plane interface between the two regions illustrated in Fig. 1. Let the bulk conductivities of regions 1 and 2 at large distances from the surfaces be κ_1 and κ_2, and the conductivities at arbitrary distances by κ_1' and κ_2', respectively. Then the total surface conductivity is

$$\lambda = \lambda_s + \lambda_a = \sum_i s_i u_i z_i +$$
$$\int_{-\infty}^0 (\kappa_1' - \kappa_1)dy + \int_0^\infty (\kappa_2' - \kappa_2)dy \quad (2.3)$$

For dilute systems, we may compute the bulk conductivities of each phase from the individual ionic contributions in the usual manner

$$\kappa_k' = \frac{1}{N} \sum_i z_i n_i(y) l_i(y) \qquad k = 1,2 \qquad (2.4)$$

where n_i is the number of ions of type i per cc. and $l_i(y)$ is the equivalent conductance of species i at position y. By considering that the equivalent conductivity is a function of distance, we allow for variations in properties of ions and solvent in the strong fields prevailing near polyions.

Calculations of the surface conductivity have been made on various double-layer models, and it already has been suggested that studies of surface conductance may permit a definitive evaluation of the merits of the Helmholtz, Gouy and Stern treat-

ments.[12] It is probable that adsorbed or bound ions may move along the surface. A particular example of this has been discussed, namely, the possibility of proton transfer on the surface of proteins in solution.[13] The importance of this effect has not been demonstrated conclusively, but the term λ_s is general and may include a contribution from it. The rest of the expression for λ refers to the ion atmospheres outside and inside the particle in question. In many cases, the internal ion atmosphere contribution may be negligible owing to low ionic concentrations and mobilities.

3. The Surface Conductivity Effect for Spheres in a Conducting Medium in a Periodic Field

We consider uniform spheres of radius a, dielectric constant ϵ_2, bulk conductivity κ_2, and surface conductivity λ in a solvent of dielectric constant ϵ_1 and conductivity κ_1, under the influence of an external electric field. The first step is to find expressions for the potentials within and outside a given sphere. In setting up the boundary value problem, we adopt the method of Böttcher[14] and consider that each sphere is surrounded by a homogeneous medium of the bulk properties of the system. This is a useful approximation for the average effect of the surrounding particles at moderate concentrations. However, it does not account for the effects of local fluctuations in the distribution of neighboring particles. We introduce polar coördinates r, θ, ϕ, with origin at the center of the sphere, and z as polar axis. Let the instantaneous value of the macroscopic field intensity be E, along the z direction. Because of the symmetry, everything will be independent of ϕ. At large distances from the sphere the electric potential will be

$$\psi = -Er \cos \theta \qquad (3.1)$$

ψ is the component of the total potential arising from the applied field. The quantities ψ and E used without subscripts refer to average values over the system. Joule heating and electrochemical effects are assumed negligible; it is well known that these become unimportant at sufficiently low fields and high frequencies. Both the sphere and the surroundings are considered to have uniform bulk conductivities and dielectric constants, so application of a field does not produce space charge within either region. Therefore we may employ Laplace's equation in both regions

$$\nabla^2\psi_2 = 0; \ \nabla^2\psi = 0 \qquad (3.2)$$

At the surface of the sphere we have the usual conditions

$$\psi_2|_a = \psi|_a \qquad (3.3)$$

and

$$\epsilon_2 \left.\frac{\partial\psi_2}{\partial r}\right|_a - \epsilon \left.\frac{\partial\psi}{\partial r}\right|_a = 4\pi\sigma \qquad (3.4)$$

It is important to realize that equation 3.4, which is obtained by application of Gauss's theorem, is valid at any instant. The quantity σ is the

density of free charge at the surface, and ϵ_2 and ϵ are the real parts of the complex dielectric constants of sphere and suspension, respectively. Since ψ_2 and ψ are complex where the field is periodic, σ will also be complex.

To solve the problem for a periodic field, given by

$$E = E_0 e^{i\omega t} \qquad (3.5)$$

we require a differential equation for σ. Here E_0 is the space mean value of the peak field intensity in the suspension, ω is the angular frequency, and $i = \sqrt{-1}$. The surface charge density undergoes a time variation as the result of two processes: (a) the transport of ions to and from an element of surface as a result of the bulk conductivities of the two media, and (b) the transport of ions along the surface as a result of the surface conductivity. For isotropic media the first contribution is

$$\frac{d\sigma_n}{dt} = \kappa \left.\frac{\partial\psi}{\partial r}\right|_a - \kappa_2 \left.\frac{\partial\psi_2}{\partial r}\right|_a \qquad (3.6)$$

Let us consider separately the transport of charge at the interface, characterized by surface conductivity λ, with $\kappa = \kappa_2 = 0$. For an axially symmetric field distribution and a spherical surface, the continuity equation for process (b) is

$$\frac{d\sigma_b}{dt} = \frac{\lambda}{a^2 \sin\theta} \frac{\partial}{\partial\theta} \left(\sin\theta \left.\frac{\partial\psi_2}{\partial\theta}\right|_a \right) \qquad (3.7)$$

Treating λ, κ and κ_2 as constants of the system, we consider that the time derivative of the surface charge density may be written as the sum of the two contributions (3.6) and (3.7), when processes (a) and (b) occur simultaneously. Thus

$$\frac{d\sigma}{dt} = \frac{\lambda}{a^2 \sin\theta} \frac{\partial}{\partial\theta} \left(\sin\theta \left.\frac{\partial\psi_2}{\partial\theta}\right|_a \right) + \kappa \left.\frac{\partial\psi}{\partial r}\right|_a - \kappa_2 \left.\frac{\partial\psi_2}{\partial r}\right|_a \qquad (3.8)$$

This equation is solved readily by standard methods, giving these results:

The potential inside the sphere is

$$\psi_2 = -3 \epsilon^* rE \cos\theta/(\epsilon_2^* + 2\epsilon^* - 8\pi i\lambda/\omega a) \qquad (3.9)$$

The external potential is

$$\psi = [a^3(\epsilon_2^* - \epsilon^* - 8\pi i\lambda/\omega a)/r^3(\epsilon_2^* + 2\epsilon^* - 8\pi i\lambda/\omega a) - 1]rE \cos\theta \qquad (3.10)$$

The density of free surface charge produced by the applied field is

$$\sigma = 3iE \cos\theta[\epsilon_2\kappa - \epsilon(\kappa_2 + 2\lambda/a)]/\omega[\epsilon_2^* + 2\epsilon^* - 8\pi i\lambda/\omega a] \qquad (3.11)$$

where

$$\epsilon^* = \epsilon - 4\pi i\kappa/\omega \qquad (3.12a)$$
$$\epsilon_2^* = \epsilon_2 - 4\pi i\kappa_2/\omega \qquad (3.12b)$$

Examination of equations 3.9, 3.10 and 3.11 reveals that the term $8\pi i\lambda/\omega a$ is always subtracted from ϵ_2^*. Comparison with equation 3.12b shows that the effect of the surface conductivity λ in this model is exactly equivalent to an increase of κ_2 by $2\lambda/a$. Thus, for spheres, the equations are the same as in a treatment involving bulk conductivities only (Maxwell–Wagner polarization) if the conductivity of the sphere is given by

$$\kappa_s = \kappa_2 + \kappa_s' \qquad (3.13)$$

where $\kappa_s' = 2\lambda/a$. Thus, κ_s may be regarded as the effective volume conductivity of a sphere electrically equivalent to our model. The important

(12) F. Urban, H. L. White and E. A. Strassner, This Journal, **39**, 311 (1935).

(13) J. G. Kirkwood and J. B. Shumaker, Proc. Natl. Acad. Sci., **38**, 855 (1952).

(14) C. J. F. Böttcher, Rec. trav. chim., **64**, 47 (1945).

difference between the true volume and the surface contributions is that the latter κ_s' varies inversely as the radius, which permits distinguishing between surface and volume conductivities when the radius can be varied independently. The complex dielectric constant of the equivalent sphere is

$$\epsilon_s^* = \epsilon_2 - 4\pi i \kappa_s / a \qquad (3.14)$$

From equation 3.9 it follows that the electric field within the sphere is

$$E_2 = \frac{3\epsilon^*}{\epsilon_s^* + 2\epsilon^*} E \qquad (3.15)$$

The dipole moment m of the free surface charge is calculable from the equation

$$m = 2\pi a^2 \int_0^\pi a(\cos \theta) \sigma \sin \theta d\theta$$

By application of (3.11)

$$m = i4\pi a^3 (\epsilon_2 \kappa - \epsilon \kappa_s) E / (\epsilon_s^* + 2\epsilon^*) \qquad (3.16)$$

4. Dielectric Increments and Conductivities of Suspensions of Spheres

Polder and van Santen[15] have given an expression for the real part of the dielectric constant, ϵ, of a suspension of randomly oriented ellipsoids of dielectric constant ϵ_2 in a medium of dielectric constant ϵ_1. For suspensions of spheres their equation becomes

$$\frac{\epsilon - \epsilon_1}{3\epsilon} = \delta_2 \frac{\epsilon_2 - \epsilon_1}{\epsilon_2 + 2\epsilon} \qquad (4.1)$$

where δ_2 is the volume fraction of the spheres, which may be uniform or polydisperse. Although this equation was derived for insulating dielectrics where the ϵ are all real, it is valid also for lossy dielectrics or conducting media where the ϵ are complex. For the present problem the complex dielectric constants ϵ_s^* and ϵ_1^* may be inserted. Then the complex dielectric constant ϵ^* of the suspension is given by

$$\frac{\epsilon^* - \epsilon_1^*}{3\epsilon^*} = \delta_2 \frac{\epsilon_s^* - \epsilon_1^*}{\epsilon^* + 2\epsilon^*} \qquad (4.2)$$

Other expressions based upon different treatments of the mixture problem may readily be obtained in a similar way.

From equations 3.13 and 3.14, it is evident that the complex dielectric constant of a sphere with surface conductivity depends upon λ. It also depends upon the size of the sphere unless λ is zero. Therefore equation 4.2 is applicable only to spheres of a given size and λ. If λ is constant or substantially independent of a, the complex dielectric constant of a heterodisperse suspension of spheres may be obtained by application of equation 13 of Polder and van Santen,[15] and equation 3.14 above, with the result

$$\epsilon^* = \epsilon_1^* \left[1 - \sum_i \delta_i (\epsilon_s^* - \epsilon_1^*)(\epsilon_s^* + 2\epsilon_1^*)/3 \right]^{-1} \qquad (4.3)$$

Here δ_i is the volume fraction of spheres of radius a, and the sum is taken over all sizes. For low concentrations, that is, $\Sigma \delta_i \ll 1$, this may be simplified to

$$\epsilon^* = \epsilon_1^* = (\epsilon_1^*/3)\Sigma \delta_i (\epsilon_s^* - \epsilon_1^*)(\epsilon_s^* + 2\epsilon_1^*) \qquad (4.4)$$

For insulating media, i.e., $\kappa_1 = 0$, it is readily confirmed that the relaxation time is given by $\tau = a(\epsilon_2 + 2\epsilon_1)/8\pi\lambda$, a result obtained earlier by a simpler method.[4] Schwan[16] has pointed out recently that this is equivalent to a result of Miles and Robertson.[10] These investigators treated the complex conductivity of a suspension of spheres with a uniformly conducting shell of finite thickness. In the limit of very thin shells, their equations for relaxation time and conductivity reduce to the above. This agreement confirms the validity of the differential equation 3.8 employed in the present treatment. Miles and Robertson did not discuss the amplitude of the dielectric dispersion, nor did they relate the parameters in their model to known ionic properties. Because of the variation of ionic concentrations within the ion atmosphere, the idealized surface layer employed here is probably as good a model as the thick uniform shell they treated, and it has the advantage of greater simplicity.

In very dilute suspensions, or $\delta_2 \ll 1$, equation 4.2 for spheres one size may be simplified by inserting ϵ_1^* for ϵ^* in the denominators on both sides, which yields an explicit equation for ϵ^*. Further simplifications occur in the limits of high and low frequencies. Thus, when $\delta_2 \to 0$, $\epsilon^* \to \epsilon_1^*$, and the following expressions can be obtained for the dielectric constant increment, $\Delta\epsilon = \epsilon - \epsilon_1$, and the dielectric loss increment $\Delta\epsilon'' = \epsilon'' - \epsilon_1'' = 4\pi i(\kappa - \kappa_1)/\omega$

$$\frac{\Delta\epsilon}{\delta_2} = 3 \frac{\epsilon_1 X + 3\epsilon_1'' Y}{Z} \qquad (4.5)$$

$$\frac{\Delta\epsilon''}{\delta_2} = 3 \frac{\epsilon_1'' X - 3\epsilon_1 Y}{Z} \qquad (4.6)$$

where

$$X = \epsilon_2^2 + \epsilon_1 \epsilon_2 - 2\epsilon_1^2 + \epsilon_s''^2 + \epsilon_1'' \epsilon_s'' - 2\epsilon_1''^2$$
$$Y = \epsilon_2 \epsilon_1'' - \epsilon_1 \epsilon_s''$$
$$Z = (\epsilon_2 + 2\epsilon_1)^2 + (\epsilon_s'' + 2\epsilon_1'')^2$$

In the limit of very low frequencies, where ionic conduction dominates the electric field distribution, it can be shown that

$$\left(\frac{\Delta\epsilon}{\delta_2}\right)_{\substack{\omega \to 0 \\ \delta_2 \to 0}} = \frac{3[(r^2 - 2r - 2)\epsilon_1 + 3\epsilon_2]}{(r + 2)^2} \qquad (4.7)$$

where $r = \kappa_s/\kappa_1$. Thus, the low frequency dielectric increment is strongly dependent upon the conductivity ratio, which involves both the bulk conductivities and the surface conductivity. This is illustrated in Fig. 2, which is a plot of equation 4.7 for $\epsilon_1 = 78.54$ (H$_2$O, 25°) and $\epsilon_2 = 3.0$. Also, at low frequencies

$$\left(\frac{\Delta\kappa/\kappa_1}{\delta_2}\right)_{\substack{\omega \to 0 \\ \delta_2 \to 0}} = 3 \frac{r - 1}{r + 2} \qquad (4.8)$$

The relative conductivity increment per unit volume fraction is $-3/2$ for $r = 0$, negative for $r > 1$, passes through zero for $r = 1$, and reaches the value 3.0 as $r \to \infty$, as shown by the dashed line of Fig. 2.

At frequencies well above the regions of dispersion, where the dielectric constants largely determine the field distribution

(15) D. Polder and J. H. van Santen, *Physica*, **12**, 257 (1946).

(16) H. P. Schwan, *Adv. Biol. and Med. Phys.*, **5**, 147 (1957).

$$\Delta\epsilon/\epsilon_1\delta_2 = 3(\epsilon_2{}^2 + \epsilon_1\epsilon_2 - 2\epsilon_1{}^2)/(\epsilon_2 + 2\epsilon_1)^2 \quad (4.9)$$
$$(\omega \rightarrow \infty, \delta_2 \rightarrow 0)$$

and

$$\Delta\kappa/\kappa_1\delta_2 = 3(\epsilon_2{}^2 - 2\epsilon_1\epsilon_2 - 2\epsilon_1{}^2 + 3\epsilon_1{}^2 r)/(\epsilon_2 + 2\epsilon_1{}^2)$$
$$(4.10)$$
$$(\omega \rightarrow \infty, \delta_2 \rightarrow 0)$$

From equation 4.9, it can be seen that the dielectric increment is independent of the conductivities where frequency is so high that the ionic currents are negligible compared to the displacement currents. In strong contrast, the conductivity increment increases with the conductivity ratio and may be very large even for a relatively low volume concentration. In this case, it may not be permissible to set $\epsilon^* = \epsilon_1^*$ in equation 4.2, except for very low concentrations. It is clear that measurements of conductivity increments at frequencies well above the dispersion region can yield important information regarding the mobilities and binding of counterions.

Employing equations 4.5 and 4.6, which are valid for any frequency, the dispersion curves were calculated assuming $\kappa_1 = 1.469 \times 10^{-4}$ (10^{-3} M KCl at 25°) and $\lambda/a = 2.0 \times 10^{-3}$ ohms^{-1} cm.$^{-1}$. The latter would correspond to 500 Å. radius spheres of $\lambda = 10^{-8}$ ohms^{-1}, or 100 Å. radius spheres of $\lambda = 2 \times 10^{-9}$ ohms^{-1}. Values of λ for glass surfaces in contact with water are of this order.[4,12] Assuming negatively charged spheres, with λ due mainly to K$^+$ counterions having their usual mobilities, the polyion valencies would be around 2500 or 200, respectively. The results are plotted in Fig. 3.

5. The Surface Contributions to the Effective Conductivities of Ellipsoids, Cylinders and Disks

In part 3, it was shown that the effect of a surface conductivity is the same as an increase of the volume conductivity by an amount $2\lambda/a$ for a sphere. We may anticipate that the surface contributions to the effective conductivities will be different along different directions in non-spherical particles. Because the electrical boundary value problems cannot be solved in closed form for irregular shapes, we shall confine the discussion to ellipsoids, for which closed solutions are available, and two figures of revolution, the cylinder and disk, which approximate limiting cases of the ellipsoid when the appropriate axial ratio is high. The latter models are of particular interest in connection with the electrical properties of solutions of large rigid rod-like macromolecules like the nucleic acids, charged α-helical polypeptides, tobacco mosaic virus, and of suspensions of plate-like colloidal particles like the bentonite clays.

To greatly simplify the calculations, we shall first see how the equation for the surface contribution, $\kappa_s' = 2\lambda/a$, to the effective conductivity of a sphere, can be obtained in an easy way, and how the procedure may be generalized to give approximate values of the surface contributions along the various axes of an ellipsoid.

Consider a section of the sphere of radius a which is perpendicular to the direction of the internal field, E_2. The radius of this section is a $\sin \theta$, where θ is the angle between a radius vector
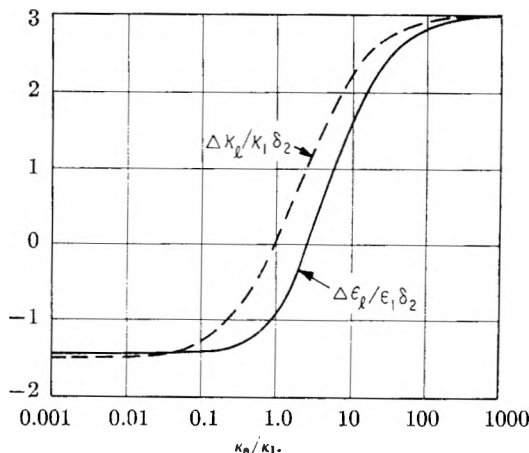
Fig. 2.—Low frequency dielectric and conductivity increments vs. conductivity ratio, κ_2/κ_1 for spheres.
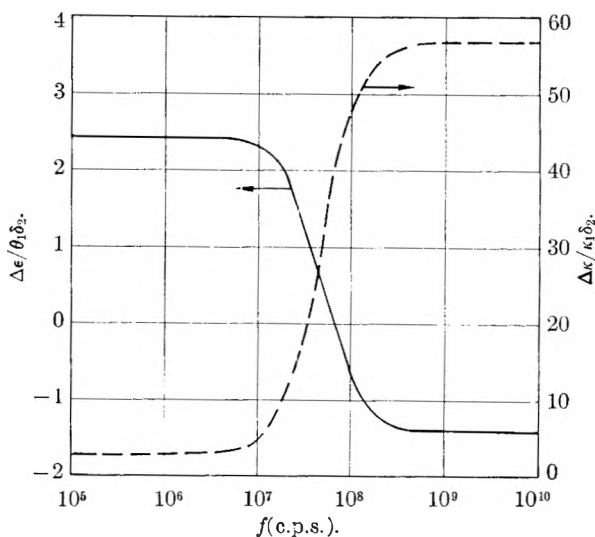
Fig. 3.—Dispersion of the dielectric constant and conductivity.

to the edge of the section and the field direction. The rate of charge transport along the surface across this section is $\lambda E_t 2\pi a \sin \theta$, where E_t is the tangential component of the internal field, equal to $E_2 \sin \theta$. The rate at which charge would be transported across the section as a result of a hypothetical volume conductivity κ_s' is $\kappa_s' E_2 A$, where A is the area of the section, equal to $\pi(a \sin \theta)^2$. Equating these two rates, one obtains $\kappa_s' = 2\lambda/a$, independent of the value of θ. Thus, the surface contribution to the effective volume conductivity is constant throughout the sphere, and may be evaluated readily by considering an equatorial section, i.e., $\theta = \pi/2$.

Ellipsoids.—We next consider an ellipsoid with electric field along one of its semi-axes, a, b or c, to evaluate the surface contributions, κ_a', κ_b', κ_c', to the effective conductivity along the respective axes. Taking equatorial sections perpendicular to the respective axes, making the assumption that the field intensity is constant across the section, as it is known to be for a homogeneous ellipsoid, and equating the expressions for surface and volume charge transport, one readily obtains

$$\kappa_a' = C(b,c)\lambda/\pi bc \qquad (5.1a)$$
$$\kappa_b' = C(a,c)\lambda/\pi ac \qquad (5.1b)$$
$$\kappa_c' = C(a,b)\lambda/\pi ab \qquad (5.1c)$$

Here $C(j,k)$ is the circumference of the ellipse with semi-axes j and k. This is approximately equal to $[2\pi(j^2 + k^2)/2]^{1/2}$ if it is nearly circular and approaches $4(j + k)$ if highly eccentric. These are equatorial values for κ'. Further consideration shows that the κ' values are not strictly constant, depending upon position along the axis, but that they are nearly constant for certain cases of special interest. Thus, for a slightly oblate or prolate spheroid, they approach the κ' evaluated for a sphere, shown to be a $2\lambda/a$ at all planes. For oblate or prolate ellipsoids of revolution ($b = c$)

$$\kappa_a' = 2\lambda/b \qquad (5.2)$$

Thus, at the equator, the surface contribution to the effective conductivity along the symmetry axis equals that of a sphere of radius b. Further detailed consideration, in which the tangential component of the internal field was evaluated as a function of position along the surface, showed that $\kappa_a'(f) = (2\lambda/b)[1 - (1 - b^2/a^2)f^2]^{-1/2}$, where f is the fractional distance along the axis a from the center to the end of the ellipsoid. If $a >> b$, κ_a' goes from $2\lambda/b$ to $1.16\,(2\lambda/b)$ as the circular section goes from the equator to $f = 0.5$. This displacement encompasses most of the volume of the semi-ellipsoid; therefore, in the present state of our knowledge, it seems adequate to consider $\kappa_a'(f)$ a constant equal to $2\lambda/b$ for a prolate ellipsoid of revolution. If $a << b$, the oblate ellipsoid approaches a disk, and $\kappa_a'(f) = (2\lambda/b)[1 + (b^2/af^2)^2]^{-1/2}$. In going from $f = 0$ to $f = 0.5$, $\kappa_a'(f)$ decreases from $2\lambda/b$ to $(a/b)(2\lambda/b)$. This is a greater change than the corresponding variation for the prolate ellipsoid, but it is not very important because, as we shall see, the transverse contribution, κ_b', is much greater than κ_a' and, in addition, positive contributions to the conductivity of the system will be much less for a circular disk with axis along the field than with axis perpendicular, as a result of the different depolarization factor A_j, defined below. It appears doubtful that a rigorous treatment, similar to the one above for a sphere, would lead to a closed solution of the boundary-value problem.

For prolate ellipsoids of revolution of high axial ratio ($a >> b = c$), the surface contributions to the effective conductivities along the transverse axes are, from equation 5.1

$$\kappa_b' = \kappa_c' \simeq 4\lambda/\pi b \qquad (5.3)$$

For thin oblate ellipsoids, approaching disks ($a << b = c$)

$$\kappa_b' = \kappa_c' \simeq 4\lambda/\pi a \qquad (5.4)$$

In both cases, the smallest dimension determines the equatorial value of κ_b'. Both values are greater than κ' for a sphere of equal volume and surface conductivity. For the long thin prolate ellipsoid of revolution, equations 5.2 and 5.3 yield $\kappa_a'/\kappa_b' \simeq \pi/2$, whereas for thin discs we find $\kappa_a'/\kappa_b' \simeq \pi a/2b$. Thus, the anistropy of the surface contribution to the effective conductivity is very weak for needles and very strong for disks. This is an interesting result from the point of view of re-

laxation behavior and particle shape studies. Because $\kappa_a' << \kappa_b'$ for a disk, use of the equatorial value for κ_b' is probably adequate for most purposes.

Cylindrical Symmetry: Rods and Disks.—Again considering the internal field to be homogeneous, i.e., neglecting end effects, we may equate the surface rate of charge transport and the volume rates for a cylinder of length $2a$ and diameter $2b$. The resulting values for the axial and transverse surface contributions to the effective conductivity are

$$\kappa_a' = 2\lambda/b \qquad (5.5)$$
$$\kappa_b' = (a + b)\lambda/ab \qquad (5.6)$$

It is seen that $\kappa_a' = \kappa_b'$ when $a = b$. At first glance this appears of interest in steady or low-frequency studies when the solvent conductivity is adjusted to equal the effective conductivity of the particle, in which case the field is uniform and end effects might be presumed non-existent. But more detailed consideration reveals that the model is not justified for the case of $a \simeq b$ because of the fundamental spatial difference between the surface and volume transport processes, i.e., end effects are probably important. In the degenerate cases, equations 5.5 and 5.6 should be good approximations, regardless of the ratio of particle and solvent conductivities. Equation 5.6 becomes

$$\text{Rods } (a >> b), \quad \kappa_b' = \lambda/b \qquad (5.7)$$
$$\text{Disks } (a << b), \quad \kappa_b' = \lambda/a \qquad (5.8)$$

The ratio between these values of κ_b' and the corresponding ones from equations 5.3 and 5.4 is $4/\pi$. Although this is a small difference, there may be a preference, to be decided by the actual shape when it is known. For rods, $\kappa_a'/\kappa_b' = 2$, and for disks, $\kappa_a'/\kappa_b' = 2(a/b)$. The relatively small anisotropy for rods does not involve a and should be present even when the ion atmosphere is comparable in thickness to b, so long as it is thin compared to a.

6. Dielectric Constant and Conductivity Increments, Non-spherical Systems

Oriented Ellipsoids, Rods and Disks.—The equations of Fricke[11] for the conductivity of dilute suspensions of isotropic ellipsoids with zero surface conductivity may be modified to obtain the more general equations appropriate to the present problem. If the ellipsoids are oriented with axis $j = a$, b or c along the direction of the field, Fricke's equation 1 may be written in the form

$$\kappa - \kappa_1 = \delta_2(\kappa_j - \kappa_1)/[1 + A_j(\kappa_j - \kappa_1)/\kappa_1] \qquad (6.1a)$$

Here, κ and κ_1 are the specific conductivities of the suspension and the solvent, respectively, κ_j is the particle conductivity along the j-axis, and A_j is the shape-dependent depolarization factor of the ellipsoid, given by

$$A_j = \int_0^\infty \frac{abc\,ds}{2(j^2 + s)[(a^2 + s)(b^2 + s)(c^2 + s)]^{1/2}} \qquad (6.1b)$$

This is equal to $abcL_j/2$ in Fricke's notation, and seems more convenient and meaningful than his L_j or x_j. Furthermore, graphs[17] and special formulas[18] for this function are available.

(17) J. A. Osborn, *Phys. Rev.*, **67**, 351 (1945).

The complex dielectric constants may be substituted for the conductivities in equation 6.1, because the boundary-value problems involving the two are mathematically identical. Alternatively, the equations of Polder and van Santen[15] derived for the static dielectric constant can be shown to give the same result in the limit of very low concentrations, after inserting the complex dielectric constants. Thus, one obtains for the dilute suspension, oriented with j-axis along the field

$$\epsilon^* - \epsilon_1^* = \delta_2(\epsilon_j^* - \epsilon_1^*)/[1 + A_j(\epsilon_j^* - \epsilon_1^*)/\epsilon_1^*] \quad (6.2)$$

Here, each complex dielectric constant, ϵ_k^*, may be written

$$\epsilon_k^* = \epsilon_k - 4\pi i\kappa_k/\omega, \ k = 1, a, b, \text{ or absent} \quad (6.3)$$

If the media exhibit dispersions, ϵ_k is the real value of the dielectric constant at the particular frequency, and κ_k would include the loss from the dispersive process. For the ellipsoid

$$\epsilon_j^* = \epsilon_j - 4\pi i\kappa_j/\omega \quad (6.4)$$
$$\kappa_j = \kappa_j^0 + \kappa_j' \quad (j = a, \ b \text{ or } c) \quad (6.5)$$

where κ_j^0 is the true volume conductivity along the j-axis, and κ_j' is the surface contribution to κ_j, the effective conductivity. For ellipsoids, values of κ_j' may be obtained from equation 5.1 or 5.2 to 5.4. If the particles are cylindrical rods or flat disks, equations 5.6 to 5.8 may be employed for the surface contributions, and the value of A_j may be taken as that of an ellipsoid of revolution of the same axial ratio. The volume fraction should be the actual external volume of the particles, determined experimentally.

Random Orientation.—For a dilute suspension of randomly oriented ellipsoids, equation 6.2 becomes

$$\epsilon^* - \epsilon_1^* = \frac{\delta_2}{3} \sum_{j=a,b,c} \frac{\epsilon_j^* - \epsilon_1^*}{1 + A_j(\epsilon_j^* - \epsilon_1^*)/\epsilon_1^*} \quad (6.6)$$

Equations applicable to more concentrated ellipsoidal systems are obtained easily by starting with Polder and van Santen's[15] equation 13. They are not presented as they cannot be solved explicitly for the dielectric constant and conductivity. Their usefulness would be doubtful because (a), the number of variables in ellipsoidal systems becomes large, and (b), ion atmosphere properties will become concentration dependent in an unknown manner when the ion atmospheres begin to overlap. Experimental tests of this theory should be confined to dilute systems, preferably by extrapolation of specific dielectric and conductivity increments to zero concentration.

The real and imaginary terms of equation 6.6 may be separated, after appropriate manipulation, to obtain the dielectric constant increment

$$\Delta\epsilon/\epsilon_1 = (\epsilon - \epsilon_1)/\epsilon_1 \quad (6.7)$$

and the dielectric loss increment

$$\Delta\epsilon''/\epsilon_1'' = (\epsilon'' - \epsilon_1'')/\epsilon_1'' = (\kappa - \kappa_1)/\kappa_1 = \Delta\kappa/\kappa_1 \quad (6.8)$$

The resulting equations are

$$\Delta\epsilon/\epsilon_1 = (\delta_2/3) \sum_{j=a,b,c} (\epsilon_j/\epsilon_1 - 1 + N_j)/D_j \quad (6.9)$$

and

(18) H. C. van de Hulst, "Light Scattering by Small Particles," John Wiley and Sons, Inc., New York, N. Y., 1957.

$$\Delta\epsilon''/\epsilon_1'' = (\delta_2/3) \sum_{j=a,b,c} (\epsilon_j''/\epsilon_1'' - 1 + N_j)/D_j \quad (6.10)$$

where

$$N_j = [(\epsilon_j - \epsilon_1)^2 + (\epsilon_j'' - \epsilon_1'')^2]A_j/(\epsilon_1^2 + \epsilon_1''^2)$$

and

$$D_j = [1 + \{(\epsilon_j\epsilon_1 + \epsilon_j''\epsilon_1'')/(\epsilon_1^2 + \epsilon_1''^2) - 1\}A_j]^2 + [(\epsilon_j''\epsilon_1 - \epsilon_j\epsilon_1'')A_j/(\epsilon_1^2 + \epsilon_1''^2)]^2$$

Numerical calculations of the dispersion may be made from these equations after appropriate simplification for a given system. Fricke's equations are for $\epsilon_a = \epsilon_b = \epsilon_c = \epsilon_2$, and $\epsilon_a'' = \epsilon_b'' = \epsilon_c'' = \epsilon_2''$, that is, he did not consider anisotropic particles. As in his case there are three relaxation times for a given ellipsoid, corresponding to the three axes. By generalization of Fricke's equation[11] 14 for anisotropic particles, the relaxation times in dilute systems are

$$\tau_j = \frac{1}{4\pi} \frac{\epsilon_j + \epsilon_1(1/A_j - 1)}{\kappa_j + \kappa_1(1/A_j - 1)} \quad (6.11)$$

where κ_j, in e.s.u., is given by equation 6.5. In the case of Maxwell–Wagner polarization, that is, zero surface conductivity, these are dependent on the shape of the particle, but independent of size. In our model they depend both upon size and shape, since κ_j', the surface contribution to the effective conductivity, clearly depends upon size as well as shape. Thus, randomly oriented polydisperse systems may be expected to show three broadened regions of dielectric dispersion, or two if there is an axis of symmetry.

If the frequency is low enough so that all dielectric constants are small relative to the corresponding loss factors, the fields are determined by the conductivities, and the equation for the dielectric increment, $\Delta\epsilon_1$, reduces to

$$\frac{\Delta\epsilon_1}{\epsilon_1} = \frac{\delta_2}{3} \sum_{j=a,b,c} \frac{\epsilon_j/\epsilon_1 - 1 + (\kappa_j/\kappa_1 - 1)^2 A_j}{[1 + (\kappa_j/\kappa_1 - 1)A_j]^2} \quad (6.12)$$

The low frequency conductivity increment is

$$\frac{\Delta\kappa_1}{\kappa_1} = \frac{\delta_2}{3} \sum_{j=a,b,c} \frac{\kappa_j/\kappa_1 - 1}{1 + (\kappa_j/\kappa_1 - 1)A_j} \quad (6.13)$$

At sufficiently high frequencies so that loss factors are all small relative to the corresponding dielectric constants

$$\frac{\Delta\epsilon_h}{\epsilon_1} = \frac{\delta_2}{3} \sum_{j=a,b,c} \frac{\epsilon_j/\epsilon_1 - 1}{1 + (\epsilon_j/\epsilon_1 - 1)A_j} \quad (6.14)$$

and

$$\frac{\Delta\epsilon_h''}{\epsilon_1} = \frac{\Delta\kappa_h}{\kappa_1} = \sum_{j=a,b,c} \frac{\kappa_j/\kappa_1 - 1 + (\epsilon_j/\epsilon_1 - 1)^2 A_j}{[1 + (\epsilon_j/\epsilon_1 - 1)A_j]^2}$$
$$(6.15)$$

For the present model and the Maxwell–Wagner model, no allowance is made for the possibility of the applied field causing large modifications of ion distributions at the boundaries, so the equations are strictly valid only for small fields. Fricke has further restricted application of his high frequency equations to frequencies "above all dispersion regions." If this is interpreted literally, his equations 22 and 23 and our 6.14 and 6.15 could only be applied above the dipolar dispersion region of polar solvents which would seriously restrict their use, for example, in aqueous systems. In obtain-

ing equations 6.14 and 6.15 from 6.9 and 6.10 here, it was seen that this restriction is not necessary. If one stays below the dipolar dispersion region of the solvent, where the dipolar contribution to ϵ_1'' is always much less than ϵ_1, the equations for $\Delta\epsilon_h$ and $\Delta\epsilon_h''$ are applicable. Thus, they may be applied for dilute aqueous solutions up to around a few hundred megacycles. When the conductivities are so high that ion atmosphere and dipolar dispersion regions overlap significantly, the more exact expressions 6.9 and 6.10 should be used. It should be kept in mind that the equations are for dilute systems, i.e., $\Delta\epsilon < \epsilon_1$ and $\Delta\kappa < \kappa_1$.

Numerical Results.—To illustrate the various effects of size, shape, magnitude of the surface conductivity, and solvent conductivity upon the dielectric and conductivity increments, numerical calculations were made for a wide range of values of the important parameters of the system. These are directed primarily at elucidation of the properties of rigid particles of relatively low dielectric constant and bulk conductivity, in a medium of high dielectric constant and low to moderate conductivity.

First, to illustrate the effect of particle shape on the primary quantities appearing in the equations, values of the depolarization factors A_a and $A_b = A_c$, and of the surface contributions to the effective conductivity, κ_a' and $\kappa_b' = \kappa_c'$, are presented in Table I. These apply to ellipsoids of revolution, where $2a$ is the symmetry axis and $2b = 2c$, with axial ratio $p = a/b$. The surface conductivity λ and the particle volume were held constant, and equations 5.1a to -c were used. The κ' values are given in units of κ_s', the value for a sphere of the same volume and surface conductivity. It is seen that κ_a' increases monotonically with increasing axial ratio, whereas κ_b' goes through a minimum at p slightly greater than one, increasing markedly for axial ratios much less than one, and somewhat less for axial ratios much greater than one. The important depolarizing factors are the smaller ones, for it is along the corresponding axis that the field exerts its greater effect.

TABLE I

DEPOLARIZING FACTORS AND SURFACE CONTRIBUTIONS TO THE EFFECTIVE CONDUCTIVITY vs. AXIAL RATIO OF SPHEROIDS

$p = a/b$	A_a	A_b	κ_a'/κ_s'	κ_b'/κ_s'
200	0.0001333	0.4999	5.848	3.724
100	.0004666	.4997	4.642	2.956
50	.001466	.4992	3.684	2.348
30	.003466	.4982	3.107	1.983
20	.006733	.4966	2.714	1.736
10	.02026	.4898	2.154	1.393
5	.05579	.4720	1.710	1.144
3	.1085	.4457	1.442	1.022
3/2	.2330	.3834	1.145	0.963
1	.3333	.3333	1.000	1.000
2/3	.4459	.2770	0.8735	1.103
1/3	.6354	.1822	.6933	1.475
1/10	.8607	.06959	.4641	3.002
1/30	.9497	.02509	.3218	6.161
1/100	.9844	.007766	.2154	13.72
1/200	.9922	.003910	.1710	21.77

Low frequency conductivity increments of randomly oriented systems were computed from equation 6.13 for a system of particles with zero volume conductivity, for varying axial ratio, again keeping the particle volume $(4\pi a_0^3/3)$ constant, for various values of $2\lambda/a_0\kappa_1 = \kappa_s'/\kappa_1$. Results are presented in Table II. No assumption regarding dielectric constants was required. For $\kappa_s'/\kappa_1 = 1$, the field is not affected by insertion of the sphere for its effective conductivity is equal to that of the medium, and $\Delta\kappa = 0$. But with highly elongated particles, the combination of small depolarization factor and increased effective conductivity along the longer axis produces positive conductivity increments. These increase rapidly for large values of p or $1/p$, and, of course, increase with κ_s'/κ_1. Thus, very large contributions to the low-frequency conductivity may occur in relatively dilute systems of highly anisometric particles with surface conductivity. The numerical calculation in Part 4 for spheres with $\lambda/a_0 = 2 \times 10^{-3}$ ohms^{-1} cm.$^{-1}$ in 10^{-3} M KCl corresponds to $\kappa_s'/\kappa_1 = 27$.

For oriented systems, the conductivity increments depend upon whether the field is oriented along the a or the b-axis, and these are designated $\Delta\kappa_a$ and $\Delta\kappa_b$, respectively. Values for parallel orientation are given in Table III. They are obtained by taking the appropriate term of the sum of equation 6.13, with the coefficient δ_2 rather than $\delta_2/3$. It is apparent that an anisotropy of the conductivity of the solution will be produced by partial orientation of the particles, and its magnitude can be obtained from these values if the degree of orientation is known.

High frequency conductivity increments for a broad range of p and κ_s'/κ_1 are given in Table IV. Equation 6.15 was employed, with $\epsilon_1 = 78.54$ (H_2O, 25°) and $\epsilon_a = \epsilon_b = \epsilon_c = 3.00$. The increments are only weakly dependent upon the latter quantity, for small ϵ_j/ϵ_1. Comparison with Table II shows that $\Delta\kappa_h$ is greater than $\Delta\kappa_l$ for large κ_s'/κ_1. This is because the local field remains large at high frequencies, but approaches zero at low frequencies for high κ_s'/κ_1. In oriented systems, $\Delta\kappa_a$ and $\Delta\kappa_b$ were computed from the appropriate term of the sum in equation 6.15. They are presented in Table V. Again, large anisotropies are observed.

The high frequency dielectric increment is independent of conductivity ratio, as seen by equation 6.14. Table VI lists values of $\Delta\epsilon_h/\epsilon_1\delta_2$ calculated for $\epsilon_1 = 78.54$ and $\epsilon_a = \epsilon_b = \epsilon_c = 3.00$. It is negative and becomes more negative at very low axial ratios, as expected from considerations of the dielectric constants of insulating particles.[15] The dielectric increments of oriented systems also are listed in Table VI.

The low frequency dielectric increments were computed for the usual axial ratios, with κ_s'/κ_1 values ranging from 1 to 100, $\epsilon_1 = 78.54$, $\epsilon_j = 3.00$, $\kappa_j^0 = 0$ and are shown in Table VII. Additional p-values were computed to delineate the interesting maximum which was found at the higher κ_s'/κ_1 values and high p. At $\kappa_s'/\kappa_1 = 1$, the low frequency dielectric increment is always negative in the range $1/100 \leqslant p \leqslant 100$. Insertion of

TABLE II
LOW FREQUENCY CONDUCTIVITY INCREMENTS vs. AXIAL RATIO FOR SPHEROIDS[a]

p	$\kappa's/\kappa_1 =$ 0.1	0.3	1.0	3.0	10	30	100
100	−0.9032	+0.05089	1.871	5.345	16.07	44.59	128.3
30	−1.120	− .3610	1.137	3.648	10.29	24.59	51.11
10	−1.258	− .6614	0.5959	2.485	6.656	10.56	14.71
3	−1.312	− .8703	.1555	1.532	3.025	3.913	4.350
3/2	−1.294	− .9100	.02190	1.248	2.350	2.858	3.071
1	−1.286	− .9130	.0000	1.200	2.250	2.719	2.912
2/3	−1.300	− .9142	.02195	1.252	2.350	2.850	3.058
1/3	−1.465	− .9452	.1643	1.619	3.030	3.733	4.039
1/10	−2.264	−1.174	.8400	3.525	6.702	8.604	9.518
1/30	−4.247	−1.567	2.411	8.089	16.27	22.15	25.29
1/100	−8.526	−1.907	6.570	20.23	44.32	65.64	78.80

[a] The numbers are relative values per unit volume fraction, $\Delta\kappa_1/\kappa_1\delta_2$.

TABLE III
LOW FREQUENCY CONDUCTIVITY INCREMENTS OF ORIENTED SPHEROIDS

p	$\kappa's/\kappa_1 =$ 0.1 a[a]	0.1 b[a]	1.0 a	1.0 b	3.0 a	3.0 b	10 a	10 b	100 a	100 b
100	− 0.536	−1.09	3.64	0.989	12.8	1.60	44.5	1.87	381	1.99
30	− .691	−1.33	2.09	.660	8.09	1.43	27.2	1.81	149	1.99
10	− .797	−1.49	1.13	.330	4.92	1.27	14.5	1.76	40.1	2.01
3	− .943	−1.50	0.422	.0223	2.44	1.08	5.46	1.80	8.66	2.20
3/2	− 1.12	−1.38	.140	− .0371	1.55	1.10	3.04	2.00	4.14	2.54
1	− 1.29	−1.29	.000	.000	1.20	1.20	2.25	2.25	2.91	2.91
2/3	− 1.54	−1.18	− .134	.100	0.941	1.41	1.74	2.66	2.19	3.49
1/3	− 2.28	−1.06	− .381	.437	.640	2.11	1.24	3.92	1.54	5.29
1/10	− 5.32	−0.736	− .995	1.76	.293	5.14	0.881	9.61	1.13	13.7
1/30	−12.0	− .388	−1.91	4.57	− .0358	12.2	.714	24.1	1.02	37.4
1/100	−26.6	+ .371	−3.45	11.6	− .543	30.6	.540	66.2	0.968	118

[a] Column a contains values of $\Delta\kappa_a/\kappa_1\delta_2$, where $\Delta\kappa_a$ is the conductivity increment for orientation of the a-axis along the field; column b contains $\Delta\kappa_b/\kappa_1\delta_2$ for orientation of the b-axis along the applied field.

TABLE IV
HIGH FREQUENCY CONDUCTIVITY INCREMENTS, $\Delta\kappa_b/\kappa_1\delta_2$, vs. AXIAL RATIO

p	$\kappa's/\kappa_1 =$ 0.1	1.0	3.0	10	100
100	−0.7770	7.192	24.90	86.88	883.7
30	−1.068	4.256	16.09	57.49	589.9
10	−1.237	2.424	10.56	39.03	405.1
3	−1.305	1.113	6.488	25.30	267.2
3/2	−1.289	0.7316	5.222	20.94	223.0
1	−1.282	.6679	5.000	20.16	215.1
2/3	−1.296	.7370	5.254	21.06	224.3
1/3	−1.426	1.250	7.197	28.01	295.6
1/10	−2.256	4.509	19.54	72.16	748.7
1/30	−4.223	12.54	49.78	180.1	1856
1/100	−7.740	23.45	92.73	335.2	3453

spheres of the same effective conductivity as the solvent does not affect the field distribution, but the dielectric constant decreases because of the lower dielectric constant of the sphere. The effect of a lower internal dielectric constant is overcome at sufficiently high values of κ_a' and κ_b', so the increment becomes positive at higher values of κ_s'/κ_1, the more so when $p \neq 1$. Large positive values at low and high p are associated with low values of the depolarizing factor, and arise from the terms containing κ_j in equation 6.12. This is of particular interest regarding the interpretation of the large dielectric increments of anisometric polyelectrolytes. If κ_j/κ_1 is large enough so $\kappa_j/\kappa_1 \gg 1$, the corresponding term of the sum approaches

TABLE V
HIGH FREQUENCY CONDUCTIVITY INCREMENTS OF ORIENTED SPHEROIDS[a]

p	$\kappa's/\kappa_1 =$ 0.1 a	0.1 b	1.0 a	1.0 b	3.0 a	3.0 b	10 a	10 b	100 a	100 b
100	− 0.536	−0.898	3.65	8.97	12.9	30.9	45.5	108	464	1094
30	− .691	−1.26	2.12	5.32	8.38	19.9	30.3	71.1	312	729
10	− .797	−1.46	1.22	3.03	5.70	13.0	21.4	47.9	223	496
3	− .942	−1.49	0.676	1.33	4.27	7.60	16.9	29.5	179	311
3/2	− 1.11	−1.38	.598	0.798	4.40	5.63	17.7	22.6	189	240
1	− 1.28	−1.28	.668	.668	5.00	5.00	20.2	20.2	215	215
2/3	− 1.53	−1.18	.877	.667	6.23	4.77	25.0	19.1	266	204
1/3	− 2.27	−1.01	1.86	.946	11.0	5.28	43.1	20.5	456	216
1/10	− 5.31	−0.730	8.78	2.37	40.1	9.27	150	33.4	1559	344
1/30	−11.9	− .379	26.7	5.44	113	18.4	413	63.7	4277	646
1/100	−24.0	+ .370	44.5	12.9	197	40.8	729	138	7576	1392

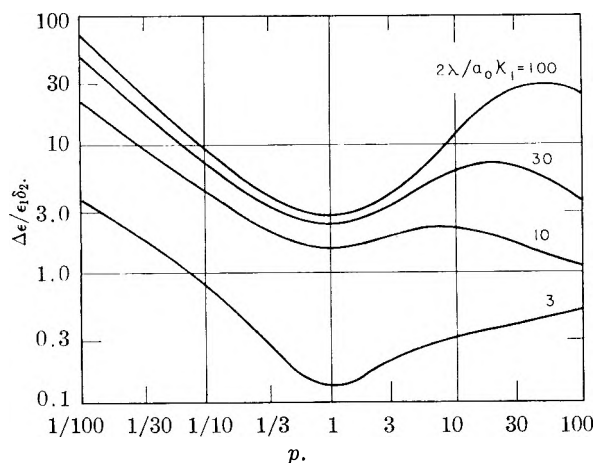[a] The numbers in column a are $\Delta\kappa_a/\kappa_1\delta_2$, in column b, $\Delta\kappa_b/\kappa_1\delta_2$.

Fig. 4.—Dielectric increments vs. axial ratio, p, for ellipsoids of revolution. Particle volume conductivity is zero. The surface conductivity and the particle volume are held constant as p changes.

TABLE VI

HIGH FREQUENCY DIELECTRIC DECREMENTS FOR COMPLETE AND RANDOM ORIENTATION

p	$-\Delta\epsilon_a/\epsilon_1\delta_2$	$-\Delta\epsilon_b/\epsilon_1\delta_2$	$-\Delta\epsilon_h/\epsilon_1\delta_2$
100	0.9622	1.852	1.555
30	.9650	1.847	1.553
10	.9809	1.818	1.539
3	1.074	1.683	1.480
3/2	1.240	1.524	1.429
1	1.416	1.416	1.416
2/3	1.684	1.311	1.435
1/3	2.473	1.166	1.602
1/10	5.586	1.031	2.549
1/30	11.11	0.9856	4.360
1/100	18.08	0.9690	6.671

TABLE VII

LOW FREQUENCY DIELECTRIC INCREMENT, $\Delta\epsilon_1/\epsilon_1\delta_2$, vs. AXIAL RATIO

p	κ_s'/κ_1				
	1.0	3.0	10	30	100
200	-0.009257	0.7073	1.025	2.307	14.08
100	- .1554	.5305	1.162	3.617	23.66
50	- .3277	.4502	1.399	5.374	29.04
30	- .4553	.3965	1.681	6.708	27.01
20	- .5543	.3571	1.934	7.217	21.90
10	- .7128	.3109	2.265	6.390	12.18
5	- .8445	.2620	2.206	4.472	6.247
3	- .9139	.2133	1.970	3.329	4.142
3/2	- .9577	.1482	1.683	2.568	2.975
1	- .9618	.1337	1.628	2.454	2.826
2/3	- .9618	.1510	1.690	2.566	2.965
1/3	- .9837	.2710	2.131	3.322	3.900
1/10	-1.427	.8075	4.420	7.415	9.088
1/30	-1.534	1.818	9.702	18.20	23.76
1/100	-2.125	3.821	22.56	49.95	72.05
1/200	-4.473	6.365	35.63	88.25	136.8

$1/A_j$, which is a large quantity along the long axes of highly anisometric particles. The maximum in $\Delta\epsilon_1$ observed for $p > 1$ is augmented and shifted to larger p at greater κ_j/κ_1. Thus, of conductivity associated with the counterions of a polyelectrolyte is a very important factor in determining $\Delta\epsilon_1$—one often ignored in past discussions with reference to theories developed for insulating systems.

The low frequency dielectric increments, $\Delta\epsilon_a$ and $\Delta\epsilon_b$, of oriented systems are presented in Table VIII. Again, $\epsilon_1 = 78.54$, $\epsilon_j = 3.00$, and $\kappa_j^0 = 0$ for all axes.

The numerical calculations have been presented in the form of tables as the wide range of values encountered would require an excessive number of curves for interpolations of reasonable accuracy. However, because low frequency dielectric increments have been widely investigated, curves of $\Delta\epsilon_1/\epsilon_1\delta_2$ vs. p for various κ_s/κ_1 are shown in Fig. 4 to portray the general trends and to facilitate interpolations over the wide range of values.

7. Applications

Proteins, Nucleic Acids and Nucleoproteins.— Dielectric dispersion has been studied in many protein solutions. The earlier work, which has been reviewed in several places,[19,20] was interpreted in terms of equations developed for insulating systems. The possibility of ionic polarization mechanisms, and variables like solvent conductivity, macromolecular charge and configuration, and counterion composition, which effect their contributions, were ignored, and the dielectric increments were attributed solely to permanent dipole orientation effects. Dielectric relaxation times were interpreted in terms of the rotational diffusion constants of rigid hydrodynamic models. From the above equations and numerical calculations, it is clear that the ion atmosphere polarization may account for the same effects previously attributed to orientation polarization. Thus, the existence of two relaxation times can be explained on the basis of a spheroidal model with surface conductivity as an alternative to one carrying a non-axial dipole moment. Either idea appears equally acceptable qualitatively and, in general, the possibility of contributions from both must be considered. However, there are several instances where the permanent dipole orientation theory is clearly inapplicable, namely, tobacco mosaic virus, hemocyanin and desoxyribonucleate.

An early suggestion of this came from a study of the Kerr effect in solutions of a large rigid macromolecule, tobacco mosaic virus (TMV), which showed very strong electric orientation which persisted at frequencies far above the expected orientational dispersion region and which was dependent upon electrolyte concentration.[21] The role of the ion atmosphere was qualitatively suggested on the basis of that study. The observed influence of electrolyte concentration can be explained through its effect on the parameters κ_j/κ_1 which strongly affect the dielectric increments, as shown above. A more quantitative treatment of the orientation effects on the present model involves additional considerations which will be discussed separately.[22] A discussion of the limiting case when κ_j/κ_1 is very large (κ_1 negligible) is con-

(19) J. L. Oncley, Ch. 22, in "Proteins, Amino Acids, and Peptides," by E. J. Cohn and J. T. Edsall, Reinhold Publ. Corp., New York, N. Y., 1943.

(20) J. T. Edsall, Forts. chem. Forschung, 1, 119 (1949).

(21) C. T. O'Konski and B. H. Zimm, Science, 111, 113 (1950).

(22) C. T. O'Konski and S. Krause, manuscript in preparation for publication.

TABLE VIII

LOW FREQUENCY DIELECTRIC INCREMENTS FOR ORIENTED SPHEROIDS[a]

p	1.0 a	1.0 b	3.0 a	3.0 b	10 a	10 b	30 a	30 b	100 a	100 b
200	− 0.957	+0.492	−0.921	1.52	−0.514	1.79	2.99	1.96	38.3	1.97
100	− .952	+ .243	− .873	1.23	− .000655	1.74	7.02	1.91	67.0	1.97
50	− .944	− .0196	− .790	1.07	+ .833	1.68	12.3	1.89	83.2	1.97
30	− .933	− .217	− .682	0.936	+1.78	1.63	16.4	1.88	77.1	1.97
20	− .921	− .371	− .563	.817	+2.63	1.59	17.9	1.86	61.8	1.97
10	− .893	− .623	− .290	.610	+3.78	1.50	15.5	1.85	32.6	1.98
5	− .864	− .835	− .00674	.396	+3.75	1.44	9.68	1.87	14.7	2.04
3	− .856	− .943	+ .129	.256	+3.08	1.42	6.12	1.93	8.13	2.15
3/2	− .896	− .989	+ .170	.137	+2.07	1.49	3.36	2.17	3.98	2.47
1	− .962	− .962	+ .134	.134	+1.63	1.63	2.46	2.46	2.83	2.83
2/3	− 1.07	− .907	+ .0705	.191	+1.30	1.89	1.89	2.91	2.13	3.38
1/3	− 1.39	− .780	− .0777	.445	+0.941	2.73	1.35	4.31	1.50	5.10
1/10	− 3.23	− .526	− .464	1.44	+ .611	6.32	0.972	10.6	1.10	13.1
1/30	− 4.14	− .230	−1.03	3.24	+ .384	14.4	.826	26.9	0.984	35.2
1/100	− 6.86	+ .244	−1.97	6.72	+ .0765	33.8	.705	74.6	.920	108
1/200	−14.7	+ .620	−0.330	9.71	− .159	144	.159	132	.889	205

[a] Columns a and b refer to $\Delta\kappa_a/\kappa_1\delta_2$ and $\Delta\kappa_b/\kappa_1\delta_2$, for orientation of the axes a and b, respectively, along the applied field.

tained in the more recent and complete study of the Kerr effect in TMV solutions.[23]

The dielectric properties of aqueous solutions of hemocyanin and sodium hyaluronate have been studied by Jacobson and co-workers.[24−26] They noted that in these systems also, the dielectric relaxation times were too short to be explained reasonably on the basis of dipolar reorientation. In studies of sodium thymonucleate partially oriented by hydrodynamic shear,[24] it was observed that the low frequency specific dielectric increments were very high. They increased with increasing velocity gradient when the electric field was along the stream lines, and decreased when the field was perpendicular. The large dielectric increments are expected on the basis of the present model, as are the changes in dielectric increment of the partially oriented systems. See Tables VII and VIII for large p and κ_s'/κ_1. Since the importance of the excess conductivity associated with the ion atmosphere and of solvent conductivity was not recognized, and the preparations studied were not well characterized, the necessary data for a quantitative interpretation on the present model are not available. Qualitative interpretations of this work subsequently were given by Jacobson,[27,28] who proposed that polyelectrolytes orient water molecules in extended ice-like hydration shells. We shall refer to this as the iceberg model. The oriented water was presumed to have a high value of the low frequency dielectric constant and dispersion properties similar to ice. It already has been pointed out on quantitative grounds that this model is inadequate to explain the electric orientation of TMV as an unreasonably thick shell of ice would be required.[23] Further tests of this proposal can be made by application of the equations

above, taking ionic conductivities to be negligible. Thus, equation 6.14 may be used to compute the low frequency dielectric increment. If one allows for the possibility of the existence of moderately thick shells, a reasonable upper value for the effective dielectric constant of the macromolecule with iceberg would be that of ice at 0°, which is 91.5.[29] The shape of Helix Pomatia hemocyanin approximates that of a prolate spheroid with axial ratio about 10.[25,30] From equation 6.14, taking ϵ_j(eff.) = 91.5, ϵ_1 = 78.54, and p = 10, one obtains $\Delta\epsilon/\epsilon_1\delta_2$ = 0.16. The reported[25] dielectric increment per gram of hemocyanin per 100 ml. of solution was 3.7 at 20°. Taking a partial specific volume of 0.7 cc./g. for the protein, $\Delta\epsilon/\epsilon_1\delta_2 = 3.7/(80.3)(7 \times 10^{-3}) = 6.6$. Thus, the iceberg model would require that around 6.6/0.16 − 1 or about 40 cc. of water be converted to ice per cc. of protein, which corresponds to a shell hundreds of ångströms thick. Reduction of this to a reasonable solvation value could be achieved only with unreasonably high assumed values for the dielectric constant of the ice.

From thermodynamic, viscosity and dielectric relaxation studies of aqueous solutions of simple electrolytes, it is well established that the effect of the high electric fields prevailing near ions is to disrupt the strongly hydrogen-bonded water structure[31] and decrease the local viscosity.[32−35] There appears to be no sound basis for supposing that a reversal of this effect, involving large masses of water, would occur in the vicinity of polyelectrolytes. Furthermore, ions are known to cause a lowering of the low-frequency dielectric constants

(23) C. T. O'Konski and A. J. Haltner, J. Am. Chem. Soc., 79, 5634 (1957).

(24) B. Jacobson, Rev. Sci. Instr., 24, 949 (1953).

(25) B. Jacobson and M. Wenner, Biochim. et Biophys. Acta, 13, 577 (1954).

(26) B. Jacobson and T. C. Laurent, J. Colloid Sci., 9, 36 (1954).

(27) B. Jacobson, Nature, 172, 666 (1953).

(28) B. Jacobson, J. Am. Chem. Soc., 77, 2919 (1955).

(29) R. P. Auty and R. H. Cole, J. Chem. Phys., 20, 1309 (1952).

(30) R. M. Pytkowicz and C. T. O'Konski, Biochim. et Biophys. Acta, 35, 466 (1959).

(31) H. S. Frank and M. W. Evans, J. Chem. Phys., 13, 507 (1945).

(32) E. C. Bingham, THIS JOURNAL, 45, 885 (1941).

(33) J. B. Hasted, D. M. Ritson and C. H. Collie, J. Chem. Phys., 16, 1 (1948).

(34) G. H. Haggis, J. B. Hasted and T. J. Buchanan, ibid., 20, 1452 (1952).

(35) F. E. Harris and C. T. O'Konski, THIS JOURNAL, 61, 310 (1957).

of solvated water.[34,35] The current view is that the first solvation shell of a small ion is radially oriented, the second is a disrupted, partially hydrogen-bonded structure, and beyond that a relatively normal water structure prevails.[35] Thus, not only is the iceberg hypothesis unnecessary but it is in contradiction with other observations as well.

Klotz[36] recently has endorsed Jacobson's iceberg hypothesis, apparently without any quantitative test, and has attempted to correlate many other observations on the basis of this model. The above considerations appear to remove the original justification for the hypothesis, and raise serious doubts regarding the validity of any interpretations of other phenomena in terms of thick ice-like shells. The long-range solvation hypothesis was actually proposed in somewhat different forms by Ostwald,[37] Hauser,[38] and Freundlich,[39] to explain the formation and the rheological properties of gels about three decades ago, only to be rejected later after more careful consideration.[40,41] The results of a recent X-ray study of hyaluronic acid by Laurent[42] constitute further evidence against the iceberg model.

To explain the larger dielectric increments of the more anisometric macromolecules, Jacobson required the additional special assumption that they crystallized out a greater amount of water than do the globular proteins. No special hypothesis is required to explain this in terms of the present model, as can be seen by reference to Fig. 4, where high dielectric increments are observed at high κ_s'/κ_1, for values of p far removed from unity.

A dielectric study of sodium thymonucleate by Jungner and Jungner[43] revealed large dielectric increments, and relaxation times shorter than expected on the basis of reorientation of the long axis of the macromolecule. These were interpreted as indicating zero dipole moment along the long axis and a transverse component which was very large, about $2 \times 10^4 d$. This appeared consistent[44] with the magnitude of the intrinsic Kerr constant reported by Benoit.[45] But it is not consistent with the negative sign of the birefringence.[46] The macromolecule has a negative optical anisotropy factor,[47] so the direction of orientation is with the long axis along the electric field, contrary to the orientation expected for a large transverse dipole moment. Since the macromolecule is known to be highly charged, it seems clear that all of the observed electrical properties can be explained in terms of ion atmosphere polarization. This does not rule out the existence of a transverse dipole

moment, but sets an upper limit to its value. To determine its magnitude would require further studies through which the effects of induced and permanent moment contributions would be separable. There now appears to be some possibility of this, by the application of the new birefringence saturation[48] and reversing field[23,49] techniques.

Proteins of smaller size than hemocyanin may have orientational relaxation times in the same frequency range as the ionic relaxation times. Then it becomes difficult to separate the contributions from the two processes from dielectric studies alone. If a more general theory combining both polarization mechanisms becomes available, it might become feasible to do this. In any event, studies as a function of pH and electrolyte composition should prove helpful. In deionized systems, the charge carriers will be H^+ and OH^-, and solvent conductivity will be relatively low. Thus, even if the acid and base groups are weakly dissociated, κ_s'/κ_1 may still be large. But the relaxation times increase with decreasing κ_s', and the ion atmosphere becomes more diffuse in salt-free solutions. Under certain conditions, the ion atmosphere relaxation time might be large compared to the reorientational relaxation times; then displacement currents will predominate over conduction currents in the reorientational dispersion region. When this is true, the previous interpretations of dielectric relaxation times[19,20] may become approximately correct. Application of theories developed for insulators may be possible for low electrolyte solutions of small spherical proteins, but each system should be subjected to appropriate tests before such theories can be applied with any degree of confidence.

A criterion of the applicability to aqueous solutions of theories developed for insulating systems is proposed. It is that $\tau_i > \tau_d$, where τ_i is the ionic relaxation time and τ_d is the orientational relaxation time. From the Debye–Stokes relation, one obtains, for spheres in water at 25°

$$\tau_d = 2.72 \times 10^{12} a_0{}^3 \qquad (7.1)$$

Applying equation 6.11 to a sphere, with the assumption that κ_1 is low, taking $\epsilon_1 = 78.5$ and $\epsilon_j = 3$

$$\tau_i = 7.1 \times 10^{-12} a_0/\lambda \ (\lambda \text{ in ohms}^{-1}) \qquad (7.2)$$

Thus, $\tau_d/\tau_i = 3.8 \times 10^{23} a_0{}^2/\lambda$. If λ is of the order of 10^{-9} ohm^{-1} it follows that $\tau_i \geqslant \tau_d$ only if $a_0 \leq 5$ Å. This is of the order of the radius of a small ion with its solvation shell. Thus, unless ionic transport at surfaces is one or two orders of magnitude less than we have reason to believe, application of dielectric theories developed for insulating systems is never fully justified for aqueous solutions at ordinary temperatures. The same statement applies for non-spherical ions.

The Kirkwood–Shumaker protonic mechanism[13] will become important if it is the major contribution to λ, and if κ_j/κ_1 is of order unity or greater. Its order of magnitude cannot be ascertained because the mobilities of the protons among the proton acceptor sites is not known from either

(36) I. M. Klotz, *Science*, **128**, 815 (1958).

(37) W. Ostwald, *Kolloid-Z.*, **46**, 248 (1928).

(38) E. A. Hauser, *J. Rheology*, **2**, 5 (1931).

(39) H. Freundlich, "Kapillarchemie," Akad. Verlag. m.b.H., Leipzig, 1932. Vol. II, p. 168–169, 624.

(40) J. L. Russell and E. K. Rideal, *Proc. Roy. Soc. (London)*, **154A**, 540 (1936).

(41) C. F. Goodeve, *Trans. Faraday Soc.*, **35**, 342 (1939).

(42) T. C. Laurent, *Arkiv Kemi*, **11**, 503 (1957); *C. A.*, **52**, 12522c (1958).

(43) A. Jungner and I. Jungner, *Acta Chem. Scand.*, **6**, 1391 (1952).

(44) I. Tinoco, Jr., *J. Am. Chem. Soc.*, **77**, 4486 (1955).

(45) H. Benoit, *Ann. Phys.*, **6**, 561 (1951).

(46) A. J. Haltner, Thesis, University of California, Berkeley, 1954.

(47) R. Cerf and H. A. Scheraga, *Chem. Revs.*, **51**, 256 (1951).

(48) C. T. O'Konski, K. Yoshioka and W. H. Orttung, THIS JOURNAL, **63**, 1558 (1959).

(49) I. Tinoco, Jr., and K. Yamaoka, *ibid.*, **63**, 423 (1959).

experiment or theory. The fluctuation polarization treatment[-3] for the low frequency dielectric increments contains the implicit assumption that the internal field is the one appropriate to insulating systems, as the solvent conductivity does not appear anywhere in the equations. To determine the possible importance of the protonic contribution, experimental results are needed on solutions of large and rigid proteins, for which the orientational and ionic contributions may be separable through analysis of dispersion data, preferably under isoionic conditions, to prevent masking by the counterion contribution.

Aqueous Suspensions, Emulsions.—The positive dielectric increments observed in aqueous colloidal suspensions—for example, V_2O_5,[50] silver halide and arsenic sulfide sols,[51] clays,[8] glass particles,[8] and polystyrene spheres[16]—can be interpreted with the aid of the above equations. Perhaps one of the best systems for experimental test of the theory is the polystyrene system, as uniform spheres of various sizes are available,[52] and polystyrene is known to be a non-hygroscopic material of low dielectric constant and negligible volume conductivity. The density of the particles[53] is close to the bulk density of polystyrene[54] so there would appear to be no complications arising from porosity. A study of Schwan and Maczu[16] on concentrated suspensions ($\sim 30\%$) is reported[55] to give reasonable values for the surface conductivity. At the high concentrations employed, particle interactions are important, and there is the possibility of anisometric aggregates. Also, the composition and concentration of the surfactant stabilizer and electrolyte were not controlled. Therefore the data cannot be employed as a definitive test of this theory, but controlled experiments of the same type on more dilute systems might be.

Wide distributions of relaxation times and the high dielectric increments observed with clay and V_2O_5 sols[8] are as expected for polydisperse systems. Dispersion studies of more monodisperse systems of this type might provide an interesting quantitative test of the theory, and yield important information regarding the distribution and properties of counterions.

Emulsions of a conducting liquid in a relatively insulating medium are expected to give positive dielectric increments at all frequencies if the dielectric constant of the suspended phase is higher than the suspending medium, and at frequencies below the Maxwell–Wagner dispersion region when the dielectric constant is lower. The effects of surface conductivity will be masked by internal volume conductivity, if $\kappa_2^0 \gg 2\lambda a_0$. When the suspending medium is the better volume conductor, adsorption of ions (*e.g.*, a dissociating surfactant) at the interface can give rise to surface

conductivities such that $\kappa_s' = 2\lambda/a_0 > \kappa_1$. Then positive dielectric increments are expected at frequencies below the dispersion region, as illustrated for $p = 1$ in Fig. 4, and the properties of adsorbed ions may be investigated with the aid of dielectric dispersion studies.

The low frequency conductivities of suspensions of glass spheres have been studied by Fricke and Curtis.[56] The computed values for the surface conductance were of the order of 10^{-9} ohms^{-1}. Unfortunately, the concentrations of the suspensions they employed were so great ($\delta_2 = 0.26$ to 0.33) that the conductivity increments were negative, particle interactions were high, and their application of Rayleigh's equation probably is not justified. A similar study on dilute suspensions, preferably at lower electrolyte concentrations and over a range of frequencies, is needed to adequately test this model.

Colloidal Electrolytes; Synthetic Polyelectrolytes.—The dielectric properties of micellar systems[8,57,58] may be interpretable in part in terms of the present model, in preference to the Debye–Falkenhagen treatment, when large or very anisometric micelles are formed. When the micelles are small, the ion atmosphere may be thick compared to all of the particle dimensions, and the equations given here would provide only a crude approximation—perhaps no better than the Debye–Falkenhagen treatment. Adding the ion atmosphere thickness to values for the semi-axes will constitute an approximate correction. When this is done, the volume average value of the dielectric constant over particle and solvent within the equivalent ellipsoid should be used in place of the particle dielectric constant. Because there is controversy regarding the shape of micelles, and the available data are limited in scope, no attempt will be made to interpret the experimental results in a quantitative way. Dielectric and conductivity dispersion studies might be of aid in answering some of the remaining structural questions.

The dielectric properties of sodium carboxymethylcellulose were investigated by Allgen and Roswall[59] who noted that the behavior was similar to that of other polyelectrolytes, such as desoxyribonucleate, nucleohistone, and sodium hyaluronate. A study of aqueous solutions of poly-4-vinyl-*n*-butylpyridinium bromide was made by Dintzis, Oncley and Fuoss.[60] They recognized qualitatively that the high dielectric increments observed probably were associated with counterion migration, and noted that the shape of the curves suggested two dispersion regions. Both observations are consistent with the present model. They recognized a similarity to both the Debye–Falkenhagen model (diffuse ion atmosphere about a point ion) and the Maxwell–Wagner model (suspension of particles with volume conductivity), and remarked, "Whether the observed increments in

(50) J. Errera, *J. phys. radium*, **9**, 307 (1928).

(51) H. R. Kruyt and H. Kunst, *Kolloid-Z.*, **91**, 1 (1940).

(52) E. B. Bradford and J. W. Vanderhoff, *J. Appl. Phys.*, **26**, 864 (1955).

(53) W. Heller, J. N. Epel and R. M. Tabibian, *J. Chem. Phys.*, **22**, 1777 (1954).

(54) R. S. Morrell, "Synthetic Resins and Allied Plastics," Oxford University Press, London, 1951, p. 696.

(55) H. P. Schwan, private communication.

(56) H. Fricke and H. J. Curtis, THIS JOURNAL, **40**, 715 (1936).

(57) M. Shirai, *Sci. Papers, Coll. Gen. Ed. Univ. Tokyo, Japan*, **7**, 23 (1957).

(58) M. Shirai and B. Tamamushi, *Bull. Chem. Soc., Japan*, **29**, 733 (1956).

(59) L. G. Allgen and S. Roswall, *J. Polymer Sci.*, **12**, 229 (1954).

(60) H. M. Dintzis, J. L. Oncley and R. M. Fuoss, *Proc. Natl. Acad. Sci.*, **40**, 62 (1954).

dielectric constant are primarily due to a Maxwell–Wagner dispersion or primarily a Debye–Falkenhagen effect, or quite possibly a combination of the two, cannot be decided on the basis of the facts available at present," and that "we must not exclude the possibility that some hitherto unsuspected effect is operating in these systems." The present view is that both the Debye–Falkenhagen and the Maxwell–Wagner treatments represent approximations incorporating the same fundamental process, ion transport, with different boundary conditions. The present treatment incorporates still another set of boundary conditions which appears more acceptable for polyelectrolytes than the Debye–Falkenhagen model, because it explains many features related to size and structure. It appears more realistic than the Maxwell–Wagner model, which requires high internal volume conductivities, as these seem unreasonable for substances with compact structures.

Anisotropy of Conductivity and Dielectric Constant.—The predictions of this treatment for the effects of orientation on the dielectric increments and conductivities already have been discussed, and it was pointed out that the observations of Jacobson and co-workers on the dielectric increments in partially oriented systems are easily explained. The qualitative features of the observations of Schindewolf,[61] Heckmann[62] and Eigen and Schwarz,[63] on the anisotropy of the low-frequency conductivity in oriented polyphosphate and soap solutions are as expected for anisometric macromolecules or micelles (cf. Table III and IV). According to this theory, the effect should exist even when the contribution of the polyions themselves to the transport process is negligible. Schwarz[64,65] has developed a theory in which the effect is attributed solely to the lower frictional coefficient of the extended polyion along its longer axis, as compared to the perpendicular axis. In terms of the present model, the polyion mobility may be negligible, and the anisotropy effect will still exist, because of the depolarizing factor in the equations for conductivity. Also, on the present model, it will depend strongly on the mobility and the degree of binding of the counterions. Furthermore, it seems clear that the anisotropy of the polyion mobility will involve an important consideration in addition to the change in frictional coefficient, namely, the change of local field at the polyion with orientation. For the present model at low frequencies, and for orientation of the j-axes along the field

$$E_j(\text{int}) = E_j(\text{ext})/[1 + (\kappa_j/\kappa_1 - 1)A_j]$$

where $E_j(\text{int})$ and $E_j(\text{ext})$ are the internal and external field intensities along the j-axis. Referring to Table I, it is seen that at high p-values, A_a becomes very small, A_b approaches 0.5, and κ_a' and κ_b' are of the same order of magnitude. Thus, when $\kappa_j/\kappa_1 > 1$, the local field effect may far exceed the frictional coefficient consideration, in de-

termining the anisotropy of the mobility of the polyion, defined in the customary way in terms of the external field. This will make the anisotropy of the polyion contribution even greater than supposed in Schwarz's treatment, but it does not follow that the polyion contribution will exceed the contributions from the relatively mobile counterions which are computed on the present model. A complete theory must include both effects. Direct observations of the polyion mobility as a function of electric field (or degree of orientation) will probably be required to evaluate contributions of polyions and other ions separately. The electric field orientation problem was treated independently by Schwarz[65] and O'Konski and Haltner[23] in terms of the limiting model in which the particles are considered very good conductors relative to the medium. In the latter study the absolute magnitude of the Kerr constant was studied in a carefully chosen model system,[23] and it was found to be significantly below the value calculated for the limiting case. The theory has been extended to the present model and will be presented elsewhere.[22]

Concentrated Systems: Biological Tissues, Polycrystalline Powders, Soils.—The above discussion on the origin and the magnitude of the surface conductivity effect, and its dependence upon particle size and shape is of interest in the further interpretation of the dielectric properties of tissues and cell suspensions, which have been reviewed recently by Schwan.[16]

As a consequence of a high localized conductivity in interfacial regions, special effects may be produced in biological systems by application of short bursts of intense high-frequency radiation, e.g., lightning strokes or high-frequency pulses. At frequencies below the dipolar dispersion region of water, the temperature rise in the ion atmosphere of polyelectrolytic components, e.g., the desoxyribonucleic acid in genes, would be expected to exceed the average temperature rise of the system until the heat can be carried away from the surface by thermal conduction. This may give rise to much greater biochemical changes in pulsed fields than expected on the basis of the mean temperature rise of the system.

The high values of the low frequency dielectric constants and the dielectric dispersion observed in crystalline powders containing very small amounts of adsorbed water vapor are very probably the result of surface conductivity produced by mobile ions in adsorbed films of water.[66,67] The presence of mobile ions on the surfaces of anisometric particles of clay probably is responsible for the large low frequency dielectric constants and the broad region of dielectric dispersion observed in soils and for the variations observed with soil type and moisture content.[68–70]

(61) U. Schindewolf, *Naturwissenschaften*, **40**, 435 (1953); *Z. physik. Chem. [N.F.]*, **1**, 129 (1954); *Z. Elektrochem.*, **58**, 697 (1954).

(62) K. Heckmann, *Z. physik. Chem. (Neue Folge)*, **9**, 318 (1956).

(63) M. Eigen and G. Schwarz, *ibid.*, **4**, 380 (1955).

(64) M. Eigen and G. Schwarz, *J. Colloid Sci.*, **12**, 181 (1957).

(65) G. Schwarz, *Z. Physik*, **145**, 563 (1956).

(66) C. T. O'Konski, *J. Am. Chem. Soc.*, **73**, 5093 (1951).

(67) E. J. Murphy and H. H. Lowry, THIS JOURNAL, **34**, 598 (1930).

(68) S. S. Banerjee and R. D. Joshi, *Phil. Mag.*, **25**, 1025 (1938); for a criticism of the method see H. R. L. Lamont, *ibid.*, **29**, 521 (1940).

(69) A. R. von Hippel, "Dielectric Materials and Applications," Technology Press, M.I.T., and John Wiley and Sons, Inc., N. Y., 1954, p. 314.

(70) C. T. O'Konski, unpublished data.

Protein Hydration from Dielectric Studies.—
Interpretation of the high frequency dielectric
decrements of protein solutions in terms of a
solvated model having a low dielectric constant[71,72]
appears to be a sound approach to the problem
for compact molecules, providing the data can be
obtained in a region where the loss contributions
from ionic processes make only small contributions
to the field distribution ($\epsilon_j'' \ll \epsilon_j$). This will be
so if $\tau_i > 1/\omega$, where ω is the angular frequency at
which the decrement is observed. Wherever
information regarding molecular asymmetry is
available, the dielectric decrement appropriate to

(71) G. H. Haggis, T. J. Buchanan and J. B. Hasted, *Nature*, **167**, 607 (1951).

(72) T. J. Buchanan, G. H. Haggis, J. B. Hasted and B. J. Robinson, *Proc. Roy. Soc. (London)*, **A213**, 379 (1952).

the macromolecular shape may be computed.[70]
From the values of $\Delta\epsilon_h/\epsilon_1\delta_2$ of Table VI, it is clear
that the calculated hydration will depend upon the
molecular shape, the variation being greater in
going from spheres to oblate ellipsoids than in
going from spheres to prolate ellipsoids.

COEFFICIENTS OF EVAPORATION AND CONDENSATION

By J. P. Hirth and G. M. Pound

Metals Research Laboratory, Carnegie Institute of Technology, Pittsburgh, Pennsylvania

A model is developed for crystal growth and evaporation which invokes the Kossel concept of a crystal surface being com-
posed of low index facets, of low binding energy for adsorbed atoms, separated by ledges of higher binding energy. The
treatment indicates that surface diffusion kinetics are important in most instances of crystal growth and evaporation.
Prior kinetic treatments, such as those involving limitations of crystal growth because of entropy effects or diffusion in the
vapor phase, are modified to include surface diffusion effects. Values for evaporation and condensation coefficient pre-
dicted by the kinetic treatment are compared with experimentally determined values.

Introduction

Since the relation between the vapor pressure of
a substance and the flux of the substance leaving
a surface in equilibrium with the vapor was de-
veloped by Hertz,[1] Knudsen,[2] and Langmuir[3]
there has been a vast research effort to investigate
the quantity α_j ambiguously called the condensa-
tion coefficient, the evaporation coefficient, or the
accommodation coefficient in the expression

$$J_i = \pm \alpha_j(p_e - p)/(2\pi mkT)^{1/2} \qquad (1)$$

where the plus sign is used for evaporation, the
minus for condensation, $J_i = J_v$ is the net vapori-
zation flux in molecules per cm.[2] per second, $J_i =
J_c$ is the net condensation flux, $j = 1, 2, 3, ---$,
dependent on the process being considered, p_e
= the equilibrium pressure, p = the actual vapor
pressure, m = molecular mass, and k and T have
their usual meaning. In general, α_j in condensa-
tion does not equal α_j in evaporation under similar
experimental conditions as was assumed by early
investigators. Also, there are often several factors
affecting α_j which may or may not be mutually
independent. Accordingly, the following treat-
ment of the various factors affecting J_i is presented
in order that the interaction of these factors might
be clarified. The various factors are considered
separately, the simpler cases being treated initially
and complexities introduced in sequence. In
each case, the consideration of surface diffusion in
the kinetics represents the new contribution of
this work.

(1) H. Hertz, *Ann. Phys.*, **17**, 177 (1882).

(2) M. Knudsen, *ibid.*, **29**, 179 (1909).

(3) I Langmuir, *Phys. Rev.*, **2**, 329 (1913).

Theory

**I. Clean Crystalline Surface with a Monatomic
Vapor Phase.**—In this case, the internal partition
functions of an atom in the crystal are vibrational
and in the vapor phase are translational. Hence,
rotational degrees of freedom are not activated in
evaporation or condensation and, as a first ap-
proximation, it is possible to use a model of evapora-
tion and growth in which atoms are considered to
be bound by near neighbor bonds.[4,5] It has been
shown by Burton, Cabrera and Frank[6] in the case
of growth and by Hirth and Pound[7] in the case of
evaporation, both following the general ideas of
Volmer,[8] that the kinetics involve the steps:
(a) adsorption or desorption to the vapor phase
from the surface; (b) surface diffusion; and (c)
movement into or out of a kink position in a mon-
atomic ledge on the crystal surface, at which the
equilibrium concentration of adsorbed atoms is
maintained, see Fig. 1.

For ideal crystals, *i.e.*, large crystals bounded
by low index planes and with no lattice imper-
fections other than the monatomic ledges and ad-
sorbed atoms, the monatomic ledges arise from
crystal edges in evaporation. The adsorbed atoms
on the surface develop the distribution shown in
Fig. 2, where it is shown that the equilibrium
concentration of adsorbed atoms is maintained at

(4) W. Kossel, *Nach. Ges. Wiss. Göttingen*, 135 (1927).

(5) I. N. Stranski, *Z. physik. Chem.*, **136**, 259 (1928).

(6) W. K. Burton, N. Cabrera and F. C. Frank, *Phil. Trans. Roy. Soc.*, **243A**, 299 (1951).

(7) J. P. Hirth and G. M. Pound, *J. Chem. Phys.*, **26**, 1216 (1957).

(8) M. Volmer, "Kinetik der Phasenbildung," Steinkopff, Dresden and Leipzig, 1939.
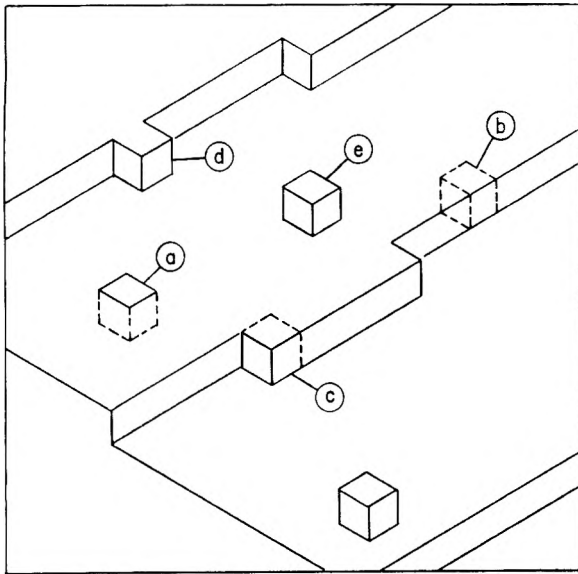
Fig. 1.—Schematic view of metal-vapor interface depicting ledges, and atoms in the following positions: a, in surface; b, in ledge; c, kink; d, at ledge; e, adsorbed on the surface.

(A) Ledge being produced from an edge.

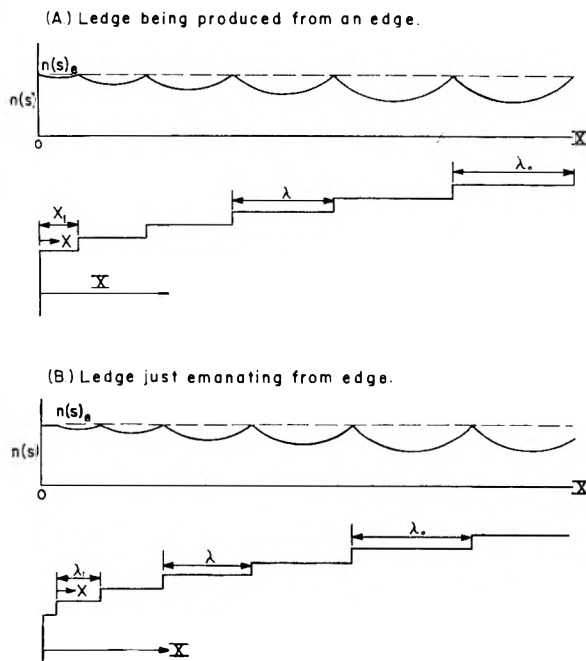(B) Ledge just emanating from edge.

Fig. 2.—Surface cross-section and the distribution of adsorbed atoms on the surface.

monatomic ledges, and that a gradient of adsorbed atoms exists. The gradient sets up a surface diffusion flux, and, invoking a condition of continuity, the divergence of this flux equals the flux of atoms evaporating into the vapor phase. Solving the differential equation corresponding to the continuity condition, Hirth and Pound[7] showed that the evaporation coefficient is given by

$$\alpha_j = (2\bar{X}/\lambda) \tanh(\lambda/2\bar{X}) \qquad (2)$$

where $\bar{X} = (D_s/\nu)^{1/2} \exp(\Delta F_{des}/2kT)$ = mean free path for random walk of an adsorbed atom on a close-packed surface, ν = vibration frequency of atoms adsorbed on the metal surface, D_s = surface self-diffusion coefficient, ΔF_{des} equals free energy of

activation for desorption of an atom from the surface to the vapor, and $\bar{\lambda}$ represents the average spacing between monatomic ledges on the crystal surface.

Now, as the spacing λ of monatomic ledges increases, the surface diffusion gradients at the ledges increase and, accordingly, the velocity of the ledges increases. Thus, in evaporation, ledges arise at crystal edges, accelerate, and finally approach a limiting velocity asymptotically when the spacing λ becomes so large that a change in λ no longer affects the gradient at the ledges. This situation arises when $\lambda = \lambda_0 = 6\bar{X}$. Referring to equation 2, it can be seen that the limiting value for α_j, i.e., the value at $\bar{X} = \lambda_0$, is $\alpha_j = 1/3$.

For real crystals, other ledge sources such as screw dislocations and grain boundaries in addition to crystal edges are effective. Grain boundaries and cracks will behave kinetically like crystal edges. Screw dislocations will lead to a different kinetic behavior as shown by Cabrera and Levine.[9] The monatomic ledge associated with a screw dislocation will wind into a spiral under the action of the evaporation kinetics outlined above. The curvature at the center of the spiral is dictated by a capillarity constraint on the spiral; the curvature at the center of the spiral will equal the curvature of a "two-dimensional" disc-shaped void in equilibrium with the undersaturated vapor phase to which the surface is exposed. With this constraint, Cabrera and Levine[9] show that the spacing λ_1 of ledges near the center of a screw dislocation spiral is

$$\lambda_1 = 19\rho_c \qquad (3)$$

where ρ_c is the critical radius of a two-dimensional nucleus on a crystal surface given approximately by

$$\rho_c = \gamma\Omega/kT \ln(p/p_e) \qquad (4)$$

in which γ = specific interfacial free energy and Ω = atomic volume. When λ_1 is less than λ_0, i.e., at large undersaturations, the ledges emanating from a dislocation will accelerate to λ_0 as outlined above, and by equation 2 α will again be $1/3$ over all the crystal except perturbed regions at the center of the dislocation spiral[10]; when $\lambda_1 > \lambda_0$, the ledges emanating from a dislocation will maintain the spacing λ_1, so that by equation 2 α_j would be less than $1/3$ if only these ledges led to evaporation. However, the ledges arising from edges will maintain a spacing λ_0 independent of undersaturation so that the ledges from edge sources will obscure ledges of spacing λ_1 arising from dislocations and α_j will be maintained at $1/3$, except for perturbations at dislocation-spiral centers. Hirth and Pound[10] showed that the concentration of dislocation-spiral centers must exceed about 10^6 per cm.^{2} before α_j becomes appreciably greater than $1/3$. Thus, the effective number of ledges from dislocation sources will vary with supersaturation but λ will in no case exceed λ_0.[10]

All of the above arguments are for large crystals bounded by low index planes. For smaller crystals, or for large crystals after long times, high index planes originating at crystal edges will be pro-

(9) N. Cabrera and M. M. Levine, Phil. Mag., 1, 450 (1956).
(10) J. P. Hirth and G. M. Pound, Acta Met., 5, 649 (1957).

duced on the crystal. This situation arises because evaporation is not steady-state, in the sense that the spacing λ of ledges at a small fixed distance from the edge source will decrease with time. Hence, an evaporating crystal will approach an end state in which it is bounded by high index planes consisting of ledges with spacing $\bar{\lambda} \ll \bar{X}$. This circumstance gives rise to an evaporation coefficient, equation 2, equal to unity.

Therefore, in evaporation, a crystal can initially have an evaporation coefficient of $1/3$ but, in any case, the evaporation coefficient will approach unity in the limit. If high index planes or many ledge sources are initially present in the crystal, the evaporation coefficient will initially be $1/3 < \alpha < 1$ and again will approach unity in the limit.

Equation 2 holds for growth where $\alpha_j = \alpha_2$, but only over a limited range. This is because ledges in growth cannot nucleate easily at crystal edges, but arise from two-dimensional nuclei or from dislocation-surface intersections as induced by Frank.[11] Thus, when for the most active dislocation source of ledges, $\lambda_1 > \lambda_0$, the spacing $\bar{\lambda} = \lambda_1$ will be maintained and

$$\alpha_2 = (2\bar{X}/\lambda_1) = (2kT\bar{X}/19\gamma\Omega)\ln(p/p_e) \quad (5)$$

The critical pressure below which this occurs is designated

$$p' = p_e \exp(19\gamma\Omega/6kT\bar{X}) \quad (6)$$

Also, at very high supersaturations, a perturbation to equation 2 occurs due to formation of stable two-dimensional nuclei between ledges, i.e., at $\lambda_0/2$ in Fig. 2. The concentration of adsorbed atoms at $\lambda_0/2$ is given by[7]

$$n_s = n_{s0}[0.1 + 0.9(p/p_e)] \quad (7)$$

where n_{se} = equilibrium concentration of adsorbed atoms. In evaporation, the minimum undersaturation of adsorbed atoms on the surface is thus 10%, under which two-dimensional nucleation of holes in the surface is negligible.[8] On the contrary, in growth the supersaturation is unlimited. It is known from two-dimensional nucleation theory[8] that the nucleation rate increases from an essentially negligible value to an essentially infinite value at a critical pressure, p''. When nucleation is rapid, the spacing between nuclei is small compared to $\bar{X}$, so that every atom striking the surface reaches a ledge and is incorporated into the crystal. Thus, α_2 will increase from the value $2\bar{X}/\bar{\lambda}$ to the value unity when $p \geq p''$ where[8,12]

$$p'' \cong p_e \exp[\pi a \gamma^2 \Omega/B(kT)^2] \quad (8)$$

in which "a" is the monomolecular step height, and $B \sim 46$ is the exponent of the frequency factor in the nucleation rate equation. Comparing (8) and (6), it is evident that p'' will be greater than p' as long as $(a^2\gamma/BkT) \exp[(\Delta F_{des} - \Delta F_D^*)/2kT]$ > unity, a condition that almost always obtains. Between p' and p'', α_2 will equal about $1/3$ as noted above. Accordingly, a typical plot of net flux versus pressure is presented in Fig. 3.[13]

(11) F. C. Frank, Disc. Faraday Soc., 5, 48 (1949).

(12) J. P. Hirth, Acta Met., 7, 755 (1959).

(13) Figure 3 obtains only for an initial crystal that is large, but finite, bounded by low index planes, and containing surface-dislocation intersections on all faces. Other starting configurations would lead to different plots, e.g., an infinite crystal with one screw dislocation
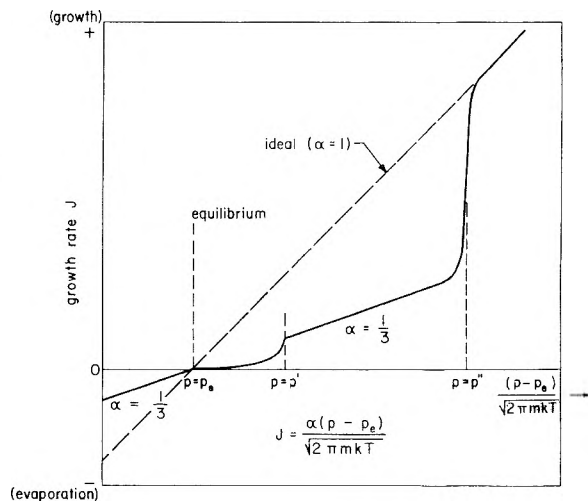
Fig. 3.—Theoretical curve of growth rate versus flux impinging on surface.

Equation 6 supposes an "active" dislocation source.[6] If there were an equal number of opposite sign dislocations intersecting the surface, and the distance between the two closest opposite sign dislocations is d^6; then for growth to occur the supersaturation must be sufficiently high that $2\rho_c < d$. Below the supersaturation corresponding to $2\rho_0 = d$, J_c drops rapidly to zero, as in the case of two-dimensional nucleation.[8]

Again, in evaporation, edge perturbations will increase as the crystal shrinks, so that α_1 will approach unity. A crystal initially bounded by close-packed planes will initially have the value $\alpha_1 = 0.33$ associated with close-packed planes. As evaporation proceeds, the high index planes initially present only at crystal corners will impinge on the close-packed planes and α_1 will approach the value unity associated with high index planes. In growth, on the other hand, the principal perturbation arises from screw dislocations; low index planes thus persist in growth; and the value of α_2 will remain constant during growth.

Thus, the vaporization coefficient α_1 does not equal the condensation coefficient α_2 for a material except in very restricted cases. Although the above treatment is elaborated for a substance with a monatomic vapor phase, it holds equally well for any crystal for which surface diffusion enters the kinetics, adsorption or desorption is the rate-controlling step, equilibrium is maintained at monomolecular ledges in the surface, and the concentration of adsorbed atoms is less than the reticular density of atoms on the plane on which the atoms are adsorbed. The latter condition obviates the necessity of treating the surface diffusion problem in a moving frame of reference.[14]

II. Clean Liquid or Amorphous Substance.—In the case of a clean liquid surface of a substance similar to the type treated in Part I, it is apparent that the surface can no longer be regarded as being composed of low index planes separated by ledges. Rather the surface will be effectively a

would, on the evaporation side of the scale, be symmetric with the condensation curve shown in Fig. 3, and the condensation curve would remain the same.

(14) W. W. Mullins, private communication; see also ref. 6.

random high index or "roughened" surface,[6] with the result that the number of available sites at the liquid–vapor interface is not restricted. Thus, the evaporation coefficient α_3 and the condensation coefficient α_4 will both equal unity subject only to the condition that the rate of evaporation is small enough that thermal equilibrium is maintained at the liquid–vapor interface, a condition which is likely to obtain.

For liquids for which the evaporating molecules have an appreciable entropy of vaporization, the above arguments are no longer valid, but absolute rate theory gives a satisfactory interpretation of the results. Hertzfeld[15] showed that, if a molecule is free to rotate in the vapor phase, but restricted in rotation in the condensed phase, the evaporation coefficient, as defined by equation 1, will be less than unity. Stearn and Eyring[16] extended this view and introduced the term δ, the "free angle ratio," to describe the restricted rotation. The absolute rate theory, in the case where a restricted rotation or torsional vibration becomes a free rotation in the activated state in the process of evaporation yields the expression for the gross evaporation rate

$$J_{VG} = (\nu/a^2)(Q^*/Q) \exp(-\Delta H_v/kT) \qquad (9)$$

where $(1/a^2)$ is the surface density of molecules in the liquid, "a" is the intermolecular spacing, Q^* is the activated rotational partition function, Q is the restricted partition function, ΔH_v is the heat of vaporization,[17] and $(Q/Q)^* = \delta$. In condensation, only a fraction δ of the molecules incident on the surface are properly oriented to condense, so that the gross condensation rate is

$$J_{CG} = \delta p/(2\pi mkT)^{1/2} \qquad (10)$$

At equilibrium

$$J_{VGe} = J_{CGe} = \delta p_e/(2\pi mkT)^{1/2} \qquad (11)$$

Further, under non-equilibrium conditions from equation 9, $J_{VG} = J_{VGe}$ so that the net condensation rate

$$J_C = J_{CG} - J_{VG} = J_{CG} - J_{CGe} = \\ \delta(p - p_e)/(2\pi mkT)^{1/2} \qquad (12)$$

A similar expression obtains for J_V; hence, evidently, in this case, $\alpha_3 = \alpha_4 = \delta$ which deviates from unity. Penner[18a] applies non-equilibrium corrections[18b] to the absolute rate treatment and obtains a result equivalent to equation 12.

Wyllie[19] has shown that a low value of δ is usually coincident with the presence of a polarized layer at the liquid–vapor interface. Under non-equilibrium conditions, the rate of transfer between this layer and the vapor phase becomes rate controlling. Because the rotation is restricted in the polar layer, this gives a physical interpretation of the correlation between δ and α_3 or α_4. An alternative possibility would be the existence of short-range order in the liquid so that restricted rotation would be required for condensation.

Thus, in this case, $\alpha_3 = \alpha_4 = \delta$, which only deviates from unity when a activational entropy obtains in evaporation or condensation.

III. Entropy Effects for Clean Molecular Crystals.

The consideration of entropy effects is more complex in the case of solids, for now the additional factor of stepwise kinetics[8] must be considered. Herzfeld,[15] Polanyi and Wigner,[20a] Pelzer,[20b] and Neumann[21] have considered evaporation probability, as reviewed by Stranski.[22] However, these treatments do not include the effect of kink and ledge concentrations in reducing the number of favorable evaporation or growth sites on the surface. Stranski[22,23] treats the stepwise problem generally, but concludes that, in the absence of effects due to δ, see Part II, α_j is unity, which is not generally the case as shown in Part I. Bradley[24] has extended the results of Polanyi and Wigner to the stepwise evaporation of KCl, but evidently does not treat the surface diffusion kinetics of adsorbed molecules. The most advanced treatment of the stepwise kinetics has been presented by Burton, Cabrera and Frank[6] as will be referred to in the following.

It is likely that the entropy term will principally affect the kinetics of transfer between kinks and adsorbed molecules, i.e., the rotational degrees of freedom, restricted in the condensed phase, are likely to be activated in the adsorbed state. Although the kinetics of evaporation and condensation are the same in such a case as those discussed in Part I, the boundary conditions are different in that equilibrium can now no longer be maintained at monatomic ledges. For example, in condensation, the concentration of adsorbed molecules at a ledge $n_s' > n_{se}$, the equilibrium concentration of adsorbed molecules. The solution for the net condensation flux is the same as the solution leading to equation 2[7]

$$J_C = (2\bar{X}/\lambda) \tanh (\lambda/2\bar{X})[P/(2\pi mkT)^{1/2} - n_s'\nu \\ \exp(-\Delta F_{des}/kT)] \qquad (13)$$

the solution leading to equation 2 differing from equation 13 only in that n_s' is replaced by n_{se}. In the case $n_s' = n_{se}$, since $p_e/(2\pi mkT)^{1/2} = n_{se}\nu\exp(-\Delta F_{des}/kT)$, equation 2 results. However, when entropy effects are present in the step adsorbed atom to ledge, $n_s' \neq n_{se}$, as noted above, and a comparison of equations 13 and 1 yields for this case the equation for the condensation coefficient

$$\alpha_6 = (2\bar{X}/\lambda) \tanh (\lambda/2\bar{X})(p - \beta p_e)/(p - p_e) \qquad (14)$$

where $\beta = n_s'/n_{se}$. Using arguments similar to those presented in Part II, and substituting from equation 2, one can solve for β in terms of δ yielding

$$\alpha_6 = f(\delta)\alpha_2/[\alpha_2 + f(\delta)] \qquad (15)$$

where $f(\delta) = 2\delta\bar{X}^2/\lambda a$. In the limit this expression reduces to $\alpha_6 = \alpha_2$ (small entropy effect) or $\alpha_6 = f(\delta)$ (large entropy effect).

(15) K. F. Herzfeld, J. Chem. Phys., **3**, 319 (1935).

(16) A. E. Stearn and H. Eyring, ibid., **5**, 113 (1937).

(17) A justification for the use of H_v in equation 9 rather than an activation enthalpy $\Delta H_v^* > \Delta H_v$, is given in Part VIII.

(18) (a) S. S. Penner, This Journal, **56**, 475 (1952); (b) T. Hirschfelder, J. Chem. Phys., **16**, 22 (1948).

(19) G. Wyllie, Proc. Roy. Soc. (London), **197A**, 383 (1949).

(20) (a) M. Polanyi and E. Wigner, Z. physik. Chem., **139A**, 439 (1928); (b) H. Pelzer, ref. 8, p. 37.

(21) K. Neumann, Z. physik. Chem., **197A**, 16 (1950).

(22) I. N. Stranski, "Progress in Metal Physics," Vol. 6, Pergamon Press, London, 1956, p. 181.

(23) O. Knacke, I. N. Stranski and G. Wolff, Z. physik. Chem., **198A**, 157 (1951).

(24) R. S. Bradley, Proc. Roy. Soc., **217A**, 524 (1953).

A similar expression obtains for the evaporation coefficient α_5 with, however, α_2 replaced by α_1.

The chief difference between condensation and evaporation once more lies in the effect of edge perturbations on α_1 in equation 15; and in dislocation-spiral control[9] affecting α_2 at p' [see discussion following equation 4].

A further modification is considered by Burton, Cabrera and Frank[6] involving diffusion along ledges. However, as shown by these authors, this effect is unlikely to be rate controlling and can generally be neglected. The conditions under which the factor becomes appreciable are presented.[6]

The critical pressure p'', see equation 8, at which two-dimensional nucleation takes place will also be higher than in the case treated in Part I. The factor B will be reduced approximately by the amount $\ln \delta$, so that p'' will accordingly be increased by a factor δ. Also, when two-dimensional nucleation takes place, the condensation coefficient will still $= \delta$, so that, while the form of Fig. 3 is maintained $\alpha_j \to \delta$ at p''. Note, too, that here p' will also be larger than in Part I.

Thus, here again, the condensation and evaporation coefficients are unlikely to be equal. Also, the introduction of entropy effects gives rise to a temperature dependence of the coefficients α_5 and α_6.

IV. Activation Energy for Evaporation.—For a limited number of valence-bonded compounds, the activation energy for evaporation, here defined as being exclusive of configuration effects, is much greater than the heat of sublimation. This case has been treated by Stranski and co-workers[25] and by Brewer and Kane.[26]

The effect is likely to be present in cases where several polymers are present in the equilibrium vapor over a crystal, but only one of the polymers participates in the interface kinetics. Also, an activation energy could arise if bond lengths of ionic molecules are different in the vapor phase from the lengths in the crystal. The vaporization will also involve δ effects. The logical development of the kinetics in this case is similar to that in Part III, and yields an expression analogous to equation 14. However, the term β will now be related to $\delta \exp(-\Delta H^*/kT)$ where ΔH^* is the activational enthalpy for condensation. Hence, the condensation coefficient

$$\alpha_8 = (2\delta \bar{X}^2/\lambda a) \exp(-\Delta H^*/kT) \qquad (16)$$

and a similar expression obtains for the evaporation coefficient α_7; p'' and p' will be much higher than in Part I. Also, α_8 will be reduced by the additional factor of diffusion of the polymer taking part in the interface kinetics through the other polymers present in the vapor. This can be obviated if only the pertinent polymer is impinged on the specimen. Again, $\bar{\lambda}$ will differ for evaporation and growth as noted in the preceding sections. Note that α_8 can be extremely small.

V. Diffusion in the Vapor Phase.—Consider first crystals where configurational entropy effects are negligible. Should the mean free path of an inert gas over the substance being tested in an evaporation or growth experiment be small with respect to that of the substance itself in its equilibrium vapor, diffusion through the inert gas will be rate controlling. The net rate of evaporation will be

$$J_v = D_v \nabla n_v \cong -D_v (\partial n_v/\partial y)_{y=0} \qquad (17)$$

where y is the distance normal to the surface, D_v the diffusion coefficient of the substance in the inert gas, and n_v the concentration of the substance in the vapor phase. The solutions to this equation and of the analogous equation for condensation are well known.[27] In the special case of a flowing inert gas

$$J_v = -D_v (n_{v_e} - n\eta)/\eta \qquad (18)$$

where $n_{v_e} = p_e/kT$ is the concentration of the equilibrium vapor, $n\eta$ is the concentration at the edge of a lamellar flow region a distance η from the surface. It is thus assumed that there is a linear concentration gradient from $y = 0$ to $y = \eta$, and a uniform concentration $n\eta$ at $y > \eta$. In experiments involving the use of flowing inert gas to carry away the evaporation product, it is assumed that equation 17 gives the same result as equation 1, so

$$\alpha_9 = -D_v(2\pi m/kT)^{1/2}/\eta \qquad (19)$$

In the general case, both surface diffusion and diffusion in the vapor will be important. The continuity equation will be[7]

$$D_s(\partial^2 n_s/\partial X^2) = -D_v(\partial n_v/\partial y)_{y=0} \qquad (20)$$

The exact solution of this equation will be quite complex. However, for the simple type of concentration gradient considered above

$$(\partial^2 n_s/\partial X^2) = (C_1/D_s)n_s - (C_2/D_s)n\eta \qquad (21)$$

where $C_1 = D_v\nu[\exp(\Delta F_{des}/kT)](2\pi mkT)^{1/2}/kT$ and $C_2 = D_v/\eta$. The solution of this equation is

$$J_v = [(2/Z\lambda) \tanh (Z\lambda/2)](D_v/\eta)$$
$$(2\pi m/kT)^{1/2}(p_e - p)/(2\pi mkT)^{1/2} \qquad (22)$$

where

$$Z = [D_v\nu(2\pi mkT)^{1/2} \exp(\Delta F_{des}/kT)/D_s\eta kT]^{1/2}$$

Thus

$$\alpha_9 = (2/Z\lambda)(D_v/\eta)(2\pi m/kT)^{1/2} \tanh (Z\lambda/2) \qquad (23)$$

α_{10}, the condensation coefficient, will be an analogous expression. Again, in the ideal case of evaporation of an otherwise perfect crystal containing a few screw dislocations, $2/Z\lambda = 1/3$, $\tanh (Z\lambda/2) = 1$ as in Part I. The difference between α_9 and α_{10} will once more lie in the dependence of $\bar{\lambda}$ on edge *versus* dislocation perturbations.

The situation where the kinetics will be partially controlled by the diffusion fluxes and partially by entropy effects will yield a result similar to equation 14, *viz.*

$$J = \alpha_9(\beta p_e - p)/(2\pi mkT)^{1/2} \qquad (24)$$

This situation is unlikely to occur in practice.

VI. Adsorption.—Adsorption can give rise to the development of macroscopic steps. For this reason, this section will be divided into two parts, the first considering the dynamics of monatomic steps, the second, macroscopic steps.

(25) I. N. Stranski and G. Wolff, *Research*, **4**, 105 (1951).

(26) L. Brewer and J. S. Kane, THIS JOURNAL, **59**, 105 (1955).

(27) W. Jost, "Diffusion," Academic Press, New York, N. Y., 1952.

A. Monatomic Steps.—Adsorption of an impurity gas, say, in condensation, or of an impurity from the crystal or vapor in evaporation can have several effects. Weak adsorption or adsorption under conditions where the flux of adsorption is small compared to the flux of the major component should have little effect on the kinetics of condensation or evaporation. Stronger adsorption should lower the energy of the kink, ledge or surface on which it takes place.[28] This adsorption could lead to the condition $n_s' > n_{s_e}$ (in condensation) and lead to the same solution given in equations 13, 14 and 15. Adsorption, however, could also change the binding energy to $\Delta F'_{des} < \Delta F_{des}$. Thus, instead of equation 13

$$J_0 = (2\bar{X}'/\lambda) \tanh (\lambda/2\bar{X}')[p/(2\pi mkT)^{1/2} - n_s'\nu \exp(-\Delta F'_{des}/kT)] \quad (25)$$

where

$$\bar{X}' = (D_s/\nu)^{1/2} \exp(\Delta F_{des}'/2kT) < \bar{X}$$

and the condensation coefficient

$$\alpha_{12} = (2\bar{X}'/\lambda) \tanh (\lambda/2\bar{X})[p/(2\pi mkT)^{1/2} - n_s'\nu \exp(-\Delta F_{des}'/kT)]/[(p - p_e)/(2\pi mkT)^{1/2}] \quad (26)$$

Hence, adsorption can reduce α_j both by decreasing $\bar{X}$ to $\bar{X}'$, and by increasing n_{s_e} to n_s'. The evaporation coefficient α_{11} will again be given by a similar expression, and evaporation will differ from condensation through the term λ as above. Also, adsorption should lower γ and (see Part I) so lower p' and p'', but as in Part II, α_{13} will not go to unity above p'' as long as dynamic adsorption of impurity obtains.

Strong adsorption could result in a diffusion solution. However, the diffusion coefficient through the adsorbed layer is difficult to estimate, so a detailed treatment is not given. A special case has been treated by Sears.[29] In the limit of strong adsorption, compound formation will take place, and the over-all kinetics will be different, involving nucleation of oxide, etc., a quite complex situation. Cabrera and Vermilyea[30] discuss the possibility of large adsorbates "pinning" monatomic ledges at points of adsorption.

B. Macroscopic Steps.—In Parts I through V, ledge kinetics are such that ledge spacings are either stable or increase. For example, considering Fig. 2, the greater the spacing λ of ledges adjoining a given ledge, the greater will be the surface diffusion gradient acting on the ledge and the faster it will move. Hence, around a macroscopic ledge (which can be considered a "bunch" of monatomic steps), the ledges adjoining the macroscopic ledge will tend to accelerate the monatomic steps at the edges of the macroscopic ledge, and the macroscopic ledge will thus be unstable and will dissociate into a spreading bunch of monatomic steps. On the other hand, Frank[31] has noted that, if an impurity is adsorbing onto a crystal in a time-dependent manner, and if the impurity slows down the ledge,

as would be the case in the kinetics leading to equation 26, then the greater the spacing of a ledge ahead of a given ledge, the *slower* the latter ledge will travel. This leads to an instability in a train of equally-spaced ledges moving across a surface in evaporation or condensation. If, by a fluctuation, one ledge spacing is increased, the following ledge will decelerate and the ledges following will pile up against the decelerating ledge, forming a macroscopic step. Thus, when such adsorption takes place, condensation or evaporation proceeds by the motion of macroscopic steps separated by essentially perfect low index planes. Such a phenomenon has been observed frequently (e.g., McNutt and Mehl[32]).

In such a circumstance, the condensation coefficient for the flat regions between steps will be (see equation 26) $\alpha_{12} = 2\bar{X}/\lambda \cong$ zero, while for the "risers" or high index planes forming the steps of height "h," the coefficient for atoms striking the rise will be $\alpha_j =$ unity. The risers will also condense atoms striking within a distance $\bar{X}$ of either side of the step, so that the effective α_j of the riser will be $\alpha_j = (h + 2\bar{X})/h$. Thus, the exact condensation (or evaporation) coefficient in such a circumstance will depend on the ratio of h to λ

$$\alpha_{13} = (h + 2\bar{X})/(h + \lambda) \quad (27)$$

if one considers the risers to contribute to the total surface area or

$$\alpha_{13} = (h + 2\bar{X})/\lambda$$

if only the close-packed planes between steps are considered to contribute to the total surface area on which the vapor impinges.

VII. Geometry Effects.—If all other coefficients are unity, the presence of sharp re-entrant crevices in the surface will not affect the condensation or evaporation rates as shown by Melville.[33] When other considerations lead to $\alpha_j < 1$ on a plane surface, a crevice will act as a quasi Knudsen cell[2] and tend to give an effective measured α_j, based on a plane surface, approaching unity. Sharp cracks will have a similar effect in condensation.

If macroscopic facets form at a small angle to the mean surface, they will raise the effective value of α_j by the ratio of the true surface area to the surface area of an assumed flat mean surface. Thus, if a high index plane tends to break up into low index facets at the temperature of evaporation or condensation measurement under an interfacial free energy criterion[34] or due to the kinetics of the process *per se*, as in Part VI, then the effective α_j will be increased by the area factor. For example, the break-up of a (100) surface into (110) facets would result in an apparent α_j greater than the true α_j by $\sqrt{2}$. Further, it is possible for a mean surface to be unstable with respect to corrugation at low temperature and stable at high temperature, so that the effective α_j can change discontinuously in a critical temperature range.

In the special case of evaporation from a Knudsen

(28) Here adsorption is confined to exclude conditions where a compound between the adsorbate and the major component would be stable.

(29) G. W. Sears, *J. Chem. Phys.*, **25**, 154 (1956).

(30) N. Cabrera and D. A. Vermilyea, "Growth and Perfection of Crystals," edited by R. H. Doremus, B. W. Roberts and D. Turnbull, John Wiley and Sons, New York, N. Y., 1958, p. 393.

(31) F. C. Frank, ref. 30, p. 411.

(32) J. McNutt and R. F. Mehl, *Trans., A.S.M.*, **50**, 1006 (1958).

(33) H. Melville, *Trans. Faraday Soc.*, **32**, 1017 (1936).

(34) C. Herring, *Phys. Rev.*, **82**, 87 (1951).

cell, geometric corrections must be made to the observed rate of emission from a cell orifice.[35] If the orifice is sufficiently large that the vapor pressure within the cell is reduced below p_e, then the other contributions to α_j must be applied to the rate at the crystal–vapor interface within the cell. In practice, this effect can be eliminated by carrying out tests for various orifice sizes and extrapolating to zero orifice size to obtain the equilibrium rate of emission at a given temperature. More complex geometry effects have been discussed by Rossman and Yarwood[36] and Bradley.[37] The effect on α_j will, however, be as discussed previously.

VII. Thermal Accommodation and Temperature Effects.

In the foregoing treatments, the thermal accommodation coefficient γ introduced by Knudsen[38]

$$\gamma = (T_I - T_R)/(T_I - T_S) \qquad (28)$$

where T_I, T_R and T_S are the temperatures of the incident atoms, reflected atoms and substrate, respectively, has been ignored. Incomplete thermal accommodation would imply that a fraction $(1 - \alpha_{14})$ of the incident atoms did not come to equilibrium with the surface, but were reflected, i.e., did not adsorb and vibrate on the surface before re-evaporating. This circumstance would lead to an evaporation or condensation coefficient $\alpha_{14} < 1$. Before discussing this topic, it is noted that, if such an effect were present, the treatments and coefficients developed in Parts I through VII would all hold, but all the coefficients would simply be multiplied by α_{14}.

Elastic reflection of atoms, which would lead to $\gamma < 1$, $\alpha_{14} < 1$, would lead to specular reflections of atomic beams. Evidence of the cosine law of evaporation[39] and of the Maxwellian distribution of energy of evaporating atoms[40] indicate that the assumption of complete thermal accommodation is substantially correct. In condensation, however, it might be supposed that the highest energy atoms impinging on the surface are elastically reflected leading to $\alpha_{14} < 1$, $\gamma < 1$.

Consider the experiment illustrated by Fig. 4. If crystal A is the crystal under consideration and crystal B is a crystal with $\gamma = 1$, then, if $\gamma \neq 1$ for crystal A, a heat flux will be developed between reservoirs A and B which are at the same temperature. This would be a violation of the second law of thermodynamics. Hence, complete elastic reflection and non-thermal accommodation cannot occur under equilibrium conditions. The above treatment supposes that the vapor phase and crystal A are composed of the substance in question, while crystal B is an inert crystal that merely emits the same flux of A atoms that impinge upon it.

Under non-equilibrium conditions, an extension of the arguments of Langmuir[41] indicates that $\gamma < 1$,

(35) (a) P. Clausing, Z. Phys., **66**, 471 (1930); (b) C. I. Whitman, J. Chem. Phys., **20**, 161 (1952).
(36) M. G. Rossman and J. Yarwood, Brit. J. Appl Phys., **5**, 7 (1954).
(37) R. S. Bradley, Proc. Roy. Soc. (London), **205A**, 553 (1951).
(38) M. Knudsen, Ann. Phys., **34**, 593 (1911).
(39) M. Knudsen, ibid., **52**, 105 (1917).
(40) I. Estermann, O. C. Simpson and O. Stern, Phys. Rev., **71**, 238 (1947).
(41) I. Langmuir, ibid., **8**, 149 (1916).

$\alpha_{14} < 1$ only if the kinetic energy of the incident molecule is of the same order or larger than ΔF_{des}. For most materials, this would only occur for T_I of the order of a million degrees. Also, if ΔF_{des} was less than kT_S, it might be that $\gamma < 1$, $\alpha_{14} < 1$. Such a circumstance is possible only in the case treated in Part VI, i.e., when strong adsorption has occurred. In short, it is felt that $\gamma = \alpha_{14} = 1$ in all cases except possibly when strong impurity adsorption obtains.

An apparent temperature dependence could arise if second-order bond melting[6] occurred, roughening the surface under study, and causing α_j to approach the value of α_j for the liquid at the critical temperature for second-order bond melting. Also, an apparent temperature effect could arise; as discussed by Littlewood and Rideal,[42] if the surface temperature is assumed to be equal to the bulk temperature when actually a temperature gradient exists between the two.

IX. Other Effects.

Consideration has been directed to cases where only one polymeric form of the substance is present in the vapor phase. When several polymers are contributing about equally to the kinetics, the computation of the kinetics becomes so complicated due to interactions between the polymers at ledges, on the surface and in the vapor, that detailed consideration of the many alternatives that arise was not felt to be worthwhile. It is noted, however, that ledge dynamics should still be important.

Similarly, if a molecular species dissociates MX → M + X during evaporation, say in the adsorbed state, the kinetics would again be complex. The considerations in such kinetics will resemble those of surface reactions as treated by Eyring, et al.[43]

It is emphasized also, as noted in earlier sections, that heat flow has been assumed never to enter the kinetics. In extreme cases where heat flow might be important, thermal gradients would tend to decrease the apparent value of α_j.

Also, only one-component systems have been considered; i.e., only the possibility of adsorption has been admitted.

Discussion

The model of unit binding assumed in this work is an approximation, but until statistical mechanical or quantum mechanical calculations of the state of a crystal surface are refined, the present model is felt to be adequate. Many values of α_j for evaporation and fewer for condensation have been obtained as reported in recent reviews.[7,8,22] However, the recent results on evaporation under ideal conditions to yield the limiting law $\alpha_1 = 1/3$ for silver[44] and cesium iodide and cesium bromide,[45] both of which gave almost exactly the theoretically predicted value, provided the motivation to extend the theory as carried out above.

Briefly mentioning other experimental work:

(42) R. Littlewood and E. Rideal, Trans. Faraday Soc., **52**, 1598 (1956).
(43) S. Glasstone, K. J. Laidler and H. Eyring, "Theory of Rate Processes," McGraw-Hill Book Co., New York, N. Y., 1941, pp. 369–400.
(44) J. P. Hirth and G. M. Pound, Trans. AIME, **215**, 932 (1959).
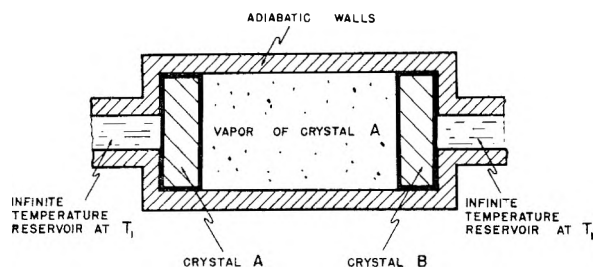(45) G. M. Rothberg, M. Eisenstadt and P. Kusch, J. Chem. Phys., **30**, 517 (1959).

Fig. 4.—Thought experiment on thermal accommodation coefficient.

Volmer and Schultze[46] give a result for condensation of iodine which fits equation 2 with the predicted value of $\alpha_2 = 1/3$, and which fits the form of Fig. 3; Wyllie[19] provides convincing evidence that $\delta = \alpha_3 = \alpha_4$; several authors[37,47,48] suppose configurational entropy contributions to evaporation which here correspond to equations 14 and 15; evaporation corresponding to equation 16 has been observed for arsenic oxide[26] and other materials; and finally Bradley and co-workers[49] obtain correlation with the spherical coördinate form of equations 17 and 19 for evaporation of liquid droplets, using the correction of Fuchs[50] for small droplets in the limit.

It seems important to carry out further Langmuir evaporation and condensation experiments in

(46) M. Volmer and W. Schultze, Z. physik. Chem., **156A**, 1 (1931).
(47) E. Rideal and P. M. Wiggins, Proc. Roy. Soc. (London), **210A**, 291 (1952).
(48) R. S. Bradley and P. Volans, ibid., **217A**, 508 (1953).
(49) R. S. Bradley, M. G. Evans and R. W. Whytlaw-Gray, ibid., **786A**, 368 (1946).
(50) N. Fuchs, Phys. Z. Sowjet. **6**, 225 (1934).

which crystal perfection, crystal size and crystallographic orientation are controlled, and in which resulting surface morphologies are specified. In particular, it is important to determine the spacings of monatomic ledges on evaporated or condensed crystals as functions of temperature and supersaturation, because differing variations of the spacings have been predicted.[6,7,9,10]

Summary.—1. Surface diffusion of adsorbed atoms is shown to limit both crystal growth from the vapor phase and evaporation at low supersaturations and undersaturations, leading to condensation or evaporation coefficients less than unity. 2. When other factors such as entropy restraints, surface contamination, diffusion in the vapor phase, or activation at the interface limit condensation or evaporation, surface diffusion also affects the kinetics. In such a case the condensation coefficient or evaporation coefficient will be less than unity, and will be a function of both surface diffusion and the other limiting factor. 3. Non-thermal accommodation of atoms impinging on a growing crystal and/or elastic reflection of such impinging atoms is shown to be unlikely except when marked impurity adsorption on the surface obtains. 4. Experimental evidence is cited that is consistent with the predicted crystal growth and evaporation kinetics. 5. It is extremely unlikely that any two of the three coefficients (the condensation coefficient, the evaporation coefficient and the accommodation coefficient) will be equal for a given material except when conditions are such that two of the coefficients are equal to unity.

HYDROTHERMAL REACTIONS BETWEEN CALCIUM HYDROXIDE AND MUSCOVITE AND FELDSPAR AT 120-220°

BY GUNNAR O. ASSARSSON

Chemical Laboratory, Geological Survey, Stockholm 50, Sweden

Received November 13, 1959

The autoclave reactions between calcium hydroxide and minerals containing alkali–alumina–silica at 120–200° are characterized by a formation of monocalcium silicate monohydrate (the tobermorite phase) and α-dicalcium silicate monohydrate, the reactions be ng similar in nature to those of the system calcium hydroxide–quartz. By a simultaneous combination of the alumina of the minerals is formed mainly cubic tricalcium aluminate hexahydrate, having 15–45% of its lattice hydroxyls replaced by silica radicals. The boundary between the monocalcium and dicalcium silicate ranges lies at about 100 mg. $CaO/m.^2$ mineral surface for the feldspar and at somewhat less than 30 mg. $CaO/m.^2$ for the muscovite. When a relatively rapid combination of calcium hydroxide–silica takes place at a silicate surface of disordered structure (ignited muscovite) the silica radical replaces hydroxyls in the cubic tricalcium aluminate hydrate in all degrees up to the percentage mentioned, as registered in the X-ray photographs as bands or sets of lines. At slow reactions at the mineral surface the aluminate phase consists almost exclusively of crystals containing a maximal silica replacement. Small amounts of a compound not positively identified but having a characteristic X-ray diffraction line at 10 Å. occur among the autoclave products of ignited muscovite and of feldspar. Its occurrence is established in the products autoclaved at 120–140° independent of the mineral and of the supply of calcium hydroxide. Some other phases not identified also occur. Because of the relatively complicated system the equilibrium conditions of the phases cannot be forecast; it must be supposed that the phases first formed are transformed successively into phases poorer in lime, as takes place in the system calcium hydroxide–quartz.

In a previous paper results were given from an investigation on hydrothermal reactions between calcium hydroxide and quartz.[1] Only ternary phases could be formed by these reactions. In

(1) G. O. Assarsson, THIS JOURNAL, **64**, 328 (1960).

those between two- or three-component silicates and calcium hydroxide other compounds will also appear. From results of experiments with silicate minerals containing only alumina, alkali and silica it should be possible to estimate the general

behavior of other minerals under similar conditions. A formation of quaternary compounds could be expected since ternary calcium silicates are produced, and some alumina remains; the alkali takes no essential part in the crystallization of the principal phases of the system.

The present paper is intended to give an account of the formation of calcium silicate hydrates and other compounds, when calcium hydroxide reacts under hydrothermal conditions with some common ternary silicates containing alumina (muscovite, feldspar). These reactions are of importance for the explanation of certain technical processes and procedures and for elucidation of the occurrence of some mineralogical paragenesis, and the investigation therefore covers the natural minerals as well as the dehydration products.

The Hydrothermal Reaction Calcium Hydroxide–Muscovite

The Muscovite Material.—Purest muscovite felsite from a large deposit at Boliden, Sweden, was used for the preparation of the mica powder. Impurities of corundum and sillimanite were removed. As is well known, the mineral is very difficult to grind to a fine powder in the agate mortar, but after repeated grinding and sieving it was possible to get a homogeneous powder.

The sample of muscovite was ground and homogenized in sufficient quantity to provide a uniform sample for all experiments. The composition given in Table I corresponds well to the theoretical composition. Samples were heated during 24 hr. to the required temperatures, and sufficient was taken for all experiments. After the heating, lumps occurring in the material were crumbled by a slight pressing, so that the grain surface area was not modified.

Table I

CHEMICAL COMPOSITION OF THE MINERAL POWDERS; % WEIGHT

Composition, calcd. from the analyses; Muscovite: $(OH. F)_{4.16}$ $(KNa)_2 \cdot [(SiTi)_{6.00} Al_{2.00}] \cdot (Al, Fe)_{4.00} O_{20}$. Feldspar: microline 78%, albite 22%.

	Feldspar, microcline	Mica, muscovite
SiO$_2$	64.9	45.6
Al$_2$O$_3$	19.2	37.7
Fe$_2$O$_3$	0.2	0.3
FeO	. . .	. . .
CaO	0.06	0.1
MgO	0.05	0.1
K$_2$O	12.9	9.2
Na$_2$O	2.4	2.2
H$_2$O	. . .	4.5
TiO$_2$	0.02	0.1

The X-ray photographs of the untreated mineral showed all the same diffraction lines reported by other investigators (Grim, Bray and Bradley[2]).

When the present muscovite sample was heated for periods of 24 hr. to 500, 900, 1,000, 1,050,

(2) R. C. Mackensie and A. A. Milne, Mineral Mag., 30, 178 (1953); N. Sundius and A. M. Bystrom, Trans. Brit. Ceram. Soc., 52, 653 (1953); R. E. Grim and W. F. Bradley, J. Amer. Ceram. Soc., 23, 248 (1943); R. Roy, ibid., 32, 202 (1949); R. E. Grim, R. H. Bray and W. F. Bradley, Amer. Mineral, 22, 813 (1937); R. E. Grim and W. F. Bradley, ibid., 33, 50 (1948).

1,150 and 1,200°, the principal change in structure took place between 1,000 and 1,050°. This 24 hr. period was sufficient to guarantee a complete transformation of the mineral grains into aggregates corresponding to a plausible equilibrium at the relevant temperatures without residual structures. The X-ray measurements of preparations heated to 1,000°, showed a small extension of the distance between the atoms. At temperatures of 1,050° and higher, new phases crystallized. They were identified as mullite and α- and β-corundum. The essential part of the heated products was an optically isotropic mass, consisting of an alkali–alumina-glass. Because of the composition of the mineral, accessory compounds (spinel and others) were not formed. The present muscovite sample can be considered to have the transition temperature between 1,000 and 1,050°, which is a little higher than that found for other samples (Roy[2]).

Heated samples of the muscovite were also autoclaved at 160 and 200° for 24 hr. The X-ray photographs of these preparations showed the same spacings as the preparations not autoclaved. This autoclave treatment, solely, therefore, does not cause a formation of new phases in amounts discernible in the X-ray photographs.

The Surface Area per g. of the Muscovite Powder

The manner in which the mineral muscovite changes its properties on heating is known from earlier investigations.[2] The results will be summarized in the following.

When heated up to about 900° the muscovite crystal loses its water while retaining its outer habitus as well as the general pattern of the remaining atoms. The change in properties is, however, connected principally with small displacements in the positions of the atoms without a formation of new phases (Grim and Bradley[2]). Above about 980° (Roy[2]) some new phases are formed, slowly at low temperature, more rapidly at higher temperatures and after continued heating. The phases that have been reported in the heated product are mullite, some types of alumina, cristobalite, leucite, and in addition a glass formed by silica, alkali and alumina.

To this short description may be added that the thermal dehydration process as well as the formation of the new phases is to some degree connected with some properties of the sample used: the rate of heating up and the period of heating time in relation to the size of the grains of the mineral, the chemical composition, and the earlier treatment of the sample (heating, repeated grinding).

The report given below on the behavior of the muscovite sample is limited to results of interest for the hydrothermal reactions.

There are questions of importance for the hydrothermal reactions that must be studied before the main problem can be treated: the change in the grain surface area per g. of the mineral brought about by dehydration and autoclave treatment and the change in mineralogical property.

The heating of the muscovite powder is accompanied by an essential change in grain surface.

It could be expected that removal of the lattice hydroxyls followed by an autoclaving should cause a splitting up of the layer structure and in this way increase the grain surface area considerably. The grain surface areas of the samples determined by the BET-method are listed in Table II.

TABLE II

MUSCOVITE GRAIN SURFACE AREA m.^{2}/g. MINERAL POWDER, AUTOCLAVED AND NOT AUTOCLAVED, DETERMINED ACCORDING TO THE BET METHOD

Phase symbols: M = muscovite; Mr = muscovite, ign. below 1000°; CO new phase (corundum, mullite, glass)

Ign. temp. 24 hr., °C.	Not autocl., m.^{2}/g.	Autocl. 200°, m.^{2}/g.	Phase
Not ign.	7.90	12.0	M
500	5.15	9.35	Mr
1000	3.55	4.30	Mr
1050	4.50	4.30	(Mr) CO
1100	4.00	4.50	CO
1150	3.65	3.90	CO
1200	2.90	3.90	CO

These measurements on the heated samples show a diminishing of the area when the mineral powder is heated to about 1,000°. After a small increase at 1,050° the area decreases when the ignition temperature rises to 1,200° or more. This course of change is in agreement with the dehydration and recrystallization of the muscovite established with X-ray measurements and with the microscope. On the other hand, the dehydration causes an extension of the cell dimensions; the effect of this should be a small increase of the area. A splitting up of the layer structure of the muscovite accompanied by an increase of the grain surface area, may in fact occur. Other reactions of an opposite character however, predominate. The muscovite ignited up to 1,000° and then autoclaved showed an increase of grain surface caused by the autoclave treatment but no change in structure. The most probable explanation of these facts might be sought in a building up of the crystals. If the crystals are formed by crystallites of dimensions just below the microscopical ones, the phenomena in question have a clear explanation. For the problems of this report, however, the results of importance are that the structure of the crystallite remains intact in spite of autoclave treatments and that the grain surface area increases to a certain degree because of these treatments, the former referring to the structure, the latter to the texture.

The Formation of the Ca-compounds

Because the properties of the muscovite samples vary according to the treatment, with subsequently far-reaching variations in the experimental conditions, the autoclave experiments were limited to three preparations, the unheated mineral and the mineral heated to 1,050 and 1,150°. The first sample represents the substance of the original structure, the second one corresponds to the very labile structure before final recrystallization, and the third one the recrystallized, glass-containing structure, the two samples last mentioned having about the same grain surface area. The calcium

hydroxide mg./m.^{2} of the mixtures used for the autoclave experiments is listed in Table III; it is referred to the grain surface area of the autoclaved samples (Table II). The rate of the combination of lime could not be studied in detail, some general observations only were made.

Compounds Formed.—The calcium silicate hydrates belonging to the system have been mentioned in earlier papers.[1] The quaternary synthetic compounds containing lime, silica, alumina and water have been studied by some authors. Hitherto known are the synthetic compounds: gehlenite hydrate, hydrogarnet, and the compound $4CaO \cdot Al_2O_3 \cdot SiO_2 \cdot 12H_2O$, some minerals: gismondite, lawsonite and scolesite, and some other compounds of zeolitic type.[3]

TABLE III

Muscovite, not ignited (M), ignited at 1050° (M_{1050}) and at 1150° (M_{1150}) mixed with calcium hydroxide, autoclaved for 4–24 hr. Symbols for the phases: Hy = hydrogarnet; T = tobermorite; Y = unknown 10-Å compound; 2A = α-dicalcium silicate monohydrate

Autoclave temp., °C.	M CaO, mg./m.^{2}	M Phase formed	M_{1050}, M_{1150} CaO, mg./m.^{2}	M_{1050}, M_{1150} Phase formed
120–140	21–44	Hy, 2A, T	56	T, Hy, 2A, Y
160–200	21–82	T, Hy, 2A	56–110	T, Hy, 2A

The investigation of the autoclave products under the microscope gave very little information concerning the compounds formed by the autoclave reactions. The crystallites were too small to permit an exact determination of the crystallographic properties. Some lumps formed were optically isotropic, some of them showed a general birefringence with a general optical refraction of about 1.6.

The principal examination of the substances was limited to X-ray investigations. The mineral muscovite gives X-ray photographs rather rich in diffraction lines. Certain important parts of the photographs, however, are free from such lines and permit an establishment of the presence of compounds formed. The first three diffraction lines of muscovite are at 10, 4.98 and 4.47 Å.; most of the identification lines of the compounds possibly formed at the reaction are to be found at Bragg-angles corresponding to d-values higher than 2.0 Å. On the other hand, the muscovite samples heated to 1,050 and 1,150° give photographs rather poor in diffraction lines; above all, the 10 Å. line of the untreated muscovite does not occur in these preparations.

Sub-X-ray crystallites are formed within the first two hours of autoclaving. They slowly grow to products easily identified (Table III). After the complete combination of lime the reaction products formed are very similar to one another; products somewhat deviating are mentioned below. Autoclaved mixtures rich in lime show generally

(3) E. P. Flint and L. S. Wells, *Bur. Standard J. Research*, **27**, 171 (1941); **33**, 471 (1944); L. S. Wells, W. F. Clarke and H. F. McMurdie, *ibid.*, **30**, 30 (1943); H. zur Strassen, *Zement-Kalk-Gips*, **11**, 137 (1943); F. H. Dorr, Unters. im System CaO-Al₂O₃-SiO₂-H₂O, Diss., Mainz 1956; H. Zeeh, Unters. im eisenfreien System CaO-Al₂O₃-SiO₂-CaSO₄-H₂O, Diss., Mainz, 1956; E. Thilo, H. Funk and E. M. Wichmann, Abh. d. Deutschen Akad. zu Berlin, Jahrg. 1950, Nr. 4.

more distinctly crystallized compounds than those poor in lime, although the composition of the phases is the same.

The tobermorite compound is considered to be present in the reaction products when the diffraction line 11.3 Å. can be established. The compound occurs in almost all of the preparations. At low temperature (120–140°), however, the natural muscovite reacts rather slowly so that the tobermorite phase could be shown only after a rather extended reaction period. The compound occurs rather well crystallized among the products of ignited muscovite (1,050, 1,150°) treated in the same way. At an autoclave temperature of 160° natural muscovite mixed in the same proportion also showed an initial crystallization of the tobermorite phase after only 2 hr. In the other autoclave products the diffraction lines of the tobermorite 11.3 Å. as well as others can be easily established.

The Hydrogarnet.—As mentioned above the alumina released by the attack of the calcium hydroxide on the silicate must be combined in some way. It is known from earlier investigation on the system $CaO–Al_2O_3–H_2O$ that the cubic tricalcium aluminate hexahydrate is the stable phase at higher temperatures.[4] This compound does not occur pure in the mixtures of the present investigation but as a solid solution with some molecules of water in the crystal structure replaced by silica (hydrogarnet $3CaO \cdot Al_2O_3 \cdot 3SiO_2/6H_2O$). The law of Vegard is here assumed to be valid for the crystals, namely, that there exists a linear correlation between the unit-cell dimensions and the chemical composition (garnet $3CaO \cdot Al_2O_3 \cdot 3$-$SiO_2$, $a = 11.86$ Å.; calcium aluminate $3CaO \cdot Al_2O_3 \cdot 6H_2O$, $a = 12.56$ Å.). This relation is an approximation. The calculations and considerations below, however, are based on the above assumption. At low temperatures (120, 140°) the unignited muscovite reacts with lime to yield the cubic compound giving diffraction lines that are very distinct. The position of the lines shows an aluminate in which the lattice hydroxyls are replaced to 40–50% by silica. No difference between the preparations at 120 and 140° was found. Muscovite ignited at 1,050°, mixed with lime and autoclaved at 120–140° yields products that show groups of successions of distinct diffraction lines. The range of these groups represents a composition of about 15 and 50% of the hydroxyls replaced by silica in the pattern. The preparations autoclaved at 160–200° show bands in the photographs instead of lines, commonly with diffuse edges, the bands obviously originating from lines of the same character as above. The measurements of those bands show a constant of 15–50% silica. In no case are bands observed corresponding to a higher content of silica.

α-Dicalcium silicate monohydrate was found in most of the preparations. At low temperature (120–140)° and with muscovite of undisturbed structure this compound was formed slowly. All the X-ray photographs of the preparations of dis-

turbed crystal structure mixed with lime and autoclaved at 120–200° and also the undisturbed muscovite crystals autoclaved at 160–200° show the characteristic spacing of the silicate mentioned. The lines are distinct without any broadening.

Other Compounds.—There occur in the X-ray photographs some diffraction lines that do not belong to the compounds mentioned above. One of them (10 Å.) appearing in the photographs of some preparations is noticeable because it seems to be a characteristic line for the present system; it occurs also in the system feldspar–calcium hydroxide. Spacings not identified are given in Table IV. The 10 Å. line is shown only in the photographs of mixtures autoclaved at 120–140° and prepared from muscovite ignited at 1,050 and 1,150°. The photographs of the unignited muscovite contain primarily a muscovite spacing of 10 Å. which makes it impossible to establish the occurrence of the compound in question. The spacing 10 Å. has not been shown in the system calcium hydroxide–amorphous silica nor in that of calcium hydroxide–quartz within the temperature range of the present experiments. It is therefore plausible that the presence of the special com-

TABLE IV

DIFFRACTION LINES, NOT IDENTIFIED IN MIXTURES MUSCOVITE (UNIGN., IGN. 1050°, 1150°)–CALCIUM HYDROXIDE, 21–120 mg. $CaO/cm.^2$, 120–200°

I	d (Å.)	I	d (Å.)
	—120–140°—		—180–200°—
w	10.0	w	4.83
w	4.19	m	4.51
ww	4.09	w	4.01
m	3.98	m	3.79
w	3.59	w	3.70
		w	3.47
		w	3.17
		w	2.93

ponents of the system, containing the component alumina are responsible for its appearance. It is probable that the phase represented by the 10 Å. line is one of the zeolites mentioned above. As the concentration of calcium ions at the surface of the mineral is rather high the conclusion may be drawn that the zeolite consists of lime, alumina and silica. A calculation of the spacings of the zeolites mentioned leads to the result that the mineral gismondite is the most plausible.

In the photographs from preparations autoclaved at 180–200° other unidentified spacings occur. Generally all these spacings show rather weak intensities probably representing relatively low content of the corresponding compounds. It may also be noted that the thorough examination of X-ray photographs provided no evidence for the occurrence of aluminum hydroxide (hydrargillite, diaspore) or other calcium aluminate hydrates among the reaction products.

The Hydrothermal Reaction
Calcium Hydroxide–Feldspar

The Feldspar Material.—A selected piece of microcline was ground in the manner described earlier for quartz.[1] The powder was not washed but purified with a magnet and with a blast of air

(4) G. Assarsson, *Z. anorg. allgem. Chem.*, **214**, 158 (1933); J. D'Ans and H. Eick, *Zement-Kalk-Gips*, **6**, 197 (1953).

TABLE V

MIXTURES FELDSPAR–CALCIUM HYDROXIDE, AUTOCLAVED AT DIFFERENT TEMPERATURES

Symbols for the crystallized phases, see Table III; CaO calc. mg./m.² mineral surface area

Auto-clave temp., °C.	75 mg. CaO Time, hr.	75 mg. CaO CaO comb., mg./m.²	75 mg. CaO Phase	165 mg. CaO Time, hr.	165 mg. CaO CaO comb., mg./m.²	165 mg. CaO Phase	220 mg. CaO Time, hr.	220 mg. CaO CaO comb., mg./m.²	220 mg. CaO Phase	330 mg. CaO Time, hr.	330 mg. CaO CaO comb., mg./m.²	330 mg. CaO Phase
120	170	75	Y	170	130	Y (Hy)	..	..	...	170	150	Y, Hy
	500	75	Y, T, Hy	500	165	Y, T, Hy, 2A	..	..	...	500	330	Y, Hy, (2A)
140	24	75	Y	24	165	Y, T, Hy, (2A)	..	..	...	24	160	Hy, (2A)
	170	75	Y, T, Hy	170	165	Y, T, Hy, 2A	..	..	...	170	330	Y, T, Hy, (2A)
160	8	75		4	95		4	135		..	..	...
	24	75	Hy	24	165	Hy, 2A	24	190	Hy, 2A	24	210	Hy, 2A
180	2	50		6	140		6	155		..	..	...
	6	70	(T, Hy)	9	165	(T, Hy)	8	220	(Hy, 2A)	24	330	(Hy, 2A)
	24	75	T, Hy	24	165	T, Hy, 2A	24	220	T, Hy, 2A	48	330	T, Hy, 2A
200	2	50		2	145		2	195		24	330	(Hy, 2A)
	4	75	(T, Hy)	4	165	(T, Hy)	4	220	(Hy, 2A)	48	330	T, Hy, 2A
	24	75	T, Hy	24	165	T, Hy, 2A	24	220	T, Hy, 2A	72	330	T, Hy

+310 mg CaO per sq. m.
×155 " " "
•65 " " "

160°

180°

200°

Extracted Alkali, mg per sq. m.
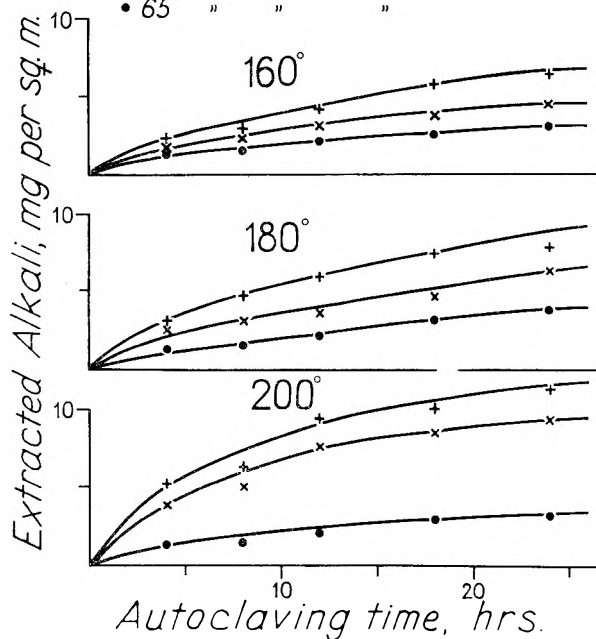
Autoclaving time, hrs.

Fig. 1.—The extraction of the feldspar alkali in the course of the autoclave treatment of mixtures feldspar–calcium hydroxide.

and finally ground to a powder of the required grain size. The composition of the feldspar is given in Table I. The grain surface area was 1.5 m.²/g. measured by the BET-method.

The Combination of Lime.—Of special interest is the course of the boundary reaction in which the lime is combined, in relation to the autoclaving temperature and time. Some experiments were performed in order to determine in an indirect way the attack of the calcium hydroxide on the feldspar. As the calcium hydroxide dissolves silica and alumina from the feldspar, a corresponding amount of alkali will be set free. By this reaction the successively proceeding destruction of the feldspar could be studied. However, as a consequence of the heterogeneous character of the reaction mixtures the results have only a rather low degree of accuracy. Results of this kind con-

cerning the autoclaving of three mixtures between 160 and 200° are given as a diagram in Fig. 1. The experiments show that the total amount of alkali that it is possible to extract during the autoclave treatment is not reached after 24 hr., although the whole amount of calcium hydroxide is consumed after this period of time (cf. Table V, corresponding experiments). The progress of the attack on the feldspar does not only depend upon the supply of uncombined lime but also upon the compounds which are formed, obviously in more than one stage.

The Phases Formed.—The microscopical examination of the samples is made very difficult by the small size of the aggregates formed. The feldspar powder itself was autoclaved at 160 and 220° for 72 hr.; no new compound could be established. The low-temperature treatment (120–160°) of mixtures feldspar–calcium hydroxide (165–330 mg. CaO/m.²) for a period of 48 hr. yielded only some spherolites without any birefringence. Specimens autoclaved at 220° for 72 hr. showed the same reaction products; some of the spherolites, however, indicated a low-moderate birefringence, some were obviously optically isotropic; most of them seem to have an optical mean index of about 1.6.

The X-ray photographs of feldspars, in the present case a perthitized microcline, contain a very large number of diffraction lines that can be measured only when a camera of very good dispersion is used. Coincidences of the feldspar can therefore be possible.

The products formed by the autoclave treatment at lower temperatures (120–140°) are very poorly crystallized. During the first period of reaction compounds are formed which show no crystallinity, although all or the greater part of the calcium hydroxide is consumed (Table V). After more extended periods of time a crystallinity of the phases appears gradually.

The tobermorite compound is formed, even at low temperatures (120–140°), as is clear by the diffraction line 11.3 Å. gradually appearing in the X-ray photographs; at higher temperatures the intensity of this line increases.

The spacings of the hydrogarnet deriving from

the autoclaved feldspar–lime mixtures have a different character from those from the muscovite–lime mixtures. At low temperatures (120°, 140°) only one set of lines occurs in the X-ray photographs, corresponding to a silica content of 40–50%. At higher temperatures and with mixtures rich in lime there appear in the X-ray photographs some other distinct lines belonging to the hydrogarnet, corresponding to about 20–30% silica; because of coincidence with other lines it is impossible to estimate the boundary of the lowest silica content. The bands observed in the photographs of the muscovite–lime mixtures do not occur.

The different lines of α-dicalcium silicate monohydrate are clearly absent from the X-ray photographs of mixtures poor in lime (75 mg. CaO/m.^{2}) autoclaved at 120–200°. In photographs of mixtures richer in lime (165–330 mg. CaO/m.^{2}) autoclaved at these temperatures, on the other hand, lines belonging to the compound do occur.

In the X-ray photographs autoclaved at 120–200° some lines also occur that have not been identified. The line at 10 Å. is discovered in these mixtures but not in those autoclaved at 160–200°. The use of this line for identification purposes is discussed above in connection with the muscovite and the same considerations are valid. Other unidentified lines of weak intensity occur in the photographs (Table VI).
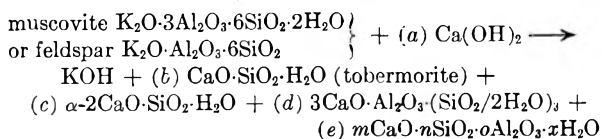
TABLE VI

DIFFRACTION LINES, NOT IDENTIFIED, IN MIXTURES FELDSPAR–CALCIUM HYDROXIDE, 75–220 mg. CaO/m.^{2}, 120–200°

I	120–140° d (Å.)	I	180–200° d (Å.)
w	10.0	m	5.58
m	6.76	w	5.16
ww	5.06	w	5.12
m	4.98	w	4.98
ww	4.75	w	4.43
w	4.12	w	4.26
w	3.49	w	3.71
m	3.34	m	3.68
m	3.03	m	2.95
m	2.74	w	2.92
		m	2.73

Discussion of Results

The above results show that different kinds of overlapping reactions take place between the alkali–alumina–silicates muscovite and feldspar and the calcium hydroxide. The essential characteristic of these reactions, however, is independent of the mineral. The conditions at the surface of the silicates can be rendered in the following way

muscovite $K_2O \cdot 3Al_2O_3 \cdot 6SiO_2 \cdot 2H_2O$
or feldspar $K_2O \cdot Al_2O_3 \cdot 6SiO_2$ $\}$ + (a) Ca(OH)$_2$ $\longrightarrow$

KOH + (b) CaO·SiO$_2$·H$_2$O (tobermorite) +
(c) α-2CaO·SiO$_2$·H$_2$O + (d) 3CaO·Al$_2$O$_3$·(SiO$_2$/2H$_2$O)$_x$ +
(e) mCaO·nSiO$_2$·oAl$_2$O$_3$·xH$_2$O

The first three silicate–aluminate members on the right part of the formula (b, c, d) are known and can generally be identified with X-ray photographs. They are the principal compounds. When the calcium hydroxide attacks the surface of the silicate the conditions for the formation of the com-

pounds depend essentially on the state of the surface of the alumina–silicate and on the proportion alumina–silica. The fourth member (e) therefore represents compounds produced when the conditions for the attack are such that the compounds of transition type or compounds corresponding to the special supply of components can be formed.

During these reactions the tobermorite phase always seems to be formed sooner or later, probably because of its being one of the more stable compounds of the system. In those cases where it is not shown, the α-dicalcium silicate is formed as a first product and later transformed by extended autoclave treatment into the tobermorite compound. The formation of the tobermorite phase is to be referred to the rate of the dissolving attack on the surface of the silicate in relation to the rate of the diffusion of calcium hydroxide through the layer at the phase boundary silicate–solution. The formation of different products has always to be referred to the periods of reaction time and to the varying amount of calcium hydroxide at the surface of the silicates present. The character of the mineral determines the type of calcium silicate. With feldspar the monocalcium silicate was observed to be an initial product when the supply of lime corresponds to 75 mg./m.^{2} mineral surface; when the concentration is 165 mg./m.^{2} the dicalcium silicate is formed. With different samples of muscovite a concentration of 33 mg CaO/m.^{2} of the mineral surface was shown to be above the lower concentration boundary for the formation of the dicalcium silicate. The boundary concentration for the formation of monocalcium–dicalcium silicates could be approximately at 100 mg. for the feldspar and 20 mg./m.^{2} for the muscovite preparation.

When calcium hydroxide attacks the surface of the silicates the alumina of the compound is very active and reacts with uncombined calcium hydroxide immediately. Being a stable phase in pure calcium hydroxide solutions at the autoclave temperatures of the present experiments, the cubic tricalcium aluminate hexahydrate is formed, its composition to a certain degree depending on the character of the surface of the silicate. It is evident from the experiments with feldspar as well as natural muscovite that at a mild attack on the surface of the minerals (low temperature, relatively undisturbed crystal structure) the cubic aluminate formed contains constant proportion silica in the pattern. Assuming 45% of the hydrogen ions to be replaced by Si ions the cubic aluminate corresponds to the formula 3CaO·Al$_2$O$_3$·1.3SiO$_2$·3.4H$_2$O. This content of silica seems to be the highest silica proportion of the system within the present experimental conditions, requiring for its formation one atom Al for 0.6 atom Si depending only slightly on the autoclave temperature within the range 120–200°. The feldspar contains one atom Al for three atoms Si, the muscovite one atom Al for one Si. The supply of alumina in relation to that of silica is therefore larger at the phase boundary of muscovite–solution than that of feldspar–solution. If the reaction runs its course slowly the

45%-silica containing cubic tricalcium aluminate will crystallize. The excess of silica will be combined as calcium silicate hydrates as the tobermorite phase or as mixtures of the dicalcium silicate and this phase. A more intensive attack of the calcium hydroxide effected either by increased temperature or by a disordered pattern of the surface of the mineral, causes a more rapid formation of the calcium aluminate. The muscovite therefore yields an aluminate, crystallizing with successively less silica as the reaction proceeds; the hydrogarnet is recorded in the X-ray photographs as bands. The more resistant pattern of feldspar contains more silica so that the formation of the hydrogarnet is retarded and the aluminate compound reaches a composition with more silica. The rate of formation of the Ca-silicate hydrates obviously regulates the successive change in composition of the solid solution.

The compound represented in the X-ray photographs by the 10 Å. line shows in the present investigation an upper existence limit between 140° and 160°. Similar considerations must be applied to the compounds shown in the preparations autoclaved at 180–200°. There also seems to be a difference between the unidentified phases of the muscovite and the feldspar preparations; the properties of the phases could probably account for the relationship.

The conditions of equilibrium between the phases of the system are difficult to establish, as some of them are not sufficiently known. Generally it can be anticipated that the compounds at the boundary silicate–calcium hydroxide solution will be transformed into those with the lowest content of calcium attainable within the system under the given experimental conditions. Several types of calcium compounds can result from the attack at the silicate surface, and these will later be transformed into others by further extraction of the components of the silicate. One may also be reminded of the varying composition of some compounds. The amount of alkali released by the attack at the mineral surface results in an increase of pH of the solutions, thus causing a change in the equilibrium conditions. The compounds can therefore not be predicted from knowledge of the reactions of the ternary systems lime–quartz–water and lime–alumina–water.

ACIDITY MEASUREMENTS WITH THE GLASS ELECTRODE IN H_2O–D_2O MIXTURES

By Kirsten Mikkelsen and Sigurd Olaf Nielsen*

Carlsberg Laboratory, Copenhagen, Denmark

Determinations at 22° of the thermodynamic dissociation constant of acetic acid in ordinary water and in deuterium-enriched water (98.0 volume % D_2O) demonstrate that an ordinary Radiometer glass electrode type G 202A under convenient experimental conditions exhibits the theoretical response to variations in the hydrogen-ion concentration in both solvents in the range between 2×10^{-2} and 2×10^{-5} M. The acidity determinations involve standardization and storage of the glass electrode in solutions in H_2O and subsequent drying of the glass electrode with mercury before immersing it in the 0.5-ml. deuterium enriched samples. From the electromotive forces observed with a saturated KCl–H_2O calomel electrode at 22° the relation between true $p(DH)$ and apparent pH in 98% D_2O is derived. $p(DH)$ = apparent $pH + 0.44$. A possibility of determining the activities, a_H and a_D, separately is considered from the point of view of extrapolating rate data obtained in H_2O–D_2O mixtures to pure D_2O.

Introduction

As the data in the literature appeared conflicting and not sufficiently accurate to serve as basis for precise acidity measurements with a calomel-glass electrode couple in mixtures of H_2O and D_2O, it was decided to reinvestigate the behavior of this electrode couple in H_2O and in water containing 98.0 volume % D_2O, i.e., 0.980 volume of D_2O per volume of water. For this purpose two calomel electrodes were used, one "light" made up with H_2O saturated with KCl and the other "heavy" made up with 98 volume % D_2O water saturated with KCl. Previously Hart[1] studied the relation

of true to apparent pH of solutions in D_2O as measured with a calomel–glass electrode couple and found the correction for DCl solutions in D_2O to be $+0.4$ pH unit. This result deviates from that of an earlier investigation[2] in which the same correction was given as $+0.26$ pH unit. Lumry, et al.,[3] gave the difference between true pD and glass electrode apparent pH as $+0.4$ pH unit in 99.8% D_2O. That the glass electrode at least under certain experimental conditions exhibits the theoretical response to variations in hydrogen ion concentration is also apparent from a number of investigations, e.g.,[4] not specifically concerned with

* Danish Atomic Energy Commission, Research Establishment, Chemistry Dept., Risø, Denmark.

(1) R. G. Hart, Nat. Research Council Canada Report CRE-423, June (1949); C. A., 46, 2887 (1952).

(2) R. B. Fischer and R. A. Potter (MDDC-715) ADD (7), 1, 458 (1947); C. A., 46, 2887 (1952).

(3) R. Lumry, E. L. Smith and R. R. Glantz, J. Am. Chem. Soc., 73, 4330 (1951).

the behavior of the glass electrode in D_2O.

Experimental

Crystalline $KH(OOCCH_3)_2$.—A mixture of 20.0 g. (0.20 mole) of analytical grade potassium acetate and 9.5 ml. of glacial acetic acid was heated to 155° and stirred until homogeneous. The mixture solidified on cooling to room temperature. Crystallization from 100 ml. of 96% ethanol yielded a crop of white needles which were recrystallized twice from 96% ethanol and once from ethanol–ethyl acetate (2:1). The crystals were washed twice with ether and vacuum-dried over silica gel at room temperature; yield 10 g. of white needles; uncorrected m.p. in closed tube 148.0–148.5°; reported[5] m.p. 148.0°. Calcd. from C_4H_7-O_4K: mol. wt., 158.2. Found: mol. wt., 159.6 by titration with 0.100 N NaOH to phenolphthalein end-point.

Water.—Deuterium oxide, D_2O, (99.78 g. D_2O per 100 g. water, d^{20}_4 1.10514) was purchased from Norsk Hydro, Norway, and used without further purification. Protium oxide, H_2O, was ordinary distilled water as obtained from a tin-coated copper distillation apparatus in this Laboratory. It was used without further purification.

Other Reagents.—Potassium chloride was Merck analytical grade dried at 110°. 1.000 N hydrochloric acid was obtained from the laboratory stock solution standardized against sodium oxalate according to Sørensen.

Electrode Assembly.—The galvanic cell had the form

$$Hg(l); \ Hg_2Cl_2(s), \ KCl(satd. \ in \ H_2O \ or \ H_2O-D_2O) \ |Soln.$$
$$X \ \| Glass \quad (I)$$

The glass electrode used (type G202A) was manufactured from Corning 015 glass and purchased from the Radiometer Company, Copenhagen. Before use the dry electrode was soaked in protium oxide. The calomel electrode was a Radiometer electrode type K 100 in which the ordinary tip had been replaced by a piece of 0.25 mm. capillary tubing. For measurements in aqueous solutions of ordinary isotopic content the whole calomel cell was filled with a saturated solution of KCl in H_2O whereas it was filled with a saturated solution of KCl in water containing 98 volume % D_2O for measurements in the deuterium-enriched samples, containing 98.0 volume % D_2O. Details of the mounting of the electrodes are shown in Fig. 1. The cell is very similar to one used previously by MacInnes and Dole.[6] The sample compartment consisted of a piece of shielded glass tubing C fitted tightly to the tip of the calomel electrode A by means of a polythene gasket D and a Teflon plug E, and partly immersed in a shielded paraffin oil-bath which in turn was immersed in a water thermostat operated at 22.2 ± 0.1°. The glass electrode B was cathetometer mounted. To facilitate cleaning of the sample compartment the interior of the glass tube was siliconized. As little as 0.40-ml. sample (see Fig. 1) would cover completely the bulb of the glass electrode.

Electrical Circuit.—The electromotive force (e.m.f.) of the calomel–glass electrode couple (right side minus left side of cell I) was measured with a 1.5 Volt Otto Wolff compensation bridge with five decades in combination with a selected Radiometer pH meter model PHM 22 serving as a high resistance galvanometer to determine when the bridge was balanced. The sensitivity of the pH meter was increased by connecting a microamp. meter to the recorder terminals of the pH meter. Its noise level and zero stability was then estimated to be better than 0.1 mv. with a 1000 Megohm resistance in the input. Also readings of the bridge during actual pH determinations could usually be made to within 0.1 mv. (<0.002 pH unit). A Weston normal cell served as voltage reference.

Procedure.—All measurements were performed in a low humidity room thermostated to 22°. The sample compartment was rinsed by washing it three times with H_2O. Remaining droplets were removed with filter paper. The capillary at the tip of the calomel electrode was flushed with a little of the saturated KCl solution from the interior of the electrode and the expelled solution removed with filter paper. Immediately thereafter the 0.500-ml. sample was
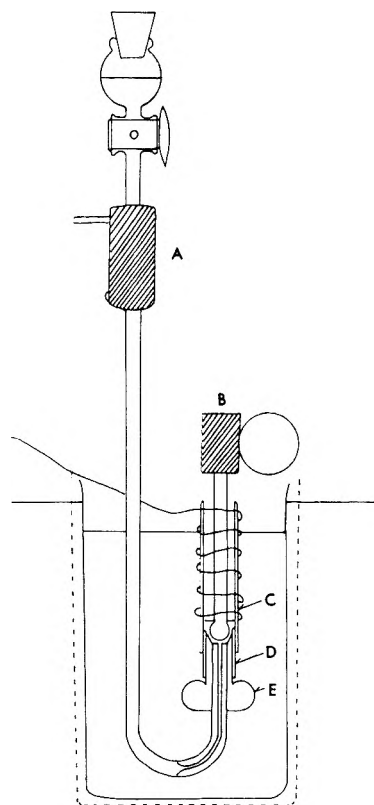
(4) D. Hubbard and G. W. Cleek, *J. Research Natl. Bur. Standards*, **49**, 267 (1952).

(5) A. W. Davidson and W. H. McAllister, *J. Am. Chem. Soc.*, **52**, 507 (1930).

(6) D. A. MacInnes and M. Dole, *J. Gen. Physiol.*, **12**, 805 (1929).

Fig. 1.—Calomel–glass electrode assembly: A, calomel electrode; B, glass electrode; C, glass tubing; D, polythene gasket; E, Teflon plug.

placed in the sample compartment and the liquid junction was allowed to develop for 3 minutes before the glass electrode was dipped into the sample. When not in use the glass electrode was kept in a 0.02 M solution of KCl in H_2O at 22.2°. For measurements in the deuterium-enriched samples the glass electrode therefore had to be dried, and it was treated before *all* measurements in the following way. The bulb was slowly dipped three times into double distilled mercury thermostated to 22.2°, whereupon the drops of aqueous solution that collected on the mercury surface each time were removed with filter paper. In order to secure proper temperature equilibration of the glass electrode it was subsequently immersed for two minutes in the mercury and immediately thereafter transferred to the waiting sample. Within the following two minutes, two readings of the balanced bridge were taken with an interval of one minute. The second reading served only as a control, experiments with pronounced drift in which the second reading deviated more than 0.2 mv. from the first being discarded. From one run to the next the asymmetry potential of the glass electrode varied considerably (Fig. 2), due to the special treatment the electrode received prior to each run. It was therefore necessary to correct each measurement of the e.m.f. of cell I (E_x) for electrode drift. This was done in the following way. Immediately before and after a measurement of E_x the sample compartment was filled with a 0.05 M $KH(OOCCH_3)_2$ + 0.1 M KCl reference solution in H_2O and the two respective electromotive forces E_{r1} and E_{r2} measured. Their average $^1/_2(E_{r1} + E_{r2})$ was subtracted from E_x to give a corrected measure

$$E = E_x - \frac{1}{2}(E_{r1} + E_{r2}) \quad (II)$$

of the acidity of solution X relative to that of the reference solution.

Results

Asymmetry Potential of the Glass Electrode.— Figure 2 shows E_r as a function of run number taken from the two experimental series reported in
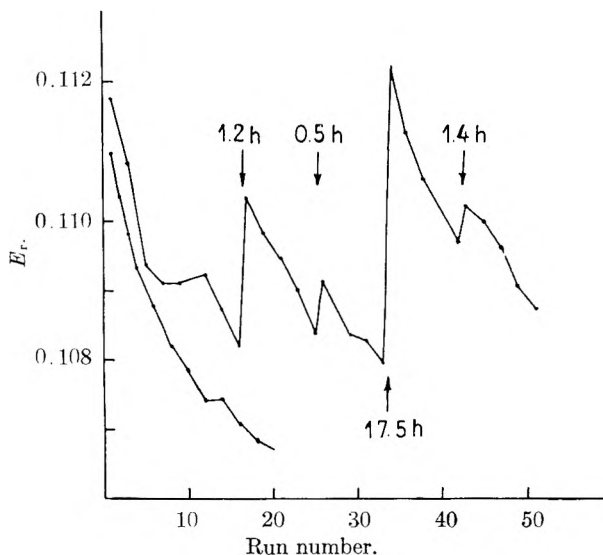
Fig. 2.—Glass electrode asymmetry potential vs. run number. Ordinate is e.m.f. (E_r) of cell I with reference solution 0.05 M KH(OOCCH$_3$)$_2$ + 0.1 M KCl in the sample compartment. Run number includes measurements on the reference solution. Average time per run 9 minutes. Upper curve, measurements in H$_2$O. The arrows indicate where the experiments were interrupted for the lengths of time given during which the glass electrode was kept at 22.2° in 0.02 M KCl in H$_2$O. Lower curve, measurements in 98.0 volume % D$_2$O.

Figs. 3–5 and 6–8. The variations of E_r in H$_2$O solutions could be very nearly eliminated if the pretreatment of the glass electrode in the mercury bath was omitted between measurements. It is obvious from Fig. 2 that it was necessary to standardize the electrode system immediately before and after each measurement of E_x, the maximal variation of the asymmetry potential being as high as 4 mv. When the measurements start with a rested glass electrode the asymmetry potential drops at first in an irregular manner. Later following an intermission in the measurements it starts to regenerate slowly. The reasons for these variations of the asymmetry potential will be considered in the Discussion. Whatever the reasons are, however, they do not seem to affect the hydrogen-ion response of the glass electrode in the two solvents investigated. This is demonstrated by the following two sets of measurements. First the electrode set-up and the extrapolation procedures employed were checked in H$_2$O solvent by determining the thermodynamic dissociation constant of acetic acid relative to the pH of dilute HCl–KCl solutions. This was followed by corresponding measurements in aqueous solvent containing 98.0 volume % D$_2$O.

Measurements in H$_2$O.—Assuming the glass electrode to have the theoretical response to variations in the hydrogen ion concentration at 22.2°

$$E = E_0 + 0.05860(\log a_H) + E_d \quad (III)$$

where E_0 is a constant, a_H is the hydrogen ion activity and E_d is a diffusion potential. Figure 3 summarizes the data obtained with dilute HCl–KCl solutions. At constant KCl concentration, c_{KCl}, and sufficiently small concentrations, c_{HCl} of HCl, employing the equation V (see ref. 7) for

log a_H, equation III may be written

$$E_a \equiv E - 0.05860(\log c_H) + 0.05860 \times 0.5066(c_{HCl} + c_{KCl})^{0.5} = E_0' + \text{constant}(c_{HCl}) \quad (IV)$$

$$\log a_H = \log c_H - 0.5066(\Gamma/2)^{0.5} + \text{constant} \times \Gamma;$$
$$\Gamma = \Sigma c_i z_i^2 \quad (V)$$

In Fig. 3 E_a is plotted against c_{HCl} and extrapolated linearly to $c_{HCl} = 0$. The points at $c_{HCl} = 0.02 M$ all fall below the corresponding straight line drawn, possibly in part due to the effect of HCl on the diffusion potential. The extrapolation in Fig. 3 is the first of three extrapolations designed to obtain thermodynamic data from the cell I with a liquid junction (compare ref. 7).

Figure 4 summarizes the data obtained with dilute KH(OOCCH$_3$)$_2$–KCl solutions. At constant c_{KCl} and appropriately small (not vanishingly small) concentrations, c_B, of KH(OOCCH$_3$)$_2$ and once more employing the expression V for the activity coefficient of a univalent ion, equation III can be written

$$pK^* = \frac{E_0' - E}{0.05860} + 0.5066(c_B + c_{KCl})^{0.5}$$
$$= -\log K' + \text{constant}(c_B) \quad (VI)$$

The appropriate value of E_0' is taken from Fig. 3. In Fig. 4 pK^* is plotted against c_B and extrapolated linearly to $c_B = 0$. Finally in Fig. 5 $-\log K'$ is plotted against c_{KCl} and extrapolated linearly to $c_{KCl} = 0$. The intercept $-\log K_H$ with the ordinate axis corresponds to the thermodynamic dissociation constant of acetic acid, HAc, at 22.2° in H$_2$O. The good agreement between the accepted value[8] at 22.2° of $-\log K_H = 4.756$ and the extrapolated value $-\log K_H = 4.74_8$ from Fig. 5 provides justification for the experimental and extrapolation procedures used.

Measurements in 98.0 Volume % D$_2$O.—The measurements were strictly analogous to those in H$_2$O. They are summarized in Figs. 6–8 which correspond closely to Figs. 3–5. Equations IV and VI were used for the first two extrapolations, neglecting the 0.4% difference[9] in dielectric constant of H$_2$O and D$_2$O at 22.2°. In equation IV $c_H = c_{HCl}$ means here the total concentration of solvated hydrogen ions, $c_H + c_D = c_{HCl} + c_{DCl}$, irrespective of isotopic species. A linear interpolation in a E_0' vs. log c_{KCl} plot (compare Fig. 3) gave the proper E_0' values to be used in equation VI.

The literature offers a number of different "authentic" values of $-\log K_{DH}$ with which to compare the extrapolated value 5.25$_0$ from Fig. 8. K_{DH} is the thermodynamic dissociation constant of acetic acid, HAc, at 22.2° in 98.0 volume % D$_2$O. At infinite dilutions

$$K_{DH} = \frac{(c_H + c_D)c_{Ac}}{c_{HAc} + c_{DAc}} \quad (VII)$$

where c_H and c_D are the concentrations of solvated protons and deuterons, respectively. The best value K_{DH} available appears to be that based on

(7) H. S. Harned and B. B. Owen, "The Physical Chemistry of Electrolytic Solutions," 2nd edition, Reinhold Publ. Corp., New York, N. Y., 1950, pp. 316–325.

(8) H. S. Harned and R. W. Ehlers, J. Am. Chem. Soc., 55, 652 (1933).

(9) I. Kirshenbaum, "Physical Properties and Analysis of Heavy Water," McGraw-Hill Book Co., New York, N. Y., 1951.

measurements by two independent methods of the relative strengths of acetic acid in H_2O and in various mixtures of H_2O and D_2O.[10] Interpolating in the results of LaMer and Chittum[10a] and using the value of K_H[8] used above one finds

$$-\log K_{DH} = \log(1.84/0.568) - \log K_H = 5.267 \quad (VIII)$$

From the good agreement[11] with the extrapolated value 5.25_0 from Fig. 8 one may conclude that the glass electrode as here employed in the range $2 \times 10^{-2} > c_H + c_D > 2 \times 10^{-5}M$ functions satisfactorily in H_2O as well as in water containing 98.0 volume % D_2O.

Acidity, pH and $p(DH)$.—Equation II defines in both solvents an acidity scale which in H_2O is simply connected with the ordinary pH scale[12]

$$pH = pH_r - \frac{E}{0.05860} \quad (IX)$$

pH_r is the pH of the reference solution. Similarly a "pH" scale may be defined by equation IX in H_2O-D_2O mixtures. This scale we shall denote by $p(DH)$ to remind us that $p(DH)$ depends on both the activities of protons and deuterons (equation X). The zero of the $p(DH)$ scale thus defined in water containing 98.0 volume % D_2O is fixed by the convention (compare references 12 and 13) that in a suitable reference solution in 98.0 volume % D_2O

$$p(DH) \approx -\log(a_H + a_D) \quad (X)$$

$a_H + a_D$ is the sum of the hydrogen- and deuterium-ion activities, calculable at high dilutions from $c_H + c_D$ and the Debye–Hückel theory of activity coefficients. The solution marked A in Fig. 7 (0.00404 M $KH(OOCCH_3)_2$ + 0.0092 M KCl in 98.0 volume % D_2O) may serve as a reference solution. Its $p(DH)$ at $22.2°$ is estimated to be $5.267 - 0.05 \pm 0.01 = 5.22 \pm 0.01$. This value and equation IX lead immediately to the apparent $p(DH)$ = 5.06 ± 0.01 of the secondary reference solution B (0.05 M $KH(OOCCH_3)_2$ + 0.1 M KCl in H_2O) used for the frequent standardizations of the electrode system. The pH of this solution is 4.63 ± 0.01. It follows that if we try to measure the pH of the reference solution B in H_2O with our $p(DH)$ meter (employing the "heavy" calomel electrode) calibrated for measurements in 98.0 volume % D_2O, the correction to apply to the measured apparent $p(DH)$ of the reference solution B in order to obtain its true pH is $4.63 - 5.06 = -0.43$ unit.

$$pH = \text{apparent } p(DH) - 0.43 \quad (XI)$$

In the course of the present investigation it was also tried to measure the $p(DH)$ of buffered solutions in 98 volume % D_2O with our calibrated pH meter (employing the "light" calomel electrode). The apparent pH values thus obtained are given in Table I together with the true $p(DH)$ values obtained by interpolation in Figs. 6 and 7. It is

(10) (a) V. K. LaMer and J. P. Chittum, *J. Am. Chem. Soc.*, **58**, 1642 (1936); (b) S. Korman and V. K. LaMer, *ibid.*, **58**, 1396 (1936).

(11) The good agreement between the extrapolated value from Fig. 8 and the value of $-\log K_{DH}$ calculated from equation VIII is still good when the value for $-\log K_H = 5 - \log 1.84 = 4.735^{10a}$ is used in equation VIII instead of the value[8] employed above.

(12) R. G. Bates, "Electrometric pH Determinations," John Wiley and Sons, Inc., New York, N. Y., 1954.

(13) S. P. L. Sørensen and K. Linderstrøm-Lang, *Compt. rend. trav. lab. Carlsberg*, **15**, no. 6 (1924).
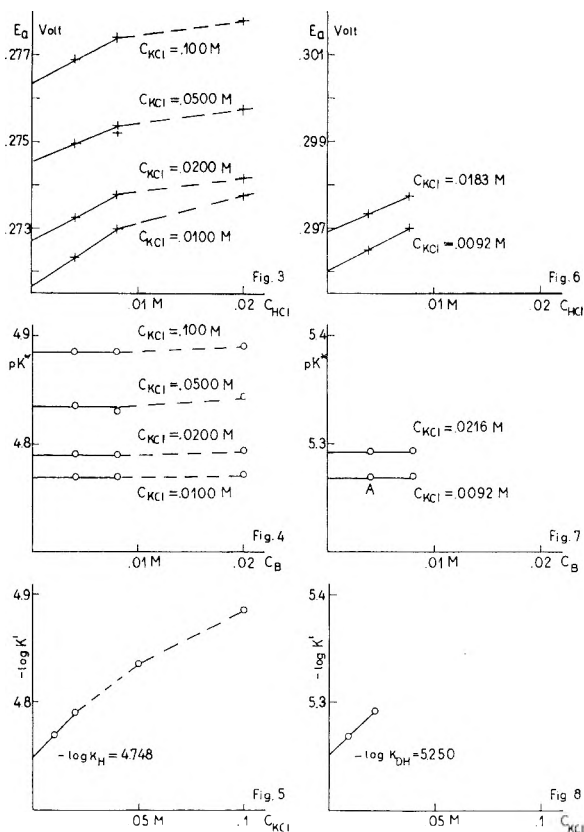
Figs. 3–5.—Measurements in H_2O. See text.
Figs. 6–8.—Measurements in 98.0 volume % D_2O. See text.

noticed that in order to obtain the true $p(DH)$ of the solutions in Table I a correction of $+0.44$ unit should be added to their apparent pH as determined by the present method. This figure is in good agreement with the $+0.4$ value reported for the same correction in D_2O by Hart[1] and by Lumry, et al.[3]

$$p(DH) = \text{apparent } pH + 0.44 \quad (XII)$$

The corrections in equations XI and XII check well numerically. This follows immediately from the approximate identity of the corresponding E values in the two columns of Table I ($\Delta E \leq 0.7$ mv.).

Discussion

The method described for determining $p(DH)$ is fairly economical in its requirements for D_2O. In addition it is so accurate that it can be used for acidity determinations in kinetic studies of acid catalysis in H_2O-D_2O mixtures. The main drawback of the method is that it is necessary to standardize the electrode system before and after each measurement. However, the total time required to determine $p(DH)$ is less than 20 minutes including one standardization.

No precautions were taken to remove dissolved CO_2 from the waters used since this amount of CO_2 affects the measurements in the rather acid range investigated to a negligible extent. A deuterium-enriched sample placed for 3–4 minutes in the sample compartment before reading its $p(DH)$ will exchange D for H with the laboratory air and with

TABLE I

RELATION BETWEEN APPARENT pH AND TRUE $p(DH)$ IN 98 VOLUME % D_2O AT 22.2°

Sample dissolved in 98 vol. % D_2O	Calibrated pH meter ("light" calomel electrode)		Calibrated $p(DH)$ meter ("heavy" calomel electrode)			
	E, v.	Apparent pH	E, v.[a]	$p(DH)$	ΔE, v.	$p(DH) - pH$ [b]
0.00387 M HCl + .0110 M KCl	0.1520	2.04	0.1515	2.48	0.0005	0.43$_8$
.00778 M HCl + .0111 M KCl	.1695	1.74	.1692	2.18	.0003	.43$_5$
.00389 M HCl + .0220 M KCl	.1519	2.04	.1512	2.48	.0007	.44$_2$
.00406 M KH(OOCCH$_3$)$_2$ +0.0109 M KCl	− .0090	4.78	− .0092	5.21	.0002	.43$_3$

[a] Interpolated values. [b] Correction to apparent pH to obtain true $p(DH)$.

H_2O adsorbed on the walls of the sample container. In addition exchange will occur with the amount of H_2O still bound to the glass electrode after drying it in the mercury bath. Estimates of the contributions of H to the D_2O–H_2O sample from each of the three sources mentioned showed them to be insignificantly small under the conditions of this investigation. This conclusion was verified by determining by an infrared spectrophotometric method[14] the increase in H content of a 0.500-ml. D_2O sample caused by an acidity determination performed as described in the experimental section. The increase in H content found corresponded to −0.03 volume % D_2O.

In Figs. 5 and 8 only the intercept with the ordinate axis can be given thermodynamical significance. The deviation of the two curves from horizontal lines measures the deviations of the activity coefficients of H^+, CH_3COO^- and CH_3COOH from the respective activity coefficients calculated with help of the Debye–Hückel limiting expression. By subtracting the function $2 \times 0.5066 \times (c_{KCl})^{0.5}$ from the curves in Figs. 5 and 8 we obtain $-\log K_c = -\log (c_H(c_{Ac}/c_{HAc}))$ at infinite dilution as a function of c_{KCl}. Using Fig. 5 and putting $c_{KCl} = 0.100\ M$ we obtain $-\log K_c = 4.885 − 0.320 = 4.565$ at 22.2°. Interpolating in the results of Harned and Hickey (ref. 7, p. 523) yields for acetic acid in 0.10 M KCl at 25° $-\log K_c = 4.545$. The agreement between the two K_c values is considered satisfactory in view of the 2.8° difference between the temperatures employed in the two investigations and the fact that the points in Fig. 5 become less accurately known with increasing c_{KCl}. The reason for this is that equation V is less adequate for extrapolation purposes the higher the ionic strength. We conclude that the glass electrode after the conditioning in mercury described above exhibits the theoretical response (estimated with help of equation V) to variations in hydrogen ion concentration between 10^{-2} and 10^{-5} M as well at low as at high ionic strengths between 0.02 and 0.1 M.

At present there is no evidence for the transfer of other ions or molecules[15] than the hydrogen ion

from the solution to the glass electrode surface layer in the electrode reaction of the glass electrode in the pH range which is of interest here. It thus appears to be a general approach to an understanding of the variations in glass electrode asymmetry potential depicted in Fig. 2 to consider them as an immediate consequence of variations in the *chemical free energy* of the hydrogen ion in the glass surface layer. This energy would depend on the state of the glass surface layer[19] and thus among other variables on the time,[17–19] the extent of hydration of the glass surface layer and apparently also on mechanical treatments like the conditioning of the electrode in mercury employed in this investigation prior to each measurement.

The single ion activities, a_H and a_D, are strictly speaking not available from any measurement[20] but their sum $a_H + a_D$ ordinarily can be determined with moderate accuracy from $p(DH)$ measurements (equation X). In order to estimate a_H and a_D separately it is necessary to make additional extrathermodynamical assumptions. This is done, e.g., in the theory of Gross and Butler[21] as recently revised by Purlee[22] who demonstrated that the revised theory is in good agreement with a large number of rate data and hydrogen ion dissociation equilibria in H_2O–D_2O mixtures. One may therefore accept the expressions for a_H and a_D given in the Gross–Butler–Purlee theory with considerable confidence at least for purposes of extrapolation of rates or hydrogen ion dissociation constants obtained in H_2O–D_2O mixtures to pure D_2O. The Gross–Butler–Purlee theory gives[22]

$$\frac{a_H}{a_D} = \frac{1 - n}{n} L^{0.5} \qquad (XIII)$$

where $n = D/[(D) + (H)]$ is the atom fraction of deuterium in the water solvent and $L = 11.0$ at 25° is the equilibrium constant for the reaction

$$2D_3O^+ + 3H_2O \rightleftharpoons 2H_3O^+ + 3D_2O \qquad (XIV)$$
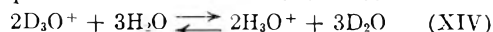
Knowing $a_H + a_D$ and a_H/a_D it is possible to calculate a_H and a_D separately. A discussion of the significance of the equilibrium constant L will be given at a later date.

(14) J. Gaunt, *Spectrochim. Acta*, **8**, 57 (1956).

(15) Dole's water-transfer theory[16] of the so-called "negative error" of the glass electrode in aqueous solutions with reduced water activity has been the subject of severe criticism.[17,18]

(16) M. Dole, "The Glass Electrode," John Wiley and Sons, Inc., New York, N. Y., 1941.

(17) E. E. Sinclair and A. E. Martell, *J. Chem. Phys.*, **18**, 224, 992 (1950); M. Dole, *ibid.*, **18**, 573, 1411 (1950).

(18) W. H. Beck and W. F. K. Wynne-Jones, *J. chim. phys.*, **49**, c97 (1952).

(19) K. Schwabe and G. Glöckner, *Z. Elektrochem.*, **59**, 504 (1955).

(20) E. A. Guggenheim, THIS JOURNAL, **33**, 842 (1929).

(21) W. E. Nelson and J. A. V. Butler, *J. Chem. Soc.*, 957 (1938).

(22) E. L. Purlee, *J. Am. Chem. Soc.*, **81**, 263 (1959).

As the transference numbers of K^+ and Cl^- vary less than 1% over the entire range of H_2O–D_2O mixtures at $25°$[23] the two types of diffusion potentials encountered in Table I are almost completely determined by the isotopic composition and the KCl concentration of the two solutions forming the diffusion boundary. Application of this principle to the chain consisting of 4 cells of type I, encountered in Table I and having a total e.m.f. $= \Delta E$, shows that ΔE should in fact be very nearly zero as found experimentally.

We shall finally examine the 0.44 correction in equation XII from the point of view of Haugaard's theory of the glass electrode[24] in moderately acid H_2O. According to this theory the proton has the same *electrochemical* potential in the surface layer of the glass electrode as in the solution X bathing the glass electrode, the *chemical* potential or the activity of the proton in the glass electrode surface layer being held constant by a large number of acid and basic groups located there. The 0.44 correction in equation XII is defined, *e.g.*, by the cell

glass1 ‖0.01 M HCl in H_2O |KCl(satd. in H_2O) |
    0.01 M (HCl + DCl) in 98% D_2O ‖glass 2   (XV)
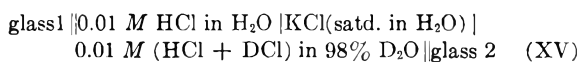
(23) L. G. Longsworth and D. A. MacInnes, *J. Am. Chem. Soc.*, **59**, 1666 (1937).

(24) G. Haugaard, *Compt. rend. trav. lab. Carlsberg*, **22**, 199 (1938).

the e.m.f. $\pi_2-\pi_1$, of which (right side positive) is 0.44 $\times$ 0.0586 = 0.025 v. In order to apply Haugaard's theory to our data we shall make the reasonable assumption that the two diffusion potentials in cell XV cancel approximately. It then follows from Haugaard's theory applied to cell XV that

$$0.44 = \frac{\pi_2 - \pi_1}{0.05860} = \log(a_H)_1 - \log(a_H + a_D)_2 \quad (XVI)$$

where $(a_H)_1$ is the constant hydrogen ion activity in the outer surface layer of glass electrode 1 and $(a_H + a_D)_2$ is the constant hydrogen ion activity in the outer surface layer of glass electrode 2. The right side of equation XVI corresponds to the change in $p(DH)$ which the buffer mixture in the glass electrode surface layer suffers when taken from H_2O to 98% D_2O. In view of the fact that the pK values of a number of acids dissolved in H_2O are increased 0.40–0.52 unit when dissolved in D_2O[25] it would appear that the 0.44 correction in equation XII tentatively may be accounted for in terms of Haugaard's theory of the glass electrode.

(25) C. K. Rule and V. K. LaMer, *J. Am. Chem. Soc.*, **60**, 1974 (1938).

THE THEORY OF DIFFUSION CONTROLLED ABSORPTION KINETICS WITH ACCOMPANYING EVAPORATION

By ROBERT S. HANSEN[1]

Contribution from the Department of Chemistry, University of Southern California, Los Angeles 7, Calif.

Received November 17, 1959

A quantitative theory is developed for diffusion controlled adsorption at the liquid–air interface with simultaneous diffusion-controlled loss of solute into the vapor phase. No essential complications result from inclusion of evaporational losses, and the general result is an integral equation equivalent to one given earlier by Ward and Tordai. A power series representation of the adsorption valid at small times and an asymptotic representation valid at large times are given, and the integral equation is solved numerically for adsorbates satisfying the Langmuir adsorption isotherm. The results explain the transient steady state observed recently by Hommelen in the surface tension of aqueous solutions of organic solutes. The infinite initial rate of adsorption predicted by diffusion-controlled adsorption theory is not in agreement with available data.

Introduction

Diffusion controlled adsorption kinetics at plane interfaces has been treated theoretically by Ward and Tordai[2] for arbitrary adsorption isotherm, by Sutherland[3] for the linear adsorption isotherm, and by Delahay and Fike[4] for the Langmuir adsorption isotherm, among others. Recently Hommelen[5] has shown experimentally that a steady-state surface tension of appreciable duration, significantly higher than that corresponding to the solution bulk concentration, may be obtained for aqueous solutions of organic compounds of intermediate chain length.

The purpose of this article is to develop a quantitative theoretical interpretation of Hommelen's

(1) Department of Chemistry, Iowa State University, Ames, Iowa. National Science Foundation Senior Postdoctoral Fellow at U. S. C.

(2) A. F. H. Ward and L. Tordai, *J. Chem. Phys.*, **63**, 485 (1946).

(3) K. Sutherland, *Aust. J. Sci. Res.*, **A5**, 683 (1952).

(4) P. Delahay and C. T. Fike, *J. Am. Chem. Soc.*, **80**, 2628 (1958).

(5) J. R. Hommelen, *J. Colloid Sci.*, **14**, 385 (1959).

result. Incident to this it will be shown that the theory of diffusion controlled adsorption kinetics is not made appreciably more complex if evaporation of solute from the interface is also considered. New general results, applicable whether or not evaporation occurs and for general form of adsorption isotherm will be developed. The special case of adsorbates satisfying the Langmuir adsorption isotherm will also be treated.

Theoretical

Let $\Gamma(c)$ be the isotherm for adsorption of solute at the liquid–vapor interface, $C_1(x,t)$ and $C_2(x,t)$ the concentration of solute in moles/cm.^{3} in liquid and gas phase, respectively, at position x and time t, D_1 and D_2 the diffusion coefficients of solute in liquid and gas phase, respectively, and K the equilibrium constant for distribution of solute between liquid and gas phases. The following boundary value problem is generated

$$D_1 C_{1xx}(x,t) = C_{1t}(x,t), \ x > 0, \ t > 0 \qquad (1)$$
$$C_1(x,0) = C_0, \ x > 0 \qquad (2)$$
$$= 0, \ x = 0$$
$$\lim_{x \to \infty} C_1(x,t) = C_0, \quad t \geqslant 0 \qquad (3)$$

$$D_2 C_{2xx}(x,t) = C_{2t}(x,t), \quad x < 0, \ t > 0 \qquad (4)$$
$$C_2(x,0) = 0, \quad x \leqslant 0 \qquad (5)$$
$$\lim_{x \to -\infty} C_2(x,t) = 0, \quad t \geqslant 0 \qquad (5a)$$

$$C_2(0,t) = K C_1(0,t), \ t \geqslant 0 \qquad (6)$$
$$D_1 C_{1x}(0,t) = \Gamma_t + D_2 C_{2x}(0,t), \ t > 0 \qquad (7)$$

(subscripts x and t denote partial differentiation after the indicated variables, e.g., $C_{1xx} = \partial^2 C_1 / \partial x^2$). It may be shown (very readily by Laplace transformation techniques) that the concentration of solute at the interface must satisfy an integral equation which may be expressed in any of the equivalent forms

$$\Gamma(t) = 2\sqrt{\frac{D_1}{\pi}} \left[C_1 t^{1/2} - \frac{1}{2}(1 + K\sqrt{D_2/D_1}) \int_0^t \frac{C_1(0,\tau)\mathrm{d}\tau}{(t-\tau)^{1/2}} \right] \qquad (8a)$$

$$= 2\sqrt{\frac{D_1}{\pi}} \left[C_0 t^{1/2} + \left(1 + K\sqrt{\frac{D_2}{D_1}}\right) \int_0^t C_1(0,\tau)\mathrm{d}(t-\tau)^{1/2} \right] \qquad (8b)$$

$$= 2\sqrt{\frac{D_1}{\pi}} \left[C_0 t^{1/2} - \left(1 + K\sqrt{\frac{D_2}{D_1}}\right) \int_0^t (t-\tau)^{1/2} \, \mathrm{d}C_1(0,\tau) \right] \qquad (8c)$$

$$= 2\sqrt{\frac{D_1 t}{\pi}} \left[C_0 - \left(1 + K\sqrt{\frac{D_2}{D_1}}\right) \int_0^{\pi/2} C_1(0,t\sin^2\theta)\sin\theta \, \mathrm{d}\theta \right] \qquad (8d)$$

Since $\Gamma(t) \equiv \Gamma[C_1(0,\tau)]$, i.e., the surface excess at any instant is in equilibrium with the subsurface concentration, the integral equations 8 suffice in principle to determine $C_1(0,t)$ if $\Gamma(c)$ is given. If D_2 or K are zero (i.e., loss of solute neglected) eq. 8b reduces to a result given by Ward and Tordai.[2] The integral equations cannot be solved to give an analytic expression for $C_1(0,t)$ for arbitrary choice of $\Gamma(c)$, but they can nevertheless be compared with experiment numerically; thus $\Gamma(c)$, the equilibrium adsorption isotherm, and $\Gamma(t)$ can be measured, $C_1(0,t)$ inferred from $\Gamma(c)$ and $\Gamma(t)$, and the integrals evaluated numerically. Thus eq. 8b, for example, asserts that the ratio $\Gamma(t)/[C_0 t^{1/2} + (1 + K\sqrt{D_2/D_1})\int_0^t C_1(0,t)\mathrm{d}(t-\tau)^{1/2}]$ is constant and equal to $2\sqrt{D_1/\pi}$ and this is subject to experimental verification.

The boundary value problem set forth in eq. 1–7 would not represent measurements of adsorption kinetics obtained by the vibrating jet method, for diffusion in the gas phase would then occur both in the direction of the jet axis and perpendicular to it. Possibly such a physical situation may be represented by boundary layer diffusion in the gas phase. Let b be the thickness of the boundary layer, and C_0' the concentration of solute on the gas phase side of the boundary layer. Eq. 4 and 5 of the original boundary value problem will not apply, and instead of eq. 7 we will have

$$D_1 C_{1x}(0,t) = \Gamma_t + \frac{D_2}{b}[K C_1(0,t) - C_0'] \qquad (9)$$

which implies that $C_1(0,t)$ must satisfy the integral equation

$$\Gamma(t) = 2\sqrt{\frac{D_1}{\pi}} \left[C_0 t^{1/2} + \int_0^t C_1(0,\tau)\mathrm{d}(t-\tau)^{1/2} - \frac{D_2}{2b}\sqrt{\frac{\pi}{D_1}} \int_0^t (K C_1(0,\tau) - C_0')\mathrm{d}\tau \right] \qquad (10)$$

Other equivalent forms similar to those in eq. 8 can be derived readily. This result could also be compared with experiment numerically; the comparison could be carried out using b and C_0' as adjustable parameters or, more satisfactorily, by devising an independent estimation of them. Since such estimates do not appear possible for data presently available we shall not pursue this aspect of the problem further at this time.

Strictly, it must be noted that loss of solute (and, in general, solvent) to the gas phase must result in displacement of the liquid–gas interface, so that one must consider a problem of diffusion with moving boundary of the type treated generally by Danckwerts.[6] The error resulting from neglect of this boundary motion can be bounded as follows: the amount of material transferred to the interface as a result of boundary motion at time t is not greater greater than $X C_0$, where X is the distance the boundary moves in time t. X is not greater than the distance the boundary would move if the diffusing components maintained their saturated vapor pressures at the boundary (i.e., no depletion at liquid side of boundary due to loss of material to the gas phase). But for a single component in this case $X_t = -v D_2 C_x(0,t) = (p_0 v/RT)\left(\dfrac{D_2}{\pi t}\right)^{1/2}$ in which v is the component molar volume in the liquid state and p_0 is its saturated vapor pressure. Hence $X = 2(p_0 v/RT)\sqrt{D_2 t/\pi}$. Suppose we consider loss of water to be the principal cause of boundary displacement. At 20° $p_0 = 17.5$ mm., $v = 18$ cc., $D_2 = 0.2$ cm.^{2}/sec., and so $X C_0 = 9 \times 10^{-6} C_0 t^{1/2}$. On the other hand, for small t the leading term in $\Gamma(t)$ is $2\sqrt{D_1/\pi} C_0 t^{1/2}$, so for $D_1 = 8 \times 10^{-6}$ cm.^{2}/sec., this term is about $3 \times 10^{-3} C_0 t^{1/2}$, or about 300 times as great as $X C_0$. Hence neglect of boundary displacement appears well justified at least for surface excesses appreciably less than their equilibrium values.

Certain consequences of eq. 8 can be deduced for arbitrary form of the adsorption isotherm; additional consequences can be deduced if the isotherm is specified. We therefore discuss these consequences in two sections, using the Langmuir isotherm to illustrate the second group.

A. General Remarks on Diffusion-controlled Adsorption Kinetics.—On consideration of eq. 8d it is apparent that the limit at large t of $C_1(0,t)$ is not C_0, but $C_0/(1 + K\sqrt{D_2/D_1})$. It is therefore of interest to consider the magnitude of the factor $(1 + K\sqrt{D_2/D_1})$ for materials of the type frequently subjected to kinetic study. Organic acids and alcohols of intermediate chain length, slightly soluble in water, in aqueous solution are such ma-

(6) P. V. Danckwerts, *Trans. Faraday Soc.*, **46**, 701 (1950).

terials. Let p_0 be the saturated vapor pressure of the organic compound in mm., m_0 its saturation concentration in water (moles/liter). Then $K = (p_0/760)/(m_0RT)$. Choosing as representative values of the diffusion coefficients $D_2 = 0.1$ cm.^{2}/ sec. (ethanol in air at 9.5°), $D_1 = 10^{-5}$ cm.^{2}/sec. (phenol in water at 18°[7] one has at 20° $K\sqrt{D_2/D_1} = 5.4 \times 10^{-3}$ (p_0/m_0). For pentanol-1 at 20°, $p_0 = 2.8$ mm., $m_0 = 0.22$ mole/liter, and therefore $K \cdot \sqrt{D_2/D_1} = 0.07$, i.e., in this system $C_1(0,t\to\infty)$ will be less than C_0 by 7%. At half coverage, $\Gamma = 4.0 \times 10^{-10}$ mole/cm.^{2}, approximately, and the predicted shift in surface tension is 0.66 dyne/cm. This is to be compared with the shift of 1.0 dyne/cm. observed by Hommelen in the aqueous hexanol-1 system.

Let $\bar{\Gamma}$ be the limiting surface excess, corresponding to $C_1(0,t) = C_0[1 + K\sqrt{D_2/D_1}]^{-1}$. Then the asymptotic behavior of $C_1(0,t)$ can also be deduced by consideration of eq. 8d; it is

$$C_1(0,t) = \frac{C_0}{1 + K\sqrt{D_2/D_1}} - \frac{\bar{\Gamma}}{\sqrt{\pi D_1 t}\,(1 + K\sqrt{D_2/D_1})}$$
$$(t \text{ large}) \quad (11)$$

For small t, and therefore for small values of $C_1(0,t)$, we may develop $C_1(0,t)$ in power series in $t^{1/2}$, substitute this series in the MacLaurin expansion of $\Gamma(c)$ and establish the coefficients in the power series by means of eq. 8d. In this way we obtain

$$C_1(0,t)/C_0 = \tau^{1/2} - \frac{1}{2}\left[C_0\left(\frac{d\ln\frac{d\Gamma}{dC}}{dc}\right)_0 + \right.$$
$$\frac{\pi}{2}(1 + K\sqrt{D_2/D_1})\Big]\tau + \frac{1}{2}\left[\left\{C_0\left(\frac{d\ln\frac{d\Gamma}{dC}}{dc}\right)_0 + \right.\right.$$
$$\frac{2}{3}(1 + K\sqrt{D_2/D_1})\left\{\left\{C_0\left(\frac{d\ln\frac{d\Gamma}{dC}}{dC}\right)_0 + \frac{\pi}{2}(1 + K\sqrt{D_2/D_1})\right\}\right.$$
$$\left. - \frac{1}{3}C_0{}^2\left(\frac{d^3\Gamma}{dC^3}\right)_0 \middle/ \left(\frac{d\Gamma}{dC}\right)_0\right]\tau^{3/2} + \cdots (\tau \text{ small}) \quad (12)$$

in which

$$\tau = 4D_1 t/\pi\left(\frac{d\Gamma}{dC}\right)_0^2$$

B. Diffusion-controlled Adsorption Kinetics in Systems Obeying Langmuir's Adsorption Isotherm. —Let

$$\Gamma(c) = \Gamma_m ac/(1 + ac) \quad (13)$$

We then introduce new variables

$$U = aC_1(0,t); \quad \bar{U} = \lim_{t\to\infty} U = aC_0/(1 + K\sqrt{D_2/D_1})$$
$$(\text{see eq. 11})$$

$$z = (2C_0/\Gamma_m)\sqrt{D_1 t/\pi}; \quad y = (2C_0/\Gamma_m)\sqrt{D_1\tau/\pi}$$

Then eq. 8a-d can be reduced to integral equations establishing $U(z)$ with a single parameter $\bar{U}$; the following are representative

$$U/(1 + U) = z - (\bar{U})^{-1}\int_0^z (z^2 - y^2)^{1/2}\, dU(y) \quad (14)$$

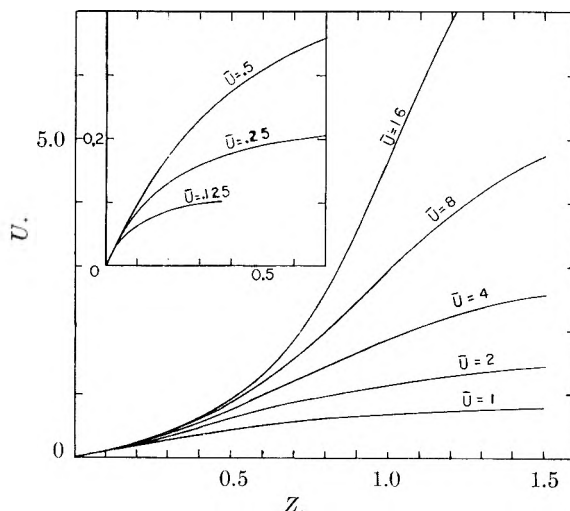$$U/(1 + U) = z\left[1 - (\bar{U})^{-1}\int_0^{\pi/2} U(z\sin\theta)\sin\theta\, d\theta\right] \quad (15)$$

(7) W. Jost, "Diffusion," Steinkopf Verlag, Darmstadt, 1957.

Fig. 1.—Dependence of reduced subsurface concentration $U = aC_1(0,t)$ on reduced square root of time $Z = (2C_0/\Gamma_m)\cdot\sqrt{D_1 t/\pi}$ for various values of the limiting reduced subsurface concentration $\bar{U} = \lim U$ for solute obeying the Langmuir adsorption isotherm.

The analogs of eq. 11 and 12 are, respectively

$$U = \bar{U}[1 - (2/\pi z)\bar{U}/(1 + \bar{U})] \quad (z \text{ large}) \quad (16)$$
$$U = z + \left(1 - \frac{\pi}{4\bar{U}}\right)z^2 + \left(1 - \frac{2}{3\bar{U}} - \frac{\pi}{2\bar{U}} + \frac{\pi}{6\bar{U}^2}\right)z^3$$
$$+ \ldots (z \text{ small, i.e., } t \text{ small}) \quad (17)$$

For intermediate values of z, let the range of z be divided into equal increments Δz; let U_n be the value of U for $z = n\Delta z$. Then the integral in eq. 14 can be approximated trapezoidally to

$$U_n/(1 + U_n) = n\Delta z - (\bar{U})^{-1}\frac{\Delta z}{2}\sum_{m=1}^{n}$$
$$[\sqrt{n^2 - m^2} + \sqrt{n^2 - (m-1)^2}](U_m - U_{m-1}) \quad (18)$$

or

$$U_n/(1 + U_n) + (\bar{U})^{-1}\frac{\Delta z}{2}U_n = n\Delta z + (\bar{U})^{-1}\frac{\Delta z}{2}U_{n-1} -$$
$$(\bar{U})^{-1}\frac{\Delta z}{2}\sum_{m=1}^{n-1}[\sqrt{n^2 - m^2} + \sqrt{n^2 - (m-1)^2}]$$
$$(U_m - U_{m-1}) \quad (19)$$

which has the form of a recurrence relation permitting evaluation of U_n in terms of U_{n-1}, U_{n-2} ...., U_0; since $U_0 = 0$, U_1, U_2, ..., can be evaluated sequentially by means of eq. 19. This procedure is exact in the limit as $\Delta z \to 0$, and can be tested for accuracy of approximation by repeating the calculation with smaller increments Δz until variation is satisfactorily small. Equation 19 was programmed for computer solution and solved in this manner for $\bar{U} = 16, 8, 4, 2, 1, 0.5$, 0.25 and 0.125 to a precision of 1% or better. Results are presented graphically in Fig. 1.

From a comparison of results obtained by numerical integration with those obtained by the asymptotic formula eq. 16, the latter formula was judged to yield a value accurate to within 1% if $U/\bar{U}$ is greater than 0.7. Similarly the sum of the first three terms in the power series in eq. 17 was found to differ from U by not more than the third term. The function $U(z)$ having been obtained, the
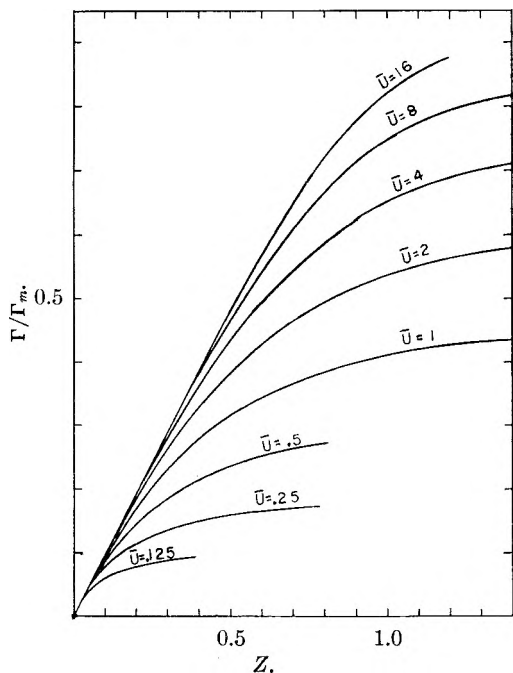
Fig. 2.—Dependence of reduced surface excess Γ/Γ_m on reduced square root of time for various values of limiting reduced subsurface concentration.
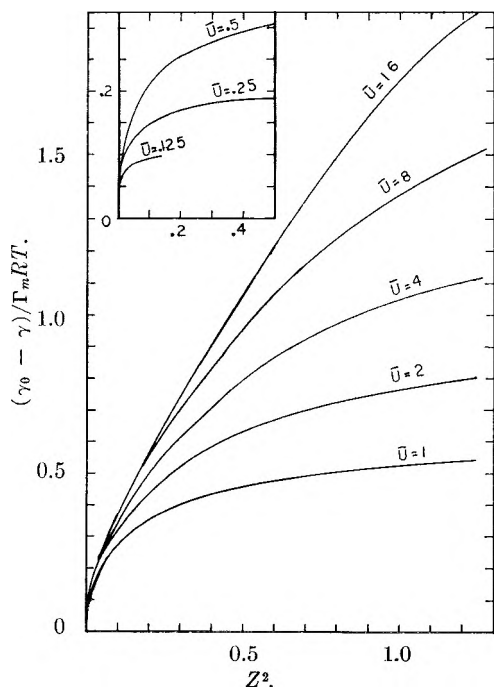

Fig. 3.—Dependence of reduced spreading pressure $(\gamma_0 - \gamma)\ \Gamma_m R T$ on reduced time $Z^2 = (2C_0/\Gamma_m)^2\ D_1 t/\pi$ for various limiting reduced subsurface concentrations.

dependence of surface excess and boundary tension on z can be obtained from eq. 20 and 21

$$\Gamma/\Gamma_m = U/(1 + U) \qquad (20)$$

$$(\gamma_0 - \gamma)/\Gamma_m R T = \ln (1 + U) \qquad (21)$$

Dependence of reduced surface excess Γ/Γ_m on z (proportional to $t^{1/2}$) is presented in Fig. 2; dependence of reduced spreading pressure $(\gamma_0 - \gamma)/\Gamma_m R T$ on z^2 (proportional to t) is presented in Fig. 3.

Discussion

The asymptotic expression eq. 11 provides a simple estimate of the time required for approximate equilibration of a new surface. Thus if $D_1 = 10^{-5}$ cm.^{2}/sec., $\bar{\Gamma} = 4 \times 10^{-10}$ mole/cm.^{2} (about half coverage in the case of straight-chain organic molecules) $C_1(0,t)$ will differ from its limiting value by less than 10% if $t > 5.1 \times 10^{-7}/\bar{C}_0{}^2$ sec., $\bar{C}_0$ being the bulk concentration in moles/liter. Further, this equation can be used with the Gibbs adsorption theorem to derive the following limiting laws for dependence of boundary tension on time

$$\gamma - \gamma_\infty = - \bar{\Gamma} R T \ln (1 - \bar{\Gamma}/C_0\sqrt{\pi D_1 t}) \qquad (22)$$

$$= \bar{\Gamma}^2 R T/C_0\sqrt{\pi D_1 t} \ (t \text{ large}) \qquad (23)$$

For the same choices of $\bar{\Gamma}$ and D_1, we find $\gamma - \gamma_\infty = 7.0 \times 10^{-4}/\bar{C}_0 t^{1/2}$. This simple formula represents within a factor two the difference between boundary tension and its equilibrium value near equilibrium (within about 3 dynes/cm.) as observed for aqueous solutions of aliphatic alcohols and acids of from 5 to 11 carbons by a variety of techniques[8-11]; the time scales over these systems vary by 10^5 and this agreement is probably as close as can be expected for an arbitrarily selected $\bar{\Gamma}$.

At sufficiently low surface ages (ages sufficiently low that back diffusion is negligible) the amount of material transported to the interface is the same as that which would have been transported into an infinite medium, initially empty; the leading term in eq. 12 corresponds to this amount, and this result is well known.[2] Equation 12 permits extension of the range in which surface accumulation at early ages can be calculated for arbitrary adsorption isotherms to third-order terms. A consequence of the $t^{1/2}$ dependence of the leading term is that the initial rate of adsorption is infinite in the diffusion-controlled model, and consequently the initial rate of surface tension depression is also infinite. Figure 3 clearly shows this behavior for a solute satisfying the Langmuir isotherm, and it should be emphasized that this result is general. The comment by Defay and Hommelen that "the surface tension does not decrease appreciably before a particular surface age has been attained —when diffusion has driven sufficient solute into the surface to form a compact layer" is simply incorrect if taken at face value, and this conclusion is an artifact of their selection of log t, rather than t, as abscissa for plotting. The infinite initial slope predicted by the diffusion-controlled adsorption mechanism is *not* in accord with experiments conducted at sufficiently early times to permit reasonably precise extrapolation of results to the origin[8-10] and, so far as can be judged from graphs presented, it is not in agreement with the data of Defay and Hommelen either.[11]

Earlier calculations of adsorption kinetics for solutes obeying the Langmuir adsorption isotherm have been presented by Delahay and Fike.[3]

(8) C. C. Addison, *J. Chem. Soc.*, 579 (1946).

(9) D. G. Dervichian, *Kolloid-Z.*, **146**, 96 (1956).

(10) R. S. Hansen and T. C. Wallace, THIS JOURNAL, **63**, 1085 (1959).

(11) R. Defay and J. R. Hommelen, *J. Colloid Sci.*, **14**, 411 (1959).

It is not possible to compare their results precisely with the present results, but they appear to differ qualitatively in two respects: (1) Fig. 1 of Delahay and Fike appears to show a linear initial dependence of adsorption on time, although it is well known and recognized explicitly by them that the initial adsorption must vary as $t^{1/2}$. (2) Neglecting evaporation and using the present notation, Delahay and Fike present $\Gamma/\bar{\Gamma}$ as a function of $\bar{U}$, D_1/Γ_m and t (i.e., one variable and two parameters); we present $\Gamma/\bar{\Gamma}_m$ (and could equally well present $\Gamma/\bar{\Gamma}$) as a function of $\bar{U}$ and $z = 2C_0/\Gamma_m \sqrt{D_1 t/\pi}$ (one parameter and one reduced variable). Since our treatment involves one less parameter than the treatment of Delahay and Fike, our treatment requires much less extensive computation and tabulation for presentation of equivalent information. An implication of their treatment with which we do not agree, however, is the following: for a given t, D_1/Γ_m the ratio $\Gamma/\bar{\Gamma}$ depends only on $\bar{U} = aC_0$, and not on a or C_0 separately. This statement is true for the linearized isotherm, but does not appear to be true for the Langmuir isotherm; since Delahay and Fike tabulate only the product aC_0 it is not possible to compare their work with the present work further.

It may be concluded that a diffusion-controlled adsorption mechanism represents rather well the approach of boundary tensions of aqueous solutions of aliphatic acids and alcohols to equilibrium, and the steady-state boundary tension observed when simultaneous evaporation of solute occurs. It does not represent at all well the initial dependence of boundary tension on time.

THE CONDUCTIVITY OF DILUTE SODIUM CHLORIDE SOLUTIONS UNDER SUPERCRITICAL CONDITIONS[1]

By James F. Corwin, Robert G. Bayless and G. E. Owen

Contribution from the Department of Chemistry, Antioch College, Yellow Springs, Ohio

Received November 18, 1959

The conductivity of aqueous sodium chloride solutions above the critical temperature for the solution differs by a considerable amount when the electrode system is located at the top of the container from that when the electrodes are at the bottom. The difference is a function of the degree of filling (steam density) and is minimized by increasing the amount of solution in the container. A concentration gradient in the solution is proposed to explain the difference and comparisons are made with existing data which were made under conditions where homogeneity was artificially maintained or ignored by equipment design.

Introduction

The variation in conductivity measurements in salt solutions under supercritical conditions was first reported by Swinnerton, et al.[2] in 1949. The measurements made at that time using similar equipment to that described in this publication showed an almost constant bottom conductivity while the conductivity at the top varied over a wide range. Equipment difficulties and lack of financial support made confirmation of the phenomena impossible until the present time. These present measurements confirm the existence of the difference in conductivity between the top and the bottom of the autoclave but show that the constant bottom conductivity reported in 1949 is in error and that the bottom conductivity varies with steam density as does the top conductivity. The presence of a two phase system suggested by the constant conductivity measurements does not explain the present results as well as the suggestion that a single phase system exists with a conductivity gradient. The present view is coincident with that found by O. Maass and co-workers[3-5] and H. D. Baehr[6] who have worked primarily with pure substances. Mayer[7-10] and co-workers have proposed an anomalous region above the critical point which most closely resembles that found in this work. Various authors have objected to this proposal and have made measurements in various ways to refute the existence of such an anomalous region. A complete review of the controversy is presented by Hirschfelder, Curtis and Bird.[11]

The experimental evidence presented here shows a continuous and reproducible conductivity difference between the top and bottom of a high pressure vessel containing sodium chloride solutions of several concentrations and steam densities at 390° which is a temperature well above the critical temperatures of such solutions. An average between

(2) A. C. Swinnerton, G. E. Owen and J. F. Corwin, *Disc. Faraday Soc.*, **5**, 172 (1949).

(3) J. S. Tapp, E. R. W. Steacie and O. Maass, *Can. J. Res.*, **9**, 217 (1933).

(4) C. A. Winkler and O. Maass, *ibid.*, **9**, 613 (1933).

(5) D. B. Pall, J. W. Broughton and O. Maass, *ibid.*, **16B**, 230 (1938).

(6) H. D. Baehr, *Z. Electrochem.*, **58**, 416 (1954).

(7) J. E. Mayer, *J. Chem. Phys.*, **5**, 67 (1937).

(8) J. E. Mayer and P. G. Ackerman, *ibid.*, **5**, 74 (1937).

(9) J. E. Mayer and S. F. Harrison, *ibid.*, **6**, 87 (1938).

(10) S. F. Harrison and J. E. Mayer, *ibid.*, **6**, 101 (1938).

(11) J. D. Hirschfelder, C. F. Curtiss and R. B. Bird, "Molecular Theory of Gases and Liquids," John Wiley and Sons, Inc., New York, N. Y., 1954, pp. 357–390.
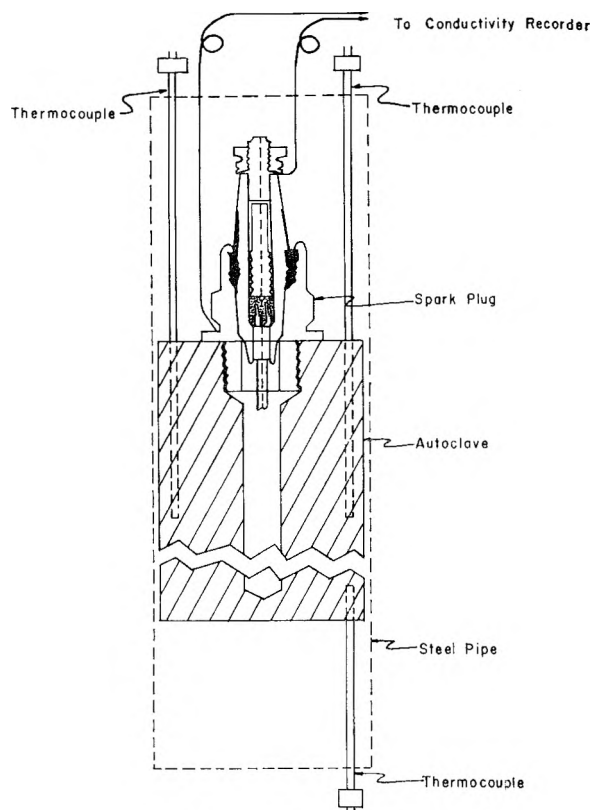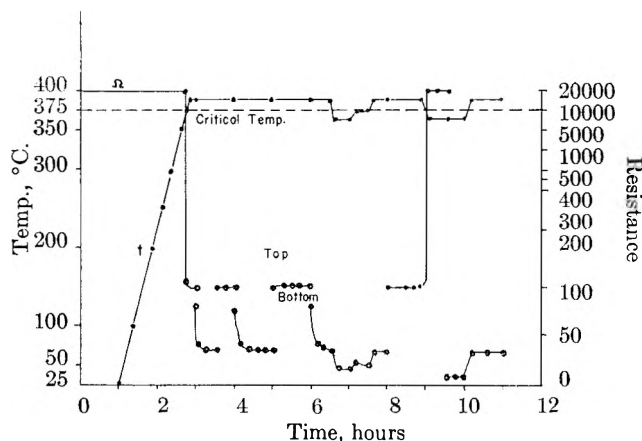
Fig. 1.—Autoclave assembly.

Fig. 2.—0.025 N KCl, steam density = 0.30.

these top and bottom conductivities compare very well with those obtained in homogeneous systems.

Apparatus.—A stainless steel autoclave containing an internal volume of 17.6 cc. and a spark plug, designed and built by the AC Spark Plug Division of General Motors Corporation were used. The autoclave was lined with platinum, 0.5 mm. thickness, extending from the base of the spark plug to the bottom of the autoclave. The spark plug surface inside the system (conducting area) was covered with gold foil, 0.002 in. thickness. These linings prevented excessive corrosion of the metal of both the spark plug and the autoclave. Figure 1 shows the autoclave-spark plug assembly.

A cylindrical furnace which was built during the initial stages of this investigation, and is the result of several trial models, was used. It was constructed by using a steel pipe, 3.5 cm. diameter, 36 cm. long, surrounded by a foamglass, insulating material, 9.0 cm. thick, 22.0 cm. diameter, and 40.0 cm. long. Nichrome resistance wire, 24 B & S gage, was wound 14 turns on the upper half of the pipe liner and an

equal number on the lower half. The whole furnace was mounted on a swivel so that the furnace and autoclave could be inverted without disturbing the connections.

The resistance of the system was measured by an automatic recording Speedomax G Electrolytic Conductivity Recorder, Model No. 1330175, built by Leeds and Northrup Instrument Company. The recorder, provided with a manual temperature compensator, was set at the value corresponding to the temperature of the electrolyte being measured at room temperature and was not changed during a measurement cycle. The recorder operated on a log scale for recording the resistance with limitations from 10 to 20,000Ω. Most of the solutions used showed resistance far above the upper limit of the instrument during a cycle when extremely small steam densities were measured, and when the electrode was not submerged. To correct for this condition, a resistance decade, Model Dr-1, built by the Heath Company, Benton Harbor, Michigan, was introduced into the measuring circuit, connected in parallel to the cell circuit. The value on this decade was set at 19,000, enough to prevent the recorder from going off scale when high resistance conditions existed.

A Brown Electronik Indicating Proportioning Controller, Model No. 156 R 16 Ps-141, built by the Brown Instrument Division of the Minneapolis-Honeywell Regulator Company, Philadelphia, Pennsylvania, was used to control the temperature input to the furnace. It proved quite satisfactory for controlling the temperature to within ±0.5° accuracy of the control point. Two variacs connected between the controllers and the furnace allowed the heating elements to be controlled for heat input.

An 8-point Speedomax Type G Recorder, Model No. 1203223, built by Leeds and Northrup Company, Philadelphia, Pennsylvania, was installed to record the temperatures throughout the hydrothermal system, and provided a continuous check so that the temperature could be kept constant.

Experimental Procedure.—Techniques common to the measurement of conductivity were used in handling the solutions and the autoclave filling except that a great deal of care was used in maintaining an oxygen-free atmosphere and oxygen-free solutions. The presence of air caused a great amount of variation in results. A measured amount of solution was added to the autoclave using a buret while a nitrogen atmosphere was maintained and the autoclave sealed with the spark plug as tightly as possible by hand. The autoclave was then transferred to a vise where the spark plug was tightened against a copper gasket using 130 to 140 foot pounds of torque.

The autoclave and solution were weighed to within an accuracy of 10 mg. on an analytical balance which had one pan substituted by a sling made to accommodate the container.

The autoclave was placed in the furnace in an upright position (spark plug at top) and the resistance of the solution measured by inverting the furnace which submerged the electrode. The furnace was then brought to the control temperature of 390° usually with the electrode at the top. Both upright and inverted positions were used without changes in results.

After reaching the control temperature, the furnace could be inverted or used upright in order to compare resistances at the top and bottom. Figure 2 represents a complete run for 11 hours with continuous measurement of resistance, and temperature of a solution of 0.025 N KCl.

At the completion of a set of measurements, the furnace was cooled to room temperature and the resistance again measured to make sure that no, or only minimum, changes in the solution were made by the heating. After cooling, the autoclave was weighed again to check for leakage.

The degree of filling of the autoclave determined the steam density and the pressure of the system. Since the pressure can be estimated from steam tables, pressures were not measured and unless the temperature was changed, the pressure was constant for any particular solution measured. The degree of filling of the container can be translated directly into steam density if one assumes that the container is full above the critical temperature.

Results

Figure 2 is representative of many experiments

TABLE I

SODIUM CHLORIDE SOLUTIONS AT 390°

Cell constant 0.073 ± 0.003 cm.$^{-1}$

Steam D, g./cc. Concn., moles/l.	0.50 T	0.50 B	0.40 T	0.40 B	0.36 T	0.36 B
Measd. resistance at 390° (ohms)						
0.1	18.0	16.0	21.0	18.0	24.0	18.0
.01	44.0	41.0	53.0	44.0	74.0	50.0
.0025	63.0	61.0	95.0	75.0	120.0	95.0
.001	76.0	67.0	120.0	95.0	150.0	105.0
.0001	155.0	145.0	210.0	155.0	320.0	215.0
Specific conductance at 390° ($L \times 10^{-4}$)						
0.1	40.6	45.6	34.8	40.6	30.4	40.6
.01	16.6	17.8	13.8	16.6	9.87	14.6
.0025	11.6	12.0	7.7	9.75	6.08	7.7
.001	9.6	10.9	6.08	7.7	4.87	6.95
.0001	4.7	5.03	3.48	4.7	2.28	3.4
Equiv. conductance at 390°						
0.1	40.5	45.6	35.0	40.5	30.4	40.4
.01	166.0	178.0	138.0	166.0	101.0	146.0
.0025	460.0	478.0	308.0	390.0	244.0	308.0
.001	960.0	1080.0	608.0	770.0	485.0	695.0
.0001	4700.0	5030.0	3480.0	4700.0	2280.0	3400.0
Steam D, g./cc.	0.32		0.25		0.20	
Measd. resistance at 390° (ohms)						
0.1	70.0	13.0	175.0	23.0	200.0	32.0
.01	95.0	55.0	280.0	105.0		
.0025	180.0	110.0	570.0	230.0	2800.0	1500.0
.001	300.0	140.0	775.0	192.0	4000.0	3500.0
.0001	470.0	285.0	1500.0	560.0	16000.0	14000.0
Specific conductance at 390° ($L \times 10^{-4}$)						
0.1	10.4	57.0	4.17	31.7	3.65	22.8
.01	7.7	13.3	2.6	6.95		
.0025	4.05	6.64	1.28	3.18	0.26	0.49
.001	2.44	5.2	0.943	3.80	0.18	0.21
.0001	1.55	2.56	0.486	1.30	0.046	0.052
Equiv. conductance at 390°						
0.1	10.5	62.0	4.2	31.7	3.65	22.8
.01	77.0	133.0	26.0	69.5		
.0025	162.0	266.0	52.0	127.0	10.4	19.4
.001	244.0	520.0	98.0	372.0	18.3	21.0
.0001	1550.0	2560.0	486.0	1300.0	45.6	52.0

to test the consistency of the apparatus. It was assumed that reproducibility of resistance measurements at the top and bottom over a period of hours showed that the measurements were real values and not due to malfunction of the apparatus with the production of temperature gradients. Each change from top to bottom measurement required that the furnace be inverted. This motion caused mixing to take place and for a time variable measurements occurred but after a time the conductivity difference was re-established. Experiments in which the autoclave was reversed in the furnace gave the same consistent results.

The most recent and, in the opinion of the authors, the most reliable results available in the literature are those reported by Fogo, Benson and Copeland[12] who worked with sodium chloride solutions in a small platinum, agitated cell and measured average conductivities at a number of temperatures,

steam densities and concentrations near and above the critical temperature. Because of the availability of these data for comparison, sodium chloride solutions were investigated at 390°. The data obtained from experiments under these conditions are collected in Table I.

These data were treated in the same manner as was done by Fogo, Benson and Copeland.[12] In order to eliminate steam density as a variable and smooth out small differences, the steam density was plotted against the log of the specific resistance (L) for all concentrations measured. The results for (L) obtained from the graph at constant steam densities were cross-plotted against log C. From these plots the specific conductance could be determined for concentrations used by Fogo, et al.,[12] and equivalent conductance could be calculated by the usual method. The graphical solutions and equivalent conductance calculations corresponding to the measured values of resistance are also listed in Table I. All of the results are based on the average

(12) J. K. Fogo, S. W. Benson and C. S. Copeland, *J. Chem. Phys.*, **22**, 212 (1954).

TABLE II

EQUIVALENT CONDUCTANCE FOR NaCl SOLUTIONS AT 390°

Steam D, g./cc. Concn. × 10⁶, moles/l.	$\sqrt{C}$	0.50		0.40		0.36	
		T	B	T	B	T	B
100	0.010	4680.0	5010.0	3200.0	3980.0	2290.0	3390.0
400	.020	1575.0	1810.0	1015.0	1440.0	705.0	1255.0
900	.030	882.0	1037.0	598.0	805.0	433.0	702.0
1,000	.0316	832.0	966.0	562.0	750.0	403.0	653.0
1,600	.040	596.0	678.0	404.0	545.0	306.0	475.0
2,500	.050	434.0	440.0	310.0	400.0	241.0	391.0
10,000	.100	166.0	190.0	129.0	162.0	107.0	145.0
100,000	.300	40.7	45.7	33.9	42.7	28.8	40.7

Steam D, g./cc. Concn. × 10⁶, moles/l.	$\sqrt{C}$	0.32		0.25		0.20	
		T	B	T	B	T	B
100	0.010	1160.0	2690.0	457.0	1290.0	186.0	490.0
400	.020	445.0	995.0	140.0	510.0	57.3	194.0
900	.030	285.0	564.0	88.2	292.0	34.4	125.0
1,000	.0316	272.0	537.0	83.2	272.0	32.4	118.0
1,600	.040	209.0	377.0	63.1	197.0	24.3	90.7
2,500	.050	163.0	283.0	49.2	149.0	19.2	73.0
10,000	.100	75.9	120.0	25.7	66.8	8.9	37.2
100,000	.300	21.1	38.0	8.4	30.6	3.6	22.9

NaCl Solutions at 390° C.

Steam Densities
.50
.40
.36
.32
.20 .25
Top

$\sqrt{C}$ 390°C

Fig. 3.

TABLE III

NaCl SOLUTIONS AT 390°

RATIO Λ TOP/Λ BOTTOM OF ALL CONCENTRATIONS AT EACH STEAM DENSITY

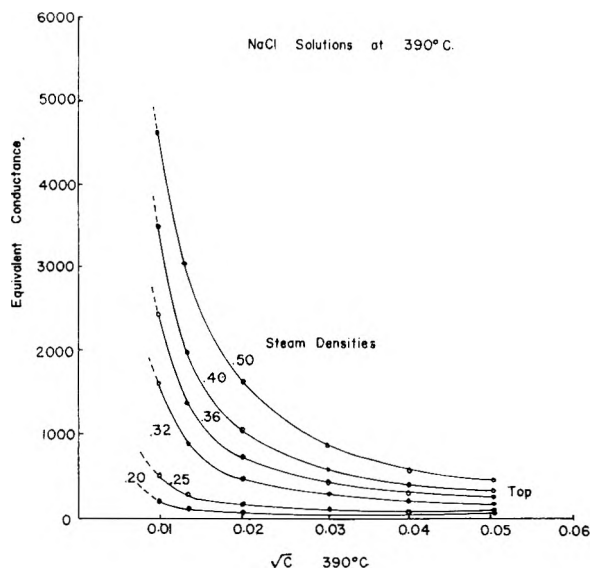| Steam D, g./cc. Concn. × 10⁶, moles/1000 cc.	0.50	0.40	0.36	0.32	0.25	0.20
100	0.935	0.805	0.675	0.543	0.354	0.380
400	.870	.705	.575	.457	.275	.296
900	.850	.745	.617	.507	.302	.275
1,000	.863	.750	.617	.507	.306	.274
1,600	.878	.743	.645	.555	.320	.378
2,500	.988	.775	.616	.576	.330	.214
10,000	.874	.796	.737	.634	.385	.239
100,000	.880	.795	.710	.555	.274	.157
Av. ratio	.886	.758	.645	.542	.313	.262

resistance measured in two separate experiments.

Table II contains equivalent conductances obtained in the same manner but listed for concentrations for which literature data are available. The values for equivalent conductance in Table II are plotted in the conventional way against the $\sqrt{C}$ in Figs. 3 and 4.

The ratio of equivalent conductivity (Λ) at the top of the autoclave to equivalent conductivity at the bottom was calculated for each concentration and steam density. The results of these calculations with the average of the ratio at each steam density is found in Table III. The averages obtained are plotted against the steam density in Fig. 5.

Discussion

The presence of differences in conductivity at the top and bottom of a vertically held container containing solutions of sodium chloride at tempera-

tures above the critical point of the solution has been established. Figure 5 which shows the ratio of the conductivities plotted against steam density indicates that as the steam density increases the difference between top and bottom becomes less. This phenomenon can be explained by the rise of the meniscus of the solution when greater than the critical volume is used. The solution expands on heating and the meniscus travels up the container and reaches the electrode at the top at about the same time as the critical temperature is reached. The measurements at 50% fillings show only the difference in conductivity between the top and bottom of the expanded liquid phase.

The selection of sodium chloride solutions for a series of experiments was made for comparison with conductivity values already in the literature[12] which were made on homogeneous systems. The only comparison that can be made is to assume that the average between top and bottom for a given concentration and steam density is the average conductivity of the system. This comparison is made in Fig. 6.

At the lower concentrations our average results are consistently higher than those in ref. 12, while at
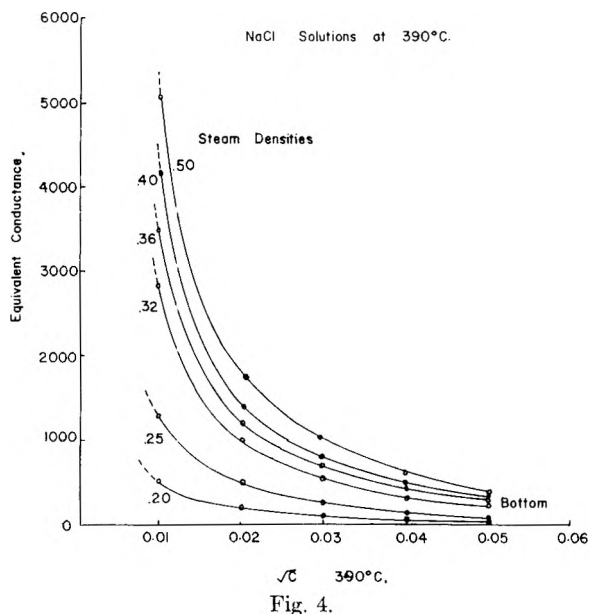
Fig. 4.

Fig. 5.

the higher concentrations our average results are lower. The cross-over point at any particular steam density occurs at concentrations between 0.0004 and 0.0010 M.

Because of conflicting effects the average of top and bottom conductivity varies with the concentration and indicates a density gradient in the autoclave. The lower density at the top contributes to lower conductivity due to the lowering of the dielectric constant of the water with steam density[13] and NaCl acts as a weaker electrolyte at the top than at the bottom. With a reduction in steam density, however, a decrease in viscosity and electrophoretic effect would cause an increase in conductivity. With a decrease in concentration the dielectric effect would be minimized and the conductivity would assume a high value, while at the higher concentrations the dielectric effect and the electrophoretic effect would overcome the viscosity effect. This explanation would account for the lower average conductivities at the higher concentrations and the higher average conductivity at the lower concentrations.

The conventional plots of equivalent conductivity, Figs. 3 and 4 against $\sqrt{C}$ have the same general shape as those reported,[12] except that at the higher steam densities the curves obtained from results reported in this paper, retain shapes similar to those at the lower densities while in ref. 12 the higher densities became almost straight lines. Since the dielectric constant[13] at 0.50 density is 9.25 at 390°, it seems that NaCl should still be acting as a weak electrolyte.

It has been suggested by some investigators[11] that the density gradient observed in fluid systems near the critical point is due to gravitational effects. The authors here hesitate to emphasize this explanation since the differences between top and bottom still occur well above the critical temperature. Experiments have been planned to examine the rate at which equilibrium measurements are ob-

(13) J. K. Fogo, S. W. Benson and C. S. Copeland, *J. Chem. Phys.,* **22**, 209 (1954).
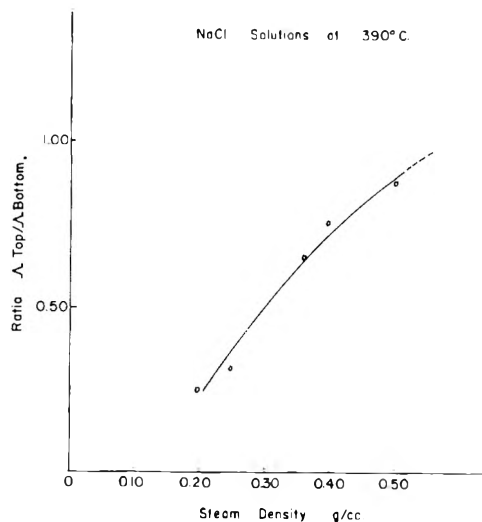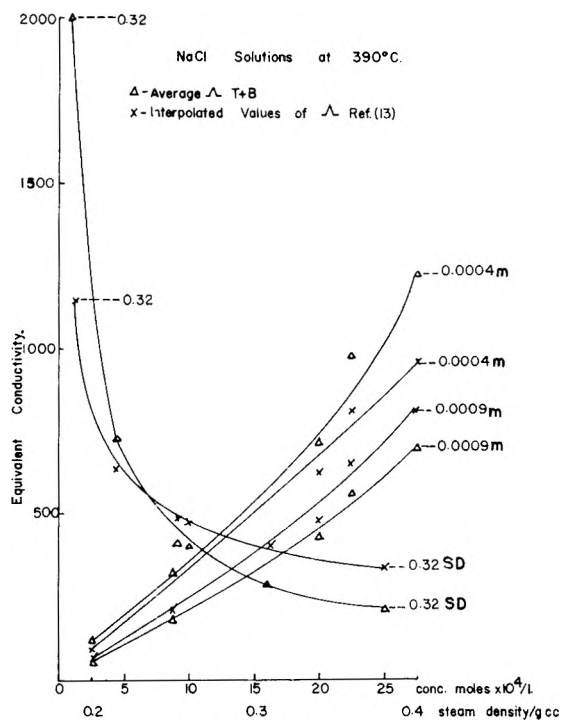
Fig. 6.

tained after an inversion of the furnace. It is hoped that a calculation of the difference in ionic "clump" size that would account for the separation would be reasonable and that gravitational attraction could be assigned to the separation.

Conclusions

The difference in conductivity, at the top and bottom in a high pressure vessel, of solutions of sodium chloride has been confirmed by a large number of measurements. A comparison of these results with a system made homogeneous by shaking shows that they are in the same order of magnitude. An explanation for the differences encountered in this comparison assumes a density gradient in the solution. An explanation of the reason for the gradient awaits further experimentation.

SELECTIVE LIQUID ADSORPTION WITH ALKALI METALS ON ACTIVE CARBON

BY W. F. WOLFF, PHILIP HILL AND G. D. McLEOD

Research and Development Department, Standard Oil Company (Indiana), Whiting, Indiana

Received November 30, 1959

Previous work has shown that the addition of metallic sodium or potassium improves the gas-adsorption characteristics of active carbon. To determine the liquid-adsorption characteristics of such carbons, percolation and batch-contacting techniques were applied to a study of the adsorption of toluene and of di-n-propyl sulfide from n-heptane. Improved liquid adsorption was observed with both sodium- and potassium-modified carbons. Calculations from the toluene–n-heptane data indicate that the alkali metal increases the selective-adsorption capacity of the carbon without affecting its selectivity. The changes in adsorption properties appear to result from modification of the pore structure of the carbon.

Introduction

When sodium or potassium is deposited on active carbon, compositions with improved gas-adsorption characteristics are formed. Optimum compositions may adsorb more than twice as much nitrogen at ordinary temperatures and pressures as the original carbon, and nitrogen can be selectively adsorbed from argon.[1] These changes in adsorption properties were attributed to the formation of narrow new pores in the carbon. They could also be explained in terms of preferential adsorption on the metal, or of electronic modification of the graphite-like carbon surfaces.[2]

To determine the effectiveness of these compositions in liquid separations and to explore further possible causes of the adsorption phenomena, selective liquid adsorptions have been carried out with unmodified carbons and with carbons modified by sodium, potassium or potassium hydroxide. Binary mixtures of n-heptane either with the corresponding seven-carbon aromatic hydrocarbon, toluene, or with the structurally analogous sulfide, di-n-propyl sulfide, were used. Percolation techniques were employed to establish the relative effectiveness of the carbons in separating both types of mixtures.

In order to obtain equilibrium data from which selective-adsorption capacities and selectivities could be calculated, batch-contacting techniques were applied to the adsorption of toluene from n-heptane, with an unmodified carbon and with the sodium-modified carbon. The adsorption capacities and selectivities were calculated by a method that has been used to study liquid separations with both alumina and silica gel.[3] Differences in the capacities and selectivities of the unmodified and sodium-modified carbons were expected to reflect the structural or electronic changes resulting from addition of the alkali metal.

Experimental

Two active carbons were used: a 12-to-20-mesh material from Burrell Corporation in the percolation runs, and an 8-to-14-mesh coconut charcoal from E. H. Sargent Company in the batch runs. Before use they were heated to 340° under a stream of high-purity nitrogen. Sodium- and potassium-modified carbons were prepared from them under a nitrogen atmosphere; the dried active carbon was stirred with the molten alkali metal until a visibly uniform product of essentially unchanged mesh size was obtained.[1,2] The concentration of metal was held at about the level that had been found to give optimum adsorption of inert gases.[1] The KOH-modified carbon was prepared by impregnating with an aqueous potassium hydroxide solution; the product was dried at 120° and then heated to 340° under a stream of high-purity nitrogen. All adsorbents were stored and used under nitrogen.

n-Heptane of 99+% purity from Phillips Petroleum Company was used in preparing the binary mixtures. Reagent grade toluene from Mallinckrodt Chemical Works and di-n-propyl sulfide from Eastman Kodak Company were used in the percolation runs. Toluene of 99+% purity from Phillips Petroleum Company was used in the batch runs.

Compositions of the toluene mixtures were calculated from the refractive indices. Refractive index data for known mixtures of toluene in n-heptane[4] were found to be satisfied by the derived equation

$$n^{20}\text{D} = 1.38764 + 0.10919 V_A - 0.0039 N_A N_B$$

where V_A is the volume fraction of toluene, and N_A and N_B are the mole fractions of toluene and n-heptane. The volume fraction and mole fractions in the equation were converted to weight fractions in order to obtain a functional relationship between the refractive index and the weight fraction of toluene, F_A. The resulting equation was solved on an electronic computer so as to obtain a table of index and weight-fraction values at intervals of $0.0005F_A$. The compositions of the propyl sulfide mixtures were calculated from the sulfur contents.

In the percolation runs, the unmodified carbon and compositions containing 10.1 weight % sodium, 9.1 weight % potassium, or 8.6 weight % potassium hydroxide were used. Thirty grams of adsorbent was charged, under nitrogen, to a percolation column 1.6 cm. in diameter; a packed section 32 cm. long was obtained. Solutions of 8.8% toluene in n-heptane or of 3.7% n-propyl sulfide in n-heptane were percolated through the adsorbent at a rate of 4 ml. per minute, and 55 ml. of percolate was collected and analyzed. The amount of toluene or propyl sulfide separated from the n-heptane then was calculated.

(1) W. F. Wolff and P. Hill, THIS JOURNAL, **63**, 1161 (1959).

(2) W. F. Wolff, *ibid.*, **63**, 1848 (1959); **62**, 829 (1958); **63**, 653 (1959).

(3) C. N. Rowe and R. W. Schiessler, *J. Am. Chem. Soc.*, **76**, 1202 (1954).

(4) We wish to thank R. W. Schiessler and C. N. Rowe for permission to use these data from the Ph.D. Thesis of C. N. Rowe, Pennsylvania State University, August, 1955.

Five series of batch runs were made with the unmodified carbon, and two series with the sodium-modified carbon. The sodium concentration was held at 11%. Unmodified carbon was dried or sodium-modified carbon was prepared directly in the three-necked 200-ml. flask to be used in selective adsorption. The flask was fitted with a Hershberg stirrer,[5] a gas-inlet stopcock, and a capillary gas vent with a removable stopcock. Temperatures were measured with a thermocouple bound to the bottom of the flask. The weight of adsorbent was determined from both the weight of the material charged and the change in weight of the flask assembly. All weighings of the flask assembly were carried out on a high-capacity analytical balance with both stopcocks closed to maintain the inert atmosphere.

In each run, high-purity nitrogen was passed slowly through the flask containing the weighed adsorbent. The vent stopcock was removed, n-heptane was introduced through the capillary with a hypodermic needle, and the increase in weight was determined. The procedure was then repeated with toluene. The mixture was stirred for about 45 minutes with cooling by a stream of air at about 27°. When thermal equilibrium had been attained, stirring was discontinued and the mixture was allowed to settle. Part of the supernatant liquid was withdrawn with a hypodermic needle, at a rate no faster than that at which nitrogen was being passed into the flask. The refractive index of this liquid was obtained on a refractometer with a precision of 0.00005.

In order that a series of equilibrations could be carried out with a single charge of adsorbent, the weight of the withdrawn liquid was determined and an additional weighed amount of toluene was introduced. The resulting mixture was stirred, and the equilibration and sampling procedure was repeated.

Results

The results of the percolation runs are given in Table I. The values for the separation of toluene and of propyl sulfide from n-heptane are consistent in that both binary mixtures place the adsorbents in the same order of effectiveness—best separations were obtained with the potassium-modified carbon, followed in order by the sodium-modified carbon, the unmodified carbon, and, finally, the KOH-modified carbon. Duplicate separations of toluene from n-heptane with the unmodified carbon agreed well.

The experimental results from the batch runs provide a basis for calculating selective-adsorption capacities and selectivities. If V^1_A is the volume fraction of the preferentially adsorbed component A in the equilibrium liquid phase[3]

$$V^1_A = \frac{V^1_A V^1_B W}{(V^i_A - V^1_A)X_v} Z_v - \frac{1}{\alpha - 1} \quad (1)$$

where V^1_B is the corresponding volume fraction of B, V^i_A is the volume fraction of A in the initial liquid, W is the weight of the adsorbent in grams, X_v is the volume of initial liquid in cubic centimeters, Z_v is the volume of selectively adsorbed liquid per gram of adsorbent, and α is the selectivity, defined[6] as $(N_A/N_B)^a/(N_A/N_B)^1$, in which N_A and N_B are the mole fractions of the components A and B, and superscipts a and 1 refer to the adsorbed and liquid phases, respectively. Equation 1 is based on the postulate that the volume of adsorbed liquid does not change with composition.[3]

If the weight of the adsorbed phase is assumed to be constant, equation 1 can be expressed in terms of weights and weight fractions

(5) F. B. Hershberg, *Ind. Eng. Chem., Anal. Ed.*, **8**, 313 (1936).

(6) B. J. Mair, J. W. Westhaver and F. D. Rossini, *Ind. Eng. Chem.*, **42**, 1279 (1950).
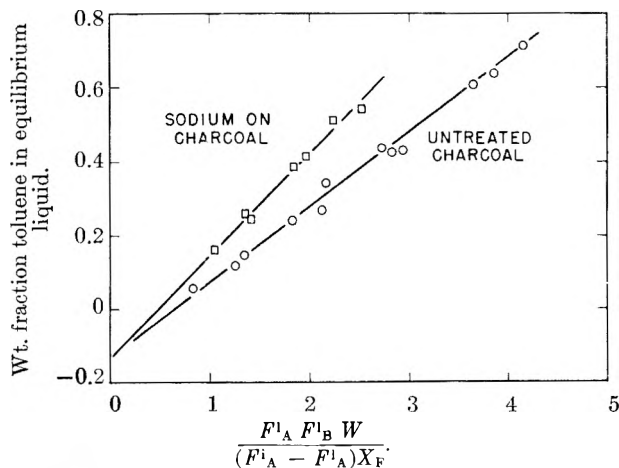

Fig. 1.—Determination of selective adsorption selectivities and capacities (toluene from n-heptane).

TABLE I

SELECTIVE ADSORPTION FROM n-HEPTANE WITH MODIFIED CARBONS

Modifier	% Adsorbed from percolate	
	Toluene	Propyl sulfide
None	47, 48	25
Sodium	58	85
Potassium	69	91
Potassium hydroxide	36	23

$$F^1_A = \frac{F^1_A F^1_B W}{(F^i_A - F^1_A)X_F} Z_F - \frac{1}{\alpha - 1} \quad (2)$$

where X_F is the weight of the initial liquid in grams, and Z_F is the weight of selectively adsorbed liquid per gram of adsorbent. The repeated weighings required by the experimental technique made it convenient to use equation 2 to calculate the adsorption capacities and selectivities. The equation was used in the form

$$F^1_A = \frac{F^1_A F^1_B W}{A^i - F^1_A (A^i + B^i)} Z_F - \frac{1}{\alpha - 1}$$

where A^i and B^i are the weights of components A and B contacted with the adsorbent. Thus, in making a series of runs with a single charge of adsorbent, the weight of the adsorbent W is determined directly; and F^1_A and F^1_B, the weight fractions of A and B in the equilibrium liquid, are determined from the refractive index of the liquid. In the first contacting, A^i and B^i are weighed out directly; the values for subsequent contacts are calculated readily from the initial weights of A and B, the weights and compositions of the liquids withdrawn, and the weights of additional portions of component A added to the mixture.

In this manner, the adsorption capacities Z_F and selectivities α for unmodified carbon and sodium-modified carbon were calculated from the data in Table II. Graphical solutions of equation 2, plotted in Fig. 1, showed

	Z_F	α
Unmodified carbon	0.203	8.7
Sodium-modified carbon	0.314	8.7

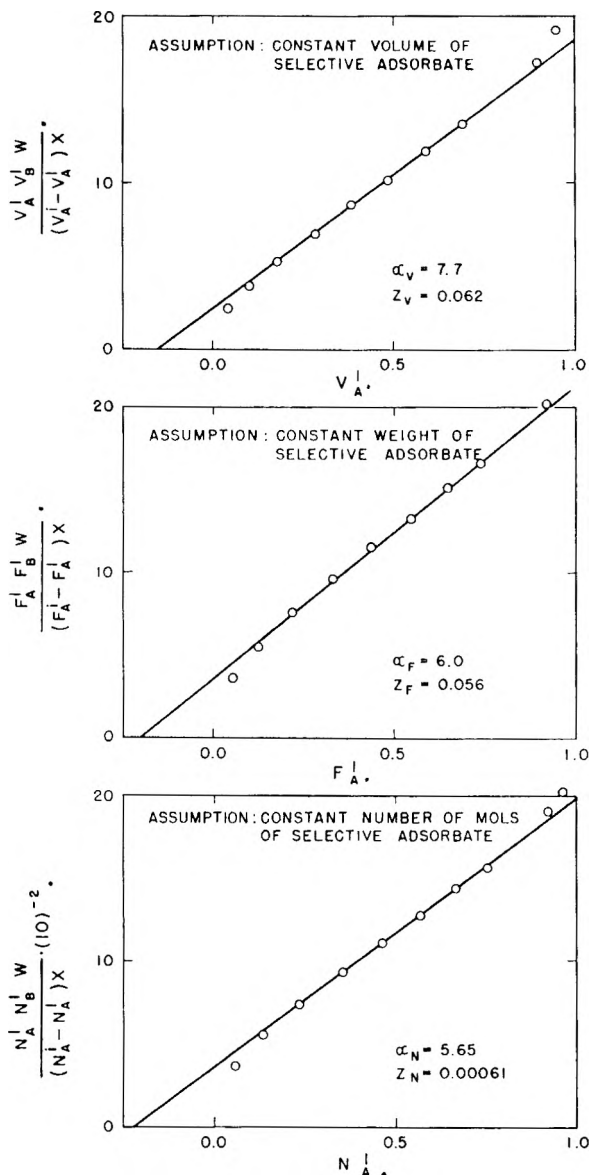where the capacity Z_F is expressed in terms of grams per gram of active carbon. These calculations indicate that sodium treatment increases the ad-

Fig. 2.—Effects of assumptions on calculated selectivities and capacities (toluene from n-heptane with alumina adsorbent).

TABLE II

SELECTIVE ADSORPTION OF TOLUENE FROM n-HEPTANE

(Batch runs at $27 \pm 2°$)

Adsorbent charged, g.	Liquid, charged g. Toluene	n-Heptane	Equilibrium liquid removed G.	n^{20}D
		Unmodified carbon		
13.7	11.52	26.83	0	1.4113
13.6	5.35	29.93	4.07	1.3978
0	5.28	0	7.34	1.4087
0	9.74	0	0	1.4278
13.75	15.69	18.44	3.51	1.4269
0	13.45	0	8.81	1.4467
0	13.12	0	0	1.4598
13.7	15.95	18.78	3.49	1.4270
0	17.41	0	0	1.4503
13.7	2.65	33.39	3.40	1.3919
0	4.23	0	4.03	1.4002
0	9.96	0	0	1.4186
		Sodium-modified carbon		
15.65	8.21	30.41	4.41	1.4014
0	4.48	0	7.15	1.4100
0	8.22	0	8.00	1.4258
0	8.04	0	0	1.4394
15.7	12.86	31.09	8.07	1.4092
0	7.91	0	8.38	1.4226
0	8.44	0	0	1.4357

sorption capacity of active carbon but has no effect on its selectivity.

Discussion

The results of the percolation runs agree with those previously reported for inert-gas adsorption.[1] The relative selective-adsorption activities of the unmodified, sodium-modified and potassium-modified carbons parallel their adsorption capacities for nitrogen and argon at room temperature. The poor selective adsorptions of toluene and propyl sulfide from n-heptane obtained with the KOH-modified carbon might be expected in view of the poor nitrogen-adsorption properties of NaOH-modified carbons.

Although the sodium-modified and unmodified carbons showed no significant difference in selectivity for the adsorption of toluene from n-heptane, previous work showed that potassium increases the selectivity of active carbon for the separation of

nitrogen from argon.[1] These results need not be considered inconsistent, but they challenge the validity of the assumption that the weight of selectively adsorbed liquid is constant. Two alternative assumptions, that the volume of selectively adsorbed liquid is constant[3] or that the number of moles of selectively adsorbed liquid is constant, would appear to be more reasonable from a theoretical point of view.

If the densities of the selectively adsorbed liquids are equal to their densities in the liquid phase, the volumes and volume fractions in equation 1 can be transformed to weights and weight fractions

$$F'_A = \frac{F'_A F'_B W}{(F'_A - F'_A)X_F} \frac{d_{B\alpha} - d_B}{d_{B\alpha} - d_A} d_A Z_v - \frac{d_A}{d_{B\alpha} - d_A} \quad (3)$$

where d_A and d_B are the densities of components A and B. Comparison of equations 2 and 3 shows that the selectivities and capacities calculated by assuming a constant weight of selectively adsorbed liquid are related to those for a constant volume of adsorbate by

$$\alpha_F = \alpha_v \frac{d_B}{d_A} \quad (4)$$

and

$$Z_F = \frac{d_B \alpha_v - d_B}{d_B \alpha_v - d_A} d_A Z_v \quad (5)$$

where selectivity is designated as either α_F or α_v, depending on the assumptions made in calculating it. For large values of α, or if d_A and d_B are about equal

$$Z_F \cong d_A Z_v \quad (6)$$

Similar relations can be derived for selectivities and capacities calculated by assuming a constant number of moles of selectively adsorbed liquid

$$\alpha_N = \alpha_v \frac{d_B M_A}{d_A M_B} \qquad (7)$$

$$Z_N = \left(\frac{d_B M_A \, \alpha_v - d_B M_A}{d_B M_A \, \alpha_v - d_A M_B}\right)\left(\frac{d_A}{M_A}\right) Z_v \qquad (8)$$

and

$$Z_N \cong \frac{d_A}{M_A} Z_v \qquad (9)$$

where M_A and M_B are the molecular weights of components A and B.

Direct evidence that equations 1 through 9 form a self-consistent set was obtained by independent calculation of Z_v and α_v, Z_F and α_F, and Z_N and α_N from the same set of data. The data are for the separation of toluene from n-heptane with an alumina adsorbent.[4] The values of Z_v and α_v were calculated by equation 1; Z_F and α_F were calculated by equation 2; Z_N and α_N were calculated from the corresponding equation in moles and mole fractions. The graphical solutions and values obtained are shown in Fig. 2; the values satisfy equations 4 through 9 within probable experimental error. Thus, the use of equation 2 in studying the selective adsorption of toluene from n-heptane seems justified, in that the capacity and selectivity are related in a known manner to Z_v and α_v, and Z_N and α_N.

According to equations 4 and 7, α_N, α_v and α_F are directly proportional to each other, the proportionality factor being a constant determined solely by the properties of the liquids. As the α_F values for the unmodified and sodium-modified carbons are identical, the α_v's, the α_N's, and thus, presumably, the true selectivities are also equal.

Conclusion

The unchanged selectivity and the increased adsorption capacity of the sodium-modified carbon are consistent with the postulate that the change in adsorption properties is primarily associated with changes in the pore structure of the adsorbent. Insofar as different surfaces might be expected to show different selectivities, the results fail to support the alternative hypotheses that the change in adsorption properties involves adsorption on the metal or electronic changes in the carbon.

The results of both the percolation and the batch runs appear consistent with the conclusions derived from the gas-adsorption studies.[1] Thus, present evidence favors the view that sodium and potassium cause structural changes in active carbon that improve its adsorption properties. The changes presumably involve the formation of new pores as well as the modification of existing ones. Other alkali metals, except lithium,[1] would be expected to cause similar changes.

DIFFUSION OF HYDROGEN IN THORIUM[1]

BY D. T. PETERSON AND D. G. WESTLAKE

Institute for Atomic Research and Department of Chemistry, Iowa State University, Ames, Iowa

The diffusivity of hydrogen in thorium was measured from 300 to 900°. Over this temperature range, $D = 2.92 \times 10^{-3} \exp(-9750/RT)$. The diffusivity increased with concentration above 600° but did not vary significantly with purity, grain size or cold working. Two different methods of determining diffusion constants were used and gave similar values.

Introduction

The effect of hydrogen on the tensile properties of thorium and the possible use of thorium containing hydrogen in nuclear applications made a measurement of the diffusivity of hydrogen in thorium valuable. No previous measurements of the diffusion constant have been reported. Diffusion was studied by measuring the rate of evolution of H_2 from cylindrical specimens and by determining the axial concentration gradient in effectively infinitely long cylinders. These methods were used rather than measurement of the permeability of a thorium diaphragm because the latter measurement is too often invalidated by contamination of the diaphragm surfaces.

Experimental

Materials.—The purity of the thorium used in this investigation is given in Table I. The Ames thorium was prepared by the method described by Wilhelm[2] and was hot rolled to 12 mm. square rod, cold swaged to 10 mm. diameter and vacuum annealed at 800°. The crystal bar thorium was made at the Ames Laboratory and arc-melted into a rod which was cold swaged to 9 mm. diameter and vacuum annealed. Cylindrical specimens were machined to size on a carefully cleaned lathe, washed in trichloroethylene, rinsed in acetone and dried. Pure hydrogen was generated by thermal decomposition of UH_3.

TABLE I
ANALYSIS OF THORIUM METAL

Element	Crystal bar Th, p.p.m.	Ames Th, p.p.m.
C	145	410
N	70	70
O	60	1300
Fe	20	130
Mn	..	20
Cr	20	20
Ni	20	20
Al	50	40
Ca	25	50
Mg	..	20
Si	..	55
Be	..	170

Apparatus.—The apparatus consisted essentially of a furnace section evacuated by a three stage mercury diffusion pump and a collection section of known volume in which the
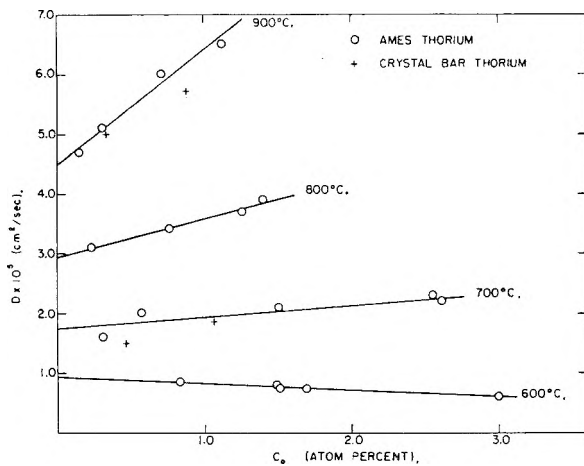
(1) Contribution No. 810. Work was performed in the Ames Laboratory of the U. S. Atomic Energy Commission.

(2) H. A. Wilhelm, "The Metal Thorium," ASM, Cleveland, Ohio, 1958.

Fig. 1.—Variation of the diffusivity of hydrogen with initial hydrogen concentration.

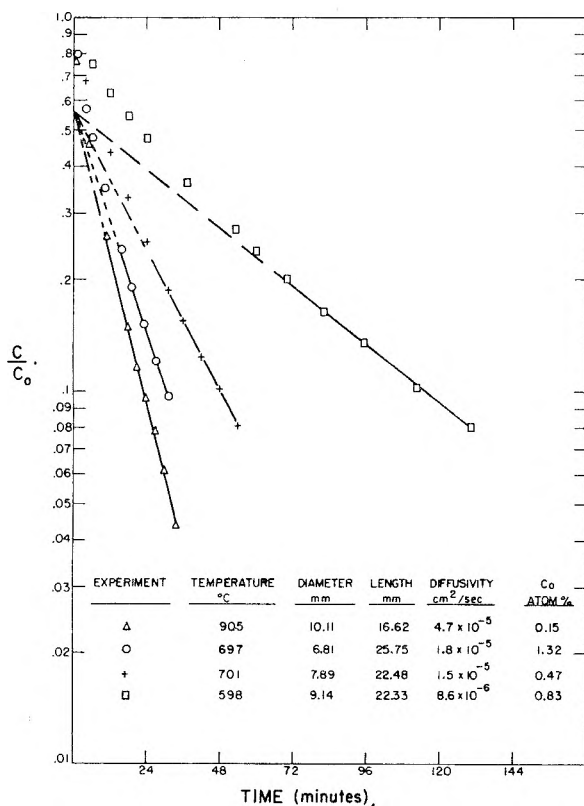| EXPERIMENT	TEMPERATURE °C	DIAMETER mm	LENGTH mm	DIFFUSIVITY cm²/sec	C₀ ATOM %
△	905	10.11	16.62	4.7×10^{-5}	0.15
○	697	6.81	25.75	1.8×10^{-5}	1.32
+	701	7.89	22.48	1.5×10^{-5}	0.47
□	598	9.14	22.33	8.6×10^{-6}	0.83

Fig. 2.—Evolution of hydrogen from a thorium cylinder.

gas evolved in the furnace section could be collected and the pressure measured. The furnace section was a horizontal Vycor tube extending through the furnace. The sample could be moved into and pushed out of the furnace by a Vycor rod. This rod had an iron rod sealed in one end and was manipulated with a magnet. The pressure in this section was measured with a manometer and a Miller Laboratories cold cathode gage. A large bore stopcock allowed the furnace section to be isolated from the diffusion pump and a liquid nitrogen trap prevented mercury vapor from the pump from reaching the sample. The collection section had a McLeod gage with a range of one to 4500 μ to measure the pressure and an auxiliary volume which could be used to hold larger volumes of gas. A mercury cut-off was used to isolate the collection section from the mechanical pump.

Procedure. (a) **Evolution Method.**—A specimen was placed in the tube and the furnace section evacuated with the furnace at the desired temperature until a pressure of 5×10^{-7} mm. was reached. The quantity of hydrogen

necessary to give the desired concentration in the specimen was admitted to the furnace section and the specimen moved to the center of the furnace and held at temperature until the concentration was uniform. The stopcock between the furnace section and the mercury diffusion pump then was opened. The diffusion pump rapidly evacuated the furnace section and maintained a pressure such that the concentration at the surface of the specimen was essentially zero. The hydrogen evolved was collected in the collection section and the pressure measured periodically. When the evolution rate had become very low, the furnace temperature was raised to 850° to extract all of the hydrogen so that the initial concentration in the sample could be measured. The measured pressures were corrected for the amount of hydrogen in the furnace section due to the equilibrium pressure over the specimen.

A solution of Fick's law for these initial and boundary conditions is given by Demerez.[3] The diffusivity was calculated from the slope of the linear portion of the log $\bar{C}/C_0$ vs. time curve. The assumption that diffusion was the rate-controlling process was verified by measuring the evolution rate with specimens of the same length and from 6 to 11 mm. in diameter; the observed diffusivity did not vary with diameter which indicates that the evolution rate was controlled by diffusion and surface reaction rates were not interfering. However, if the sample surface were contaminated by incomplete degassing of the furnace tube or use of abrasive paper to prepare the surface, the evolution rate was much slower and log $\bar{C}/C_0$ did not become linear with time. The specimen surface was usually darker after runs in which this occurred and the evolution rates were not reproducible. Thus, surface contamination could be detected and the results of such experiments rejected. The evolution method did not give satisfactory results below 600°, and surface contamination was much more frequent at 600° than at higher temperatures.

(b) **Absorption Method.**—A specimen, 9 mm. diameter by 60 mm. long, was placed in the furnace tube, the furnace section degassed to 5×10^{-7} mm. and the specimen moved into the center of the furnace and heated for one hour at 800°. The furnace was adjusted to the desired temperature, and an amount of hydrogen sufficient to form a hydride layer about 0.2 mm. thick was allowed to react with the sample. After a measured length of time, the specimen was pushed from the furnace and cooled. The thorium hydride layer was removed by machining on a lathe and annular sections, excluding the portion 10 mm. from each end, were turned off. The turnings from each section were analyzed for hydrogen by warm extraction at 850°. The ratio $(C - C_0)/(C_s - C_0)$, was plotted against r/a, where C was the hydrogen concentration in the annular section whose mid-point was a distance r from the center, C_s was the constant surface concentration, C_0 was the initial hydrogen content (in this case, zero) and a was the radius of the cylinder. The value of C_s was determined by trial and error so that the experimental curves fit the curves given by Crank.[4] The appropriate value of Dt/a^2 was estimated and the diffusivity, D, calculated.

Results and Discussion

The diffusivity of hydrogen above 600° measured by the evolution method increased with the initial hydrogen concentration. The values at each temperatures are plotted in Fig. 1 against the initial hydrogen concentration. The variation with concentration at 600° was small, in fact, hardly more than the experimental uncertainty. At 900°, the variation was much larger. Whether the diffusivity remained independent of or decreased with increasing concentration below 600° could not be determined as the evolution method did not give reproducible results below this temperature. Although the solution of Fick's law which was used was based on a constant diffusivity, the evolution

(3) A. Demerez, A. G. Hock and F. A. Meurier, *Acta Met.*, **2**, 214 (1954).

(4) J. Crank, "Mathematics of Diffusion," Oxford University Press, Oxford, England, 1956.

curves (several are shown in Fig. 2) followed the expected form. Because the concentration of the specimen was changing continuously during an evolution experiment, the observed diffusivity must be some mean value for a range of concentrations below the initial concentration.

The logarithm of the diffusivity, extrapolated to zero hydrogen concentration, was plotted against reciprocal temperature in Fig. 3. The values obtained from the concentration gradient method were included on this figure. The data fell very close to a straight line and were fit by least squares to a relationship $\log D = -2.536 - 2134/T$. The value of D_0 was 2.92×10^{-3} cm.^{2}/sec. and $\Delta H = 9.75$ kcal.

The concentration gradient measurements gave no indication of a concentration dependence of the diffusivity. A typical gradient is shown in Fig. 4. A small change of D with concentration would not be detected but, if D changed by a large amount, the data would not have fit any of the theoretical curves. The concentration gradient measurement does not involve a surface reaction and, consequently, the observed values would not be influenced by a slow surface reaction of hydrogen gas. As the diffusivities determined by both methods fit the same temperature dependence equation, the assumption that the evolution rate was diffusion controlled is strongly supported.

The surface concentration observed in the concentration gradient samples should be the saturation solubility of ThH_2 in thorium if the surface concentration were constant during the experiment as postulated as one of the boundary conditions. In Table II are given C_s and the solubilities of ThH_2 in crystal bar thorium reported by Peterson and Westlake.[5] The solubility in crystal bar thorium should be close to the lattice solubility, whereas the apparent solubility in Ames thorium reported by these investigators was the lattice solubility plus the hydrogen precipitated as a more stable thorium–hydrogen–carbon ternary compound. The close agreement of C_s and the solubility confirms the validity of this boundary condition.

TABLE II
SURFACE CONCENTRATION IN GRADIENT SPECIMENS AND SOLUBILITY OF ThH_2 IN THORIUM

Temp., °C.	C_s, atom% hydrogen	Solubility
298	0.90	0.84
409	2.3	2.6
504	5.5	5.5
602	9.0	9.6

Purity, grain size and cold work had only small effects on the rate of diffusion. The results of four evolution experiments with crystal bar thorium are given in Fig. 1. Although the values are all lower than for Ames thorium, the difference is not appreciably greater than the experimental error. The diffusivity in cast Ames thorium, grain size 25 grains per sq. mm., was 2.7×10^{-5} at 800° compared to 3.1×10^{-5} for swaged and annealed metal with a grain size of 2600 grains per sq. mm.

(5) D. T. Peterson and D. G. Westlake, *Trans. AIME,* **215**, 444 (1959).
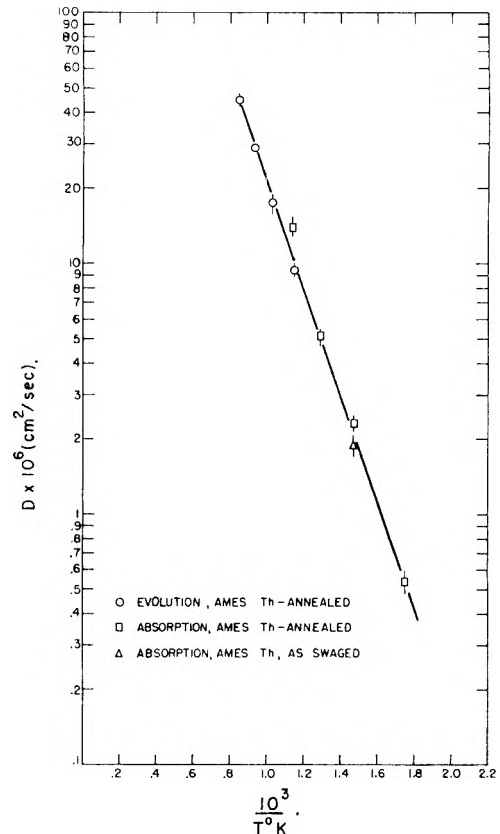
Fig. 3.—Logarithm of the diffusivity of hydrogen vs. reciprocal temperature.
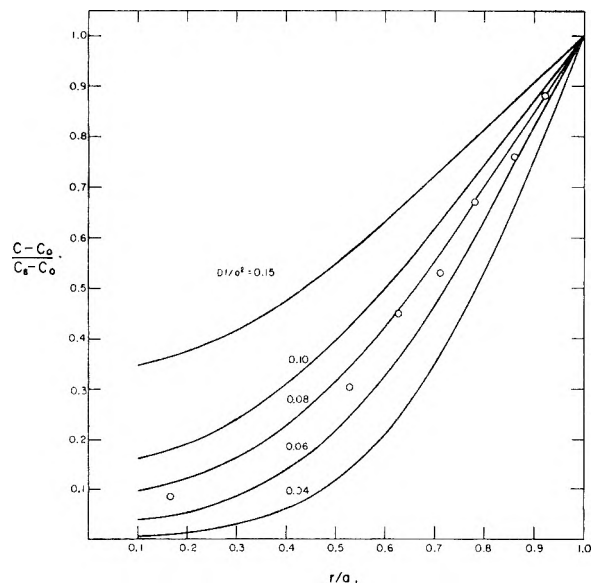
Fig. 4.—Typical radial concentration gradient in an infinitely long thorium cylinder.

This small difference between samples with greatly different grain size indicates that grain boundary diffusion is of minor importance. The solubility and rate of diffusion of hydrogen in some metals are very sensitive to cold working. This was not found for thorium as at 409° the diffusivities in cold swaged and in annealed metal were 1.9×10^{-6} and 2.3×10^{-6}, respectively, and the same surface concentration was found in both specimens.

ELECTROMOTIVE FORCE STUDIES IN AQUEOUS SOLUTIONS AT ELEVATED TEMPERATURES. I. THE STANDARD POTENTIAL OF THE SILVER–SILVER CHLORIDE ELECTRODE[1]

By Richard S. Greeley, William T. Smith, Jr., Raymond W. Stoughton and M. H. Lietzke

Contribution from the Chemistry Division, Oak Ridge National Laboratory,[2] Oak Ridge, Tennessee, and the Department of Chemistry, University of Tennessee, Knoxville, Tennessee

The electromotive force of the cell Pt–H$_2$(p) |HCl(m) |AgCl–Ag was measured at temperatures from 25 to 200° and in some cases to 275° using hydrochloric acid concentrations from 0.005 to 1.0 m and hydrogen pressures of about one atmosphere. A closed, static, high pressure system was used which consisted of a fused silica vessel contained tightly in a steel autoclave with a Teflon interliner. The measurements were reproducible to within ±0.5 mv. from 25 to 225°, ±2 mv. at 250°, and ±5 mv. at 275°. At 25 to 90° the results agreed satisfactorily with previous investigations. Calculations were made of the standard potential of the silver–silver chloride electrode and the resulting values may be expressed by $E^0 = 0.23735 - 5.3783 \times 10^{-4}t - 2.3728 \times 10^{-6}t^2$ volts with a standard error of fit of 0.19 mv. from 25 to 200°.

Introduction

The standard electrode potential of the silver–silver chloride electrode has been measured from 0 to 60° by Harned and Ehlers[3,4] and from 0 to 95° by Bates and Bower,[5] but no measurements of the standard potential at higher temperatures have been reported. Since the silver–silver chloride electrode shows promise of being useful as a reference electrode at temperatures well above 100°,[6] it was decided to determine its standard potential to as high a temperature as possible. Also, it was of interest to study the behavior of the hydrogen electrode at elevated temperatures. Therefore, the cell

$$\text{Pt–H}_2(p)/\text{HCl}(m)/\text{AgCl–Ag}$$
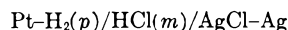
was investigated over the concentration range 0.005 to 1.0 m HCl, the temperature range 25 to 275°, and at hydrogen pressures of about one atmosphere.

Experimental

The Autoclave Assembly.—The primary containment vessel for the solution was a cylindrical liner made of fused silica for corrosion resistance. It fitted into a Teflon interliner which in turn fitted snugly into a type 347 stainless steel autoclave. The Teflon interliner, having a relatively high coefficient of thermal expansion, expanded as the autoclave was heated and filled the space between the steel body and the quartz liner completely. This prevented condensation of water vapor between the liner and the body. A lip on the Teflon interliner served as a gasket for sealing the autoclave head to the autoclave body. The total volume of the autoclave available for solution and vapor was 160 ml.

Corrosion of the silica liner and other silica parts was measured during several tests and it was found that the rate was low enough to be neglected as a source of error. For instance, in 0.0075 m HCl the loss in weight of all of the silica exposed to solution in a 36-hour test to 225° was 0.3 mg. The Teflon interliner was also a possible source of

contamination since it was observed previously at this Laboratory that Teflon evolves low molecular weight material at temperatures as low as 150°.[7] Consequently the interliners were heated to 275° in a trial run before use in an actual test.

The autoclave head was machined from commercially pure titanium and is shown in detail in Fig. 1. A valve was installed directly in the head which allowed the vapor space to be evacuated through the stainless steel capillary tube. Hydrogen was also vented through this line during the initial bubbling. A platinum capillary tube connecting the autoclave interior with the pressure gauges was inserted through the center of the titanium valve stem and was sealed in at the top of the valve stem with a Teflon gasket and a steel nut. The platinum capillary tube was connected at its other end to a two-way, two-stem autoclave valve mounted outside of the oven which in turn was connected to the hydrogen supply system and to the pressure gauges. The electrode leads were passed through the bomb head as shown in Fig. 1 and were connected to the electrodes by firm crimping.

The titanium autoclave head was resistant to corrosion by the vapor above the acid solutions under all conditions except during the tests with 0.5 and 1.0 m HCl. Above 225° with the former and 125° with the latter solution an increase in pressure with time at constant temperature was noticed. The extent of the reaction was followed by the change of pressure and e.m.f. with time and the results were corrected as discussed below. On opening the autoclave after the two tests in which corrosion occurred, a white deposit, determined spectrographically to be TiO$_2$, was found on the titanium. Therefore the corrosion reaction was assumed to be

$$\text{Ti} + 2\text{H}_2\text{O} \longrightarrow \text{TiO}_2 + 2\text{H}_2 \qquad \text{(A)}$$
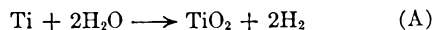
Agreement was obtained between the observed pressure increase and the pressure increase calculated from the change in solution concentration due to the loss of water in accordance with reaction (A).

The titanium autoclave head was held onto the autoclave body by eight steel lugs supported in a stainless steel cap screwed onto the autoclave body. The lugs acted on a Belleville spring washer designed so that the thermal expansion and contraction of the Teflon gasket (the lip on the Teflon interliner) was matched by compression and expansion of the spring.[8]

The Oven and the Measuring Equipment.—The autoclave was placed in a large, cylindrical, aluminum block inside an electrically heated, forced-draft oven which was controlled to within ±1°. Within the autoclave this temperature fluctuation was smoothed to less than ±0.001°. The temperature of the autoclave head was measured with a platinum resistance thermometer inserted in the thermowell shown in Fig. 1. The thermometer had been calibrated by the National Bureau of Standards at the ice,

(1) Based on a thesis submitted by R. S. Greeley in partial fulfillment of the requirements for the degree Doctor of Philosophy, University of Tennessee. Presented at the 135th Meeting of the American Chemical Society, Boston, Mass., April 6, 1959.

(2) Operated for the United States Atomic Energy Commission by the Union Carbide Corporation.

(3) H. S. Harned and R. W. Ehlers, *J. Am. Chem. Soc.*, **54**, 1350 (1932).

(4) H. S. Harned and R. W. Ehlers, *ibid.*, **55**, 2179 (1933).

(5) R. G. Bates and V. E. Bower, *J. Research Natl. Bur. Standards*, **53**, 283 (1954).

(6) M. H. Lietzke and J. V. Vaughen, *J. Am. Chem. Soc.*, **77**, 876 (1955); R. N. Roychoudhury and C. F. Bonilla, *J. Electrochem. Soc.*, **103**, 241 (1956); V. Prazák, *Werkstoffe u. Korrosion*, **9**, 524 (1958).

(7) W. C. Waggener, Oak Ridge National Laboratory, private communication.

(8) J. O. Almen and A. Laszlo, *Trans. Am. Soc. Mech. Engrs.*, **58**, 305 (1936).

steam and sulfur points and the ice point was rechecked before each run.

Pressures were measured using two Heise precision bourdon gages connected with water-filled stainless steel capillary tubes to the valves and to the platinum capillary discussed above. One of the gauges had a range 0 to 250 p.s.i.g. and an accuracy of 0.25 p.s.i. It was used at temperatures to 200°. The other gauge had a range 0 to 1000 p.s.i.g. and accuracy of 1 p.s.i. The gauges were calibrated using a Consolidated Electrodynamics Corp. primary pressure standard of the pneumatic dead weight type.

The e.m.f. was measured with an Applied Physics Corp. Model 30 vibrating reed electrometer and a Rubicon type B potentiometer, and was displayed on a Brown recording potentiometer. The e.m.f. values were precise to ±0.02 mv.

The Electrodes.—The hydrogen electrode was made to float at the surface of the solution in order to come quickly to equilibrium with the hydrogen in the vapor phase. A 1-in. length of 24 gauge platinum wire was attached to a projection on a fused silica float with fine 40 gauge platinum wire and formed around the float so as to be held at the surface of the solution and parallel to it. Another fine platinum wire was welded onto the 24 gauge wire in order to connect it with the platinum lead wire in the autoclave head. The platinum was platinized as directed by Bates.[9] On several occasions the floating electrode was compared with a foil electrode, prepared in the usual way,[10] in dilute hydrochloric acid saturated with hydrogen. The two types of electrodes exhibited the same potential to within ±0.02 mv.

The silver–silver chloride electrodes were of the thermal type.[11] For the first series of tests, which went only to 200°, a four-inch length of $^1/_8$ in. dia. o.d. soft glass tubing was used to support the platinum wire of the electrode. Six electrodes were prepared simultaneously, and, after cooling, they were immersed in hydrochloric acid of the same composition as that to be used in the test, and interconnected. The solution was heated to 75° and allowed to cool overnight as suggested by Ashby, Crooke and Datta.[12] The next day the electrodes were within ±0.05 mv. of each other. Two electrodes reading within 0.02 mv. of the average were chosen for the experiment and fastened onto the platinum leads through the autoclave head.

It was found that dilute hydrochloric acid attacked the soft glass electrode support at 250°. Therefore, in the succeeding series of tests, which went to 275°, the soft glass holder was omitted and the entire length of the platinum wire electrode was coated with the silver–silver chloride deposit. Only one pair of these electrodes was made and they were used for the entire second series of experiments covering the range 25 to 275°. Thermal cycling appeared to improve the characteristics of these electrodes. With care being taken to avoid mechanical strain, the results at all temperatures in common with the first series were entirely comparable.

A silica tube containing a sintered silica disk was placed around each silver–silver chloride electrode. Excess solid silver chloride was placed inside the silica tube prior to each run.

The Solutions and Materials.—All solutions were made from conductivity water; all apparatus was given final rinsings with the same; and all chemicals were recrystallized or washed in conductivity water as deemed necessary. The hydrochloric acid solutions were made up by weight dilutions from twice-distilled constant boiling hydrochloric acid which had been analyzed gravimetrically and found to agree with values given by Foulk and Hollingsworth.[13] Silver oxide was made according to the procedure given by Bates[14] and was washed twenty-five times with distilled water and ten times with conductivity water. Silver chlorate was made according to the procedure given in "Inorganic Syntheses."[15] Silver

(9) R. G. Bates, "Electrometric pH Determinations," John Wiley and Sons, Inc., New York, N. Y., 1954, p. 167.

(10) Ref. 9, p. 166.

(11) C. K. Rule and V. K. LaMer, J. Am. Chem. Soc., **58**, 2339 (1936).

(12) J. H. Ashby, F. M. Crooke and S. P. Datta, Biochem. J., **56**, 190 (1954).

(13) C. W. Foulk and M. Hollingsworth, J. Am. Chem. Soc., **45**, 1223 (1923).
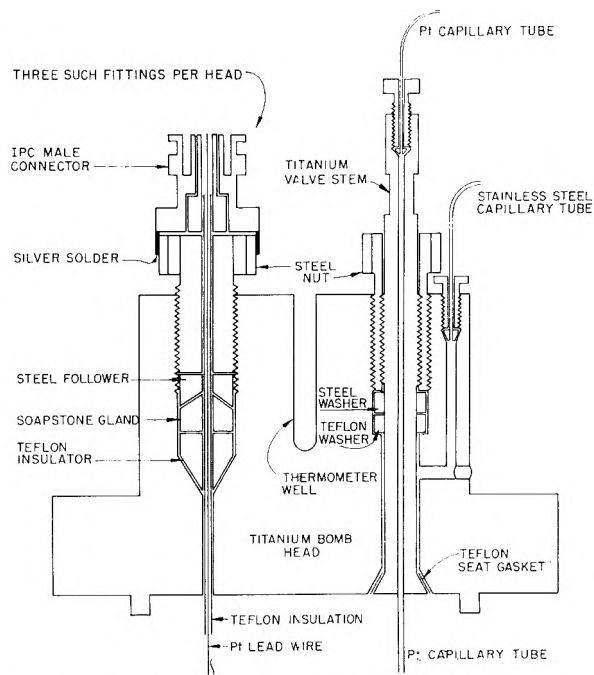
(14) R. G. Bates, ref. 9, p. 206.

Fig. 1.—Titanium bomb head for use with autoclave assembly.

chloride was made according to the procedure given by Zimmerman[16] except that the starting material was Baker and Adamson reagent grade silver nitrate. The absence of bromide from all solutions and silver compounds was checked by the method of Pinching and Bates.[17] Electrolytic hydrogen obtained in commercial cylinders was passed over Ascarite, Drierite and a platinized catalyst bed before passing through two bubble towers containing solutions identical to that under test and then into the autoclave.

General Procedure.—After the autoclave containing the electrodes and solution had been put into the aluminum block in the oven and all connections made, the vapor space was evacuated and hydrogen was admitted carefully. The process was repeated twice and then hydrogen was bubbled through the solution for several hours (titration of the solution before and after this procedure in several trials showed that the concentration changed less than one part per thousand). When the chart record of the e.m.f. showed that equilibrium was attained, the valve in the head of the autoclave was closed, the hydrogen supply was shut off, and the valve to the pressure gages was opened. An initial reading of temperature, pressure and electromotive force was taken, and then the temperature was raised to the next level desired. After equilibrium, the second set of readings was taken and the temperature again raised.

After the final set of readings had been taken at the highest temperature, the oven was cooled to room temperature and another set of readings taken. It should be noted that the autoclave was entirely static during the test and that hydrogen was bubbled through the solution only at the beginning of the test, not during any of the subsequent measurements.

Results and Calculations

Temperature and Concentration Range.—The first series of tests was conducted on seven solutions from 0.005 to 1.0 m HCl at 25, 60, 90, 125, 150, 175 and 200°. Several duplicate tests were made and the e.m.f. values taken at the same temperature were reproducible to within about ±0.4

(15) D. C. Nicholson and C. E. Holley, Jr., "Inorganic Syntheses," Edited by W. C. Fernelius, Vol. 11, 1st Ed., McGraw–Hill Book Co., New York, N. Y., 1946, p. 4.

(16) W. Zimmerman, III, J. Am. Chem. Soc., **74**, 852 (1952).

(17) G. D. Pinching and R. G. Bates, J. Research Natl. Bur. Standards, **37**, 311 (1946).

mv. In one test, measurements were made during both ascending and descending temperatures with good agreement between values taken at the same temperature, but otherwise measurements were made only during ascending temperatures (except for the final measurement at room temperature). Agreement between initial and final values at 25° averaged 0.5 mv.

In the second series of tests, measurements were extended to include 225, 250 and 275° (the 60 and 90° points generally were omitted) with nine solutions from 0.005 to 0.5 m. A 1.0 m solution was measured to 200°.

Molality and Ionic Strength of the Solutions.— It was found that, besides the two tests in which corrosion occurred, the e.m.f. did not stay constant after thermal equilibrium had been attained at the higher temperatures, but showed a steady, linear decrease with time. This effect was noticed by Anderson[18] and he attributed it to the reduction of silver ion by hydrogen. This reaction both increased the acid concentration and decreased the hydrogen pressure according to the reaction

$$^1/_2H_2 + AgCl \longrightarrow Ag + HCl \qquad (B)$$
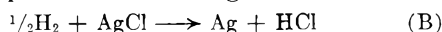
The rate of the reaction increased with increasing temperature and with decreasing acid concentration.

Since no provision was made for sampling the solution at the time of each measurement, it was found necessary to calculate the concentration of the solution from the slope of the recorder trace of e.m.f. vs. time. Therefore each measurement of temperature, pressure and e.m.f. was delayed until the slope of the recorder trace had been established after attainment of thermal equilibrium. Table I is a list of the rate of change of the e.m.f. and the total extent of the change at each temperature for several of the tests. The change in e.m.f. was assumed to be due entirely to reaction B at 0.01 to 0.2 m and to reaction A at 0.5 and 1.0 m, since no corrosion was observed below 0.5 m and since the estimated rate of reaction B at 0.5 and 1.0 m was negligible. The total extent of the change depended on the time the system was held at each temperature as well as on the rate of change.

The values listed in columns three and four of Table I were corrected for the change in e.m.f. due to the increase or decrease in hydrogen pressure and the corrected change in e.m.f. then was converted to the change in molality during the period of measurement by the equation

$$\Delta m = m \left[\left(\text{antilog} \frac{F}{4.6RT} \Delta E \right) - 1 \right] \qquad (1)$$

These changes in molality are listed in column five of Table I and were cumulative during each run. Molality changes during temperature changes were calculated using an average value of the e.m.f.– time slope determined at the upper and lower temperatures. No changes in concentration occurred below the lowest temperature listed for each concentration.

A check on the calculation at each temperature during a test was obtained by adding up all the

(18) N. J. Anderson, Ph.D. thesis, University of Chicago, Chicago, Ill., 1945, p. 12–17.

TABLE I

RATE AND EXTENT OF REACTIONS A AND B DURING SEVERAL TESTS

Concn., m	Temp., °C.	Rate of change of e.m.f. mv./hr.	Total change in e.m.f., mv.	Calcd. equiv. change in molality, parts/ thousand
0.01[a]	175	0.25	0.50	6
	200	0.51	1.27	16
	225	2.79	3.95	52
	250	5.0	7.1	149
0.05[a]	200	0.30	2.33	29
	225	0.57	1.53	20
	250	1.17	1.46	17
	275	2.0	7.0	77
0.1[a]	200	0.07	0.20	2
	225	.20	0.40	5
	250	.41	1.62	19
	275	.8	1.2	13
0.2[a]	250	.08	0.80	9
	275	.63	2.51	27
0.5[b]	250	.33	2.97	6
	275	1.18	7.87	15
1.0[b]	125	0.17	1.80	1
	150	0.89	6.00	5
	175	1.78	6.60	5
	200	1.73	1.87	1

[a] Reaction B: $^1/_2 H_2 + AgCl \rightarrow HCl + Ag$. [b] Reaction A: $Ti + 2H_2O \rightarrow 2H_2 + TiO_2$.

changes in molality and comparing the result with the value obtained by titrating the solution after the run. The agreement between calculated and titrated concentrations averaged 0.6% in the first series and 2.4% in the second series.

A further correction to the molality was made necessary by the increase in concentration due to the loss of water from solution to the vapor space. This was calculated from the vapor density of steam[19] and the vapor volume (calculated assuming that the expansion of the solutions with temperature was equal to that of pure water).

An additional factor, for which no correction was made, was the presence of hydrogen chloride in the vapor phase above solutions. In two preliminary experiments the vapor above 0.01 and 0.1 m HCl was sampled at 200 and 250° and the chloride content of the condensate determined by radioactivation analysis. The samples were withdrawn dropwise through a water-cooled platinum capillary tube fitted into the bomb head in place of one of the electrodes. It was found that the vapor space contained 0.2% or less of the total hydrogen chloride originally present.

Lietzke and Stoughton have pointed out[20] that it is necessary to know the solubility of silver chloride as a function of temperature and hydrochloric acid concentration in order properly to interpret the electromotive force data. Hence the recent solubility values of Raridon[21] were fitted by

(19) "VDI-Wasserdampftafeln," Edited by E. Schmitt, 4th Ed. Springer-Verlag, Berlin, 1956.

(20) M. H. Lietzke and R. W. Stoughton, J. Am. Chem. Soc., **79**, 2067 (1957).

(21) R. J. Raridon, Ph.D. thesis, Vanderbilt University, Nashville, Tenn., 1958, p. 93.

the method of least squares[22] to equations which enabled the solubility of silver chloride to be obtained as needed for the succeeding calculations. Complete dissociation of HCl and AgCl was assumed in all of the calculations and the solution was assumed to be saturated with silver chloride.

Hydrogen Pressure.—The hydrogen pressure was obtained by subtracting the vapor pressure of the solution from the observed total pressure. The former was obtained by taking the vapor pressure of pure water at the temperature of measurement from the steam tables[19] and correcting for the presence of the HCl in solution by Raoult's law. A further minor correction was the effect of the presence of hydrogen on the vapor pressure of the solution. This correction was calculated from the formula

$$\Delta P_{H_2O} = (\bar{v}/RT)P_{H_2O} \times P_{H_2} \quad (2)$$

where $\bar{v}$ is the molal volume of liquid water, R is the gas constant, T is the absolute temperature, P_{H_2O} is the steam pressure in the absence of hydrogen, and P_{H_2} is the hydrogen pressure.

Each experimental e.m.f. value was then corrected to exactly 1.00 atm. hydrogen pressure by subtracting the Nernst term $(RT/2F) \ln f_{H_2}$ in which the hydrogen fugacity f_{H_2} was taken to be equivalent to the hydrogen pressure.

In order to get an idea of the magnitude of the error involved in taking the fugacity to be equivalent to the pressure, equations 19 and 33b of Hildebrand and Scott[23] were used to make a detailed calculation for one temperature, viz., 200°. An average value of the hydrogen pressure was taken, 1.600 atm., and the fugacity found to be 1.642 atm. The corresponding correction to the electromotive force would be +0.56 mv. Therefore the error may be significant, although there are no experimental data at 200° presently available to confirm the calculation. The data of Pollitzer and Strebel[24] taken at 50 and 70° would indicate the error to be considerably less than that calculated.

Calculation of $E^{0''}$.—The further treatment of the data was similar to that of Bates and Bower,[5] and a Debye–Hückel equation in extended form was used

$$\log \gamma \pm = -\frac{1.8252 \times 10^6 \sqrt{\rho_0 I}}{(DT)^{3/2}(1 + A\sqrt{\rho_0 I})} +$$
$$BI - \log(1 + 0.03604m) + Ext \quad (3)$$

where ρ_0 = density of water, D = dielectric constant of water,[25] T = absolute temperature, I = ionic strength of solution = $m_{HCl} + s_{AgCl}$ (i.e., the sum of the molalities of HCl and AgCl), A = denominator coefficient = $50.2904 (DT)^{-1/2} \mathring{a}$, $\mathring{a}$ = ion size parameter, B = linear term coefficient, $\log(1 + 0.03604m)$ = corrn. from rational to practical scale, Ext = extended terms of Gronwall, LaMer and

(22) M. H. Lietzke, "An ORACLE Code for Least Squares," Oak Ridge National Laboratory—CF-59-2-20, Feb. 4, 1959.

(23) J. H. Hildebrand and R. L. Scott, "The Solubility of Nonelectrolytes," 3rd ed., Reinhold Publ. Corp., New York. N. Y., 1950, Chapter XIV.

(24) F. Pollitzer and E. Strebel, Z. physik. Chem., **110**, 768 (1924).

(25) G. C. Åkerlöf and H. I. Oshry, J. Am. Chem. Soc., **72**, 2844 (1950).

Sandved.[26] The values of the fundamental constants were taken from Cohen, Crowe and Dumond.[27] Inserting equation 3 into the Nernst equation and collecting terms, $E^{0''}$ is defined as

$$E^{0''} = E + \frac{2RT}{F} \ln m\pm + 2.3026 \frac{2RT}{F}$$
$$\left[\frac{-1.8252 \times 10^6 \sqrt{\rho_0 I}}{(DT)^{3/2}(1 + A\sqrt{\rho_0 I})}\right] + Ext' \quad (4)$$

where E = e.m.f. at 1 atm. H_2 at temperature T, $m\pm$ = mean molality of solution = $[m_{H^+} m_{Cl^-}]^{1/2} = [(m_{HCl})(m_{HCl} + s_{AgCl})]^{1/2}$, and $Ext' = 2.3026 (2RT/F) [Ext - \log(1 + 0.03604m)]$.

A set of $E^{0''}$ values was calculated for all of the electromotive force values for each of several values of the ion size parameter $\mathring{a}$. The $\mathring{a}$ values were varied in 1 Å. increments over a wide range at each temperature. Each set of $E^{0''}$ values then was fitted at each temperature by the method of least squares to

$$E^{0''} = E^0 + bI \quad (5)$$

for concentrations up to and including 0.1 m where E^0 is the standard potential of the silver–silver chloride electrode. Finally, the standard errors of fit (σ_{fit}) from the least squares lines at each temperature were plotted versus $\mathring{a}$ and that value of $\mathring{a}$ which gave the lowest σ_{fit} was taken to be the correct value.

Determination of E^0 and B.—Having assigned the value of $\mathring{a}$ at each temperature, the values of E and b became established from the intercept and slope of the least squares line. The value of the linear term coefficient B was calculated from $B = -b(F/4.606RT)$. Table II is a list of the values of E^0, B, their standard errors, $\mathring{a}$, and the standard error of fit at each temperature of interest from 25 to 275°.

TABLE II

VALUES OF E^0, B, AND $\mathring{a}$ FROM LEAST SQUARES FIT OF
$E^{0''} = E + bI$

Temp., °C.	E^0, v.	σ_{E^0},[a] mv.	B, m^{-1}	σ_B[a]	$\mathring{a}$, Å.	σ_{fit},[a] mv.
25	0.22233	0.08	+0.152	0.011	4.3	0.22
60	.1968	.23	− .025	.028	6.0	.41
90	.1696	.20	− .125	.023	7.0	.36
125	.1330	.14	− .116	.013	7.0	.23
150	.1032	.10	− .250	.010	8.0	.21
175	.0708	.17	− .274	.015	9.0	.36
200	.0348	.30	− .422	.024	11	.68
225	− .0051	.34	− .578	.020	12	.29
250	− .054	2.16	−1.1	.12	15	2.57
275	− .090	4.74	−0.95	.23	20	3.89

[a] σ = standard error.

Smoothed Values of the Electromotive Force.—For the purpose of comparison with previous and possible future work, smoothed values of the electromotive force up to 0.1 m HCl were calculated from the E^0 and B values using equations 4 and 5. These values are listed in Table III. It should be noted that a solution originally exactly the concentration listed will not have the same concentration

(26) T. H. Gronwall, V. K. LaMer and K. Sandved. Physik. Z., **29**, 358 (1928).

(27) E. R. Cohen, K. M. Crowe and J. W. M. Dumond, "The Fundamental Constants of Physics," Interscience Publishers, Inc., New York, N. Y., 1957.

Table III

Smoothed Values of the Electromotive Force of the Cell

$$Pt-H_2(p)|HCl(m)|AgCl-Ag$$

At One Atmosphere Hydrogen Pressure

m	25°	60°	90°	125°	E_{smooth} (volts) 150°	175°	200°	225°	250°	275°
0.001	0.57904	0.5953	0.6036	0.6063	0.6014	0.5897	0.5698	0.5422	0.504	0.474
.002	.54415	.5565	.5617	.5620	.5571	.5474	.5308	.5067	.471	.443
.005	.49838	.5055	.5063	.5023	.4952	.4846	.4689	.4474	.415	.390
.0075	.47830	.4831	.4820	.4758	.4674	.4559	.4407	.4183	.387	.363
.01	.46411	.4672	.4648	.4571	.4478	.4354	.4185	.3970	.366	.342
.02	.43017	.4295	.4238	.4124	.4007	.3859	.3673	.3447	.314	.290
.025	.41932	.4174	.4107	.3982	.3856	.3701	.3508	.3277	.297	.272
.05	.38576	.3802	.3705	.3543	.3396	.3215	.3002	.2758	.246	.219
.075	.36619	.3587	.3473	.3290	.3132	.2936	.2713	.2463	.218	.189
.1	.35228	.3435	.3310	.3112	.2948	.2742	.2514	.2261	.200	.168
.2	.31891	.3063	.2906	.2685	.2499	.2269	.2025	.1754	.142	.098
.5	.27245	.2546	.2357	.2085	.1871	.1633	.1309	.0968	.057	.024
1.0	.23340	.2124	.1907	.1614	.1384	.1128	.0853			

at elevated temperatures due to reaction B and hence will not give the electromotive force listed. However, for short times at temperatures up to 200° and for solutions greater than 0.005 m the difference is not large. The solubility of silver chloride was taken into account in calculating the values for Table III.

Also listed in Table III are smoothed electromotive force values at 0.2, 0.5 and 1.0 m. These were obtained simply by averaging the experimental values at each concentration and temperature, after correcting to even molalities by the term $2RT/F \ln (m_{obs}/m_{even})$ where necessary.

Discussion

The values of E^0 measured in this study are compared in Table IV with those obtained by Bates and Bower.[5] It can be seen that the agreement at 25° is excellent, i.e., within 0.01 mv. Bates and Bower critically reviewed the data at 25° reported in the literature and discussed the surprising 0.18 mv. discrepancy between their data and those of Harned and Ehlers. Taniguchi and Janz[28] attributed this discrepancy to slight differences in thermal strain of the silver–silver chloride electrodes. Since the electrodes used here were in a sense thermally annealed by heating and cooling in solution, it would appear that our data confirm the value of Bates and Bower.

In order to compare the data at higher temperatures, the E^0 values of Bates and Bower were extrapolated in two ways. Their measured values were fitted by the method of least squares first to a quadratic function of the centigrade temperature to give

$$E^0 = 0.23683 - 5.2004 \times 10^{-4}t - 2.5241 \times 10^{-6}t^2 \quad (6)$$

and also to an equation involving a $T \log T$ term in the absolute temperature to give

$$E^0 = -0.06864 - 0.0037345T \log T + 0.0102177T \quad (7)$$

Values calculated from these equations are shown in Table IV and it can be seen that the measured values fall between the two extrapolated values except at 250°.

(28) H. Taniguchi and G. J. Janz, J. Electrochem. Soc., 104, 124 (1957).

Table IV

Standard Electrode Potential of the Silver–Silver Chloride Electrode

Temp., °C.	Measured, this study	Eq. 8	Bates and Bower Measured	Eq. 6	Eq. 7
25	0.22233	0.2224	0.22234	0.22225	0.22232
60	.1968	.1955	.19649	.19654	.19648
90	.1696	.1697	.1695	.1696	.1696
125	.1330	.1330		.1324	.1331
150	.1032	.1033		.1020	.1040
175	.0708	.0706		.0685	.0725
200	.0348	.0349		.0319	.0387
225	− .0051	− .0038		− .0080	.0028
250	− .054	− .045		− .051	− .035
275	− .090	− .090		− .097	− .075
300		− .138		− .146	− .117

For comparative purposes the following equation was obtained by fitting the measured E^0 values of this study over the range where the data were the more accurate and numerous, 25 to 200°

$$E^0 = 0.23755 - 5.3783 \times 10^{-4}t - 2.3728 \times 10^{-6}t^2 \quad (8)$$

The standard error of fit of the data from 25 to 200° to this equation was 0.19 mv.

The smoothed values of the e.m.f. at 25, 60 and 90° were compared with Harned and Ehlers[4] and with Bates and Bower[5] as shown in Table V. As can be seen, the agreement is satisfactory. Part of the discrepancy between the present results and those of Harned and Ehlers at 60° is that $å$ was taken to be 6.0 instead of their value of 4.3 Å. Also, at 90°, 7 Å. was used instead of the value of 6 Å. used by Bates and Bower.

The agreement with the data of Bates and Bower is particularly valuable since their study was over a wider temperature range than any previous work and they used many more cells at each temperature. Since their electrodes were of the thermal-electrolytic type and their methods somewhat different, support is lent to the view that systematic errors in the present study were minimized.

One previous investigation of the cell at elevated temperatures was that of Roychoudhury and Bonilla.[29] Their e.m.f. values were compared with values calculated using the E^0 and $\gamma^{\pm}$[30] values

(29) R. N. Roychoudhury and C. F. Bonilla, J. Electrochem. Soc. 103, 241 (1946).

TABLE V

COMPARISON OF RESULTS WITH THOSE OF PREVIOUS INVESTIGATORS

Temp., °C.	HCl concn., m	E_{smooth} (volts)		
		This study	Harned and Ehlers	Bates and Bower
25	0.005	0.49838	0.49841	0.49840
	.01	.46411	.46416	.46412
	.05	.38576	.38587	.38579
	.1	.35228	.35239	.35233
	.2	.31891	.31871	
	1.0	.23340	.23328	
60	0.005	.5054	.5049	.5052
	.01	.4672	.4667	.4669
	.05	.3802	.3797	.3797
	.1	.3435	.3425	.3428
	.2	.3063	.3055	
	1.0	.2124	.2123	
90	0.005	.5063		.5063
	.01	.4648		.4648
	.05	.3705		.3703
	.1	.3310		.3304
	.2	.2906		
	1.0	.1907		

of the present study and found to agree within about 5 and 10 mv. at 100 and 150°, respectively. However, the difference between calculated and observed values was 35 mv. at 250° and in the opposite direction from that calculated by Lietzke[31] in his interpretation of their data. The discrepancy might be due to the fact that they used silver chloride electrodes chloridized on the surface only. This surface coating could have dissolved at 250° giving an unsaturated solution of silver chloride in hydrochloric acid.

Roychoudhury and Bonilla found a discrepancy from the theoretical effect of hydrogen pressure on the electromotive force. This effect was attributed to an effect of hydrogen on the silver–silver chloride electrode which Lietzke suggested might be due to hydrogen electrode sites on that electrode. In the present study in an experiment in 0.05 m HCl at 150° the Nernst slope was obeyed upon increasing the hydrogen pressure from 1.5 to 3 atm. However, Roychoudhury and Bonilla's pressures were as high as 40 atm.

If hydrogen electrode sites were established on the silver–silver chloride electrode the electromotive forces would indeed be lower than in the absence of hydrogen. Since Anderson[18] found that a platinized platinum electrode covered with finely divided silver still gave the same potential as a fresh platinized surface, it would appear that the hydrogen electrode reaction can readily occur on a finely divided silver surface. However, whether hydrogen electrode sites exist on the silver–silver electrode or not, the electromotive force values determined here were reproducible and apparently reversible and thus the E^0 values are usable standard potentials for the particular electrode processes occurring under the conditions of the tests.

The cell used in this study is ordinarily referred to as a cell "without liquid junction." However, in the present case the solubility of silver chloride became appreciable as the temperature increased and since the silver chloride was prevented from diffusing into the main body of solution by the silica frit there was a definite liquid junction. The junction potential was assumed to be negligible in relation to the other effects noted above since the concentration of dissolved silver chloride was generally small in comparison to the hydrochloric acid concentration. For instance the solubility of silver chloride at 200° ranged between 0.001 and 0.002 m.

A further consideration, viz., the difference in ionic strength between the solution within the silica tube surrounding the silver–silver chloride electrode and the bulk solution, was neglected for the same reason. The ionic strength of the solution within the silica tube was used in the calculations. Of course, the actual ionic strength depends upon the species of complex ions which are present and these are not known at the higher temperatures.

In addition to the junction potential caused by dissolved silver chloride, a further junction potential would have been caused by reaction B if the HCl produced had remained within the silica tube. However, it is believed that the high mobility of hydrogen ion, particularly at the higher temperatures, and the presence of HCl in the vapor phase would have allowed sufficient transport of HCl to prevent any significant difference in HCl concentration between the solution in the silica tube and in the bulk solution.

The Debye–Hückel equation in extended form was found to be entirely applicable over the range of temperatures studied. Straight lines were obtained for $E^{0\prime\prime}$ vs. I that were within the limits of experimental error and which readily allowed extrapolation to infinite solution. However, the magnitude of the ion-size parameter, $\mathring{a}$, at the higher temperatures was so large as to suggest that $\mathring{a}$ in these cases is simply an adjustable constant at each temperature and bears no relation to ion size. Lietzke and Stoughton[32] found that for solubility calculations up to 200°, when the denominator term in the Debye–Hückel expression for the activity coefficient was set equal to $(1 + A_s \sqrt{I})$ where A_s was independent of temperature, better agreement was obtained with experiment than with the full expression $(1 + 50.29\mathring{a} \, (DT)^{-1/2} \sqrt{\rho_0 I})$.

(30) See Part II in this series of papers.
(31) M. H. Lietzke, J. Am. Chem. Soc., 77, 1344 (1955).
(32) M. H. Lietzke and R. W. Stoughton, THIS JOURNAL, 63, 1183 (1959).

VAPOR PRESSURE AND VISCOSITY RELATIONSHIPS FOR A HOMOLOGOUS SERIES OF α,ω-DINITRILES

By Alan L. Woodman, Warren J. Murbach and Martin H. Kaufman

U. S. Naval Ordnance Test Station, China Lake, California

Received November 30, 1959

Densities, viscosities and vapor pressures of six α,ω-dinitriles, $NC(CH_2)_nCN$ for $n = 3$ through 8, have been measured; the vapor pressure of succinonitrile ($n = 2$) also has been determined. Constants in the viscosity–temperature relation $\log \eta = A + B/(C + T)$ and in the vapor pressure–temperature relation $\log p = A' - B'/T$ were calculated. Empirical equations, one relating vapor pressure, temperature and n, the other relating the heat of vaporization and n were established. An equation, derived by L. A. Girifalco, was found to give a linear relation between vapor pressure, viscosity and temperature for the α,ω-dinitriles.

Introduction

The densities, viscosities and vapor pressures of six α,ω-dinitriles, $NC(CH_2)_nCN$, where n equals 3 through 8, were measured; vapor pressures of succinonitrile also were measured. The densities and viscosities were measured at 15, 25 and 35°, and the vapor pressures were measured in the range of 5 to 70°. The viscosity, vapor pressure and temperature data for the α,ω-dinitriles were found to fit an equation derived by Girifalco.[1]

Experimental

Reagents.—All of the dinitriles except suberonitrile and azelaonitrile were obtained from commercial sources. Succinonitrile was obtained from the Matheson Co. and needed no purification since sublimation and recrystallization failed to change the vapor pressure or the freezing point (57.4°; lit.[2] 56.9°).

The infrared spectra of glutaronitrile, adiponitrile, pimelonitrile and sebaconitrile indicated the presence of small quantities of carbonyl containing impurities. These impurities were removed by treating the dinitriles with either 10% aqueous KOH or methanolic KOH solution. In most instances one distillation sufficed to give spectroscopically pure material. Using the above procedure the following materials were obtained: glutaronitrile, b.p. 94.9° (1.1 mm.), $n^{25}D$ 1.4332 (lit.[3] $n^{20}D$ 1.42947); adiponitrile, b.p. 101.5–101.7° (0.7 mm.), $n^{25}D$ 1.4366 (lit.[4] $n^{20}D$ 1.4369); pimelonitrile, b.p. 116.0–116.1° (0.9 mm.), $n^{25}D$ 1.4398 (lit.[5] $n^{20}D$ 1.4472); and sebaconitrile, b.p. 127.0° (0.2 mm.) $n^{25}D$ 1.4462 (lit.[5] $n^{20}D$ 1.4474).

Suberonitrile.—A solution of 205.6 g. (3.0 moles) of 95% KCN in 250 ml. of water and 875 ml. of 95% ethanol was heated to reflux. The heating mantle was removed, and then 408.6 g. (1.21 moles) of 1,6-diiodohexane was added over a period of 35 minutes. When the exothermic reaction had subsided, the mixture was refluxed for two hours. Approximately 900 ml. of ethanol–water then was removed by distillation under reduced pressure. The suberonitrile layer was separated, and the aqueous phase extracted with benzene. The extracts were combined with the crude dinitrile and washed, respectively, with water, 10% sodium thiosulfate and saturated sodium chloride solution, and then dried over anhydrous magnesium sulfate. Distillation of the crude dinitrile gave a material which contained halogen but no carbonyl impurities. To remove the halogen-containing impurities the dinitrile was treated with methanolic KOH. One distillation gave 113.6 g. (68.9%) of pure suberonitrile, b.p. 120.1–120.3° (0.8 mm.), $n^{25}D$ 1.4419 (lit.[6] $n^{22}D$ 1.4448).

Azelaonitrile.—A mixture of 338.8 g. (1.8 moles) of azelaic acid and 1000 ml. of thionyl chloride was heated to reflux over a period of 1.5 hours and then refluxed for four hours when evolution of SO_2 and HCl had ceased. Excess thionyl

chloride was removed *in vacuo* and the residue was distilled to yield 364.7 g. (90.0%) of azelaoyl chloride; b.p. 96.7–102.0° at 0.2 to 0.4 mm.

A 4-liter beaker, fitted with an efficient stirrer, thermometer, fritted glass delivery tube and cooled in an ethanol–ice bath, was charged with 3000 ml. (44.4 moles NH_3) of NH_4OH precooled to 0°. Additional ammonia (170 g., 10.0 moles) was added from a tank. Then 364.7 g. (1.62 moles) of azelaoyl chloride was added dropwise over a one-hour period at 0 to 5° while a second 170-g. portion of ammonia was added through the gas delivery tube. After 1.5 hours the white precipitate was collected, washed with water and dried under vacuum at 60°. The yield of azelaamide was 291.2 g. (96.5%); m.p. 173.4–178.1° (lit.[6] m.p. 175°).

The azelaamide (1.56 moles) in 1250 ml. of pure thionyl chloride was heated to reflux over a period of four hours and then refluxed for an additional seven hours when no more gas was evolved. Excess thionyl chloride was removed *in vacuo*, and the residue was dissolved in 500 ml. of 1,2-dichloroethane. After washing with 10% KOH, water and saturated sodium chloride solution and then drying over anhydrous potassium carbonate, the solvent was removed. Two distillations gave 196.6 g. (83.9%) of pure azelaonitrile, b.p. 105.0–105.2° (0.1 mm.); $n^{25}D$ 1.4439 (lit.[7] $n^{25}D$ 1.4426).

Density.—The densities were measured with a one-milliliter Sprengel-type pycnometer which had been calibrated with water; the densities at 15, 25 and 35° are given in Table I. The temperature of the bath was controlled to within ± 0.02°.

Viscosity.—The viscosities, at 15, 25 and 35°, were measured with an Ubbelohde-type viscometer which had been calibrated with distilled water; the values for the viscosity of water were obtained from the data of Weber[8] and were based on an absolute viscosity of 1.0020 centipoise at 20°. Kinetic energy corrections were made where necessary.

Vapor Pressure.—The vapor pressures, using between 0.5 and 1.0 ml. of sample, were measured with the piston manometer apparatus of Pitman and Ernsberger.[9] No change in vapor pressure was observed over a period of about a week indicating the absence of more volatile impurities not detectable by the infrared spectra. The temperature of the bath was controlled to within ±0.007° and was read to the nearest 0.01° on a thermometer which had been calibrated with a National Bureau of Standards platinum resistance thermometer.

Results

The plot of the logarithm of the viscosity against the reciprocal of the absolute temperature gave non-linear curves; however, a suitable equation, given by Gutmann and Simmons,[10] was found to be

(1) L. A. Girifalco, *J. Chem. Phys.*, **23**, 2446 (1955).

(2) A. van de Vloed, *Bull. soc. chim. Belg.*, **48**, 229 (1939).

(3) G. H. Jeffery and A. I. Vogel, *J. Chem. Soc.*, 674 (1948).

(4) A. E. Kulikova, E. N. Zil'berman, T. N. Roginskaya and M. M. Smirnova, *Zhur. Priklad. Khim.*, **32**, 227 (1959); *C. A.*, **53**, 11217i (1959).

(5) R. Paul and S. Tchelitcheff, *Bull. soc. chim. France*, 470 (1949).

(6) I. Heilbron and H. M. Bunbury, eds., "Dictionary of Organic Compounds," Oxford University Press, New York, N. Y., 1953, Vol. I, p. 224.

(7) D. T. Mowry and E. L. Ringwald, *J. Am. Chem. Soc.*, **72**, 4439 (1950).

(8) W. Weber, *Z. angew. Phys.*, **7**, 96 (1955).

(9) H. W. Pitman and F. M. Ernsberger, *Rev. Sci. Instr.*, **26**, 584 (1955).

(10) F. Gutmann and L. M. Simmons, *J. Applied Phys.*, **23**, 977 (1952).

TABLE I

DENSITIES OF THE DINITRILES

Compound	d^{15}_4	d^{25}_4	d^{35}_4	Lit. values
Glutaronitrile	0.9892	0.9811	0.9733	d_4 1.00293, d^{15}_4
				0.99112, d^{30}_4
				0.97930[a]; d^{35}_4
				0.97661[b]; d^{20}_4
				0.9879[c]
Adiponitrile	.9664	.9579	.9515	d^{19}_{19} 0.951[d] d_{20}
				0.9610[e]
Pimelonitrile	.9497	.9414	.9344	d_4 0.96181, d^{15}_4
				0.95070: d^{30}_4
				0.93961[a]; d^{20}_4
				0.948[f]
Suberonitrile	.9347	.9269	.9186	d^{22}_4 0.940[f]
Azelaonitrile	.9255	.9178	.9115	d^{19}_4 0.929[f]
Sebaconitrile	.9179	.9107	.9033	d^{20}_4 0.913[f]

[a] H. Serwy, *Bull. soc. chim. Belg.*, **42**, 483 (1933). [b] R. Legrand, *ibid.*, **53**, 166 (1944). [c] Reference 3. [d] I. Heilbron and H. M. Bunbury, eds., ref. 6, Vol. I, p. 34. [e] Reference 4. [f] Reference 5.

$$\log \eta = A + \frac{B}{C + T} \qquad (1)$$

in which η is the viscosity in centipoise and T is the absolute temperature. The constants A, B and C, determined by a least squares analysis, are given in Table II for each of the dinitriles. The standard percentage error (s.p.e.) of fit, defined by

in which N is the number of experimental points, is given in the last column of Table II for each compound.

$$\text{s.p.e.} = 100 \left[\frac{\sum \left(\frac{\eta_{calc} - \eta_{obs}}{\eta_{obs}} \right)^2}{N} \right]^{1/2} \qquad (2)$$

TABLE II

VISCOSITIES OF DINITRILES, CONSTANTS IN THE EQUATION

$$\log \eta \text{ (cp)} = A + \frac{B}{C + T (\degree K.)}$$

Compound	A	B	C	S.p.e.
Glutaronitrile	−0.9025	233.83	−159.12	0.01
Adiponitrile	−0.8016	201.92	−171.52	.01
Pimelonitrile	−0.9017	224.59	−168.31	.00
Suberonitrile	−1.0664	267.03	−159.75	.01
Azelaonitrile	−0.9849	250.16	−166.63	.00
Sebaconitrile	−1.0172	264.18	−166.56	.01

The vapor pressure data are given in Table III. The vapor pressure of sebaconitrile has been reported previously.[11] The data are believed to be accurate to within 1%.[9] Table IV lists the constants in the equation

$$\log p \text{ (microns)} = A' - B'/T \qquad (3)$$

calculated from a least-squares treatment of the log p vs. $1/T$ data. The heats of vaporization as calculated from B' are given in column 3 of Table IV, and are essentially constant over the temperature range studied.

Discussion

It is interesting to note that when the constants in equation 3, except those for succinonitrile, are

(11) M. H. Kaufman and A. G. Whittaker, *J. Chem. Phys.*, **24**, 1104 (1956).

TABLE III

VAPOR PRESSURES OF THE DINITRILES

Compound	Temp., °C.	p (μ) (obsd.)	p (calcd.)	% Dev.
Succinonitrile	6.24	1.156	1.154	+0.2
	10.16	1.742	1.751	−0.5
	13.06	2.370	2.365	+0.2
	16.15	3.238	3.238	0.0
	17.74	3.798	3.797	0.0
	19.63	4.589	4.576	+0.3
	25.14	7.774	7.784	−0.1
				±0.2
Glutaronitrile	4.51	1.115	1.119	−0.4
	10.16	1.991	1.993	−0.1
	14.16	2.966	2.958	+0.3
	18.14	4.355	4.334	+0.5
	25.54	8.590	8.584	+0.1
	30.65	13.45	13.50	−0.4
				±0.3
Adiponitrile	12.66	0.753	0.756	−0.4
	17.05	1.189	1.186	+0.3
	20.13	1.612	1.614	−0.1
	25.84	2.815	2.810	+0.2
	30.15	4.222	4.212	+0.2
	36.26	7.341	7.332	+0.1
	41.35	11.40	11.44	−0.3
				±0.2
Pimelonitrile	33.98	2.275	2.293	−0.8
	34.46	2.405	2.400	+0.2
	40.06	4.065	4.039	+0.6
	44.21	5.879	5.872	+0.1
	45.20	6.421	6.411	+0.2
	57.08	17.59	17.64	−0.3
				±0.4
Suberonitrile	30.70	0.966	0.969	−0.3
	33.37	1.262	1.264	−0.2
	37.34	1.872	1.863	+0.5
	40.41	2.503	2.497	+0.2
	42.09	2.936	2.925	+0.4
	50.59	6.304	6.342	−0.6
	65.02	21.66	21.58	+0.4
				±0.4
Azelaonitrile	35.67	0.787	0.783	+0.5
	40.00	1.213	1.206	+0.6
	42.06	1.460	1.476	+1.1
	45.00	1.979	1.961	+0.9
	48.27	2.664	2.671	−0.3
	53.60	4.304	4.364	−1.4
	67.70	14.96	14.85	+0.7
				±0.8

plotted as a function of the number of methylene groups, n, in the dinitrile, two straight lines are obtained, thus

$$A' = (0.222 \pm 0.002)n + (11.936 \pm 0.014) \qquad (4)$$

and

$$B' = (173 \pm 4)n + (2996 \pm 24) \qquad (5)$$

By substituting the empirical relationships found in equations 4 and 5 for the constants A' and B'

Table IV

Dinitrile Vapor Pressure Equations, Constants in the
Equation $\log p \, (u) = A' - B'/T$

Compound	A'	B'	Ht. of vap. (kcal./mole)
Succinonitrile	13.1473	3656	$16.73^a \pm 0.03$
Glutaronitrile	12.6177	3490	$15.97 \pm .02$
Adiponitrile	12.8166	3698	$16.92 \pm .02$
Pimelonitrile	13.0289	3891	$17.81 \pm .05$
Suberonitrile	13.2686	4036	$18.47 \pm .03$
Azelaonitrile	13.4964	4201	$19.22 \pm .07$

^{a} Heat of sublimation.

in equation 3, the following equation is determined

$$\log p = 0.222n + 11.936 - (173n + 2996)/T \quad (6)$$

The vapor pressure data for sebaconitrile are included in this calculation. Most of the vapor pressures calculated from equation 6 agree with the experimental values to within 2%, and all of the calculated values agree to within 4%.

An equation was also determined which relates the heats of vaporization to the number of methylene groups (n) in the dinitrile. This equation is

$$\Delta H = (0.79 \pm 0.02)n + (13.71 \pm 0.11) \quad (7)$$

in which ΔH is the heat of vaporization in kcal./mole. Extrapolation of the line to $n = 2$ (succinonitrile) gives a value of 15.29 kcal./mole for the heat of vaporization. Subtraction of this value from the heat of sublimation given in Table IV yields 1.44 kcal./mole for the heat of fusion of suc-

cinonitrile; the heat of fusion at the melting point and atmospheric pressure was found to be 2.79 kcal./mole.[2] Upon consideration of the fact that the heat of fusion was obtained as the difference of two rather large numbers both of which contain some error, of the difference in temperature and of the error arising from some probable association of the dinitrile in the vapor state, no better agreement between the two values could be expected.

The viscosity and vapor pressure data over a 30° range in temperature were plotted in a number of previously published equations relating these two quantities.[1,12,13] The data best fit Girifalco's equation[1]

$$n' = kX + m + \frac{J}{\log \eta_0/\eta} \quad (8)$$

in which $n' = (\log p - \log p_0)/(\log \eta_0 - \log \eta)$, $X = (1/T_0 - 1/T)/\log(\eta_0/\eta)$, p_0 and η_0 are the pressure and viscosity at T_0, and k, m and J are constants. The plot of n' vs. X for water is linear showing that the third term in the equation does not contribute appreciably to the variation in n'. The data for the dinitriles give a linear plot for n' vs. X, thus showing that here, too, the third term is very small.

(12) A. K. Mukherjee, J. Ind. Chem. Soc., 30, 725 (1953).

(13) S. S. Mitra and D. N. Chakravarty, J. Chem. Phys., 22, 1775 (1954).

DESTRUCTIVE AUTOXIDATION OF METAL CHELATES. I. EFFECTS OF VARIATION OF LIGAND AND METAL ON INITIAL RATE

By Morris Mendelsohn, Edward M. Arnett[1] and Henry Freiser[2]

Contribution from the Department of Chemistry, University of Pittsburgh, Pittsburgh, Penna., and the University of Arizona, Tucson, Arizona

Results are presented of a systematic study of the effect of structure and conditions on the irreversible autoxidation of a series of metal chelates under pure oxygen at atmospheric pressure at about 100° in diphenyl ether as solvent. A convenient apparatus for autoxidation studies is described which gives a reproducibility of about 1% for initial rates. Main products of the autoxidation of iron(III) acetylacetonate are: carbon dioxide, water, biacetyl, acetic acid, acetylacetone, mesityl oxide and an amorphous iron residue approximating the formula $FeC_7H_8O_{4.85}$. Substitution of dibenzoylmethane for acetylacetone as the ligand increased the rate by better than seven times while the use of 3-phenylacetylacetone, 3-benzylacetylacetone or dipivaloylmethane made the chelate inert. Variation of the metal in a series of acetylacetonates gave in decreasing order of rates: V(III) > Ce(IV) > Ni(II) > Mn(III) > Fe(III) > Co(II) > Co(III) > Th(IV): some other chelates were inert under these conditions: Al(III), Zr(IV), Be(II), Cr(III), In(III). Comments and interpretations are given.

Introduction

In the last several decades a large number of studies have been directed toward an understanding of the attack of molecular oxygen on organic molecules. A description of this work and the conclusions derived from it are available in several excellent reviews.[3,4] The effects of metallic com-

pounds on the reaction recently have been summarized also.[5]

To our knowledge the only systematic studies that have yet been made of the autoxidation of chelates are those which apply to "oxygen-carrying" compounds.[6] In contrast, we have been concerned with what might properly be called "destructive autoxidation" of chelates in which the at-

(1) Department of Chemistry, University of Pittsburgh, Pittsburgh 13, Pennsylvania. Inquiries should be sent to this author.

(2) Department of Chemistry, University of Arizona, Tucson, Arizona.

(3) C. Walling, "Free Radicals in Solution," John Wiley and Sons, Inc., New York, N. Y., 1957, Chapter 9.

(4) G. Russell, J. Chem. Ed., 36, 111 (1959).

(5) F. Basolo and R. Pearson, "Mechanisms of Inorganic Reactions," John Wiley and Sons, Inc., New York, N. Y., 1958, Chapter 8.

(6) A. E. Martell and M. Calvin, "Chemistry of the Chelate Compounds," Prentice-Hall, New York, N. Y., 1952, Chapter 8.

tack of oxygen produces irreversible changes in the ligand and the metal. Although it is possible that "destructive autoxidation" of chelates takes place through a combination of the complexing reactions of the oxygen-carrying chelates and the classical peroxide and hydroperoxide mechanisms of organic autoxidation, one may well expect that the incorporation of the metal directly into the organic structure will open up possibilities for new reaction pathways that have not been observed previously.

Experimental

Apparatus.—The oxidation apparatus consists essentially of a special reaction flask connected to a gas-reservoir and measuring system of the type traditionally used for measuring rates of oxygen uptake at constant pressure. The reaction vessel is cylindrically shaped (260 × 38 mm.) and equipped with a "Lew" Magnetic Stirrer[7] with the magnetic impeller enclosed in a sealed chamber. Hung about midway inside the reactor, and coaxial with the stirrer shaft which passes through it, is an open cylindrical vessel containing Molecular Sieves.[8] This material serves as an absorbent for the removal of volatiles formed during the oxidation which would produce a back-pressure and reduce the apparent rate of oxygen uptake. Some other workers[9] have employed gas absorbers during autoxidation studies for the removal of volatile products, using a pumping system for the circulation of the gases. We have found the placing of the absorbent inside the reactor vessel itself to be very convenient and a number of careful control experiments have shown that no obvious errors are introduced by this modification. It is well known that oxygen is not appreciably absorbed by Molecular Sieves at temperatures above −20° whereas all of the volatiles formed by the reaction (see Product Study below) are strongly held.

Directly attached to the reaction vessel through a ground-glass cock is a container in which the chelate solution may be heated under nitrogen before the reaction is begun. Upon rotation of this container through 90 degrees the two orifices of the ground-glass cock are aligned so that the chelate solution can flow into the reaction vessel containing pure oxygen which also has been preheated. The entire assembly is immersed in a thermostated oil-bath. Thus we have made provision for bringing the reactants to the desired temperature before mixing and for the removal of volatile products as fast as they are formed.

The gas measuring system is of conventional design consisting of a gas buret, manometer (filled with dibutyl phthalate) and a mercury leveling bulb. Constant oxygen pressure is maintained by adjusting the height of the leveling bulb and the quantity of oxygen consumed is determined from readings of the gas buret. Gas volumes consumed are corrected for temperature and pressure.

Reagents and Purification.—U.S.P. oxygen was used after passage through a two foot Drierite column. The chelate solution was protected during the heat-up period with prepurified nitrogen.

Phenyl ether was used as the solvent because of its inertness to oxidation and pyrolysis under the working conditions. A mass spectrometric analysis of the products of the oxidation of iron(III) acetylacetonate in this solvent did not show evidence of any aromatic compounds. In addition, identical rates of oxygen uptake were observed when ethylene dibenzoate and Dow-Corning 550 fluid, a phenylmethyl-polysiloxane oil, were substituted for the phenyl ether. Eastman White Label phenyl ether was further purified[10] by shaking with 1 N KOH solution, water washing, drying over Drierite and distillation. The purified phenyl ether was analyzed for impurities with a Burrell Kromo-Tog Model 1 gas chromatograph using nitrogen at a flow rate of 40 ml./min. as carrier with a 2.5 meter column of Apiezon L grease on Celite at 200°. It was found to be free of contaminants.

Acetylacetone and dibenzoylmethane were purchased from the Carbide and Carbon Chemicals Company and

Eastman Kodak Company, respectively. Dipivaloylmethane[11] and 3-phenylacetylacetone[12] were prepared according to the methods of Hauser. 3-Benzylacetylacetone was prepared by heating sodium acetylacetonate with benzyl chloride.[13]

Ce(IV) acetylacetonate was made as follows. An acidified aqueous solution of cerous chloride was treated with ammonium acetylacetonate prepared by the addition of 135 g. (1.35 moles) of acetylacetone to a solution of 54 g. of concd. ammonium hydroxide (Baker's Analyzed Reagent, 28.7% NH₃) and 100 g. of distilled water. The ammonium acetylacetonate solution was added slowly with stirring to 100 g. (0.27 mole) of CeCl₃·7H₂O in 74 g. of a 10% HCl solution. 3% NH₄OH was then added slowly with rapid stirring until the pH reached 5. The mixture was stirred for about ¹/₂ hour and then refrigerated overnight. Filtration and washing of the precipitate with cold, acidified water (pH 4.5) followed. Cerium(III) acetylacetonate in about 80% yield was obtained. The yellow product was then oxidized almost quantitatively to cerium(IV) acetylacetonate by heating in benzene exposed to the air. During this heating the chelate dissolved slowly in the benzene to a give a solution of dark red color. Needle-shaped crystals of the Ce(IV) chelate of the same color were obtained after evaporating some benzene, adding n-heptane and cooling. Recrystallization from benzene–petroleum ether solution followed. *Anal.* Calcd. for $C_{20}H_{28}O_8Ce$: C, 44.8; H, 5.3; Ce, 26.0. Found: C, 44.5; H, 5.5; Ce, 26.1.

All of the other metal acetylacetonates (2.4-pentanedionates) were prepared according to methods described in the literature.[14] The other β-diketone chelates were prepared similarly except that about three times more methanol was used than for the corresponding acetylacetonates. All of the chelates were recrystallized at least twice from mixtures of benzene–petroleum ether or water–methanol. In every case the elemental analysis was in very good agreement with the calculated value. A sample of iron(III) acetylacetonate was further purified by column chromatography through a two-foot tube of Woelm alumina using mixtures of benzene–petroleum ether as eluent. This additional purification had no effect on the rate of autoxidation.

Control Experiments and Errors.—Our rates were mostly measured at atmospheric pressure and at temperatures close to 100°. As is customary when dealing with highly complex reactions only initial rates were taken. In our case this turned out to be quite simple since the reaction usually had a very short induction period or none at all and almost immediately gave a plot of ml. of oxygen consumed *vs.* time which held linear for 10–15 minutes until about ¹/₂ mole of oxygen per mole of chelate had been absorbed and which was remarkably reproducible under identical conditions. It is the slope of this linear portion, corrected to standard conditions of temperature and pressure, which is taken as the rate k for comparing one run with another. Results are presented in terms of moles of oxygen/mole chelate-hour.

Primary sources of error seem to lie in the actual readings of oxygen uptake and in measuring the quantity of chelate solution added from the preheater to the reactor. Most of the incremental error in reading oxygen volumes is compensated for by the fact that the readings are cumulative, a number of them being plotted to give a straight line. The cumulative error for reading volume is about ±0.1 ml. which would affect k by about ±0.5%. It is estimated that the same error applies to transfer of the chelate solution from the preheater to the reactor. Control of temperature to within ±0.04° at 98.5° and pressure to within ±0.1 mm. at 740 mm. introduced negligible error from these sources.

Agitation was shown to be more than adequate for preventing the reaction from becoming diffusion-controlled. No effect on rate was observed between runs stirred at 625 and 1260 r.p.m. During one run the stirring speed was abruptly changed from 923 to 625 r.p.m. and no change in

(7) Obtainable from Scientific Glass Apparatus Co.

(8) Trade name, Linde Division, Union Carbide Corp.

(9) G. Von Fuchs and H. Diamond, *Ind. Eng. Chem.*, **34**, 927 (1942).

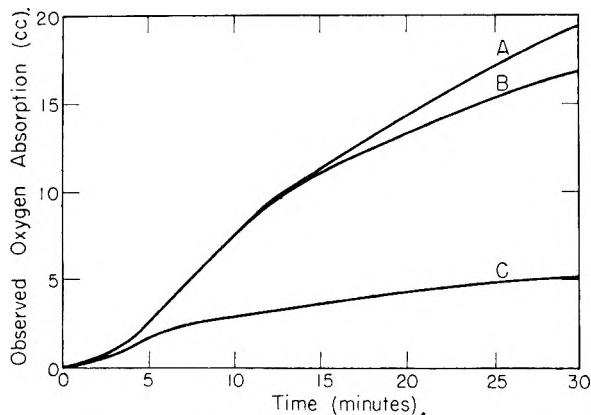(10) D. R. Hill and M. Davis, *Trans. Faraday Soc.*, **49**, 395 (1953).

(11) B. O. Linn and C. R. Hauser, *J. Am. Chem. Soc.*, **78**, 6066 (1956).

(12) J. T. Adams and C. R. Hauser, *ibid.*, **66**, 345 (1944); **67**, 284 (1945).

(13) G. T. Morgan and C. J. A. Taylor, *J. Chem. Soc.*, **127**, 797 (1925).

(14) R. G. Charles and M. Pawlikowski, THIS JOURNAL, **62**, 440 (1958).

Fig. 1.—Oxidation of ferric acetylacetonate in diphenyl ether at 98.5°; 1.01×10^{-3} mole of chelate, concentration—0.128 molal; curves show effect of absorbants: A, mixture of equal parts 5A and 13X Linde molecular sieves; B, Ascarite, C, no absorbant.

slope observed. Several oxidations not described here have gone at rates much faster than the normal chelate runs. The fact that oxygen could be absorbed very rapidly in these runs shows that the apparatus was not imposing limits on the rate at which it was being supplied in the much slower runs described in this report. Charles[14,15] and co-workers have observed that the thermal decomposition of many of the chelates we have studied at temperatures above 150° leads to the formation of acetone and carbon dioxide in considerable quantities as well as other gaseous products. Although their results imply clearly that no pyrolysis of the chelate should occur at temperatures close to 100°, we checked this point by heating one of our usual reaction mixtures of chelate at 100° under an atmosphere of pure nitrogen. No pressure build-up was observed over a period much longer than is usually taken for our rate runs.

In order for our rates to be at all meaningful the Molecular Sieves must absorb the volatile products instantly and completely. This crucial requirement for our apparatus was checked in several independent ways. A sample of Molecular Sieves used in a regular rate experiment was transferred to a vacuum line. It was found that the vapor pressure over this sample did not differ appreciably from a control sample that had merely been exposed to experimental conditions in the absence of chelate. The slight vapor pressure observed in both cases could be attributed entirely to diphenyl ether. Secondly, a sample of Ascarite used to absorb carbon dioxide in our initial experiments before we began using Molecular Sieves removed CO_2 so effectively that during a four hour run only a trace could be detected by mass spectrometric examination of the residual gases. Finally, and most important, several runs were made in which the *amount* of chelate oxidized was varied from $0.500-1.27 \times 10^{-3}$ mole but the *concentration* of chelate was held constant. In all cases the k for rate of oxygen absorbed per mole of chelate per hour was the same, showing that even though far more volatiles were being produced in the case of the larger sample, the apparatus was capable of reproducibly supplying oxygen as demanded and removing the volatiles formed.

Deliberate contamination of the reaction mixture with pieces of Molecular Sieve did not affect the rate. A control experiment in which the reaction mixture was completely protected from light gave the usual rate.

To test the reproducibility of the rates, a group of seven replica runs using iron(III) acetylacetonate at a concentration of 3.198% in diphenyl ether at 98.5° was made. The mean value of k was 1.935 mole oxygen/mole chelate hour with an estimated standard deviation of ±0.029 mole oxygen/mole chelate hour or an interval of 1.917 to 1.955 at the 95% confidence level.

Results and Discussion

Product Study.—Mass-spectrometric studies of the gas phase following oxidation of iron(III)

(15) J. Von Hoene, R. G. Charles and W. Hickam, This Journal, 62, 1098 (1958).

acetylacetonate showed the formation of considerable carbon dioxide and other volatiles. That most of the gas was formed in the early stages of reaction is CO_2 and water was shown by nearly identical rates when Ascarite was replaced by Molecular Sieves 5-A and 13-X in equal parts. Differences between the slopes of the curves obtained in the presence and absence of absorbent were greatest in the early stages of reaction showing that this is when most of the volatiles are formed. These curves are presented in Fig. 1 which also shows that the apparent rate is much slower in the absence of absorbents due to the back-pressure of volatiles formed by the reaction.

A mass-spectrometric examination of the vapor following a reaction run for 48 hours at 150° in a sealed, totally immersed flask, showed the formation of carbon dioxide and water in relatively large amounts, moderate quantities of acetone, acetic acid, methanol, and methyl acetate and traces of mesityl oxide and acetylacetone. This is reminiscent of the results of Charles[14,15] and co-workers who found that large quantities of acetone and carbon dioxide are formed in the pyrolysis of these chelates at higher temperatures.

In order to obtain a more complete picture of the main products of reaction, a large scale continuous autoxidation was performed at 106°. Purified oxygen was bubbled though a 3.24% solution of iron (III) acetylacetonate in diphenyl ether for 24 hours, the volatile products being collected in a series of traps at room temperature, 0 and −78°, a long Ascarite tube and finally a large pneumatic trough gas-collector. Nothing except oxygen could be found in the gas-collector. From 0.81×10^{-2} mole of original chelate oxidized, 1.062×10^{-3} mole of CO_2 was found in the Ascarite tube.

Yellow products were found in the traps at room temperature and −78° but nothing was discovered in the ice trap. Most of the products were in the Dry Ice trap and its contents were analyzed by mass-spectrometer to show the composition

Component	Mole %
Water	50.04
Biacetyl	31.29
Acetic acid	15.63
Acetylacetone	2.37
Mesityl oxide	0.67

The material remaining in the reactor was vacuum distilled yielding only diphenyl ether in the distillate. The solid residue was extracted exhaustively in a Soxhlet extractor with methyl ethyl ketone, acetone, methanol, dioxane, tetrahydrofuran, diethyl ether and trichloroethylene, and yielded only unreacted chelate in the soluble portion and an insoluble black residue. *Anal.* Fe, 25.18; C, 34.49, H, 3.38; O, 36.95. This material was very slightly soluble in a large excess of 5% hydrochloric acid thus eliminating iron(III) acetate as a possible structure. Material balances could be made to account for 105% of the iron, 99% of the carbon and 107% of the hydrogen in the original sample of chelate. The combined oxygen content of the products showed 3.86 moles of oxygen absorbed per mole of chelate.

For the observed stoichiometry of this continuous oxidation we may write Fe(III) acac$_3$ + 3.86 O$_2$ → 0.0272 Mesityl oxide + 1.26 Biacetyl + 0.096 Acetylacetone + 0.64 Acetic acid − 2.02 H$_2$O + 1.31 CO$_2$ + insoluble iron products. A sample of the insoluble product from a normal kinetic run gave nearly the same analysis: Fe (24.78%), C (37.05%), H (3.95%), O (34.22%) corresponding to FeC$_7$H$_8$O$_{4.85}$. It was examined by X-ray diffraction using the powder method by Dr. A. Taylor of the X-ray section of the Westinghouse Research Laboratories and found to consist of amorphous organic matter and to be free of iron oxides, iron carbonates, and free of carbon or other inorganic substances.

In the continuous run there is a conspicuous absence of acetone among the products while no biacetyl appears in the products of the 48 hour static run at 150°. This probably is due to the swift removal of biacetyl as it is formed during the continuous run. During the static run the biacetyl is exposed longer to more drastic conditions and so could be oxidized to yield acetone and carbon dioxide and also perhaps be a precursor for the formation of methanol and methyl acetate.

Although the results of this extended destructive oxidation need not apply directly to the products obtained during the first 10 or 15% of reaction during a kinetic run, it is similar in that in both cases the volatile products are removed from the hot zone of the reactor and stored in a cooler place. Biacetyl was easily detected as a product in all of our runs at 98.5° by its powerful odor.
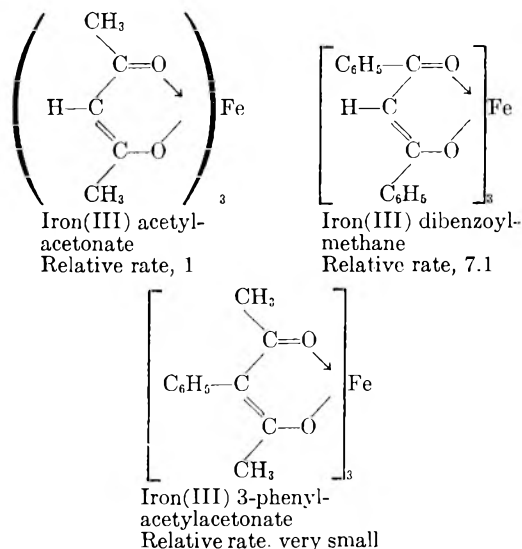
Variation of Ligand Structure.—Most of our studies have been performed on metal acetylacetonates because these are structurally the simplest chelates we have encountered that have appreciable solubility in non-polar solvents and also because they are easily made and have been fairly well studied. Iron(III) acetylacetonate was chosen for most of our work because it had good solubility and gave conveniently measured rates; however, the acetylacetonates of a number of other important metals were insufficiently soluble in diphenyl ether to be examined.

The harsh conditions of the reaction and the generally accepted radical mechanism for autoxidation of hydrocarbons caused us to expect a radical chain mechanism as the most likely course for the autoxidation of chelates. The preceding product study is consistent with this showing a complex mixture of products including biacetyl which may be produced by the coupling of acetyl radicals. Accordingly, it seemed instructive to try variations in the ligand part of the molecule for effect on rate.

The iron(III) chelate of dibenzoylmethane was prepared and, although it was not very soluble in diphenyl ether, its autoxidation rate could easily be measured at 98.5° and was found to be about 7.1 times faster than that for the acetylacetonate under the same conditions. This is not due to any peculiar sensitivity of the ligand as such since dibenzoylmethane itself shows no oxygen uptake under these conditions.

We now replaced the lone hydrogen in the 3-position with a phenyl group. Iron(III) 3-phenyl

acetylacetonate was found to be inert to autoxidation under our conditions. Its ability to catalyze normal hydrocarbon autoxidation was demonstrated by using it as a catalyst in the autoxidation of tetralin for which it is fully as effective as is iron(III) acetylacetonate. Likewise iron(III) 3-benzyl acetylacetonate and the corresponding iron(III) chelate of dipivaloylmethane were inert to autoxidation.

Iron(III) acetyl-
acetonate
Relative rate, 1

Iron(III) dibenzoyl-
methane
Relative rate, 7.1

Iron(III) 3-phenyl-
acetylacetonate
Relative rate, very small

The rate of attack by a radical is generally believed to be conditioned mainly by the density of electrons at the site of attack and the stability of the new radical formed. In our case we are probably dealing with a very complex chain reaction in which the observed rate of oxygen uptake is determined by a balance of a number of propagation and termination steps. This balance, as well as individual rates, may very well change a good deal from one compound to another. The results above suggest that in the case of iron(III) dibenzoylmethane a radical involved in one of the propagation steps is being stabilized by the phenyl groups thereby enhancing the rate.

The inertness of the 3-phenyl and 3-benzyl compounds may be interpreted as evidence that the 3-hydrogen is the site of attack in an important step and that this pathway is blocked by the replacement of the hydrogen. The inertness of the dipivaloylmethane chelate then may be the result of hindrance by the flanking *t*-butyl groups to attack on the 3-position.

These experiments indicate clearly the wide effects that variation in structure of the organic part of the chelate can have on the sensitivity of the molecule to attack by oxygen. They also show in the case of dibenzoylmethane that a molecule which by itself is inert to the attack of oxygen under these rather severe conditions may be converted into an easily oxidizable material by chelation. This parallels the observation that free acetylacetone is far more resistant to pyrolysis than are its metal chelates.[16] The inertness of the 3-phenyl chelate, which however catalyzes the autoxidation of tetralin as well as the acetylacetonate, does suggest that the

(16) Private communication from R. Charles.

autoxidation of chelates may not proceed simply through oxidation of the organic part of the molecule by means of the usual metal-catalyzed mechanism for autoxidation of hydrocarbons.

Variation of the Metal.—The literature of autoxidation[3-5] contains many accounts of the widely varying effects of different metal salts on autoxidation of hydrocarbons. The metals are usually incorporated into the solution through a compound of ill-defined structure such as a resinate, naphthenate or salt of a long-chain fatty acid. Many salts of transition metals are renowned for their effectiveness in promoting autoxidation while those of metals less prone to exhibit variable valence such as aluminum or magnesium are usually without effect. Much evidence is available to show that the metal is mainly effective by oxidizing hydroperoxides to peroxy radicals which in turn attack the hydrocarbon in what is often the rate-limiting step. The reduced metal is then subsequently oxidized again and is able to repeat its role indefinitely. Clearly ability to function properly in this way is contingent upon a metal's having energetically favorable paths for electron gain and loss.

In addition to the possibility of the metal functioning in the classical way described above, one might expect in the case of chelates that initial attack could occur at the metal and that further reaction could take place by a series of steps some of which might be intramolecular and available only in the case of chelates but not in the free ligand.

The above considerations underline the importance of varying the coördinating metal as well as the organic part of the molecule in a systematic examination of the factors that could effect rate. The results of a series of comparable oxidations of 0.128 molal solutions of metal acetylacetonates in diphenyl ether at 98.5° under 730–745 mm. of pure oxygen, all other variables likewise being held constant, are given in the adjoining tabulation. In the cases of the chelates that are listed as unreactive, we mean that no perceptible change in oxygen

Metal chelate	$k, \dfrac{\text{moles oxygen}}{\text{moles chelate, hr.}}$
Vanadium(III) acac$_3$	7.81
Cerium(IV) acac$_4$	4.17
Nickel(II) acac$_2$	4.07
Manganese(III) acac$_3$	2.73
Iron(III) acac$_3$	2.26
Cobalt(II) acac$_2$	1.64
Copper(II) acac$_2$	0.55
Cobalt(III) acac$_3$	0.28
Thorium(IV) acac$_4$	0.19
Al(III) acac$_3$	0
Zr(IV) acac$_4$	0
Be(II) acac$_2$	0
Cr(III) acac$_3$	0
In(III) acac$_3$	0

volume was apparent after 90 minutes in contrast to the others where usually several milliliters of oxygen had been absorbed within the first five minutes. Usually induction periods were very short or non-existent so that the inertness of the unreactive chelates cannot be attributed to this.

We notice at least two important facts about this series. First, there is a marked difference between the rates of chelate oxidation and this works to separate the chelates into two large groups: those that give easily measurable rates and those that are inert. The chelates that are sensitive to oxidation are just the ones that have metals capable of easy reduction–oxidation cycles and the ones that are stable are mostly those which cannot undergo easy electron transfer. Secondly, we notice that the differences in rates among the chelates which do oxidize is far from dramatic, covering a rather small range of rates.

MICROWAVE ABSORPTION AND MOLECULAR STRUCTURE IN LIQUIDS. XXXI. ANALYSIS IN TERMS OF TWO RELAXATION TIMES FOR SOME AROMATIC ETHERS[1]

By Klaus Bergmann, Dominic M. Roberti[2] and Charles P. Smyth

Contribution from the Frick Chemical Laboratory, Princeton University, Princeton, N. J.

Received December 19, 1959

Dielectric measurements on diphenyl ether, dibenzyl ether, anisole and o-dimethoxybenzene have been analyzed in terms of two relaxation times. The results are consistent with the interpretation of a large relaxation time due to molecular rotation and a smaller relaxation time due to intramolecular motion, notably methoxy group rotation for anisole and o-dimethoxybenzene. The data for dibenzyl ether have also been analyzed in terms of a distribution of relaxation times between two limiting values.

The Cole–Cole arc plot has proved a very useful method of representing the relationship between dielectric constant and dielectric loss and of calculating dielectric relaxation time. Its assumed symmetrical distribution of relaxation times around a most probable value commonly cannot be distinguished by the few points experimentally obtainable at microwave frequencies from other possible distributions. Considerations of structure in some cases render more probable a distribution of relaxation times between two limiting values.[3,4] A number of relaxation times have been found which are much lower than would be expected for the molecules in the media in question. Although, in several of these cases, the deviation of the observed points from a Cole–Cole arc is little, if any, greater than the possible experimental error, it appears certain that the dielectric relaxation process involves an intramolecular orientation process with a very short relaxation time in addition to the normal molecular orientation process. The extent to which the observed relaxation time is shortened below that to be expected for the molecular orientation process depends upon the relative importance of the intramolecular process. It is the purpose of the present paper to analyze the dielectric relaxation of certain of these substances in terms of two relaxation times, one for the molecular orientation process and one for the intramolecular.

If there are two relaxation times and one is much larger than the other, the two dispersion regions are distinct, and each may be examined independently of the other.[5] More often there is overlapping of the dispersion regions and the observed relaxation time is lower than would be expected from the size of the molecule, as Fischer[6] found for diphenyl ether. A previously described[7] indirect method of analysis for such a case has been applied to measurements on four aromatic ethers.

(2) Gulf Oil Fellow in Chemistry, 1957–1958.

(3) H. Fröhlich, "Theory of Dielectrics," Oxford University Press, London, 1949, p. 94.

(4) K. Higasi, K. Bergmann and C. P. Smyth, to be published.

(5) M. Davies and R. J. Meakins, *J. Chem. Phys.*, **26**, 1584 (1957).

(6) E. Fischer, *Z. Naturforsch.*, **4A**, 707 (1949).

(7) K. Bergmann, Doctoral Dissertation, Freiburg/Breisgau, West Germany, 1957.

Analysis

Dielectric relaxation with two mutually independent relaxation times may be considered to follow the equations[7]

$$\frac{\epsilon' - \epsilon_\infty}{\epsilon_0 - \epsilon_\infty} = c_1 \frac{1}{1 + (\omega\tau_1)^2} + c_2 \frac{1}{1 + (\omega\tau_2)^2}$$
$$\frac{\epsilon''}{\epsilon_0 - \epsilon_\infty} = c_1 \frac{\omega\tau_1}{1 + (\omega\tau_1)^2} + c_2 \frac{\omega\tau_2}{1 + (\omega\tau_2)^2} \quad (1)$$

where ϵ' and ϵ'' are the measured dielectric constant and loss at frequency ω, ϵ_0 and ϵ_∞ are the static and high frequency or optical dielectric constants, τ_1 and τ_2 are the two relaxation times, and c_1 and c_2 are the relative weights of each relaxation term, where $c_1 + c_2 = 1$. The values of ϵ_0, ϵ' and ϵ'' are measured quantities, while ϵ_∞ must be estimated in the absence of very high frequency measurements. In this work, ϵ_∞ was estimated by taking the atomic polarization plus electronic polarization as larger than the electronic polarization by a factor γ, where

$$\frac{\epsilon_\infty - 1}{\epsilon_\infty + 2} = \gamma \frac{n_D^2 - 1}{n_D^2 + 2}$$

γ is an empirical parameter, which, for a given substance, may be taken as constant over the temperature ranges under consideration in the present work.

A graphical method[7] was used to select the values of τ_1, τ_2, c_2 and ϵ_∞ of eq. 1 which gave the best fit for the experimental data. Equation 1 may be written in the form

$$Y = c_1 Y_1 + c_2 Y_2 \quad (2)$$
$$Z = c_1 Z_2 + c_2 Z_2$$

where

$Y = \epsilon''/(\epsilon_0 - \epsilon_\infty)$	$Z = (\epsilon' - \epsilon_\infty)/(\epsilon_0 - \epsilon_\infty)$
$Y_1 = \omega\tau_1/(1 + \omega^2\tau_1^2)$	$Z_1 = 1/(1 + \omega^2\tau_1^2)$
$Y_2 = \omega\tau_2/(1 + \omega^2\tau_2^2)$	$Z_2 = 1/(1 + \omega^2\tau_2^2)$

By referring to Fig. 1, it may be seen that the point (Y,Z) lies on the chord between the points (Y_1, Z_1) and (Y_2, Z_2) of the normalized Debye semi-circle and divides the chord in the ratio $b/a = c_1/c_2$. The graphical analysis consists of plotting the normalized experimental points on a complex plane (Fig. 1) and drawing various chords of the semi-circle through the points until a set of parameters is found which is consistent for all the points.

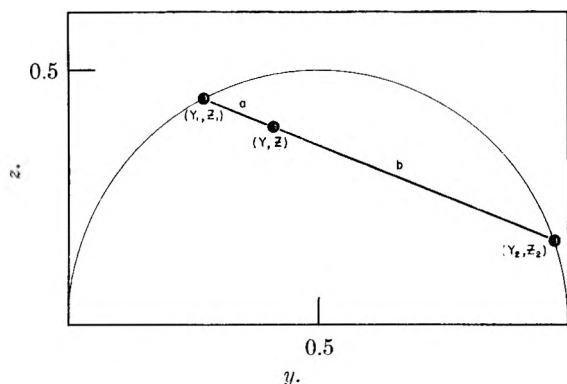The experimental measurements on diphenyl ether have been published previously,[8] while those

Fig. 1.—Plot of normalized semicircle according to eq. 1 and 2.

Results of Calculations

on dibenzyl ether,[9] anisole,[10] and o-dimethoxybenzene[10] have been submitted for publication.

In Table I are shown the values obtained for the two relaxation times, τ_1 and τ_2, and for the weight, c_2. Three sets of values are given for anisole because it was impossible to choose the best value of γ. In this case all the values of γ from 1.05 to 1.15 gave a good fit. An indication of the accuracy of the analysis is given in Table II, where, for each line of Table I, are given the corresponding observed dielectric constants and losses, and the values calculated from eq. 1 using the values of τ_1, τ_2 and c_2 of Table I. The parameter S is a measure of the deviation of the calculated from the observed values, as given by

$$S = 10^4 \sum_\lambda [(\epsilon_{calcd}' - \epsilon_{obsd}')\lambda^2 + (\epsilon_{calcd}'' - \epsilon_{obsd}'')^2\lambda]$$

(3)

Although the data for dibenzyl ether have been analyzed in terms of two relaxation times, it seems of interest in this case, because of the greater complexity of the molecule, to try an analysis in terms of a distribution of relaxation times between two limiting values. Using a graphical method,[3,4,7] the parameters A, τ_s and $\tau_1 = \tau_s e^A$ were determined for the equations[3]

$$\frac{\epsilon' - \epsilon_\infty}{\epsilon_0 - \epsilon_\infty} = 1 - \frac{1}{2A}\ln\frac{1 + e^{2A}\omega^2\tau_s^2}{1 + \omega^2\tau_s^2}$$

(4)

$$\frac{\epsilon''}{\epsilon_0 - \epsilon_\infty} = \frac{1}{A}[\tan^{-1}(e^A\omega\tau_s) - \tan^{-1}(\omega\tau_s)]$$

This method of analysis gives a plot of Y vs. Z in the form of an ellipse, as contrasted with the semicircle given by the Cole–Cole analysis. Table III gives values of the small limiting relaxation time, τ_s, the large limiting relaxation time, τ_1, the Fröhlich parameter, A, which is proportional to the eccentricity of the ellipse, and the values of S calculated by means of eq. 3.

Discussion of Results

Diphenyl ether shows two relaxation times at 40 and 60°, but at 80° the smaller relaxation time, presumably arising from some sort of intramolecu-

(8) J. H. Calderwood and C. P. Smyth, J. Am. Chem. Soc., **78**, 1295 (1956).

(9) D. M. Roberti, O. F. Kalman and C. P. Smyth, ibid., **82**, in press (1960).

(10) D. M. Roberti and C. P. Smyth, ibid., **82**, 2106 (1960).

TABLE I

RELAXATION TIMES BY THE CHORD METHOD FOR SOME AROMATIC ETHERS

	$t,$ °C.	γ	τ_1 ($\times 10^{11}$ sec.)	τ_2 ($\times 10^{11}$ sec.)	c_2
Diphenyl ether	40	1.10	2.0	0.50	0.76
	60	1.10	1.3	.44	0.87
	80	1.10	...	.40	1.0
Dibenzyl ether	20	1.05	3.3	.39	0.21
	40	1.05	2.5	.42	.31
	60	1.05	1.7	.42	.33
Anisole	20	1.05	1.46	.20	.22
	20	1.10	1.46	.26	.20
	20	1.15	1.53	.59	.26
o-Dimethoxy-benzene	25	1.05	4.6	.34	.67

TABLE II

COMPARISON OF CALCULATED AND OBSERVED VALUES

$t,$ °C.	λ (cm.)	ϵ' Calcd.	ϵ' Obsd.	ϵ'' Calcd.	ϵ'' Obsd.	S
		Diphenyl ether				
40	1.10	1.25	3.16	3.17	0.400	0.397	7.3
		3.22	3.43	3.43	.296	.295
		10.0	3.58	3.56	.138	.123
60	1.10	1.25	3.17	3.18	.371	.360	2.2
		3.22	3.39	3.39	.223	.222
		10.0	3.46	3.46	.083	.085
80	1.10	1.25	3.16	3.19	.322	.312	10.3
		3.22	3.31	3.31	.162	.162
		10.0	3.35	3.35	.055	.061
		Dibenzyl ether				
20	1.05	1.25	2.79	2.79	.308	.285	15.3
		3.22	3.02	3.03	.460	.460
		10.0	3.53	3.56	.462	.461
40	1.05	1.25	2.83	2.81	.357	.358	24
		3.22	3.11	3.11	.452	.461
		10.0	3.52	3.56	.340	.357
60	1.05	1.25	2.83	2.84	.390	.387	15.1
		3.22	3.17	3.17	.428	.431
		10.0	3.46	3.49	.229	.251
		Anisole				
20	1.05	1.25	3.07	3.05	.706	.713	13.0
		3.22	3.73	3.75	.816	.797
		10.0	4.28	4.28	.412	.402
20	1.10	1.25	3.03	3.05	.678	.713	17.5
		3.22	3.74	3.75	.801	.797
		10.0	4.28	4.28	.404	.402
20	1.15	1.25	3.07	3.05	.716	.713	4.2
		3.22	3.75	3.75	.800	.797
		10.0	4.28	4.28	.402	.402
		o-Dimethoxybenzene				
25	1.05	0.31	2.92	2.96	.37	.41	80
		1.25	3.47	3.42	.427	.449
		3.22	3.67	3.67	.316	.316
		10.0	3.90	3.87	.278	.218

TABLE III

ANALYSIS IN TERMS OF A DISTRIBUTION OF RELAXATION TIMES BETWEEN LIMITS FOR DIBENZYL ETHER

$t,$ °C.	γ	A	τ_s ($\times 10^{11}$ sec.)	τ_1 ($\times 10^{11}$ sec.)	S
20	1.10	2.0	1.1	7.9	55
40	1.10	1.6	0.8	4.2	42
60	1.10	0.8	0.8	1.9	33

lar motion, becomes completely predominant. Dibenzyl ether also shows two relaxation times with a tendency for the smaller one to become more important at higher temperatures. In both cases, the smaller relaxation time shows relatively little dependence on temperature, as might be expected for an intramolecular relaxation process. The small relaxation times in Table III, presumably associated with intramolecular motion, are seen to be little dependent on temperature and hence on viscosity, while the large relaxation times are strongly dependent, as would be expected if they were associated with orientation of the molecule as a whole. These values may be compared with the single most probable values obtained from the Cole–Cole plot, 2.76×10^{-11} sec. at $20°$, 1.87 at $40°$, and 1.32 at $60°$, with almost negligible values for the distribution parameter α, 0.06, 0.04 and 0.02, respectively.

Anisole shows excellent agreement of the calculated and observed values in Table II for values of γ of 1.05, 1.10 and 1.15, but the value obtained for τ_2 appears sensitive to that chosen for γ. The values of the smaller relaxation time for anisole are near enough to that for o-dimethoxybenzene to indicate that both probably are associated with the rotation of the methoxy group. The reduced relaxation time, τ_1/η, is the same for both molecules, 1.4, indicating that, in both cases, τ_1 is the relaxation time for the orientation of the molecule as a whole, although one would expect

the slightly larger o-dimethoxybenzene molecule to have a slightly larger value. The small relaxation time is more prominent, that is, c_2 is larger, in o-dimethoxybenzene than in anisole, which is qualitatively consistent with the existence of two methoxy groups instead of one.

It is evident that the dielectric behavior of certain molecules with abnormally low relaxation times can be represented in terms of two relaxation times, one corresponding to orientation of the polar molecule as a whole and a smaller one corresponding to an intramolecular motion or shift of charge. An analysis based on so few points in a frequency region where two different relaxation processes may overlap cannot be expected to give accurate values for the two relaxation times, or, in some cases, even to establish the existence of a second relaxation process, if there is no other reason to expect its presence. Indeed, the need for caution in the use of this method is emphasized by the fact that the few experimental points available for each substance may often be represented by a distribution around a most probable value or by a continuous distribution between limits. However, the relaxation time values obtained by analysis in this way, though very approximate, are consistent with what might be expected from the molecular sizes and structures and should be valuable in the study of molecular structure and behavior.

THE RELATIVE EFFECTS OF THE URANYL SULFATE COMPLEXES ON THE RATE OF EXTRACTION OF URANIUM FROM ACIDIC AQUEOUS SULFATE SOLUTIONS

By Kenneth A. Allen

Oak Ridge National Laboratory, Oak Ridge, Tennessee[1]

At constant sulfuric acid activity, constant low total uranium concentration and constant extractant concentration, the rate of extraction of uranyl sulfate by tri-n-octylamine sulfate in benzene decreases with increasing aqueous sulfate ion activity as a linear function of the corresponding decrease in the fraction of the aqueous uranium present as the dipositive uranyl ion. On the basis of the reasonable hypothesis that the first-order behavior of the system as a whole extends to the species UO_2^{++}, UO_2SO_4 and $UO_2(SO_4)_2^{=}$, it is shown that the data permit estimation of the individual rate constants for these species. The ratios of these constants to each other, in turn, indicate that UO_2^{++} is about six times as effective as either UO_2SO_4 or $UO_2(SO_4)_2^{=}$ in transferring uranium from such aqueous systems to an extracting phase.

Introduction

The equilibria involved in uranium extraction from acidic aqueous sulfate solutions by long chain amine sulfates in benzene have been described in previous papers,[2] and the effects of the various aqueous uranium species (UO_2^{++}, UO_2SO_4, UO_2-$(SO_4)_2^{=}$) on these equilibria have been shown to lead to new estimates of the formation constants of the uranyl sulfate complexes, which are in reasonable agreement with other reported values.[3]

A question which arises frequently in discussions concerning these systems asks which of the three aqueous uranium species is most effective in transferring uranium to the organic phase during such an extraction, and what, if any, are the relative effects of the others. Since this question deals with processes occurring during a transition from one state to another, it is apparent at the outset that no conceivable combination of equilibrium experiments, which deal only with initial and final states, can possibly provide the required informa-

(1) Operated for the U.S.A.E.C. by Union Carbide Nuclear Company.

(2) Cristiane Boirie, *Bull. Soc. Chim. France*, 1088 (1958); Doctoral Dissertation, University of Paris, May 20, 1959; W. J. McDowell and C. F. Baes, This Journal, **62**, 777 (1958); K. A. Allen, *J. Am. Chem. Soc.*, **80**, 4133 (1958).

(3) S. Ahrland, *Acta Chem. Scand.*, **5**, 1151 (1951); K. A. Kraus and F. Nelson, Chap. 23, p. 349, "The Structure of Electrolytic Solutions," W. J. Hamer, Editor, John Wiley and Sons, Inc., New York, 1959; M. H. Lietzke and R. W. Stoughton, *J. Phys. Chem.*, **64**, in press (1960).
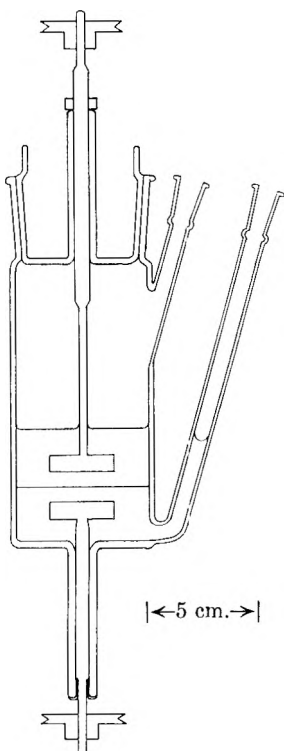
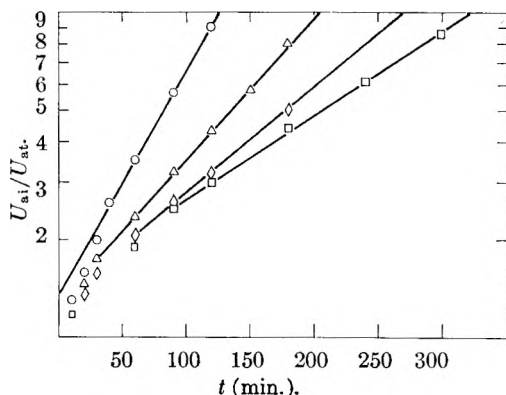Fig. 1.—Cell for studying liquid-liquid extraction kinetics.

Fig. 2.—Typical experimental data; added Na₂SO₄ molarities are: ⊙, 0; △, 0.05; ◇, 0.30; □, 0.90.

tion. Non-equilibrium measurements, on the other hand, might be of value in gaining insight into these processes. The present paper describes a series of kinetic studies on a typical uranyl sulfate-amine sulfate extraction system $(H_2O-H_2SO_4-Na_2SO_4-UO_2SO_4)$: C_6H_6-TOAS (tri-n-octylamine sulfate) which did indeed yield reasonably unambiguous indications as to the relative effectiveness of each of the three species.

Experimental

The materials and analytical methods have been described elsewhere.[2-4] The cell used for the rate measurements is shown in Fig. 1. During the runs the cell was immersed in a $25.00 \pm 0.01°$ bath, and that part of the aqueous phase present in the long side tube, which allowed sampling with an ordinary pipet, was pulsed up and down several centimeters every few seconds by a small bellows pump, in order to ensure thorough mixing.

The aqueous phases were prepared by combining H_2SO_4

(4) K. A. Allen, *Anal. Chem.*, **28**, 1144 (1956); This Journal, **62**, 1119 (1958).
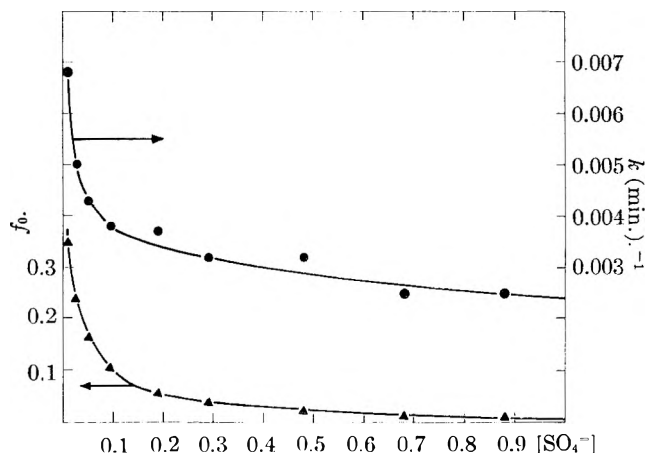
Fig. 3.—Rate constants (●) and f_0 (▲) as functions of the aqueous sulfate ion molarity.

and Na_2SO_4 solutions in such a way as to vary the sulfate ion activity while keeping the acid activity constant at $a_{H_2SO_4} = 4[H_2SO_4]^2[H_2SO_4 + Na_2SO_4]\gamma_{\pm}^3 = (4.8 \pm 0.1) \times 10^{-6}$. For the pure acid this activity corresponds to $[H_2SO_4] = 0.0250$; at the highest sulfate level used $([Na_2SO_4] = 0.900)$ it was necessary to increase $[H_2SO_4]$ to 0.0460. These and the intermediate compositions were computed from Baes' relationships,[5] and then were checked experimentally at the termination of each run by determining $[H_2SO_4]_{org}$. Whenever the latter varied more than 1% from the predicted value[6] the run was repeated with an appropriately adjusted aqueous phase. The TOAS solutions in benzene were prepared by pre-equilibrating 0.1 M TOA with 0.0250 M H_2SO_4, and were therefore already at the proper sulfate level initially for each run.

In commencing a run 100 ml. of an aqueous phase containing 0.001 M UO_2SO_4, in addition to H_2SO_4 and Na_2SO_4 as described above, was pipetted into the cell, followed by 100 ml. of TOAS solution, care being taken to avoid undue mixing. The paddles were then driven at 25 r.p.m. in opposite directions by synchronous motors, and the side tube was pulsed as described. At predetermined time intervals the motors were stopped and 0.5 ml. of aqueous solution was transferred directly to the automatic uranium titrator.[4] A typial sampling schedule was (in minutes) 10, 10, 10, 30, 30, 30, and then hourly until $[UO_2SO_4]_{aq}$ fell below 0.0001 M. No attempt was made to replace the liquid removed for analysis. However, since the same procedure was used for all the runs, the rather complex relationships necessary for estimating the true rate constants corresponding to constant total volumes of both phases were ignored.

Results and Discussion

In computing the fractions of the aqueous uranium in the forms of the various species (*i.e.*, $f_0 = [UO_2^{++}]/[\Sigma U]_{aq}$, $f_1 = [UO_2SO_4]/[\Sigma U]_{aq}$, and $f_2 = [UO_2(SO_4)_2^=]/[\Sigma U]_{aq}$), the relationships derived in reference 2 were used,[7] working back-

(5) C. F. Baes, Jr., *J. Am. Chem. Soc.*, **79**, 5611 (1957).

(6) At $a_{H_2SO_4} = 4.8 \times 10^{-6}$, 0.1 M TOA in C_6H_6 becomes 0.056 molar in H_2SO_4 (K. A. Allen, This Journal, **60**, 239 (1956)).

(7) The relationships from ref. 2 for computing the f_i are

$$K_{a1} = \frac{[UO_2SO_4]}{[UO_2^{++}][SO_4^=]} \quad G_1 = 580$$

$$K_{a2} = \frac{[UO_2(SO_4)_2^=]}{[UO_2^{++}][SO_4^=]^2} \quad G_2 = 3450$$

$$\log G_i = -0.509\Delta(Z_i^2)\sqrt{I}(1 + 2.3\sqrt{I})^{-1}$$

$$\Delta(Z_1^2) = \Delta(Z_2^2) = -8$$

$$I = 1/2 \sum_j c_j Z_j^2 = [H_2SO_4] + [Na_2SO_4] + 2[SO_4^=]$$

and finally

$$f_0 = \frac{[UO_2^{++}]}{[\Sigma U]_{aq}} = \left(1 + \frac{K_{a1}}{G_1}[SO_4^=] + \frac{K_{a2}}{G_2}[SO_4^=]^2\right)^{-1}$$

wards from the constants and making the same one-parameter Debye–Hückel ionic strength corrections as were used in obtaining the constants in the first place. Also as in that work, of course, we have the almost indispensably simplifying experimental condition that $[\Sigma U]_{aq} << [SO^=]_{aq}$ throughout. In addition to the assumptions affecting the original evaluation of the constants (absence of medium effects, applicability of Debye–Hückel activity variation over the range of ionic strengths used, and assignment of the aqueous molarity of the neutral species, UO_2SO_4, as a linear function of the activity of the aqueous uranyl sulfate), there are others peculiar to the kinetic considerations of interest here. The two most important of these are, first, that activity coefficient variations do not seriously affect the ratio U_{ai}/U_{at}[8] over the range of values used in computing the rate constants, and, second, that as a given extraction at a given sulfate level proceeds, the rates of re-adjustment of the f_i are fast compared with the over-all rate of extraction.

Typical kinetic data are shown in Fig. 2. In each run the first few points showed spuriously high rates, due to unavoidable mixing which occurred while the run was being set up. However, it is apparent that the limiting behavior in each case is first order, in agreement with the results of other studies of similar systems.[9]

In view of the complexity of the chemical reactions involved,[2] such behavior suggests that the rate-controlling step is Fick's first law diffusion through one, or possibly both, of the stationary layers at the liquid–liquid interface. The fact that the changes observed were due entirely to experimentally controlled variations in the aqueous phase suggests that diffusion on the aqueous side of the interface is the slower, and therefore the rate-determining process.

The rate constants derived from the slopes of the lines in Fig. 2 and other similar plots are shown as a function of the calculated sulfate ion molarities in Fig. 3. Similarly, on the same plot, the fractions f_0 of the aqueous uranium in the form of the uranyl ion are shown as a function of the same

$$f_1 = \frac{[UO_2SO_4]}{[\Sigma U]_{aq}} = f_0 \frac{K_{a1}}{G_1} [SO_4^=]$$

$$\text{and } f_2 = \frac{[UO_2(SO_4)_2^=]}{[\Sigma U]_{aq}} = f_0 \frac{K_{a2}}{G_2} [SO_4^=]^2$$

(8) The subscript abbreviations are as follows:

U_{ai} = initial molarity of aq. uranium = total taken
U_{at} = $[U]_{aq}$ at time t
U_{ae} = $[U]_{aq}$ at equilibrium

The log function plotted in Fig. 2 derives from assignment of the difference $U_{at} - U_{ae}$ as the driving force

$$dU_{at} = -k(U_{at} - U_{ae})dt, \text{ whence}$$

$$\log \frac{U_{ai} - U_{ae}}{U_{at} - U_{ae}} = kt, \text{ and since}$$

in all of the present extractions $U_{ae} \ll U_{ai}$ and $U_{ae} \ll U_{at}$ also, for the data actually used in computing rate constants, there follows at once the obvious simplification to the expression used in the plots.

(9) J. B. Lewis, Chem. Eng. Sci., 8, 295 (1958); 3, 248, 260 (1954); R. P. Wischow, Doctoral Dissertation, Vanderbilt University, 1958; A. D. Ryon, F. L. Daley and R. S. Lowrie, Amex and Dapex manuscripts in preparation for issue as ORNL topical reports (1960), to mention a few.
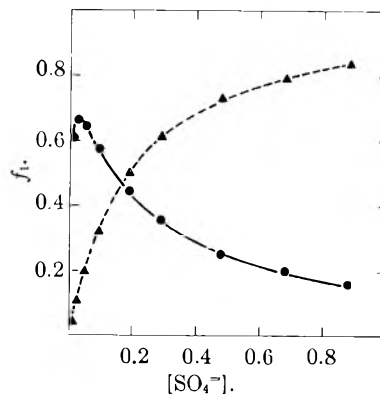

Fig. 4.—The fractions of the mono (f_1, ●) and disulfate (f_2, ▲) complexes computed for the sulfate range shown in Fig. 3.
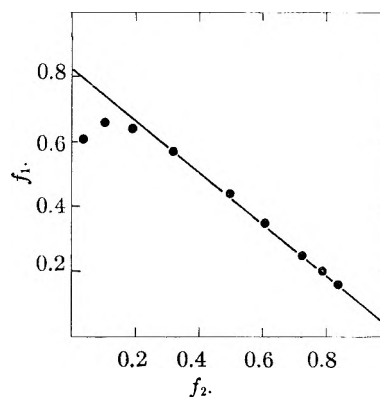

Fig. 5.—Plot for determining an approximately constant linear combination of f_1 and f_2.
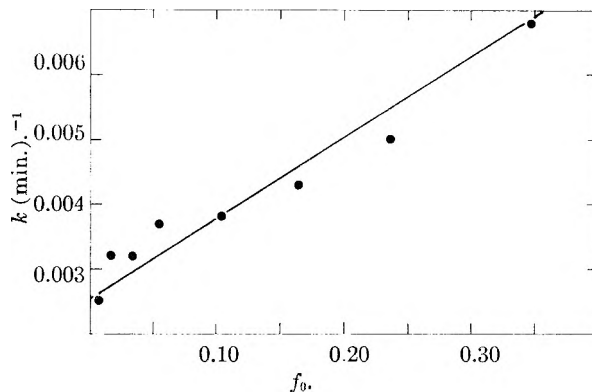

Fig. 6.—The rate constant as a linear function of f_0. The line shown was computed from the linear combination $0.015f_0 + 0.0025f_1 + 0.0025f_2$.

variable. The almost astonishing similarity between the two curves suggests immediately that the uranyl ion is of paramount importance in controlling the rate of transfer of uranium to the organic phase. The other two fractions, f_1 and f_2, computed for the same experimental points, are shown in Fig. 4; neither of these curves shows any apparent correlation with the rate constants.

A necessary hypothesis for further interpretation is the quite reasonable one that the first-order behavior evidenced by the system as a whole extends to the aqueous uranium species individually as well. It follows that the over-all rate can be expressed as a linear combination of the fractions

f_i. *I.e.*, we can write $k = k_0 f_0 + k_1 f_1 + k_2 f_2$, where the k_i are the respective first-order rate constants for the individual species.[10] From these considerations and the appearance of the curves in Fig. 3 the simplest approach is to ascribe the changes in the rate constants entirely to the corresponding changes in f_0. Obviously, however, since f_0 vanishes at high sulfate levels while k levels off at an asymptotic value, there remains an approximately constant contribution from the mono- and disulfate complexes. The next question revolves around whether or not such a contribution is possible, as a linear combination of f_1 and f_2. If it is, then some number A can be expressed as

$$A = Bf_1 + Cf_2, \text{ from which}$$

$$f_1 = \frac{A}{B} - \frac{Cf_2}{B}$$

The plot of f_1 against f_2 in Fig. 5 shows, indeed, that with the exception of a few points at the low sulfate end the fractions provide satisfactory evaluations of A/B and C/B. Now, since the rate constants are to be expressed as a linear function of one variable, f_0, plus a constant term, it is necessary only to plot k against f_0 in order to determine the coefficients k_0, k_1 and k_2. Such a plot is shown in Fig. 6. Here, admittedly, the fit is less than satisfying. Nevertheless, there is no apparent

(10) The rates of transfer of the individual species are

$$d[UO_2{}^{++}] = -k_0[UO_2{}^{++}]dt$$
$$d[UO_2SO_4] = -k_1[UO_2SO_4]dt$$
$$d[UO_2(SO_4)_2{}^=] = -k_2[UO_2(SO_4)_2{}^=]dt$$

Adding these expressions

$$d([UO_2{}^{++}] + [UO_2SO_4] + [UO_2(SO_4)_2{}^=]) = dU_{at}$$
$$= -kU_{at}dt = -(k_0[UO_2{}^{++}] + k_1[UO_2SO_4] + k_2[UO_2(SO_4)_2{}^=])dt$$

From which, finally

$$k = k_0 f_0 + k_1 f_1 + k_2 f_2$$

indication that the data suggest a fundamental inadequacy in the present treatment.

It is concluded, within the degree of uncertainty indicated by the scatter in Fig. 6, that the overall rate constant can indeed be expressed as a linear combination of the f_i, the coefficients of which are themselves the first-order rate constants of the individual species. The values resulting from the plots in Fig. 5 and 6 are $k_0 = 0.015 \pm 0.005$, $k_1 = 0.0025 \pm 0.0010$, and $k_2 = 0.0025 \pm 0.0010$ min.$^{-1}$.

The absolute magnitudes of these numbers, of course, are dependent on the measuring device. On the other hand, however, their ratios, which are dimensionless, should be indicative of the behavior of the chemical system *per se*, in any sort of liquid–liquid contactor.[11] These ratios indicate that, mole for mole, the uranyl ion is about six times as effective as either of the other two species in transferring uranium from acidic sulfate aqueous solutions to amine sulfate extractants in benzene. In view of the fact that the three complex species must make their contributions entirely on the aqueous side of the interface, it is quite reasonable to suppose that their relative effects would be similar in similar aqueous phases regardless of the nature of the extracting phase. Further work, aimed at resolving the correctness of this and other suppositions in the present treatment through straight diffusion measurements coupled with kinetic studies of other extractants, will be described in subsequent papers.

(11) Possible exceptions to this generalization are contacting methods which result in anomalous equilibria due to violence of agitation (K. A. Allen and W. J. McDowell, THIS JOURNAL, **64**, in press (1960)). However, as far as is known at present, such anomalies are encountered only very infrequently.

LITHIUM SALTS AS SOLUTES IN NON-AQUEOUS MEDIA. I. THE TERNARY SYSTEM LiNO₃-LiClO₄-CH₃OH AT 25°

By Meyer M. Markowitz and Robert Harris

Contribution from the Chemicals Division, Research and Development Laboratories of the Foote Mineral Company, Berwyn, Penna.

The isothermal invariant point for the system LiNO₃–LiClO₄–CH₃OH at 25°, in weight per cent., corresponds to 0.7% LiNO₃, 63.7% LiClO₄ and 35.6% CH₃OH. Only the unsolvated salts exist as the equilibrium solids. Lithium perchlorate has a significant salting-out effect on lithium nitrate in methyl alcohol solutions. This phenomenon is interpreted as indicating solvation of the perchlorate ion in methyl alcohol.

The systematic studies of Willard and Smith[1,2] demonstrated the exceptionally high equilibrium solubility of anhydrous lithium perchlorate in organic solvents with an oxygen-containing functional group.

Similar solubility characteristics have been found for lithium nitrate in such oxygenated solvents as glacial acetic acid,[3] ethyl alcohol[4] and isoamyl alcohol.[5] The conductance behavior of dilute solutions of lithium perchlorate in methyl alcohol[6]

(1) H. H. Willard and G. F. Smith, *J. Am. Chem. Soc.*, **45**, 286 (1923).

(2) G. F. Smith, *ibid.*, **47**, 762 (1925).

(3) A. W. Davidson and H. A. Geer, *ibid.*, **55**, 642 (1933); **60**, 1211 (1938).

(4) A. N. Campbell and R. A. Bailey, *Can. J. Chem.*, **36**, 518 (1958).

(5) R. Mueller, *Z. anorg. allgem. Chem.*, **142**, 130 (1925).

and in ethyl alcohol[7] and of dilute solutions of lithium nitrate in ethyl alcohol[7] show the solutes to be strong electrolytes in these nonaqueous solvents. Analogous results have been found for lithium nitrate and perchlorate in N,N-dimethylacetamide.[8] Undoubtedly, the conductivity and solubility phenomena must be related to solvation reactions between the solute ions and the solvent molecules.[9]

The extensive solvation of the lithium ion in aqueous solution is well-established[10-13] and is frequently reflected in the occurrence of crystalline hydrates[14] such as $LiClO_4 \cdot 3H_2O$[15] and $LiNO_3 \cdot 3H_2O$.[16] Conductance investigations of concentrated solutions of lithium nitrate in ethyl alcohol and in ethyl alcohol–water mixtures point to the transition of lithium ion solvation from a water molecule sheath to an ethyl alcohol molecule sheath.[17] Attempts at isolating a solid alcoholate in the ternary phase system: lithium nitrate–ethyl alcohol–water, were unsuccessful.[4,16] We thought that a sterically smaller solvent, such as methyl alcohol, would be more likely to give solid solvated lithium compounds. Lithium perchlorate[1] and lithium nitrate[18] dissolve readily in methyl alcohol and the electrical conductivity of concentrated solutions of the latter salt is known. Accordingly, an isothermal study of the ternary system lithium nitrate–lithium perchlorate–methyl alcohol at 25° was undertaken.

The isothermal diagram does not indicate the existence of any solvated solid at equilibrium but does point to the possibility of solvation of the perchlorate ion as part of the driving force for the solution process of lithium perchlorate in methyl alcohol.

Experimental Procedures

The preparations of anhydrous lithium perchlorate and of anhydrous lithium nitrate have been detailed elsewhere.[19]

The lithium perchlorate was analyzed by precipitation as nitron perchlorate.[20] Analysis of product: ClO_4^-, 94.0 (calcd., 93.5). The lithium nitrate was analyzed by a modified Kjeldahl procedure using Devarda's alloy to reduce the nitrate group to ammonia.[20] Analysis of product:

(6) E. D. Copley and H. H. Hartley, *J. Chem. Soc.*, 2488 (1930).

(7) E. D. Copley, D. M. Murray-Rust and H. H. Hartley, *ibid.*, 2492 (1930).

(8) G. R. Lester, J. W. Vaughn and P. G. Sears, *Trans. Kentucky Acad. Sci.*, **19**, 28 (1958).

(9) L. F. Audrieth and J. Kleinberg, "Non-aqueous Solvents," John Wiley and Sons, Inc., New York, N. Y., 1953, pp. 19–20.

(10) R. A. Robinson and R. H. Stokes, "Electrolyte Solutions," Butterworth Scientific Publications, London, 1955, p. 320.

(11) A. N. Campbell, E. M. Kartzmark and A. G. Sherwood, *Can. J. Chem.*, **36**, 1325 (1958).

(12) A. N. Campbell, J. B. Fishman, G. Rutherford, T. P. Schaefer and L. Ross, *ibid.*, **34**, 151 (1956).

(13) A. N. Campbell, G. H. Debus and E. M. Kartzmark, *ibid.*, **33**, 1508 (1955).

(14) A. F. Wells, "Structural Inorganic Chemistry," Oxford University Press, London, 1945, pp. 370–373.

(15) J. P. Simmons and C. D. L. Ropp, *J. Am. Chem. Soc.*, **50**, 1650 (1928).

(16) A. N. Campbell and E. M. Kartzmark, *Can. J. Chem.*, **34**, 1405 (1956).

(17) A. N. Campbell and G. H. Debus, *ibid.*, **34**, 1232 (1956).

(18) M. A. Klochko and J. G. Grigor'ev, *Izvest. Sektora Fiz.-Khim. Anal., Inst., Obshchei Neorg. Khim., Akad. Nauk S.S.S.R.*, **21**, 311 (1952); *cf. C.A.*, **48**, 6220c (1954).

(19) M. M. Markowitz, THIS JOURNAL, **62**, 827 (1958).

(20) F. P. Treadwell and W. T. Hall, "Analytical Chemistry," Vol. II, John Wiley and Sons, Inc., New York, N. Y., Ninth English Edition, 1942, pp. 383–384.
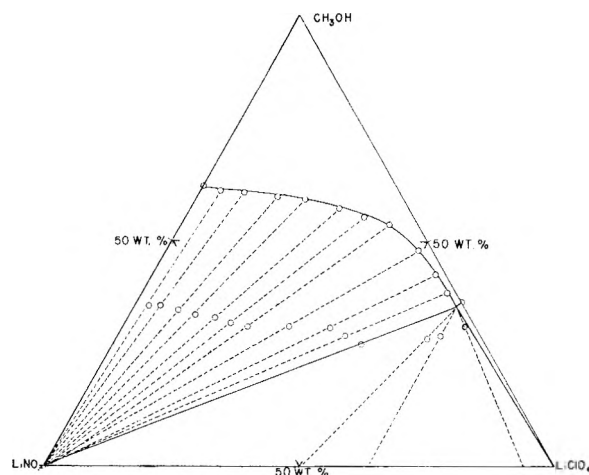
Fig. 1.—The ternary system $LiNO_3$–$LiClO_4$–CH_3OH at 25°.

NO_3^-, 90.1 (calcd., 89.9). It was subsequently found that nitrate could be determined in this fashion without interference from the presence of perchlorate. Anhydrous methyl alcohol was prepared by refluxing the solvent with magnesium metal turnings, and then fractional distillation.[21] Analysis of the product by the Karl Fischer technique showed it to contain less than 0.01% water.

The study was carried out by the "Synthetic Method."[22] Complexes were equilibrated in a constant temperature bath maintained at 25.0 ± 0.02°. Equilibration was ascertained by the constancy of the refractive index of the solutions. The solutions were analyzed for methyl alcohol content by the weight loss encountered upon evaporation and drying of the sample under vacuum for two hours at 150°. The remaining solids were then analyzed for nitrate content by the method described earlier; perchlorate content was taken by difference.

The composite data are given in Table I and are shown diagrammatically in Fig. 1. Extrapolation of the tie lines to the solid phases was facilitated by the algebraic method.[23]

TABLE I

LITHIUM NITRATE–LITHIUM PERCHLORATE–METHANOL AT 25°

Complex compn., wt. %		Soln. compn., wt. %		
$LiNO_3$	$LiClO_4$	$LiNO_3$	$LiClO_4$	Solid phase
. . .	. . .	37.8	. . .	$LiNO_3$
61.9	2.2	35.0	3.6	$LiNO_3$
59.4	4.7	30.4	8.8	$LiNO_3$
56.7	8.9	24.1	15.8	$LiNO_3$
53.3	13.0	19.6	21.7	$LiNO_3$
50.2	16.9	13.1	29.6	$LiNO_3$
47.4	20.5	9.4	35.1	$LiNO_3$
44.2	24.2	6.1	41.0	$LiNO_3$
36.2	32.3	2.6	49.4	$LiNO_3$
28.1	40.3	1.5	55.5	$LiNO_3$
26.1	44.7	1.1	60.0	$LiNO_3$
24.2	48.6	0.7	63.7	$LiNO_3$
10.8	61.0	0.8	63.7	$LiNO_3 + LiClO_4$
7.4	63.4	0.7	63.9	$LiNO_3 + LiClO_4$
1.7	67.2	0.8	63.6	$LiNO_3 + LiClO_4$
0.8	67.9	0.7	63.8	$LiNO_3 + LiClO_4$
. . .	. . .	. . .	63.8	$LiClO_4$

Discussion

It is apparent from Fig. 1 that the unsolvated

(21) A. Weisberger, E. S. Proskauer, J. A. Riddick and E. E. Toops, Jr., "Organic Solvents," Vol. VII of "Techniques Organic Chemistry," Interscience Publishers, Inc., New York, N. Y., 1955, pp. 333–337.

(22) F. F. Purdon and V. W. Slater, "Aqueous Solution and the Phase Diagram," Edward Arnold and Co., London, 1946, pp. 65–69.

(23) A. E. Hill and J. E. Ricci, *J. Am. Chem. Soc.*, **53**, 4305 (1931).

salts are the only equilibrium solids present in the system at 25°. The isothermal invariant point corresponds to the average composition in weight per cent., of 0.7% $LiNO_3$, 63.7% $LiClO_4$ and 35.6% CH_3OH.

A particularly interesting feature of the system is the very small univariant region for the solid lithium perchlorate–solution equilibrium. Lithium perchlorate exerts a marked salting-out effect on lithium nitrate in methyl alcohol. Figure 1 is quite similar to the isothermal diagrams determined for the systems $LiCl$–$NaCl$–H_2O at 25°,[24] and $LiCl$–KCl–H_2O at 25°[25]; in each instance lithium chloride manifests a strong salting-out of the other alkali metal chloride. This phenomenon has been attributed to the strong hydration of the lithium ion.[24,25]

(24) A. Smits, J. Elgersma and M. E. Hardenberg, *Rec. trav. chim.*, 43, 671 (1924).

(25) A. N. Campbell and E. M. Kartzmark, *Can. J. Chem.*, 34, 672 (1956).

In the present system where the two salts possess a common cation, it appears that the depressant effect of lithium perchlorate on the solubility of lithium nitrate in methyl alcohol might be related to differences in solvent–anion interaction. An interpretation of the conductivity of concentrated solutions of lithium nitrate in absolute ethyl alcohol[17] has led to the suggestion that the nitrate ion is solvated in this medium. Ultrasonic studies[26] aimed at resolving complex formation in acetone solutions of lithium perchlorate have been used as the basis for the tentative proposal of perchlorate ion solvation as part of the solution mechanism of this salt. Solvation of the lithium ion in hydroxylic solvents involves association with the oxygen atom of the solvent molecule[27]; oxyanion solvation in these solvents in all likelihood arises through hydrogen-bonding.

(26) P. G. T. Fogg, *J. Chem. Soc.*, 4111 (1958).

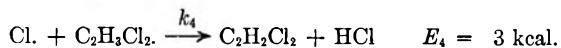(27) A. D. E. Pullin and J. Pollock, *Trans. Faraday Soc.*, 54, 11 (1958).
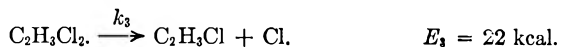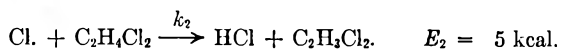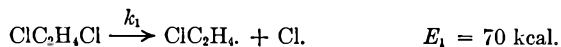

NOTES

THE PHOTOLYSIS OF 1,2-DICHLOROETHANE

By Wm. F. Yates and L. J. Hughes

Contribution from the Research Department, Plastics Division, Monsanto Chemical Company, Texas City, Texas

The thermal decomposition of 1,2-dichloroethane has been studied in detail by Barton and Howlett.[1] These authors have established essentially that the reaction proceeds by a radical chain mechanism and is a homogeneous gas phase decomposition. The mechanism they propose, with subsequent refinement of the initiation step by Howlett[2] is as shown; with the estimated energies given

$$ClC_2H_4Cl \xrightarrow{k_1} ClC_2H_4. + Cl. \qquad E_1 = 70 \text{ kcal.}$$

$$Cl. + C_2H_4Cl_2 \xrightarrow{k_2} HCl + C_2H_3Cl_2. \qquad E_2 = 5 \text{ kcal.}$$

$$C_2H_3Cl_2. \xrightarrow{k_3} C_2H_3Cl + Cl. \qquad E_3 = 22 \text{ kcal.}$$

$$Cl. + C_2H_3Cl_2. \xrightarrow{k_4} C_2H_2Cl_2 + HCl \qquad E_4 = 3 \text{ kcal.}$$

When Barton and Howlett[1] estimated the activation energy (22 kcal.) for step three in the sequence they used a value of 80 kcal. for the energy of the C–Cl bond in 1,2-dichloroethane. Howlett[2] has subsequently argued for the value of 70 kcal. as shown above, and if his argument for the initiation step is accepted then some correction must be made in the 22 kcal. value for step three.

If one examines the over-all rate equation for the observed disappearance of dichloroethane

(1) D. H. B. Barton and K. E. Howlett, *J. Chem. Soc.*, 155 (1949).

(2) K. E. Howlett, *Trans. Faraday Soc.*, 48, 25 (1952).

$$d[C_2H_4Cl_2]/dt = (k_1k_2k_3/k_4)^{1/2}[C_2H_4Cl_2] = k_0[C_2H_4Cl_2]$$

it is seen that the over-all temperature coefficient for a photochemically induced reaction should be given by

$$d \ln k_0/d(1/T) = -(E_2 + E_3 - E_4)/2R$$

since the initiation rate can be held to a constant independent of the temperature. Because E_2 and E_4 are accepted as being small[3] and have different signs in the expression above, the over-all activation energy should be determined largely by the value of E_3.

Experimental

Materials.—The 1,2-dichloroethane used was the commercial product prepared by reaction of ethylene and chlorine. It was fractionally distilled until a gas chromatogram, sensitive to 10 p.p.m. of hydrocarbon and chlorinated hydrocarbon impurities, could detect no impurities.

Apparatus.—The photolysis cell was made of a cylindrical Pyrex tube 30 cm. long and 3.8 cm. i.d. fitted with a quartz window at one end. It had inlet and outlet tubes at the ends, an opening for a thermometer, and was electrically heated and insulated. The source of illumination was a 200 watt xenon lamp (Type 510B1, Hanovia Lamp Div., Engelhard Ind., Inc.) located about 2 cm. from the quartz window.

Procedure.—Helium was saturated with 1,2-dichloroethane by passage through a thermostated bubbler and conducted through a rotameter to the photolysis cell. The contact time within the cell then could be regulated by the rate of helium flow. The outlet tube of the cell was connected directly to the sample line of a gas chromatograph for analysis of the products.

Results and Discussion

Measurements of the rate of photochemically induced decomposition of 1,2-dichloroethane were carried out at various temperatures from 110 to

(3) E. W. R. Steacie, "Atomic and Free Radical Reactions," Vol. II, A.C.S. Monograph No. 125, Reinhold Publ. Corp., New York, N. Y., 1954, p. 505, 508.
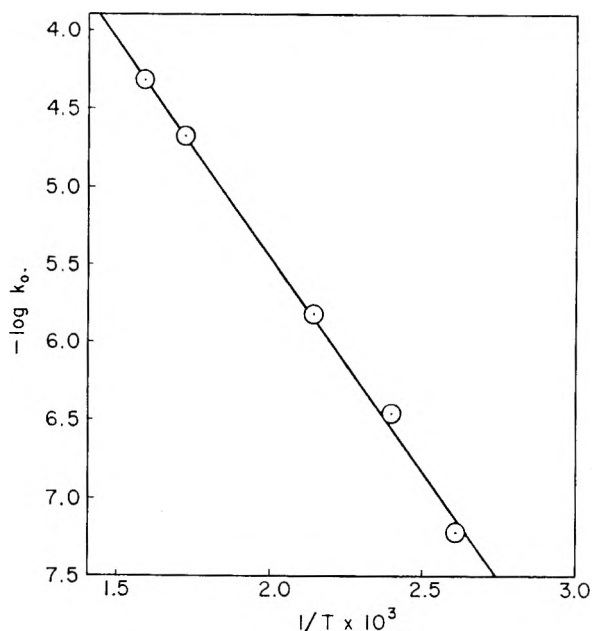
Fig. 1.—Effect of temperature on the photolysis of 1,2-dichloroethane.

360°. It is clear that thermal initiation at these temperatures is negligible. Conversions of 1,2-dichloroethane were kept low, generally less than 1%, in order to avoid possible secondary photolysis and absorption of active radiation by the products. Some acetylene was observed in some of the runs at higher temperature. It also was determined that vinyl chloride does not photolyze under the conditions employed here, so it may be inferred that the presence of acetylene is a consequence of the chain reaction or arises from dichloroethane directly. In any case, the amount of acetylene could be considered to have a negligible effect on the results here. Table I summarizes the results obtained in these experiments. The reaction rate constants shown should not be taken as absolute rate constants because they contain the undetermined initiation rate constant, which is a function of light intensity. They should be good relative rate constants, however, for the determination of the temperature coefficient.

Figure 1 is a plot of the rate constants as a function of $1/T$ from which an over-all activation energy of 12.5 kcal. can be obtained. Using this value to estimate E_3 one gets 23 kcal., which is in reasonable agreement with the value of 22 kcal. calculated by Barton and Howlett. The conclusion one then reaches is that the C–Cl bond energy in 1,2-dichloroethane is nearer to 80 kcal. than 70.

TABLE I

EFFECT OF TEMPERATURE ON THE RATE OF PHOTOLYSIS OF 1,2-DICHLOROETHANE

Temp., °C.	Contact time range, sec.	k_0 (sec.$^{-1}$) $\times 10^8$
110	0–120	6.06
146	0–90	34.6
194	0–90	152
310	0–60	2090
360	0–20	4820

THE GAS CHROMATOGRAPHIC DETERMINATION OF HYDROGEN, DEUTERIUM AND HD

BY W. A. VAN HOOK AND PAUL H. EMMETT

Department of Chemistry, The Johns Hopkins University, Baltimore, Md.

Received November 6, 1959

A consideration of the results obtained in this Laboratory with an aluminum oxide chromatographic column operating at $-195°$ for the separation of ortho- and parahydrogen as well as those reported by Moore and Ward[1] for the separation of ortho and paradeuterium and ortho and parahydrogen made it seem probable that a separate peak would be found for HD. Such a peak would make possible the analysis of an H_2–HD–D_2 mixture by gas chromatography. The present paper reports the successful production of a chromatogram showing peaks for parahydrogen, orthohydrogen plus HD, and deuterium using helium as a carrier gas; and for HD and D_2 using hydrogen as a carrier gas.

Experimental

Apparatus.—The chromatographic assembly consisted of a twelve foot $1/4$ inch coiled copper column filled with 20/40 mesh activated alumina in series with a manometer type flow meter and a Gow-Mac TE 1997 thermal conductivity cell connected to a Leeds and Northrup Speedomax type G recorder. All runs were made with the column immersed in liquid nitrogen and with the cell at room temperature. Alumina was selected as a good diamagnetic adsorbent which, at $-195°$, would not catalyze the ortho–para conversion or the hydrogen–deuterium exchange. It was activated by heating at 120° for 48 hours.

Flow rates were in the range 100 to 150 cc. per minute; retention times were between 5 and 7 minutes. Following a suggestion of Moore and Ward,[1] the hydrogen, HD and deuterium were converted to water over copper oxide prior to analysis in the thermal conductivity cell.

The mass spectrograph was a Consolidated Electronics Company type 21–611 instrument with an attached Varian G-10 recorder.

Results

Deuterium and Hydrogen.—Good separation of deuterium and of ortho and parahydrogen was obtained. However, ortho- and paradeuterium did not separate on the column used in this work (cf. Fig. 1b).

Deuterium, HD and Hydrogen.—All chromatograms of mixtures containing these three isotopes show the HD and the orthohydrogen peaks superimposed (Fig. 1c compared with Fig. 1b). A knowledge of the orthohydrogen to parahydrogen ratio or of the HD:D_2 ratio would therefore be necessary for a quantitative analysis.

In order to test the utility of the chromatograms for the analysis of typical H_2–HD–D_2 mixtures, results obtained with a mass spectrometer were compared with those obtained gas chromatographically. It became apparent that to make even an approximate analysis one would have to correct for the tailing of the HD plus orthohydrogen peak into the deuterium peak. Since pure HD or a mixture of HD and orthohydrogen could, for obvious reasons, not be obtained for use in estimating quantitatively the tailing effect, an approximate and semi-empirical method illustrated in Fig. 1c

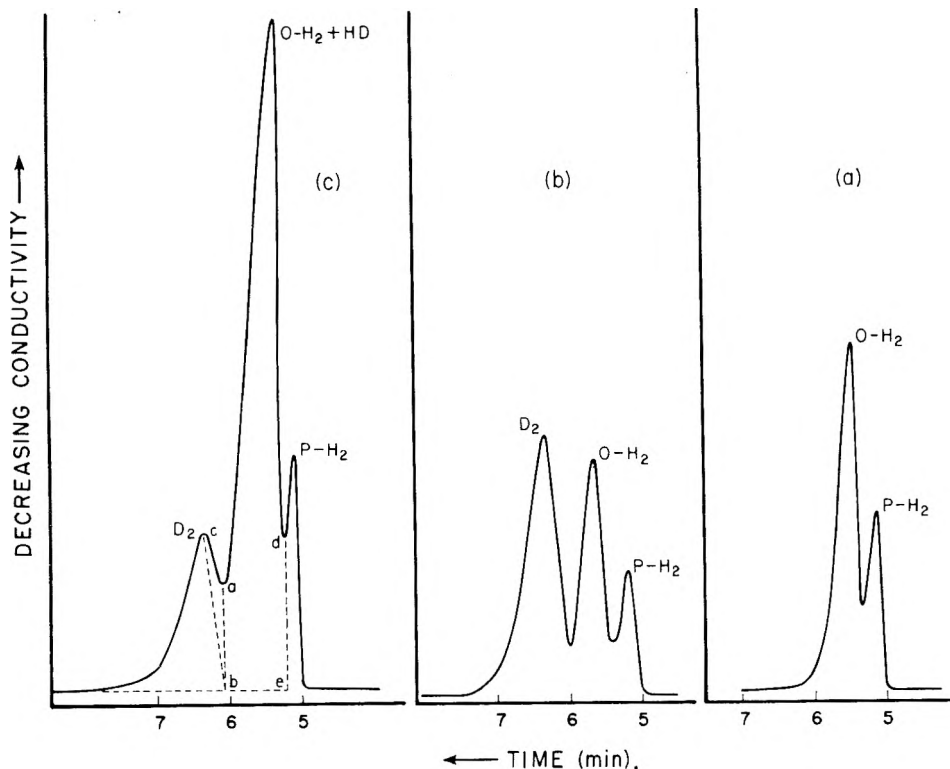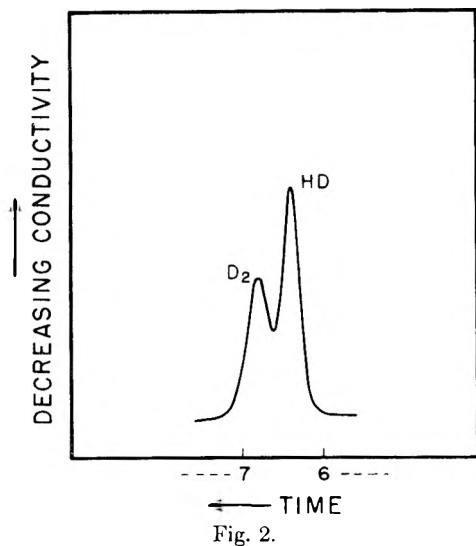(1) W. R. Moore and W. R. Ward, J. Am. Chem. Soc., **80**, 2909 (1958).

Fig. 1.

Fig. 2.

runs 1 to 4 containing small amounts of HD. This is understandable when it is realized that the total hydrogen is taken as four times the value deduced from the peak for parahydrogen, and the orthohydrogen is three times the para peak. This orthohydrogen value must of course be subtracted from the combined orthohydrogen plus HD to obtain a value for HD. Hence, any slight error in the value for parahydrogen will appear as a larger error for HD.

The above method of analysis for H_2-HD-D_2 mixtures seems promising. For high accuracy a chromatographic column capable of giving greater separation of the respective peaks would have to be found.

Deuterium–HD Ratio.—As pointed out above, if the ortho to parahydrogen ratio were not known, one would have to know another ratio such as that of deuterium:HD in order to obtain a complete analysis from chromatograms of the type shown in Fig. 1c. This ratio can be determined using hydrogen as a carrying gas and a Linde Molecular Sieve column[2] as described by Ohkoshi, Fugita and Kwan[3] and by Riedel and Uhlmann.[4] It can also be done using the same alumina column employed in the present work for H_2-D_2-HD mixtures. Such a chromatogram is shown in Fig. 2.

It is our conclusion that the methods here described can be used for an inexpensive and convenient method of analysis of both mixtures of

was adopted. A vertical line was dropped from the crotch between the D_2 and HD peaks at point "a" and a straight line drawn from point "b" to the D_2 peak at point "c." The area to the left of line cb was then assigned to D_2 and that to the right of de to parahydrogen. The remaining area was assumed to be due to the combined effect of orthohydrogen and HD. Using this method and knowing that the ortho to parahydrogen ratio in our samples was 3:1 we obtained results shown in Table I for seven different mixtures of hydrogen, deuterium and HD.

The agreement between the gas chromatographic and mass spectrographic results is very satisfactory for mixtures 5, 6 and 7 containing large amounts of HD. The error however is much greater in

(2) D. Rittenberg, W. Bleakney and H. C. Urey, *J. Chem. Phys.*, **2**, 48 (1934).

(3) (a) S. Ohkoshi, Y. Fugita and T. Kwan, *Bull. Chem. Soc. J.*, **31**, 770 (1958); (b) S. Ohkoshi, S. Tenma, Y. Fugita and T. Kwan, *ibid.*, **31**, 772 (1958); (c) S. Ohkoshi, Y. Fugita and T. Kwan, *ibid.*, **31**, 773 (1959).

(4) O. Riedel and E. Uhlmann, *Z. Anal. Chem.*, **166**, 433 (1959).

TABLE I

Run	% HD C.[a]	% HD M.S.[b]	% D₂ C.	% D₂ M.S.	% H₂ C.	% H₂ M.S.
1	7.2	6.3	67.0	66.2	25.6	27.6
2	9.0	11.3	25.0	25.6	65.8	63.2
3	13.3	14.6	26.4	25.6	60.3	59.8
4	14.0	13.1	49.7	50.1	36.3	36.8
5[c]	46.2	46.8	19.7	18.2	34.2	35.0
6[c]	45.6	47.0	16.8	19.3	37.6	33.8
7[c]	46.3	47.0	19.4	19.9	34.3	33.1

[a] C = chromatographic. [b] M.S. = mass spectrographic. [c] Samples for 5, 6 and 7 were taken from an H_2-D_2 mixture which was allowed to equilibrate by standing over an iron catalyst at room temperature for approximately two weeks. The equilibrium constants obtained were

Run	M.S.	C.	Lit.[2] (25°C.)
5	3.44	3.17	
6	3.40	3.29	3.28
7	3.36	3.22	
Av.	3.40	3.23	

ortho and parahydrogen (Fig. 1a) and of hydrogen, deuterium and HD in which the HD concentration is larger than about 10%. For lower percentages of HD larger errors are to be expected unless the present alumina column can be improved sufficiently to give more completely resolved peaks.

Acknowledgment.—This work was financed by the Atomic Energy Commission. Our thanks are also due to the Leeds and Northrup Company for supplying the recorder used in this work.

THE THERMAL DECOMPOSITION OF RUBIDIUM PERMANGANATE

By P. J. Herley and E. G. Prout

Chemistry Department, Rhodes Univ., Grahamstown, South Africa

Received November 11, 1959

The thermal decomposition of whole crystals of $KMnO_4$[1] and $CsMnO_4$[2] takes place in three stages. A period of slow reaction is followed by one of rapid acceleration which in turn passes into a decay stage. The first stage, in the case of $CsMnO_4$, is described by the expression

$$p^{1/2} = kt + c \qquad (1)$$

and is considered to consist of the two-dimensional growth of a fixed number of nuclei on the external surfaces. This stage with $KMnO_4$ follows the linear relationship

$$p = k_1 t + c_1 \qquad (2)$$

The acceleratory and decay stages for both substances obey the Prout–Tompkins equation

$$\log p/(p_f - p) = kt + c \qquad (3)$$

where p_f is the final pressure. Two values of k are necessary, one (k_2) holding over the acceleratory period and the other (k_3) during the decay period. The Prout–Tompkins equation was originally applied to the decomposition of $KMnO_4$ and was derived theoretically on the premise that the formation of product molecules induces strain in the crystal which produces cracks and thus forms fresh

(1) E. G. Prout and F. C. Tompkins, *Trans. Faraday Soc.*, **40**, 488 (1944).

(2) P. J. Herley and E. G. Prout, *J. Chem. Soc.*, 3300 (1959).

surfaces in which decomposition can occur. These cracks spread in a branching manner into the crystal over the acceleratory period. The branching mechanism breaks down ultimately due to the interference of the branching planes, and after the time of maximum velocity the rate is controlled by the number of unreacted molecules remaining.

It was of interest to study the decomposition of rubidium permanganate to determine whether the kinetics were similar to those of $CsMnO_4$ or $KMnO_4$. A knowledge of the kinetics of unirradiated $RbMnO_4$ is also necessary for a systematic study of the effects of pre-irradiation by thermal neutrons and ^{60}Co γ-rays on the subsequent decomposition of the permanganates of the alkali metals.

Experimental

Crystals of $RbMnO_4$ (2.5 × 0.5 mm.) were obtained by cooling 75 ml. of an aqueous solution containing 5 g. of "AnalaR" $KMnO_4$ and 3.6 g. of $RbCl$ (B.D.H.) from 60° to room temperature. The crystals were twice recrystallized from aqueous solution. They were skeletal or hopper crystals and were markedly elongated parallel to the b crystallographic axis. The co-zonal faces r, c and a, were prominently striated parallel to each of these three faces. The apparatus and experimental procedure were similar to that previously described.[1] Approximately 20 mg. of material was decomposed in each run. Pre-illumination of the salt with ultraviolet light was done in air with a quartz–mercury vapor lamp (full arc) running off 200 volts and at a distance of 10 cm. Pre-irradiation with cathode rays was done in an apparatus similar to that used in the study of the decomposition of mercuric oxalate.[3] Pre-irradiation with γ-rays was performed in the spent fuel facility at Harwell. The dose rate was 4 Mrad. hr.$^{-1}$.

Results

In general, the pressure–time plots for the decomposition of whole crystals resemble those for the decomposition of whole crystals of $KMnO_4$ and $CsMnO_4$ in that a slow reaction precedes the acceleratory period which is followed by the usual decay (Fig. 1). The curves, however, most closely resemble those for the decomposition of $KMnO_4$ since the evolution of gas during the slow reaction is linear. The acceleratory and decay periods conform to the Prout–Tompkins equation if the origin is taken at the p, t values corresponding to the end of the linear part of the curve (Fig. 1). Crystals ground in an agate mortar and then decomposed, yielded p-t plots which were fitted over almost the entire curve by the Prout–Tompkins equation (Fig. 2). The linear rate was thus eliminated by grinding. With $KMnO_4$, fracture of the crystals by crushing, as distinct from grinding, effected a loss of sharpness of the slow reaction, *i.e.*, the velocity during this time was higher, but the subsequent acceleratory effect less than for whole crystals. With finely crushed crystals the slow reaction was eliminated.[4] Similar effects were found with crushed whole $RbMnO_4$ crystals, the Prout–Tompkins equation becoming applicable from times closer to the origin as the degree of crushing was increased.

The mathematical analysis of the p-t plots for the decomposition of whole crystals indicated changes in the mechanism of decomposition at

(3) E. G. Prout and F. C. Tompkins, *Trans. Faraday Soc.*, **43**, 148 (1947).

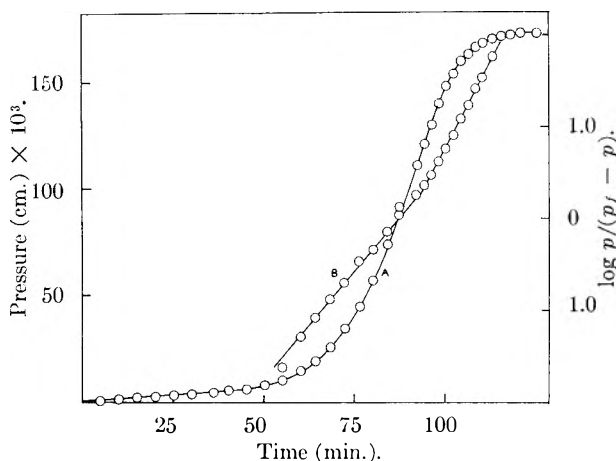(4) E. G. Prout, Thesis, Natal University College, South Africa, 1943.

Fig. 1.—Curve A, pressure–time plot for decomposition of whole crystals of RbMnO₄ at 245°; curve B, plot of log $p/(p_f - p)$ vs. t for curve A.
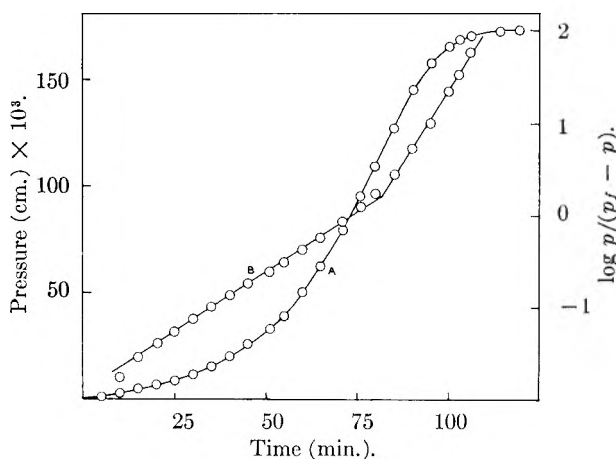

Fig. 2.—Curve A, pressure–time plot for decomposition of ground crystals of RbMnO₄ at 245°; curve B, plot of log $p/(p_f - p)$ vs. t for curve A.

times corresponding to the end of the slow reaction and the inflection point. This was supported by visual observation of a decomposing single large crystal. Referring to Fig. 1, from $t = 0$ to $t = 50$ min. the crystal broke into a few large splinters, longitudinal splitting being preferred. From $t = 55$ min. the fragments broke down randomly and at a high rate until $t \approx 68$ min. after which it was difficult to detect any change with the naked eye. Consequently, specimens were withdrawn at various times during a run and examined and measured microscopically. After $t = 5$ min. all external surfaces of the crystal were covered by a steel-blue layer of product material. Examination from $t = 5$ to $t = 50$ min. showed that the main change was a loss of sharpness of the edges and ridges of the crystal and splinters. At $t = 64$ min. the fragments were of different sizes, but the average dimensions were 0.08×0.3 mm. This average size decreased as decomposition proceeded until at the inflection point the average value was $(4 \times 10^{-2}) \times (8 \times 10^{-2})$ mm. Thereafter no decrease in size occurred. Reproducibility of results was satisfactory; k_1 at 240° for three consecutive runs was 0.7253×10^{-4}, 0.7250×10^{-4}, 0.7493×10^{-4} cm. min.⁻¹; k_2, 2.632, 2.550,

2.713 × 10⁻² min.⁻¹; and k_3, 3.704, 3.640, 3.488 × 10⁻² min.⁻¹, for whole crystals. For ground crystals the values were, k_2, 1.463, 1.438, 1.397 × 10⁻² min.⁻¹, k_3, 3.381, 3.214, 3.109 × 10⁻² min.⁻¹. There was no mass effect. The analysis of the p–t plots are summarized in Tables I and II.

TABLE I
SUMMARY OF KINETIC DATA FOR WHOLE CRYSTALS

Temp., °C.	$k_1 \times 10^4$, cm. min.⁻¹	$k_2 \times 10^2$, min.⁻¹	$k_3 \times 10^2$ min.⁻¹
255	1.673	7.595	11.81
250	1.160	5.199	8.451
245	0.8365	3.529	5.882
240	.7250	2.632	3.704
235	.5438	1.860	2.308
230	.4143	1.183	1.807
227	.3246	0.8824	1.288
224	.2339	.7653	0.9093
220	.1908	.5376	.7673
215	.1450	.3452	.4177

TABLE II
SUMMARY OF KINETIC DATA FOR GROUND CRYSTALS

Temp., °C.	$k_2 \times 10^2$, min.⁻¹	$k_3 \times 10^2$, min.⁻¹
255	4.375	9.836
250	3.015	5.882
245	1.888	4.959
240	1.463	3.214
235	1.099	2.174
230	0.6985	1.416
226	.5313	1.119
220	.3140	0.6451

The log k against $1/T$ (°K.) plots are well defined straight lines from which the activation energies, E_1, E_2 and E_3 for whole crystals are found to be 31.4, 39.5 and 40.2 kcal./mole, respectively. The values of E_2 and E_3 for ground crystals were 38.3 and 39.3 kcal./mole, respectively.

The chemical nature of the decomposition is best represented by

$$4RbMnO_4 \longrightarrow 2Rb_2O + 4MnO_2 + 3O_2$$
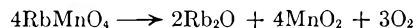
The percentage decomposition, in terms of this, was 82.7 and 82.4% for whole and ground crystals, respectively. Variations of temperature or mass did not significantly alter these percentages. Complete decomposition did not occur since the end product gave the characteristic permanganate color in water.

The addition of end products, either to whole or ground crystals, had no effect. Decomposition in the presence of oxygen (pressure 1.5×10^{-2} cm.) also had no effect. Interruption of the reaction by sudden cooling and subsequent reheating to the original temperature after 24 hr. produced no change in the p–t plot. Preirradiation by ultraviolet light (2 hr.) or bombardment with cathode rays (10 min.) at room temperature prior to decomposition had no effect. The effect of pre-irradiation by γ-rays (10 Mrad.) was marked and is shown in Fig. 3. A detailed account of the effect of pre-irradiation will be published later.

Discussion

The decomposition of $RbMnO_4$ resembles that of $KMnO_4$ and $CsMnO_4$ in the effects which are produced by ultraviolet light, cathode rays and γ-rays. Similarly, in all cases the end products do not catalyze the reaction and interruption of the reaction has no effect. The kinetics of the decomposition of whole crystals must closely resembles that of $KMnO_4$ since the three stages of decomposition obey the equations 2 and 3. As well, there is no significant difference between the activation energies for the acceleratory and decay periods. Such a difference does exist with $CsMnO_4$, and it was suggested that the discrepancy is associated with diffusion of oxygen through the network of cracks in the crystal during the main acceleratory period; the crystal does not splinter over the acceleratory period but collapses just prior to the onset of the decay stage. With both $KMnO_4$ and $RbMnO_4$ disintegration is extremely rapid in the early stages of the acceleratory period and it seems that escape of the oxygen is easier in these cases than with $CsMnO_4$.

The mechanism proposed for $KMnO_4$ is considered to be applicable here since $RbMnO_4$ (orthorhombic; unit cell of 4 molecules $a:b:c = 0.8311 : 1:1.3323$)[5] differs largely in geometric form and dimensions from one of the products, MnO_2 (body centered tetragonal cell; $c/a = 0.65$, $a = 4.38$ Å.).[6] It has been shown for $KMnO_4$ and $RbMnO_4$ that fracture of the crystals, e.g., by crushing, produces new surfaces from which an accelerating reaction commences far more rapidly than from the original crystal face. It is assumed, therefore, that initially, over the period of slow reaction, the product increases in thickness on the crystal faces until sufficient strain is produced in the reactant surface to initiate cracks down which reaction proceeds in a branching manner as postulated in the Prout–Tompkins theory for $KMnO_4$.

The induction period was not considered in detail for $KMnO_4$ but we have re-examined the results[4] and the values of k_1 for whole crystals at various temperatures are given in Table III

TABLE III

KINETIC DATA FOR WHOLE CRYSTALS OF $KMnO_4$

Temp., °C.	$(k_1 \times 10^4)$, cm. min.$^{-1}$	Temp., °C.	$(k_1 \times 10^4)$, cm. min.$^{-1}$
200	0.0885	215	0.1850
205	.1163	220	.2701
210	.1400	225	.3603

The plot $\log k_1$ against $1/T(°K.)$ is a well defined straight line and the calculated activation energy is 25.5 kcal./mole. Thus, for both $RbMnO_4$ and $KMnO_4 (E_2 = 38.5, E_3 = 38.8$ kcal./mole) there is a discrepancy between the values for the slow reaction and main reaction. It is suggested that the gaseous pressure measured during the slow reaction is in the main due to reaction from a fixed number of nuclei and proceeding along the crystal dislocations. Decomposition along such imperfections would be preferred and would have a lower activation energy. If the critical thickness of the
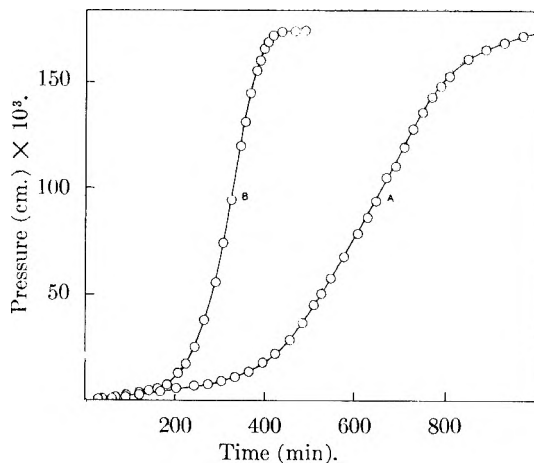
(5) T. V. Barker, *J. Chem. Soc.*, **89**, 1120 (1906).

(6) A. St. John, *Phys. Rev.*, **21**, 389 (1923).

Fig. 3.—Effect of pre-irradiating whole crystals of $RbMnO_4$ with γ-rays (dose 10 Mrad): Curves A and B, un-irradiated and irradiated crystals, respectively, dec. at 215°.

product layer is not large then the contribution to the gaseous pressure by this process will be small.

The longitudinal splitting of the crystal over the slow reaction is probably not of any significance relative to the main decomposition. The mechanical stresses which the crystal suffers on being raised rapidly from room temperature to $\sim 240°$ possibly opens up cleavage planes without actually disrupting the crystal. The growth of product on these cleavage faces ultimately forces the faces apart.

Roginsky, et al.,[7] have made a qualitative study of the permanganates of a series of metals and find that the thermal decomposition of all the compounds investigated has a sharply autocatalytic character. They measured the temperature ($KMnO_4$, 255°, $RbMnO_4$, 240°) at which the maximum velocity was reached in the same time (120 min). Using the value of 38.6 kcal./mole for $KMnO_4$ the heat of activation of $RbMnO_4$ would be 37.5 kcal./mole which is in reasonable agreement with the values found here.

THE DECARBOXYLATION OF MALONIC ACID IN BENZYL ALCOHOL, BENZALDEHYDE AND CYCLOHEXANOL

By LOUIS WATTS CLARK

Contribution from the Department of Chemistry, Saint Mary of the Plains College, Dodge City, Kansas

The systematic investigation of the kinetics of the decomposition of malonic acid in polar solvents, initiated several years ago, has yielded valuable data on the mechanism of the reaction as well as on the electron properties of 38 solvents comprising representatives of 10 homologous series.[1] The

(1) L. W. Clark, THIS JOURNAL, **64**, 41 (1960), and previous articles in this series.

electrophilic carbonyl carbon atom of malonic acid apparently coördinates with an unshared pair of electrons on a nucleophilic atom of a polar molecule forming a transition complex, thus facilitating the subsequent cleavage of malonic acid into acetic acid and carbon dioxide.[2] If the reaction proceeds by the indicated mechanism, it was reasoned that the unshared electrons on the oxygen atom of aldehydes and alcohols ought to entice the malonic acid to coördinate, thereby promoting decarboxylation. Preliminary tests having verified this deduction, kinetic studies were carried out on the decomposition of malonic acid in three closely related solvents in these two categories, namely, benzyl alcohol, benzaldehyde and cyclohexanol. Results of this investigation are reported herein.

Experimental

Reagents.—(1) The malonic acid was 100.0% assay. (2) The solvents were reagent grade chemicals, each sample of which was distilled directly into the dried reaction flask immediately before the beginning of each experiment.

Apparatus and Technique.—The kinetic experiments were conducted in a constant-temperature oil-bath ($\pm0.05°$) by the technique previously described.[3] Temperatures were determined by means of a thermometer calibrated by the U. S. Bureau of Standards. In each experiment a 0.1857-g. sample of malonic acid (the amount required to produce 40.0 ml. of CO_2 at STP on complete reaction) was introduced in the usual manner into the reaction flask containing a weighed sample of solvent saturated with dry CO_2 gas.

Results

Decarboxylation experiments were carried out in each solvent over approximately a twenty-degree temperature interval. Two or three experiments were performed at each temperature in each solvent. In every experiment a plot of log ($a - x$) vs. t (where a is the maximum theoretical yield of CO_2 and x the volume evolved at time t) yielded a straight line over about the first 75% of the reaction. (Evidently a very slow esterification reaction was taking place simultaneously with the decarboxylation.) The maximum actual yield of CO_2 in any experiment was about 38.0 ml. (correct to STP). The reaction generally was carried out in approximately 50 ml. of solvent. However, as in the case of previous studies conducted in various types of solvents, variation in the ratio of solvent to solute had no appreciable effect upon the rate of reaction.[1]

The average values of the apparent first-order rate constants for the reaction in the three solvents at the various temperatures studied, obtained from the slopes of the experimental logarithmic plots, are listed in Table I. The parameters of the Eyring equation are shown in Table II. Data for the decarboxylation of malonic acid in anisole are included for comparison.

Discussion of Results

A comparison of the kinetic data for the decarboxylation of malonic acid in benzyl alcohol and its isomer, anisole (lines 1 and 4 of Table II), shows that ΔH^* for the reaction differs by less than half of a kcal. in these two liquids. In anisole the electron deficit on the oxygen atom occasioned by the

(2) G. Fraenkel, R. Belford and P. E. Yankwich, *J. Am. Chem. Soc.*, **76**, 15 (1954).

(3) L. W. Clark, THIS JOURNAL, **60**, 1150 (1956).

TABLE I

APPARENT FIRST-ORDER RATE CONSTANTS FOR THE DECARBOXYLATION OF MALONIC ACID IN SEVERAL LIQUIDS

Solvent	Temp., °C. cor.	No. of runs	$k \times 10^4$, sec.$^{-1}$
Benzyl alcohol	117.96	3	3.52 ± 0.03^a
	125.12	3	$7.20 \pm .04$
	132.28	3	$14.28 \pm .05$
	137.53	3	$23.20 \pm .06$
Benzaldehyde	128.77	3	$2.89 \pm .06$
	135.23	3	$5.05 \pm .05$
	141.04	2	$8.24 \pm .04$
	148.35	3	$15.02 \pm .06$
Cyclohexanol	112.40	2	$3.47 \pm .02$
	115.35	2	$4.38 \pm .03$
	119.20	2	$5.91 \pm .02$
	130.22	2	$13.62 \pm .02$
	133.15	2	$16.94 \pm .02$

^{a} Average deviation.

TABLE II

KINETIC DATA FOR THE DECARBOXYLATION OF MALONIC ACID IN SEVERAL LIQUIDS

Solvent	ΔH^*, kcal.	ΔS^*, e.u.	$\Delta F^*_{140}°$, kcal.	$k_{140}° \times 10^4$, sec.$^{-1}$
(1) Benzyl alcohol	29.7	$+1.0$	29.3	29.0
(2) Benzaldehyde	27.9	-7.0	30.8	7.6
(3) Cyclohexanol	23.0	-15.0	29.3	27.0
(4) Anisole[4]	30.17	-3.67	31.7	1.4

strong $-I$ effect of the phenyl group is partially restored by the $+I$ effect of the methyl group. In benzyl alcohol the presence of a methylene group between the ring and the oxygen atom partially inhibits the electron withdrawing action of the aromatic nucleus. As a result, the effective negative charge on the oxygen atom is about equal in these two diverse liquids. Furthermore, it is obvious that the malonic acid would experience considerably more steric hindrance in attempting to reach the unshared pair of electrons on the oxygen atom in anisole than in benzyl alcohol. This would be expected to result in a lower value of ΔS^* for the reaction in anisole provided no other complicating factor (*e.g.*, association) intervened. We find, in fact, that ΔS^* is about 5 e.u. lower in anisole than in the benzyl alcohol. Inasmuch as ethers definitely do not associate due to the absence of hydrogen bonding, the fact that ΔS^* for the reaction is higher in benzyl alcohol than in anisole suggests that association is negligible in benzyl alcohol.

On going from benzyl alcohol to benzaldehyde the ΔH^* for the reaction decreases by nearly 2.0 kcal. (see lines 1 and 2 of Table II), indicating that the unshared pair of electrons attached to the carbonyl oxygen atom of the aldehyde are more loosely held than those in benzyl alcohol when coördination occurs. We may infer from this that the effective positive charge on the carbonyl carbon atom of malonic acid evokes a $-E$ effect on the carbonyl oxygen atom of the aldehyde, at the precise moment of reaction, partially nullifying the $-I$ effect of the conjugated aromatic nucleus and increasing the effective negative charge on the oxygen of the aldehyde. The decrease in ΔS^*

(4) L. W. Clark, *ibid.*, **62**, 1468 (1958).

on going from benzyl alcohol to benzaldehyde indicates that benzaldehyde is a more complex molecule than is benzyl alcohol. This fact suggests that the benzaldehyde molecules may exist in some associated form, involving coördination of the electrophilic carbonyl carbon atom of one molecule with the nucleophilic oxygen atom of a second molecule.[5]

On comparing lines 1, 3 and 4 of Table II we see that the addition of hydrogen atoms to the double bonds of the benzene ring results in a lowering of ΔH^* of the reaction by about 7.0 kcal. (passing from anisole or benzyl alcohol to cyclohexanol). Instead of a $-I$ effect of the phenyl group we now have a $+I$ effect of a cyclohexyl group, resulting in a considerable increase in the effective negative charge on the hydroxyl oxygen atom. Another example of this effect has been reported in a study of the relative basicities of aniline and cyclohexylamine.[6] The large decrease in ΔS^* on going from benzyl alcohol or anisole to cyclohexanol may be attributed to the larger extent of association of the alicyclic alcohol.

Acknowledgments.—The support of this research by the National Science Foundation, Washington, D. C., is gratefully acknowledged.

(5) W. Hückel, "Theoretical Principles of Organic Chemistry," Vol. II, Elsevier Publishing Co., New York, N. Y., 1958, p. 322 et seq.

(6) (a) N. F. Hall and M. R. Sprinkle, J. Am. Chem. Soc., **54**, 3469 (1932); (b) E. A. Braude and F. C. Nachod, "Determination of Organic Structures by Physical Means," Academic Press, Inc., New York, N. Y., 1955, p. 581.
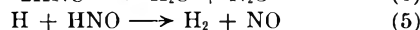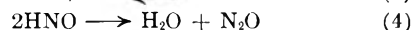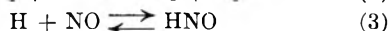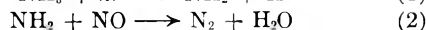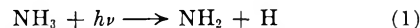

THE PHOTOLYSIS OF AMMONIA ($N^{15}H_3$) IN THE PRESENCE OF NITRIC OXIDE[1]
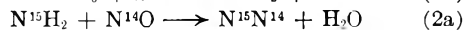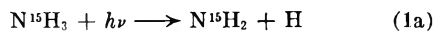
BY R. SRINIVASAN

Department of Chemistry, University of Rochester, Rochester 20, New York

Received November 13, 1959

It was observed by Serewicz and Noyes[2] that the photolysis of ammonia in the presence of nitric oxide led to the formation of nitrogen, nitrous oxide, water, and small amounts of hydrogen. For moderate pressures of nitric oxide (1 to 8 mm.), they proposed the following sequence of reactions to account for these products

$$NH_3 + h\nu \longrightarrow NH_2 + H \qquad (1)$$
$$NH_2 + NO \longrightarrow N_2 + H_2O \qquad (2)$$
$$H + NO \rightleftarrows HNO \qquad (3)$$
$$2HNO \longrightarrow H_2O + N_2O \qquad (4)$$
$$H + HNO \longrightarrow H_2 + NO \qquad (5)$$

The present study was undertaken to obtain confirmatory evidence for this mechanism by the use of nitrogen[15] to label the nitrogen atom in the ammonia molecule. Steps 1 to 4 would then be

$$N^{15}H_3 + h\nu \longrightarrow N^{15}H_2 + H \qquad (1a)$$
$$N^{15}H_2 + N^{14}O \longrightarrow N^{15}N^{14} + H_2O \qquad (2a)$$
$$H + N^{14}O \rightleftarrows HN^{14}O \qquad (3a)$$
$$2HN^{14}O \longrightarrow H_2O + N_2^{14}O \qquad (4a)$$

(2) A. Serewicz and W. A. Noyes, Jr., THIS JOURNAL, **63**, 843 (1959).
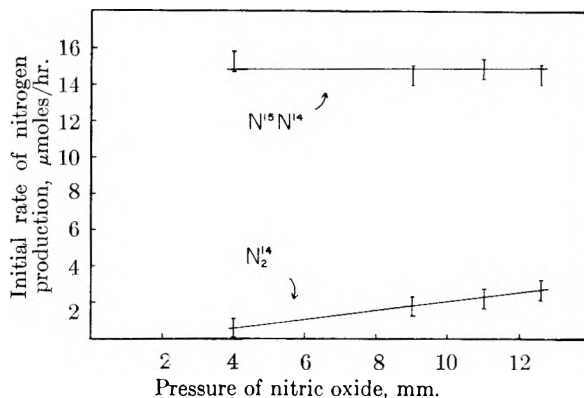

Fig. 1.—Rate of nitrogen production *vs.* pressure of nitric oxide.

The mechanism predicts that the nitrogen molecules formed will be exclusively mass 29 and the nitrous oxide exclusively mass 44.

Experimental

$N^{15}H_3$ was obtained from Isomet Corporation, N. J. It had a stated isotopic purity of 99.4%. Nitric oxide was purified as described by Serewicz and Noyes.[2]

Photolyses were carried out in a quartz cell 20.0×3.9 cm. The gases were mixed prior to photolysis and in the middle of a run by repeated expansion into a large volume. While this was not a very satisfactory way to keep the reactants well mixed during a run, it was adopted in order to keep the dead space small, and thus conserve material. The source of radiation was an unfiltered Hanovia S-100 medium pressure mercury arc.

Separation of the products and unreacted material was achieved as described in the earlier work.[2] Hydrogen and water were not determined. Mass spectrometric analysis of nitrogen and nitrous oxide were made with a Consolidated Engineering Co. type 21-620 mass spectrometer. Standard cracking patterns and sensitivities for nitrogen, nitric oxide, nitrous oxide and ammonia on this instrument were determined by the use of pure samples of each gas. On the basis of this information, corrections for the small amount of nitric oxide found in the nitrogen fraction, and ammonia in the nitrous oxide could be made. The sensitivity of the instrument to the parent peaks of $N^{15}N^{14}$ and N_2^{14} was assumed to be the same.

Results

At room temperature, and at a pressure of ammonia of 40 ± 1 mm., the initial rate of production of $N^{15}N^{14}$ and N_2^{14} are plotted as a function of nitric oxide pressure, in Fig. 1. In all these experiments there was no evidence for more than a trace of N_2^{15}, while the nitrous oxide was found to be wholly $N_2^{14}O$. The ratio of nitrous oxide to nitrogen was observed to vary from 0.21 at 4.0 mm. of nitric oxide to 0.27 at 12.5 mm. This may be compared with the values of 0.36 to 0.26 for the same pressure range found by Serewicz and Noyes.[2] Since they observed that a change in the surface to volume ratio of the cell changed the ratio of the products, a better agreement between the relative rates of production of nitrous oxide and nitrogen may not be expected.

In one experiment, the cell was filled with 11.5 mm. of nitric oxide alone. The light beam passed through a 4.4 cm. long filter cell filled with ammonia ($N^{15}H_3$) at 198 mm. pressure, before it entered the nitric oxide cell. After irradiation for 60 minutes, the nitric oxide was found to contain a mere trace of nitrogen.

Discussion

The results indicate that at pressures of nitric oxide of 4 mm. or less, the nitrogen contained 95% or more of $N^{15}N^{14}$ and the nitrous oxide was wholly $N_2^{14}O$. In this narrow range of conditions, the mechanism of Serewicz and Noyes[2] may be said to be confirmed. These workers have observed that with an increase in the pressure of nitric oxide, the stoichiometry of the products is in increasingly unsatisfactory. The present study points out why this is so. As indicated in Fig. 1, up to 4 mm. of nitric oxide, the rate of formation of N_2^{14} is no more than the uncertainty in the results. But at higher pressures of nitric oxide this is no longer true. It also was found by Serewicz and Noyes[3] and confirmed in the present instance, that at room temperature, under otherwise constant conditions, the rate of production of nitrogen increases with an increase in the nitric oxide pressure. If the light absorbing species is only ammonia, and the reactions 1-6 are the only important steps, this trend cannot be explained. On the other hand, the rate of production of $N^{15}N^{14}$ alone is seen to be constant with nitric oxide pressure within experimental error.

While it is clear that in addition to step 2a, nitric oxide gives rise to nitrogen in a second way—since this is the only way N_2^{14} may be formed—it is not obvious by what reaction this takes place. Both nitric oxide and ammonia absorb in the same general wave length region[3] but most of the light is absorbed by the ammonia since its extinction coefficient is many times greater than that of nitric oxide. Since the absorption spectrum of ammonia is discrete down to at least 2175 Å., it is possible that some particular mercury line or lines may be absorbed by nitric oxide even in the presence of ammonia. However, this appears to lead to very little decomposition in view of the meager yield of N_2^{14} in the photolysis of nitric oxide with light filtered by ammonia.

The transfer of energy from an excited ammonia molecule to a nitric oxide through a collision appears to be excluded by the fact that in its excited state, the ammonia molecule has a very short lifetime.[3]

Further speculation on the mode of formation of nitrogen from nitric oxide in this system must await a more detailed analysis of the products of the photolysis at high nitric oxide pressures.

Acknowledgment.—The author wishes to thank Professor W. Albert Noyes, Jr., for his advice and encouragement.

(3) For references and a summary see W. A. Noyes, Jr., and P. A. Leighton, "The Photochemistry of Gases," Reinhold Publ. Corp., New York, N. Y., 1941, pp. 135. 370.

A SPECTROPHOTOMETRIC STUDY OF THE HYDROLYSIS OF PLUTONIUM(IV)[1]

By S. W. Rabideau and R. J. Kline

University of California, Los Alamos Scientific Laboratory, Los Alamos, New Mexico

The hydrolysis quotients of some of the tetravalent actinides have been determined both with electromotive force methods[2,3] and with spectrophotometric procedures.[4-6] Also, from kinetic studies of the reaction between Pu(VI) and Pu(III) a value has been adduced for the hydrolysis quotient of Pu(IV) in D_2O which is larger than that in H_2O.[7] Since with a spectrophotometric method the K_H/K_D ratios were found to be greater than unity for U(IV) and Np(IV) in perchlorate solution,[6] this method was employed in a similar study of the effect of solvent upon the hydrolytic equilibrium for Pu(IV). The temperature coefficients of the equilibria both in H_2O and in D_2O have been measured.

Experimental

The Cary Model 14 recording spectrophotometer was used together with a double-chambered 10 cm. spectrophotometric absorption cell described previously.[8] The Pu(IV) stock solutions, prepared as described below, were added from a weight buret to one leg of the mixing cell. To the other leg, a pipetted volume of filtered sodium perchlorate solution of known concentration was added. The sodium perchlorate solution was used to maintain the ionic strength at a constant value of two. After the solutions had attained temperature equilibrium in a water thermostat, they were mixed quickly, and the cell was placed in a temperature-controlled water thermostat in the cell compartment of the spectrophotometer. First readings of optical densities were made within 20 sec. of the time of mixing. In general, the diminution of the optical densities with time as a result of the disproportionation of Pu(IV) was small, and extrapolations were made to zero time with little difficulty.

Spectrophotometric measurements were made at the Pu(IV) peak of 4692 Å. and also on the shoulder at 3300 Å. In D_2O solutions, the Pu(IV) peak shifted to 4684 Å. Better precision in the values computed for the Pu(IV) hydrolysis quotient was achieved in the use of the measurements at 3300 Å. At this wave length, the observed molar absorptivities increased with decreasing acidity. Thus, the hydrolyzed form, $PuOH^{+3}$, has a molar absorptivity greater than that of Pu^{+4} at this wave length.

Stock solutions of Pu(IV) were prepared fresh daily by the dissolution of purified plutonium metal in the appropriate weight of standardized 71% perchloric acid, followed by dilution and by the oxidation of Pu(III) to Pu(IV) with a weighed aliquot of a standard potassium dichromate solution. Only enough oxidant was added to convert 90% of the Pu(III) to Pu(IV) to avoid both the formation of higher oxidation states and the presence of excess dichromate. Although no slowness has been reported previously[9] in the oxidation of Pu(III) to Pu(IV) by dichromate, it has been found in the present study that in solutions of Pu(III) in which the perchloric acid concentration was 0.1 M or less, the yellow color of the dichromate disappeared gradually, and the maximum optical density at 4692 Å. was reached only after about a minute at 2.4°. Accordingly, the stock solutions of Pu(IV) were made either 2.000 or 4.000 M in perchloric acid, since under these conditions no slowness is observed and also the rate of disproportionation of Pu(IV) is negligibly small.

The final acidity of the Pu(IV) solutions in the spectrophotometer cell was calculated from the weight of the combined solutions in the cell together with the measured solution density and the volume and acidity of the Pu(IV) stock

(1) This work was done under the auspices of the U. S. Atomic Energy Commission.

(2) S. W. Rabideau and J. F. Lemons, *J. Am. Chem. Soc.*, **73**, 2895 (1951).

(3) S. W. Rabideau, *ibid.*, **79**, 3675 (1957).

(4) K. A. Kraus and F. Nelson, *ibid.*, **72**, 3901 (1950).

(5) R. H. Betts, *Can. J. Chem.*, **33**, 1775 (1955).

(6) J. C. Sullivan and J. C. Hindman, THIS JOURNAL, **63**, 1332 (1959).

(7) S. W. Rabideau and R. J. Kline, *ibid.*, **62**, 617 (1958).

(8) S. W. Rabideau, *ibid.*, **62**, 414 (1958).

(9) R. E. Connick, "The Actinide Elements," Natl. Nuclear Energy Ser., McGraw-Hill Book Co., Inc., New York, N. Y., Div. IV, 14-A, 1954, p. 262.

solutions. The acid consumed in the solution of the plutonium metal and in the oxidation of Pu(III) to Pu(IV) by dichromate and the acid produced by the hydrolysis of Pu(IV) were all taken into consideration in the computation of the acidity of the diluted Pu(IV) stock solution.

The Pu(IV) stock solutions in D_2O were prepared as for the H_2O solutions with the exception that D_2O was substituted for all the dilutions. The sodium perchlorate solutions were prepared from the anhydrous salt and the mole fraction of D_2O was about 0.95 in all those experiments in which D_2O was used as the solvent.

In the computation of the corrected optical densities of the Pu(IV) solutions, the contributions of Cr^{+3}, Pu^{+3}, and the acid–salt blank were subtracted. These corrections were determined separately under experimental conditions of temperature and solution composition as nearly as possible simulating those used in the hydrolysis quotient determinations.

Calculations

Under appropriate conditions of metal ion concentration and acidity, the hydrolysis of Pu^{+4} can be represented by the reaction

$$Pu^{+4}(aq.) + H_2O = PuOH^{+3}(aq.) + H^+(aq.) \quad (1)$$

The hydrolysis equilibrium quotient for equation 1 is

$$K = [PuOH^{+3}][H^+]/[Pu^{+4}] \quad (2)$$

It can be shown easily that the relationship between the experimentally observed optical density, OD, and the molar absorptivities of the unhydrolyzed and hydrolyzed forms of Pu(IV), ϵ_1 and ϵ_2, respectively, is

$$OD = (\epsilon_1[H^+] + \epsilon_2 K) 10[Pu(IV)]/([H^+] + K) \quad (3)$$

where [Pu(IV)] represents the total concentration of plutonium in the tetravalent state and the factor 10 corresponds to the cell length in centimeters. The unknowns in equation 3 are ϵ_1, ϵ_2 and K. Sets of equations of the type shown in equation 3 were obtained, one corresponding to each hydrogen ion concentration used. Instead of using a trial and error procedure in the evaluation of K, use was made of a computer program developed at Los Alamos Scientific Laboratory for the least squares solution of non-linear equations[10] using the IBM-704 machine. Values of ϵ_1, ϵ_2 and K together with their standard deviations were obtained which minimized the sum of the squares of the difference, $(OD_{calcd} - OD_{exptl})$. Although it is possible that other minima may exist in the parameter space, the requirement of positive values for ϵ_1 and ϵ_2 and K, together with the availability of reasonable estimates of these quantities, seriously limits the number of such minima. Moreover, the procedure used was verified by supplying significantly different initial estimates of the parameters, yet through the iterative machine calculation, identical final values of the parameters were obtained.

Results

Medium Effects.—In the spectrophotometric determination of the Pu(IV) hydrolysis quotient, it is necessary to assume that the molar absorptivities of Pu^{+4} and $PuOH^{+3}$, ϵ_1 and ϵ_2, respectively, are not functions of the medium. A series of measurements was made at 2.4° at a wave length of 4692 Å. in perchlorate solutions of ionic strength

(10) R. H. Moore and R. K. Zeigler, "The Solution of the General Least Squares Problem with Special Reference to High-Speed Computers," Report LA-2307, October 15, 1959.

4.00 in an attempt to examine the validity of this assumption. The acidity of the Pu(IV) solutions was varied between 2.000 and 4.000 M. The total Pu(IV) concentration was held constant and sodium perchlorate was added to maintain the ionic strength at a constant value of 4.00. Values of 59.86, 59.72, 59.67 and 59.30 M^{-1} cm.$^{-1}$ were obtained for four different solutions in the above acid concentration range. It can be concluded that ϵ_1 is not sensitive to the substitution of Na^+ for H^+ under these conditions. Little can be said of the constancy of ϵ_2 from these measurements because of the small fraction of this species present in the solutions studied.

In the experimental measurements of the Pu(IV) hydrolysis quotient in solutions of ionic strength two, it can be considered that the medium changes from 1.90 M $NaClO_4$-0.10 M $HClO_4$ to 1.99 M $NaClO_4$-0.01 M $HClO_4$, rather than from 2 M $HClO_4$ to essentially 2 M $NaClO_4$ since, in general, values of ϵ_1, ϵ_2 and K were not significantly different with or without the inclusion of data above 0.10 M $HClO_4$. Thus, large medium effects do not seem to be present in the spectrophotometric evaluation of K.

Beer's Law Tests.—Conformity to Beer's law within 1% was observed for Pu(IV) solutions at 2.4° in either perchloric acid solutions of 0.050 or 2.000 M at constant ionic strengths of two at 3300 and 4692 Å. The Pu(IV) concentrations were varied by as much as fourteen-fold.

Pu(IV) Hydrolysis Quotients.—In the analysis of the spectrophotometric data, it was found that the results obtained at 3300 Å. were especially useful in the evaluation of the Pu(IV) hydrolysis quotients. The precision of the values of K as measured by the standard deviation was better by nearly an order of magnitude from data obtained at 3300 than at 4692 Å. This result occurs because the molar absorptivity of the hydrolyzed species is much larger at the lower wave length ($\epsilon_2 = ca.$ 300 M^{-1} cm.$^{-1}$ at 3300 Å. $vs.$ $ca.$ 20 M^{-1} cm.$^{-1}$ at 4692 Å.). In Table I are given the results of measurements at 25 and 15.4° in the solvents H_2O and D_2O.

TABLE I

PU(IV) HYDROLYSIS QUOTIENTS IN PERCHLORATE
SOLUTIONS OF IONIC STRENGTH TWO

Solvent	Temp., °C.	No. expts.[b]	K(3300Å.)	σ^a	No. expts.[b]	K(4692Å.)	σ^a
H_2O	25.0	6	0.0226	0.0038	6	0.0234	0.014
		6	.0183	.0004	6	.0438	.012
		4	.0196	.0011	5	.0347	.013
	15.4	8	.0112	.0013	8	.0220	.015
		6	.0122	.0018			
D_2O	25.0	6	.0101	.0011	7	.020	.008
		6	.0134	.0013	4	.015	.006
	15.4	6	.0096	.0048	6	.0103	.010
		6	.0038	.0005			

[a] Estimated standard deviation obtained by least squares methods. [b] Number of measurements made at acidities between 0.01 and 2 M with a given Pu(IV) stock solution.

Although the data are presented for both the 3300 and 4692 Å. wave lengths, the results obtained at the latter wave length have such large uncertainties that they define K only poorly. With weights assigned to the 3300 Å. data of Table I in propor-

tion to $1/\sigma^2$, weighted mean values of 0.0185 ± 0.0004 and 0.0115 ± 0.0008 were calculated for the Pu(IV) hydrolysis quotients at 25° in the H$_2$O and D$_2$O solvents, respectively. The uncertainties of the weighted means correspond to $2\sigma = 2(1/\Sigma w_i)^{1/2}$, where w_i is the weighting factor. Thus, a K_H/K_D ratio of 1.6 is obtained at 25° from these spectrophotometric measurements. This result is similar to observations[6] in the cases of Np(IV) and U(IV) for which K_H/K_D ratios were found to be 1.6 and 1.2, respectively. This result is not in agreement with the conclusion reached in the kinetic studies of the Pu(VI)–Pu(III) reaction.[7] In this latter work, the results seemed to indicate a K_H/K_D ratio less than unity. This discrepancy is unresolved.

Kraus and Nelson[4] give spectrophotometric data obtained at 4700 Å. from which it is possible to calculate a value for K in perchlorate solutions of ionic strength 0.5 at 25° with the criterion that the sum of the squares of the difference, ($\epsilon_{calcd} - \epsilon_{exptl}$), is made a minimum. Whereas these authors found an average value of 0.0249 for K by a trial and error procedure, with the use of their data and the above criterion together with the computer program used in this study, a value of 0.019 ± 0.002 was obtained. The parameters ϵ_1 and ϵ_2 which together with the above value of K produced this minimum least squares sum had values of 54.7 ± 0.3 and 9.9 ± 3 M^{-1} cm.$^{-1}$, respectively.

From the temperature dependence of the Pu(IV) hydrolysis quotient as given in Table I, a value of 8.5 ± 0.9[11] kcal./mole is computed for ΔH for reaction 1 in H$_2$O. This result is in agreement with the value of 7.3 ± 0.5 kcal./mole obtained for ΔH from electromotive force measurements of the acidity dependence of the Pu(III)–Pu(IV) couple.[3] A somewhat higher ΔH is found for the hydrolysis reaction in D$_2$O, namely, 19.4 ± 1.3[11] kcal./mole. A wider temperature difference over which K was evaluated would have been desirable. Attempts were made to evaluate K in H$_2$O and in D$_2$O at a temperature of 2.4°; however, it was not possible to obtain a sufficient change in the values of the observed molar extinction coefficients to provide meaningful data. At temperatures greater than 25°, the disproportionation of Pu(IV) makes the extrapolation to zero time more difficult.

In the evaluation of the hydrolysis quotient of Pu(IV) from measurements of the formal potentials of the Pu(III)–Pu(IV) couple, a value of 0.054 was obtained for K at 25° in perchlorate solutions of ionic strength two.[3] It is not clear why such discordant values of the hydrolysis quotient have been obtained by the spectrophotometric and potentiometric methods.

Acknowledgments.—The authors wish to express their appreciation to Drs. J. F. Lemons and C. E. Holley, Jr., for helpful discussions and to R. H. Moore and R. E. Vogel for their assistance in the computer programming and in the statistical treatment of the data.

(11) The uncertainties given for the values of ΔH were computed by the method of propagation of errors with the use of the expression, $\pm \sigma \Delta h = \pm \{1/(1/T_1 - 1/T_2)^2 [\sigma^2 K_1/K_1^2 + \sigma^2 K_2/K_2^2] \}^{1/2}$.

THERMOCHEMISTRY OF DIMETHOXYBORANE

By W. J. COOPER AND J. F. MASI

Callery Chemical Company, Callery, Pennsylvania

Received November 30, 1959

Dimethoxyborane was first prepared by Burg and Schlesinger[1] from the reaction of diborane with methyl alcohol. They found the compound to be unstable above 0°, disproportionating according to the equation

$$6HB(OCH_3)_2 \rightleftarrows B_2H_6 + 4B(OCH_3)_3 \quad (1)$$
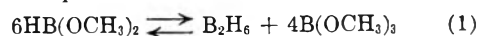
More recently Uchida,[2] have reported the kinetics of the vapor phase disproportion in which the reaction was found to be second order with respect to dimethoxyborane and surface dependent.

A determination of the heat of formation of dimethoxyborane would not only enable one to calculate the heat of the disproportionation reaction but also afford a means of estimating the strength of the B–H bond in a somewhat different manner than from the heat of formation of BH$_3$.[3]

Preliminary investigation of the heat of combustion of dimethoxyborane showed that the combustion was insufficiently complete for an accurate determination. Since the hydrolysis was reported to proceed readily,[1] the heat of hydrolysis was studied and found to be a satisfactory measurement for heat of formation determination.

Experimental

Sample Preparation and Purity.—The dimethoxyborane was prepared by reaction of diborane and methyl alcohol and was purified by distillation in a low-temperature Podbielniak column. The purity, as determined by hydrolyzable hydrogen, was found to be greater than 98%. As an additional check on the purity, the 0° vapor pressure (275 mm.) was measured prior to filling the hydrolysis sample bulbs.

The sample bulbs of thin-walled Pyrex were filled by vacuum condensation and sealed while frozen at liquid nitrogen temperature. To minimize disproportionation, the sample bulbs were stored in liquid nitrogen until they were weighed prior to introduction into the calorimeter.

Calorimeter.—The calorimeter was of a design similar to that described by Van Artsdalen and Anderson.[4] The calorimeter vessel was a 250-ml. silvered dewar flask. The calorimeter heater, approximately 25 ohms, was of No. 32 constantan wound non-inductively on the stirrer well. This heater was used both for electrical calibration and for adjustment of the calorimeter temperature. The platinum resistance thermometer had a resistance at 0° of 25.506 ohms and was calibrated by the National Bureau of Standards. The calorimeter was immersed in a water-bath maintained at 25 ± 0.05°. An outlet tube connected to a gas measuring buret provided for collection and measurement of the evolved hydrogen.

Calibration and Hydrolysis Reaction.—A series of electrical calibrations of the calorimeter system was made, as shown in Table I. In addition, a calibration was run in conjunction with each hydrolysis experiment. No significant differences in energy equivalents were observed between initial and final states.

The amount of dimethoxyborane which reacted was determined from the weight of sample, with completeness of

(1) A. B. Burg and H. I. Schlesinger, *J. Am. Chem. Soc.*, **55**, 4023 (1933).

(2) H. S. Uchida, H. B. Kreider, A. Murchison and J. F. Masi, THIS JOURNAL, **63**, 1414 (1959).

(3) R. E. McCoy and S. H. Bauer, *J. Am. Chem. Soc.*, **78**, 2061 (1956).

(4) E. R. Van Artsdalen and K. P. Anderson, *ibid.*, **73**, 579 (1951).

reaction being checked by measurement of evolved hydrogen and by titration of the final solution for boric acid. As a separate check on the state of the reaction products, a portion of the final solution from one of the runs was analyzed for methyl borate by infrared spectrometry. No lines of methyl borate were observed. Hydrolysis of a sample of methyl borate also went to completion under the same conditions as the dimethoxyborane hydrolysis. The heat of hydrolysis of the methyl borate sample was observed to be -4.65 kcal. mole^{-1} as compared to the value of -4.615 reported by Charnley, Skinner and Smith.[5]

All results are in terms of the defined calorie (4.1840 absolute joules). No correction was applied for the small amount of water vaporized from the calorimeter with the evolved hydrogen.

Results and Discussion

The average observed heat of hydrolysis, as given in Table II, refers to the over-all reaction

$$HB(OCH_3)_2(l) + (n + 3)H_2O(l) \longrightarrow$$
$$H_2(g) + (H_3BO_3(aq.) + 2CH_3OH)(aq.) \cdot nH_2O(l) \quad (2)$$
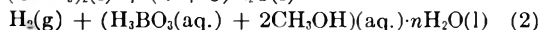
In the hydrolysis reactions, n was made sufficiently large to approach infinite dilution $(n > 1000)$. In deriving the heat of formation, therefore, these standard heats of formation of the products at infinite dilution were used

$$CH_3OH(aq, \infty) \; \Delta Hf^0 = -58.77^6$$
$$H_3BO_3(aq, \infty) \; \Delta Hf^0 = -256.92^7$$

TABLE I
CALORIMETER CALIBRATION

Mass H₂O, g.	Energy input, joules	Energy equiv., cal./ohm
190.0	1422.5	2274.2
190.0	1427.3	2289.5
190.0	1439.5	2295.2
190.0	1444.8	2271.8
190.0	1426.6	2291.4
190.0	1407.2	2286.4
Mean energy equiv.		2284.8
Stand. dev. of mean		±3.9

TABLE II
HYDROLYSIS MEASUREMENTS

Mass sample, g.	$-\Delta H_{obsd}$, kcal. mole
0.7122	24.55
.7026	23.88
.2885	24.44
.2967	23.93
.6396	23.99
.5826	24.65
.9208	24.24
Mean obsd. heat	24.24
Std. dev. of mean	+0.12

The resulting heat of formation of liquid dimethoxyborane is -145.3 kcal. mole^{-1}. The uncertainty of this value is estimated from the uncertainties of the calibration and hydrolysis measurements to be ±1.5 kcal.

From the reported value of 6.138 kcal. mole^{-1}

for the heat of vaporization at $25°$,[1] the heat of formation of gaseous dimethoxyborane is -139.2 kcal. mole^{-1}.

The heat of disproportionation, reaction 1, may then be calculated to be -16.8 kcal. for the liquid phase reaction and -20.5 kcal. for the vapor phase.

The energy of dissociation of the B–H bond has been estimated previously from the heat of formation of BH_3 to be 91.2 kcal. Since the heat of formation of BH_3 was based on an indirect series of measurements, a check on the B–H bond energy would be of value. Using the data of Charnley, Skinner and Smith[5] corrected for the more recent heat of sublimation of boron[8] of 135 kcal., the mean dissociation energy of the B–OCH$_3$ bond may be calculated to be 116.5 kcal. From this and the heat of formation of dimethoxyborane, the dissociation energy of the B–H bond is calculated to be 92.5 kcal. This result is in good agreement with that obtained from BH_3.

(8) Thermochemistry and Thermodynamics of Some Boron Compounds, NBS Report No. 6252.

PHYSICAL ADSORPTION ON CHEMISORBED FILMS

By D. S. MacIver and H. H. Tobin

Gulf Research & Development Company, Pittsburgh 30, Pa.

Received December 5, 1959

It is generally considered[1] that the presence of a layer of chemisorbed gas does not interfere with the measurement of the surface area of solids by the BET gas adsorption method provided that there is no blocking of adsorbent pores by the chemisorbate. There are in the literature, however, several indications that exceptions to this statement may exist. Thus Stone and Tiley[2] found that the chemisorption of carbon monoxide by a copper oxide film decreased the krypton BET monolayer volume by some 20%; oxygen, on the other hand, had no effect. In contrast to these results, Joy and Dorling[3] reported that the chemisorption of carbon monoxide by an iron Fischer–Tropsch catalyst did not influence the subsequent physical adsorption of nitrogen. Teichner and Morrison[4] have found that the prior chemisorption of either carbon monoxide or oxygen by nickel oxide reduces the BET V_m value for argon. More recently, it has been shown by Sastri, Viswanathan and Nagarjunan[5] that the chemisorption of carbon monoxide on cobalt catalysts decreases the subsequent physical adsorption of nitrogen. These authors claim, although they do not demonstrate, that this decrease is tantamount to a suppression of the monolayer volume.

In general, while it would appear from the preceding discussion that a chemisorbed film may influence subsequent physical adsorption, a question

(5) T. Charnley, H. A. Skinner and A. B. Smith, *J. Am. Chem. Soc.*, **74**, 2288 (1952).

(6) "Selected Values of Chemical Thermodynamic Properties." NBS Circular 500.

(7) Thermodynamic Properties of Some Boron Compounds, NBS Report No. 4943.

(1) P. H. Emmett, "Catalysis," Vol. I, ed. by P. H. Emmett, Reinhold Publ. Corp., New York, N. Y., 1954, p. 51.

(2) F. S. Stone and P. F. Tiley, *Nature*, **167**, 654 (1951).

(3) A. S. Joy and T. A. Dorling, *ibid.*, **168**, 433 (1951).

(4) S. J. Teichner and J. A. Morrison, *Trans. Faraday Soc.*, **51**, 961 (1955).

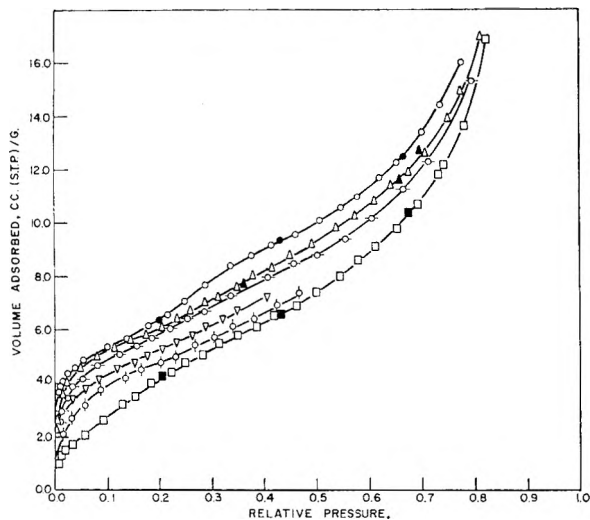(5) M. V. C. Sastri, T. S. Viswanathan and T. S. Nagarjunan, THIS JOURNAL, **63**, 518 (1959).

Fig. 1.—Argon adsorption on chromia surfaces at −195°. Open and solid symbols represent adsorption and desorption, respectively: O, clean surface; △, oxygen surface; -○-, carbon dioxide surface; □, carbon monoxide surface; ▽, oxygen + carbon monoxide surface; ◊, carbon dioxide + carbon monoxide surface.
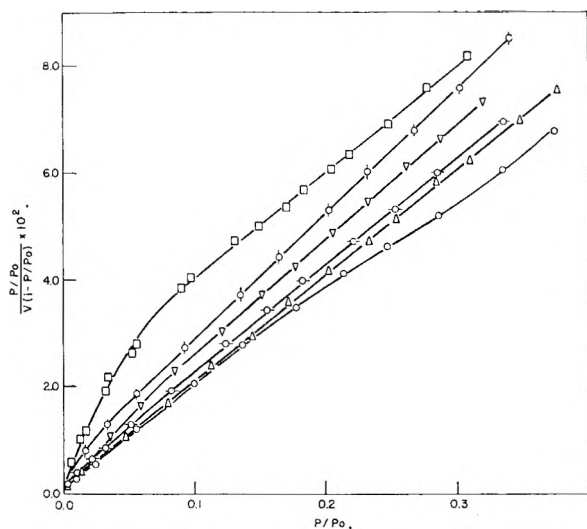

Fig. 2.—BET plots of argon adsorption on chromia surfaces at −195°: O, clean surface; △, oxygen surface; -○-, carbon dioxide surface; □, carbon monoxide surface; ▽, oxygen + carbon monoxide surface; ◊, carbon dioxide + carbon monoxide surface.

remains as to the concurrent effect upon the parameters of the BET equation. Obviously this is a point of some importance because of the widespread use of the BET formulation in determining surface areas. The purpose of the present note is to describe some observations of the effects of chemisorption upon the physical adsorption of argon by a chromia surface and to discuss these effects in terms of the BET theory.

Experimental

The adsorption measurements were carried out in a standard volumetric gas adsorption apparatus; a description of this equipment and of the gases used may be found in an earlier publication.[6] The chromia was the same sample

(6) D. S. MacIver and H. H. Tobin, Symposium on Theoretical Aspects of Heterogeneous Catalysis, Division of Colloid Chemistry, A.C.S. Meeting, September, 1959; Paper No. 6, to be published.

used previously[6] and was stabilized by alternate oxidation and reduction at 500°.[6,7] Before use the chromia was pretreated by oxidation in a stream of oxygen for three hours at 500°, atmospheric pressure, and a gaseous hourly space velocity of 5000, reduction in hydrogen for six hours under the same conditions, and finally evacuation for 16 hours at 500°. An argon isotherm then was determined in the usual fashion at −195° and the physically adsorbed argon removed by evacuation for one hour at −78°. A chemisorbed phase then was introduced by exposing the adsorbent to several millimeters pressure of the chemisorbate for an hour at −195° and then evacuating for an hour at −78°. After recooling the adsorbent to −195°, another argon isotherm was measured. At this point either the original surface was regenerated by repeating the pretreatment or a second chemisorbate introduced by a repetition of the procedure just described and another argon isotherm obtained. In determining the argon isotherms adsorption points were taken only after the pressure had remained constant for at least 15 minutes; in some instances points were checked by equilibration for periods as long as 16 hours. The liquid vapor pressure of argon[8] was used to compute relative pressures and a value of 16.9 Å.[2] was employed for the cross-sectional area of a physically adsorbed argon atom.[9] Upon completion of the series of experiments described in this note the entire sequence was repeated; the results of the two sets of measurements were in essential agreement. Despite the several regenerative treatments required, no appreciable change in adsorbent surface area was observed during the course of the work.

Results and Discussion

The chemisorbates employed in the present study were carbon monoxide, oxygen and carbon dioxide; as shown earlier[6] these were chemisorbed to the extent of 0.14, 0.10 and 0.12 cc. (STP)/m.^{2}, respectively. In addition, the oxygen covered-surface chemisorbed 0.03 cc.(STM)/m.^{2} of carbon monoxide while the carbon dioxide-covered surface chemisorbed either 0.06 cc.(STP)/m.^{2} of oxygen or 0.04 cc. (STP)/m.^{2} of carbon monoxide. It was possible, therefore, to study the physical adsorption of argon on chemisorbed layers of the three individual gases or on mixed layers of oxygen and carbon monoxide, oxygen and carbon dioxide, or carbon dioxide and carbon monoxide.

The argon isotherms obtained on the clean, reduced surface and on the same surface after introduction of various chemisorbed layers are shown in Fig. 1; the corresponding BET plots are given in Fig. 2 and a summary of all the BET parameters in Table I. For the sake of graphical clarity the argon

TABLE I

BET PARAMETERS FOR ARGON ADSORPTION ON CHROMIA SURFACES AT −195°

Surface	V_m cc. (STP)/g.	C
Clean	4.9	197
0.10 cc. (STP) O$_2$/m.^{2}	4.8	131
.12 cc. (STP) CO$_2$/m.^{2}	4.9	67
.14 cc. (STP) CO/m.^{2}	5.0	11
.12 cc. (STP) CO$_2$ + 0.06 cc. (STP) O$_2$/m.^{2}	4.9	49
.12 cc. (STP) CO$_2$ + 0.04 cc. (STP) CO/m.^{2}	4.2	43
.10 cc. (STP) CO + 0.03 cc. (STP) O$_2$/m.^{2}	4.5	40

isotherm on the surface containing both carbon dioxide and oxygen has been omitted from the

(7) S. W. Weller and S. E. Voltz, J. Am. Chem. Soc., 76, 4695 (1954).

(8) A. M. Clark, F. Din, J. Robb, A. Michels, T. Wassenaar and T. Zweitering, Physica, 17, 876 (1951).

(9) H. L. Pickering and H. C. Eckstrom, J. Am. Chem. Soc., 74, 4775 (1952).

figures; this isotherm was quite similar to that for the surface containing only carbon dioxide but was displaced slightly lower with respect to the ordinate.

It is readily apparent from Fig. 1 that the physical adsorption of argon on the clean, reduced chromia surface is anomalous in that a fairly sudden rise or step in the volume adsorbed takes place starting at a relative pressure of about 0.2. This is reflected in the corresponding BET plot of Fig. 2 by a tendency of the plot to be concave with respect to the pressure coördinate. The general shape of the isotherm is similar to those found on certain moderately graphitized carbon blacks where the presence of steps in the isotherms has been considered as characteristic of relatively homogeneous surfaces for physical adsorption.[10] In the present case, while an oxide such as chromia would ordinarily be expected to exhibit a fairly heterogeneous surface, it is conceivable that the stabilization of the surface by repeated oxidation and reduction at elevated temperatures could have resulted in a more homogeneous surface than is usual. On this basis the effect of chemisorbing oxygen or carbon dioxide would be to introduce sufficient heterogeneity so as to eliminate the stepwise feature of the isotherm. As may be seen in Fig. 1 such chemisorption appeared to have just this effect; the argon isotherms on the oxygen-covered and the carbon dioxide-covered surface have the usual sigmoidal shape and seem to show normal BET behavior.

In the case of homogeneous surfaces it has been suggested[11] that data at fairly low relative pressures (i.e., in the vicinity of a statistical monolayer) be employed in the BET equation. Accordingly, the portion of the BET plot of Fig. 2 for the clean, reduced surface up to a relative pressure of 0.14 was used to calculate the corresponding BET parameters of Table I; the V_m value so obtained agrees quite well with the values derived from the normal BET plots of the oxygen-covered and carbon dioxide-covered surfaces. This agreement would seem to validate the use of the low pressure region to obtain the area of the clean surface.

The chemisorbed carbon monoxide which covered essentially the entire surface[6] had a much more drastic effect on subsequent physical adsorption than did the other chemisorbates. In Fig. 1 it is apparent that the carbon monoxide layer not only removed the stepwise character of the isotherm but also caused a large decrease in the amount of argon physically adsorbed at any given relative pressure; in particular, it should be noted that the sharply-defined bend in the vicinity of a monolayer is missing. Despite these changes, however, a BET plot of the data, shown in Fig. 2, seems fairly linear above 0.10 relative pressure and indicates a V_m in good agreement with the earlier values. The principal effect of the chemisorption, in terms of the BET formulation, was to decrease the C-value by a factor of about 20. This low C-value is indicative of a low heat of physical adsorption and it is thereby apparent that the argon interaction with the chemisorbed film was much weaker than the inter-action with the clean surface. In general, the effect reported here of the carbon monoxide chemisorption was quite similar to the effect, described by Singleton and Halsey,[12] of physically adsorbing a layer of xenon on carbon black or silver iodide prior to the argon adsorption.

It might be thought that the lowering of the argon isotherm by the carbon monoxide was caused, at least in some part, by a blocking of adsorbent pores by the chemisorbate. Several points would seem to argue against this interpretation. First of all, the BET monolayer volume obtained with argon appears to indicate that the entire surface was accessible to the argon atoms. Secondly, no evidence could be obtained that any small pores were present in the adsorbent; this is indicated by the lack of any appreciable hysteresis in the isotherms of Fig. 1.[13] Finally, it seems unlikely that any pores blocked by carbon monoxide would not also be blocked by chemisorbed carbon dioxide.

It may be seen in Fig. 1 that when two chemisorbed species were present the argon isotherms were definitely modified in comparison to the clean surface isotherm, although in no case was the effect as pronounced as that found when the surface was completely covered with carbon monoxide. In each instance of dual chemisorption the BET plots were linear over the "usual" range of relative pressures (i.e., 0.05 to 0.35). Despite this linearity, however, the data in Table I show that when one of the chemisorbates was carbon monoxide the monolayer volume was somewhat lower than the expected value. Thus while the V_m value for the surface containing both carbon dioxide and oxygen was the same as for the clean surface, substituting carbon monoxide for the oxygen reduced the apparent V_m by some 14%.

In summary, carbon monoxide was the only chemisorbate studied which seemed to have a significant effect on the BET surface area; further, this effect was not found when the entire surface was covered with carbon monoxide. While a quantitative explanation for this behavior cannot be offered at this time, it is suggested that the presence of adsorption sites characterized by widely separated C-values (i.e., heats of adsorption) may be responsible. Thus the chemisorption of carbon dioxide (high C-value) and carbon monoxide (low C-value) may produce a dual surface of the nature discussed by Walker and Zettlemoyer.[14] As these workers have shown, it is possible in such a case to obtain a V_m value somewhat smaller than the true value. A similar explanation has been advanced by Stone and Tiley[2] to account for their results; it may be noted that in this latter work and in that of Teichner and Morrison[4] the carbon monoxide coverages were less than unity. Finally, it should be remarked that in the present case of chromia, the depression in the physical adsorption isotherms upon carbon monoxide chemisorption did not appear to have been caused by a change in the density

(10) M. H. Polley, W. D. Schaeffer and W. R. Smith, THIS JOURNAL, **57**, 469 (1953).

(11) D. S. MacIver and P. H. Emmett, ibid., **60**, 824 (1956).

(12) J. H. Singleton and G. D. Halsey, ibid., **58**, 330 (1954).

(13) The desorption points in these isotherms were obtained after the relative pressure had been increased to a value greater than 0.98 (based on the solid phase saturation pressure for argon).

(14) W. C. Walker and A. C. Zettlemoyer, THIS JOURNAL, **52**, 47 (1948).

of packing in the physically adsorbed phase as postulated by other workers[5] for the case of a metallic surface.
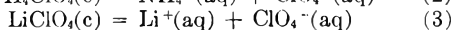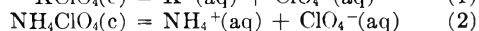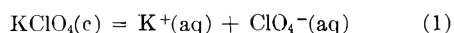

THERMOCHEMISTRY OF SOME PERCHLORATES AND AQUEOUS PERCHLORATE ION

By Merritt M. Birky and Loren G. Hepler[1]

Contribution from Cobb Chemical Laboratory, University of Virginia, Charlottesville, Va.

Received December 9, 1959

Partly because of recent interest in perchlorates as components of solid propellants, the heats of solution have been determined

$$KClO_4(c) = K^+(aq) + ClO_4^-(aq) \qquad (1)$$
$$NH_4ClO_4(c) = NH_4^+(aq) + ClO_4^-(aq) \qquad (2)$$
$$LiClO_4(c) = Li^+(aq) + ClO_4^-(aq) \qquad (3)$$

These data are used in several thermodynamic calculations.

Experimental

The solution calorimeter has been described previously.[2,3] The Leeds and Northrup type H. S. galvanometer used for null readings with the Mueller bridge has been replaced by a Beckman d.c. breaker amplifier (Model 14) and voltmeter. Sensitivity and zero stability are a little better than with the galvanometer and the experiments are much easier to carry out with the amplifier.

All heat determinations were carried out at $25.0 \pm 0.2°$ in 950 ml. of water.

Two samples of $KClO_4(c)$ were prepared by adding Baker and Adamson reagent grade $HClO_4$ (70–72%) to a solution of Fisher's KOH. Each sample was recrystallized three times and then dried. Sample 1 was dried for one week in a desiccator over P_2O_5. Sample 2 was dried for 8 hours in an air oven at 50–55°. Sample 3 was prepared from Baker and Adamson reagent grade perchloric acid and Mallinckrodt analytical grade anhydrous potassium carbonate, recrystallized twice, and dried for 8 hours at 100°. Sample 4 was prepared by recrystallizing some of sample 1 and drying for 30 minutes at 100°.

Baker and Adamson reagent grade perchloric acid was added to a cold (0°) solution of Baker and Adamson reagent grade ammonium nitrate. The precipitated ammonium perchlorate was recrystallized twice. Sample 1 was dried for 1 hour at 100°. Sample 2 was dried for 4 hours at 100°. Sample 3 was dried for 2 months in a desiccator with P_2O_5. Sample 4 was prepared by recrystallizing some of samples 1 and 2 and, after drying for 3 hours at 100°, was analyzed by the Karl Fischer method[4] and found to contain 0.05% water. The end point was detected electrometrically.

Baker and Adamson reagent grade perchloric acid (70–72%) was added to a saturated solution of Fisher purified lithium hydroxide and the resulting lithium perchlorate was recrystallized twice before being fused at 300° *in vacuo*. Sample 1 was found by the Karl Fischer method to contain 0.14% water. Sample 2 was prepared by adding perchloric acid to an aqueous paste of Mallinckrodt analytical grade lithium carbonate. The recrystallization and drying were the same as for sample 1 and the water content was found to be 0.15%. Samples 3 and 4 were prepared in the same manner as sample 1 but were dried for 3 days at 195°.

All perchlorate samples were checked with aqueous $AgNO_3$ to test for Cl^-; no precipitates of AgCl were observed.

Results

The values obtained for the heats of solution of $KClO_4(c)$, $NH_4ClO_4(c)$ and $LiClO_4(c)$ are given in Tables I, II and III.

(1) Alfred P. Sloan Research Fellow.

(2) R. L. Graham and L. G. Hepler, *J. Am. Chem. Soc.*, **78**, 4846 (1956).

(3) C. N. Muldrow, Jr., and L. G. Hepler, *ibid.*, **79**, 4045 (1957).

(4) J. Mitchell, Jr., and D. M. Smith, "Aquametry," Vol. 5, Interscience Publishers, Inc., New York, N. Y., 1948.

Table I
Heats of Solution of $KClO_4(c)$

Sample	Moles $KClO_4 \times 10^3$/ 950 ml.	ΔH_1 (kcal./mole)
1	3.836	12.33
1	8.003	12.31
2	8.860	12.31
2	6.961	12.31
2	6.475	12.32
3	8.781	12.33
4	7.409	12.32

Table II
Heats of Solution of $NH_4ClO_4(c)$

Sample	Moles $NH_4ClO_4 \times 10^3$/ 950 ml.	ΔH_2 (kcal./mole)
1	8.536	8.01
1	6.544	8.02
1	6.879	8.05
2	4.596	8.02
3	1.178	8.03
4	1.323	8.06

Table III
Heats of Solution of $LiClO_4(c)$

Sample	Moles $LiClO_4 \times 10^2$/ 950 ml.	ΔH_3 (kcal./mole)
1	1.373	−6.28
1	1.235	−6.24
2	0.740	−6.30
2	1.114	−6.25
3	1.534	−6.31
3	0.848	−6.24
3	0.520	−6.25
3	1.346	−6.34
4	1.681	−6.31

Heats of dilution of aqueous $KClO_4$ have been determined[5,6] and we have used these heats of dilution with data in Table I to calculate $\Delta H_1^0 = 12.31 \pm 0.06$ kcal./mole for the standard heat of solution of $KClO_4(c)$. Our estimate of the *total* maximum uncertainty is ± 0.06 kcal./mole.

Because heats of dilution of aqueous NH_4ClO_4 and $LiClO_4$ are not available, we have estimated these values on the basis of known heats of dilution of NH_4NO_3, NH_4Cl, $LiNO_3$, $NaClO_4$ and $KClO_4$ and calculated $\Delta H_2^0 = 8.02 \pm 0.07$ kcal./mole $NH_4ClO_4(c)$ and $\Delta H_3^0 = -6.31 \pm 0.13$ kcal./mole $LiClO_4(c)$ from the data in Table II and III.

Johnson and Gilliland[7] at the Bureau of Standards recently have investigated the heat of decomposition of $KClO_4(c)$ into $KCl(c)$ and $O_2(g)$ as in the equation

$$KClO_4(c) = KCl(c) + 2O_2(g) \qquad (4)$$
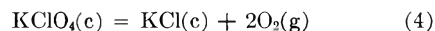
and found $\Delta H_4^0 = -0.96 \pm 0.10$ kcal./mole. This heat of decomposition with the heat of formation of $KCl(c)$[6] leads to -103.22 kcal./mole for the standard heat of formation of $KClO_4$ (c). We have used this heat of formation with the heat of formation of $K^+(aq)$ and our ΔH_1^0 in calculating -30.87 kcal./mole for the standard heat of formation of $ClO_4^-(aq)$. We believe this is the

(5) M. Andauer and E. Lange, *Z. physik. Chem.*, **A165**, 89 (1933).

(6) "Selected Values of Chemical Thermodynamic Properties," Circular 500, National Bureau of Standards, 1952.

(7) W. H. Johnson and A. A. Gilliland, National Bureau of Standards, personal communication.

best available heat of formation of $ClO_4^-(aq)$ because Johnson and Gilliland's value for the heat of decomposition appears to be far more reliable than any older value. Our heat of solution of $KClO_4(c)$, ΔH_1^0, is 0.19 kcal./mole more endothermic than that reported by Latimer and Ahlberg.[8]

We have calculated the standard partial molal entropy of $ClO_4^-(aq)$ to be 43.9 cal./mole deg. For this calculation we have used the solubility of $KClO_4(c)$ determined by Noyes, et al.,[9] the entropy of $KClO_4(c)$,[8] the entropy of $K^+(aq)$,[6] our ΔH_1^0 and Latimer and Ahlberg's[8] estimated activity coefficient for $KClO_4(aq)$ in saturated solution. It is to be noted that our entropy differs from that of Latimer and Ahlberg[8] because we used different values for ΔH_1^0 and the entropy of $K^+(aq)$. The heat of formation and entropy of $ClO_4^-(aq)$ with NBS[6] data lead to -2.14 kcal./mole for the standard free energy of formation of $ClO_4^-(aq)$.

We have used our values for the heats of solution of $NH_4ClO_4(c)$ and $LiClO_4(c)$, ΔH_2^0 and ΔH_3^0, with the above heat of formation of $ClO_4^-(aq)$ and NBS[6] heats of formation of $NH_4^+(aq)$ and Li^+ (aq) in calculating the standard heats of formation of $NH_4ClO_4(c)$ and $LiClO_4(c)$ to be -70.63 and -91.11 kcal./mole, respectively. Our heat of solution of $NH_4ClO_4(c)$ is not in good agreement with that obtained by Berthelot.[10] Markowitz, et al.,[11] recently have investigated the heat of solution of $LiClO_4(c)$ in more concentrated solutions than we used and report a value in agreement with our heat data.

The standard free energy of solution of NH_4ClO_4 (c) can be calculated from the solubility and the activity coefficient of $NH_4ClO_4(aq)$ in saturated solution. We have taken the solubility at 25° from Seidell[12] (2.12 molal) and have estimated the desired activity coefficient to be 0.52 after comparison of activity coefficients of $NaCl(aq)$, $NaNO_3(aq)$, $NaClO_4(aq)$, $NH_4Cl(aq)$ and $NH_4NO_3(aq)$[13] at the same concentration. From these values we have calculated $\Delta F^0 = -RT \ln m^2 \gamma^2 = -115$ cal./mole which has been used with the standard free energies of formation of $NH_4^+(aq)$[6] and $ClO_4^-(aq)$ (this paper) to give -21.02 kcal./mole for the standard free energy of formation $NH_4ClO_4(c)$. The standard free energy and heat of solution lead to $\Delta S^0 = 27.3$ cal./mole deg. This value for ΔS^0 and the partial molal entropies of NH_4^+ (aq)[6] and $ClO_4^-(aq)$ (this paper) lead to 43.6 cal/mole deg. for the standard entropy of $NH_4ClO_4(c)$ at 298°K.

(8) W. M. Latimer and J. E. Ahlberg, J. Am. Chem. Soc., 52, 549 (1930).

(9) A. A. Noyes, C. R. Boggs, F. S. Farrell and M. A. Stewart, ibid., 33, 1650 (1911).

(10) M. Berthelot, Ann. chim. phys., [5] 27, 214 (1882).

(11) M. Markowitz, R. F. Harris and H. Stewart, Jr., THIS JOURNAL, 63, 1325 (1959).

(12) A. Seidell, "Solubilities of Inorganic and Metal Organic Compounds," D. Van Nostrand Co., Inc., New York, N. Y., 1940.

(13) R. A. Robinson and R. H. Stokes, "Electrolyte Solutions," Butterworths Publications Ltd., London, 1955.

LEAD SULFATE: HEAT CAPACITY AND ENTROPY FROM 15–330°K.[1]

By K. Gallagher, G. E. Brodale and T. E. Hopkins

Contribution from the Low Temperature Laboratory, Departments of Chemistry and Chemical Engineering, University of California, Berkeley, Cal.

This paper presents low temperature calorimetric data on $PbSO_4$. The entropy and other quantities are of interest particularly in connection with the thermodynamics of the lead storage cell.

Preparation of Sample.—The crystals of $PbSO_4$ were prepared by adding K_2SO_4 to a solution of $Pb(NO_3)_2$ in 1 N HNO_3 as described by O'Connor and Buchanan.[2] The average size of the crystals formed was 3–4 mm. Spectroscopic analysis showed no K^+ in the crystals. The sample inadvertently contained 0.054 g. of H_2O per mole of $PbSO_4$ as determined by the high heat capacity at 271.05°K. A 317.632-g. sample of $PbSO_4$ was used.

Apparatus for Calorimetry.—The heat capacities were measured in a copper calorimeter similar to one used by Giauque and Archibald.[3]

One defined calorie was taken as 4.1840 absolute joules and 0°C. = 273.15°K. Laboratory thermocouple W-26 was used as a reference for the gold resistance thermometer-heater. The thermocouple had been recalibrated recently at the triple (13.94°K.) and boiling (20.36°K.) points of hydrogen and the triple (63.15°K.) and boiling (77.34°K.) points of nitrogen.

Low Temperature Heat Capacities of $PbSO_4$.—The experimental heat capacity measurements are given in Table I. Smoothed values of the thermodynamic properties given in Table II are corrected for the small amount of water present. The entropy values include an extrapolated amount of 0.67 gibbs[4] mole^{-1} below 15°K.

TABLE I

HEAT CAPACITY OF PbSO₄

Sample containing 0.054 g. H_2O per mole of $PbSO_4$ as determined by the high heat capacity at 271°; 0°C. = 273.15° K., gbs. mole^{-1}

T, °K.	C_p	T, °K.	C_p
12.17	1.08	143.07	17.35
13.30	1.29	151.82	17.72
14.90	1.63	160.55	18.16
18.95	2.53	169.12	18.69
21.21	3.06	177.59	19.14
23.56	3.59	186.01	19.65
25.98	4.11	194.58	19.94
28.47	4.64	202.98	20.53
31.14	5.21	211.49	20.98
34.95	6.00	220.04	21.44
39.38	6.92	228.77	21.86
43.81	7.82	237.37	22.23
47.60	8.54	245.94	22.72
52.40	9.37	254.21	23.07
58.77	10.34	262.64	23.49
64.47	11.10	271.05	24.34
70.77	11.81	279.10	24.15
78.40	12.65	287.08	24.37
86.46	13.47	295.12	24.62
94.37	14.06	302.87	24.86
102.21	14.65	298.55	24.64
110.56	15.28	307.82	25.04
118.77	15.90	316.09	25.11
126.89	16.38	324.67	25.52
135.02	16.89		

TABLE II

THERMODYNAMIC PROPERTIES OF PbSO$_4$

Mol. wt. = 303.28, 0°C. = 273.15°K., gbs. mole^{-1}

T, °K.	C_p	S	$\frac{H^0 - H_0^0}{T}$	$\frac{-(F^0 - H_0^0)}{T}$
5	(0.085)	0.028	0.021	0.007
10	(0.643)	.223	.167	.056
15	1.623	.668	.490	.178
20	2.780	1.289	.913	.375
25	3.899	2.031	1.400	.631
30	4.970	2.837	1.906	.931
35	6.009	3.681	2.418	1.263
40	7.046	4.551	2.932	1.619
45	8.052	5.440	3.445	1.994
50	8.963	6.336	3.952	2.384
55	9.777	7.229	4.445	2.784
60	10.510	8.112	4.921	3.191
70	11.750	9.828	5.811	4.017
80	12.818	11.468	6.621	4.847
90	13.703	13.032	7.362	5.670
100	14.408	14.516	8.035	6.481
110	15.235	15.933	8.656	7.277
120	15.934	17.289	9.234	8.055
130	16.578	18.590	9.774	8.816
140	17.150	19.840	10.281	9.559
150	17.691	21.042	10.757	10.285
160	18.205	22.200	11.207	10.993
170	18.727	23.319	11.633	11.686
180	19.274	24.405	12.043	12.362
190	19.817	25.462	12.438	13.024
200	20.356	26.492	12.820	13.672
210	20.895	27.498	13.192	14.306
220	21.415	28.482	13.554	14.928
230	21.924	29.446	13.907	15.539
240	22.406	30.389	14.251	16.138
250	22.875	31.313	14.587	16.726
260	23.317	32.219	14.914	17.305
270	23.717	33.107	15.233	17.874
280	24.077	33.976	15.542	18.434
290	24.442	34.827	15.844	18.984
298.15	24.667	35.509	16.083	19.426
300	24.717	35.660	16.137	19.525
310	24.995	36.475	16.419	20.058
320	25.277	37.273	16.692	20.584
330	25.555	38.055	16.957	21.102

(3) W. F. Giauque and R. C. Archibald, *J. Am. Chem. Soc.*, **59**, 561 (1937).

(4) W. F. Giauque, E. W. Hornung, J. E. Kunzler and T. R. Rubin, *J. Am. Chem. Soc.*, **82**, 62 (1960). 1 gbs. (gibbs) = 1 defined calorie (deg. K.)$^{-1}$.

HYDROTHERMAL SYNTHESIS OF ZINC OXIDE AND ZINC SULFIDE[1]

BY R. A. LAUDISE AND A. A. BALLMAN

Bell Telephone Laboratories, Inc., Murray Hill, N. J.

Large relatively flawless crystals of quartz[2,3] and sapphire[4] have been prepared by hydrothermal crystallization and their rates of growth and the phase equilibria involved in the systems used for

(1) This work was described in part at the American Chemical Society meeting, Boston, Mass., April, 1959.

(2) A. C. Walker and E. Buehler, *Sci. Monthly*, **69**, 148 (1949).

(3) R. A. Laudise, *J. Am. Chem. Soc.*, **81**, 562 (1959).

(4) R. A. Laudise and A. A. Ballman, *ibid.*, **80**, 2655 (1958).

their preparation have been studied. Zinc oxide like quartz and sapphire is an amphoteric oxide and it might be expected to crystallize under hydrothermal conditions in a basic solution. Hüttig and Möldner[5] have studied the phase equilibria in the system ZnO–H$_2$O up to about 40° and found ZnO (zincite) to be the stable solid phase at pressures above about 50 mm. and temperatures above 35°. However, growth of ZnO on a seed has never been reported in detail under hydrothermal conditions. Indeed, the preparation of ZnO crystals has been confined until recently to growth by sublimation or vapor phase reaction and has not yielded crystals much larger than fractions of a millimeter.

Since ZnO sublimes (1720°) before it melts (above 2000°)[6] and is virtually insoluble at room temperature, many conventional crystal growth methods are not practicable. Growth from flux and hydrothermal growth appear as the most feasible methods. Nielsen and Dearborn[7] have grown ZnO from molten PbF$_2$ with much success and indeed seed material from their preparations was invaluable in this work. However, ZnO prepared from a flux tends to contain flux inclusions, strains, and crucible impurities and is not suitable for most electronic studies where control over impurities and stoichiometry is indispensable. Furthermore ZnO grown from PbF$_2$ tended to crystallize as platelets whose principal face was (0001) and whose thickness was insufficient for many applications. A. C. Walker[8] had grown ZnO hydrothermally in this Laboratory and preliminary indications were that large crystals could be prepared provided conditions were controlled carefully.

Zinc sulfide is dimorphic changing from the β or cubic modification (sphalerite) at about 1020° to the α or hexagonal modification (wurtzite).[9] ZnS sublimes at 1185° and melts at 1850° with a vapor pressure of 150 atmospheres.[9] Consequently most conventional crystal growth techniques are not suitable for its preparation especially if the cubic modification is desired. Small crystals (< 1 mm.) of ZnS have been prepared by sublimation and vapor phase reaction but their size, purity, stoichiometry and perfection preclude certain electrical and luminescence studies. Few phase equilibria studies involving sulfides have been conducted under hydrothermal conditions. Allen and Crenshaw[10] and Kremheller and Levine[11] have crystallized ZnS isothermally under hydrothermal conditions but the increase in particle size was rather small (5 μ) and no attempts to grow on a seed were made. However, it was felt that ZnS could be grown in a hydrothermal system where the required supersaturation was produced by a temperature gradient.

Experimental

Two sorts of studies were necessary in order to grow crys-

(5) G. F. Hüttig and H. Möldner, *Z. anorg. Chem.*, **211**, 368 (1933).

(6) G. F. Hüttig and K. Toischer, *ibid.*, **207**, 273 (1932).

(7) J. W. Nielsen and E. F. Dearborn, to be published.

(8) A. C. Walker, *J. Am. Ceram. Soc.*, **36**, 250 (1953).

(9) "Handbook of Chemistry and Physics," Chemical Rubber Publishing Co., 27th Ed., 1943, p. 489.

(10) E. T. Allen and J. L. Crenshaw, *Am. J. Sci.*, **34**, 341 (1912).

(11) A. Kremheller and A. K. Levine, *Sylvania Technologist*, **10**, 67 (1957).

tals of ZnO and ZnS. First it was necessary to conduct phase equilibria studies. For this work a platinum lined vessel of the sort described by Morey[12] sealed with a plunger covered with a platinum sheet was used. The cylindrical cavity within the vessel had internal dimensions of 3/4″ diameter × 4″ length, with a wall thickness of 3/4″ and could contain pressures up to 8,000 p.s.i. at about 400°. This autoclave could be conveniently maintained nearly isothermal for phase equilibria studies by the use of furnaces and control equipment previously described.[3,4] In some experiments where crystal growth was desired, the furnace was arranged to produce a temperature differential from bottom to top of the vessel of from 5–50° as measured by strapped external thermocouples.

The vessel principally used for the growth of crystals was a cylindrical steel welded closure autoclave 1″ in internal diameter by 12″ in internal length with a wall thickness of $1/2''$. This vessel and its associated furnace equipment has been described previously.[3,4] The vessel was capable of containing pressures in excess of 35,000 p.s.i. at temperatures up to 470°. The furnace assembly used was capable of producing any desired temperature difference from bottom to top of the autoclave, as measured on strapped external thermocouples, of from 5–70°. Temperatures as reported in this work are estimated to be accurate within ±3° and previous studies[3] seem to indicate that they represent quite closely the true internal temperature within the vessel.

In the bottom of the vessel there was placed starting material or nutrient. This was finely powdered (100 mesh) reagent grade zinc oxide, zinc hydroxide, zinc sulfide or sintered zinc oxide rods. In runs where crystal growth was desired, there was placed directly above the nutrient a perforated metal disc or baffle the fraction of whose open area was 0.10. The baffle has been shown to serve to localize the temperature difference in the baffle region.[3,4] The vessel was filled to a predetermined fraction of its free volume or per cent. of fill with the desired solvent and closed. Runs of from 2 to 40 days were made. Above the baffle in the growth region were suspended seed crystals prepared either by carefully building up spontaneously nucleated hydrothermal crystals (ZnO and ZnS) or prepared from molten PbF₂ (ZnO) by Nielsen and Dearborn. Extremely small seed crystals were placed in a wire basket, larger crystals were drilled and mounted on a wire frame. Rates of growth were determined by the measurement of appropriate dimensions before and after growth and by weight changes. Phases were identified by X-ray diffraction. Pressures reported in this work are the p–v–t pressures of pure water, as determined by Kennedy.[13] Measurements in the system Na₂O–H₂O–SiO₂ under hydrothermal conditions[14] show pressures 10–20% lower than the p–v–t pressures for pure water and similar effects might be expected in the systems studied in this work.

Results

ZnO.—The systems NaOH–H₂O–ZnO and H₂O–ZnO were investigated at fills from 30 to 85% at temperatures between 200 and 400° in a search for conditions where ZnO could best be grown. Figure 1 shows the temperatures and pressures where ZnO was found to form in 1.0 M NaOH. Superimposed in Fig. 1 is the phase diagram ABC deduced by Hüttig and Möldner.[5] According to Hüttig and Möldner, the temperature for the Zn(OH)₂–ZnO transition should coincide nearly with the (H₂O)g–(H₂O)l equilibrium line in the region A–B. That is the pressure of water over Zn(OH)₂–ZnO should nearly equal the vapor pressure of water up to 35°. At water pressures between 40 and 70 mm. the transition line B–C is temperature independent. Above 70 mm. the data of Hüttig and Möldner would imply continued temperature independence. Studies of the corundum-diaspore
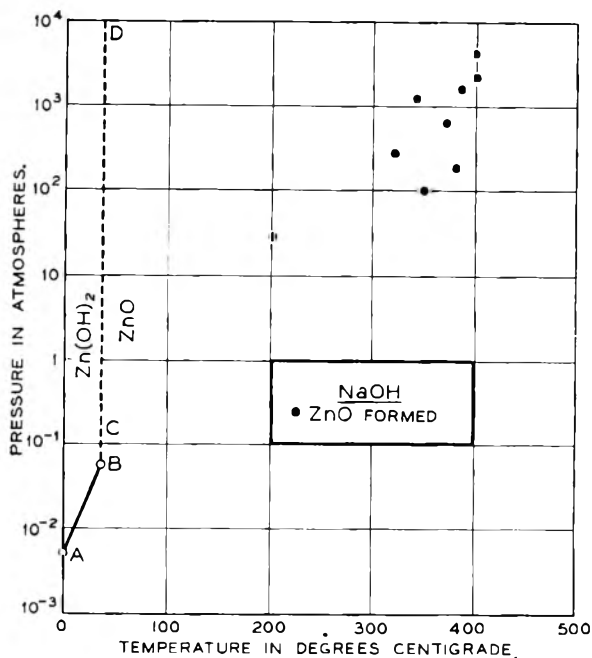
(12) G. W. Morey, *Am. Min.*, **22**, 1121 (1937).

(13) G. C. Kennedy, *Am. J. Sci.*, **258**, 540 (1950).

(14) R. A. Laudise and R. A. Sullivan, *Chem. Eng. Prog.*, **55**, 55 (1959).
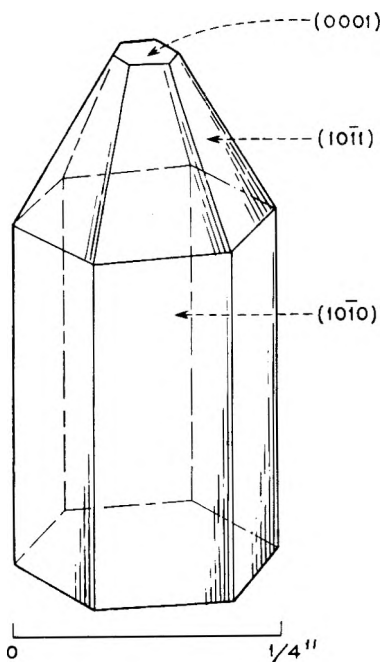
Fig. 1.—ZnO–H₂O phase equilibria.

Fig. 2.—Idealized ZnO habit under hydrothermal conditions.

transition in Al₂O₃–H₂O[15] and Al₂O₃–NaOH–H₂O[4] systems have shown that in those systems transition temperature is not altered by low concentrations of NaOH and this assumption is probably valid in ZnO–H₂O systems. Consequently it is probably valid to extrapolate Möldner and Hüttig's transition in the region C–D and to assume that the phase diagram is valid in low concentrations of NaOH. As the points of Fig. 1 show, no data in contradiction to these assumptions were found. Closer approach to the transition line was not attempted in our studies because it was ob-

(15) G. Ervin and E. F. Osborn, *J. Geol.*, **59**, No. 4, 387 (1951).

served that at temperatures much below 200° the rate of growth of ZnO was rather low.

Seeds used in the studies were mainly plates prepared from flux[7] whose principal faces were (0001). Since ZnO is hexagonal (wurtzite structure) one would expect that these plates would be bounded by (10$\bar{1}$0) faces and indeed after short periods of growth under hydrothermal conditions these faces together with the capping (10$\bar{1}$1) faces began to appear. The habit of both spontaneously nucleated crystals and (0001) seeds grown for a reasonable period of time approached that shown in Fig. 2. Especially noteworthy is the fact that (0001) is not a stable face under hydrothermal conditions in contrast to its persistence in molten PbF$_2$.[6] The rate of growth in the $\langle 0001 \rangle$ direction has been observed to be about twice as fast as that in the $\langle 10\bar{1}0 \rangle$ direction and $\langle 0001 \rangle$ growth tends to be flawed except at very low supersaturation in a manner reminiscent of crevice flawing in quartz.[3] This is as would be expected since unstable faces generally grow faster and with lower perfection than stable faces. The growth rate in the $\langle 10\bar{1}1 \rangle$ seems to be intermediate between those of the $\langle 0001 \rangle$ and $\langle 10\bar{1}0 \rangle$ directions and reasonable rates without flawing seem most practicable in this direction.

The dependence of rate on experimental parameters seems to be qualitatively similar to that found with quartz.[3] The parameters of principal importance have been found to be growth zone temperature, temperature difference between nutrient and growth zones (Δt), per cent. of fill and concentration of NaOH. As any of these is increased, the rate tends to increase. Growth zone temperature above about 350°, per cent. of fill above about 70 and NaOH concentration in the neighborhood of 1.0 M seem to be required for appreciable growth rates. Runs in pure water yielded little growth. To prevent excessive spontaneous nucleation on the walls and to aid in decreasing crevice flawing on the (0001) surface it was found that Δt's could not exceed about 10-15°.

Typical conditions where good growth was achieved were:

ZnS.—For the hydrothermal growth of ZnS the systems ZnS–H$_2$O–Na$_2$S and ZnS–H$_2$O–NaOH were investigated. In Na$_2$S runs were made between 50 and 80% fill, between 250 and 405° and at concentrations of Na$_2$S between 1.0 and 2.0 M. Under all these conditions β-ZnS was found to be the stable solid phase. In NaOH runs were made between 50 and 80% fill, between 345 and 410°, and between 1.0 and 10 M NaOH. Under all these conditions β-ZnS again was found to be the stable solid phase. Typical conditions for good growth were 80% fill, growth temperature 380°, Δt 30° and 2 M NaOH. There seemed to be little difference between the ease of crystallization in Na$_2$S and that in NaOH. However, since Na$_2$S solutions attack the autoclave walls in steel and silver plated vessels NaOH solutions were found more suitable for all of the studies at higher pressures where platinum lined equipment was not available.

No large seeds were available so it was necessary to select spontaneously nucleated crystals for seeds. The best condition for growth on a seed seemed to be: fill above 70%, growth temperature above 350°, and sodium hydroxide concentration above 2.0 M. Crystals up to about 2 mm. have been prepared and growth on a seed appears nearly as rapid as in the case of ZnO. X-Ray powder and single crystal studies showed the crystals to be cubic but there was found to be either a stacking fault or twinning along one of the $<111>$ directions. The distance between stacking faults must be rather high since no optical birefringence could be found. Crystals were yellow to white in color and contained appreciable quantities of iron.

Physical measurements of the grown crystals both ZnO and ZnS, further rate studies, and growth of high purity controlled stoichiometry crystals are in progress.

Especially interesting in this work was the discovery that even in 10 M NaOH, ZnS could not be converted to ZnO at all temperatures studied (up to nearly 400°). One would think that the equilibrium

$$\text{ZnS} + 2(\text{OH})^- = \text{ZnO} + (\text{S})^= + \text{H}_2\text{O}$$

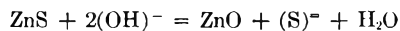| Crystaln. temp. °C.	Δt °C.	% Fill	Solvent	
387 (pressure $\sim$ 37,000 p.s.i.)	8	85	2 M NaOH	$\langle 0001 \rangle \sim 10$ mil./day, considerable flawing
				$\langle 10\bar{1}0 \rangle \sim 5$ mil./day, good quality
				$\langle 10\bar{1}1 \rangle \sim 5$-10 mil./day, good quality
430 ($\sim$ 21,000 p.s.i.)	30	70	1 M NaOH	$\langle 0001 \rangle \sim 15$ mil./day, some flawing
400 ($\sim$ 30,000 p.s.i.)	10	80	1 M NaOH	$\langle 0001 \rangle \sim 10$ mil./day, considerable flawing

The grown ZnO crystals some of which were as large as several grams were hemimorphic, amber in color, and rather heavily contaminated with iron as evidenced by their high conductivity. Hemimorphism would be expected considering the lack of a center of symmetry in the sphalerite unit cell.

might be shifted to the right at sufficiently high (OH)$^-$ concentration. Evidence that the weight solubility of ZnS does not exceed 5%[11] leads to the conclusion that K_c when concentrations are expressed in moles per liter for the above equilibrium must be equal to or less than 10^{-6}. Therefore one would feel that for the hydrothermal

crystallization of other sulfides of low solubility product $(OH)^-$ in quite high concentrations may be efficacious in increasing the solubility without causing oxide formation. It is interesting to note that Linares[16] has observed that in molten NaOH at temperatures between the melting point and 700° ZnS is converted to ZnO.

Acknowledgments.—The authors wish to thank S. Geller and C. G. B. Garrett for discussions concerning the structure of ZnS, S. Geller and M. Reid for X-ray work and J. W. Nielsen for ZnO seeds. A. J. Caporaso performed some of the experimental work.

(16) R. C. Linares, private communication.

STUDIES ON THE CHEMISTRY OF HALOGENS AND OF POLYHALIDES. XX. FORMATION CONSTANT OF DIOXANE–ICl COMPLEX

By Alexander I. Popov,[1] Carla Castellani-Bisi[2] and Willis B. Person

Department of Chemistry, State University of Iowa, Iowa City, Iowa

Received December 28, 1959

Dioxane is known to be a fairly strong electron donor, capable of forming addition compounds with halogen, interhalogen and pseudohalogen molecules. The formation constant of the iodine complex has been determined both in the ultraviolet[3] and in the infrared regions[4] and the respective values of the formation constant for a 1:1 complex were 0.86 and 0.7 l. mole⁻¹ which is very good agreement. The formation constant of the dioxane–ICN complex was found to be 1.2 from infrared measurements.[5] Lilich and Presnikova[6] have determined the formation constants of bromine, iodine, iodine bromide and iodine monochloride complexes with dioxane in carbon tetrachloride solutions using the Benesi–Hildebrand method[7] in the ultraviolet spectral region. The values of these formation constants for Br₂, I₂, IBr and ICl complexes were, on a molarity basis, 0.356, 0.997, 14.5 and 60.6, respectively. In all of the above cases only a 1:1 complex was assumed. It is interesting to note that Hassel and Hvoslef have obtained a solid complex Diox·2ICl[8] by the reaction the two components in the vapor phase. There does not seem to be an *a priori* reason why this 1:2 complex cannot exist in solution.

In connection with our study of charge-transfer complexes by infrared absorption,[5,9] it was decided

(1) College of Liberal Arts and Sciences, Northern Illinois University, DeKalb, Illinois.

(2) On leave of absence from Institute of General Chemistry, University of Pavia, Pavia, Italy.

(3) J. A. A. Ketelaar, C. van de Stolpe, A. Goudsmit and W. Dzcubas, *Rec. trav. chim.*, **71**, 1104 (1952).

(4) D. L. Glusker and H. W. Thompson, *J. Chem. Soc.*, 471 (1955).

(5) A. I. Popov, R. E. Humphrey and W. B. Person, *J. Am. Chem. Soc.*, **82**, 1850 (1960).

(6) L. S. Lilich and O. E. Presnikova, *Uchenye Zapiski Leningrad. Gosudarst. Univ. im. A. A. Zhdanova*, No. 163, Ser. Khim. Nauk No. **12**, 3 (1953).

(7) H. A. Benesi and J. H. Hildebrand, *J. Am. Chem. Soc.*, **71**, 2703 (1949).

(8) O. Hassel and J. Hvoslef, *Acta Chem. Scand.*, **10**, 138 (1956).

(9) W. B. Person, R. E. Humphrey, W. A. Deskin and A. I. Popov, *J. Am. Chem. Soc.*, **80**, 5346 (1958); W. B. Person, R. E. Humphrey and A. I. Popov, *ibid.*, **81**, 273 (1959).

to check the formation constant of dioxane–ICl complex. Since preliminary results disagree with those of Lilich and Presnikova, a more thorough study of this constant was indicated.

Experimental Part

The source and purity of iodine monochloride, of carbon tetrachloride, and dioxane as well as experimental details of spectral measurements have been described in previous publications.[5,9]

In a typical run a series of eight solutions was prepared containing small and constant concentrations of iodine monochloride and varying large excesses of dioxane. Concentration of iodine chloride was determined by an iodometric titration. Dioxane solutions were prepared by the addition of a given amount of dioxane from a weight buret to a given volume of carbon tetrachloride and diluting to the desired concentration. Solutions used for infrared measurements had to be quite concentrated, and because of the difficulties involved in working with concentrated iodine monochloride solutions which were described earlier,[9] the concentrations of these solutions were known only with an accuracy of ±10%.

Absorption spectra of ICl-dioxane mixtures were determined in the visible and ultraviolet regions; since the uncomplexed ICl showed some absorption in this region, the method of Ketelaar, *et al.*,[3,10] was used for computing the formation constant. The data were treated by the method of least squares and are summarized in Table I.

TABLE I

ABSORBANCE DATA AND FORMATION CONSTANT OF DIOXANE–ICl COMPLEX

C_{ICl}^{tot}	C_{diox}^{tot}	Absorbance			
		355 mμ	345 mμ	355 mμ	365 mμ
7.848 × 10⁻³	...	0.022	0.025	0.048	0.120
7.848 × 10⁻³	0.051	.370	.500	.613	.695
7.848 × 10⁻³	.102	.460	.635	.755	.865
7.848 × 10⁻³	.153	.520	.705	.865	.950
7.848 × 10⁻³	.204	.535	.742	.910	.995
7.848 × 10⁻³	.255	.555	.770	.938	1.025
7.848 × 10⁻³	.357	.590	.805	.975	1.065
7.848 × 10⁻³	.510	.620	.845	1.015	1.110
$a_{Complex}$		83.0	114.6	139.1	150.9
K_f		23.86	23.12	23.07	23.03
$K_{av.}$		23.27 ± 0.34			

For the infrared studies, solutions of dioxane and ICl in CCl₄ also were used. In one series of experiments a solution of 0.05 M ICl was studied with concentrations of dioxane ranging from 1.0 to 0.1 M. In another series, the ICl concentration was 0.1 M, while the dioxane concentration was varied from 0.1 to 0.0125 M. These concentrations were not the most desirable values, but we were limited by the reactivity of the halogen to fairly dilute solutions. However, the concentration of the complex must be high enough so that its absorbance can be measured. This imposes rather narrow limits on the range of concentration which can be studied.

As seen from Table I, the average value for the formation constant measured in the ultraviolet region is 23.3, which is much lower than the value reported by Lilich and Presnikova.[6] However, a personal communication from Professor Lilich disclosed that they also obtained a lower value for K_f in a series of solutions in which a very large excess of dioxane was used, but attributed it to an experimental error.

The results of Lilich and Presnikova, as well as those of Hassel and Hvoslef[8] point to a distinct possibility that in solutions with only a small excess of dioxane, a diox·2ICl complex might be forming, to some extent at least. This would decrease the concentration of free iodine monochloride and would account for the higher value of the calculated formation constant. On the other hand, with a large excess of dioxane only the 1:1 complex has a chance to form. While it might be possible to prove the existence of the

(10) A. I. Popov, C. Castellani-Bisi and M. Craft, *ibid.*, **80**, 6573 (1958).

second complex spectrophotometrically and even to determine its formation constant, such measurements would have to be carried out in solutions having an excess of iodine monochloride which has a considerable absorption in the near ultraviolet region and the results would not be too reliable. Also, concentrated ICl solutions have a tendency to halogenate organic compounds and such a side reaction with dioxane would render the measurements valueless.

The procedure used to analyze the infrared data was that described earlier.[5] However, in using the Benesi–Hildebrand–Scott equation, we made two modifications. Instead of using the *initial* concentration of dioxane as the independent variable, we used the *actual* concentration (obtained by assuming a value for K_f). Also, we used the *integrated* absorbance, Bnl, instead of the absorbance, A_s. The resulting value of K_f was 35 l./mole. However, the experimental scatter of the data was sizable, and lines could be drawn through the data giving values of K_f as high as 55 and as low as 25. It should be noted that the infrared measurements were made on solutions with relatively high concentrations of ICl. Thus, it is possible that the higher value of K_f is significant, and due to some contribution to our data from the 2:1 complex.

Because of the correlations found earlier[9,11] in studies of the infrared spectra of charge-transfer complexes it is of some interest to determine the values of the frequency, half-intensity width, and intensity for the I–Cl absorption band in the complex. These were, respectively, $\nu = 352$ cm.$^{-1}$, $\Delta\nu_{1/2} = 13$ cm.$^{-1}$, and $B = 4000$ cm.$^{-1}$ millimole^{-1} (darks). From this, $\Delta k/k = 0.12$ and $\epsilon_a = 2.6D/\text{Å}$. (see the references cited for definitions). This value of ϵ_a is quite high for the corresponding value of $\Delta k/k$, and the resulting point falls quite high on the correlation plot (Fig. 7 of ref. 11) and outside the average deviation of the values shown in that plot. This may also be due to the presence of a two-to-one complex.

Acknowledgment.—The authors are grateful to Professor L. Lilich for the discussion of this problem.

(11) W. B. Person, R. E. Ericksonand R. E. Buckles, *J. Am. Chem. Soc.* **82**, 29 (1960).

THE EFFECT OF HIGHER FATTY ACIDS ON THE DECARBOXYLATION OF MALONIC ACID

By Louis Watts Clark

Contribution from the Department of Chemistry, Saint Mary of the Plains College, Dodge City, Kansas

Kinetic studies have been reported on the decomposition of malonic acid in forty-seven non-aqueous solvents comprising representatives of fourteen homologous groups.[1] The rate-determining step of the reaction in every case appears to be the formation of a transition complex, the nucleophilic carbonyl carbon atom of un-ionized malonic acid coördinating with an unshared pair of electrons on an electrophilic atom of the solvent molecule, facilitating cleavage. The delicate affinity of un-ionized malonic acid for unshared electrons, made manifest by the different rates of evolution of carbon dioxide, makes possible its use as a tool or technique for studying the electron and steric structures of all kinds of polar molecules. Interesting results have been obtained previously from a study of the reaction in several of the lower fatty acids and their derivatives.[2] For the sake of completeness it was believed worthwhile to extend the investigation into some of the higher members of the series.

(1) L. W. Clark, This Journal, **64**, 508 (1960).
(2) L. W. Clark, *ibid.*, **64**, 41 (1960).

The present paper describes the results of kinetic studies carried out in this Laboratory on the decarboxylation of malonic acid in four additional monocarboxylic acids, namely, 2-methylbutanoic acid, *n*-valeric acid, hexanoic acid and decanoic acid, making now a total of 51 solvents in which the reaction has been investigated.

Experimental

Reagents.—(1) Reagent grade malonic acid, 100.0% assay, was used in this investigation. (2) Solvents: The fatty acids used in this research were either reagent grade or highest purity chemicals. Each sample of each liquid was fractionally distilled at atmospheric pressure into the reaction flask immediately before the beginning of each experiment.

Apparatus and Technique.—The details of the apparatus and technique have been described previously.[3] In these experiments a sample of malonic acid weighing 0.1857 g. (corresponding to 40 ml. of CO_2 at STP on complete reaction) was weighed into a fragile glass capsule blown from 6 mm. soft-glass tubing weighing approximately 0.1 g. A weighed quantity of solvent (saturated with dry CO_2 gas) was placed in the 100-ml., 3-neck, standard-taper flask immersed in the oil-bath. The temperature of the thermostat controlled oil-bath (maintained to within $\pm0.01°$) was determined using a thermometer graduated in tenths of a degree and calibrated by the U.S. Bureau of Standards.

Results

Decarboxylation experiments were carried out in each solvent at three or four different temperatures over approximately a 20° temperature range. Two or three experiments were performed at each temperature in each solvent. First-order kinetics were observed for the first 50–75% of the reaction, after which the reaction rate constant decreased slightly with time, due, undoubtedly, to slower side reactions. About 50 ml. of solvent was the amount generally used in the experiments. However, a wide variation in the ratio of solvent to solute did not appear to have any effect upon the rate of reaction.

The average values of the apparent first-order rate constants for the reaction in the four acids at the various temperatures studied, obtained from the slopes of the experimental logarithmic plots, are listed in Table I. The parameters of the Eyring equation are shown in Table II. Corresponding data for the reaction in propionic acid and butyric acid, as well as for the decarboxylation of molten malonic acid, are included for comparison.

Discussion of Results

In the case of the decarboxylation of malonic acid in the lower monocarboxylic acids it has been shown that the transition complex is probably formed by the coördination of the electrophilic carbonyl carbon atom of the malonic acid with one of the unshared pairs of electrons on the hydroxyl oxygen atom of the solvent molecule.[2] Since the ΔH^* of the reaction decreases as the effective negative charge on the nucleophilic atom of the solvent increases[4] the decrease in ΔH^* on going from propionic acid to *n*-butyric acid (lines 5 and 6 of Table II) is consistent with the fact that the ethyl group exerts a greater positive inductive effect than does the methyl group.[6] The slight

(3) L. W. Clark, *ibid.*, **60**, 1150 (1956).
(4) K. J. Laidler, "Chemical Kinetics," McGraw–Hill Book Co., Inc., New York, N. Y., 1950, p. 138.

TABLE I

APPARENT FIRST-ORDER RATE CONSTANTS FOR THE DE-
CARBOXYLATION OF MALONIC ACID IN SEVERAL HIGHER
FATTY ACIDS

Solvent	Temp., °C. cor.	No. of runs	$k \times 10^4$, sec.$^{-1}$
2-Ethylbutanoic acid	130.97	2	1.24 ± 0.01^a
	139.84	3	$2.46 \pm .01$
	145.37	2	$5.12 \pm .02$
	151.74	2	$9.23 \pm .01$
n-Valeric acid	134.45	2	$1.58 \pm .01$
	138.06	2	$2.23 \pm .02$
	146.00	3	$4.78 \pm .04$
	154.07	3	$10.10 \pm .02$
Hexanoic acid	138.14	2	$2.10 \pm .01$
	142.85	3	$3.89 \pm .02$
	148.14	2	$6.33 \pm .01$
	158.53	2	$16.37 \pm .01$
Decanoic acid	134.33	3	$1.89 \pm .02$
	142.94	3	$3.84 \pm .01$
	147.49	2	$5.48 \pm .01$
	153.25	3	$8.57 \pm .01$

^{a} Average deviation.

TABLE II

KINETIC DATA FOR THE DECARBOXYLATION OF MALONIC
ACID IN SEVERAL ACIDS

Solvent	ΔH^*, kcal.	ΔS^*, e.u.	ΔF_{140}^*, kcal.	$k_{140} \times 10^4$, sec.$^{-1}$
(1) 2-Methylbutanoic acid	32.1	+1.4	31.5	1.8
(2) n-Valeric acid	32.2	+2.4	31.1	2.5
(3) Hexanoic acid	32.5	+3.2	31.2	2.4
(4) Decanoic acid	26.6	−11.0	31.1	2.5
(5) Propionic acid[2]	33.6	+6.1	31.1	2.5
(6) n-Butyric acid[2]	32.3	+2.5	31.3	2.2
(7) Molten malonic acid[5]	33.0	+4.5	31.1	2.5

decrease in ΔH^* on going from n-butyric acid to 2-methylbutanoic acid (lines 6 and 1 of Table II) reflects the small increase in the I effect due to the branched alkyl group in the latter. It is apparent, however, on comparing lines 1, 2, 3 and 6 of Table II, that there is very little difference in the ΔH^* of the reaction in n-butyric acid, 2-methylbutanoic acid, n-valeric acid or hexanoic acid—a result which is not surprising in view of the fact that all normal alkyl groups beyond the 3–4 carbon stage possess about the same inductive effect.

The decrease in the ΔS^* of the reaction on going from propionic acid to n-butyric acid (lines 5 and 6 of Table II) is indicative of the increased complexity of the butyric acid dimer over that of propionic acid.[2] On going from n-butyric acid to 2-methylbutanoic acid (lines 6 and 1 of Table II) ΔS^* decreases by only 1.1 e.u. This decrease does not appear to be commensurate with the greater steric hindrance one would expect from the presence of the branched methyl group. The addition of a methyl group to the α carbon atom of butyric acid apparently interferes to some extent with the tendency toward dimerization (screening effect).[7]

(5) C. N. Hinshelwood, J. Chem. Soc., 117, 156 (1920).

(6) C. K. Ingold, "Structure and Mechanism in Organic Chemistry," Cornell University Press, Ithaca, N. Y., 1953, p. 71.

(7) W. Hückel, "Theoretical Principles of Organic Chemistry," Vol. II, Elsevier Publishing Co., New York, N. Y., 1958, p. 363.

Both the ΔH^* and ΔS^* of the reaction in n-butyric acid and in n-valeric acid are very nearly equal (lines 6 and 2 of Table II). This suggests that the 5-carbon acid is not as extensively dimerized as is the 4-carbon acid.

The ΔS^* of the reaction in hexanoic acid is slightly higher than it is in n-butyric acid or n-valeric acid (lines 6, 3 and 4 of Table II). The addition of another carbon atom to the chain has undoubtedly resulted in considerable interference with the tendency toward dimerization, so that, in spite of the larger size of the monomer of hexanoic acid, the reduction in the degree of dimerization actually results in a simpler transition complex with malonic acid than in the case of n-butyric acid or n-valeric acid.

At first glance the data for the decarboxylation of malonic acid in decanoic acid (line 4 of Table II) appear rather surprising. If all alkyl groups beyond the 3–4 carbon stage have about the same inductive effect one would have expected the ΔH^* of the reaction in decanoic acid to be approximately the same as in n-valeric acid, n-butyric acid or n-caproic acid. We find, instead, that the ΔH^* of the reaction in decanoic acid is almost six kilocalories lower than it is in hexanoic acid. Evidently, the nine-carbon alkyl group in decanoic acid has profoundly changed the electron properties of the carboxyl group to which it is attached. Steric hindrance due to the complexity of the hydrocarbon chain probably entirely prevents the formation of the dimer, and strongly hinders the formation of the transition complex, as evidenced by the very large decrease in ΔS^*.

It has been pointed out that in the case of the lower molecular weight alkanoic acids the H-bond in the dimer (being formed between the hydroxyl group of one molecule and the carbonyl oxygen atom of another molecule) probably is stronger than that which is formed between two hydroxyl groups.[8] This strong hydrogen bonding in the dimer will obviously decrease the electron density on the hydroxyl oxygen atom. Consequently, in the case of fatty acids which do not dimerize, the electron density on the hydroxyl oxygen atom would be expected to be considerably greater than it would be for those acids which exist largely in the dimeric form. The large decrease in ΔH^* on going from hexanoic acid to decanoic acid is in line with these considerations.

Of considerable interest is a comparison of Hinshelwood's data for the decomposition of molten malonic acid with that for the decomposition of malonic acid in propionic acid (lines 5 and 7 of Table II). (It is worth noting that a period of nearly 40 years intervened between these two sets of data.) The transition complex for the reaction in propionic acid is formed by coördination of the carbonyl carbon atom of the malonic acid with the hydroxyl oxygen atom of the propionic acid.[2] In molten malonic acid the transition complex is formed evidently by coördination between the electrophilic carbonyl carbon atom of one molecule of malonic acid and one of the unshared pairs of electrons on the hydroxyl oxygen atom of a second

(8) W. Hückel, ref. 7, p. 341.

molecule of malonic acid. (A certain analogy exists between these two acids inasmuch as they are both carboxylic acids containing three carbon atoms.) The specific reaction velocity constant for the decarboxylation of molten malonic acid at 140° is the same as that for the decomposition of malonic acid in propionic acid at that temperature. Furthermore, the ΔH^* of the reaction is nearly equal in both cases, being slightly less in molten malonic acid than in propionic acid. Also, the ΔS^* of the reaction decreases by 1.6 e.u. on going from propionic acid to molten malonic acid.

All these results are easily explicable on the basis of the known properties of the mono- and dicarboxylic acids.[9] It is known that dimerization in the case of the dicarboxylic acids proceeds beyond the dimer stage, however the associated complex which forms still possesses a carboxyl group at both ends. Consequently, in molten malonic acid, the transition complex represents a larger aggregate than in propionic acid, resulting in a lowering of ΔS^*. The fact that there are free carboxyl groups at the termini of the associated complex results in a slightly higher effective negative charge on the hydroxyl oxygen atom of molten malonic acid than in the case of propionic acid, and hence in a somewhat lower value of ΔH^*.

Further work on this problem is contemplated.

Acknowledgments.—The support of this research by the National Science Foundation, Washington, D. C., is gratefully acknowledged.

(9) W. Hückel, ref. 7, p. 329, et seq.

AN EXTRACTABLE COMPLEX OF DIBUTYL PHOSPHATE AND PHOSPHORIC ACID[1]

By B. J. THAMER

Contribution from Los Alamos Scientific Laboratory of the University of California, Los Alamos, New Mexico

The extraction of uranium by a several-fold greater concentration of dialkyl phosphate has been formulated as

$$UO_2^{+2}(aq) + 2H_2D_2(org) =$$
$$UO_2(HD_2)_2(org) + 2H^+(aq) \quad (1)$$
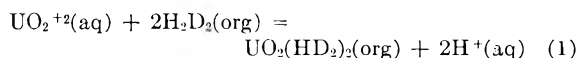
by Baes, et al.,[2] in the extraction into n-hexane with di-(2-ethylhexyl) phosphate and by Dyrssen[3] in the extraction into chloroform with di-n-butyl phosphate. It was the purpose of the present experiments to investigate further the state of the extractant without uranium under the conditions of the author's study of uranyl phosphate complexes.[4] The aqueous phases thus were $HClO_4$–$NaClO_4$ solutions having 0–3.76 M total H_3PO_4, 0.510 M H^+, and 1.07 for the ionic strength, and the previous kerosene was used.

(1) Work performed under the auspices of the Atomic Energy Commission.

(2) C. F. Baes, Jr., R. A. Zingaro and C. F. Coleman, THIS JOURNAL, **62**, 129 (1958).

(3) D. Dyrssen, "Recent Investigations on Extractable Metal Complexes," in Italian National Research Council, et al., "Chemistry of the Co-ordinate Compounds, a Symposium, Sept. 15–21, 1957," Pergamon Press, Inc., New York, 1958, p. 291–295.
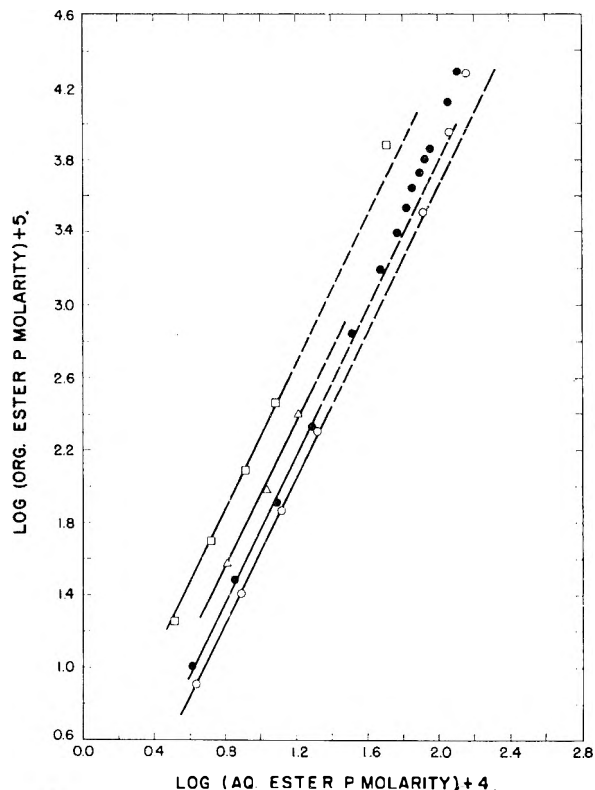
(4) B. J. Thamer, J. Am. Chem. Soc., **79**, 4298 (1957).

Fig. 1.—Ester phosphorus molarities, organic vs. aqueous: $\bigcirc$, no H_3PO_4; $\bullet$, 1.004 M H_3PO_4; $\triangle$, 2.008 M H_3PO_4; $\square$, 3.76 M H_3PO_4.

The dibutyl phosphate was prepared by further purifying the previously used material mixed with P^{32}-labelled dibutyl phosphate from the Volk Radiochemical Company. Any pyro- and triesters were removed from the mixture by the procedure of Peppard, et al.,[5] followed by acidification, extraction into the kerosene, extensive washing with water to remove monobutyl phosphate, and drying. The kerosene solutions of the dibutyl phosphate were equilibrated in the previous manner[4] with the desired aqueous phase, after which the dibutyl phosphate concentration was determined in each phase by β-γ counting. The method thus was similar to that of Dyrssen.[6]

Figure 1 contains a log-log plot of the ester concentrations at equilibrium. The lines have been drawn with a slope of 2. This slope is verified in the absence of H_3PO_4 for gross organic concentrations of ester of 0.00008 to 0.002 M, but it increases rapidly when the concentration is raised above 0.03 M where higher polymers apparently become important. The presence of H_3PO_4 augments the extraction of the ester into the organic phase, thus indicating one or more extractable, probably uncharged, complexes between the two. The series of points of each of the three concentrations of H_3PO_4 each shows a slope of 2 within 10^{-4} to 0.002 M ester in the organic phase. Higher concentrations of ester give higher slopes. However, the average extracted complex probable has the combination $2HD \cdot xH_3PO_4$ within the region of a slope

(5) D. F. Peppard, J. R. Ferraro and G. W. Mason, J. Inorg. Nuclear Chem., **7**, 231 (1958).

(6) D. Dyrssen, Acta Chem. Scand., **11** (2), 1771 (1957).

of 2 where only H_2D_2 is important. Equilibria in the aqueous phase may be sufficiently represented by Dyrssen's data.[6] The four points without H_3PO_4 then give $k = 325 \pm 12\ M^{-1}$ for $2HD(aq) = H_2D_2(kerosene)$. The other data within the region of a slope of 2 might be interpreted with the additional equilibrium

$$H_2D_2(org) + xH_3PO_4(aq) = (2HD \cdot xH_3PO_4)(org) \quad (2)$$
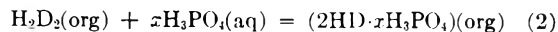
The best single numerical value of x is 1.8 ± 0.1, and the associated value for the formation constant is 0.31 ± 0.03. It is likely that the present experimental conditions produce principally a species containing $2HD \cdot 2H_3PO_4$ with a formation constant in equation 2 of 0.2–0.3 M^{-2}.

From the foregoing it may be said that the author's study of the second and third uranyl phosphate complexes by solvent extraction[1] involved UO_2 $(HD_2)_2$, polymers of dibutyl phosphate beyond the dimer, and an extractable complex between H_3PO_4 and dibutyl phosphate. A recalculation does not seem warranted owing to the present incomplete knowledge of the dibutyl phosphate reactions.

RADIOLYSIS OF ORGANIC LIQUIDS CONTAINING DISSOLVED ICN[1]

By Gordon Hughes[2] and Warren M. Garrison

Crocker Laboratory, Lawrence Radiation Laboratory, University of California, Berkeley, California

In an earlier communication[3] we described some preliminary observations related to the use of ICN as a scavenger of labile intermediates formed in the radiolysis of organic liquids. Of particular interest was the finding that I_2 is a major product of radiation-induced reactions between ICN and the lower alcohols. In the present note we consider the mechanism of I_2 production in the ICN–methanol system. Brief reference is given to comparative data obtained with other organic solvents.

Experimental

The ICN was prepared by addition of I_2 to an aqueous solution of KCN (in excess).[4] Final purification was accomplished by sublimation under nitrogen. The colorless crystalline product contained less than 10^{-3} mole % I_2. Labelled compounds were prepared by direct exchange of ICN with NaI^{131} or $NaC^{14}N$. Methanol (Baker analyzed reagent) was redistilled over 2,4-dinitrophenylhydrazine and chromotropic acid. Cyclohexane (Phillips pure grade) was redistilled and twice recrystallized. All other chemicals were reagent grade and were used without further purification.

Irradiations were made with γ-rays from a 1500-curie cobalt source.[5] Dosages were calculated from calibrations made with the Fricke dosimeter $[G(Fe^{+3}) = 15.5]$.[6,7] Energy absorption in the various solutions was assumed proportional to density.

(1) The work reported in this paper was performed under the auspices of the Atomic Energy Commission.

(2) Department of Chemistry, University of Liverpool, England.

(3) G. Hughes and W. M. Garrison, Abstracts, Am. Chem. Soc. Paper No. 90 (133rd meeting, San Francisco, California, April 1958, Division of Physical and Inorganic Chemistry).

(4) *Org. Syntheses*, **32**, 29 (1952).

(5) We are indebted to the Bio-organic Chemistry Group of the Lawrence Radiation Laboratory for the irradiation facility.

(6) C. J. Hochanadel and J. A. Ghormley, *J. Chem. Phys.*, **21**, 880 (1953).

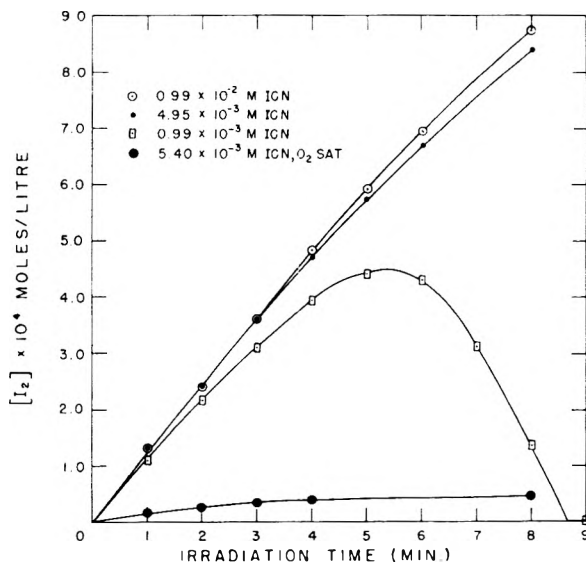(7) R. M. Lazo, H. A. Dewhurst and M. Burton, *ibid.*, **22**, 1370 (1954).

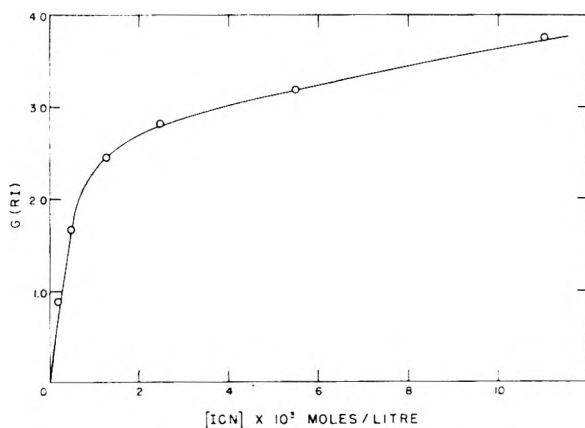Fig. 1.—Iodine production in ICN–methanol solutions.

Fig. 2.—Organic iodide production in ICN–cyclohexane solutions.

Iodine was determined spectrophotometrically in an absorption cell that formed an integral part of the irradiation vessel. Measurements were made at the wave length of maximum absorption by I_2 in each solvent. This value ranged from 450 mμ in methanol to 520 mμ in cyclohexane. Formation of organic iodides in $I^{131}CN$–cyclohexane solutions was measured in terms of I^{131} retention by the solvent after extraction of excess $I^{131}CN$ with aqueous sodium sulfite. In studies with $IC^{14}N$, sulfite treatment was followed by acid hydrolysis and ether extraction. Aliquots of the latter were evaporated to dryness and assayed for C^{14} activity. Control runs established that solutions prepared by addition of ICN to each of the solvents both pure and pre-irradiated were stable in the dark for at least 24 hours.

Figure 1 shows typical data on I_2 production in evacuated ICN–methanol solutions. The initial rate is essentially independent of ICN concentration and corresponds to $G(I_2) = 3.4$. The data obtained with solutions initially 10^{-3} M show that ICN is converted almost quantitatively to I_2 before any appreciable decrease in the rate of I_2 production occurs. Formation of I_2 in the earliest stages of the irradiation we attribute to reduction of ICN by H and(or) CH_2OH, the principal radical products from methanol.[8-10]

$$H + ICN \longrightarrow HCN + I \quad (1)$$
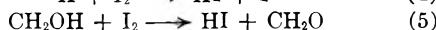$$CH_2OH + ICN \longrightarrow HCN + I + CH_2O \quad (2)$$

(8) W. R. McDonell and A. S. Newton, *J. Am. Chem. Soc.*, **76**, 4651 (1954).

(9) G. E. Adams and J. H. Baxendale, *ibid.*, **80**, 4215 (1958).

(10) N. N. Lichtin, This Journal, **63**, 1449 (1959).

$$2I \longrightarrow I_2 \qquad (3)$$

As soon as first traces of I_2 appear, the competing processes

$$H + I_2 \longrightarrow HI + I \qquad (4)$$

$$CH_2OH + I_2 \longrightarrow HI + CH_2O \qquad (5)$$

can occur. However, no net change in the rate of production of I_2 is introduced by reactions 4, 5 as long as excess ICN is present because HI reacts quantitatively and almost instantly with ICN in organic media.[11,12]

$$HI + ICN \longrightarrow I_2 + HCN \qquad (6)$$
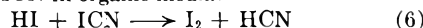
Substantiating evidence for reaction 5 as written has been obtained from separate studies in which excess ICN was added to pre-irradiated I_2-methanol solutions. It was found that the I_2 concentration is immediately restored to within 90 to 95% of the initial value.[13] This observation is consistent with our proposal that the principal radical products from methanol, viz., H and CH_2OH, both react with I_2 to form HI.

On the basis of the mechanism given by reactions 1 through 6 inclusive, the total radical yield from methanol as measured by I_2 production in ICN–methanol solutions is given by $2G(I_2) = 6.8$. This measurement is in fairly good agreement with the values 6.1[9] and 6.3[14] recently obtained for methanol by use of ferric ion scavengers.

The radiation chemistry of ICN–hydrocarbon systems is considerably different from that of the alcohols. No net production of I_2 is found on radiolysis of cyclohexane and n-hexane containing ICN. However, we have established through the use of $I^{131}CN$ that alkyl iodides are formed as major products in both cases. Typical data on alkyl iodide production in evacuated ICN–cyclohexane solutions are shown in Fig. 2. The value $G(RI)$ increases rapidly with ICN concentration over the range 10^{-4} to 10^{-3} M but does not appear to approach a limiting value at ICN concentration as high as 10^{-2} M. At 10^{-3} M ICN, $G(RI) \simeq 2.2$. From corresponding studies with $IC^{14}N$ we estimate that the yield of nitriles $G(RCN)$ is less than 0.1. Since bond-energy data[15] indicate reactions of the type $R + ICN \rightarrow RI + CN$ are endothermic by about 15 kcal., we venture the opinion that organic halides are formed predominantly by reaction of alkyl radicals with I_2 that is produced through H-atom reduction of ICN via reaction 1 above. Since alkyl radicals are produced in excess of H, no net production of I_2 from ICN is observed; direct experimental evidence for formation of H atoms in cyclohexane with a G-yield of ~2.1 recently has been reported.[16,17] It is likely that the increase in $G(RI)$ observed with increasing ICN concentration above 10^{-3} M is related to processes of charge and(or) energy transfer. Some preliminary data recently obtained with ICN–benzene solutions appear to be interpretable only if such processes are invoked. These effects will be considered in a subsequent report.

(11) R. B. Mooney and H. G. Reid, J. Chem. Soc., 1318 (1933).

(12) Any removal of H via H + $CH_3OH \rightarrow H_2 + CH_2OH$ does not affect the kinetics or I_2 production in this system, since no change in the total number of (reducing) radicals is involved.

(13) The fact that the observed recovery of I_2 is not quantitative in these experiments may be explained in terms of the reaction $CH_3 + I_2 \rightarrow CH_3I + I$. Methyl radicals apparently account for some 5 to 15 per cent. of the total radical yield from methanol (ref. 8–10).

(14) E. A. Cherniak, E. Collinson, F. S. Dainton and G. M. Meaburn, Proc. Chem. Soc., 54 (1958).

(15) T. L. Cottrell, "The Strengths of Chemical Bonds," Butterworths Scientific Publications, London, 1954, p. 178.

(16) G. Meshitsuka and M. Burton, Radiation Research, 9, 152 (1958).

(17) We have found that addition of ICN to γ-irradiated solutions of I_2 in cyclohexane liberates I_2 (HI + ICN $\rightarrow$ I_2 + HCN) in amounts corresponding to $G(HI) \simeq 2$.

TABLE OF DISSYMMETRIES AND CORRECTION FACTORS FOR USE IN LIGHT SCATTERING

By W. H. Beattie and C. Booth

Shell Chemical Corporation, Synthetic Rubber Division, Torrance, California

Tables of dissymmetries and correction factors

calculated for particles of various shapes have been published by several authors.[1-3] The tables differ with respect to the methods of calculation used, e.g., graphical integration,[2] conversion to tabulated functions,[1,4] and direct computation.[3] It is not surprising then that comparison of these tables reveals several points of disagreement.

We recently have taken the opportunity of re-calculating these and other light scattering functions for particles of several shapes. Our calculations were made using an IBM 650 electronic computer and are, therefore, internally consistent. The accuracy of the programmed calculation was verified by hand computation of several widely spaced values. The results provide an interesting comparison with the earlier calculations as well as a more convenient and extensive table for use in practical light scattering work than those hitherto available.

The mathematical relations giving particle scattering factors for discs of negligible thickness, spheres, rigid rods of negligible diameter, and linear coiling molecules (in which the distribution of mass obeys Gaussian statistics) are given below.[5-7] These formulas apply only to monodisperse samples, and only to particles having a refractive index close to that of the surrounding medium.[8]

Disc

$$P(\theta) = \frac{x^0}{1} - \frac{x^2}{6} + \sum_{n=3}^{n=\infty} \frac{x^{2(n-1)} \cos (n+1)\pi}{(2n + b_{n-1}/b_{n-2})b_{n-1}} \qquad (1)$$

Sphere

$$P(\theta) = [(3/x^3)(\sin x - x \cos x)]^2 \qquad (2)$$

Rod

$$P(\theta) = (1/x) \int_0^{2x} \left(\frac{\sin w}{w}\right) dw - \left(\frac{\sin x}{x}\right)^2 \qquad (3)$$

Coil

$$P(\theta) = (2/\mu^2)[e^{-\mu} - (1 - \mu)] \qquad (4)$$

where

$x = (2\pi D/\lambda') \sin \theta/2$

$b_n = $ denominator of nth term in eq. 1; $b_1 = 1$; $b_2 = 6$

$\mu = 2x^2/3$

$w = $ variable over which integration is taken

$\lambda' = $ wave length of light in soln. (equal to wave length in a vacuum divided by refractive index of solvent)

$D = $ major dimension of particle
    sphere: diameter
    rod: length
    disc: diameter
    coil: root mean square distance between ends of coil

The dissymmetries, $P(45)/P(135)$, and correction factors, $1/P(90)$, calculated directly from equations 1–4 are given in Table I. The values are believed to be correct to ±0.002. Comparison with earlier tables shows deviations, especially at large D/λ', up to 2%[1] and 3%[3] for discs, 0.4%[1] and 10%[2]

(1) W. M. Cashin, Technical Report to Reconstruction Finance Corporation, Office of Rubber Reserve, CR 2472, September 12, 1950.

(2) P. Doty and R. F. Steiner, J. Chem. Phys., 18, 1211 (1950).

(3) P. Becher, This Journal, 63, 1213 (1959).

(4) F. Bueche, P. Debye and W. M. Cashin, J. Chem. Phys., 19, 803 (1951).

(5) P. Debye, This Journal, 51, 18 (1947).

(6) P. Debye and E. W. Anacker, ibid., 55, 644 (1951).

(7) B. H. Zimm, R. S. Stein and P. Doty, Polymer Bulletin, 1, 90 (1945).

(8) H. C. Van de Hulst, "Light Scattering by Small Particles," John Wiley and Sons, Inc., New York, N. Y., 1956, p. 85.

TABLE I

DISSYMMETRIES AND CORRECTION FACTORS

D/λ'	Discs $\dfrac{P(45)}{P(135)}$	Discs $\dfrac{1}{P(90)}$	Spheres $\dfrac{P(45)}{P(135)}$	Spheres $\dfrac{1}{P(90)}$	Rods $\dfrac{P(45)}{P(135)}$	Rods $\dfrac{1}{P(90)}$	Coils $\dfrac{P(45)}{P(135)}$	Coils $\dfrac{1}{P(90)}$
0.04	1.009	1.005	1.009	1.006	1.005	1.004	1.009	1.007
.06	1.017	1.012	1.020	1.014	1.011	1.008	1.022	1.016
.08	1.030	1.021	1.037	1.026	1.020	1.014	1.040	1.028
.10	1.048	1.033	1.058	1.040	1.031	1.022	1.063	1.044
.12	1.069	1.049	1.084	1.059	1.045	1.032	1.090	1.064
.14	1.095	1.067	1.117	1.081	1.061	1.043	1.124	1.088
.16	1.126	1.088	1.156	1.107	1.080	1.057	1.162	1.115
.18	1.163	1.112	1.202	1.138	1.102	1.072	1.206	1.147
.20	1.204	1.141	1.257	1.173	1.126	1.090	1.255	1.183
.22	1.252	1.173	1.320	1.214	1.153	1.109	1.310	1.223
.24	1.307	1.208	1.395	1.260	1.183	1.131	1.370	1.268
.26	1.368	1.249	1.481	1.313	1.216	1.154	1.436	1.317
.28	1.438	1.294	1.582	1.373	1.250	1.180	1.507	1.371
.30	1.516	1.344	1.700	1.440	1.288	1.207	1.583	1.430
.32	1.604	1.400	1.838	1.517	1.328	1.237	1.663	1.495
.34	1.703	1.461	2.000	1.604	1.370	1.269	1.748	1.564
.36	1.813	1.529	2.192	1.702	1.414	1.304	1.838	1.639
.38	1.936	1.605	2.420	1.814	1.460	1.341	1.931	1.720
.40	2.073	1.688	2.692	1.941	1.508	1.379	2.027	1.806
.42	2.224	1.780	3.021	2.086	1.556	1.421	2.126	1.898
.44	2.391	1.881	3.420	2.251	1.606	1.464	2.227	1.996
.46	2.574	1.992	3.912	2.441	1.656	1.510	2.329	2.100
.48	2.775	2.115	4.522	2.660	1.705	1.558	2.433	2.210
.50	2.991	2.249	5.292	2.912	1.754	1.608	2.538	2.325
.52	3.224	2.397	6.276	3.205	1.802	1.660	2.642	2.447
.54	3.472	2.560	7.559	3.548	1.848	1.714	2.747	2.575
.56	3.732	2.738	9.266	3.949	1.892	1.770	2.850	2.709
.58	4.000	2.932	11.59	4.423	1.933	1.827	2.953	2.849
.60	4.273	3.145			1.972	1.886	3.054	2.995
.62	4.544	3.376			2.007	1.946	3.154	3.148
.64	4.808	3.627			2.040	2.006	3.251	3.306
.66	5.059	3.899			2.069	2.068	3.347	3.469
.68	5.291	4.192			2.095	2.130	3.440	3.639
.70	5.498	4.506			2.118	2.193	3.530	3.815
.72	5.678	4.841			2.139	2.256	3.618	3.996
.74	5.829	5.196			2.156	2.318	3.703	4.183
.76	5.951	5.570			2.172	2.380	3.785	4.376
.78	6.045	5.961			2.185	2.442	3.864	4.574
.80	6.114	6.366			2.197	2.503	3.940	4.778
.82	6.162	6.783			2.207	2.563	4.014	4.988
.84	6.195	7.208			2.216	2.622	4.084	5.203
.86	6.215	7.637			2.225	2.681	4.152	5.424
.88	6.227	8.066			2.232	2.738	4.217	5.650
.90	6.235	8.492			2.239	2.795	4.279	5.881
.92	6.243	8.911			2.246	2.850	4.338	6.118
.94	6.252	9.321			2.252	2.905	4.395	6.361
.96	6.265	9.719			2.258	2.958	4.449	6.609
.98	6.281	10.10			2.264	3.012	4.501	6.862
1.00	6.304	10.48			2.270	3.064	4.551	7.121

for spheres, $0.5\%^2$ for rods, and $0.6\%^2$ and $1.5\%^1$ for coils. When high accuracy is desired, the present table is preferred. For most light scattering purposes, the dissymmetries and correction factors are quoted at intervals which are small enough to allow direct interpolation.

The calculations for spheres were terminated at a dissymmetry value of 10 since experimental measurements of dissymmetries greater than this value are inaccurate owing to large reflectance corrections.[9] It may be noted, however, that the dissymmetry of spheres goes to infinity at $D/\lambda' \approx 0.774$ (see equation 2) and then decreases.

(9) A. Oth, J. Oth and V. Desreux, J. Polymer Sci., 10, 551 (1953).

NUCLEAR MAGNETIC RESONANCE STUDIES OF SOME METHYL DERIVATIVES OF THE GROUP IVB ELEMENTS

By M. P. Brown[1] and D. E. Webster[1,2]

Contribution from the Mallinckrodt Chemical Laboratory of Harvard University, Cambridge, Mass.

The proton magnetic resonance spectra of the tetramethyl derivatives of the Group IVB elements have been studied previously,[3] and it was concluded that in these compounds the relative electronegativities are C > Pb > Ge > Sn > Si, contrary to the usually accepted values.

The effect of various organic groups and of chlorine in a variety of silanes has shown that electronegativity is not the only factor to be considered in interpreting the n.m.r. spectra of this type of compound.[4]

To study further the various effects, we have examined the proton magnetic resonance spectra of the methylchloro-derivatives of carbon, silicon and tin, and hexamethylethane, di-*t*-butyl ether and the corresponding derivatives of silicon, germanium and tin.

Experimental

Proton Magnetic Resonance Spectra.—The measurements were made at a fixed frequency of 40.01 mc. on a Varian Model V-4300B high resolution n.m.r spectrometer equipped with a super-stabilizer, sample-spinner, audio-oscillator, Hewlett–Packard 521-C frequency counter and a Sanborn 151 recorder. An internal standard (Me$_4$Si) was used throughout. The solvent, carbon tetrachloride, the sample of concentration 2–10% and 1% Me$_4$Si (pure grade, Anderson Laboratories, Inc.) were sealed, under vacuum, in 5 mm. o.d. "Pyrex" tubes.

All of the peaks were singlets and were measured to the nearest 0.1 cps., the average of at least 6 determinations being used for each value recorded. The sidebanding technique of Tiers[6] was used for these determinations.

Materials.—The di-*t*-butyl ether was prepared by the method of Erickson and Ashton.[6]

The bis-(trimethyltin) oxide was prepared by the reaction of trimethyltin hydroxide with sodium in boiling benzene,[7] and distillation under vacuum. The yield was very low, but the compound was identified by its infrared absorption spectrum.[8] The proton magnetic resonance spectrum showed only one type of hydrogen.

The hexamethylethane was very kindly supplied by Dr. E. Clinton, The Ethyl Corporation, Detroit, Michigan.

The other hexamethyl derivatives were prepared at the University, Southampton, England.[9]

All other compounds were commercially available, or had been prepared previously in this Laboratory.

Results

It has been shown[3] that the shielding of the protons of the methyl groups attached to the

(1) Research Fellow in Chemistry at Harvard University, 1958–1959.

(2) The University, Hull, England.

(3) A. L. Allred and E. G. Rochow, *J. Inorg. Nucl. Chem.*, **5**, 269 (1958).

(4) D. E. Webster, *J. Chem. Soc.*, in press.

(5) G. V. D. Tiers, This Journal, **62**, 1151 (1958).

(6) J. L. E. Erickson and W. H. Ashton, *J. Am. Chem. Soc.*, **63**, 1769 (1941).

(7) T. Harada, *Sci. Papers Inst. Phys. Chem. Research*, **38**, 115 (1940).

(8) See, R. Okawara, D. E. Webster and E. G. Rochow, *J. Am. Chem. Soc.*, **82**, in press (1960).

(9) M. P. Brown and G. W. A. Fowles, *J. Chem. Soc.*, 2811 (1958).

Group IVB elements in the tetramethyl compounds increases in the order C < Pb < Ge < Sn < Si. Upon successive replacement of the methyl groups by the more electronegative chlorine atoms in the carbon, silicon and tin compounds, we find, as expected, that the shielding decreased, as shown in Table I, where the shielding values (τ in p.p.m.) are reported.

Table I

PROTON MAGNETIC RESONANCE SHIELDING VALUES FOR
Me$_x$MCl$_{4-x}$
(x = 1 to 4)(M = C, Si or Sn)

Compd.	τ, p.p.m.[a]	Compd.	τ, p.p.m.[a]
Me$_4$C	9.073 ± 0.002[b]	Me$_2$SiCl$_2$	9.200 ± 0.002[d]
Me$_3$CCl	8.404 ± .005[c]	MeSiCl$_3$	8.858 ± .005[d]
Me$_2$CCl$_2$	7.828 ± .014	Me$_4$Sn	9.930 ± .005[b]
MeCCl$_3$	7.257 ± .007[c]	Me$_3$SnCl	9.368 ± .012
Me$_4$Si	10.000	Me$_2$SnCl$_2$	8.835 ± .007
Me$_3$SiCl	9.578 ± .002[d]	MeSnCl$_3$	8.353 ± .005

[a] τ, in p.p.m. = $[10.000 - 10^6 (\nu_{\text{obsd}} - \nu_{\text{Me}_4\text{Si}})/\nu_{\text{Me}_4\text{Si}}]$. Increasing values of τ signify increasing shielding of the proton. Error values are standard deviations for the measurements (see ref. 5) [b] These values agree with those previously reported (ref. 3) when H$_2$O was used as the external standard. [c] Also determined by G.V.D. Tiers, "Characteristic N.M.R. Shielding Values for Hydrogen in Organic Structures," Central Research Department, Minnesota Mining and Manufacturing Company, St. Paul, Minnesota, March, 1958. [d] The values for these compounds differ from those previously obtained in this Laboratory (E. Schnell and E. G. Rochow, *J. Inorg. Nucl. Chem.*, 6, 303 (1958). These earlier values are now known to be incorrect. The values reported here are in excellent agreement with values determined independently by Tiers (personal communication).

The change in the shielding of the protons of the methyl group with each successive replacement of a methyl group by chlorine is nearly constant within each of the series. A noticeable difference is that the change is larger in the carbon series than in the silicon series. This also has been found in similar series where the resonance of the proton attached directly to the silicon or the central carbon was studied.[4] This difference may be explained by double bonding between the silicon and chlorine[10] which would return electrons to the silicon and hence increase the shielding.

The change in the tin series more closely parallels the carbon rather than the silicon series. These results are consistent with the tin–chlorine bond not having as much double-bond character as the silicon–chlorine bond.

We have also examined the proton magnetic resonance spectra of the methyl protons in the hexamethyl derivatives of carbon, silicon, germanium and tin, and the corresponding compounds with oxygen between the two central atoms. The shielding values (τ) are given in Table II. The shielding values of the tetramethyl compounds also are given, for comparison.

The protons of the methyl groups in the hexamethylethane are found to be more shielded than in the tetramethyl compound. This is in contrast to the other hexamethyl derivatives, where the protons of the methyl groups are less shielded than in their tetramethyl analogs. In all four series

(10) L. Pauling, "The Nature of the Chemical Bond," 2nd Ed., Cornell Univ. Press, Ithaca, N. Y., 1946, p. 228.

TABLE II

PROTON MAGNETIC RESONANCE SHIELDING VALUES FOR
Me_4M, Me_6M_2 AND Me_6M_2O (M = C, Si, Ge or Sn)

Compd.	τ, p.p.m.[a]	Compd.	τ, p.p.m.[a]
Me_4C	9.073 ± 0.005	Me_6Ge_2	9.788 ± 0.005
Me_4Si	10.000	Me_6Sn_2	$9.790 \pm .005$
Me_4Ge	9.873^b	Me_6C_2O	$8.752 \pm .005$
Me_4Sn	$9.930 \pm .005$	Me_6Si_2O	$9.950 \pm .005$
Me_6C_2	$9.130 \pm .007$	Me_6Ge_2O	$9.700 \pm .010$
Me_6Si_2	$9.963 \pm .002$	Me_6Sn_2O	$9.730 \pm .002$

[a] As ref. *a*, Table I. [b] Value taken from A. L. Allred and E. G. Rochow (ref. 3).

the shielding decreases on putting the electronegative oxygen between the two central atoms. It is again noticeable that the changes in the silicon series are much smaller than in the other series, particularly the carbon series.

Acknowledgment.—The authors wish to thank Professor E. G. Rochow for helpful discussions.

A CONTINUOUS FLOW COUNTING RADIOCHEMICAL TECHNIQUE FOR THE STUDY OF SOLUTION KINETICS[1]

BY J. B. HYNE[2] AND RICHARD WOLFGANG

Contribution No. 1573 from The Sterling Chemistry Laboratory, Yale University, New Haven, Conn.

The use of radio-isotope tracers in kinetics has nearly always involved a sampling technique wherein a series of aliquots is removed from the reaction mixture and analyzed.[3–5] This technique, while convenient when penetrating radiation is involved, is quite laborious and of limited accuracy for the soft emitters, tritium, C^{14} and S^{35} that are most useful in organic reaction studies. The recent development of simple gas-flow counters[6] has prompted the use of a new technique of continuous flow counting of swept out volatile reaction products. This method, as described here, is quite simple, rapid and eliminates the irreproducibility in counting conditions which is the main limitation and source of error of the aliquot technique. It is seldom possible to achieve an accuracy of better than $\pm5\%$ in the rate constant by such aliquot techniques. While this is adequate for many purposes the precision study of many organic reaction rates in solution requires an accuracy of $\pm1\%$ or better.

In many solvolytic reactions where ions are created or replaced conductimetric rate determinations have been made with better than 1% ac-

curacy.[7–9] Since the conductimetric method depends upon the ionizable species behaving as a strong electrolyte the technique is restricted to solvent media of relatively high dielectric constant. It was as a result of efforts to devise a kinetic method of accuracy comparable to that of the conductimetric method but without the limitations of the latter that the radiochemical method described here was developed.

The Method

The radiochemical method described here is applicable to the determination of the rate of any reaction in the liquid phase which liberates as a product a volatile liquid or real gas which can be labelled with any radioactive atom. For the purposes of illustration the hydrolysis of dimethyl *t*-butyl sulfonium iodide in 0.001 M aqueous solution is considered since the radiochemical rate determinations can be compared with the conductimetric rate determinations on the same system. A small amount (*ca.* 2%) of the elimination prod-

uct, isobutylene, is known to form in this reaction[10] but it has been shown that the rate-determining step in this reaction is the S_N1 formation of the *t*-butylcarbonium ion and the elimination of dimethyl sulfide.

In the experimental system used nitrogen is bubbled at a constant flow rate through a sintered glass plate in a cell containing the reaction mixture immersed in a thermostat. As is shown in the Analysis of Data the constancy of the gas flow rate is critical. The flow rate can be controlled adequately, however, by a good two stage reduction regulator on the nitrogen cylinder in conjunction with a tube type flowmeter. Thermal equilibrium is established in the cell within ten minutes after introduction of the cold reaction mixture. The volatile dimethyl sulfide is carried in the nitrogen stream to a proportional gas flow counter of the type previously described by Wolfgang and MacKay.[6] In this type of counter the radiation penetrates a thin (1 mg./cm.^{2}) extensive aluminized Mylar window. The pulses are registered on a scaling circuit having a 1 millivolt sensitivity (Technical Measurement Corp. Model SG2A) and recorded on a moving chart event recorder (Esterline–Angus). Because the plateau is quite independent of the material being counted the window flow counter is generally slightly preferable for C^{14} and S^{35}. However, an internal flow counter[6,11] may also be used and if the very weak H^3 is being counted its use is almost mandatory. If the internal flow counter is used a gas with suitable counter characteristics must be used as the sweep gas. This should be no limitation since inert low boiling mixtures such as $He–CH_4$ are very satisfactory.

Analysis of Data.—Figure 1 illustrates typical data obtained plotted as the logarithm of the count rate *versus* time at two different nitrogen flow rates. The rate at which the labelled dimethyl sulfide is carried to the counter is dependent on two separate rate processes, one chemical the other physical. The net observed counting rate, therefore, measures the over-all behavior of two con-

(1) This work was supported in part by a Frederick Gardner Cottrell Grant from Research Corporation and in part by the Atomic Energy Commission.

(2) Department of Chemistry, Dartmouth College, Hanover, New Hampshire.

(3) P. J. Manno and W. H. Johnson, *J. Am. Chem. Soc.*, **79**, 807 (1957).

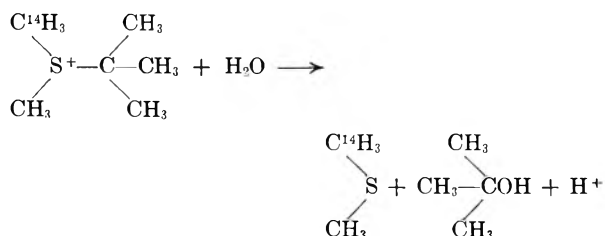(4) D. Conway and W. F. Libby, *ibid.*, **80**, 1077 (1958).

(5) S. Levine and R. M. Noyes, *ibid.*, **80**, 2401 (1958).

(6) R. Wolfgang and C. MacKay, *Nucleonics*, **16**, 69 (1958).

(7) R. E. Robertson, *Can. J. Chem.*, **33**, 1536 (1955).

(8) B. L. Archer and R. F. Hudson, *J. Chem. Soc.*, 3259 (1950).

(9) J. B. Hyne and R. E. Robertson, *Can. J. Chem.*, **35**, 623 (1957).

(10) E. D. Hughes and C. K. Ingold, *J. Chem. Soc.*, 1571 (1933); E. D. Hughes, C. K. Ingold and L. I. Woolf, *ibid.*, 2084 (1948).

(11) R. Wolfgang and F. S. Rowland, *Anal. Chem.*, **30**, 903 (1958).
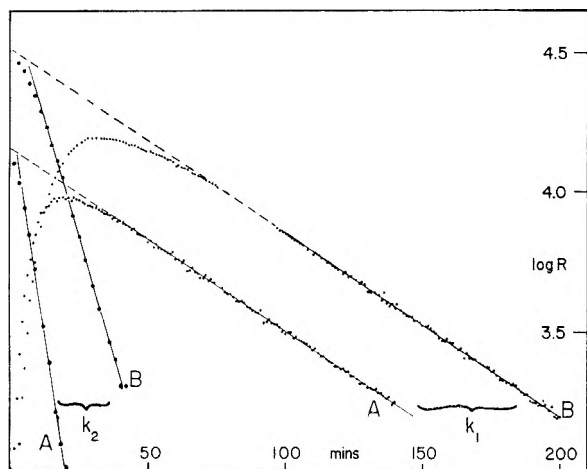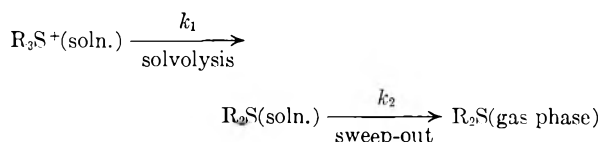
Fig. 1.—Hydrolysis of dimethyl t-butylsulfonium iodide at 75.76°; log R (count rate) vs. time for nitrogen flow rates (A) 15 cc./min. and (B) 7 cc./min. all other conditions identical.

$$R_3S^+(\text{soln.}) \xrightarrow[\text{solvolysis}]{k_1}$$

$$R_2S(\text{soln.}) \xrightarrow[\text{sweep-out}]{k_2} R_2S(\text{gas phase})$$

secutive first-order reactions. The chemical rate k_1 is pseudo first order due to the great excess of the second reactant, namely, solvent, and the sweep out rate k_2 is assumed to be first order proportional to the concentration of dimethyl sulfide in solution at constant nitrogen flow rate. This presumption is shown to be valid by the subsequent analysis.

If n is the number of tagged dimethyl sulfide molecules in solution at any time t and n_0 is the total number of tagged species in the original salt at time zero then by the usual methods of analysis of consecutive first-order reactions[12] we have

$$n = [k_1 n_0/(k_2 - k_1)][e^{-k_1 t} - e^{-k_2 t}] \qquad (1)$$

If the sweep-out rate is first order as assumed then the counting rate R will be given by

$$\begin{aligned} R = Ck_2 n &= [Ck_2 k_1 n_0/(k_2 - k_1)][e^{-k_1 t} - e^{-k_2 t}] \\ &= K[e^{-k_1 t} - e^{-k_2 t}] \qquad (2) \end{aligned}$$

where C is a proportionality constant depending on the geometry of the counter and the rate of passage of the gas through the counter. Provided $k_2 > k_1$ or $k_1 > k_2$ equation 2 becomes, at large t

$$R = Ke^{-k_1 t} \text{ or } R = Ke^{-k_2 t} \qquad (3)$$

A plot of log R vs. t should therefore approach linearity as t becomes large as in Fig. 1. Once one of the rate constants has been determined from the slope of this linear section the second rate constant can be easily determined graphically by plotting, versus time, the logarithm of the difference between the initial observed count rates and the values obtained at corresponding times by back extrapolating the linear section to zero time. These plots are also shown in Fig. 1. The data from a run under a single set of conditions, however, do not enable identification of the rate constants obtained with the corresponding rate processes; by running the

(12) A. A. Frost and R. G. Pearson, "Kinetics and Mechanism," John Wiley and Sons, Inc., New York, N. Y., 1953, pp. 152–153.

system at a different nitrogen flow rate, however, it is clear from Fig. 1 that it is the faster rate in this case which is dependent on flow rate and hence must be the sweep-out rate k_2. Clearly, however, the analysis would also be valid if the chemical rate k_1 were faster than the sweep out rate. The method of calculation is inapplicable when $k_1 = k_2$ but since one of the rates is variable at will this is unlikely to prove a limitation in the method.

Comparison of Results.—Table I shows the radiochemically determined solvolysis rates k_1 at two nitrogen flow rates and solvolysis rates determined conductimetrically for comparison by established methods.[7] Robertson[13] has evaluated the constants for the equation describing the temperature dependence of the rate of hydrolysis of sulfonium salts in water, namely, log $k = -7462.919/T -2.7207 \log T + 24.7096$ and the rate computed from this equation at the corresponding temperature is also shown in Table I. The parts of the curve in Fig. 1 over which the least mean squares fitting was carried out are shown by full lines. The sweep out rates are determined from the initial portions of each run and are good first-order plots, the initial curvature being due to lack of thermal equilibrium in the cell in the early stages of the run. The ratio of the two sweep out rates is also in good agreement with the ratio of the nitrogen flow rates. The initial assumption that the sweep out rate was first order in concentration of dimethyl sulfide in solution and proportional to the nitrogen flow rate is therefore borne out by this analysis.

TABLE I

RATES OF HYDROLYSIS OF SULFONIUM SALT AT 75.76 ± 0.01°

Method and conditions	Chemical rate $k_1 \times 10^4$, sec.$^{-1}$	Sweep-out rate $k_2 \times 10^3$, sec.$^{-1}$
Radiochemical ($N_2 = 15$ cc./min.)	2.50[a]	2.63
Radiochemical ($N_2 = 7$ cc./min.)	2.53[a]	1.28
Conductimetric (3 determinations)	2.53; 2.52; 2.51[b]	
Computed from Robertson eq.[13]	2.529	

[a] Determined by least mean squares fit   [b] Conductimetric determinations were carried out with both "dead" and active samples of the salt; no evidence of an isotope effect was found.

The comparison of results in Table I establishes the precision of the radiochemical kinetic method reported here as of the order of ±1%, comparable with the conductimetric technique but not subject to the limitations of this latter method.

Experimental

Preparation of Labelled Dimethyl t-Butylsulfonium Iodide.—Methyl t-butyl sulfide, n_D 1.4395, was prepared by the method of McAllan, et al.,[14] and treated with a 185 mg. sample (50 microcuries) of NENEX C^{14}-methyl iodide in 0.5 ml. of nitromethane. The sulfide was present in about 10% mole excess. After 8 hours an 88–95% yield of crystalline labelled sulfonium salt was recovered and washed quickly

(13) R. E. Robertson, private communication.

(14) D. T. McAllan, T. V. Cullum, R. A. Dean and F. A. Fidler, J. Am. Chem. Soc., 73, 3627 (1951).

with ether. No further recrystallization was carried out; m.p. 159.5–160.2°.

Kinetic Working Solutions.—Ninety ml. of 0.001 M labelled t-butyldimethylsulfonium iodide solution was required for each run. Labelled and "dead" salt was mixed in 1:2 proportions in each case giving a total activity of each working solution of the order of 5 to 8 microcuries. This activity gave a maximum count rate of the order of 10^4 counts per minute in the early stages of the runs reported here.

Notes on Kinetic Procedure.—1. The count rate obtained is dependent not only on the activity of the sample used but also on the flow rate of the carrier gas. An increase in flow rate will result in a faster sweep-out rate and a more rapid attainment of the linear portion of the rate plot (see Fig. 1) but will also increase the speed at which the active material passes through the counter and hence lower the count rate. Optimization of the flow rate is therefore of considerable importance in obtaining the best results. With the experimental design used in this work flow rates between 5 and 40 cc./min. were found to be within the optimum range.

2. The temperature in the cell is measured directly and is always lower than that of the thermostating fluid due to the cooling effect of the solvent run back from the efficient condenser above the cell. The temperature of the thermostat is set prior to a run at a given cell temperature by duplicating reaction conditions in all respects except inclusion of the reactant in the solvent. The temperature differential between the thermostating fluid and the reaction mixture is principally dependent on both the flow rate of the nitrogen and the thermostat temperature relative to the boiling point of the solvent. At 76° with water as solvent and a flow rate of 40 cc./min. (at STP) solvent loss over a period of six hours was less than 0.5%; with pure ethanol as solvent under the same conditions the maximum solvent loss noted was 1%.

3. Background count was of the order of 130 to 140 counts per minute and was subtracted from the observed count rate before computation of the rate since although insignificant in the early stages of each run the background attains a relatively greater significance when the count rate drops to the order of 10^3 per minute. In all runs the reaction was followed over at least six half-lives and the linear portion of each plot which was least mean squared was never less than three half-lives.

Acknowledgment.—The authors wish to record their thanks to Mr. Z. Hall for technical assistance in this work.

THE NUCLEAR MAGNETIC RESONANCE SPECTRA OF SOME METHYLHYDROPOLYSILOXANES

By D. E. Webster[1,2] and R. Okawara[1]

Contribution from the Mallinckrodt Chemical Laboratory of Harvard University, Cambridge, Mass.

Recently a series of methylpolysiloxanes containing hydrogen bonded directly to the silicon have been prepared.[3] It has been noted[4] that in the infrared absorption spectra of these compounds the Si–H stretching vibration occurred at different positions depending on whether the Si–H grouping was part of a chain-forming (D′) or chain-terminating (M′) unit.[5] When a molecule containing both units was examined (*e.g.*, M′D′M′) a broad band, which could not be resolved, was obtained.

(1) Research Fellow in Chemistry at Harvard University 1958–1959.

(2) The University, Hull, England.

(3) R. Okawara and M. Sakiyama, *Bull. Chem. Soc. Japan*, **29**, 236, 547 (1956).

(4) M. Sakiyama, *ibid.*, **31**, 67 (1958).

(5) In this paper a shorthand notation based on that of Wilcock (*J. Am. Chem. Soc.*, **69**, 477 (1947)) will be used. M = $(CH_3)_3SiO_{1/2}$, M′ = $H(CH_3)_2SiO_{1/2}$, D′ = $H \cdot CH_3SiO$.

It also has been found that the cleavage of the Si–H bond by copper oxide occurs when it is part of an end unit (*e.g.*, M₂′), but not when it is a chain unit in a cyclic compound (*e.g.*, D₅′). Also, cleavage of the siloxane chain by active clay occurs without cleavage of the Si–H bonds in the D′ unit, but with cleavage of the Si–H bonds in the M′ units.[6]

To obtain more information about these compounds, the proton magnetic resonance spectra have now been studied.

Experimental

Proton Magnetic Resonance Spectra.—The conditions for obtaining the spectra already have been described.[7] The n.m.r. standard was Me_4Si (internal).

Materials.—The preparation of the compounds has been described previously.[3]

Discussion

The proton magnetic resonance spectra of the methylhydropolysiloxanes M₂′, D₅′ and MD$_n$′M (n = 1–5) have been examined. In all cases the spectra consisted of two groups of lines, those at high field being due to the protons of the methyl groups, and those at low field due to the protons attached directly to silicon. The positions of the lines are as given in Table I (the τ-values are those of the centers of the multiplets).

TABLE I

PROTON MAGNETIC RESONANCE SHIELDING VALUES FOR M₂′, D₅′ AND MD$_n$′M (n = 1 TO 5)

Compd.	Si–H proton Peak mult.	Si–H proton τ, p.p.m.^{c}	C–H proton Peak mult.	C–H proton τ, p.p.m.^{a}
M₂′	7	5.342 ± 0.010	2	9.828 ± 0.002
D₅′	m^b	$5.324 \pm .020$	2	$9.795 \pm .005$
MD′M	4	$5.402 \pm .005$	2	$9.932 \pm .002^c$
MD₂′M	4	$5.366 \pm .005$	2	$9.870 \pm .002^j$
MD₃′M	5	$5.339 \pm .020$	2	$9.823 \pm .005^c$
MD₄′M	5	$5.329 \pm .024$	2	$9.825 \pm .005^c$
MD₅′M	5	$5.329 \pm .012$	2	$9.825 \pm .005^c$

^{a} τ, in p.p.m. $= [10.000 - 10^6 (\nu_{obsd} - \nu_{Me_4Si})/\nu_{Me_4Si}]$. Increasing values of τ signify increasing shielding of the proton. Error values are standard deviations for the measurements.[8] ^{b} m is an unresolved multiplet. ^{c} There is also a much larger single line at τ = 9.890 ± 0.005 p.p.m. due to the methyl protons of the M unit.

The spectrum of M₂′ consists of a doublet at high field and a group of seven lines at low field, as would be expected from spin-spin interactions. That of D₅′ consisted of a doublet at high field and an unresolved multiplet at low field. The positions of the Si–H resonances in these two compounds were the same, within experimental error, although a difference in the Si–H stretching frequency in the infrared absorption spectra had been found.

The spectra of the series MD$_n$′M are interpreted by assuming that the chain-forming units (D′) are of three types, D$_\alpha$′, D$_\beta$′ and D$_\gamma$′, where D$_\alpha$′ is a D′ unit between two M units, D$_\beta$′ is a D′ unit between an M and a D′ unit, and D$_\gamma$′ is a D′ unit between two other D′ units.

(6) R. Okawara, to be published in *Bull. Chem. Soc. Japan*.

(7) M. P. Brown and D. E. Webster, This Journal, **64**, (1960).

(8) G. V. D. Tiers, *ibid.*, **62**, 1151 (1958).

The compound MD'M contains one D_{α}' unit and $MD_2'M$ contains two D_{β}' units. From the positions of the resonance lines of these two molecules the τ values for the proton of the Si–H group in a D_{α}' and a D_{β}' unit are centered at 5.402 and 5.366 p.p.m., respectively. The spin–spin splitting in each case is 0.036 p.p.m. (fortuitously the same as the difference between D_{α}' and D_{β}'), and the peaks are each a 1 : 3 : 3 : 1 quadruplet. As there is a constant change from D_{α}' to D_{β}' to D_{γ}', it is reasonable to assume that the D_{γ}' quartet will be centered about 5.330 p.p.m., although there is no linear molecule containing only D_{γ}' units with which this can be experimentally verified. The expected spectra for $MD_3'M$, $MD_4'M$, and $MD_5'M$ can now be predicted, and the predicted and experimental spectra are the same in both peak position and relative intensities.[9]

This movement of the Si–H proton resonance is paralleled by the resonance of the hydrogen of the methyl groups of the D' unit. In a D_{α}' unit the methyl group doublet is centered on 9.932 p.p.m., in a D_{β}' unit it is centered on 9.870 p.p.m., and in a D_{γ}' unit on 9.823 p.p.m., the spin–spin coupling being 0.036 p.p.m. There is also a strong singlet at 9.890 p.p.m. due to the methyl groups of the M units.

Since the Si–H protons of the D' units differ in the proton magnetic resonance spectra depending upon the position of the D' unit in the chain, it is likely that the force constants of the Si–H bonds differ and thus it need not be surprising that in the infrared spectrum a broad band has been obtained. It may also be concluded that as the shielding values of the Si–H protons of the M' and the D' units are not appreciably different, the noticeable chemical differences probably are due to other than electronic factors.

Acknowledgments.—We wish to thank Professor E. G. Rochow for helpful discussions.

(9) The success of this treatment suggests that no serious complications are introduced by the fact that the compounds are mixtures of diastereoisomers.

THE DIFFUSION OF HYDROCARBONS IN POLYISOBUTYLENE

By George Blyholder[1] and Stephen Prager

Contribution from the Department of Chemistry, University of Minnesota Minneapolis, Minnesota

The diffusion of a number of light hydrocarbons in polyisobutylene has been studied by Prager, Bagley and Long[2,3] using a technique which measures the rate of sorption and desorption from a film. In the present work this systematic survey of a series of closely related systems is extended to larger molecules and to cyclic as well as branched and straight chain hydrocarbons.

Experimental Procedure

Measurements were made by Barrer's time lag method,[4] suitably modified to deal with the low vapor pressures of some of the penetrants used, as well as the inability of polyisobutylene films to support for long a pressure difference of much more than 1 mm. The apparatus consists essentially of a diffusion cell, a gas metering system and various pressure measuring devices.

The cell itself was made by cutting and grinding off half of the ball from each of two ball-and-socket joints. By placing the poly-isobutylene film between the two halves so obtained and clamping them together, a most satisfactory vacuum tight seal was produced, with the film serving as its own gasket. The lower half of the diffusion cell was fitted with a Pirani gauge, made from the filament of a 60 watt light bulb.

The polyisobutylene was Vistanex B-100, obtained from the Standard Oil Company of New Jersey. The films were prepared from a cyclohexane solution of the polymer, by the previously described technique[2] of casting on a mercury surface, their thickness being measured by weighing a piece of known area. The hydrocarbons were the "pure" grade furnished by the Phillips Petroleum Company, and were used without further purification.

To make a run the assembled diffusion cell was attached to the remainder of the apparatus by the two tapered joints, and the entire system thoroughly outgassed by means of a diffusion pump, the liquid hydrocarbon contained in a bulb being frozen out by immersion in liquid air for this purpose. Hydrocarbon vapor was then admitted and a small quantity was metered by means of a section of tubing between two stopcocks. The diffusion cell was immersed in a water thermostat at the desired temperature. The vapor was then admitted to the top half of the diffusion cell, the pressure in that part of the system being measured by means of a silicone oil manometer, and the ensuing permeation of vapor through the film was followed by measuring the pressure in the bottom half of the cell with a Pirani gauge.

Results

The diffusion coefficient D was calculated from the resulting data by the usual relation.[4]

$$D = \frac{l^2}{6t_0}$$

where l is the thickness of the film and t_0 the time lag obtained by extrapolating the asymptote of the pressure–time plot back to the time axis. While the permeability method should in principle permit the calculation of the penetrant concentration on the high pressure side of the film, such results are not given here because relatively few calibrations of the Pirani gauge were obtained, especially for some of the larger hydrocarbons; however, it was estimated that the weight fraction of penetrant in general did not exceed 2–3 × 10^{-4}.

Values of t_0 and D for a variety of hydrocarbons are given in Table I. It will be observed that in spite of the very low penetrant concentrations in the film, the time lag t_0 shows an appreciable pressure dependence. This is probably to be attributed to the deformation of the film by the pressure difference which it supports: as the pressure in the top half of the cell increases, the film decreases in thickness and increases in area, leading to lower values of t_0. Whenever possible, therefore, the data were extrapolated to zero pressure to give t_∞. The diffusion coefficient for *n*-pentane in polyisobutylene at 35° obtained in this way (2.55 ×

(1) Department of Chemistry, University of Arkansas, Fayetteville, Arkansas.

(2) S. Prager and F. A. Long, *J. Am. Chem. Soc.*, **73**, 4072 (1951).

(3) S. Prager, E. Bagley and F. A. Long, *ibid.*, **75**, 1255 (1953).

(4) R. M. Barrer, "Diffusion in and Through Solids," Cambridge University Press, London, 1941.

TABLE I

DATA FOR DIFFUSION COEFFICIENTS FOR FILM NO. 1, 2 AND 3 WITH THICKNESSES 9.4, 4.3 AND 5.7 $\times$ 10^{-3} CM., RESPECTIVELY

Gas	Film No.	P, mm.	T, °C.	t_0, min.	t_∞	$D \times 10^9$
n-C_5	1	0.344	25.1	165		1.5
n-C_5	1	.342	35	71.5 ± 0.5		3.4
n-C_5	1	.329	45	32.5 ± 0.5		7.5
n-C_5	1	.358	45	35		7.0
n-C_5	1	.321	55	16.3 ± 0.7		15.0
n-C_6	1	.350	55	15.5 ± 0.5		15.8
n-C_5	2	.362	35	16.7		3.0
n-C_5	2	.379	45	7.7		6.7
n-C_5	3	.404	25	74.8 }	84	1.08
n-C_5	3	.178	25	80 }		
n-C_5	3	.390	35	30 }		
n-C_5	3	.359	35	30.3 }	35.7	2.55
n-C_5	3	.133	35	34 }		
n-C_5	3	.384	35	32 }		
n-C_6	2	.404	35	17		2.99
n-C_7	3	.419	35	26.2 }	29.9	3.04
n-C_7	3	.270	35	27.5 }		
n-C_8	3	.155	25	62 }	78.6	1.17
n-C_8	3	.080	25	70 }		
n-C_8	3	.082	35	27.3 }		
n-C_8	3	.072	35	28.4 }	28.8	3.16
n-C_8	3	.281	35	24.1 }		
n-C_8	3	.617	35	21.5		
2-Methylpentane	2	.390	35	28.5		1.8
3-Methylpentane	3	.392	35	56		1.6
2,2,5-Trimethyl C_6	1	.385	35	214		1.15
2,2,5-Trimethyl C_6	1	.351	45	104		2.36
2,2,5-Trimethyl C_6	1	.370	45	98		2.50
2,2,5-Trimethyl C_6	1	.376	65	24.5		
2,2,5-Trimethyl C_6	3	.063	25	216 }	230	0.395
2,2,5-Trimethyl C_6	3	.204	25	184 }		
2,2,5-Trimethyl C_6	3	.056	35	89.5 }	93	0.98
2,2,5-Trimethyl C_6	3	.129	35	85 }		
Cyclohexane	1	.398	45	94		2.6
Cyclohexane	1	.449	65.0	23.3		10.5
Cyclohexane	2	.388	35	43		1.2
Methylcyclohexane	1	.384	35	180		1.36
Methylcyclohexane	1	.382	35	187		1.31
Methylcyclohexane	2	.399	35	37		1.37
Methylcyclopentane	2	.399	35	34		1.5

10^{-9} cm.^{2}/sec.) proved to be in good agreement with the value given by Prager and Long[2] for the same system (2.64×10^{-9} cm.^{2}/sec.).

So far as comparison between the different hydrocarbons is concerned, the trends indicated by the earlier work continue: within the limits of the experimental error, the diffusion coefficients of n-pentane, n-hexane and n-octane at 35° are equal, but greater than those of cyclohexane, methylcyclohexane and methylcyclopentane, which in turn are about equal to those for the branched hydrocarbons 2-methylpentene and 2,2,5-trimethylhexane. Thus, as expected, branching and cyclization seem to have comparable effects. The activation energies for n-pentane, n-octane, and 2,2,-5-trimethylhexane are 15.7, 18.4 and 16.6 kcal./mole, respectively. They show some variation, but because of the small range of temperatures employed in most cases the significance of this is somewhat doubtful; thus if the temperature range used is 10°, a $\pm 5\%$ error in the diffusion coefficient, (which is approximately the experimental error indicated by the reproducibility of the data) leads to an error of about ± 2 kcal./mole in the activation energy.

MAGNESIUM–HYDROGEN RELATIONSHIPS[1]

BY J. A. KENNELLEY, J. W. VARWIG AND H. W. MYERS

Mallinckrodt Chemical Works, Uranium Division, St. Charles, Missour

Investigations in our laboratory have required an accurate knowledge of equilibrium dissociation

pressures of magnesium hydride in the region between 100 and 1000 mm. We have employed a modified Sievert's apparatus to determine the equilibrium pressures, to follow the rate of magnesium hydride decomposition, and for preliminary observations on the kinetics of magnesium hydride formation in this pressure range. Commercially available magnesium hydride was used as the starting material for these experiments. Previous work on decomposition pressures for magnesium hydride and rate constants for the magnesium–hydrogen reaction were reported by Ellinger, et al.,[2] in the pressure range above four atmospheres.

The temperature–pressure relationship is given by the equation $\log P_{mm} = -3857/T + 9.78$. In determining experimental values, equilibrium was approached from the high and low pressure sides. For most of the measurements, several days of constant temperature control ($\pm 1.0°$) were required to obtain a single equilibrium pressure reading. The heat of formation calculated from these data is 17.7 ± 0.7 kcal./mole at the 95% confidence level.

By using very finely divided magnesium (B.E.T. surface area of 3.6 sq. m./g.) and hydrogen produced from the decomposition of UH_3, we have established that the formation of magnesium hydride is governed by the first-order relationship $k = (2.303/t)(\log W_0/W)$, where W_0 is the initial weight of magnesium present and W the quantity unreacted, and k is the specific reaction rate constant. Values for k are 0.087 hr.$^{-1}$ and 0.052 hr.$^{-1}$ at 255 and 281°, respectively.

The rate of decomposition and the equilibrium dissociation pressure increase rapidly with temperature. We have observed that the decomposition of magnesium hydride (B.E.T. surface area = 3.1 sq. m./g.) at constant volume satisfies the rate equation $\log (P_0 - P) = -(k/2.303)t + \log P_0$, where P_0 is the equilibrium hydrogen pressure at a particular temperature, P is the hydrogen pressure at time t, and k the rate constant. Rate constants at 234, 256 and 278° are 2.59 $\times$ 10^{-2}, 1.47 $\times$ 10^{-1}, and 3.39 $\times$ 10^{-1} hr.$^{-1}$, respectively.

(1) This work was supported by the U.S.A.E.C., Contract W-14-108-Eng.-8.

(2) F. H. Ellinger, C. E. Holley, Jr., B. B. McInteer, D. Pavone, R. M. Potter, E. Staritzky and W. H. Zachariasen, J. Am. Chem. Soc., 77, 2647 (1955).

THE X-RAY PATTERN OF CRYSTALLINE XYLANS

By R. H. MARCHESSAULT AND T. E. TIMELL

Contribution from the Research and Development Division, American Viscose Corporation, Marcus Hook, Penna., and Pulp and Paper Research Institute of Canada, Montreal, Que.

Several authors[1-4] have reported X-ray diagrams of various crystalline xylans. The purpose of this communication is to point out that xylans readily form a crystalline hydrate giving an X-ray pattern which is distinctly different from that of the dry polysaccharide. Failure to appreciate this fact has caused some confusion in the literature[1,2] where the two different diagrams have been presented without any mention of this fact.

Two different X-ray diagrams (Table I) were obtained with both a neutral esparto xylan[5] and with two 4-O-methyl-glucuronoxylans from the wood[6] and the bark[7] of white birch. It was possible to transform one form into the other by wetting, or by drying at 80° in vacuo overnight, exposure at 80% relative humidity for ten days was not sufficient to cause the dry form to revert to the hydrate modification. Gravimetric analyses suggested that the hydrated xylans contained approximately one water molecule per D-xylose residue. However, since polymers are not perfectly crystalline this is probably a lower limit. The crystalline perfection depended greatly on the pretreatment, and solvent-exchange to non-polar solvents was most detrimental in this respect, while drying from an aqueous medium appeared to give maximum enhancement of crystallinity.

TABLE I

Cu $K\alpha$ X-RAY REFLECTIONS OF CRYSTALLINE XYLANS

v. w. = very weak; w = weak; n = normal; s = strong.

Xylan hydrate	Xylan	Xylopentaose
7.76n	7.32w (diffuse)	7.55w (diffuse)
6.71n		5.30w
5.31v.w.	4.98s	4.93s
4.44s		4.70v.w.
3.79w		4.55n
3.43w	4.15n	4.15n
2.74v.w.		3.95v.w.
		3.20w
	2.98w	3.00n
		2.85n
		2.65w
	2.53v.w.	2.53v.w.

The resolution of the diagrams of the 4-O-methylglucuronoxylans was greatly improved by mild hydrolysis (pH 4, 120°, 15 min.).[4] Uronic anhydride and infrared analyses indicated that the acid groups, which were present in the salt form, had not been removed. The close resemblance between the X-ray diagrams of the dry xylans and that exhibited by a pure sample of xylopentaose[8] suggested that the acid groups are not an integral part of the unit cell. It is worth noting that the spacings for the xylan in Table I are slightly different from those reported earlier.[2]

(1) B. G. Rånby, Svensk Papperstidn., 55, 115 (1952).

(2) P. A. Roloefson, Biochim. Biophys. Acta, 13, 592 (1954).

(3) C. T. Bishop, Can. J. Chem., 31, 793 (1953).

(4) A. P. Yundt, Tappi, 34, 89 (1951).

(5) S. K. Chanda, E. L. Hirst, J. K. N. Jones and E. G. V. Percival, J. Chem. Soc., 1289 (1950).

(6) C. P. J. Glaudemans and T. E. Timell, J. Am. Chem. Soc., 80, 941, 1209 (1958).

(7) A. Jabbar Mian and T. E. Timell, unpublished results.

(8) Kindly donated by Professor R. L. Whistler, Purdue University.

CHEMICAL ENGINEER

ADVANCE DEVELOPMENT OF SEMICONDUCTOR DEVICES

PHD, MS or equivalent to expand and design processes and techniques to obtain stable device surfaces, surface protectants, and precise surface ambients during transistor encapsulation.

WRITE: M. D. Chilcote, Div. JPC-5
Semiconductor Products Dept.
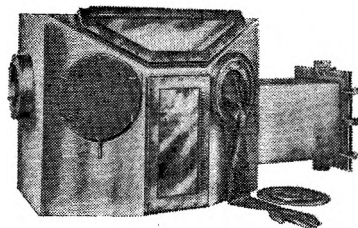Electronics Park, Syracuse, New York

GENERAL ⊛ ELECTRIC

PHYSICAL CHEMIST

ADVANCE DEVELOPMENT OF SEMICONDUCTOR DEVICES

PHD, MS or equivalent with a background in surface-gas reactions, diffusion, surface reaction kinetics or electrochemical phenomena to develop basic processes for the stabilization of semiconductor device surfaces.

WRITE: M. D. Chilcote, Div. JPC-5
Semiconductor Products Dept.
Electronics Park, Syracuse, New York

GENERAL ⊛ ELECTRIC

PHYSICIST

ADVANCE DEVELOPMENT OF SEMICONDUCTOR DEVICES

PHD, MS or equivalent with a background in solid state physics or electronics to analyze the operation of high frequency devices leading to the development of new device structures.

WRITE: M. D. Chilcote, Div. JPC-5
Semiconductor Products Dept.
Electronics Park, Syracuse, New York

GENERAL ⊛ ELECTRIC

2037
3 √σ